UNIVERSITY OF MICHIGAN
DEPARTMENT OF MECHANICAL ENGINEERING
CAVITATION AND MULTIPHASE FLOW LABORATORY

UMICH 014571-4-T

STUDY OF LIQUID FILMS, FINGERS AND DROPLET MOTION FOR STEAM TURBINE BLADING EROSION PROBLEM

by

Wontaik Kim

Approved by: F. G. Hammitt

Financial Support provided by: National Science Foundation
Grant No. ENG 75-2315 and University of Michigan (SEP)
funds.

September, 1978

ABSTRACT

STUDY OF LIQUID FILMS FINGERS AND DROPLET MOTION
FOR STEAM TURBINE BLADING EROSION PROBLEM

by

Wontaik Kim

Chairman: Frederick G. Hammitt

Some phenomena leading to large steam turbine blading erosion have been investigated experimentally. Primarily these are the behavior of thin liquid films, and their subsequent break-up into droplets and fingers at the trailing edge of a stationary blade in the University of Michigan low-pressure wet-steam tunnel.

Both high-speed (5000 Hz) cinematography and still photography have been used to visualize the pertinent phenomena and measure the important parameters. Also electrical conductivity microgages were used to measure liquid film thickness.

A film "Transition Map" for various flow regimes has been constructed, based on the author's results. Three film flow regimes were delineated: rivulet, wavy-film and an entrainment regime.

Critical conditions for rivulet flow were obtained experimentally. Comparison with existing theoretical models shows that the wetting contact angles required in these models are much smaller than those measured here and elsewhere for static conditions. "Bulges" at the film-rivulet stagnation point, and waviness in the film, have been

observed and may be responsible for discrepancies between the author's observations and earlier theoretical models.

Film wave characteristics have been measured, showing some waviness always. These wavelets are either two-dimensional or three-dimensional depending on the flow conditions. A shear perturbation instability mechanism for wave generation seems pertinent for the present thin film case, while pressure perturbation is pertinent for thick-film cases. The author's wave propagation speed measurements show that for two-dimensional waves, the classical capillary-gravity wave propagation model is suitable, while for the high-subsonic waves Wurz's model[W14] correlates the results well.

For the entrainment regime, a correlation has been found based on the author's film thickness measurements. This correlation explains horizontal film flow data well (including the author's), but not vertical passage data.

At the trailing edge, time-dependent liquid finger behavior has been observed. It is found that Karman vortex shedding in the steam is not a controlling factor, rather surface tension and other dynamic forces of the steam play more important roles for finger formation.

The author's measured wake droplet trajectories show two important phenomena which were not reported previously in the literature. These are periodic deceleration of wake droplets and break-up time-dependence upon droplet Weber number. The primary cause of periodic deceleration of drops

may be steam vortex-shedding from the blade into the wake. Direct measurements of such vortices were not attempted in this study.

Droplet break-up time dependence on inverse Weber number is explained well by classical wave growth theory.

STUDY OF LIQUID FILMS, FINGERS, AND DROPLET MOTION FOR STEAM TURBINE BLADING EROSION PROBLEM

by

Wontaik Kim

A dissertation submitted in partial fulfillment
of the requirements for the degree of
Doctor of Philosophy
(Mechanical Engineering)
in The University of Michigan
1978

Doctoral Committee;

Professor Frederick G. Hammitt, Chairman
Professor Vedat S. Arpaci
Professor James W. Daily
Professor Jerzy R. Moszynski, University of Delaware
Professor Charles M. Vest

ACKNOWLEDGEMENTS

The author is very grateful for the support and assistance of many individuals towards the completion of this work. In particular, he would like to express his appreciation to Professor Frederick G. Hammitt for his careful and consistent advice during this thesis work; Dr. S. Krzeczkowski for his useful suggestions and assistance while he was here as a Visiting Scientist; Professor Vedat S. Arpaci for his many discussions and encouragement during the author's most difficult time in the graduate work; to Professors James W. Daily, Jerzy R. Moszynski and Charles M. Vest for their serving as a doctoral committee members.

Thanks are also due to large number of student assistants for their time and effort in the test operation and data reduction.

The assistance of Ms. Ruth Howard in the preparation of the thesis manuscript is most greatly appreciated.

The author also gratefully acknowledges the financial support by the National Science Foundation, Grant ENG 75-2315, internal University of Michigan Funds (SEP) and University Fellowship.

And finally the author extends his appreciation to his wife, Songmin, and daughter, Christina, who provided shelter and comfort throughout the entire graduate work.

Dedicated to my father

Mr. Kyung-Suk Ma

TABLE OF CONTENTS

LIST OF TABLES

LIST OF FIGURES

NOMENCLATURE

Symbol	Description	Unit
a_F	Frozen speed of sound	m/sec
A_C	Cross sectional area of the test section	m^2
Am	Measured droplet acceleration	m/sec^2
As	Droplet acceleration using Serafini drag coefficient	m/sec^2
a,b	Widths of test section walls	cm
A	Wave amplitude	cm
A_D	Projected area of droplet in the axial direction $(\frac{\pi D^2}{4})$	cm^2
B	Blade thickness	cm
C	Wave propagation speed	cm/sec
C'	Non-dimensional wave speed $(= C/V_f)$	
C*	Non-dimensional wave speed $(= C/\sqrt{\tau_i / \rho_f}$ Wurz$)$	
C_D	Drag coefficient	
D	Liquid droplet diameter	cm
D_o	Initial liquid droplet diameter	cm
D_H	Hydraulic diameter $(= 4 \times \frac{\text{area}}{\text{periphery}})$	cm
f	Film friction coefficient	
f_i	Interfacial film friction coefficient	
F	Henstock-Hanratty Parameter $(= \frac{\gamma \, Re_f}{Re_s^{0.9}} (\frac{\nu_f}{\nu_s}) (\frac{\rho_f}{\rho_s})^{1/2})$	
g	Gravitational acceleration	cm/sec^2

Symbol	Description	Unit
G	Reciprocal Froude number $(= \frac{gh}{V_f^2})$	
h	Film thickness	μm
h_p	Film thickness of wavy crest	μm
H_{hg}	Mercury manometer head	cm or inch
h^+	Non-dimensional film thickness $(= \frac{h\,(\tau_i/\rho)^{1/2}}{\nu_f})$	
K_i	Isentropic expansion, index	
Kn	Knudsen number $(= \frac{\text{mean free path of vapor molecule}}{\text{diameter of droplet}})$	
K	Von Karman's constant	
k	Wave number $(= \frac{2\pi}{\lambda})$	cm^{-1}
L	Maximum finger length	cm
$\bar{L}$	Time averaged maximum finger length	cm
L*	Non-dimensional finger $(= \frac{\bar{L}}{\lambda_f})$	
M	Mach number	
N	Number of fingers	
P_o	Pressure	N/m^2
ΔP	Pressure drop	N/m^2
P_k	Negative pressure differential due to curvature of wave $(\propto \rho_s (U_s - c)^2 (\frac{A}{\lambda}))$	N/m^2
P_s	Surface tension stress $(\propto \frac{\sigma}{\lambda}\frac{A}{\lambda})$	N/m^2

Symbol	Description	Unit
q	Specific liquid flow rate per unit width	$cm^3/cm.sec$
Q	Non-dimensional flow, i.e. ratio of dynamic steam pressure on the droplet surface to upstream dynamic steam pressure $\left(= \frac{\rho_g U_g^2}{\rho_s U_s^2} \right)$	
Q_m	Maximum Q	
Re_d	Droplet Reynolds number $\left(= \frac{U_r D}{\nu_s}\right)$	
Re_f	Liquid film Reynolds number $\left(= \frac{V_f h}{\nu_f}\right)$	
R	Ratio of measured to Serafini's acceleration $\left(= \frac{Am}{As}\right)$	
$\bar{R}$	Time averaged acceleration ratio	
S_{f_1}	Finger Strouhal number $\left(= \frac{\bar{L}}{\Delta T\ V_f}\right)$	
S_{f_2}	Finger Strouhal number $\left(= \frac{\bar{L}}{\Delta T\ U_s}\right)$	
S_B	Strouhal number for droplet deceleration $\left(= \frac{B}{U_s \Delta t}\right)$	
T_o	Steam temperature	°C
t_b	Break-up time of droplet	sec
T	Reciprocal Weber number $\left(= \frac{\sigma}{\rho_f V_f^2 h}\right)$	
ΔT	Finger formation period	sec
Δt	Droplet deceleration period	sec
T_b	Non-dimensional break-up time $\left(= \frac{U_r\ t_b}{D_o} \left(\frac{\rho_s}{\rho_f} \right)^{1/2}\right)$	

Symbol	Description	Unit
U	Droplet Velocity	cm/sec
U_r	Relative steam velocity ($= U_s - U$)	cm/sec
U_s	Bulk average steam velocity in the test section	m/s
u^*	Friction velocity ($= \sqrt{\tau_i / \rho_f}$)	m/s
v	Specific volume of steam	cm^3/gm
v_o	Volume of a liquid droplet ($= \frac{\pi D^3}{6}$)	cm^3
V_f	Film surface velocity	cm/sec
V_c	Capillary - Gravity propagation speed ($= (\frac{g}{k} + \sigma \frac{k}{\rho})^{1/2}$)	cm/sec
W_w	Mass flow rate of steam	Kg/hr
$W_{(y)}$	Velocity profile in rivulet	cm/sec
We_h	Weber number ($= \frac{\rho_f h V_f^2}{\sigma}$)	
We_p	Weber number ($= \frac{\rho_f h_p V_f^2}{\sigma}$)	
We_s	Finger Weber number ($= \frac{\rho_s \bar{L} U_s^2}{\sigma}$)	
We_b	Droplet break-up Weber number ($= \frac{\rho_s U_r^2 D_o}{\sigma}$)	
x	Steam quality	
X	Transverse span in finger formation	cm
ρ_g	Density of gas or density of steam far ahead of droplet	gm/cm^3
ρ_s	Density of steam	gm/cm^3
ρ_f	Density of liquid	gm/cm^3
λ	Film wave length	cm

Symbol	Description	Unit
λ_f	Finger wave length (= X/N)	cm
ν_s	Kinematic viscosity of steam	cm^2/sec
ν_f	Kinematic viscosity of liquid	cm^2/sec
τ	Non-dimensional finger formation period $\left(= \frac{U_s \Delta T}{\bar{L}} \left(\frac{\rho_s}{\rho_f}\right)^{1/2}\right)$	$dyne/cm^2$
τ_i	Interfacial shear stress	$dyne/cm^2$
τ_s	Shear stress due to smooth wall	$dyne/cm^2$
μ	Dynamic viscosity	gm/cm.sec
ϵ	Sand roughness	cm
θ	Wetting angle	
σ	Surface tension	dyne/cm
α	Non-dimensional wave number (= k.h)	
η (X,t)	Non-dimensional sinusoidal perturbation profile	
II	Non-dimensional normal perturbation stress	
Σ	Non-dimensional tangential perturbation stress	

CHAPTER I

GENERAL PROBLEMS ASSOCIATED WITH STEAM WETNESS

One might ask the question, "Now that steam turbines have been used and improved since the late 17th century, why do we still need further research thereon?" That may seem a plausible question because the first substance discussed in elementary thermodynamics courses is steam, and all power engineers must have thoroughly studied the properties and behavior of steam, concepts of steam turbine efficiencies, etc. Nevertheless, there continue to be many on-going research programs, particularly relating to wet steam flow in steam turbines which, being multiphase flow, is itself a very complex subject. Therefore, it is of benefit to review the history of the various problems concerning steam turbines, specifically in the area of the author's research.

From the early days of steam turbines, designers have made substantial efforts to improve the efficiency of the steam cycle. The most promising way of accomplishing this was to raise the temperature and pressure of steam to as high a value as would be compatible with the best construction materials available at an acceptable price. It became apparent soon that the limits set to the temperature of highly stressed parts were rather strict, while the limits concerning the pressure in the boiler and turbine inlet could be raised more easily by improved design.

As seen in Fig. 1.1 an increase of steam pressure P_o,

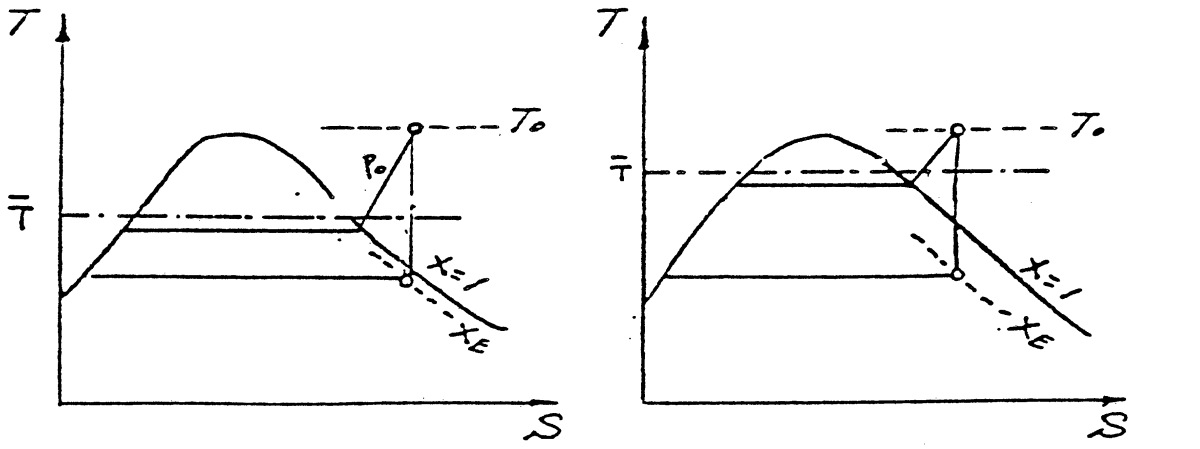

(a) Low P_o ;
Low Carnot efficiency
Low exit wetness $(1 - X_E)$

(b) High P_o ;
High Carnot efficiency
Higher exit wetness $(1 - X_E)$

Fig 1.1 : Steam Cycle Characteristics (Temperature and Entropy Diagram)

Fig 1.2: Wetness Loss Data From Tests on Laboratory Turbines (Miller, 1972)

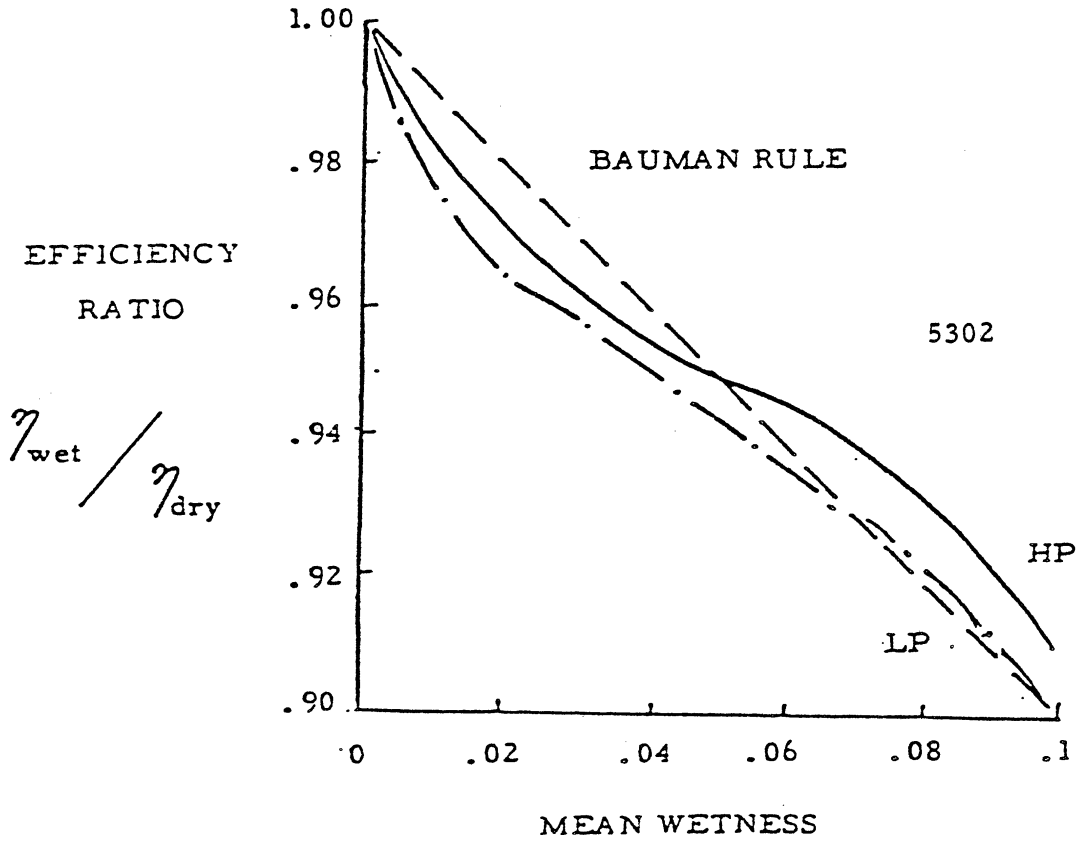

at constant steam temperature, T_o, raises the mean temperature, $\bar{T}$, of heat addition to the cycle, which means an improved Carnot efficiency. However, it was also necessary to limit pressure. Practical pressure limits were set both by stress considerations and limitations on wetness fraction at turbine exit.

For increased exit wetness, two problems are noted. First, severe erosion damage to the low-pressure blading occurs. After a few months or years of service, poorly designed low-pressure rotor blades can be significantly damaged, i.e., seriously roughened, pitted or even broken. To prevent grave erosion damage as well as substantial loss of efficiency, limitation of exit wetness to $\sim$ 12% (by mass) was found necessary. Thus wetness became as severe a limiting factor to the attainable efficiency of steam turbine plants as the temperature and pressure resistance of materials.

Second, it was found that the aerodynamic efficiency of turbine stages operating in the wet steam region was considerably lower than that of dry stages. One of the earliest empirical correlations of turbine efficiency to account for wetness loss was that of Baumann[B1]. He concluded that 1% of mean wetness reduces efficiency by 1%. It was also experimentally verified[M1] that supersaturation produces a significant part of the total loss in efficiency (Fig. 1.2).

Sources for this efficiency loss include the thin wavy film of deposited droplets on the casing wall and blades which results in higher friction loss than would a dry wall.[C1]

Also a part of the vapor energy is spent in accelerating the liquid droplets. This energy term does not add to turbine power output.

The fact that present day large water-cooled nuclear reactors produce only saturated high pressure steam forces the study of moisture effects in steam flow. For typical plants (such as PWR) the high pressure (45-65 bar) saturated or near-saturated steam enters and expands in the high-pressure turbine with ~15% or more of wetness developing at a pressure of ~5 bar. Continued expansion would give ~25% wetness at turbine exit which is clearly not acceptable. Figures 1.3 and 1.4 show the events leading to steam turbine erosion in such plants.

A. CONDENSATION OF STEAM

In many technical processes, such as expansion, compression or heating and cooling, the wet steam is subjected to rapid changes of state. In such processes, time is not sufficient for full phase equilibrium. The necessary evaporation and condensation is limited by many factors. Therefore, non-equilibrium processes take place, which are characterized by finite temperature differences between and within phases. Equality of pressure between vapor and liquid phase is usually maintained, because pressure disturbances propagate at acoustic speed. Thus supersaturated (or subcooled) steam and superheated liquid may coexist. However, these states are very unstable. They occur only

EROSION PROCESS

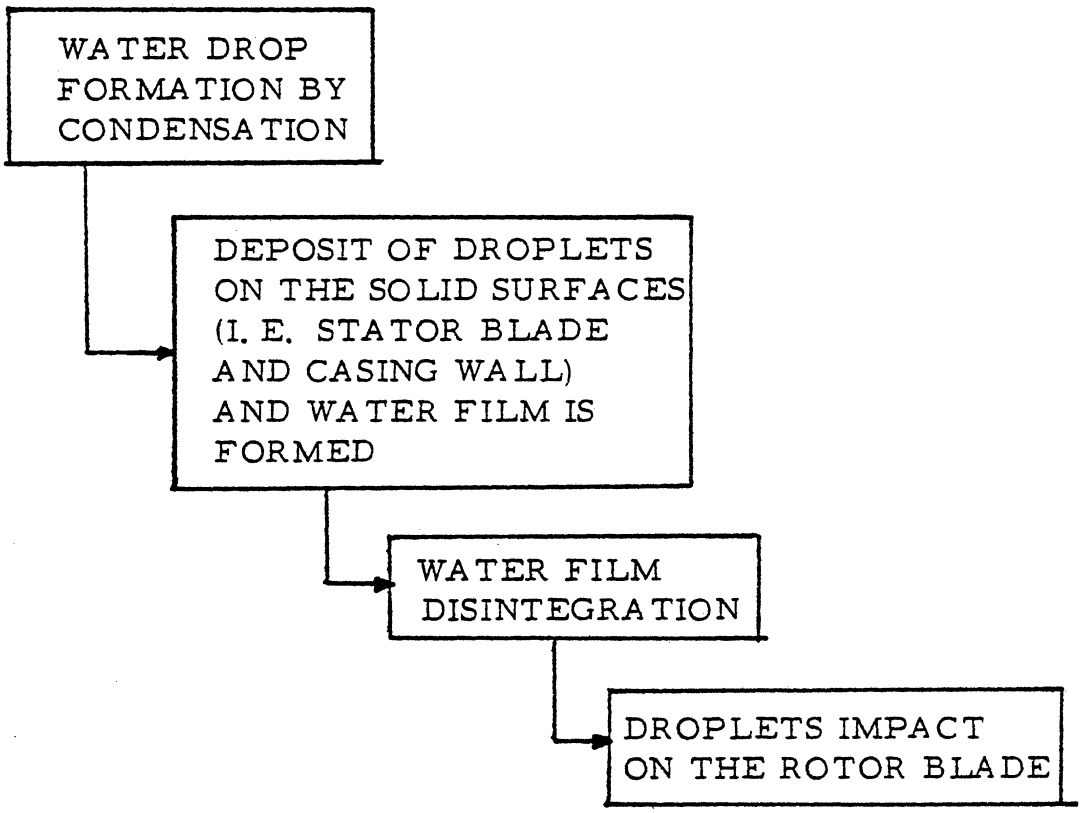

Figure 1.3 : Summary of Erosion Process.

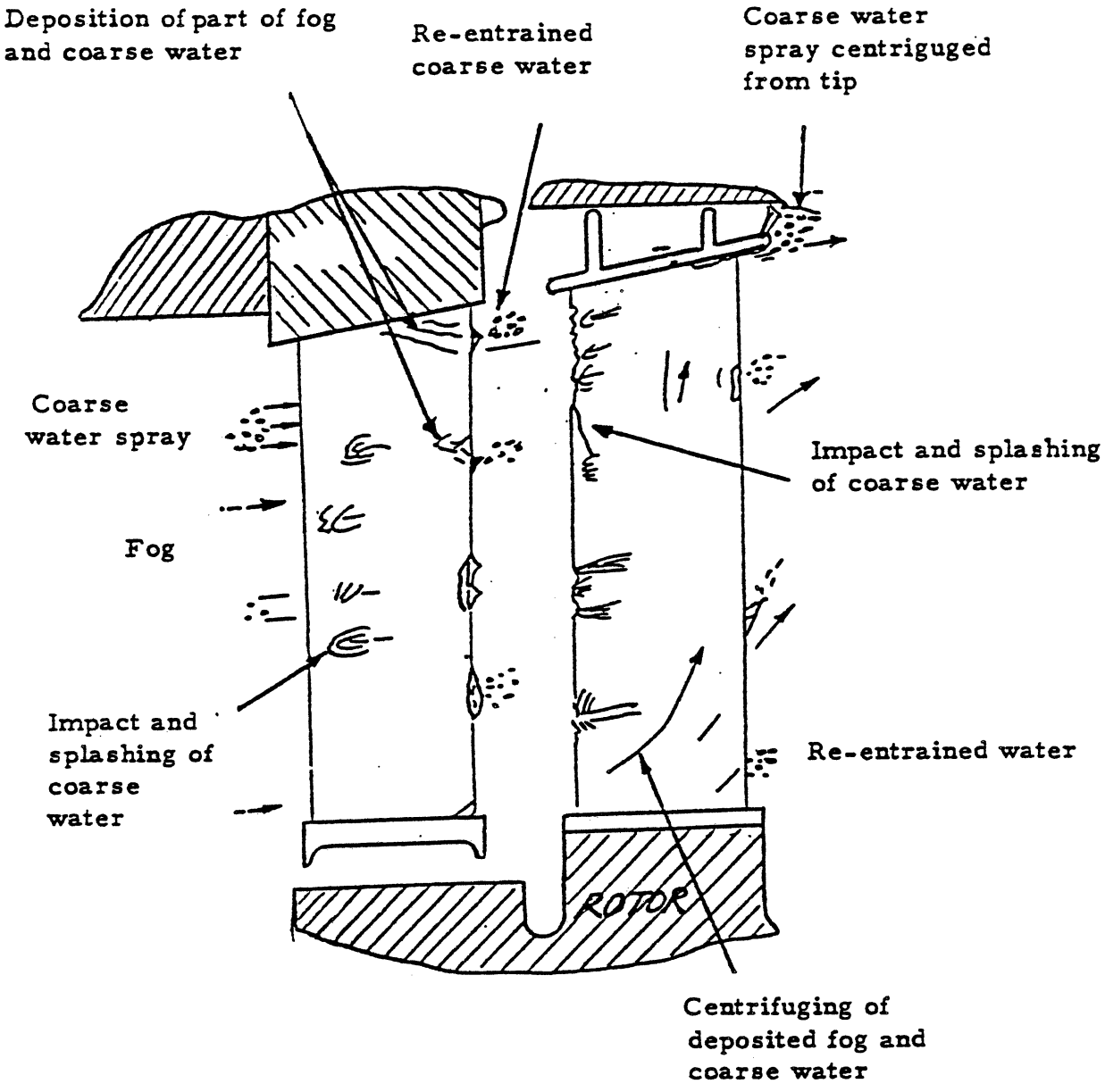

Fig 1.4 : Diagram of the Forms of Water in a Wet-Steam Turbine Stage.

during dynamic processes, and disappear when equilibrium is recovered. Thus in the fast steam expansion in a turbine, steam condenses in the so-called "Wilson zone"[W6]. Numerous investigators such as Yellot[Y1,Y2] Gyarmathy[G1,G2] and Ryley[R1] found that the "Wilson zone" lies at ~5 % equilibrium wetness.

The size of droplets in spontaneous condensation is known to be in the range of 0.01~ 0.1 μm.[G1,P1,V1] Also the number density of droplets per unit volume has been estimated to be $\sim 10^{15}/m^3$, assuming a uniform size of 0.1 μm [G2]. Droplets formed at the Wilson zone will grow in the following downstream expansion region. The growth rate of droplets has attracted the attention of many researchers. Hill[H1] developed a growth law from kinetic theory considering the droplet growth rate to be the difference between the molecular impingement rate of the vapor at the droplet surface and the evaporation rate of the droplet.

Gyarmathy[G2] used Fick's diffusion law and Fourier's law of heat conduction to develop a growth rate for spherical droplets in a continuum environment of arbitrary supersaturation and moisture fraction. Moses and Stein[M2] compared their experiment with several growth laws and concluded that Gyarmathy's model is more accurate than the others. Whether the vapor behaves with regard to a droplet as a continuum or as a free-molecular gas depends on the value of the Knudsen Number,

$$K_n = \frac{\text{mean free path of vapor molecule}}{\text{diameter of droplet}}$$

i.e., Kn $\leq$ 0.01; continuum flow

Kn $\geq$ 4.45; free molecular condition prevals.

Most primary droplets studied in steam turbines fall between these extremes.

B. DEPOSITION OF PRIMARY DROPLETS ON THE BLADE SURFACES

Primary steam droplets are not in general large enough to cause erosion damage by direct impact. Rather water from deposition of primary drops is collected on blade surfaces, and then torn from the stationary blades in larger "droplets" which then cause erosion of the next rotating row. Traupel[T1] has shown that the thermal boundary layer will maintain blading surfaces in a superheated condition. Thus evaporation rather than condensation is expected, so that direct condensation on the blade is unlikely.

Gardner[G4] proposed two possible mechanisms of collection, "Brownian Diffusion" for drops smaller than 0.1 μm and "Eddy Impaction" for those larger than 0.1 μm. For the Brownian diffusion model, molecular diffusion controls near the surface and eddy diffusion at a distance. The efficiency of collection decreases as drop size increases. On the other hand, for the eddy impaction mechanism, particles approach the wall by eddy diffusion, and proceed the remaining distance by already gathered inertia, dissipated by viscous resistance. Contrary to Brownian diffusion, the

collection efficiency increases as drop size increases.

Crane[C2] carried out experiments for the "collection efficiency" of the eddy impaction mechanism. Some typical results for HP and LP turbine blades are shown in Fig. (1.5).

Recently Ganic and Rohsenow[G5] proposed a modified deposition mechanism, considering lift forces, due to drop rotation within the laminar sublayer caused by high vapor velocity gradients, and reaction forces due to asymmetrical drop evaporation inside the laminar sublayer. In addition inertia, drag, bouyancy, and gravitational forces were included.

C. FILM FLOW AND SECONDARY DROP FORMATION

The deposited drops form a very thin water film, or sometimes separate rivulets on the stator blades. This water will flow along the blades under the influence of steam "drag" (interfacial shear). Finally the film is torn away at the trailing edge or at the wave crests of a wavy film upstream of this edge, depending on the prevailing conditions. Droplets detached from such films are in fact much larger than the primary droplets, and cause the observed erosion damage to downstream rotating blades. Thus the behavior of these thin films, and the size of the secondary drops, their acceleration and their break-up and time of break-up into smaller though still large droplets, must provide the design bases to avoid steam turbine blade erosion. This is the major subjects of author's present research.

Information about the droplet acceleration is very

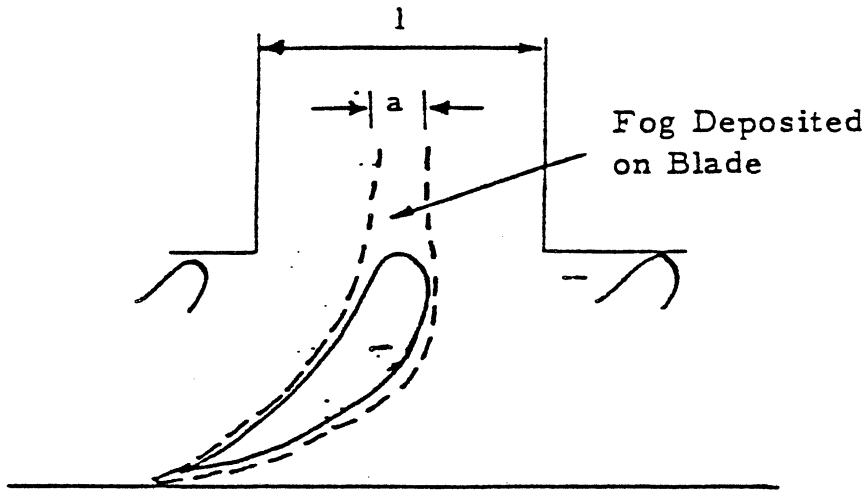

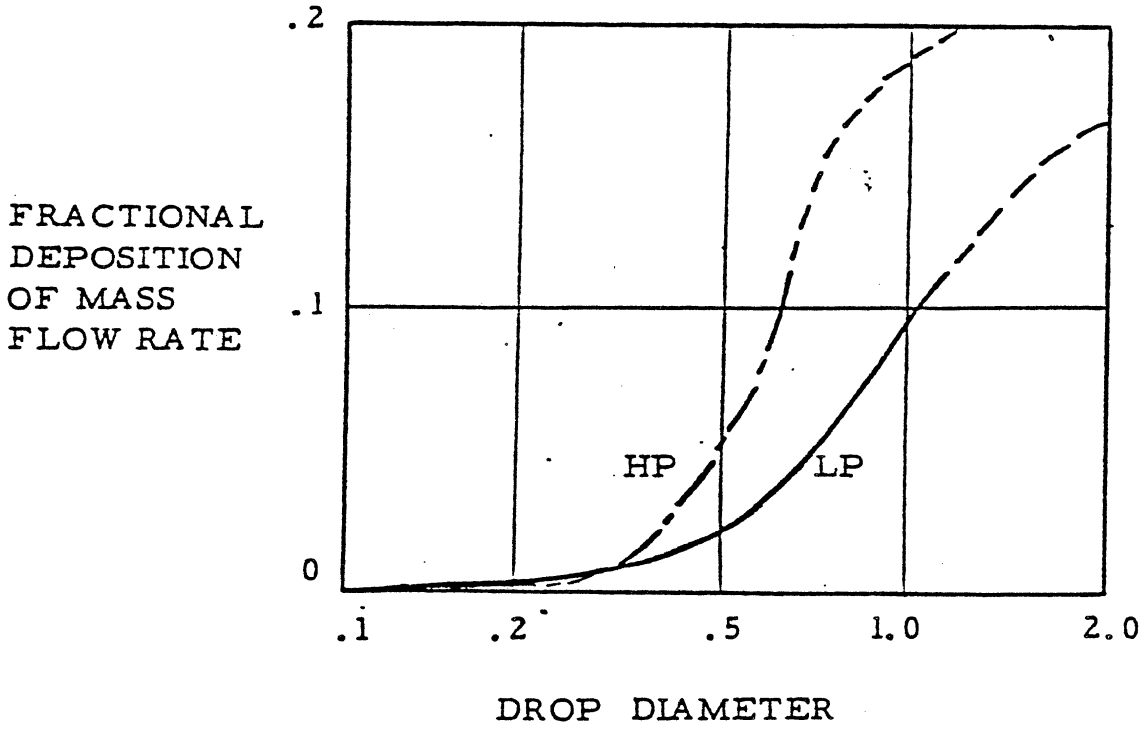

5305

Fig 1.5 : Approximate Fractional Deposition of Fog Drops on Blading. (C2)

important,since the closer the velocity of the droplets approaches the main steam velocity,the less will be the normal impact velocity between the droplet and the blade surface,thus causing less damage.(see Fig.1.6). It is generally agreed that only the normal component of droplet velocity contributes to the erosion damage. Example of damaged blade is shown in Fig. 1.7.

D. VELOCITY OF SOUND IN WET STEAM

Mach number is an important design parameter in steam turbines, and the steam flow is generally in a compressible flow regime. For this reason,steam velocities are here usually presented in terms of Mach number.

Theoretical and experimental studies of acoustic velocity are due to many researchers[D1,C3,P2,G6]. Petr's results[P2] are summarized graphically. The speed of sound(Fig.1.8) was expressed in terms of the "frozen" speed of sound, which is defined as : $a_F^2 = \frac{K_i P}{\rho_g}$

where K_i is isentropic expansion index, a_F is the gas phase speed of sound, inferring that there is no interaction with the liquid phase(which is frozen). Petr considered the effect of frequency on the sound wave speed. As seen in Fig.1.8, acoustic velocity approaches a_F as frequency is increased. For reduced wetness fraction and increased density of the gas phase, the mixture tends towards the single-phase acoustic speed a_F. This is used in this thesis.

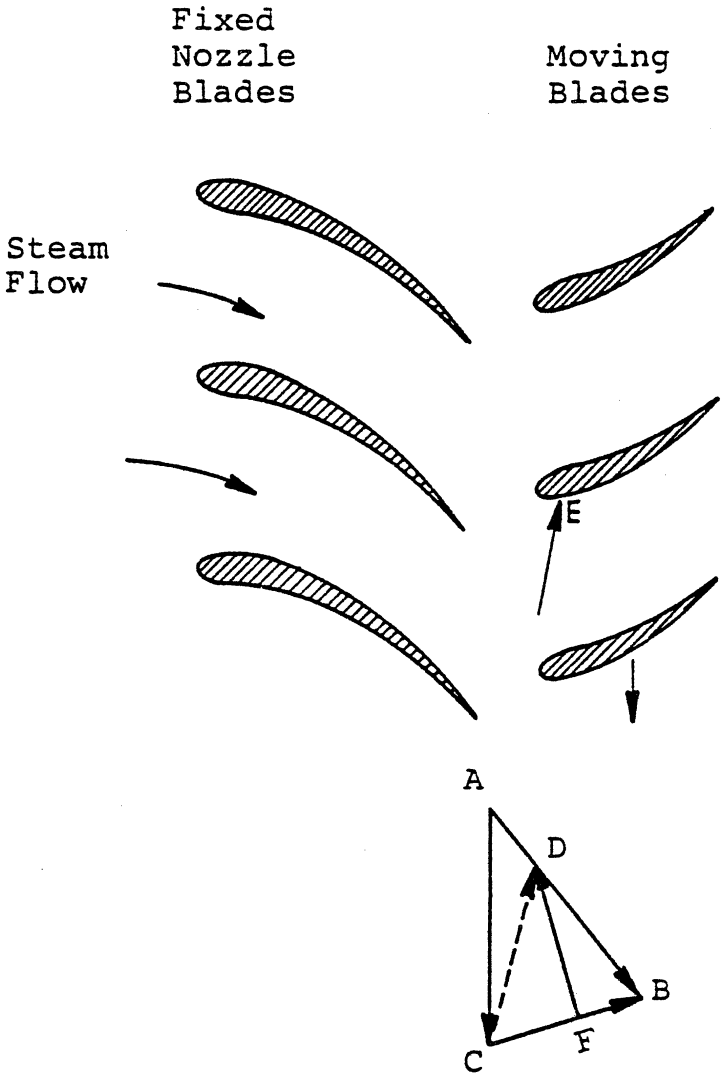

AC - Moving Blade Velocity

AB - Steam Velocity Leaving Fixed Blade

CB - Steam Velocity Relative to Moving Blade

AD - Velocity of Entrained Water Drops at Entry to Moving Blades

CD - Velocity of Drops Relative to Moving Blade at Impact Point E Where Erosion Takes Place

FD - Normal Component of Drop Velocity Relative to Moving Blade

Fig. 1.6 Vector Diagram of Steam Flow in Turbine

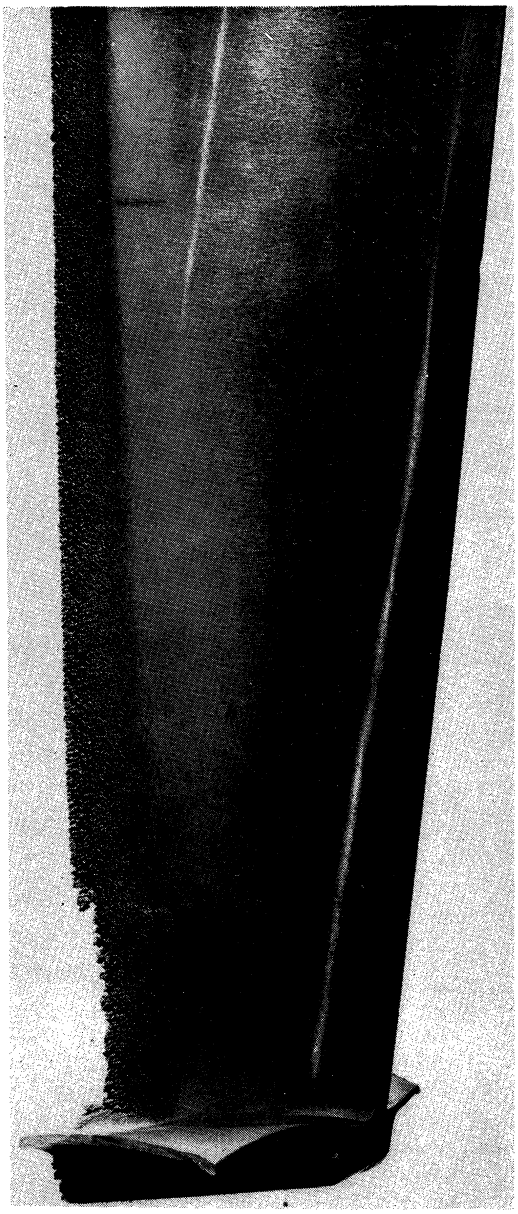

Fig. 1.7 Notching of Moving Blade at Inlet Edge by Water
(Taken by Christie and etc. , 1966 (c19))

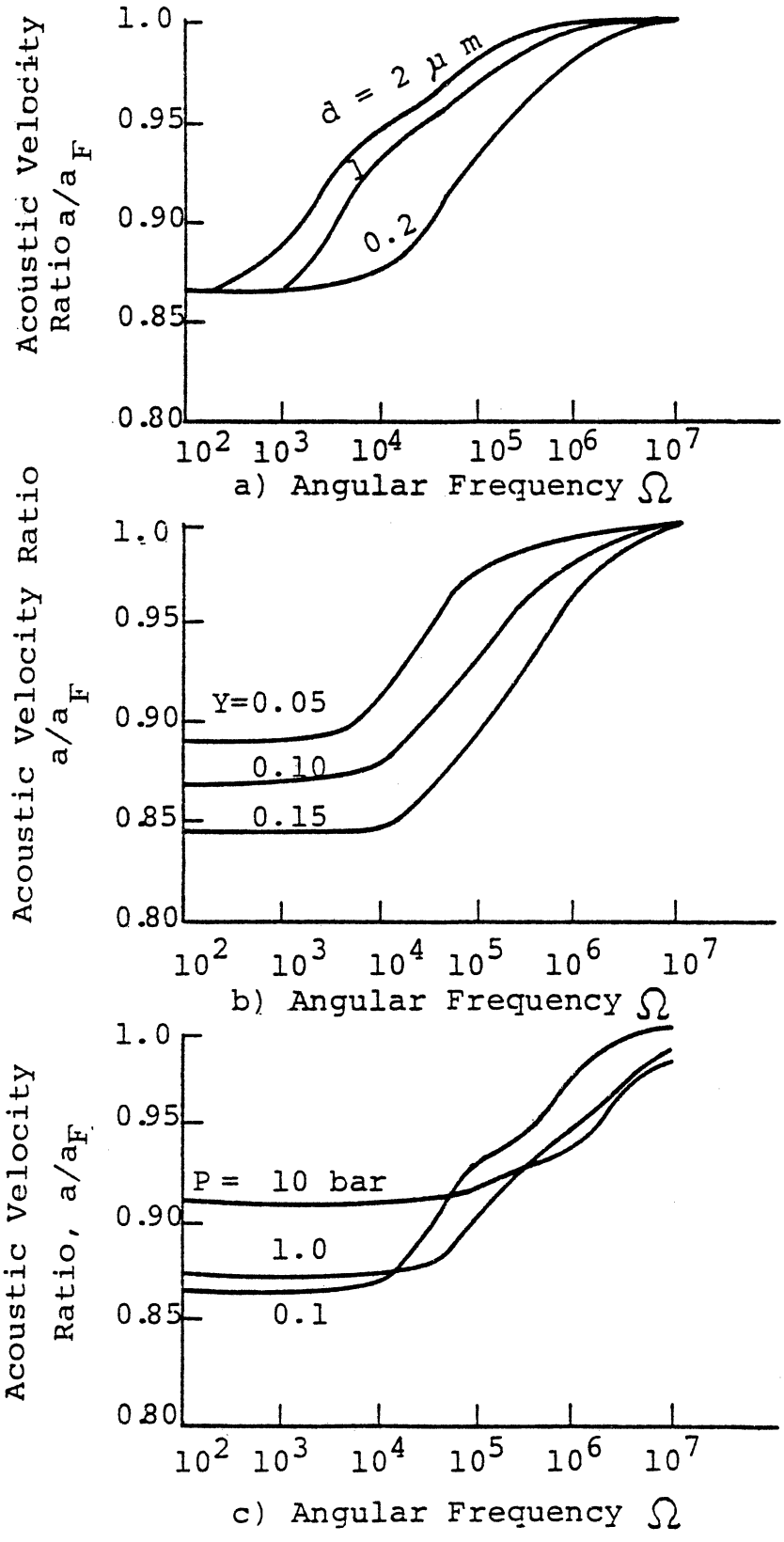

Fig. 1.8

Effects of a) Drop Size, b) Moisture Content, and c) Pressure on Acoustic Velocity Ratio, a/a_F, where $a_F^2 = k_i \frac{p}{\rho}$, Ω; Frequency of Acoustic Wave Propagation

(From Petr's results[P2])

CHAPTER II

INTRODUCTION

The behavior of a horizontal thin liquid film driven by interfacial shear from a cocurrent high-velocity subsonic, low-pressure wet steam flow and its subsequent break-up in the wake of a simulated turbine blade into relatively large droplets have been researched in detail. Conditions are nominally adiabatic.

The results include the identification of several wavy film regimes under various flow conditions, and the construction of a flow-regime transition "map". Important parameters governing the different map regimes, such as film thickness and the detailed wave characteristics like amplitude, form, and propagation celerity, have been measured using electrical conductivity microgages and high speed photography including both still and motion picture. Author's experimental results concerning the critical parameters controlling the transitions between regimes, and the wave characteristics have been compared to other studies in the literature. Where important discrepancies exist between analytical and experimental results of other investigators and author's data, new theoretical analyses or plausible sources of the discrepancies have been suggested.

Liquid phase behavior in the blade wake is highly important, having obvious direct application to the steam

turbine blade erosion problem. Measurements of the "liquid finger" characteristics and the observed periodic decelerations of large droplets are "firsts" from this study, as are the detailed high-speed motion pictures. Due to the overall complexity of the problem and non-existence of previous comparable experimental or analytical results in many cases, much of the experimental data have been reduced using dimensional analysis, rather than direct solution of the required differential equations.

The following sections are descriptions of author's overall results, including pertinent literature surveys. They consider primarily two subjects: 1) the behavior of the liquid film flow and 2) the formation of "liquid fingers" and secondary "droplets", and their subsequent trajectories. These phenomena are of major importance for the erosion-resistant design of the subsequent rotating turbine rows. Some results are also pertinent to the "loss of coolant accident" of liquid-cooled nuclear powerplants such as PWR.

A. FILM FLOW

As explained in previous chapter, understanding of the thin liquid film behavior on turbine stator blades, and its subsequent break-up into liquid droplets, are essential to improved steam turbine blade design, concerning particularly erosion. However, besides the steam turbine application, the study of such liquid film flows has many other important applications. Conveying of liquids by co-current gas

streams in oil pipelines, "loss of coolant accident" and emergency core cooling in liquid-cooled nuclear reactors, internal boiler tube flow, transpiration cooling systems for re-entry vehicle nose cones are pertinent examples. The family of liquid film flows is categorized in Fig. 2.1 .

To allow a study of this range of phenomena and applications, a high-velocity, low-pressure, wet steam tunnel had been designed here and constructed. A simulated turbine blade (in this study, a thin flat plate, Fig. 3.3) is inserted parallel to the flow direction along the axis of a transparent rectangular test section. For film thickness measurement, electrical conductivity microgages were developed,[M10] calibrated and installed at various suitable locations flush with the blade surface. The various attainable film flow regimes, together with wavelet characteristics, were observed using both high-speed cinematography and a still polaroid camera with a 1.2 μs flash and flood lights.

Most previous investigations involving film thickness measurements were for relatively large film Reynolds numbers, because of their interest in relatively thick liquid films occurring in pipe flow applications,(Fig. 2.2). Author's film Reynolds number (pertinent to the steam turbine case) is very low ($Re_f < 56$).*

As injected liquid film flow rate is increased from zero at fixed steam velocity, various film-flow regimes have been observed here. A film-flow "map" from this study is thus

*Based on surface film velocity and mean film thickness.

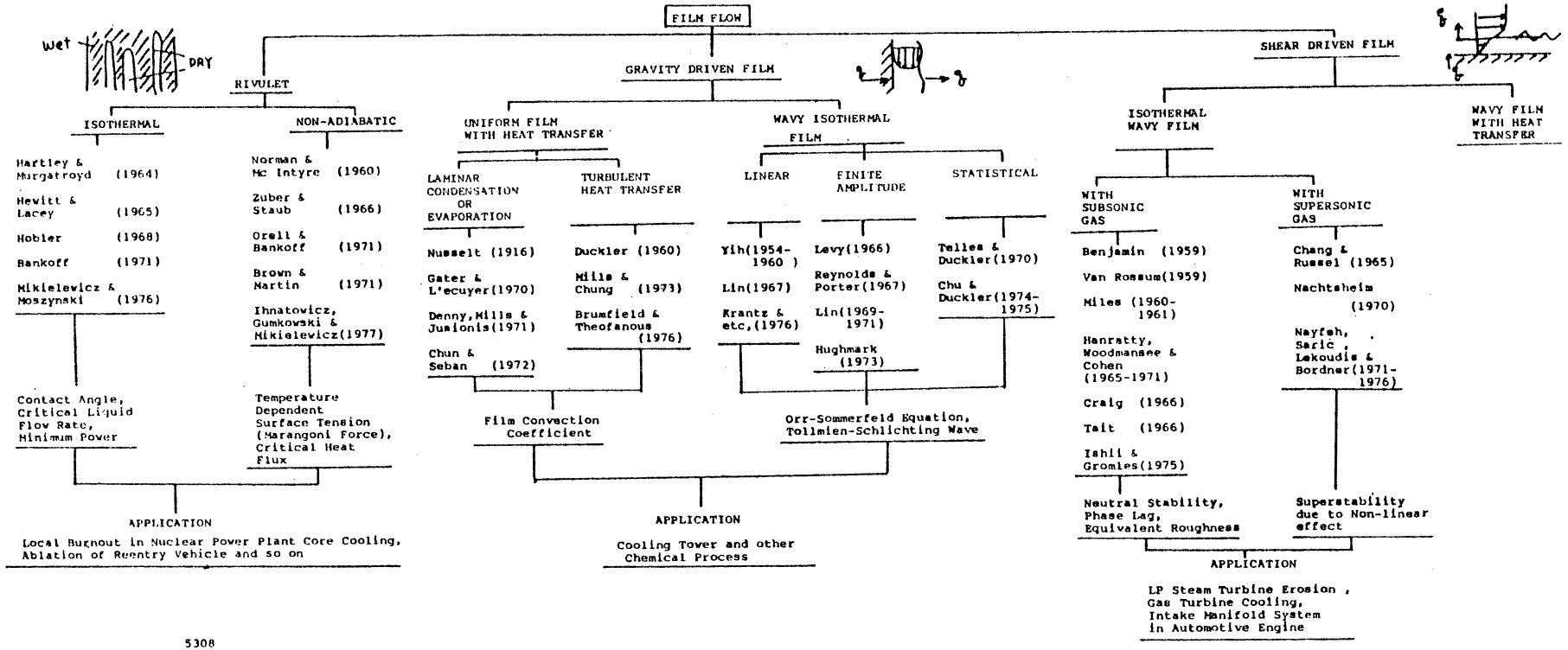

5308

Fig. 2.1 Categorization of Liquid Film Flow Study

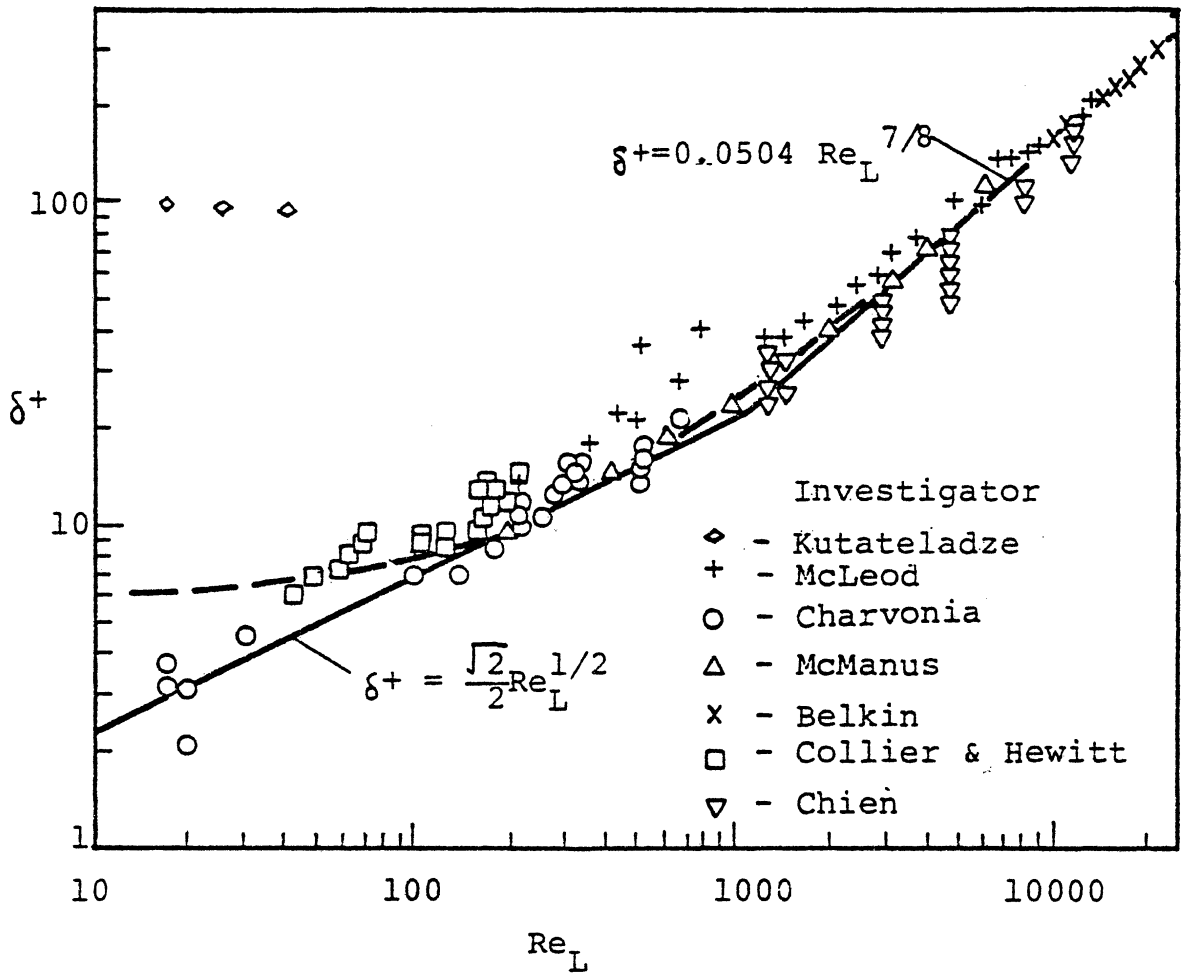

Fig. 2.2 Liquid Film Thickness Measurement Data
(Kosky, 1971 (K 10))

presented here. The film flow regimes are;

i. Rivulet flow (partly dry and partly wet)

ii. Two-dimensional wavy film (small wave)

iii. Three-dimensional wavy film (large wave)

iv. Entrainment regime (droplet formation at the crest of waves)

1. Rivulet Flow Regimes

The transition between regimes (i) and (ii) is of particular interest for safety considerations of nuclear powerplant core cooling (dry-spot formation) as well as to turbine stator blades at the low pressure end.

Hartley and Murgatroyd's analysis[H2] in 1964 was the first attempt to predict a critical liquid flow rate and thickness corresponding to continuous film break-down into rivulets. The mechanism initiating such dry patches was not discussed. The study was concerned rather with whether once a dry patch is formed, will it remain dry or become rewetted. They suggested two criteria. One was based on a force balance at the upstream stagnation point of a dry patch; the other on a minimum total power criterion based on kinetic and interfacial energy in a transversely unrestrained stream. Their minimum power criterion did not include any influence of the contact angle, which since has appeared to be very important in this regard.

Based on Hobler's analysis[H3], where a minimum power criterion allowed for the effect of contact angle, Mikielewicz and Moszynski[M3] suggested an improved criterion.

Both Hartley-Murgatroyd's force balance (H-M) and the Mikielewicz-Moszynski models (M-M) included contact angle criteria. Comparing with author's experimental minimum flow rate criterion, contact angle, θ, needs be $\sim 6°$ and $\sim 10°$ respectively for these models to be compatible with author's data. The static contact angle between a stainless-steel plate and a water droplet (in air) is believed to be $49 \pm 4°$. (H4) However for a single curvature such as in the case of a rivulet, the measured angle (M15) was found approximately half of that static angle. Anyway the wetting angles necessary to make the H-M and M-M models realistic are too small to be exactly valid. Of course contact angle is dependent on surface conditions, i.e., roughness, cleanliness, etc. and also on gas phase. Such aspects were not considered in the theoretical analyses.

Author's photographic studies (Fig. 4.1), show an abrupt liquid bulge just upstream of the stagnation point for a dry-patch. Some analyses (M12,I1) mentioned this particular geometry. This may be partially responsible for the large discrepancies in contact angle between observation (M15) and requirement to match the H-M and M-M criticality models.

Non-Adiabatic Dry Patch Formation

For cases with strong heat flux, Zuber and Staub (Z1) considered surface tension variation with temperature. Orell and Bankoff (O1) added the liquid pressure due to the thrust of evaporating molecules. Both these analyses are based on the Hartley-Murgatroyd model. (H2) These studies are not direct-

ly applicable to author's case which was nominally adiabatic.

2. Wavy Film Regime

If liquid flow rate is further increased at fixed steam velocity, the blade surface is completely wetted and the dry patch or rivulet regime no longer exists; rather a wavy film regime appears. This is shown from author's photographic results confirmed by film thickness gage output. The interaction of the external driving vapor flow with the liquid interface produces two important effects. The first is the establishment of a velocity profile in the liquid due to the shear stress at the liquid-vapor interface. The second is the action of perturbations in the normal and tangential stresses exerted by the vapor due to the appearance of waves.

The main steam flow may be considered inviscid because of the high Re ($>10^5$). In our case it is also subsonic ($M < 0.8$). The pressure perturbations in the liquid are then in phase with the amplitude of the surface waves. In fact the pressure perturbation from the vapor would be 180° out of phase with the wave amplitude due to the resultant vapor streamline curvature. Thus there is an energy transfer from the vapor flow to and from the wavelets in the liquid layer (Fig. 2-3a). This is the classical Kelvin-Helmholtz instability mechanism for wave formation. In real cases, however, the pressure distribution in the liquid is not, in general, precisely in phase with the surface wave amplitude.

As seen in Fig. (2-3b) the perturbation distribution upon the profile slopes leads to a resultant stress in the

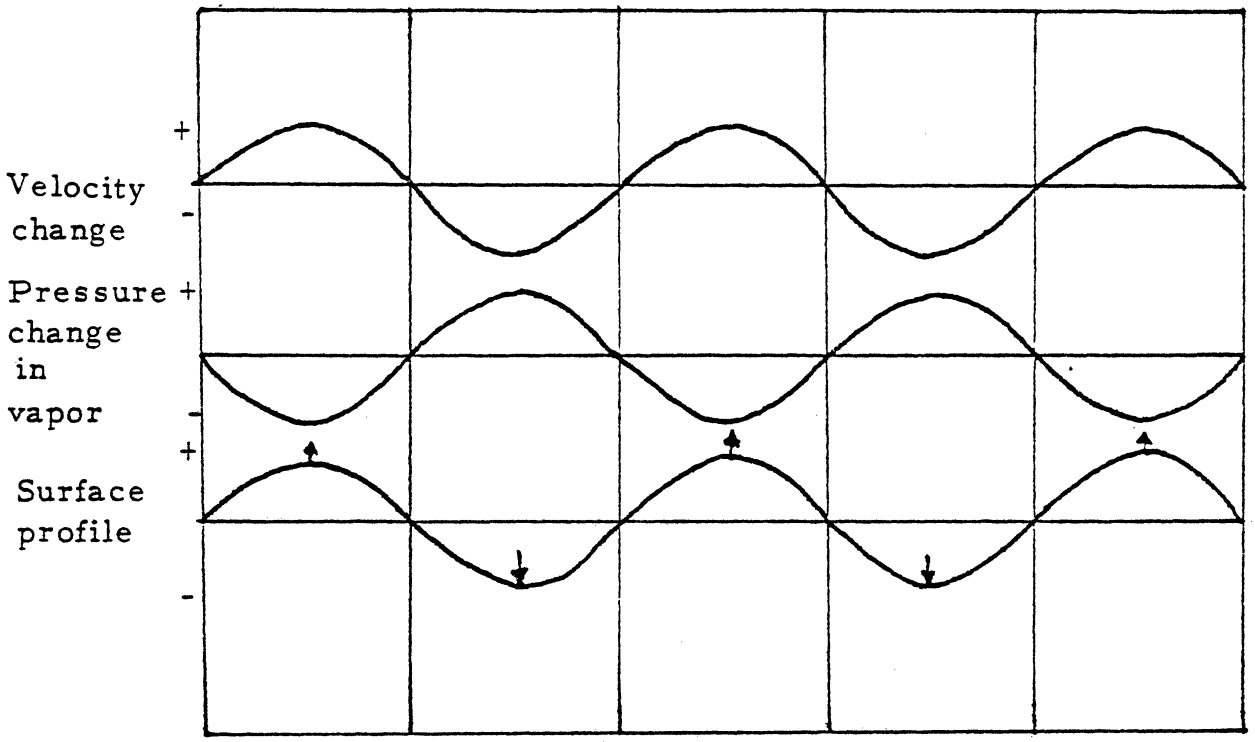

a) Kelvin-Helmholtz Mechanism
pressure changes lag surface profile by π

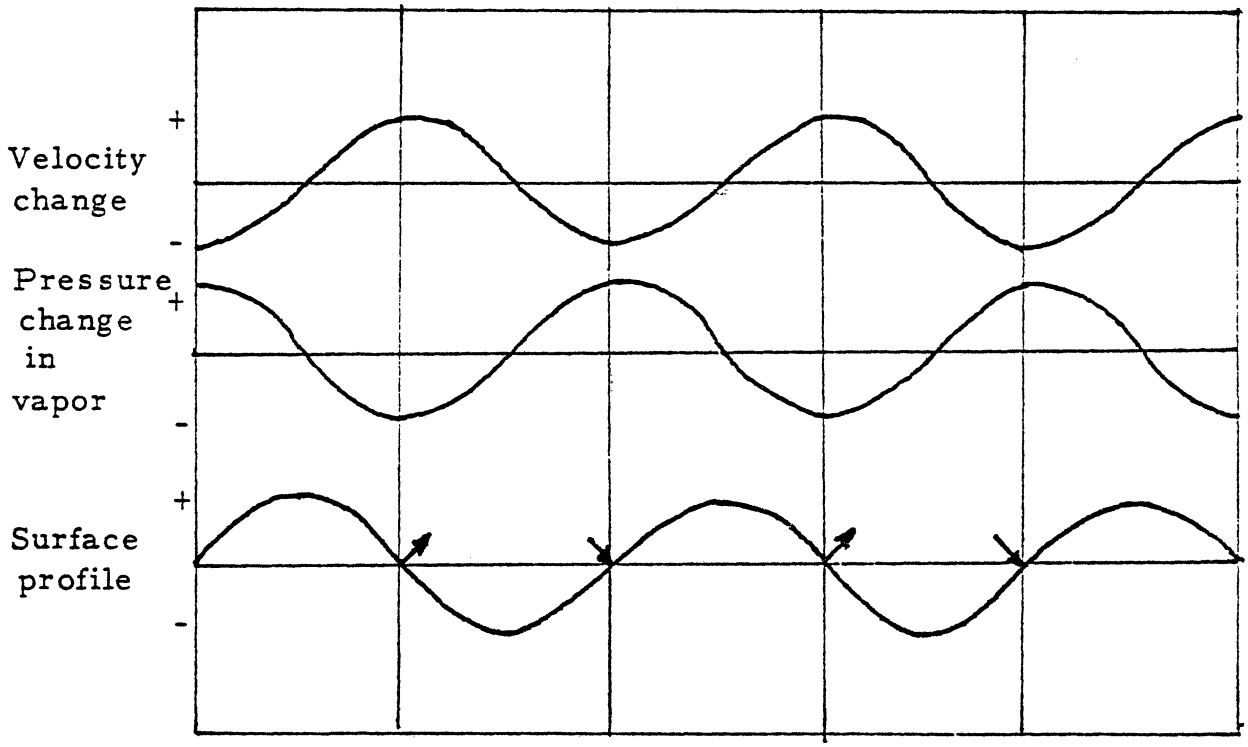

b) Pressure changes lag surface profile by $\pi/2$

Fig 2-3: Velocity and pressure changes in flow over wavy surface.

flow direction, and does work on the waves. This interfacial stress, derived from the normal pressure distribution near the boundary, is sometimes called "form drag".

Since the behavior of the liquid film is largely governed by stresses exerted upon its surface by the vapor flow, good estimates of these stresses are obviously desirable. In general, the vapor stream is turbulent, and consequently random fluctuations of stresses exist at the liquid interface. Although the resonant response of a liquid surface to random pressure fluctuations is important in the generation of ocean waves[P5], such a resonance mechanism is not important in the author's present problem, since the convected velocities of the vapor flow fluctuation are always much greater than the wave velocities in the liquid film. Thus only a very weak response of the surface is possible.

The surface stresses produced by interaction of the mean steam flow with small periodic perturbations of the boundary surface have been evaluated by Miles[M4,M5,M6] and Benjamin[B4] for mean vapor-velocity profiles of the boundary-layer type. However, their approaches lead to great mathematical complexity.

Miles[M4] proposed the "Tollmien-Schlichting" instability mechanism for large film Reynolds number. In this mechanism, the unstable disturbances receive their energy from the mean flow of the liquid layer, rather than from the vapor, by way of the Reynolds stresses in the liquid near the wall. The disturbances receive their energy either from the mean flow

of liquid or vapor depending on whether the wave speed is less than or greater than the interface velocity. Miles concluded that a necessary condition for instability, assuming a Tollmien-Schlichting mechanism, is $Re_f > 203$. Saric and Marshall[S2] verified this mechanism experimentally for supersonic gas flow, and concluded Re_f must be >100 for this mechanism to occur.

The analysis and experiments of Craik[C10] with an incompressible air flow showed that thinner films may be more unstable than thickner ones. His expression for shear perturbation in phase with wave slope is inversely proportional to film thickness; the thinner the film the larger the shear perturbation. Because of this thin film consideration, author's experimental results can best be compared to Craik's model.

The analysis of Nayfeh and Saric[N3] extended Craik's work to include an arbitrary body force. External flow was supersonic and a long-wave analysis was used. A simple relation between the wave speed and growth rate was derived. This author's vapor velocity is subsonic. However an interesting result was reported for the supersonic vapor flow case. Nayfeh and Saric's non-linear analysis[N4,N5] showed that stable linear disturbances die faster whereas unstable disturbances achieve steady-state amplitude instead of growing indefinitely if disturbance boundary layer is larger than subsonic boundary layer. This was verified experimentally[S3] by observing no liquid removal even for supersonic gas flow.

3. Entrainment Regime

From author's photographic study, for higher steam velocities, as liquid flow rate is further increased, the waves grow and crests are broken, much like ocean "breakers". Droplets are then shed from the wave crests into the vapor flow. From the viewpoint of turbine blade erosion, this entrainment mechanism, at least the parameters controlling its inception, is important. Since the entrainment takes place along the stator blading or casing wall, the flight time of such entrained droplets is different from those generated at the trailing edge.

Experimental inception criteria for droplet entrainment in horizontal two-phase film flow have been measured by many (V2,W2,W4) and numerous inception criteria for vertical pipe flow have also been proposed by others.(C16,S4,G7,G8) All of these used air-water, relatively high film Reynolds number ($Re_f > 100$) and low gas velocity. The tests were generally performed in low velocity wind tunnels.

Attempts(W5,H6) have been made to correlate the various data available. However, these were empirical and fit only the limited range of data used. In general these do not fit the high-velocity, thin-film data of present interest. Results are conflicting due to effects of flow orientation, i.e., horizontal, or vertically up or down. Zhivaikin's data(Z2) shows that the inception of droplet entrainment depends on flow direction at low liquid Reynolds number, while Wallis(W7) indicates that onset is independent of flow

direction.

An extensive entrainment inception model was proposed by Ishii and Grolmes.[I2] Based on Zuber's analysis,[Z1] they considered the wave amplitude and flow within the wave crest. They assumed that the interfacial shear force at the top of the wave induces an internal velocity of same order as film velocity, and that the velocity of the wave crest with respect to the film is proportional to film velocity. Using Hughmark's correlation[H6] for the effective interfacial friction factor, they concluded that critical non-dimensional vapor velocity for entrainment inception is proportional to $(-\frac{1}{3})$ power of film Reynolds number for relatively thick films ($Re_f > 160$). For low film Reynolds number flow they speculated upon the similarity between Hinze's critical droplet disintegration mechanism[H8] and their entrainment inception. They concluded that non-dimensional vapor velocity for entrainment is proportional to $(-\frac{1}{2})$ power of the film Reynolds number. Compared to author's experimental results, their correlation for low film Reynolds number criterion is high.

B. LIQUID FINGERS AT BLADE TRAILING EDGE AND SECONDARY DROPLET FORMATION

Liquid films formed on the stator blade can be partially removed by suitable separators or by the entrainment mechanisms already discussed. However, the remaining film is entrained by shear force of the driving vapor from the blade trailing edge, forming into "secondary droplets" in the steam wake.

The liquid droplet motion in the wake near the trailing edge is very important to the erosion problem, controlling the upper size limit for drops reaching the rotor blade. Since the erosion potential of droplet impact increases strongly with droplet size [P6,S9], this is an extremely important question for blading erosion.

1. Formation of Liquid Fingers

In author's experiment, liquid film detachment from the trailing edge is never continuous, but appears as discrete "fingers". An extensive study of the time-averaged shape of such fingers, together with the time parameters involved in the frequency of finger formation has been made. It is important to secondary droplet formation, directly pertinent to blade erosion potential. Surface tension, together with shear, inertial forces and film flow conditions at the trailing edge are governing parameters for finger behavior.

Axial finger length and finger wave length (distance between fingers) as function of time have been measured from numerous high-speed motion pictures for the various steam and liquid flow conditions. The frequency for the formation of longer fingers was especially studied, since these are of particular importance from the erosion viewpoint, transporting large slugs of liquid into the path of the next rotating row.

Dimensional analyses were used to study the effects of surface tension, inertial and viscous forces of the vapor

and liquid flow on the frequency of formation of the longer fingers and wave lengths of fingers. It is shown that Strouhal number based on formation frequency, finger length and liquid film velocity decreases with increasing steam Reynolds number.

2. Acceleration of Secondary Droplets

When droplets are detached from the fingers, they are accelerated by drag forces due to vapor flow in the wake region. Information concerning droplet acceleration is most important, since the closer the droplet velocity appoaches steam velocity, the less their erosion potential, since impact damage is a strong function of normal velocity alone.(P6)

Many studies of liquid droplet acceleration have been motivated by aircraft and missile rain erosion problems. In such cases the velocity is supersonic, so that droplet desintegration is influenced by shock-wave patterns. Thus the trajectories and acceleration of droplets just after passing through a shock wave is of interest.(L7,S5,S6) Nevertheless, an important, partially unknown parameter is the drag coefficient for droplets as a function of Mach number and shape. This of course is also a function of drop Reynolds number. Empirical or theoretical drop or bubble drag coefficients have been reported because of their importance in heat and mass transfer.(A1,C14) All of these drag coefficient correlations considered single droplets with external gas or vapor flow. Also of interest is the drag coefficient for a drop in the presence of other drops

of varying sizes. Tam[T2] derived a formula for the drag exerted on a cloud of spherical particles of a given particle size distribution at low Reynolds number. Based on the statistical concept of distributed particles, he concluded that the drag experienced for a particle depends only on the first three moments of the distribution function.

None of these correlations can be directly applied to author's particular case, because author's flow regime is the wake region of a tapered flat blade. Author's experimental droplet accelerations, when plotted as a function of time, show periodic abrupt changes, i.e., an accelerating droplet suddenly decelerates, sometimes reverses direction, and then accelerates again. This observed phenomenon can best be explained by the trailing vortices shed from the blade, similar to a Karman vortex street. The presence of a discrete vortex near a droplet would produce an induced velocity field which may be responsile for the observed changes in droplet acceleration. The periodic vortices shed from the droplets themselves may also be important. A very similar observation is reported by Tyler and Salt[T4] for solid spheres in free-flight. The periodic behavior is assumed due to Karman vortices shed from the spheres.

3. Break-Up of Droplets

In the higher steam velocity ranges, the disintegration of the droplets was found to occur more rapidly. Author defined the break-up time, t_b, as the duration from the time when discrete droplet forms from fingers, to the time when

the droplet becomes amorphous or disintegrates. Non-dimensional break-up time based on initial drop diameter and vapor flow conditions was found to be approximately inversely proportional to the droplet Weber number.

CHAPTER III

EXPERIMENTAL FACILITY AND MEASUREMENT CONDITIONS

A. STEAM TUNNEL GENERAL

Figures 3.1 and 3.2 are a schematic and a photograph of the low pressure wet-steam tunnel facility, "Wet Steam Tunnel," at the University of Michigan. This wet steam tunnel was designed[K5,H9,H10] to produce flow parameters in the test section which would generally match the average steam parameters in the last stages of large steam turbines.

Mean static steam conditions in the test section are near saturation, probably never superheated, showing varying degrees of moisture depending primarily upon test section velocity,(Table 3.1).* Of course, wetness increases with velocity head for fixed supply conditions. Actually in many cases, upstream of the throttle valve has rather low quality (almost hot water according to pressure and temperature measurements at the upstream orifice under low flow conditions). However, after traversing the valve, water is trapped in the "stilling tank" so that the quality of steam reaching the test section is still nearly dry. This is confirmed by the fact that water build-up is not observed on the blade or in the test section. The test section temperature (which is almost stagnation temperature) does cover a certain temperature range (usually decreasing as steam flow rate is reduced). It is assumed for present purposes that supply conditions are constant, though this is not precisely true.

*These are "typical" conditions, not entirely accurate.

Fig.3.1 Facility Schematic

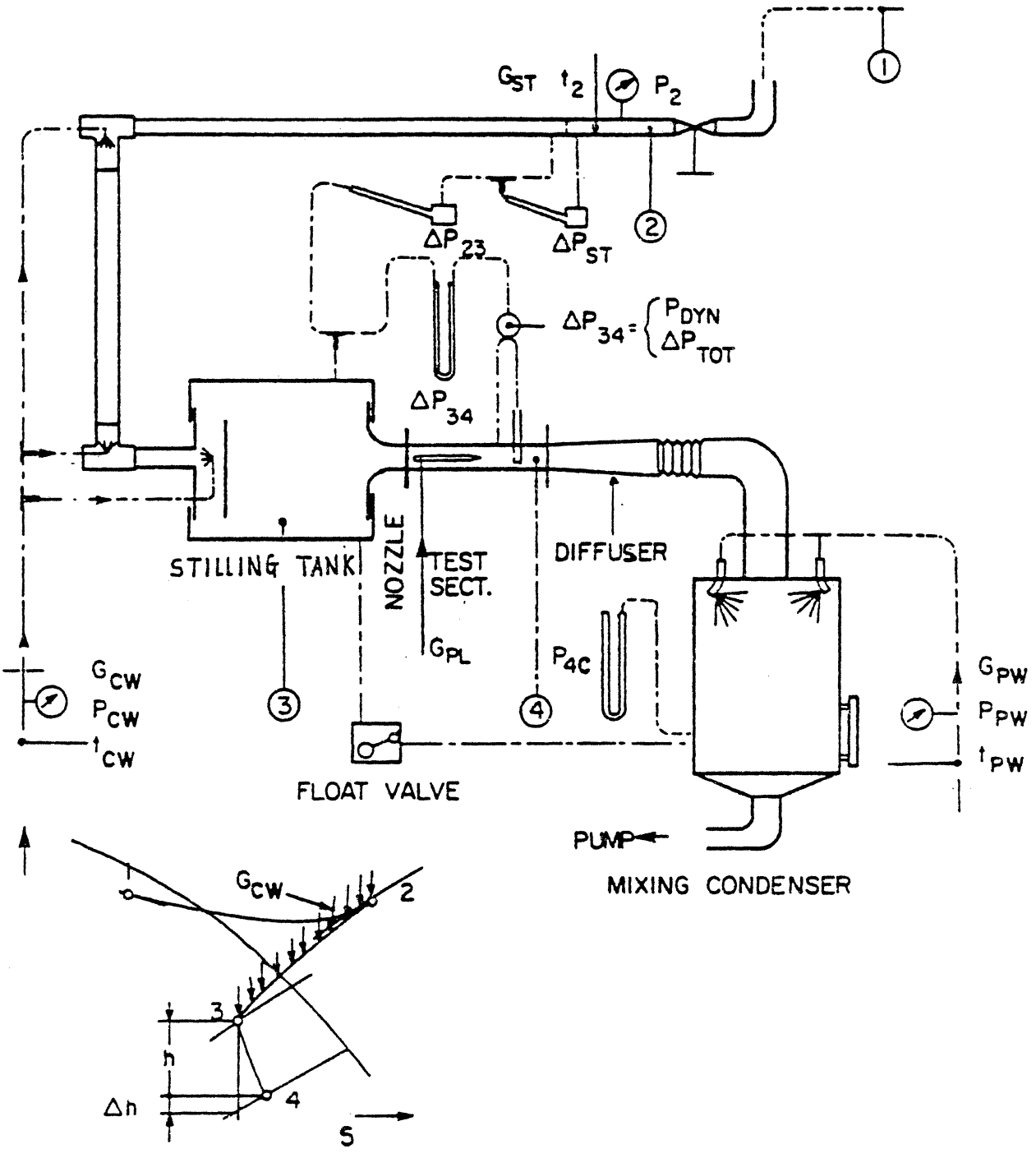

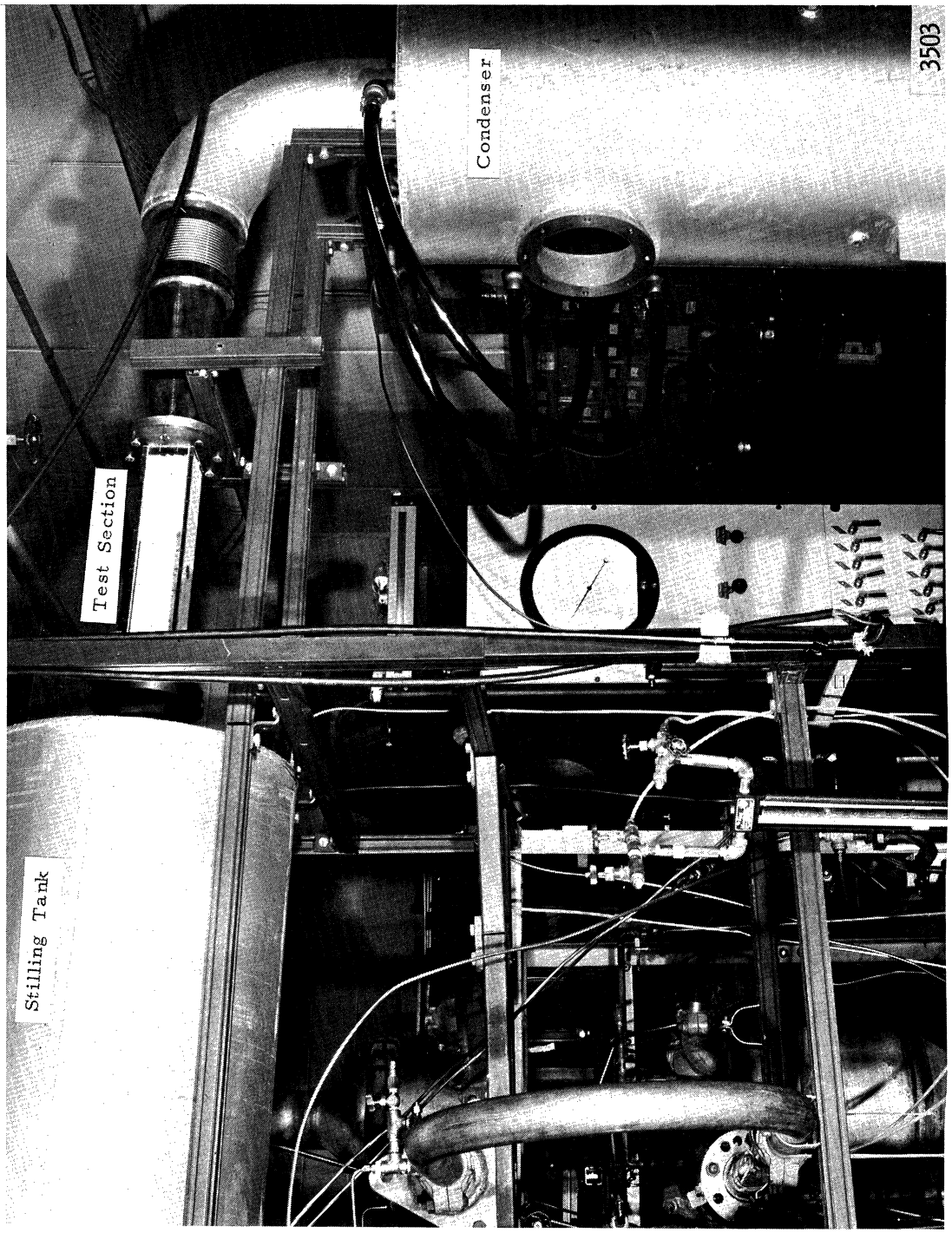

Fig. 3.2 Photograph of the Overall Steam Tunnel Facility

5375

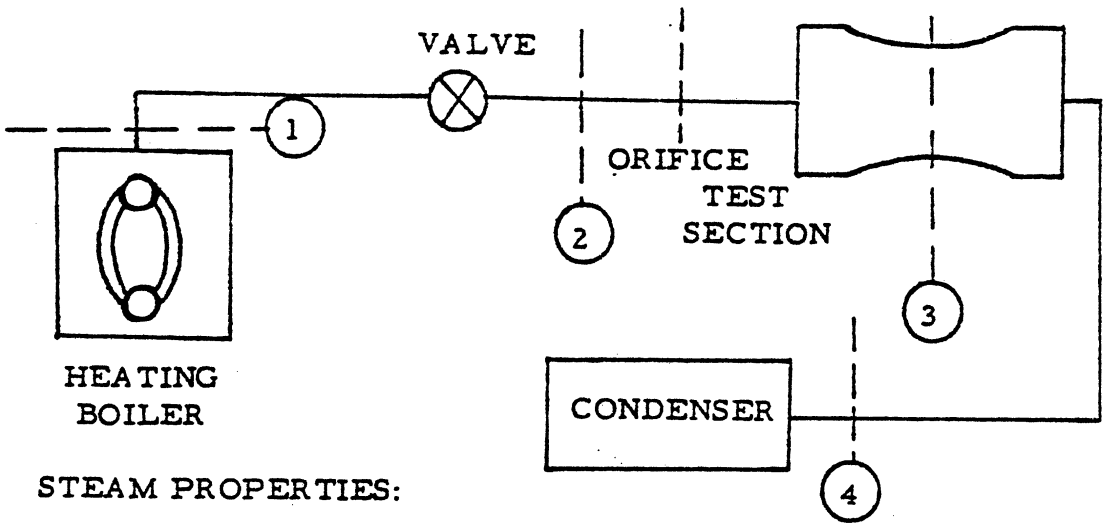

STEAM PROPERTIES:

V_{steam} ft/sec	T_3 °F	P_3 lb/in^2	h_3 BTU/lbm	S_3 BTU/lbm F	X_3	T_1 °F	P_1 lb/in^2	X_1	h_1 BTU/lbm	S_1 BTU/lbm F
200	130	2.225	1107.456	1.894	.99	227.96	20	.95	1108.225	1.662
600			1101.065	1.877	.98					
1500			1063.316	1.825	.95					

Note: Conditions at "3" and "4" approx. same

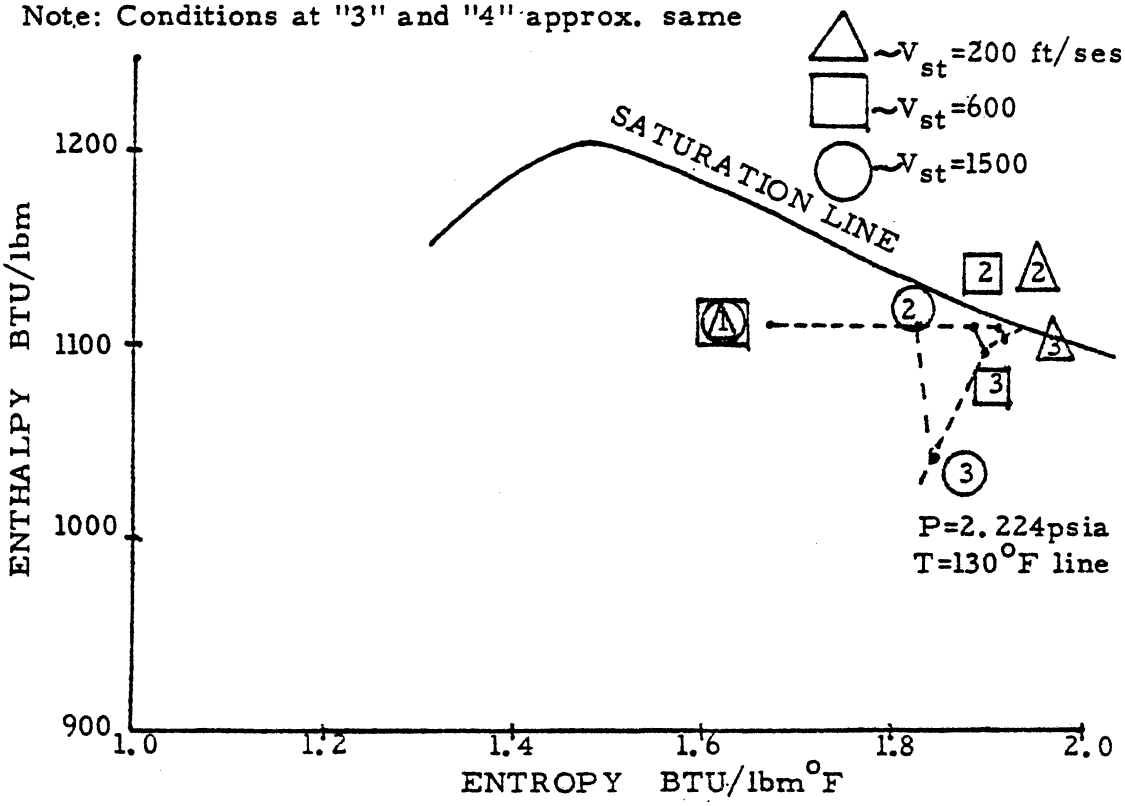

Table 3.1 Thermodynamic Operating Conditions of Steam Tunnel

The supply is from the building heating boiler. No actual measurements of steam quality in the test section have been made, but only conventional thermodynamic calculations. However, precise knowledge of test section steam wetness is not of great importance for present purpose, where liquid film is injected and conditions are nominally adiabatic.

Test section steam velocity can be measured either by a Pitot tube installed in the test section or by the upstream orifice. Once agreement between these devices was established, only the flow orifice was used, to avoid the flow perturbations caused by the presence of the Pitot tube. The relationship used for measurement of steam velocity is as follows:

$$U_s = \frac{W_w \, v}{3600 \, A_c} \qquad (3.1)$$

where:

U_s = bulk average steam velocity, in the test section (ft/sec)

W_w = mass flow rate of steam (lbm/hr)

v = specific volume of the steam (ft^3/lbm)

A_c = cross-sectional area of the test section (ft^2). For the present geometry $A_c = 0.069$ ft^2. And from the handbook, "Principles of Flow Meter Engineering" (S10).

$$w_w = 2781.72 \left(H_{hg} \left(\frac{P_2}{T_2} \right) \right)^{1/2}$$

where

H_{hg} = manometer head, inches of mercury

T_2 = steam line temperature (°R)

P_2 = saturation pressure at the steam line temperature (lb/in^2-abs.)

More details of the steam flow measurement and related data reductions are available in reference.[M9]

Static pressure was measured along the side wall of the test section. Three pressure taps were installed; the first opposite the leading edge of the blade, the second 11.5 cm downstream with respect to the leading edge, and the third 25.5 cm downstream from the leading edge (5.5 cm downstream of the trailing edge). These static pressures were read using a precision Heise gage as negative gage pressures. Ann Arbor atmospheric pressure of course varies from day to day. The average pressure, however, is 14.3 psia (9.86×10^4 N/m^2). Thus the average absolute test section static pressure ranged between 1.2 and 1.3 psia (0.83×10^4 and 0.89×10^4 N/m^2). One thermocouple was embedded flush with the side wall of the test section. The temperature reading obtained there was always higher than the saturation temperature corresponding to the test section pressure. This positive temperature differential is of course due to the boundary layer recovery of part of the kinetic temperature in this high velocity steam flow near the wall.[S8]

Average parameters in the test section, i.e. position #4 of Fig. 3.1 are:

P_4 = 0.09 bar	(1.25 psia)	test section pressure
T_4 = 43°C	(109.4°F)	saturation temprature at P_4
X_4 = 0.95		estimated steam quality
v_4 = 16 m^3/Kg	(256.47 ft^3/lbm)	steam specific volume

$U_{s\ max}$ = 335 m/s (1100 ft/s), maximum obtainable steam velocity

The test section (8 cm x 8 cm x 100 cm) is constructed of clear transparent plastic (Lexan) which allows the necessary photographic studies. A simulated turbine blade, i.e., essentially a thin flat plate with tapered ends (Fig. 3.3), with electrical conductance microgages on the blade to measure liquid film thickness, including time variations, is inserted along the centerline and parallel to the flow axis.

The design and calibration of these gages is discussed in Appendix A. The "stilling tank" (Fig. 3.1) provides a honeycomb flow straightener to produce uniform flow in the test section. The condenser is of the jet type (rather than conventional shell-and-tube design). Jets of tap water are used to condense the steam in a counterflow vertical tank. The bottom of the tank serves as a "hot-well" from which a centrifugal condensate pump takes suction. The pump then exhausts the combined flow into the laboratory drain system. To improve condensing, and hence obtain increased vacuum and steam velocity, perforated trays were installed in the condenser to produce more efficient mixing. In addition, a mechanical vacuum pump (Kinney Hi-Vacuum pump, Model KC-15) was used to increase the test section-condenser vacuum still further.

B. BLADING PROFILE AND ELECTRICAL CONDUCTANCE MICROGAGES

As shown in Fig. 3.3, a thin flat plate used to simulate the steam turbine blade was designed, fabricated

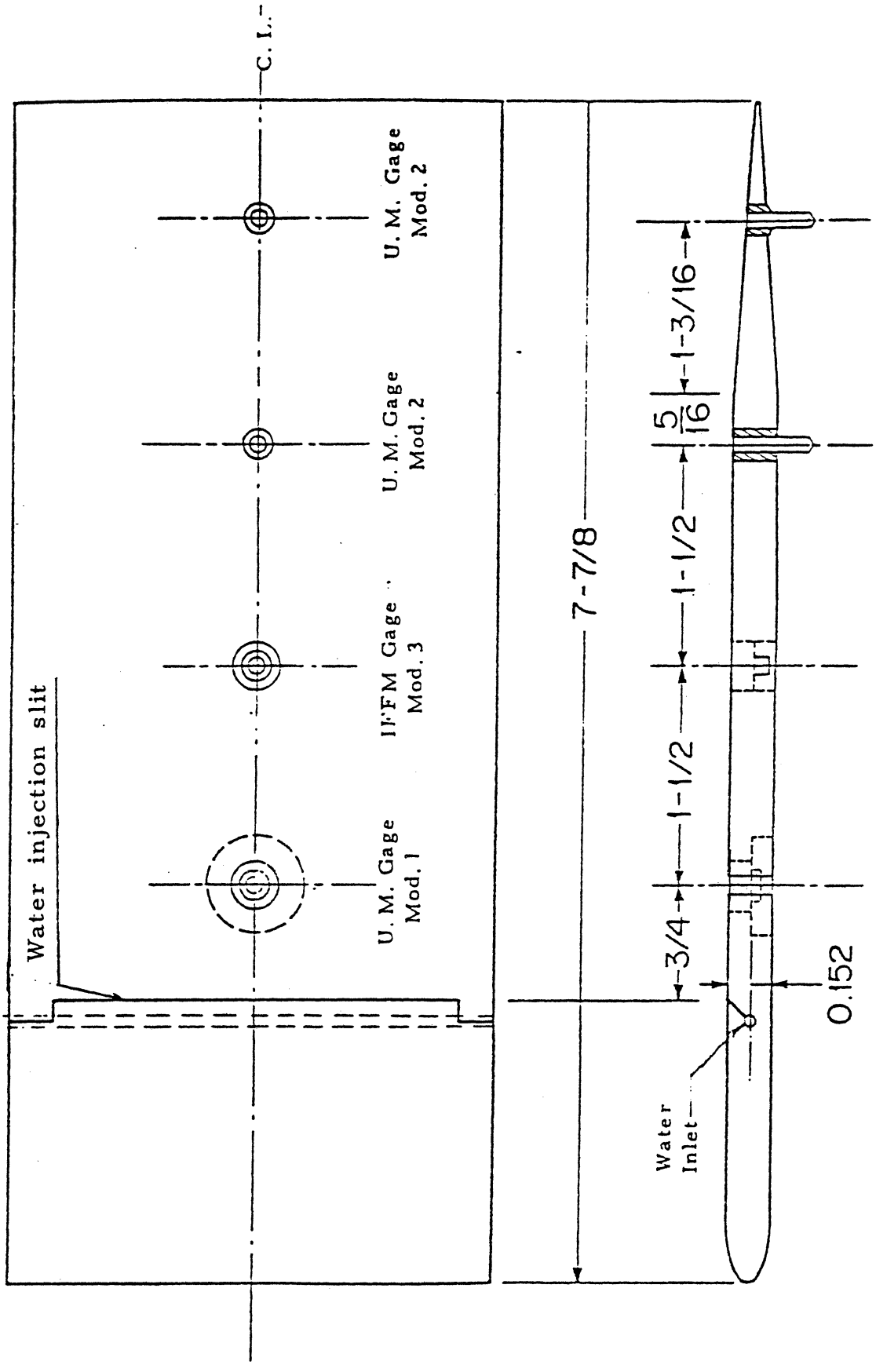

Fig. 3.3 Test Section Blade

and installed in the test section for these tests. In one version, a liquid film is injected through a small slit normal to the tunnel axis, to simulate the liquid film flow condition encountered naturally in the turbine stator blades.

Minimum film injection rate depends upon the measuring and throttling capability of the flow meter, and is 5 cm^3/min (0.625 cm^3/min-cm, "specific" liquid flow rate per unit blade width). The maximum rate used was 100 cm^3/min (12.5 cm^3/min-cm). The pressure differential for film injection from the open reservoir used is due to the vacuum in the test section (~1.25 psia) plus an elevation head between liquid reservoir and the test section.

Electrical conductance microgages were installed flush with the blade surface to measure the liquid film thickness variation with respect to time. Since detailed decriptions of gage design and calibration are given in Appendix A, only a few important aspects are discussed here. Essentially, the electrical conductance of a thin liquid film connecting the central pole of the gages with an external annulus (separated by an electrical insulator), all installed flush with the blade surface (Fig. 3.3), is measured by an a.c. circuit including a Wheatstone bridge. The output is connected to a dual-beam oscilloscope, so that the simultaneous output of two gages can be compared at a given instant of time. An a.c. circuit is used to avoid problems of electrostatic charge. While results depend somewhat on circuit frequency,(C15,H19) it was found that the response is flat

with a frequency in the range of 1 kHz (H10,F1), which was thereafter utilized. The output in terms of circuit conductivity was found to be approximately linear for small film thickness, but gage output becomes "saturated" at higher thickness (>300 μm). (M10,F1,H10,H11,H18)

Thus the useful operating range of the gages is limited to $\lesssim$ 300 μm. (See Appendix A and references F1, M10). This is sufficient for present purposes.

C. PHOTOGRAPHIC FACILITIES

Photographs were made using both a still polaroid camera (4x5 Busch precision camera, Model D) and a modified high speed Wollensac Fastax camera (WF-1) for the investigation of wavy films, finger formation, and droplet trajectories.

In the Fastax WF-1 camera, film is transported continuously past the aperture while a rotating prism, geared to film motion, produces an image which is stationary with respect to time. Individual frames (16 mm x 8 mm) constitute the 100 ft. rolls of film used. (Kodak Tri-X reversal 7278 film).

A "Wollensac-Goose" control regulates the camera motor speed. The motor continuously accelerates the film, which is initially at rest. The maximum acceleration, and hence framing rate, is determined by the film strength. Since the film is initially at rest, the framing rate changes continuously, so that the maximum framing rate occurs only near the end. The exact framing rate at a given point is determined from timing marks placed along the edge of the film using a 60 Hz timing light.

For present work, the framing mechanism was removed and a magnetic coil installed near the drive sprocket. Framing was achieved using the magnetic pickup coil, which is triggered by the drive sprocket. Pulses are then delivered to a strobo-trigger circuit (EG&G high-speed stroboscope Type 501), which fires the flash lamp (EG&G-FX2). Synchronization of camera and strobe is thus ensured at all film speeds. An EG&G stroboscopic light source which produces high intensity 1.2 μs light pulses at a maximum rate of 6,000 flashes/sec was used to reduce the exposure time per frame. Since the Fastax camera has a rated top speed of ~ 14,000 frames per sec., framing rate was limited in the present case by the flash rate of the light source, which was in fact sufficient.

The Fastax cinematography was sufficient to "freeze" all droplet and wave motions, as was the still photography used. By using the timing marks on the film, the time increment between frames could be determined accurately for the purpose of establishing wave propagation speed and droplet accelerations and break-up times.

For the still photography, two sets of flood lights were employed (Color Trans Quartz-King dual 650, Model no. 160-011). The lens settings were selected as required. Film used was Polaroid 4x5 land-film/Type 57. Typical exposure time was 5 ms with two flood lights. This relatively long exposure time was sufficient, even though much shorter exposure times were used for the Fastax. These different exposure time requirements are due to the combined effects

of light intensities and film speeds used.

D. EXPERIMENTAL MEASUREMENT CONDITIONS

The range of experimental parameters and measurements is listed in Table 3.2 below:

TABLE 3.2 - Experimental Parameters

Independent Variables	
Steam Velocity, U_s,	- 20 to 335 m/s (Mach No. = 0.05 to 0.81)
Specific Liquid Flow Rate, q	- 0.010 to 0.208 $cm^3/cm\text{-}sec$ (Re_f = 1.4 to 56.2)
Dependent Variables	
Wavy Films	(see Fig. 3.4)
Film Thickness, h,	- 1 to 10 mils (25.4 to 254 um)
Film Wave Length, λ	- 5 to 12 mm (small waves)
	10 to 20 mm (large waves)
Wave Propagation Speed, C,	-20 to 200 cm/s (small waves)
	100 to 1500 cm/s (large waves)
Finger Formation and Droplet Motion (see Fig. 3.5)	
Finger Length, L,	- 3 - 30 mm
Finger Wave Length, λ_f, (average distance between fingers)	- 2 to 10 mm
Frequency of Large Finger Formation, f,	- 8 to 16 $sec.^{-1}$
Initial Size of Largest Drop in Wake, D_o,	- 0.5 to 2.0 mm
Droplet Acceleration, A_m,	- 300 to 400 $m.sec.^{-2}$ ($\cong$ 30 to 40 g)
Duration of Large Droplets, t_b,	- 0.001 to 0.02 sec.

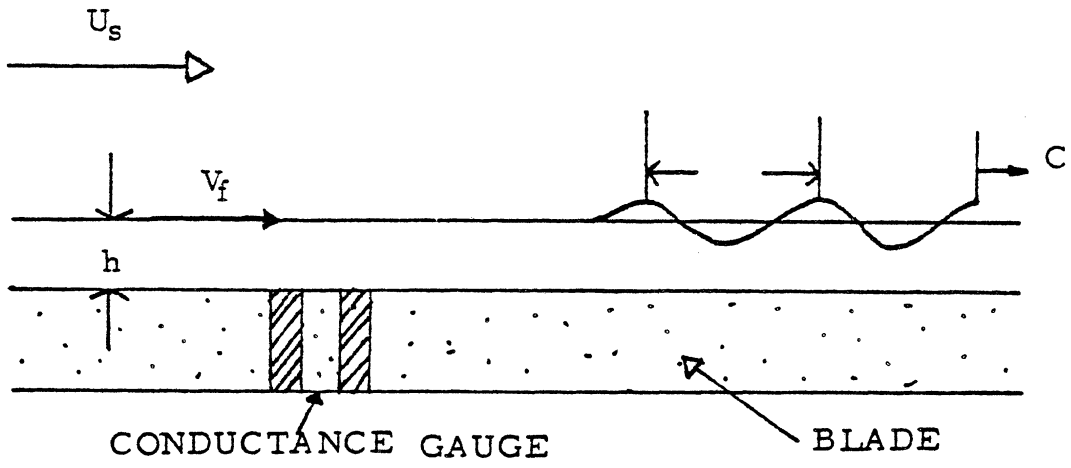

Fig 3.4 : Schematic of Wavy Film Characteristics

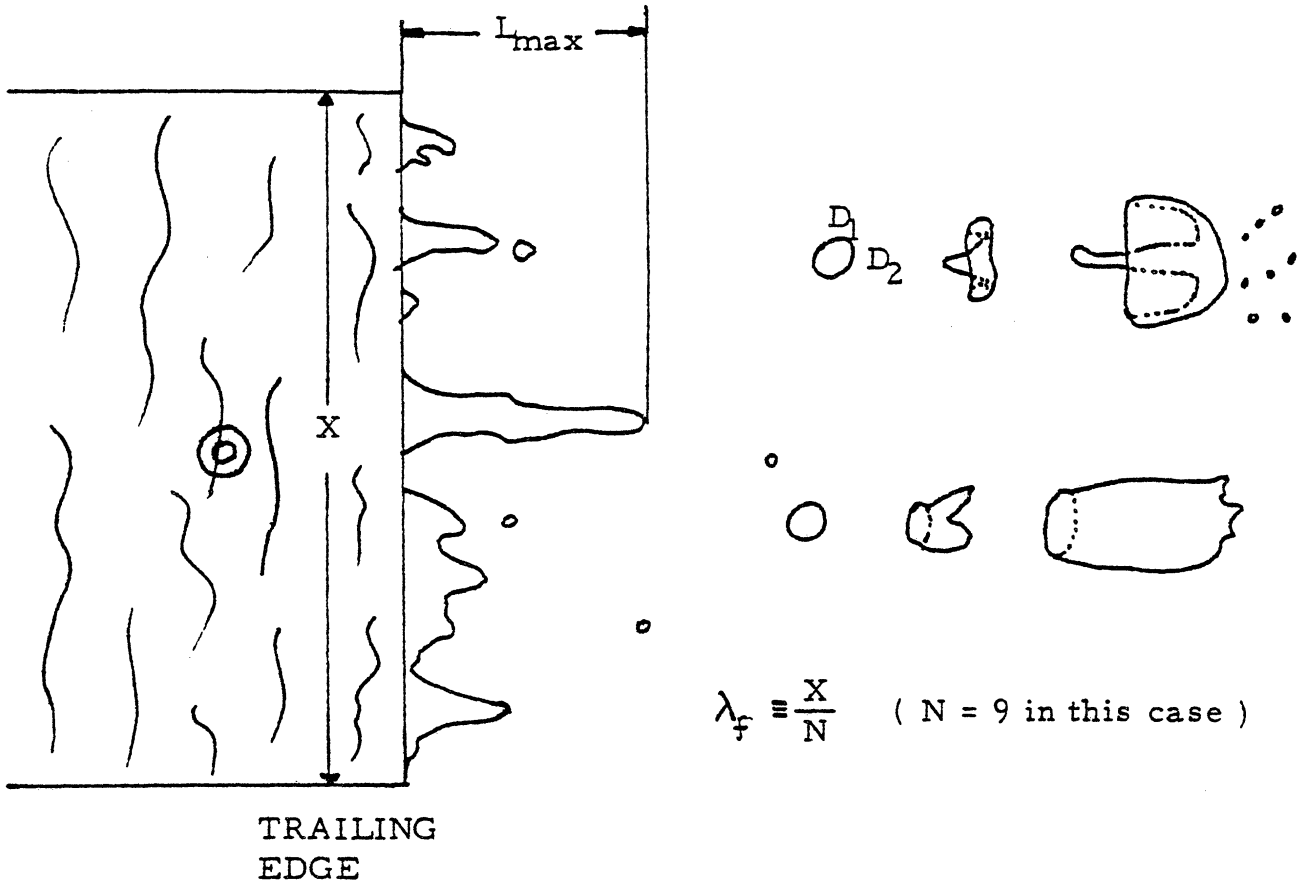

Fig 3.5 : Schematic of Finger Formation and Secondary Droplet Motion

CHAPTER IV

BEHAVIOR OF LIQUID FILM

A. VISUAL OBSERVATION OF WAVY FILM

One of the most important features of film flow are the wave patterns which appear at the free surface or interface between the liquid and vapor phases. Such wavy film flows are highly complex. Thus no satisfactory general theory has yet been evolved; rather only specialized and simplified models are available. Further, the complete experimental determination of the parameters characterizing very thin wavy film patterns, as in the present case, is extremely difficult.

To study the wavelet patterns in detail, about one thousand still photographs have been taken at various steam and liquid flow conditions, as well as $\sim$100 rolls of 100 feet length of Fastax high speed motion pictures. Oscilloscope photos of film thickness conductivity gage voltage output were taken, simultaneously with the wavelent pattern photos. The photographs of Fig. 4.1 show the various wavy film patterns for different flow conditions. For different steam velocities, the transition points between various wavy pattern regimes, as the liquid flow rate is increased, have been observed. Plate Series #1 of Fig. 4.1 show the various wavy patterns for steam velocity, U_s=30 m/s, which is the minimum steam velocity used for this investigation. Instrumentation limitations prevent the use of still lower steam velocities. As can be seen in plate 1.1 for minimum

Table 4.1 FLOW CONDITIONS AND OSCILLOSCOPE SET UP FOR FIGURE 4.1

Plate No	Steam Velocity U_s(m/s)	Liquid Flow Rate q, $cm^3/cm.s$	Oscilloscope Set Up X ms/unit	Y V/ unit	Features
P1.1	30	0.010	10	0.5	Rivulet Flow
P1.2	30	0.021	10	0.5	Ripples
P1.3	30	0.043	10	0.5	Smooth and 2-D wave
P1.4	30	0.083	10	0.5	Ripples and 2-D wave
P1.5	30	0.125	10	0.5	2-D and 3-D wave
P1.6	30	0.167	10	0.5	3-D waves
P1.7	30	0.208	10	0.5	3-D waves
P2.1	50	0.010	10	0.5	Dry patch and abrupt bulge at the stagnation point
P2.2	50	0.021	10	0.5	Dramatic dry patch and apparent wave appearance
P2.3	50	0.043	10	0.5	2-D waves
P2.4	50	0.083	10	0.5	2-D waves
P2.5	50	0.125	10	0.5	3-D waves
P2.6	50	0.167	20	1.0	3-D waves
P2.7	50	0.208	10	1.0	3-D waves
P3.1	80	0.010	10	0.5	Rivulet Flow
P3.2	80	0.021	10	0.5	2-D wave and dry patch
P3.3	80	0.083	10	0.5	2-D and complicated ripples
P3.4	80	0.125	10	0.5	3-D waves
P3.5	80	0.167	10	0.5	3-D waves
P3.6	80	0.208	10	1.0	3-D waves

Table 4.1

P4.1	144	0.010	10	0.1	Wavy rivulet
P4.2	144	0.021	10	0.5	2-D waves
P4.3	144	0.043	10	0.5	2-D and 3-D waves
P4.4	144	0.083	10	0.5	3-D waves
P4.5	144	0.125	20	0.5	Entrainment
P4.6	144	0.167	10	0.5	Entrainment
P4.7	144	0.208	10	0.5	Entrainment
P5.1	227	0.010	10	0.5	2-D waves
P5.2	227	0.021	10	0.5	2-D waves
P5.3	227	0.043	10	0.5	3-D waves
P5.4	227	0.083	20	1.0	Entrainment
P5.5	227	0.125	20	1.0	Entrainment
P5.6	227	0.167	20	1.0	Entrainment
P5.7	227	0.208	20	1.0	Entrainment
P6.1	305	0.010	10	0.5	2-D wave
P6.2	305	0.021	10	0.5	3-D wave
P6.3	305	0.043	10	0.5	3-D wave
P6.4	305	0.083	10	0.5	Entrainment
P6.5	305	0.125	10	0.5	Entrainment
P6.6	305	0.167	10	0.5	Entrainment
P6.7	305	0.208	10	0.5	Entrainment

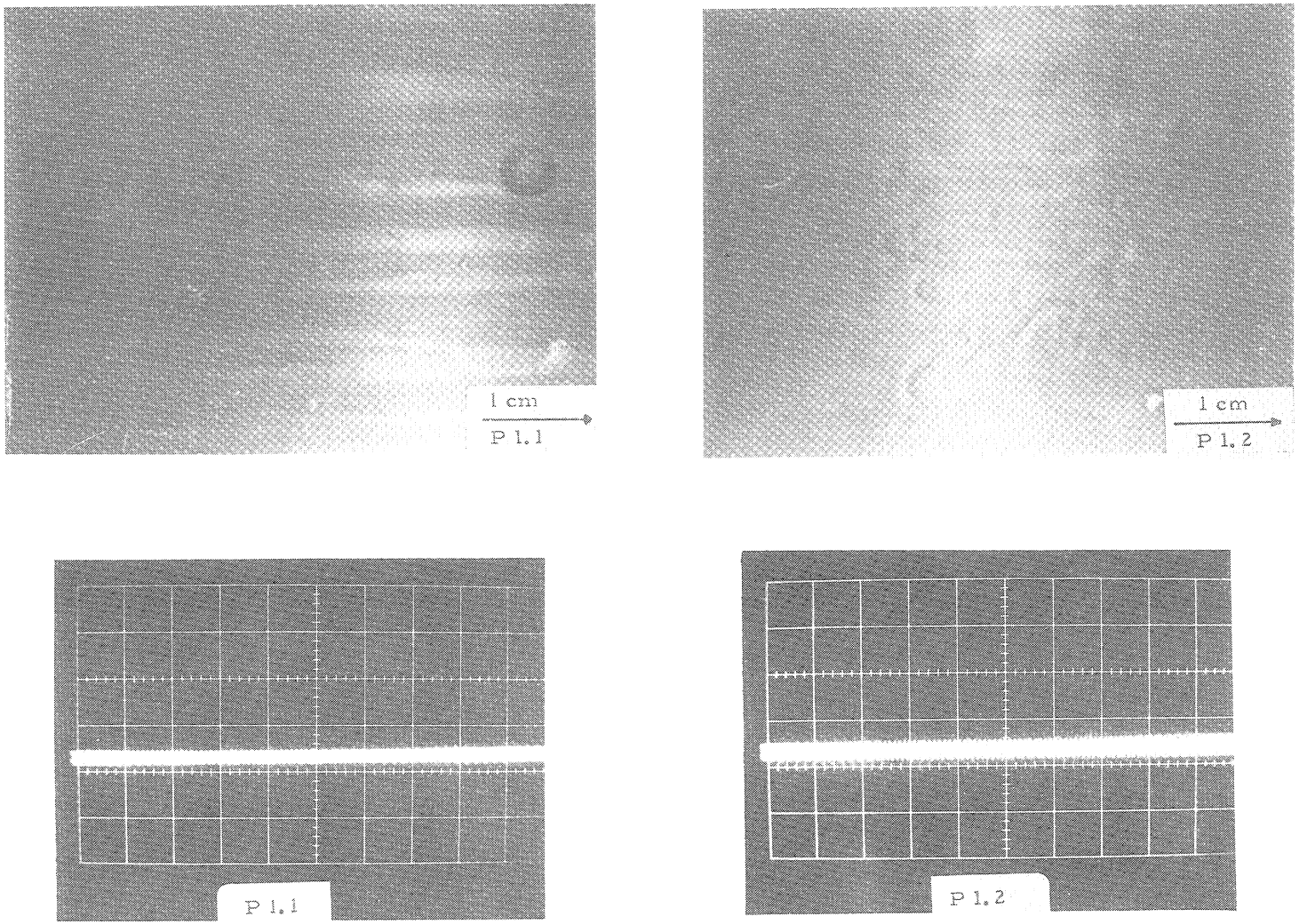

Fig. 4.1 Photographs of Wavy Films Under Various Flow Conditions

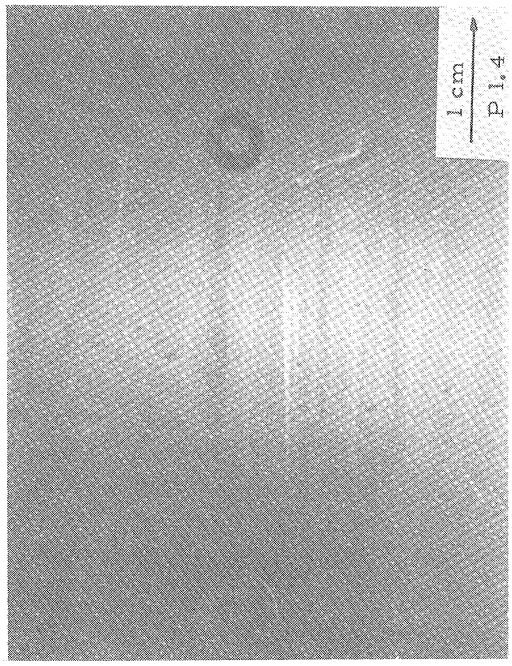

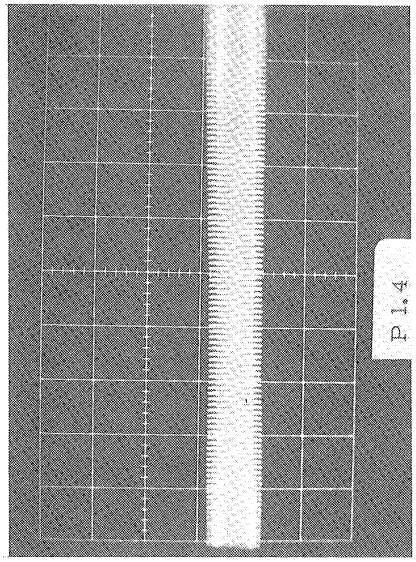

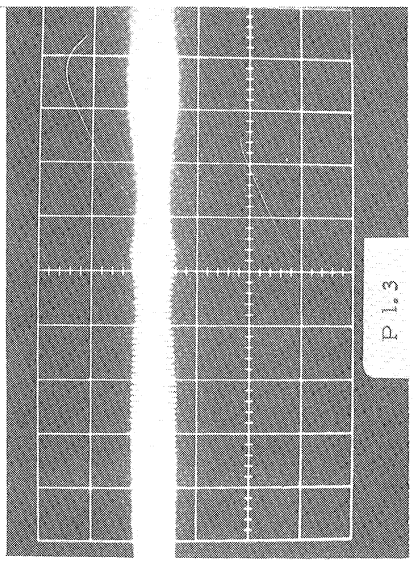

Fig. 4.1 Continued

5377

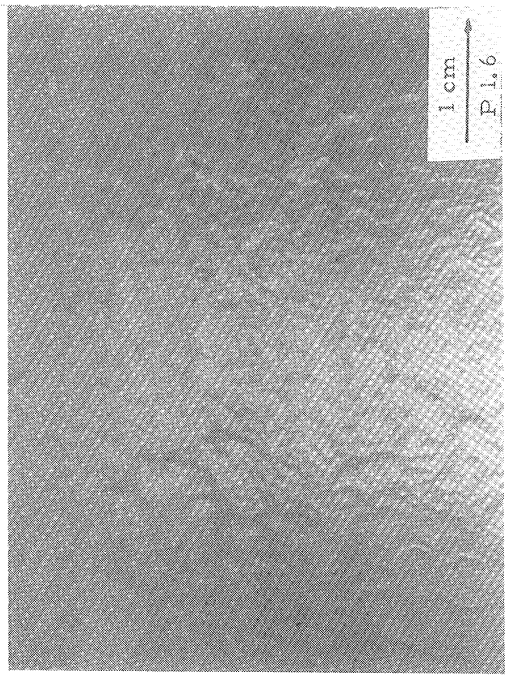

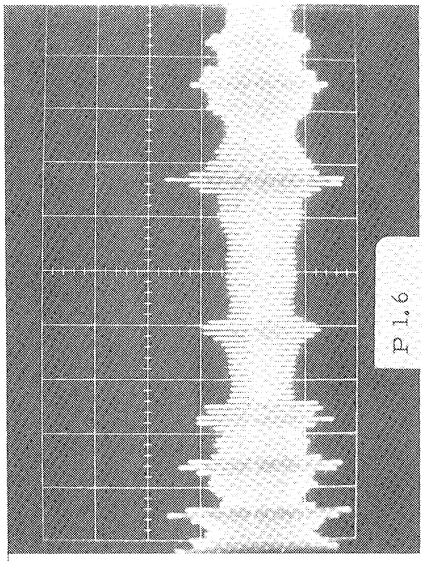

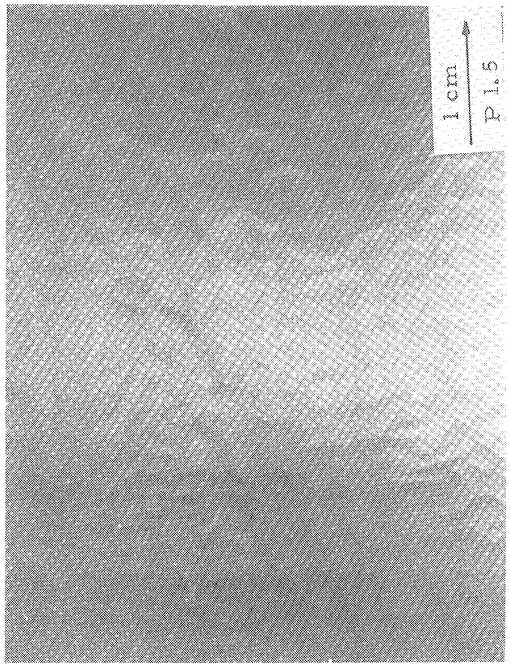

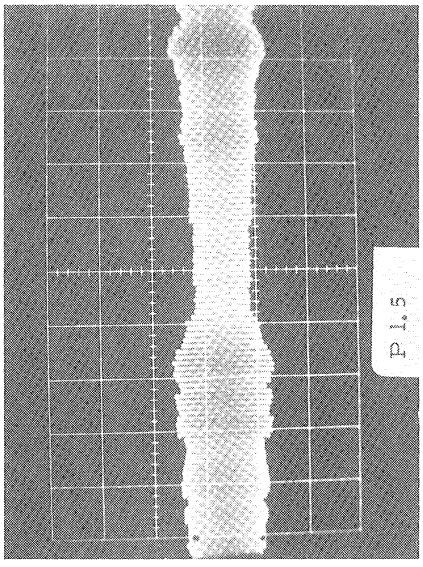

Fig. 4.1 Continued

5378

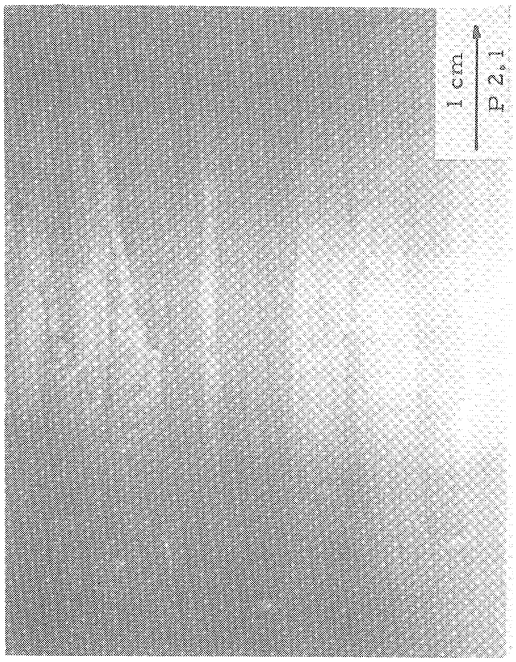

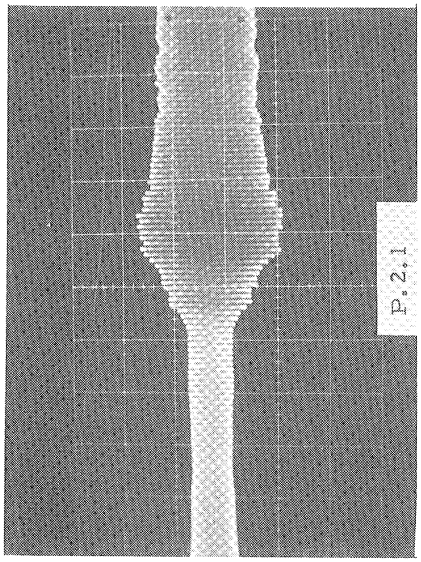

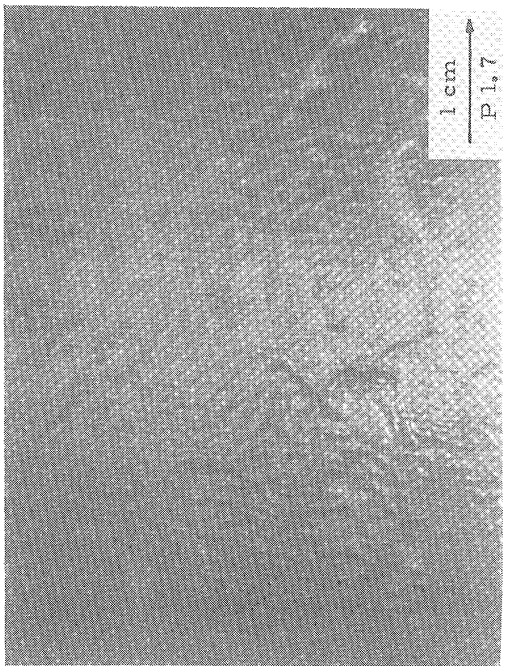

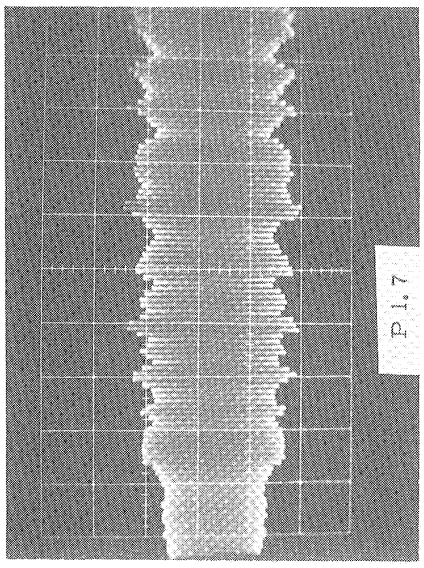

Fig. 4.1 Continued

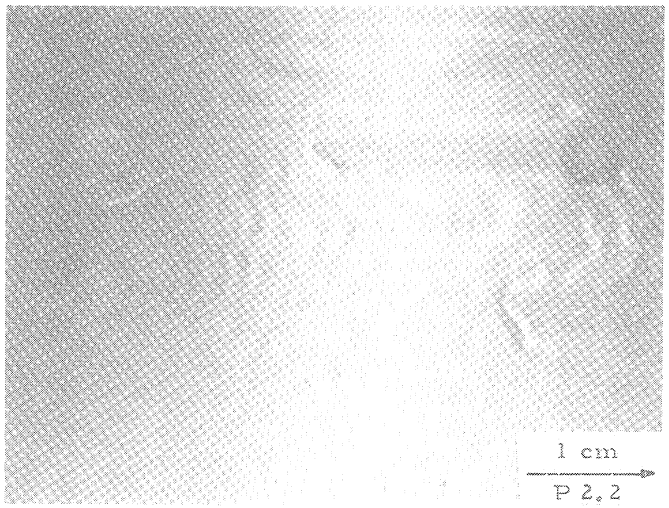

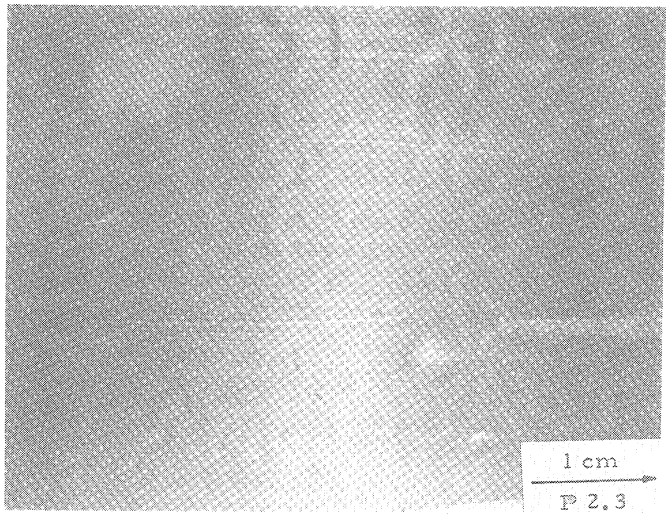

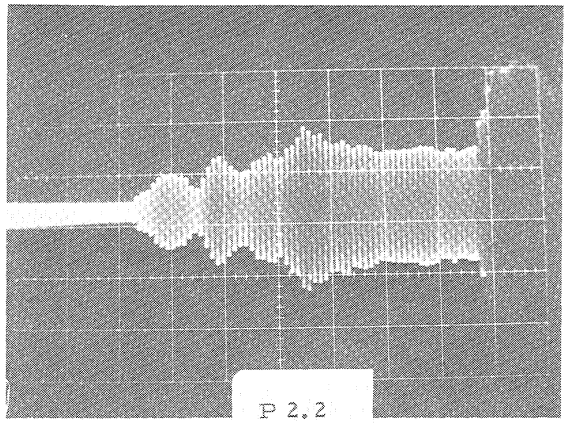

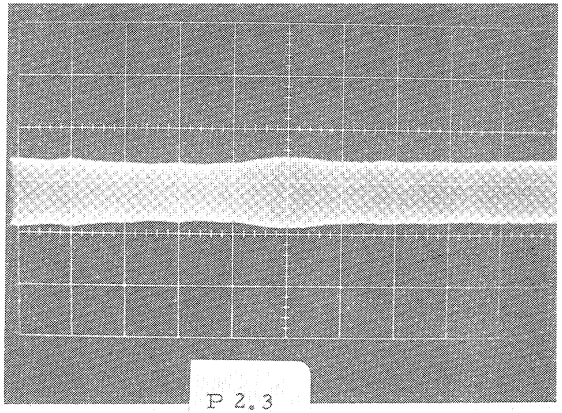

Fig. 4.1 Continued

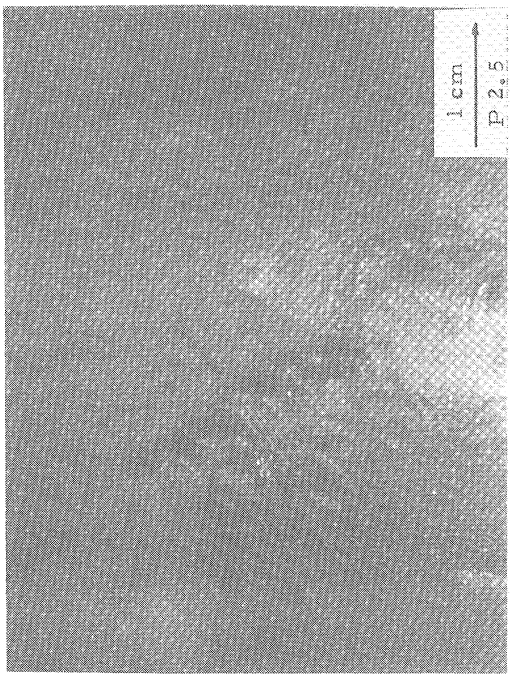

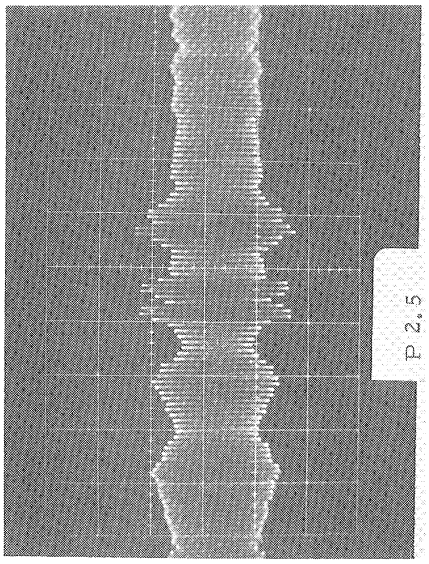

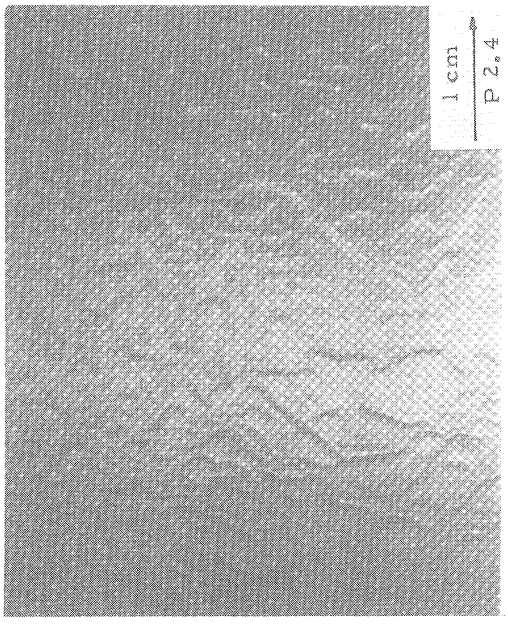

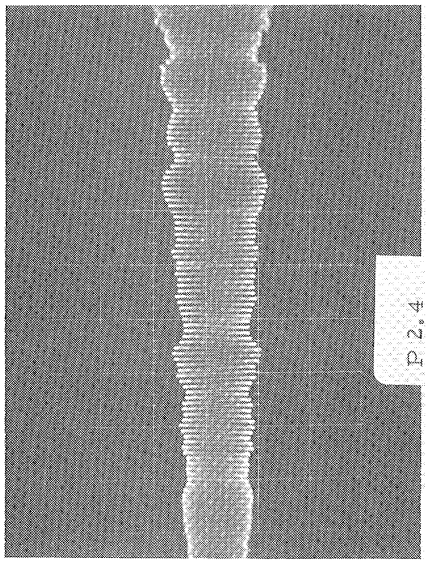

Fig. 4.1 Continued

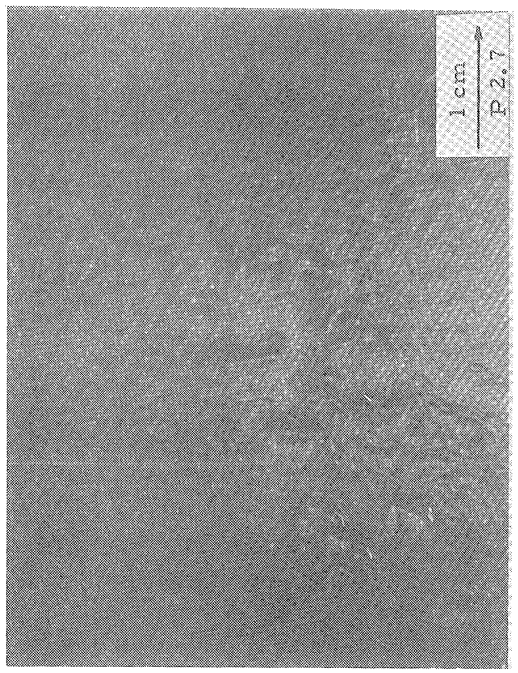

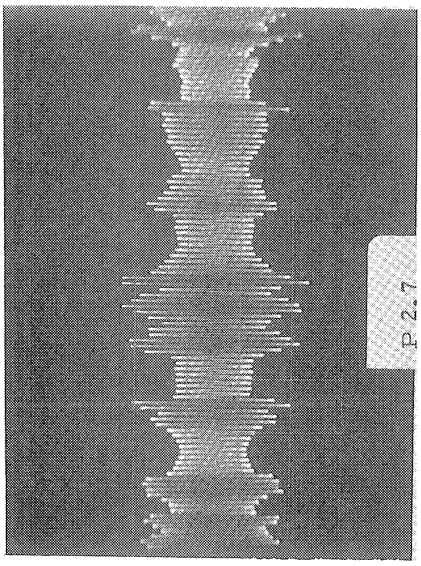

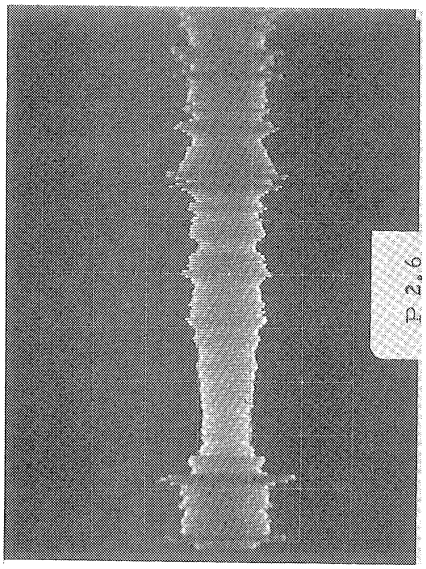

Fig. 4.1 Continued

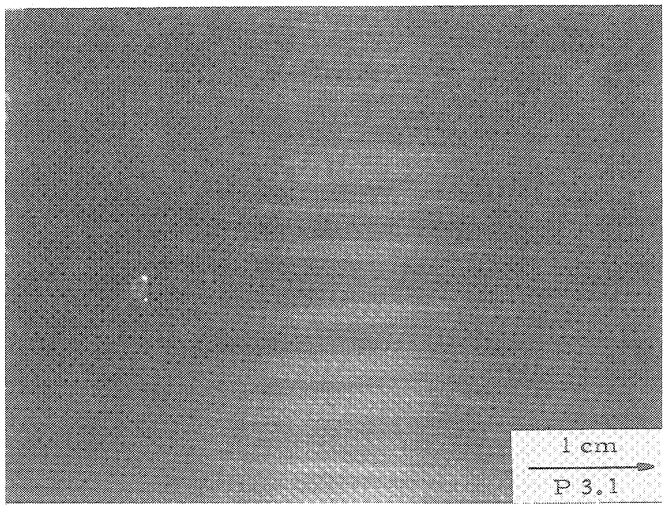

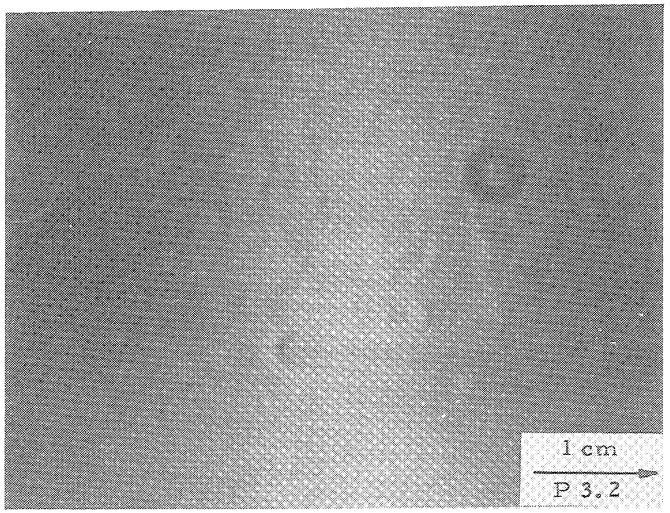

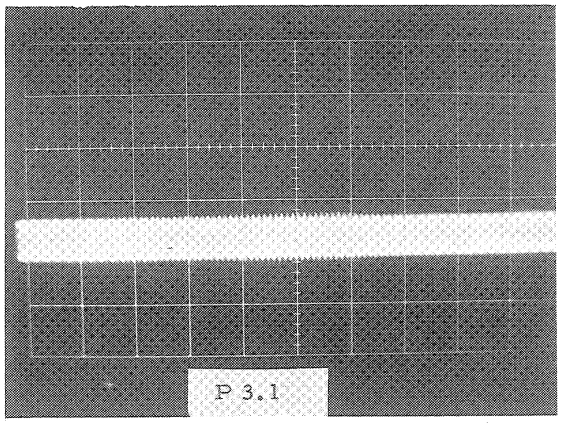

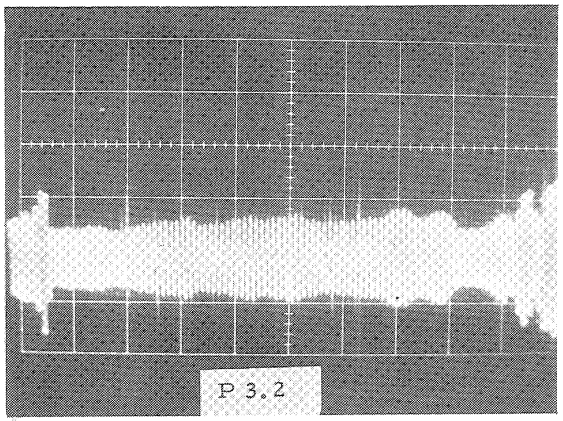

Fig. 4.1 Continued

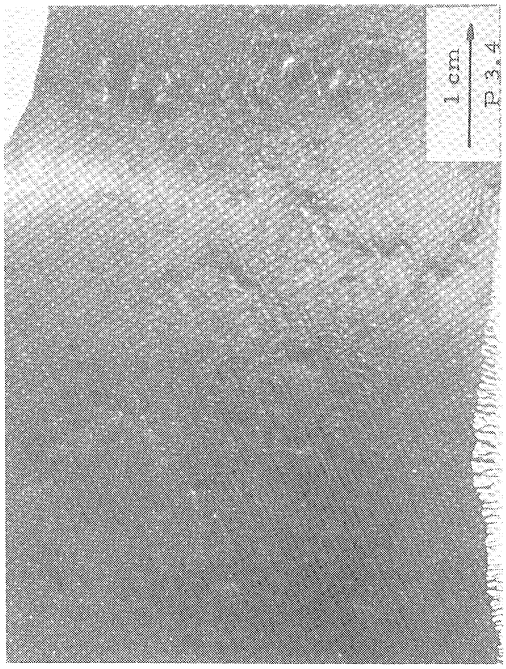

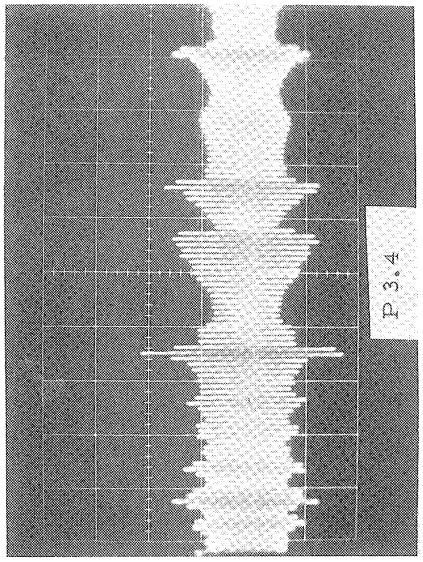

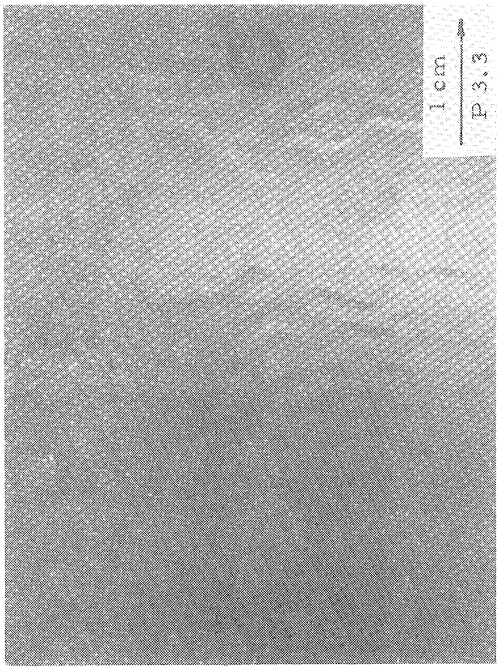

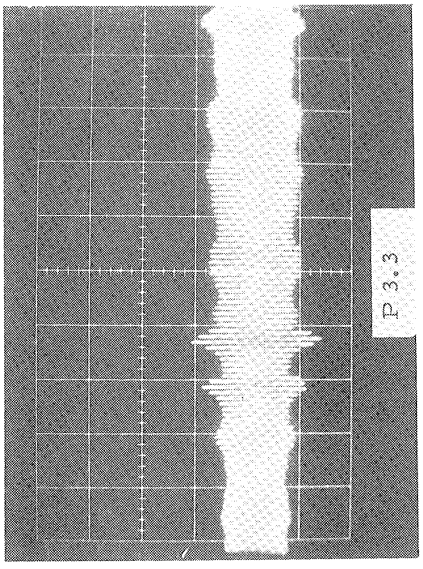

Fig. 4.1 Continued

5384

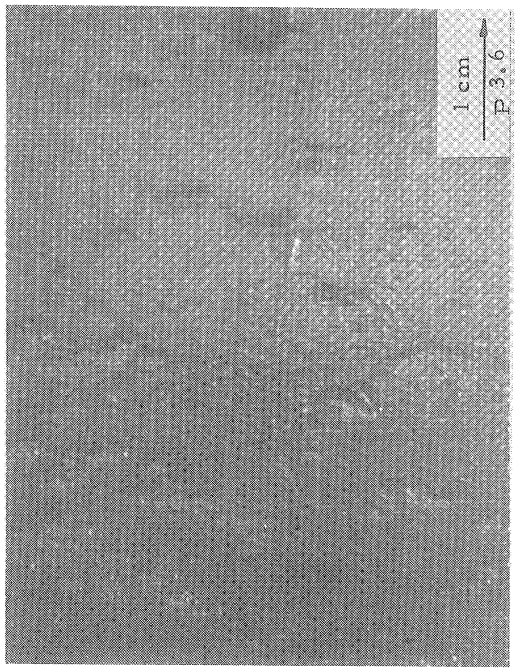

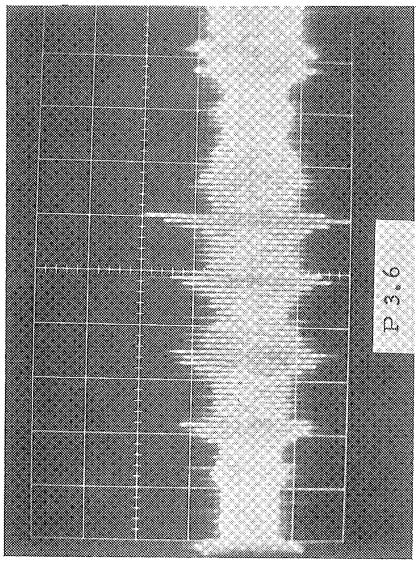

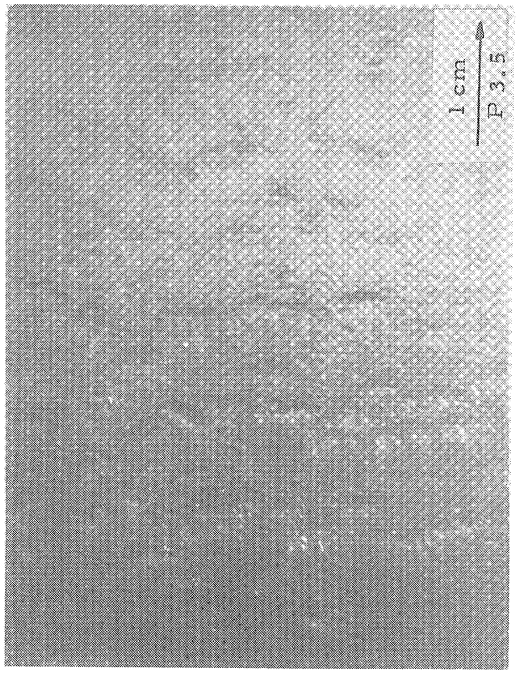

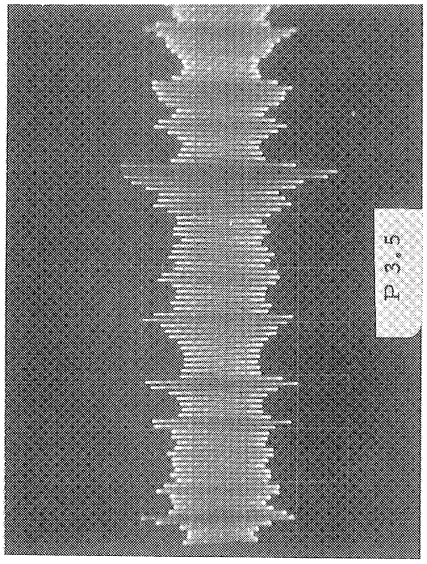

Fig. 4.1 Continued

5385

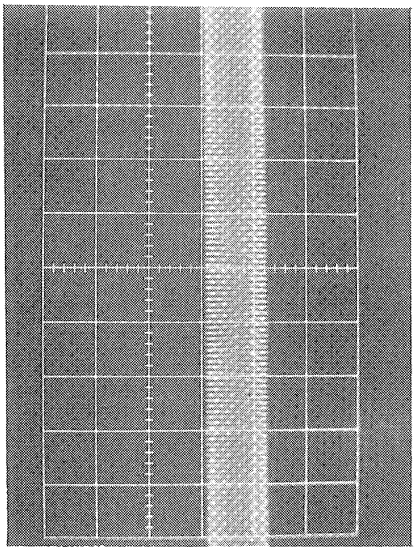

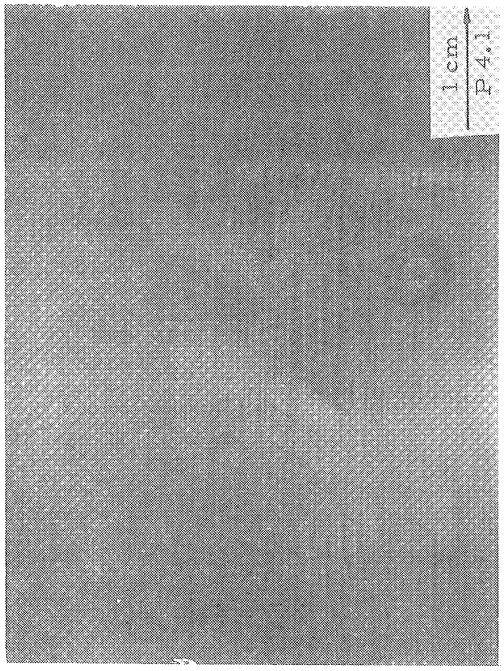

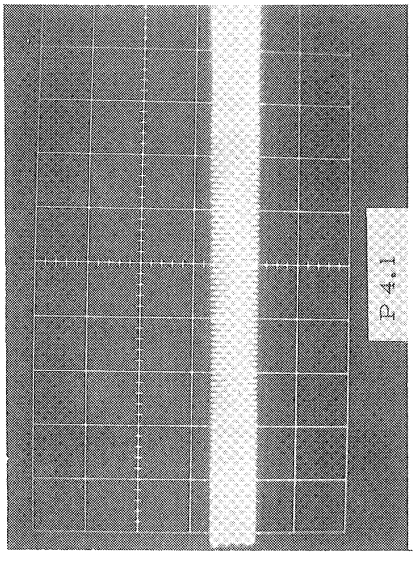

Fig. 4.1 Continued

5386

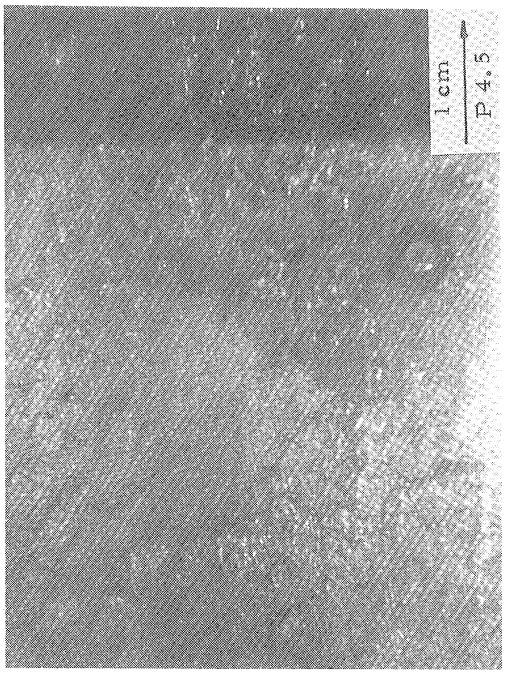

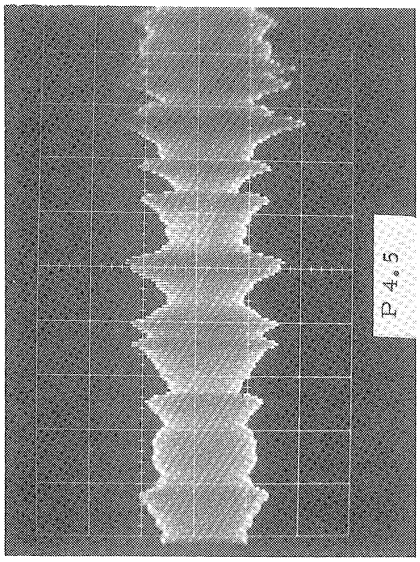

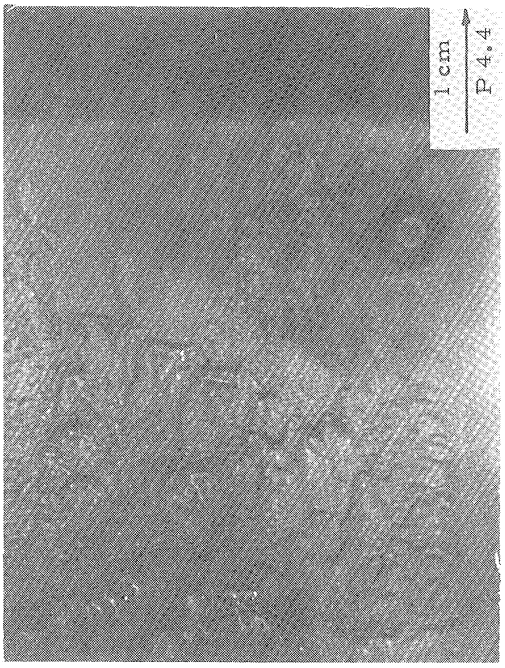

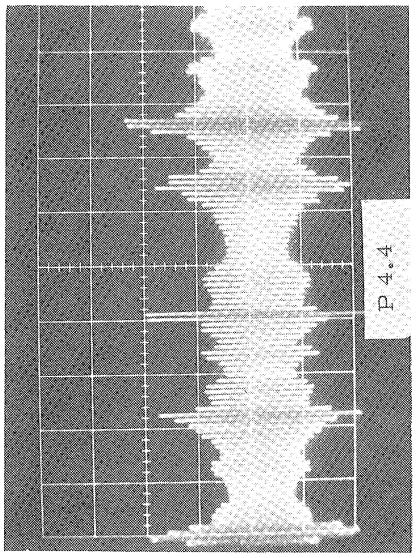

Fig. 4.1 Continued

5387

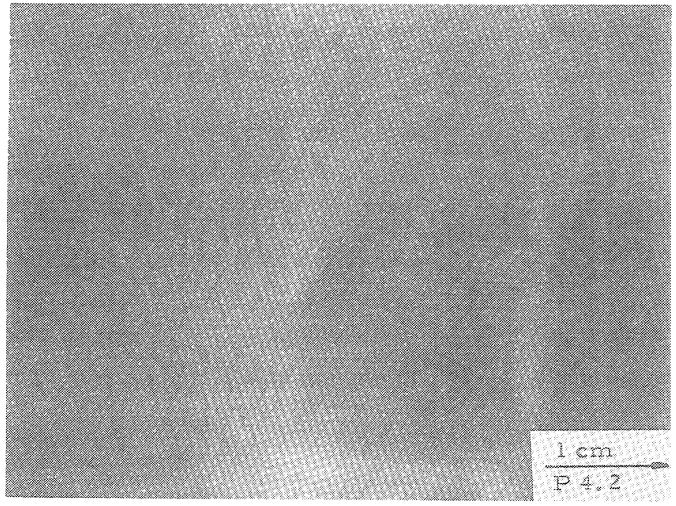

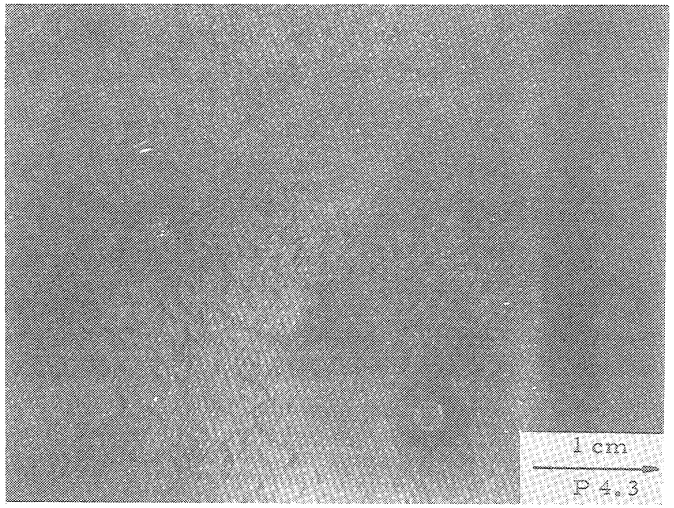

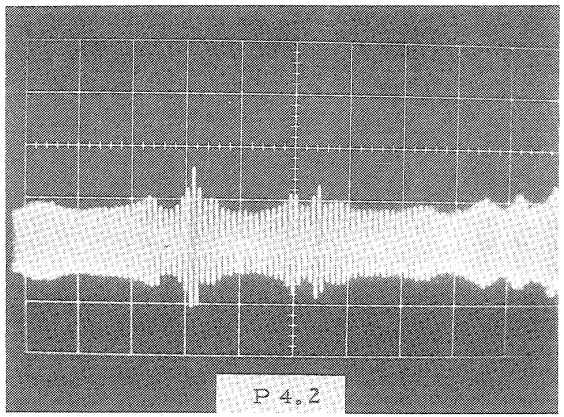

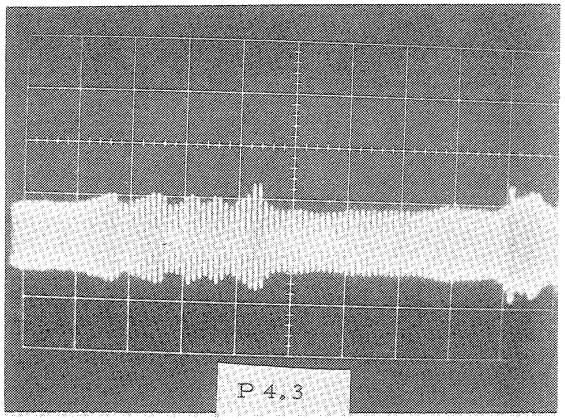

5388

Fig. 4.1 Continued

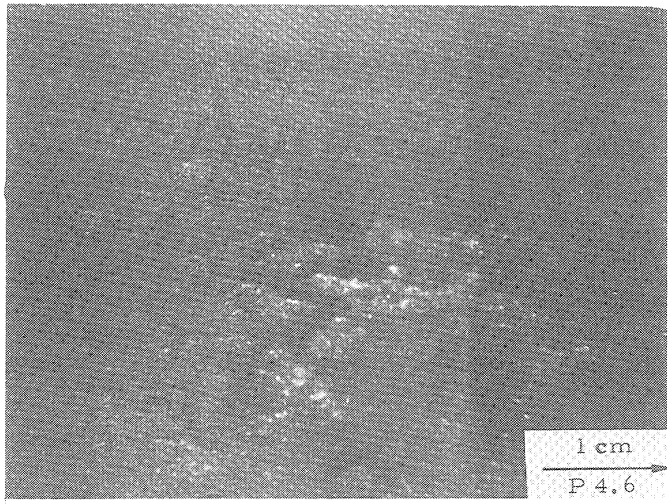

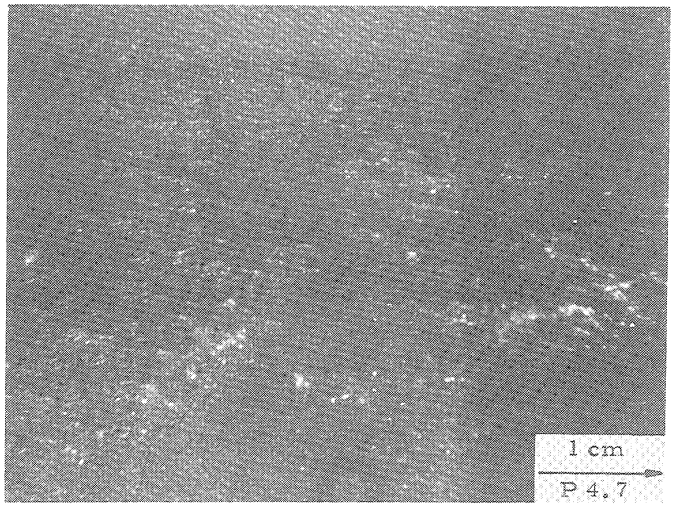

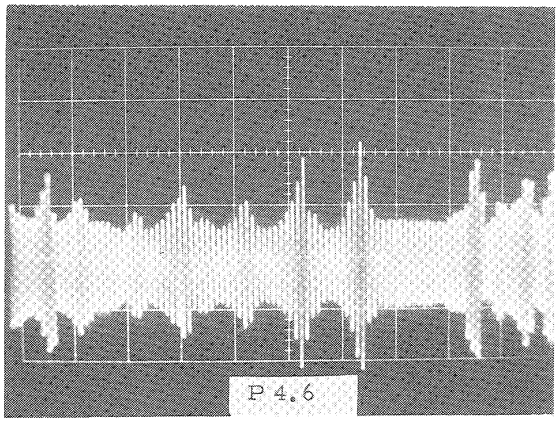

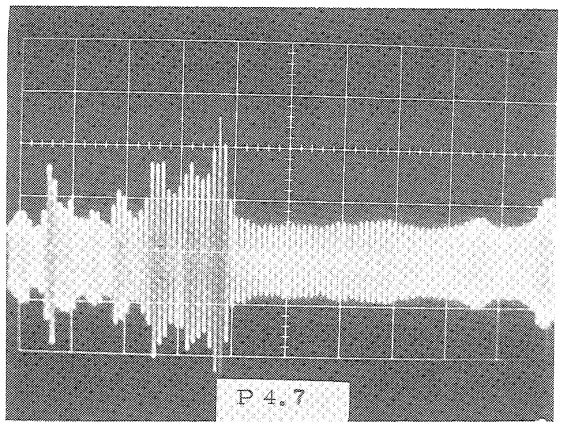

Fig. 4.1 Continued

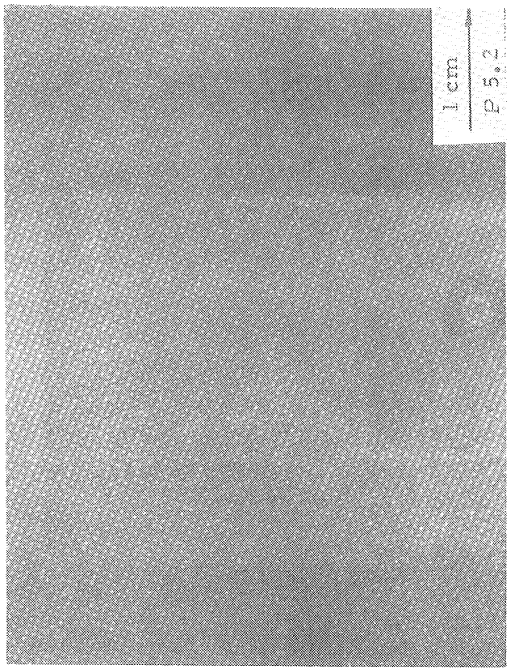

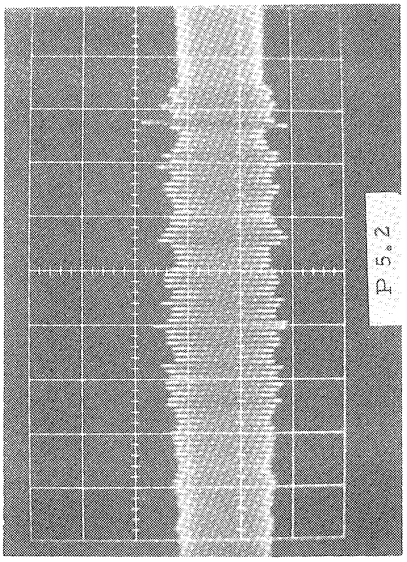

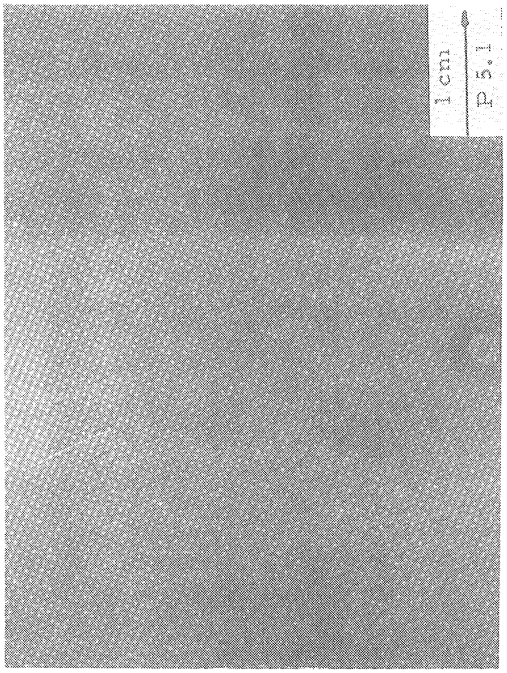

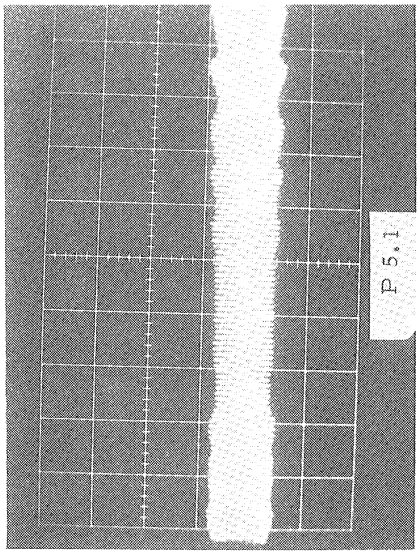

Fig. 4.1 Continued

5390

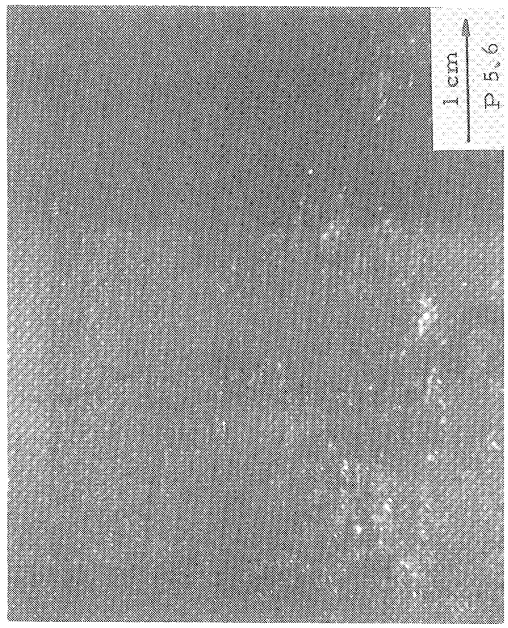

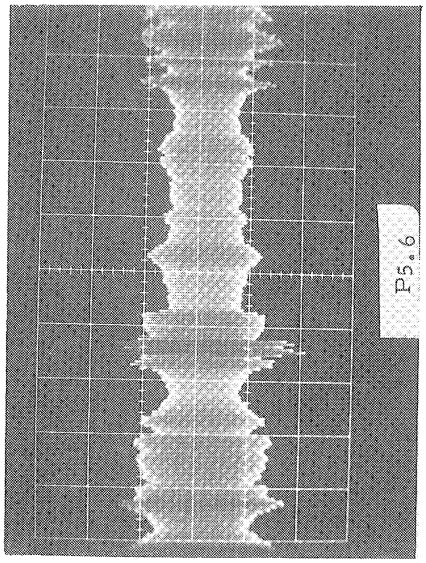

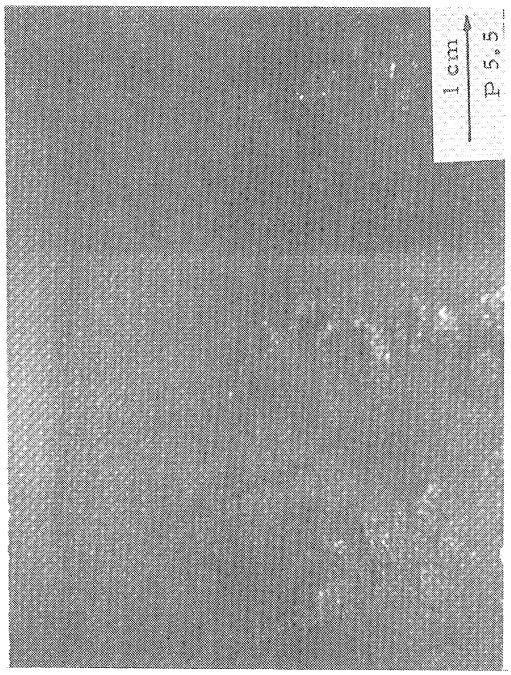

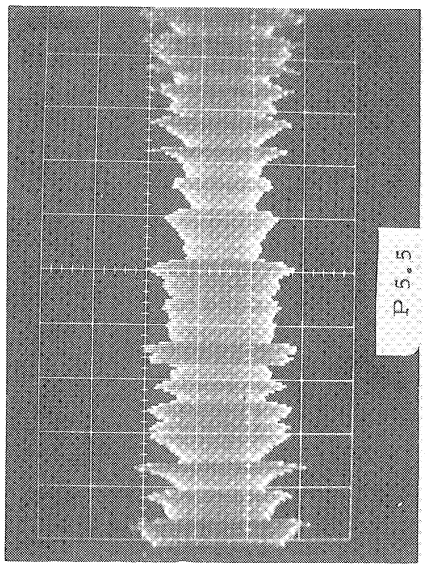

Fig. 4.1 Continued

5391

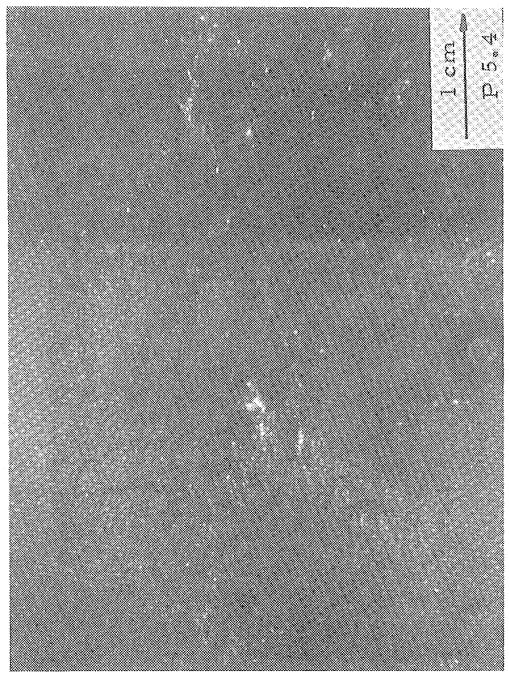

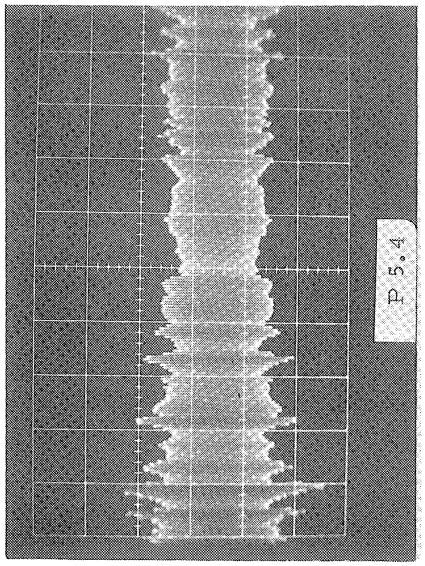

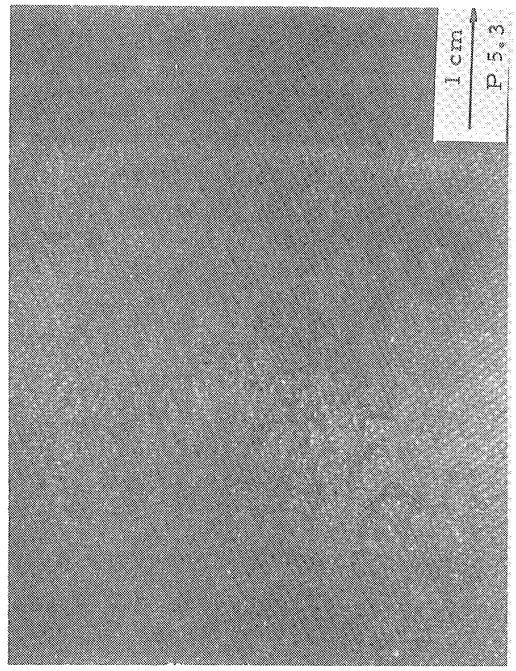

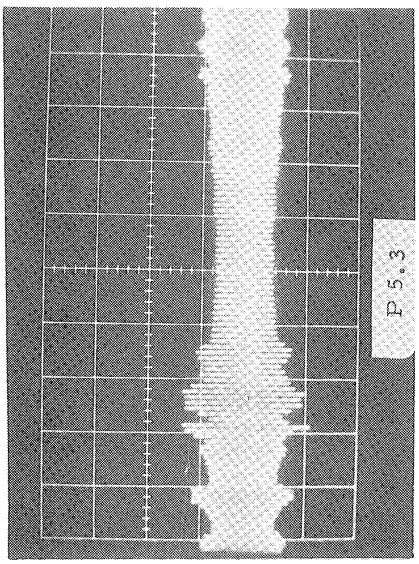

Fig. 4.1 Continued

5392

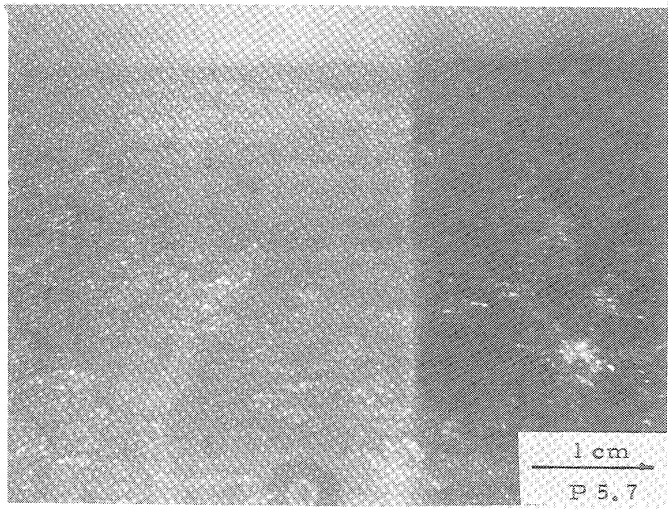

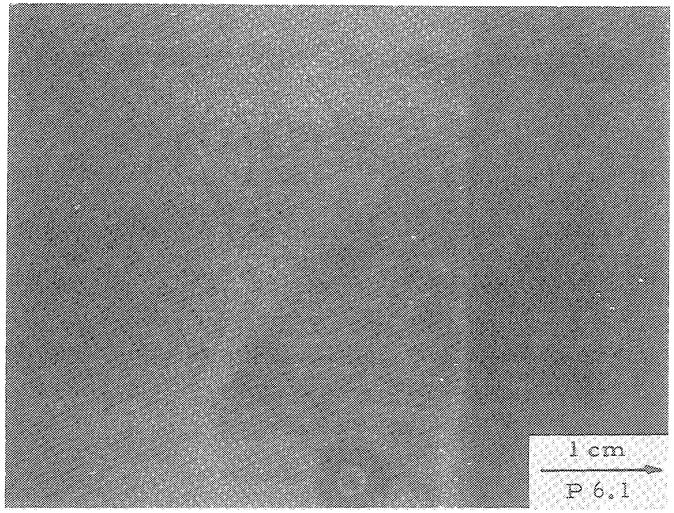

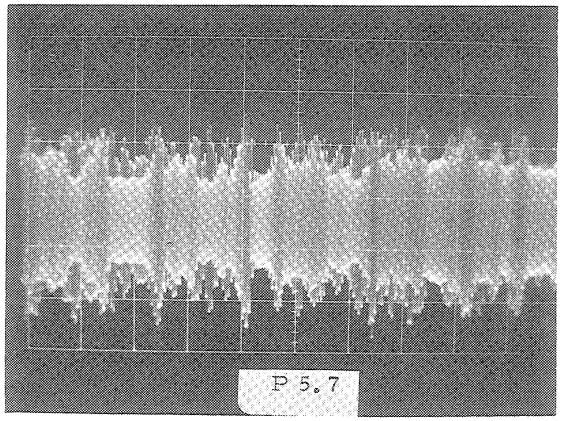

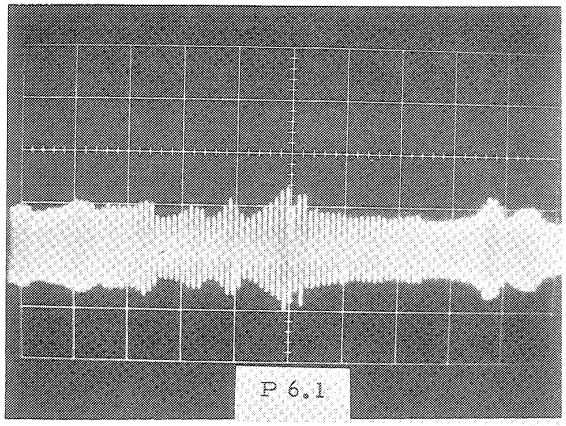

Fig. 4.1 Continued

Fig. 4.1 Continued

5394

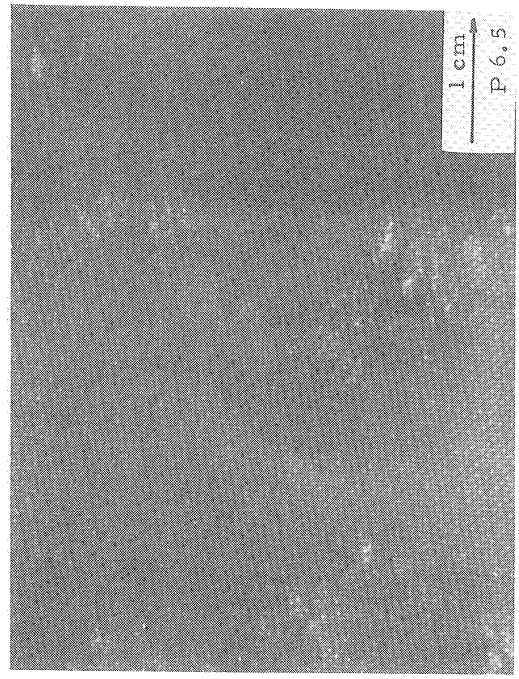

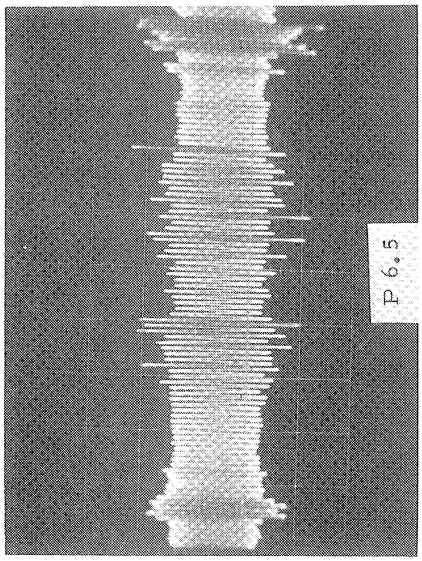

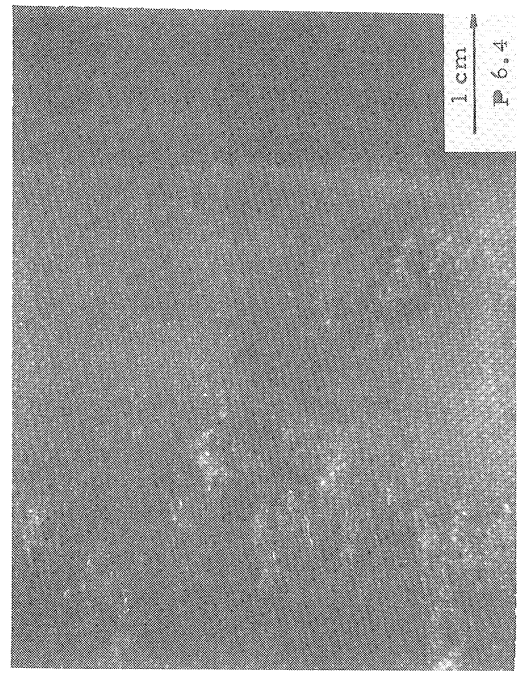

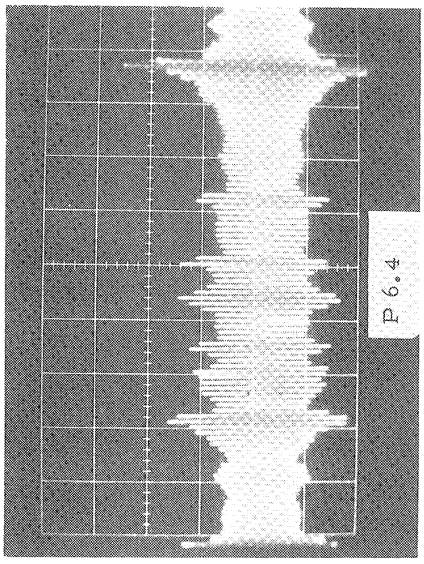

Fig. 4.1 Continued

5395

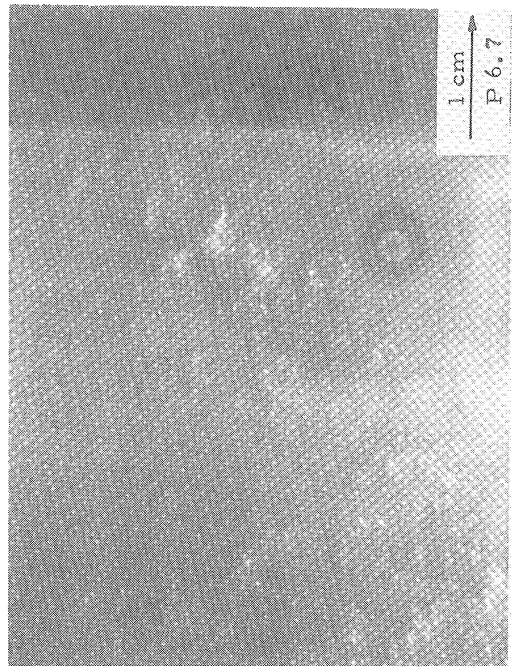

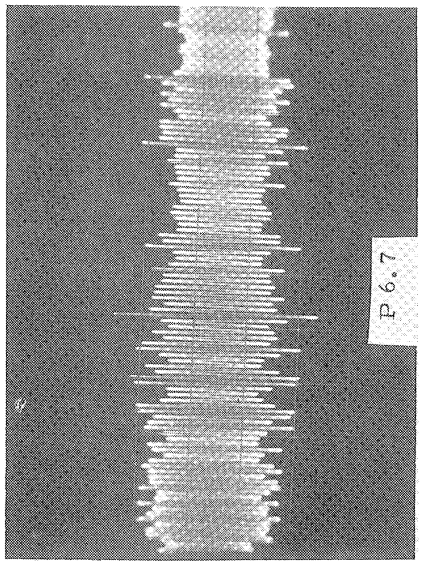

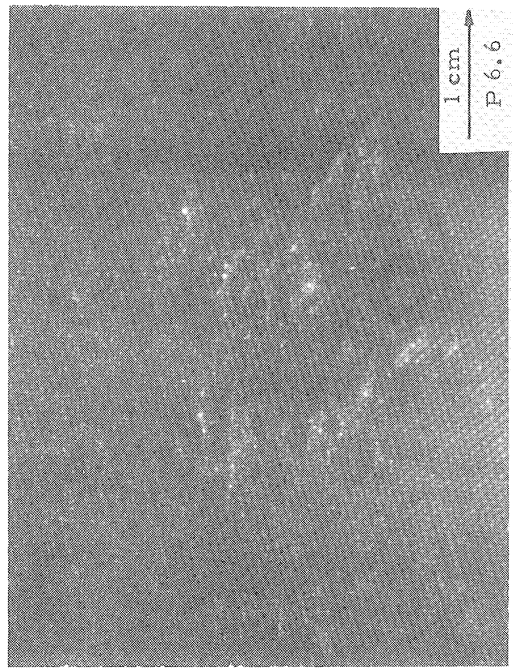

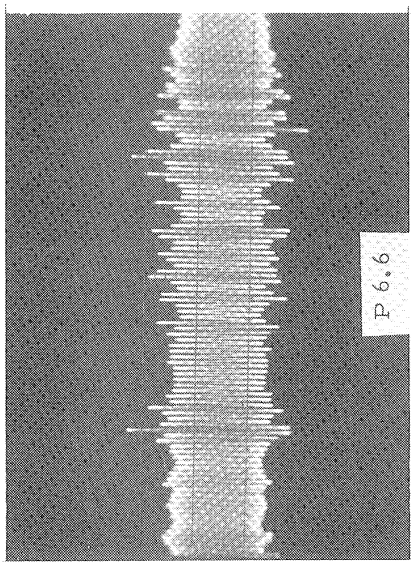

Fig. 4.1 Continued

5396

film flow ($q = 0.01$ $cm^3/cm.sec$), the liquid film on the blade is not continuous but contains "dry spots", i.e., one region is dry, and contiguous regions are covered with a thin liquid film.

To be consistent with existing literature,[M3,M8] this flow pattern is called "rivulet flow". The existence of rivulet flow requires a balance of the various applicable forces at the junction of wet and dry regions. These are due to surface tension, shear, inertia and gravity. Surface tension and shear(viscosity)are strong functions of temperature. Thus for strong heat flux (not present case) temperature dependence of these properties need be considered. The films are never waveless in author's experiments (Plate 1.1). Thus a fully realistic analysis is very difficult.

If the liquid flow rate is further increased, as in plates 1.2 and 1.3 ($q = 0.02$ $cm^3/cm.sec$), the blade surface becomes completely covered with a thin liquid film which remains relatively smooth. Plate 1.3 includes portions of both wavy and relatively smooth films.

Further increasing liquid flow rate, q, one finds more complicated wave patterns of the liquid on the blade. Plate 1.5 ($q = 0.125$ $cm^3/cm.sec$) shows relatively symmetrical wave patterns about a plane parallel to the axis, while plates 1.6 and 1.7 show patterns which are non-symmetrical about this axis. These symmetrical waves will be called "two dimensional waves", and the non-symmetrical waves "three-dimensional waves". The important differences

between these wave forms will be discussed later.

Plates of series #2 of Fig. 4.1 for a somewhat higher steam velocity (U_s = 50 m/s) are quite similar to Series #1 in showing the wavy film pattern transitions. There are, however, a few peculiar features not found in the plate #1 series. In plate #2.1, a more irregularly shaped rivulet forms than that of plate #1.1. Also, at the junction of dry and wet regions, a bulge in film thickness is observed. The bulge geometry is of interest, because of its possible influence on vapor flow patterns near the stagnation point. Hartley and Murgatroyd[H2] assumed the liquid film thickness to decrease smoothly from the up-stream value to zero at the stagnation point. The forces acting on the stagnation point due to changes in vapor flow pattern could then be relatively easily estimated. However, with an abrupt liquid bulge at the stagnation point as in author's case, the vapor flow pattern around the stagnation point becomes more complicated and difficult to estimate. Some[M12,I1] considered this geometry but did not get fully acceptable results. The significance of this particular flow geometry will be discussed in more detail in section C of this chapter.

Plate #2.2 ($q = 0.021$ $cm^3/cm.sec$) shows a relatively unique rivulet formation. There are only two dry spots, one at the center, and the other a little further down-stream near blade axis. In most "rivulet" photos, there are many rivulets along with parallel dry strips. Here also

a film thickness bulge is seen at the stagnation point. Again, there are waves in the liquid film ahead of the stagnation point bulge.

Plates #2.3 (q = 0.043 cm^3/cm) and #2.4 (q = 0.083 cm^3/cm sec) show typical "two-dimensional waves" formed on the blade. In plate #2.3 only relatively faint wave outlines are observed, while those in plate #2.4 are more clearly defined. In both photos, the wave fronts are nearly straight, and most are perpendicular to the flow direction. Since the wave length in plate #2.3 is greater than in plate #2.4, it appears that wave length decreases as liquid flow rate is increased.

As liquid flow rate is further increased, the shape of waves becomes less regular and their cross-sections attain a relatively steep front with long tail (see plates #2.5, q= 0.125 cm^3/cm sec) , #2.6 (q = 0.157) and #2.7 (q = 0.208)). Usually each such three-dimensional wave is preceded by a number of small satellite wavelets. The wave lengths from plate #2.7 are smaller than those from plate #2.6 or 2.5. Also the transverse length of the three-dimensional wave front is reduced, and consequently a more "pebbly" shape appears, as the film flow rate is further increased.

From inspection of the oscilloscope photos, the wave heights can be estimated. In a particular case (plate #2.4) the wave amplitude is ~20% of the average film thickness. It is ~100% of average film thickness in plate #2.7. The amplitude of the "three dimensional" waves is typically as

large as the mean film thickness itself.

Plates #3 are photos of wavy films for a larger steam velocity (U_s = 80 m/s). These show the same transition of wavy films as do the #1 and #2 series. Plates #3.4, 3.5 and 3.6 indicate very typical "three-dimensional" waves, with pebbly wave fronts.

Plates #4 are for steam velocity, U_s = 144 m/s. In plate #4.1 (q = 0.01 cm^3/cm sec), wavy liquid filaments are in good contrast with the adjacent dry strips. Plate #4.2 (q = 0.021 cm^3/cm sec) shows two-dimensional waves, parallel to each other and with wave fronts perpendicular to the flow direction. Further, the wave lengths are relatively uniform. Plate #4.3 (q = 0.043 cm^3/cm sec) shows three-dimensional and two-dimensional waves at the same time with relatively irregular wave lengths; i.e., waves with longer wave lengths are accompained by three or four small satellite waves.

Plate #4.4 (q = 0.083 cm^3/cm sec) also shows three-dimensional waves (with steep fronts) as well as a dry spot at the upper right of the picture. Dry spots in the vicinity of three-dimensional waves are not common. Plate #4.4 is one of a very few pictures obtained showing such dry spots near three-dimensional waves in author's entire experiment. Such a complicated wave shape in front of the stagnation point associated with the dry spot makes the analysis of this particular film breakdown phenomenon difficult.

A different phenomenon can be observed in plate #4.5

($q = 0.125$ cm^3/cm sec), i.e., a white blur apparently above the film appears in the picture. The blurred portion, though somewhat out of focus appears to be a spray of liquid. It can thus be presumed that the crest of the three-dimensional wave has been entrained into the main stream flow. This type of liquid entrainment also is observed in plates #4.6 ($q = 0.167$ cm^3/cm sec) and #4.7 ($q = 0.208$ cm^3/cm sec).

This entrainment mechanism is of considerable interest having application to many mass transfer problems in various chemical and aerospace processes, besides that of steam turbine erosion. If relatively large slugs of liquid, formed on the stator blade, are removed by this entrainment mechanism, the probability of forming large droplets at the trailing edge of the blade may be less than without entrainment beforehand. The largest droplets from the trailing edge of the blade are of order 2 mm[K4]. However droplets entrained from the wave crest are much smaller, and thus have much less erosion potential. Also they are formed further from the next rotating row. Thus they have more time for acceleration to main steam velocity, losing some erosive potential (Fig. 1.6).

Plates #5 are for steam velocity of 227 m/s. Even for very small film flow rates, (plate #5.1, $q = 0.010$ cm^3/cm sec) no rivulet flow regime was observed. Because of the limitations of the instrumentation, liquid flow rates less than $q = 0.010$ cm^3/cm sec were not investigated, but presumably a rivulet regimes would have been found there.

Plates #5.1 and 5.2 (q = 0.02) show two-dimensional waves with relatively small wave lengths. Plate #5.3 shows three-dimensional waves, while all the plates between #5.4 (q = 0.083) and #5.7 (q = 0.208) show the entrainment regimes.

Plate #6 series is for the steam velocity of 305 m/s. Trends concerning wavy film transition are the same as found in the plates #5. Plate #6.1 (q = 0.01 cm^3/cm sec) shows two-dimensional waves. Plates #6.2 (q = 0.021 cm^3 cm sec) and 6.3 (q = 0.043 cm^3/cm sec) show three-dimensional waves, and all the plates between #6.4 (q = 0.083 cm^3/cm-sec) and #6.7 (q = 0.208 cm^3 cm sec) show the entrainment regimes.

The entrainment regime pictures do not show any peculiar differences for the various steam and liquid flow conditions. Rate of entrainment is of considerable interest in light of mass transfer, but no measurements of entrainment rate were possible. Flow conditions and oscillogram scales are listed in Table 4.1.

Based on all the above, a liquid film "Transition Map" (Fig. 4.2) for the experimentally attainable steam and liquid flow conditions was made.[K6] From this map (Fig. 4.2) the wavy film regimes can be identified for given steam and liquid flow conditions. Physical interpretation of the transition zone will be discussed next in as simple a manner as possible, without losing the basic physics.

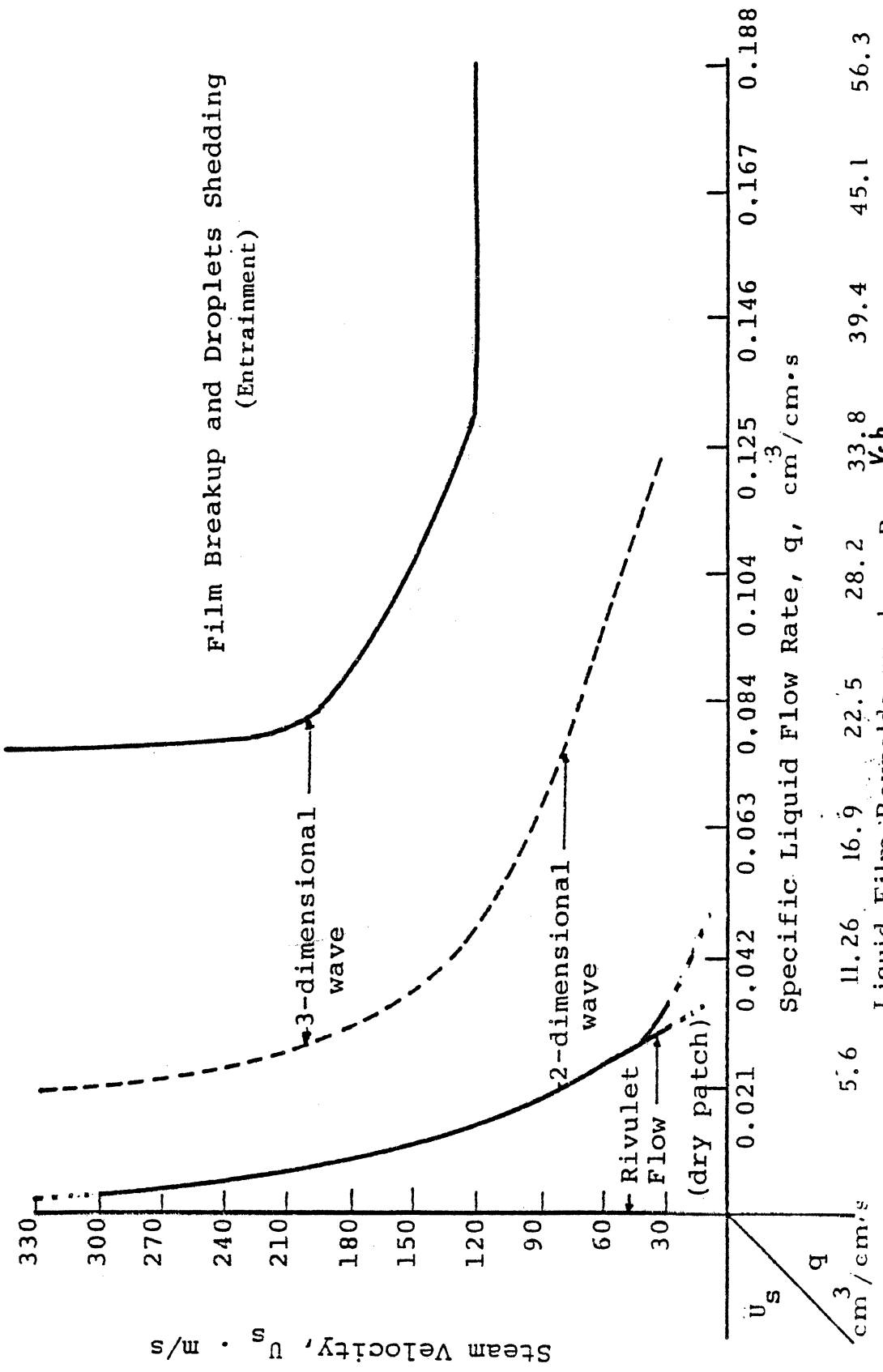

Fig. 4.2.a Transition Map, U_s vs q

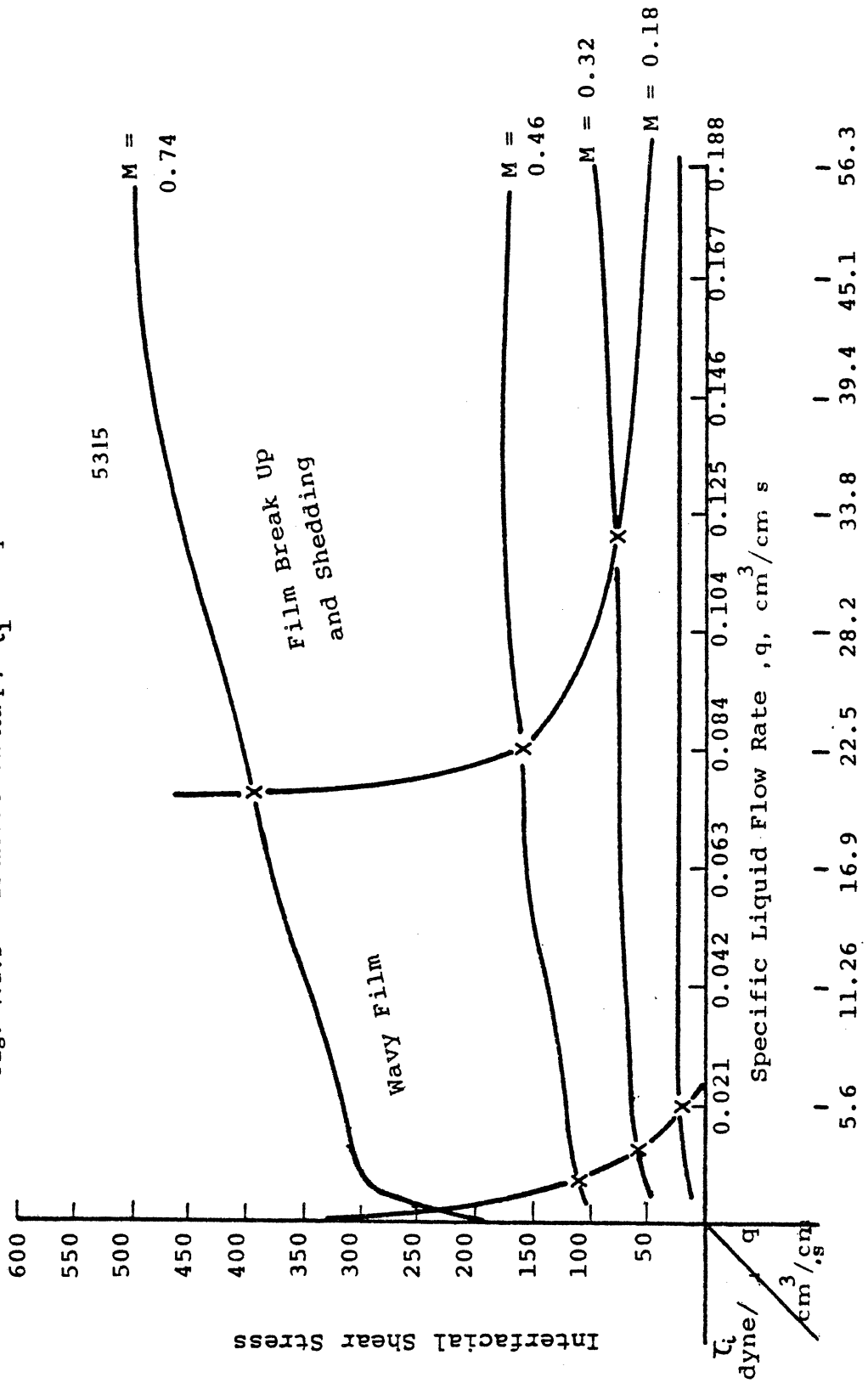

Fig. 4.2.b Transition Map, τ_i vs q

B. MEASUREMENT OF FILM THICKNESS AND ESTIMATE OF INTERFACIAL SHEAR STRESS

Liquid film thickness measurements have been made using electrical conductance microgages previously discussed. The use of a "generalized characteristic curve" to reduce the data is explained in Appendix A. Some initial film thickness measurements were already reported.[H10,H11,K7] Among the most important parameters determining the thin-film flow regime are the film thickness itself, since it is necessary to compute the interfacial shear caused by the high velocity steam flow.

The vapor flow establishes an approximate Couette-type velocity profile in the liquid, i.e. constant shear imposed at the interface. Wavelets are also initiated due to perturbations in the normal and tangential stresses exerted by the vapor. Increased flow resistance (axial pressure drop) is found when waves are present, due to their effect on "roughness". Consequently, the velocity profiles in both phases may be affected according to the different interfacial wave structures.

It is convenient to describe the effect of the interface structure by comparing the drag on the liquid surfaces with that on roughened solid surfaces. Cohen and Hanratty[C9] were perhaps the first to measure the increased drag due to wavy liquid films in terms of an equivalent sand roughness. Utilizing the "universal velocity profile" for the vapor phase,

$$U = \frac{2.303}{K} u^* \log \frac{Y+}{Z} \qquad (4.1)$$

where u* is "friction velocity", $y+ = y\ u^*/\nu$, K = 0.4 is Von Karman's constant. From Nikuradse's measurements[S8] of the friction factor and their own experiments, they concluded the ratio between equivalent sand roughness and root-mean-square wave amplitude of the liquid film (~2 mm of mean thickness) to be ~4.2. Their velocity profiles were also found to be different from those reported for flows over sand-roughened surfaces.

Kordyban[K9] obtained similar results from his experiments for thick liquid films (min. water depth ≅ 30 mm) in an air tunnel (max. air vel. ≅ 6 m/s).

Numerous empirical two-phase pipe flow studies are reported[L5,W7,H13] which generally present the interfacial shear stresses in the form,

$$\tau_i = f_i \frac{\rho_g V_r^2}{2} \tag{4.2}$$

where τ_i is interfacial shear stress, f_i is interfacial friction factor, ρ_g is density of the gas or vapor phase, and V_r is relative velocity between liquid and gas.

For the present study, a simple but physically defensible analysis has been made. The film thickness data from the electrical conductivity gages has been used to compute

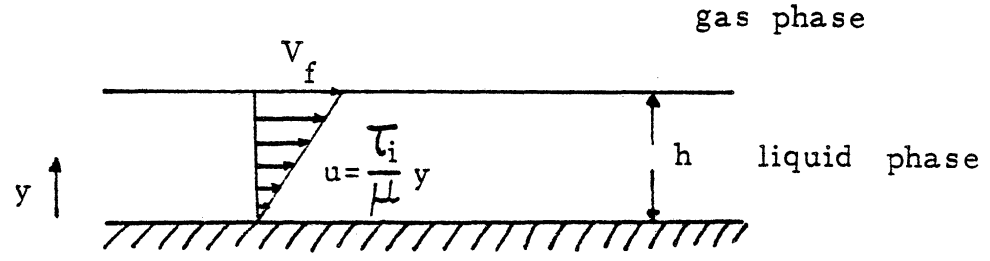

the shear, assuming a classical constant shear, Couette flow i.e., a thin laminar film with smooth and flat vapor-liquid interface, and linear velocity profile. A film Reynolds number, Re_f is defined,

$$Re_f = \frac{V_f h}{\nu_f} \tag{4.3}$$

where V_f is the nominal average film surface velocity, h, film thickness, ν_f kinematic liquid viscosity. The velocity profile can then be expressed as

$$u = \frac{\bar{\tau}_i}{\mu_f} Y \tag{4.4}$$

where $\bar{\tau}_i$ is the effective shear stress, μ_f absolute liquid viscosity. The effective shear stress $\bar{\tau}_i$ is discussed later in detail.

Specific flow rate, q, i.e., volume flow rate per unit blade width, is obtained by integrating the velocity profile

$$q = \int_o^h u \, dy = \bar{\tau}_i h^2 / 2\mu_f$$

$$= V_f h/2 \tag{4.5}$$

so

$$Re_f = \frac{2q}{\nu_f} \tag{4.6}$$

Then from equations (4.5) and (4.6)

$$\frac{(\bar{\tau}_i/\rho_f)^{1/2} h}{\nu_f} = Re_f^{1/2} \tag{4.7}$$

Figure 4.3 shows schematically the flow regime in the test section. The cross-section of the active portion of the steam flow channel consists of three "Lexan" plates, and the liquid film surface on the blade. Flow is from

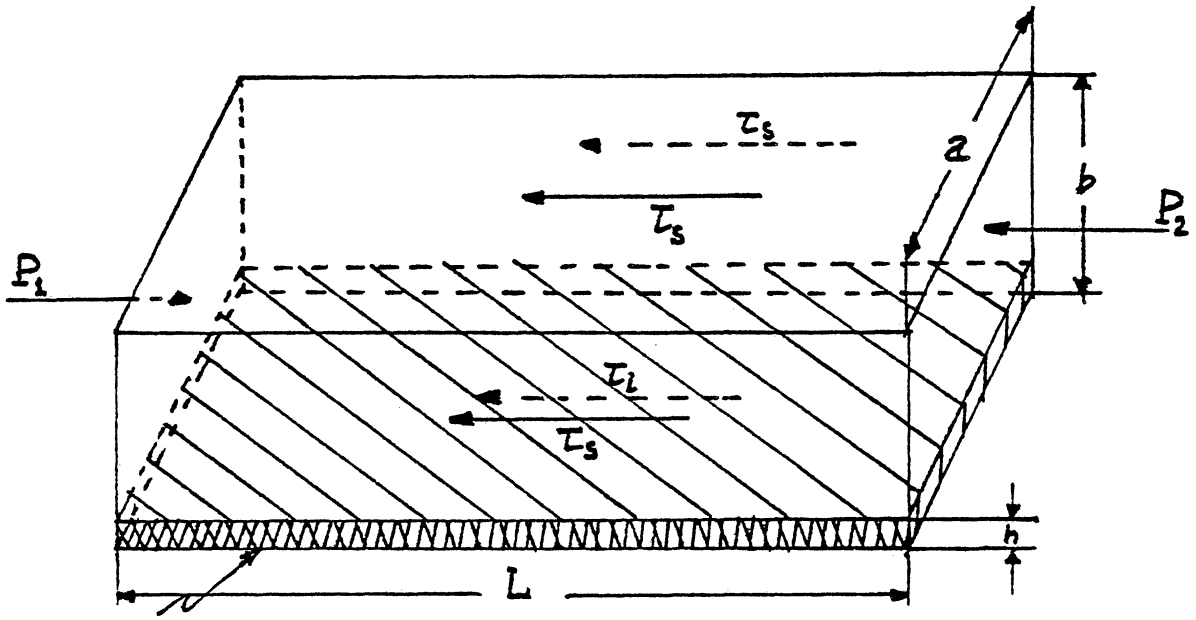

τ_s : shear stress from smooth wall

τ_i : shear stress from wavy film

L : axial length of the section

h : average film thickness

P : pressure

Fig. 4.3: Shear stress schematic of test section with liquid film

left to right. Shear stresses exist with the three (hydraullically smooth) Lexan plates and the liquid film, which has an effective roughness due to surface wavelets in most cases. Applying an axial force balance to this geometry, one obtains the following relation:

$$a\ b\ \Delta p = (a+2b)\ L\ \tau_s + a\ L\ \tau_i \tag{4.8}$$

where a and b are the widths of the Lexan walls, L is the test section axial length considered, i.e., blade length, and ΔP is the axial pressure drop for distance L. τ_s is the shear stress due to the smooth plastic wall, and τ_i that due to the roughened liquid film. Also the pressure drop Δp can be expressed as:

$$\Delta p = f \frac{L}{D_H} \frac{\rho_s U_s^2}{2} \tag{4.9}$$

where f is friction factor, D_H is hydraulic diameter, ρ_s the steam density, and U_s is steam velocity.

If it were assumed that approximately the interfacial shear stress τ_i is the same as the smooth wall shear stress, τ_s, then

$$\tau_i = \tau_s = \tau_o \tag{4.10}$$

Combining Eq. (4.8), (4.9), and (4.10) one obtains

$$\tau_o\ 2\ (a+b)\ L = f \frac{L}{D_H} \frac{\rho_s\ U_s^2}{2} \tag{4.11}$$

Substituting the actual dimensions and conversion factors, Eq. (4.11) becomes:

$$\tau_o = 5.4 \times 10^{-3} \left(f \frac{\rho_s U_s^2}{2}\right) \tag{4.12}$$

where dimension of τ_o is lbf/in^2, ρ_s lbm/ft^3, U_s ft/sec.

To improve the precision of Eq. (4.10) separate friction factors can be considered for the walls and the film. Then, weighting f according to wetted perimeters one obtains:

$$\tau_o = 5.4 \times 10^{-3}\left(\frac{a+2b}{2(a+b)} f_s + \frac{a}{2(a+b)} f_i\right)\frac{\rho_s U_s^2}{2} \tag{4.13}$$

where f_s is the friction factor due to solid walls, and f_i to the film. f_s is a function of steam Reynolds number, Re_s, only but f_i is a function of Re_s, and film equivalent sand roughness, $\frac{\epsilon}{D_H}$; i.e., (4.14)

$$f_i = f_i\left(Re_s, \frac{\epsilon}{D_H}\right) \tag{4.15}$$

Using Eqs. (4.5) and (4.15), one obtains the equivalent sand roughness as a function of film thickness, h; i.e. $\epsilon = \epsilon(h)$. An iteration method was used, involving liquid flow rate q, measured film thickness h, steam velocity U_s, and the density and viscosity of each fluid. First results using this method have been already reported.(K7) Figures 4.4a through 4.4g show the measured film thickness as functions of steam velocity and liquid flow rate, and equivalent sand roughness as a function of average measured film thickness. Interfacial shear stress, τ_i, equivalent sand roughness, $\epsilon(h)$, and friction factor, f_i, as functions of steam velocity and liquid flow rate are listed in Table 4.2.

In Fig. 4.5 the variation of friction factor, f_i, is

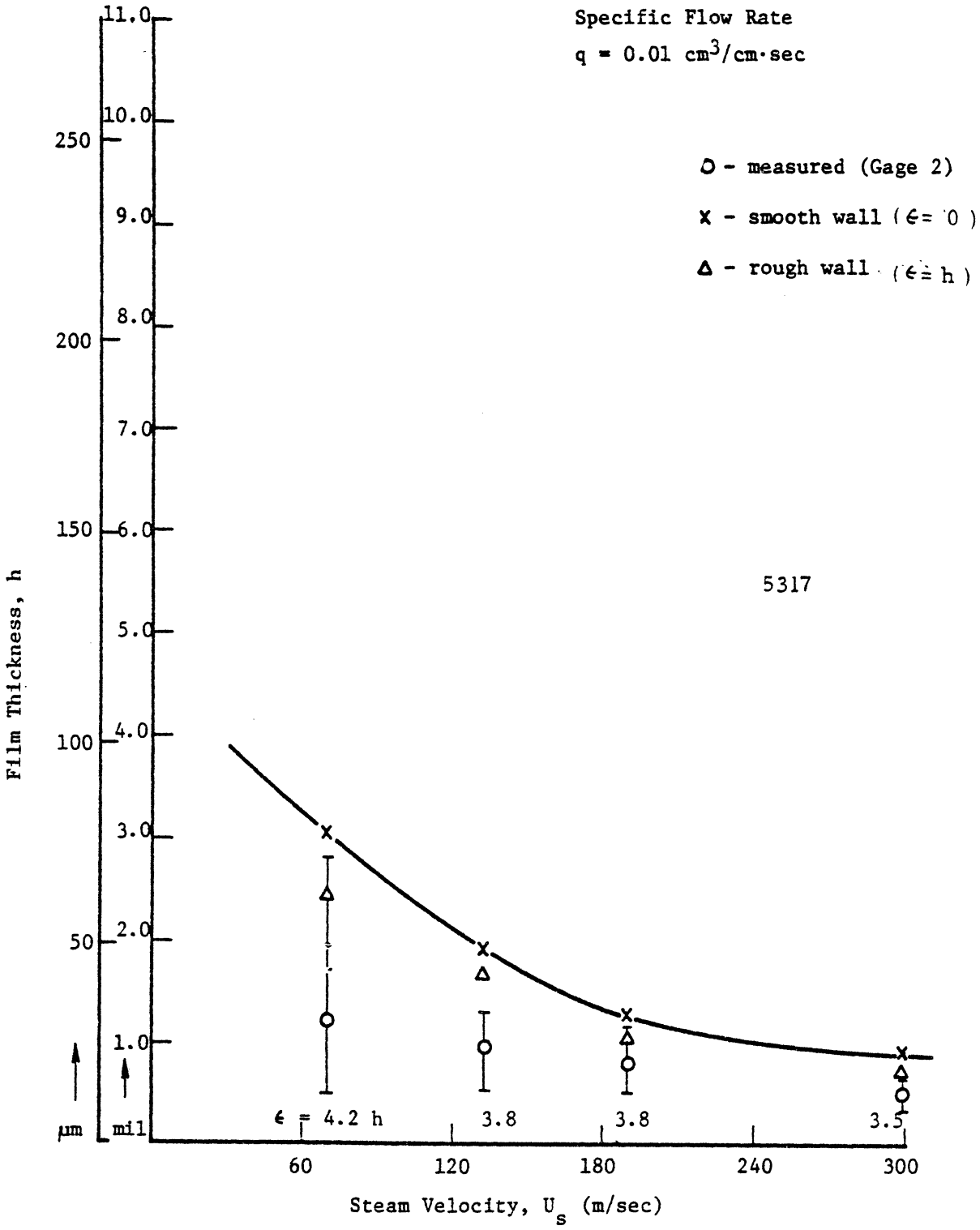

Fig. 4.4.a Flim Thickness vs. Steam Velocity

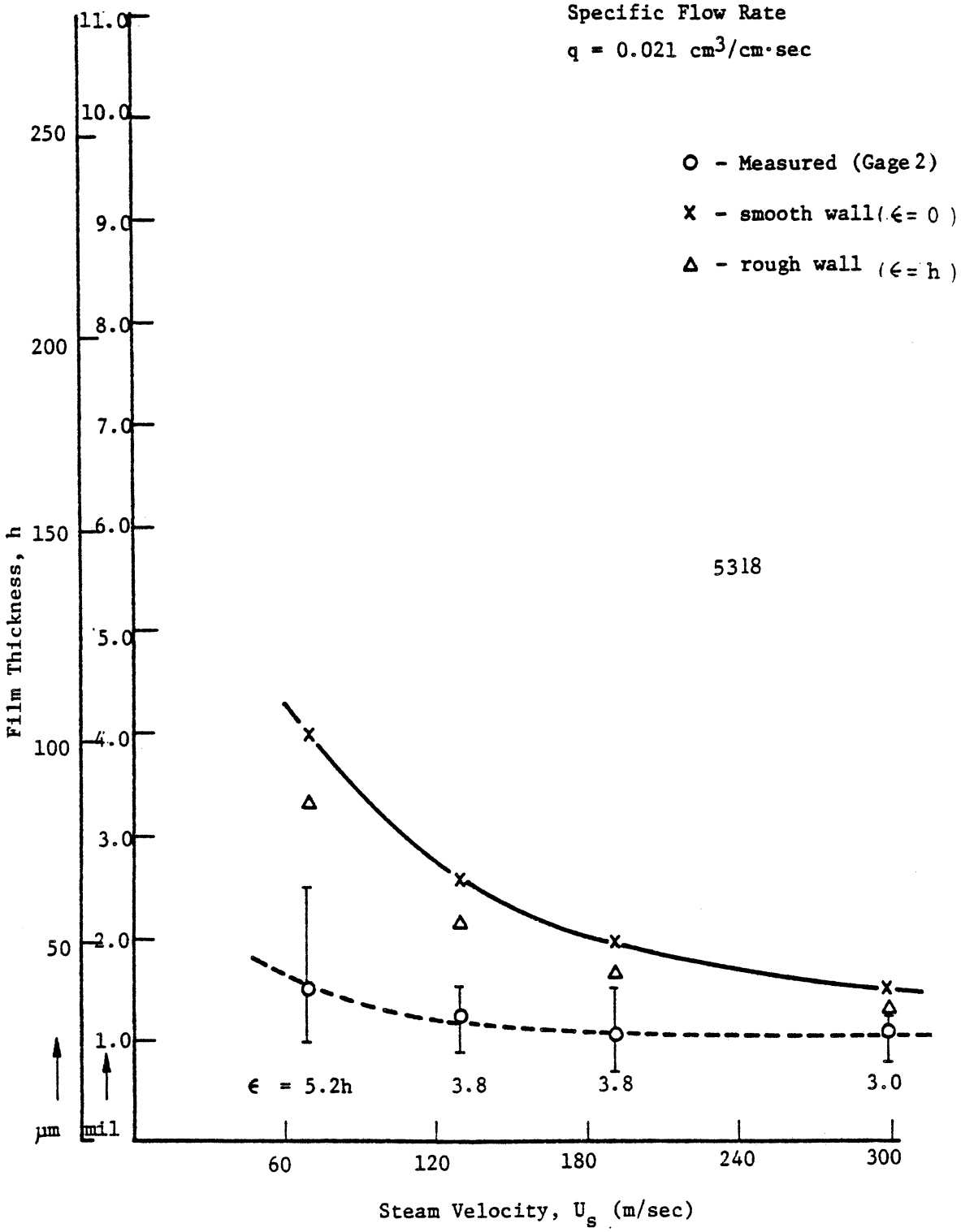

Fig. 4.4.b Film Thickness vs. Steam Velocity

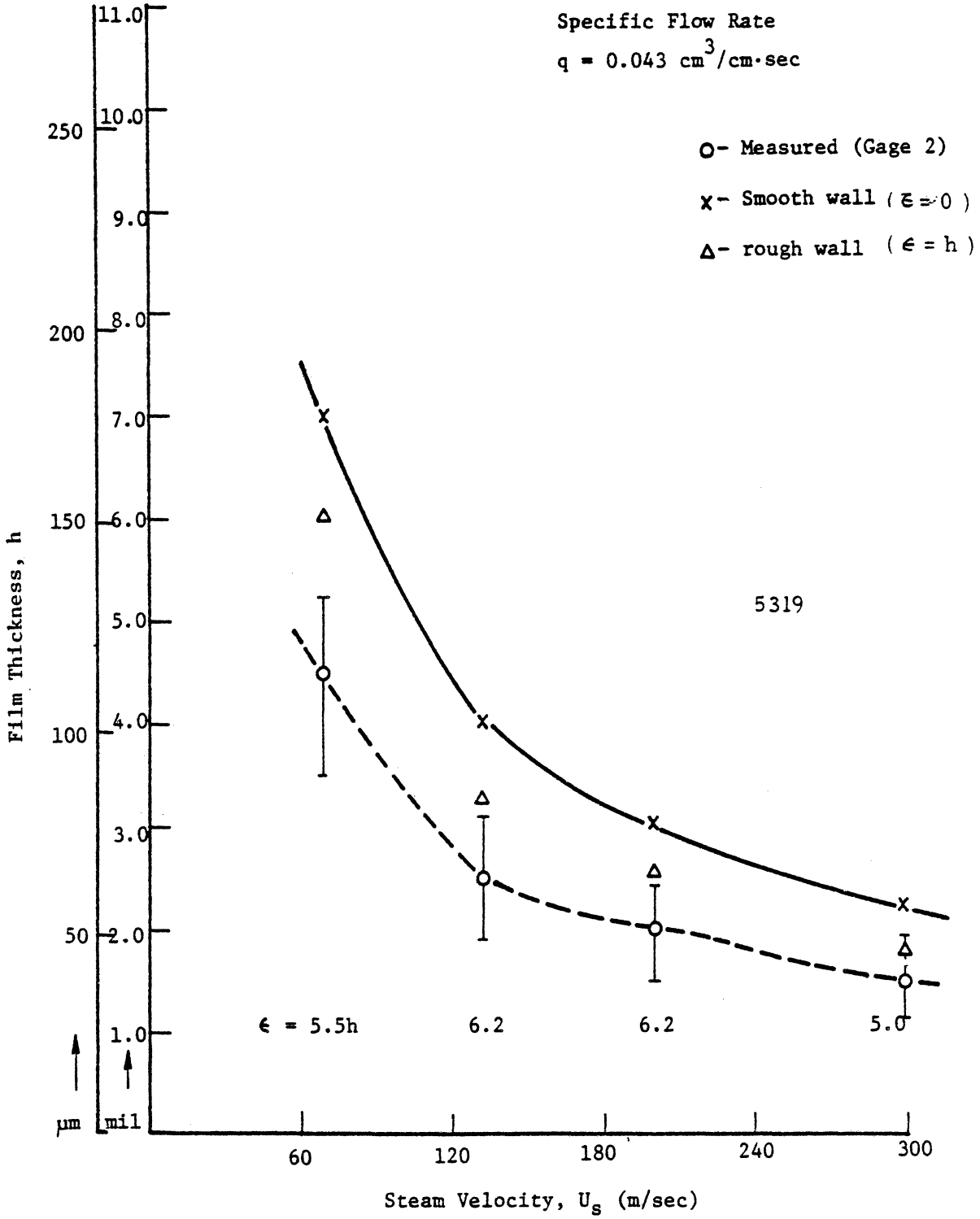

Fig. 4.4.c Film Thickness vs. Steam Velocity

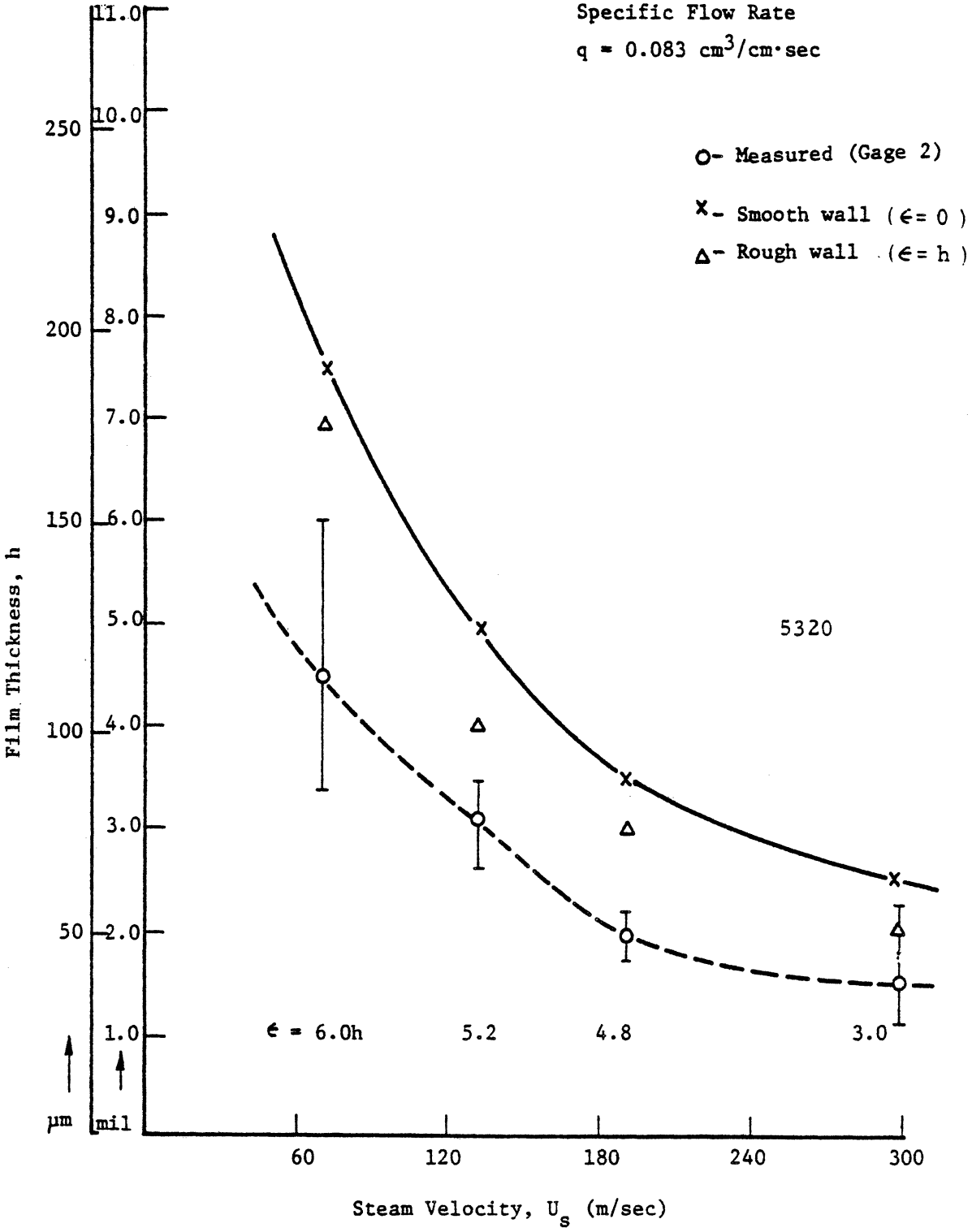

Fig. 4.4.d Film Thickness vs. Steam Velocity

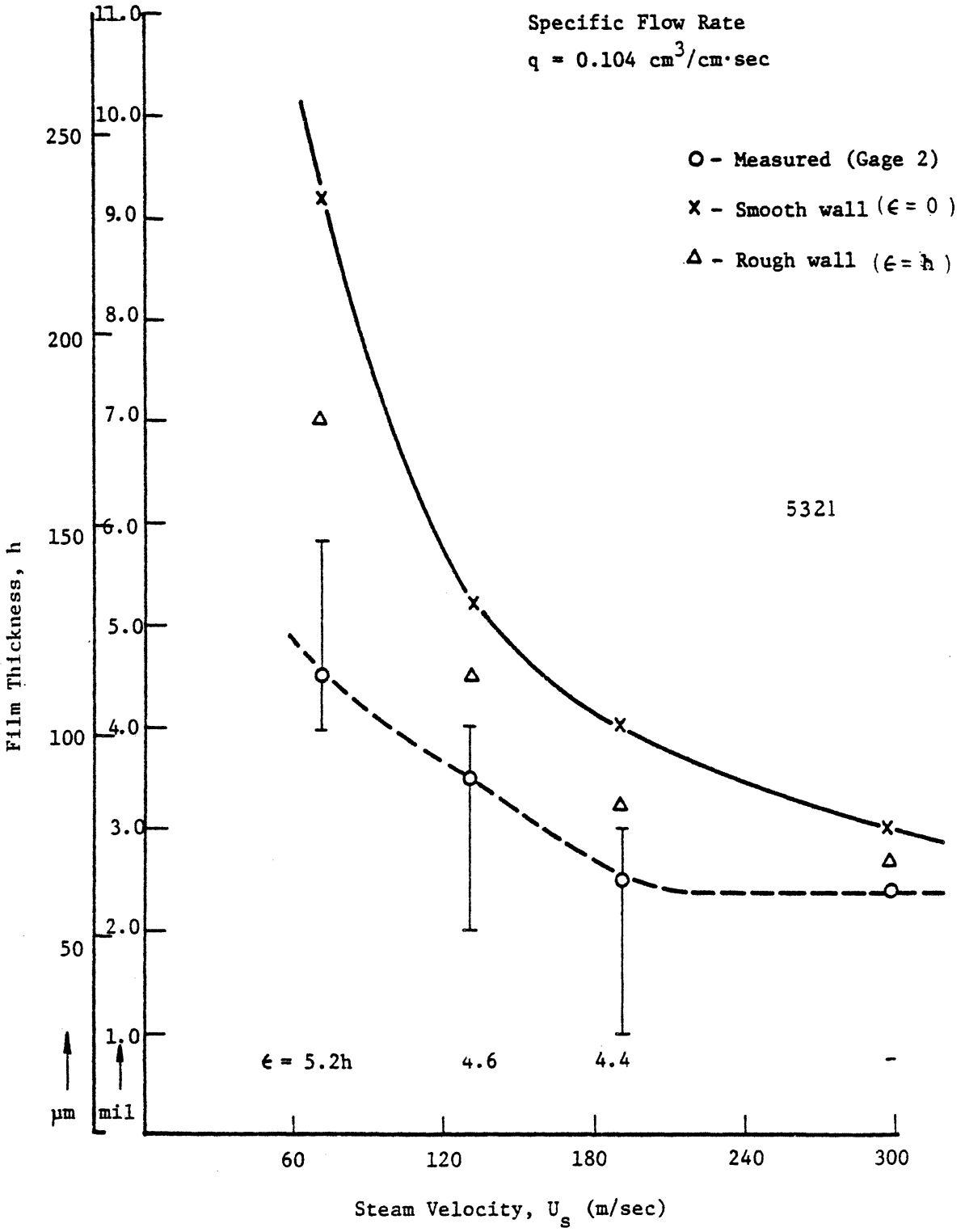

Fig. 4.4.e Thickness vs. Steam Velocity

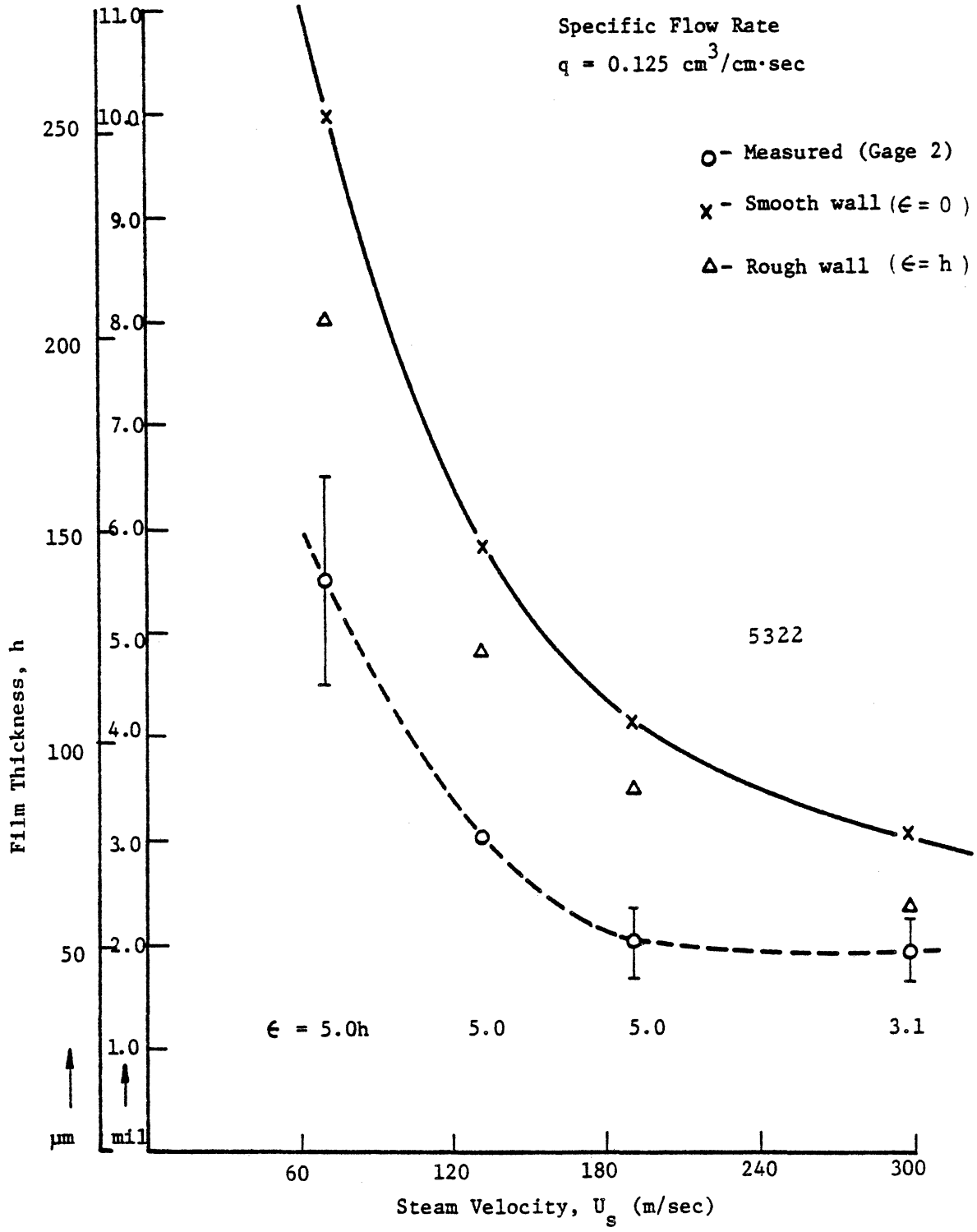

Fig. 4.4.f Film Thickness vs. Steam Velocity

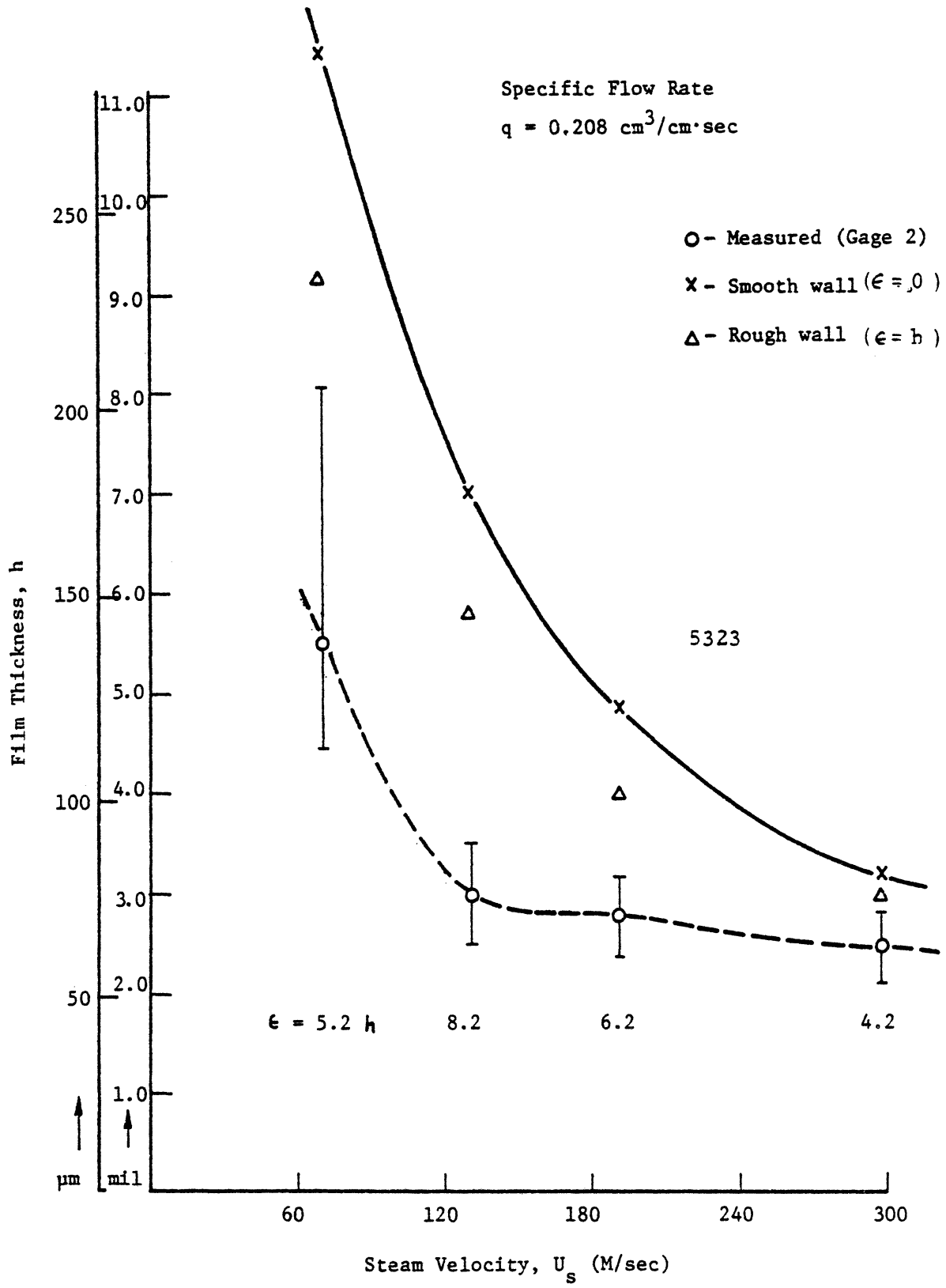

Fig. 4.4.g Film Thickness vs Steam Velocity

Table 4.2: ESTIMATE OF INTERFACIAL FRICTION FACTOR

$$f_i = \frac{\tau_i}{\frac{1}{2}\rho_s V_s^2}$$

ϵ_s : equivalent sand roughness

dyne/cm^2		τ_s = 18.1	τ_s = 47.09	τ_s = 81.87	τ_s = 196.48
V_s (fps)		240 (73.2m/s)	435 (133m/s)	625 (191m/s)	1000 (305m/s)
Q (cc/min)	Re_s	4.2x10^4	7.6x10^4	1.1x10^5	1.75x10^5
q(cm^2/s)	M	0.18	0.32	0.46	0.74
Re_f					
5	f_i	0.006	0.0059	0.0059	0.0059
0.010	ϵ_s	4.2 h	3.8 h	3.5 h	3.5 h
2.8	τ_i	17.68	57.16	118.00	302.08
10	f_i	0.0065	0.0065	0.0062	0.0061
0.021	ϵ_s	5.2 h	3.8 h	3.8 h	3.0 h
5.6	τ_i	19.6	62.97	124.00	312.32
20	f_i	0.0073	0.0075	0.0068	0.0067
0.043	ϵ_s	5.5 h	6.2 h	6.2 h	5.0 h
11.26	τ_i	21.53	72.66	136.00	343.04
30	f_i	0.0076	0.0077	0.0077	0.0077
0.063	ϵ_s	4.5 h	4.5 h	4.0 h	4.0 h
16.9	τ_i	22.41	74.6	154.00	394.24
40	f_i	0.0075	0.0079	0.0078	0.0077
0.083	ϵ_s	5.2 h	4.5 h	4.5 h	4.0 h
22.5	τ_i	22.12	76.53	156.0	394.24
50	f_i	0.0080	0.0080	0.0083	0.0085
0.104	ϵ_s	5.2 h	4.6 h	4.4 h	-
28.2	τ_i	22.12	77.51	166.0	435.20
60	f_i	0.0078	0.0088	0.0090	0.0120
0.125	ϵ_s	5.0 h	5.0 h	5.0 h	3.1 h
33.8	τ_i	23.00	85.26	180.00	614.4
80	f_i	0.0090	0.0090	0.0088	0.0095
0.167	ϵ_s	8.0 h	6.2 h	6.0 h	2.5 h
45.1	τ_i	26.54	87.19	176.00	486.40
100	f_i	0.010	0.012	0.015	0.0098
0.208	ϵ_s	5.2 h	8.2 h	4.2 h	4.2 h
56.3	τ_i	29.49	116.25	300.00	501.76

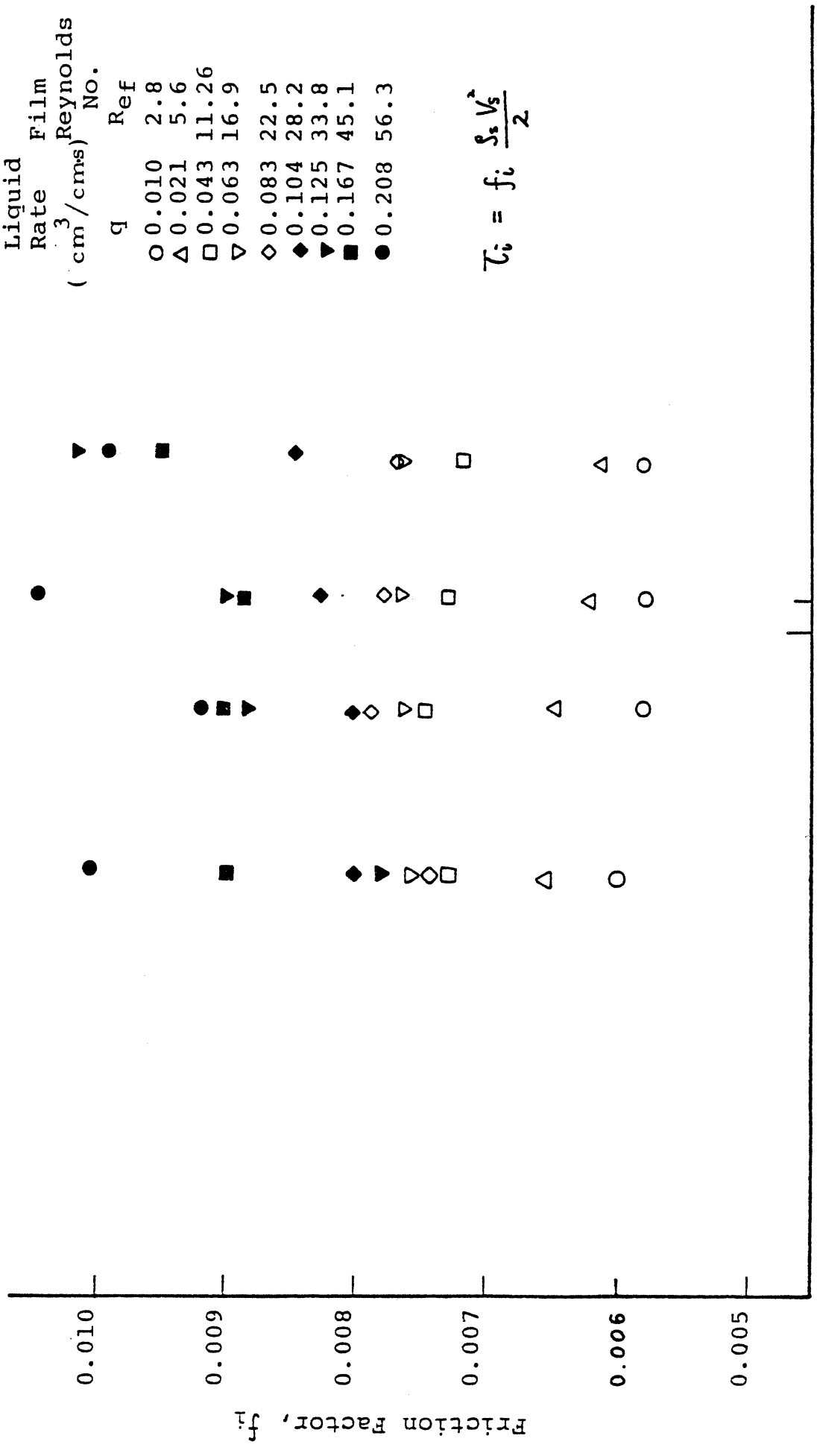

Fig. 4.5 Friction Factor vs. Steam Reynolds Number

shown to be more dependent on the liquid film Reynolds number than on the steam Reynolds number. In general, friction factor increases for an increasing film Reynolds number, Re_f. This is as expected, since film waviness and thus equivalent roughness, increase with Re_f.

For high Re_f, f_i increases for an increase in steam Reynolds number, Re_s, indicating that increased steam turbulence increases waviness, as expected. However, no direct analytical confirmation is available. Author's photographs show large three-dimensional waves and the entrainment of wave crests at these conditions. Both phenomena would likely increase effective friction factor.

In Fig. 4.6 and Table 4.3 ratios of measured to predicted film thickness, based on the smooth wall assumption, are shown. These are always smaller than 1, indicating an effective film roughness for the film, and generally increase with Re_s. The average ratio of the measured film thickness to the predicted film thickness in the author's experimental range is:

$$\frac{h_m}{h_t} \cong 0.55 \qquad (4.16)$$

for $2.8 < Re_f < 56.2$

$4.0 \times 10^4 < Re_s < 1.75 \times 10^5$

There are numerous thickness measurements for high film Reynolds number, ($Re_f > 100$), particularly for pipe flow. These are well summarized in reference (K10). However, for the low film Reynolds number range (author's case), such

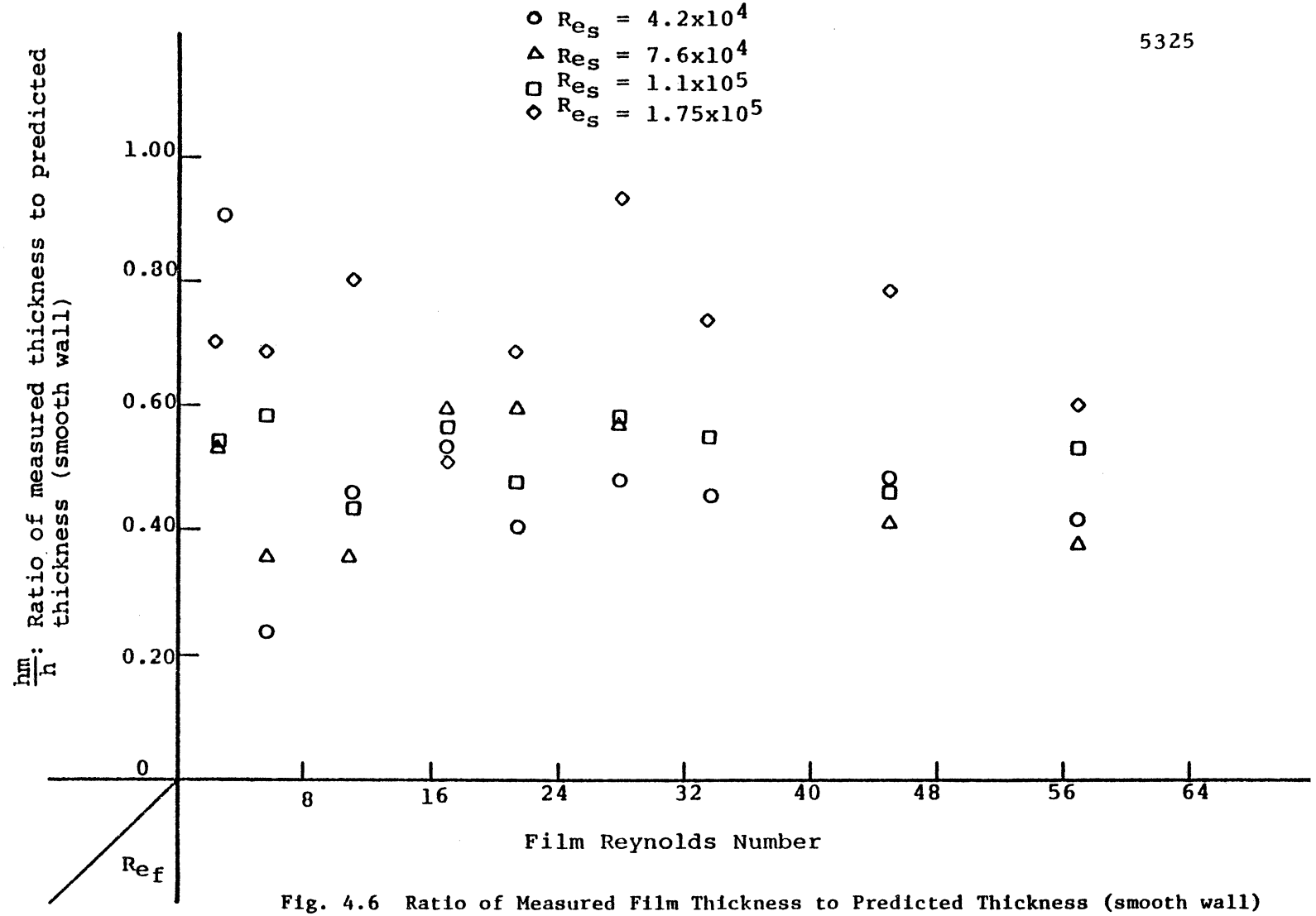

Fig. 4.6 Ratio of Measured Film Thickness to Predicted Thickness (smooth wall)

Table 4.3: COMPARISON OF AVERAGE MEASURED FILM THICKNESS AND PREDICTED FILM THICKNESS (SMOOTH WALL)

h_m : Measured film thickness (mils)

h_t : Predicted film thickness (mils)

h_m/h_t : Ratio of above two thickness

V_s (fps) / Q cc/min / Re_s / q (cm^2/s) / Re_f / M		240 (73.2m/s) 4.2×10^4 0.18	435 (133m/s) 7.6×10^4 0.32	625 (191m/s) 1.1×10^5 0.46	1000 (305m/s) 1.75×10^5 0.74	Average $\frac{h_m}{h_t}$
5	h_m	2.67	0.90	0.67	0.55	
0.010	h_t	2.92	1.69	1.24	0.79	
2.8	h_m/h_t	0.91	0.53	0.54	0.70	0.67
10	h_m	1.00	0.87	1.00	0.75	
0.021	h_t	4.12	2.39	1.74	1.11	
5.6	h_m/h_t	0.24	0.36	0.58	0.68	0.47
20	h_m	2.67	1.22	1.07	1.25	
0.043	h_t	5.82	3.38	2.47	1.57	
11.26	h_m/h_t	0.46	0.36	0.43	0.8	0.51
30	h_m	3.83	2.50	1.73	1.00	
0.063	h_t	7.14	4.14	3.03	1.93	
16.9	h_m/h_t	0.54	0.6	0.57	0.52	0.56
40	h_m	3.40	2.88	1.63	1.52	
0.083	h_t	8.24	4.78	3.49	2.23	
22.5	h_m/h_t	0.41	0.60	0.47	0.68	0.54
50	h_m	4.45	3.03	2.27	2.35	
0.104	h_t	9.21	5.35	3.90	2.49	
28.2	h_m/h_t	0.48	0.57	0.58	0.94	0.64
60	h_m	4.65	-	2.37	2.00	
0.125	h_t	10.10	5.86	4.28	2.73	
33.8	h_m/h_t	0.46	-	0.55	0.73	0.58
80	h_m	5.57	2.85	2.25	2.45	
0.167	h_t	11.65	6.76	4.94	3.15	
45.1	h_m/h_t	0.48	0.42	0.46	0.78	0.54
100	h_m	5.43	2.88	3.00	2.10	
0.208	h_t	13.03	7.56	5.52	3.52	
56.3	h_m/h_t	0.42	0.38	0.54	0.60	0.49
Avg	h_m/h_t	0.49	0.48	0.52	0.71	0.55

thickness measurements hardly exist, even for the pipe flow case. In Fig. 4.7 a non-dimensional film thickness, $h^+ = \frac{h\left(\frac{\tau_i}{\rho_f}\right)^{1/2}}{\nu_f}$ is plotted as a function of Re_f. The form of h^+, generally accepted in most thickness measurement literature, is based on the previously estimated shear stress, τ_i. The only available data, in this low Re_f range, is from the measurements of Charvonia[C12] and Collier-Hewitt.[C13] They both studied air-water flow in a vertical pipe. This data is graphed using solid symbols, while the author's data is plotted with open symbols. The first solid line represents the ideal case, with the shear stress of Eq. (4.7) found assuming a smooth wall.

The second solid line is the empirical correlation of Hughmark,[H16] based on data obtained by others for upward flow in vertical pipes. The shear stress used in the friction velocity term for the dimensionless film thickness was not clearly specified. It appears that he used wall (rather than liquid film) shear stress.

The author's data can be correlated by the following expression, using the previously estimated interfacial shear stress,

$$h^+ = 0.6\ Re_f^{1/2} \qquad (4.17)$$

This curve is the best-fitting curve for all the data points in author's entire experimental range. Comparing with the Charvonia and Collier-Hewitt data, one finds that their non-dimensional film thicknesses are always higher than the author's data for the same Re_f.

Fig. 4.7 Film Thickness Factor as a Function of Film Reynolds Number (Comparison with Hughmark Correlation, 1973) (H6)

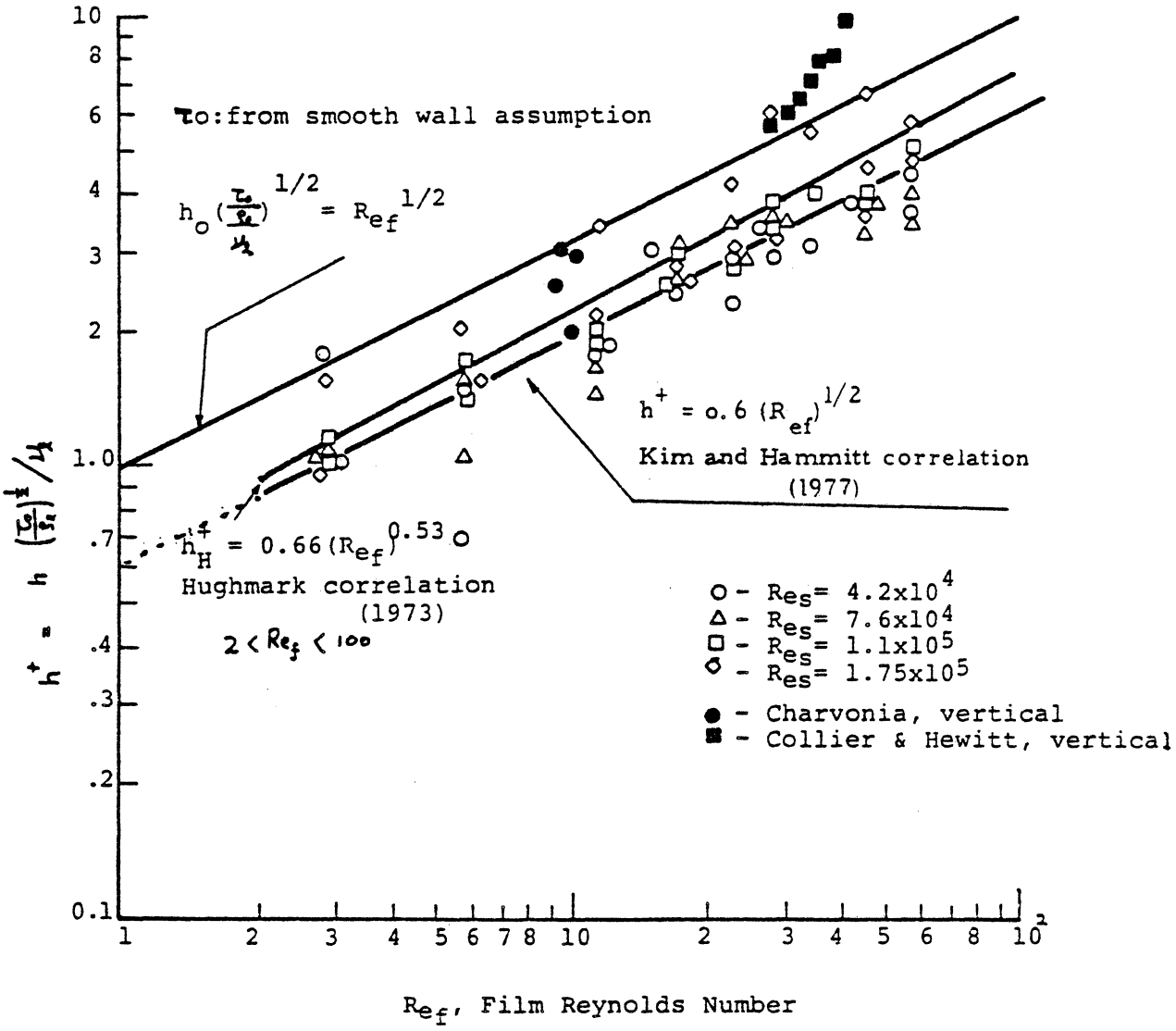

These deviations can be explained in that their data is for a relatively thicker film and lower gas velocity, while the author's data is for very thin films with very high steam velocity, sometimes accompanying the entrainment of liquid film.

In Fig. 4.8 author's data is plotted in terms of the Henstock-Hanratty[H7] parameter

$$F = \frac{\gamma \, Re_f}{Re_s^{0.9}} \frac{\nu_f}{\nu_s} \left(\frac{\rho_f}{\rho_s}\right)^{1/2} \tag{4.18}$$

which is a Martinelli-type flow parameter.[H7] Here.

$$\gamma = [(0.707 \, Re_f^{0.5})^{2.5} + (0.379 \, Re_s^{0.9})^{2.5}]^{0.4} \tag{4.19}$$

Their correlation

$$\frac{h}{D_H} = \frac{6.95 \, F}{(1+850 \, F)^{1/2}} \tag{4.19}$$

was only tentatively suggested due to the lack of sufficient data. This correlation over-estimates the author's data.

C. RIVULET FLOW REGIME

As already discussed, a thin liquid film flowing over a solid surface under an applied shear stress due to a high speed steam or gas velocity, may separate into a number of filaments (Figs. 4.1 and 4.2). Such rivulets may then occur on turbine stator blade surfaces. In such cases, the spectrum of detached droplets impinging on the next rotating row depends on the rivulet characteristics. This type of film break-up is also related to boiling "dry-spots" in

Fig. 4.8 Nondimensional Film Thickness as a Function of F
(Comparison with Henstock and Hanratty Prediction, 1976)

$$\frac{h}{D_H} = \frac{6.59F}{(1+850F)^{1/2}}$$

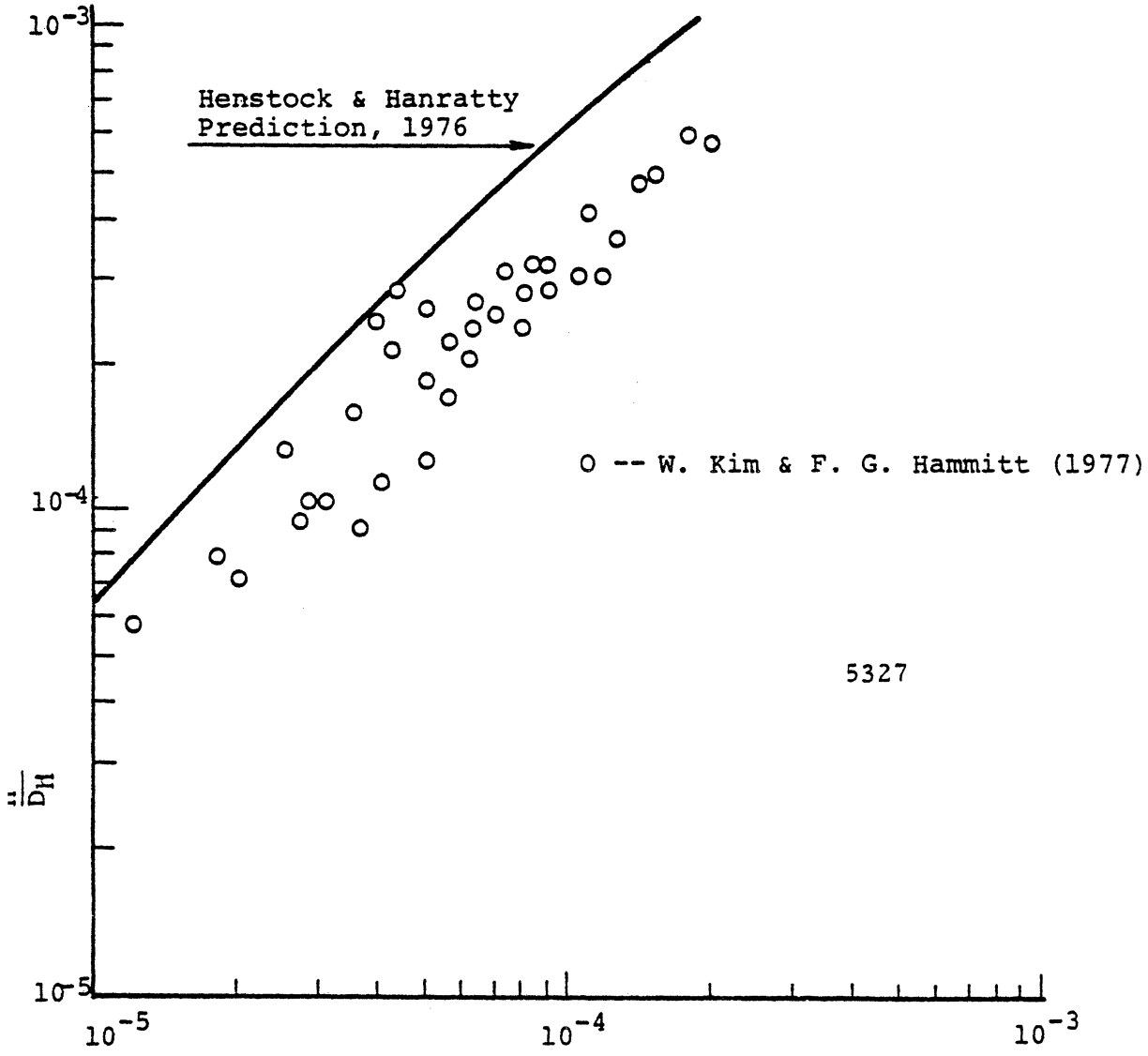

$$F = \frac{\gamma(R_{ef})}{R_{es}^{0.9}} \frac{\nu_f}{\nu_s} \sqrt{\frac{\rho_f}{\rho_s}}$$

$$\gamma = [(0.707\ R_{ef}^{0.5})^{2.5} + (0.0379\ R_{ef}^{0.9})^{2.5}]^{0.4}$$

emergency cooling of nuclear powerplants, as well as to various chemical engineering applications. Because of applications to numerous important engineering problems, several models describing such dry-patch or filament stability have been suggested[H2,H3,B2,M3]. These analyses are generally based on force or power balances at the junction between rivulets or dry patches and the continous film. Since the surface tension plays an important role along with the dynamic pressures of liquid and vapor flow at the stagnation junction, the relations for critical (or minimum) flow conditions for rivulet stability should include the contact (or "wetting") angle, θ, between liquid and solid. Unfortunately, θ depends heavily upon other parameters such as surface condition.

Experimental studies on the formation of rivulet flow were also conducted by Hewitt and Lacey[H4] for air-water flow in a vertical pipe. Even though their experimental geometry and flow conditions are quite different and thus cannot be directly compared with the author's experimental results, some pertinent points should be made. The upward air velocity used in the Hewitt-Lacey work ranged from 18 to 95 m/s, while the downward flow critical liquid film thickness from 30 to 210 μm. This thickness was not directly measured, but estimated using the Hartley-Robert's model[H14]. The film breakdown was studied by artificially producing a dry patch using an air jet directed perpendicularly toward the tube wall. It would no doubt have been more

realistic had they produced the rivulet or dry patches without using such an air jet.

They concluded that for the higher gas flow regime, minimum wetting rate (which Hartley and Murgatroyd[H2] used to express the minimum liquid flow rate required to re-wet the surface after the formation of a dry patch) decreases with an increase in the gas flow rate. At lower gas flow rates, however, the minimum wetting rate passes through a maximum, and then begins to decrease with a decreasing gas flow rate. They ascribed these results to a flow regime change between the climbing film regime and "churn flow", which occurs at higher gas flows in this vertical annular pipe flow. Such a maximum critical wetting rate was not found by present author.

They also observed that at liquid flow rates above the minimum wetting rate, the patch was more or less circular. Rewetting of the surface occurred in a complex manner, usually by splitting of the dry patch by filaments, followed by the disappearance of the ends and sides of the resultant secondary patches. This kind of rewetting process, Fig. 4.9, also was observed on a laboratory turbine blade.[F2]

For cases with strong wall heat flux, additional effects need to be considered. Examples are the thermocapillary effect[Z1] due to the temperature dependent surface tension and vapor-thrust effect[N1,Z1,O1] caused by surface evaporation. These models show that such thermal effects become dominant for the strong wall heat flux cases in determining

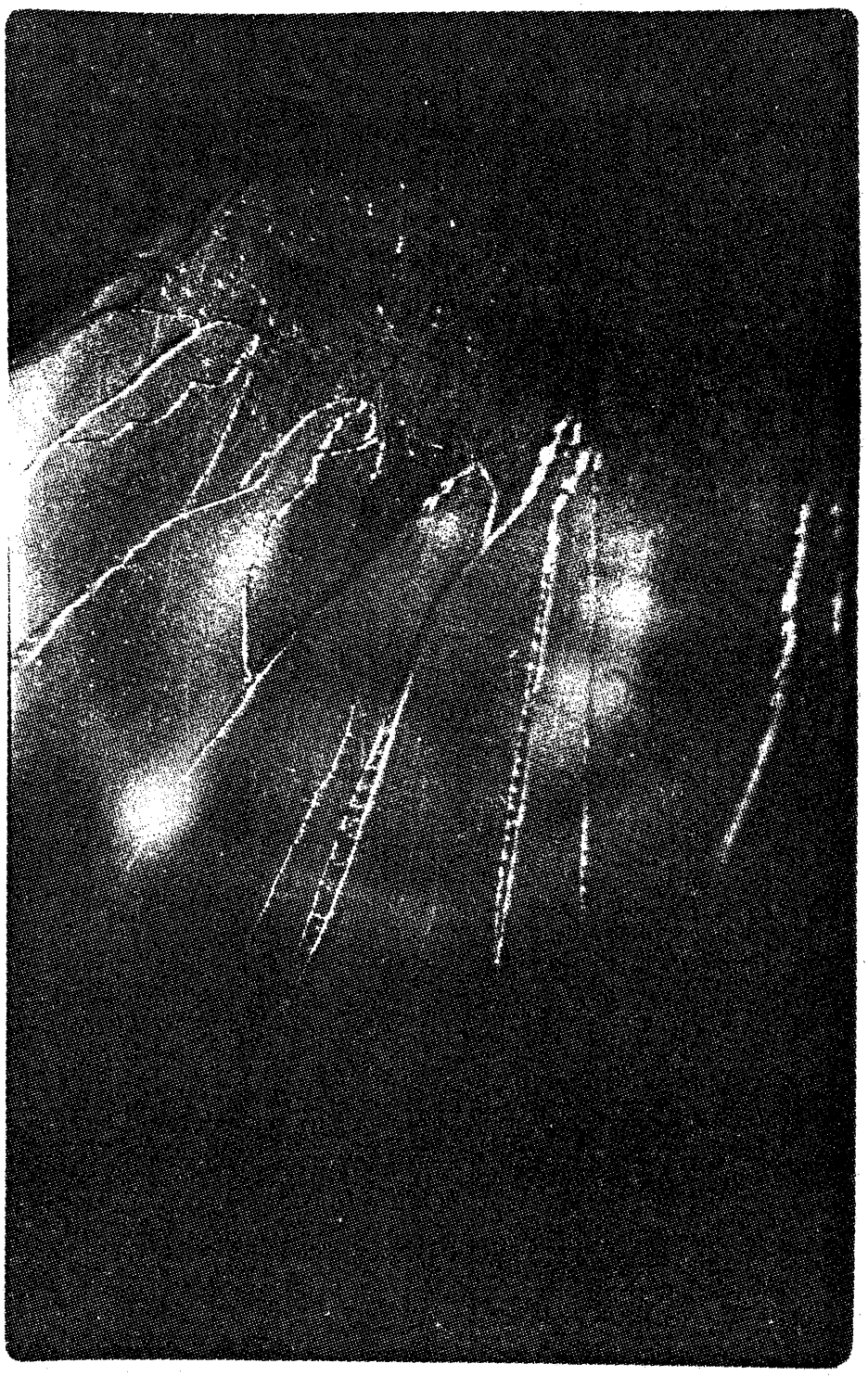

5397

Fig. 4.9 Rivulet Formation on Experimental Turbine Blade
= 5000 rpm, d= 380 mm, M_{steam}=0.7, p=0.6 bar

(supplied by Visiting Scientist , Dr. O. Povarov,
Moscow Power Institute)

the stability of dry patches. These thermally dominated situations are most directly applicable to the nuclear power plant "loss of coolant accident" (LOCA), while the isothermal considerations of stability of dry patches are directly pertinent to the steam turbine problem here emphasized.

No new analytical model was developed by author since many models already exist. The need for better experimental data seemed more pressing. However, some modifications of existing models are suggested in the following discussions considering author's experimental results.

Hartley and Murgatroyd (H-M model)[H2] present the first relatively comprehensive theory for the stability of dry patches. Mikielewicz and Moszynski (M-M model)[M3] involves a more complete analysis, which can more usefully be compared to author's experimental criteria.

H-M Model[H2]

Hartley and Murgatroyd suggested two models for the stability of dry patches. The first model was based on the balance of forces at the liquid flow stagnation point between dry and wetted regions (points G in Fig. 4.10a).

If the dry patch is stable, the surface tension forces must balance the fluid pressures over the stagnation line $G_s G_p$ in Fig. 4.10a . Surface tension and pressure terms can be expressed respectively as,

$$F_\sigma = dX \cdot \sigma \cdot (1-\cos\theta)$$

$$F_p = dX \int_0^{\delta_{AB}} \rho_f [W(y)]^2/2 \, dy$$

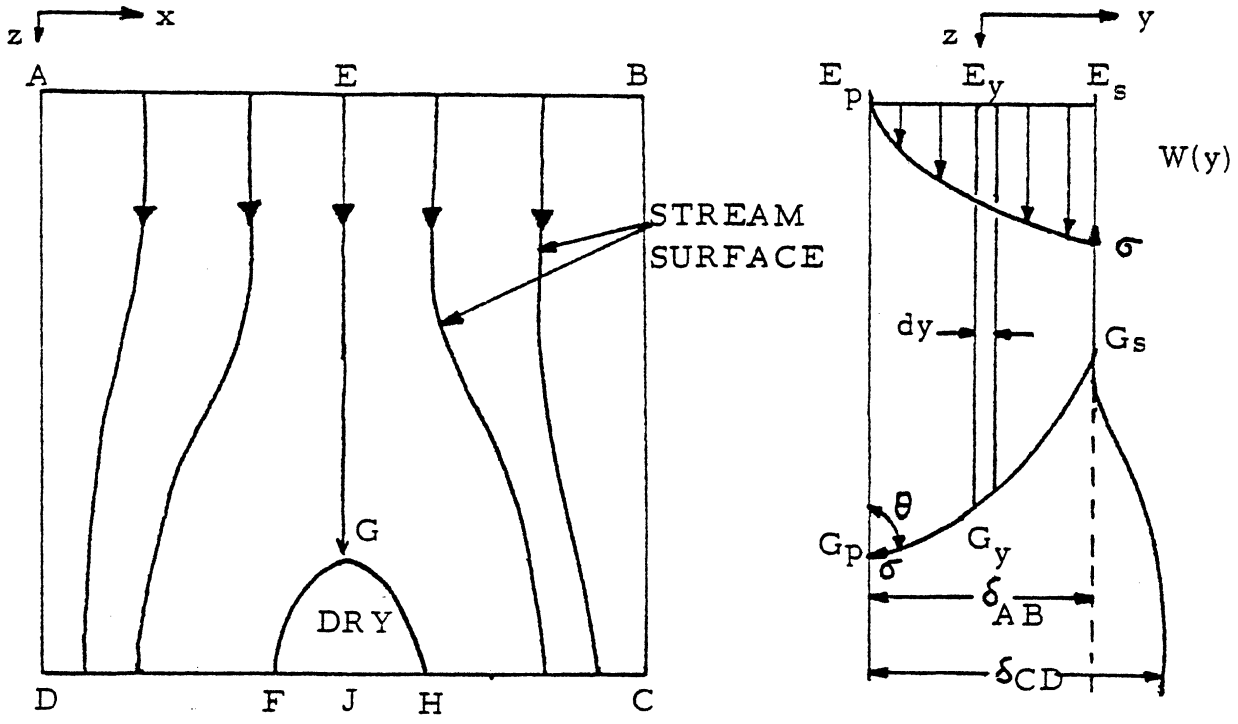

$$F_p = dx \int_0^{\delta_{AB}} \rho_f \left[W(y)\right]^2/2 \, dy$$

$$F_\sigma = dx \cdot \sigma \cdot (1 - \cos\theta)$$

By $F_p = F_\sigma$

$$h_c = 1.82 \left[\sigma(1 - \cos\theta)/\rho_f\right]^{1/3} (\mu_f/\tau_i)^{2/3}$$

$$q_c = 3.3 (\rho_f \mu_f/\tau_i)^{1/3} \left[\sigma (1 - \cos\theta)\right]^{2/3}$$

θ should be $4 \sim 8^\circ$ in comparison with our data

Fig 4.10.a : RIVULET FLOW MODEL
HARTLEY and MURGATROYD (1964)

1. FORCE BALANCE MODEL

where θ is the contact angle between the liquid and solid

σ liquid surface tension, dX the unit length in X direction, W(y) the velocity profile, δ_{AB} the fluid thickness before the stagnation point.

Assuming a linear velocity profile and $F_\sigma = F_p$ for neutral equilibrium, the minimum (or critical) film thickness and flow rate become,

$$h_c = 1.82\ [\sigma (1-\cos\theta)/\rho_f]^{1/3}\ (\mu_f/\tau_i)^{2/3} \qquad (4.20)$$

$$q_c = 3.3\ [\sigma (1-\cos\theta)]^{2/3}\ (\rho_f\ \mu_f/\tau_i)^{1/3} \qquad (4.21)$$

where h_c is the critical film thickness and q_c the critical flow rate, μ_f the liquid viscosity, τ_i the interfacial shear, and ρ_f the liquid density.

A comparison between author's experimental criterion observed from the "map", Fig. 4.2 , and Eq. (4.21) discloses that the contact angle, θ, would need to be between $4 \sim 8°$ (see Table 4.4). However, the static contact angle of a water drop on stainless steel is known to be about 50° (see Fig. 4.11 and Ref. H4) at room temperature and atmospheric pressure. Thus the values required by the H-M model are not realistic. Of course, the contact angle is dependent on many parameters such as temperature and surface conditions (wet or dry, cleanliness, roughness, time of exposure*, etc). A possible source of this apparent discrepancy is the geometric consideration of the stagnation point in their model. (See point G of Fig. 4.10a).

*Shown by author's work measuring changes in θ as droplet size decreased due to evaporation (Fig. 4.11).

Table 4.4 CRITERIA OF RIVULET FORMATION

COMPARISON WITH MIKIELEWICZ-MOSZYNSKI (M-M) AND HARTLEY-MURGATROYD (H-M) THEORIES

U_s (m/s)	73.2	133	191	305
Q (cm^3/min)	10	7.5	2.5	2.5
Re_f	5.6	4.2	1.4	1.4
τ_o ($dyne/cm^2$)	22	60	110	280
h [$\times 10^3$ cm	8.13	4.57	2.69	1.78
h [mils	3.2	1.8	1.06	0.70
h^+	0.0060	0.0058	0.0060	0.0070
θ (M-M) -deg	10	9.5	10	11
θ (H-M) -deg	8.4	5.5	4.7	3.8

$\rho_f = 1\ gm/cm^3$

$\mu = 7.4 \times 10^{-3}$ dyne sec/cm^2

$\sigma = 72.8$ dyne/cm

$h^+ = \rho_f \tau_o^2 h^3 / 6 \mu^2 \sigma$

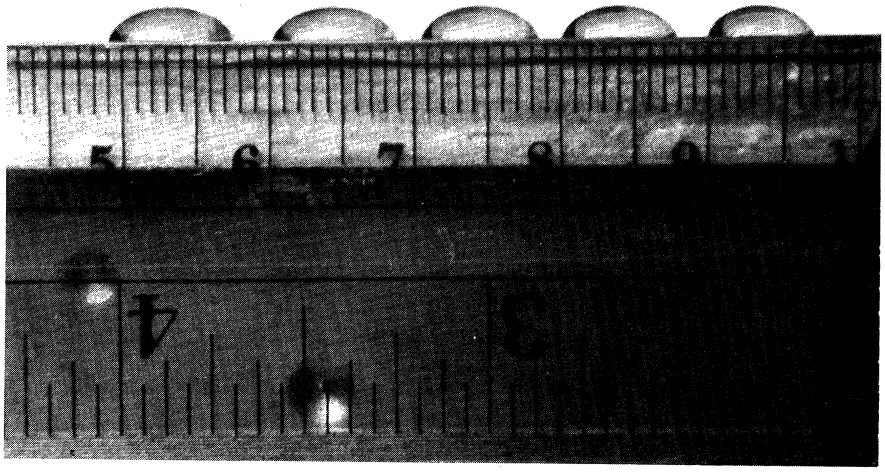

5398

Fig. 4.11 Photograph of Contact Angle Between Water Droplets and Stainless Steel Plate at Room Temperature.

(taken by H. Hamed and W. Kim, 1977)

In the H-M model (Fig. 4.10a), the stagnation line $G_s G_p$ is assumed to decrease smoothly from the upstream thickness δ_{AB}. However, author's rivulet pictures (plates #2.1,2.2 and 3.2 of Fig. 4.1) show an abrupt bulge in the liquid at the stagnation point ahead of a dry patch. There is no doubt that the bulge geometry may change the force balance considerably.

Another factor, which complicates an adequate modeling, is the existence of waves in the upstream liquid film. Such waves always exist in the author's rivulet pictures. They suggest that a modification of the H-M force balance model to include their effect is necessary.

The other H-M model, called "minimum power model", is based on the assumption that the film will attain a condition such that the sum of surface and kinetic energy across a rivulet cross-section will be a minimum.

For such a stable rivulet (Fig. 4.10b), the kinetic energy flux E_k is

$$E_k = X \int_0^{\delta_{PQ}} \frac{\rho_f [W(y)]^3}{2} \, dy$$

where $W(y)$ is the velocity at element $P_y Q_y$. Also surface energy flux E_σ is

$$E_\sigma \cong X \cdot \sigma \cdot W(\delta_{PQ}).$$

Then the total energy flux, E_T is

$$E_T = E_k + E_\sigma$$

The minimum for E_T is obtained by setting

$$\partial E_T / \partial \delta = 0$$

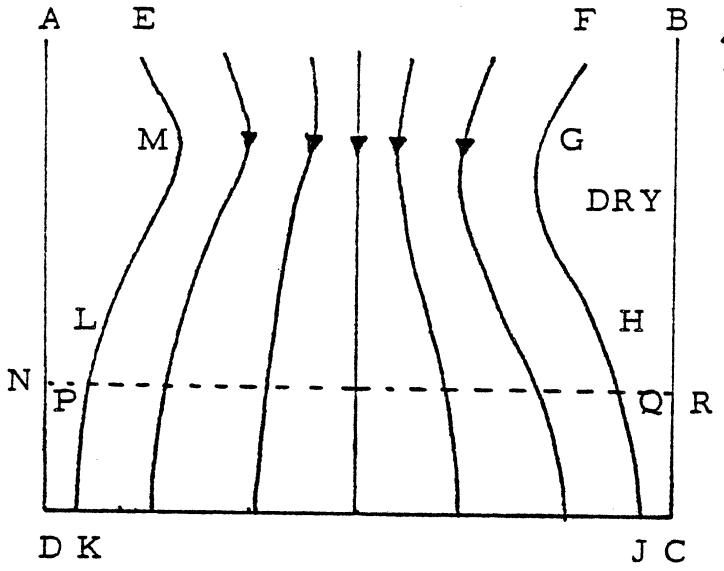

$$E_K = x \int_0^{\delta_{PQ}} \frac{\rho}{2} \left[W(y) \right]^3 dy$$

$$E_\sigma = x \cdot \sigma \cdot W(\delta_{PQ})$$

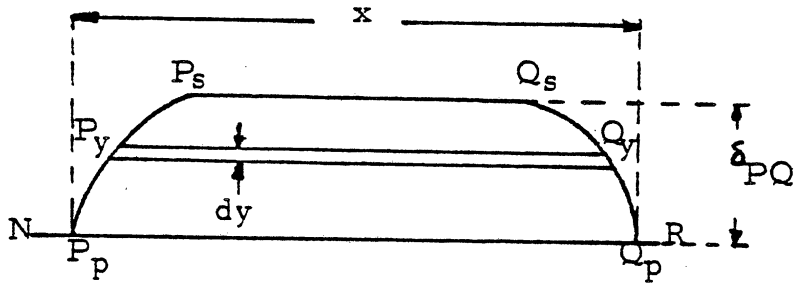

$$E_T = E_p + E_\sigma$$

By $\partial E_T / \partial \delta = 0$

$$h_c = 1.59 \, (\sigma / \rho_f)^{1/3} \, (\mu_f / \tau_i)^{2/3}$$

$$q_c = 2.52 \, (\rho_f \mu_f / \tau_i)^{1/3} \, \sigma^{2/3}$$

Fig 4.10.b : RIVULET FLOW MODEL
HARTLEY and MURGATROUD (1964)

2. MINIMUM ENERGY MODEL

Assuming a linear velocity profile in the liquid as in the first H-M model and author's analyses, one obtains the critical flow rate as

$$h_c = 1.59 \left(\sigma/\rho_f\right)^{1/3} \left(\mu_f/\tau_i\right)^{2/3} \tag{4.22}$$

$$q_c = 2.52 \left(\rho_f \mu_f/\tau_i\right)^{1/3} \sigma^{2/3} \tag{4.23}$$

Equations (4.22) and (4.23) do not include the contact angle, rather assuming the rivulet cross section to be rectilinear, i.e. $\theta = 90°$. Thus a portion of the surface energy of the rivulet was neglected.

Comparison between author's direct measurement of the critical film thickness and the H-M power model (Eq. 4.22) shows that the predicted critical film thickness is $\sim 4x$ that measured by present author (Table 4.5). A partial explanation of the difference may be their assumption of a rectilinear rivulet cross-section. In light of the minimum surface energy, the cross-section should not be flat but rather it approaches a circular segment. This shape requires less energy than a flat form. Present author observed from his rivulet photographs (plates #1.1 and 3.1 of Fig. 4.1) that a stable approximately flat cross sectional rivulet continued to be stable. Of course, the exact rivulet shape is not known at this time.

Another possible reason for the difference in measured and predicted critical stability parameters is the negligence of wave effects in the rivulets for the H-M minimum power model. Two-dimensional waves moving in the rivulet flow

V_s (m/s) / h_c x10^3(cm)	73.2	133	191	305
Measured (W. Kim)	8.13	4.57	2.7	1.78
Predicted (H&M)	32	16	11	6

Predicted Critical Film Thickness is $\sim$ 4 times larger than Measured Film Thickness.

Table 4.5: COMPARISON OF THE MEASURED AND PREDICTED MINIMUM POWER CRITERION OF H-M MODEL

direction were observed (see plates in Fig. 4.1) and should be considered in any rivulet film flow stability model.

M-M Model

More recently Mikielewicz and Moszynski[M3] proposed a modified H-M minimum power model based on Hobler's[H3] basic approach. As an improvement over the H-M model, they assumed the rivulet cross-section to be a circular segment.

Assuming that the rivulet is stable when the total energy flux (kinetic plus surface) is minimum, they obtained the following equation for the critical film thickness for critically stable rivulet flow,

$$h^+ = 3.2^{-2/3}\left(\frac{\theta}{\sin\theta} - \cos\theta\right)^{1/3} h^{+2/3}\, g(\theta)^{2/3}\, \frac{\sin\theta}{\phi(\theta)}\,(1-\cos\theta) \qquad (4.24)$$

where

$$h^+ = \frac{\rho_f\, \tau_i^2\, h^3}{\mu_f^2\, \sigma}$$

is the non-dimensional thickness,

$g(\theta) = -1/4\cos^3\theta - \frac{13}{8}\cos\theta + \frac{15\,\theta}{8\sin\theta} - \frac{3}{2}\theta\sin\theta,$

$\phi(\theta) = \sin\theta - \frac{1}{3}\sin^3\theta - \theta\cos\theta.$

In this analysis, the velocity profile of the liquid film was assumed linear. They presented a graphical solution for the above expressions (Fig. 4.12).

Comparing the author's critical film thickness measurement with the predicted M-M model, the contact angle θ should be about 10° for the model to be compatible with the experiments. (see Table 4.4). This presents substantial improvement

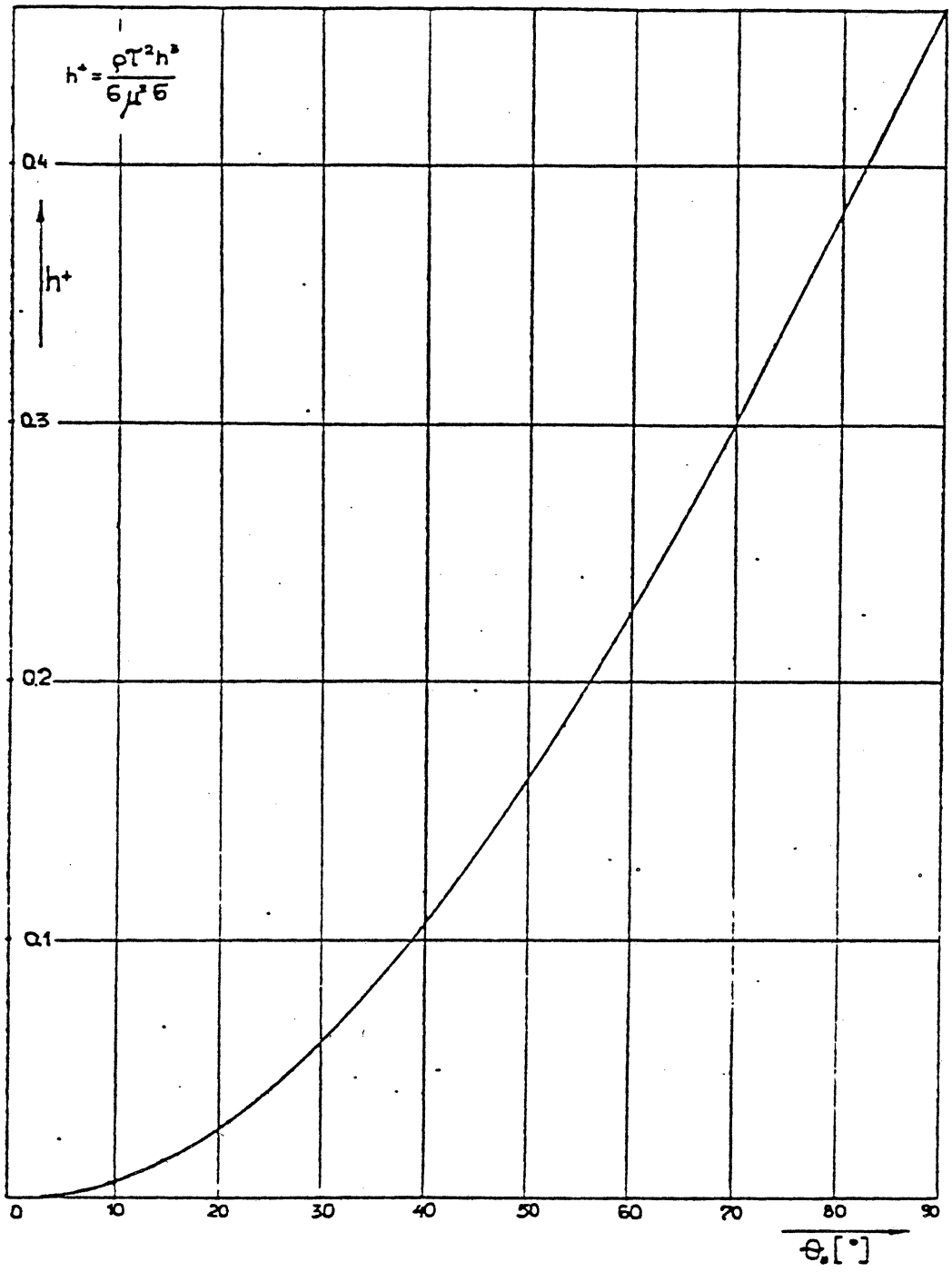

$$h^+ = 3 \cdot 2^{-\frac{1}{2}} \left(\frac{\theta_0}{\sin\theta_0} - \cos\theta_0 \right)^{\frac{1}{2}} h^{+\frac{3}{2}} g(\theta_0)^{\frac{1}{2}} \frac{\sin\theta_0}{\phi} - (1 - \cos\theta_0),$$

where

$$h^+ = \frac{\rho\tau^2 h_0^3}{6\mu^2 \sigma_{2-3}}.$$

Fig. 4.12 Dimensionless Minimum Film Thickness as a function of the Contact Angle (Mikielewicz-Moszynski, 1975)

over the H-M minimum power model, but still the required contact angle, θ, is less than half that of measured contact angle ($\sim 25°$) [M15] in such a single curvature flow as rivulet. An important reason for the discrepancy with author's experiment may well be the neglect of rivulet film waviness.

D. WAVY FILM REGIME

When the liquid flow rate is increased at fixed steam velocity, the liquid film covering the blade surface becomes continuous, and rivulets and dry patches disappear.

For the range of steam velocities here used, the surface of the liquid film is only rarely entirely smooth. Rather it is nearly always somewhat wavy (see plates in Fig. 4.1). The shape of these wavelets for low steam velocities and liquid flow rates is two-dimensional with relatively small wave lengths ($\sim$0.5 cm) in direction of flow. With further increase of liquid flow rate or steam velocity, the wavelet shape becomes more complicated with much larger wave lengths ($\sim$2 cm). The author has defined this wave form as "three-dimensional." These larger waves are usually preceded by a parasitic group of much smaller wavelets. In the "film map" Fig. 4.2, the division between two dimensional and three-dimensional wave regimes is indicated by the broken line. This division is not "sharp", so that in the three dimensional wave region (Fig. 4.2), two dimensional waves sometimes exist, appearing and disappearing.

Extensive measurements of film thickness, wave length, and wave propagation speed have been performed for the

different steam and liquid flow conditions attainable. Test points (Tables 4.6, 4.7) were selected to cover with adequate detail the full range of steam velocity (steam Mach number) and film flow (film Reynolds number). Calculated results include interfacial shear stress (section B of Chapter IV) wave number, capillary wave celerities and other important parameters.

The measured wave length data for the two-dimensional and three-dimensional waves are shown in Figs. 4.13 and 4.14. Figure 4.13 shows that the wave length, λ, of two-dimensional waves decreases as the liquid film Reynolds number, Re_f increases, for lower steam velocities, while it slowly decreases with increasing Re_f for very high steam velocity. The Mach number is then high subsonic (M=0.61 and 0.72), so that compressibility may importantly influence the flow. In general, the wave length, λ, decreases with increasing steam velocity or Mach number for a given Re_f. Also the data scatter decreases with increasing steam velocity, perhaps because the relative precision of the measurement of these larger parameters improves.

For three-dimensional large waves, λ, deceases with increasing Re_f at lower steam velocities, but increases with Re_f for higher velocities. This trend is not found for the two-dimensional waves.

Figures 4.15a and 4.16 show measured data on propaga_ tion speed of two and three dimensional waves for various Re_f and steam Mach numbers, M. These were directly measured

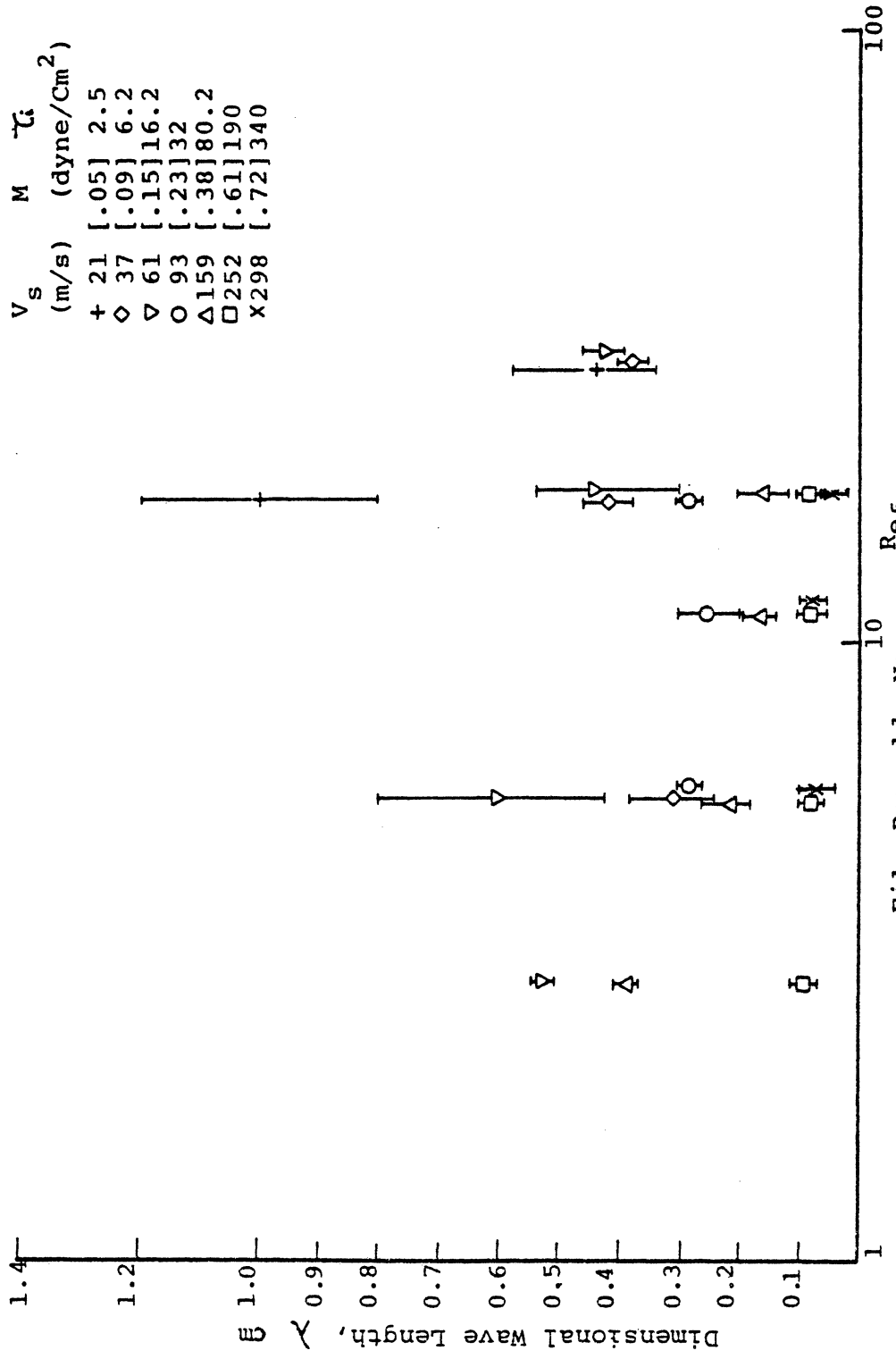

Fig. 4.13 Wave Length, , vs Film Reynolds No. Re_f
(2-D waves)

5331

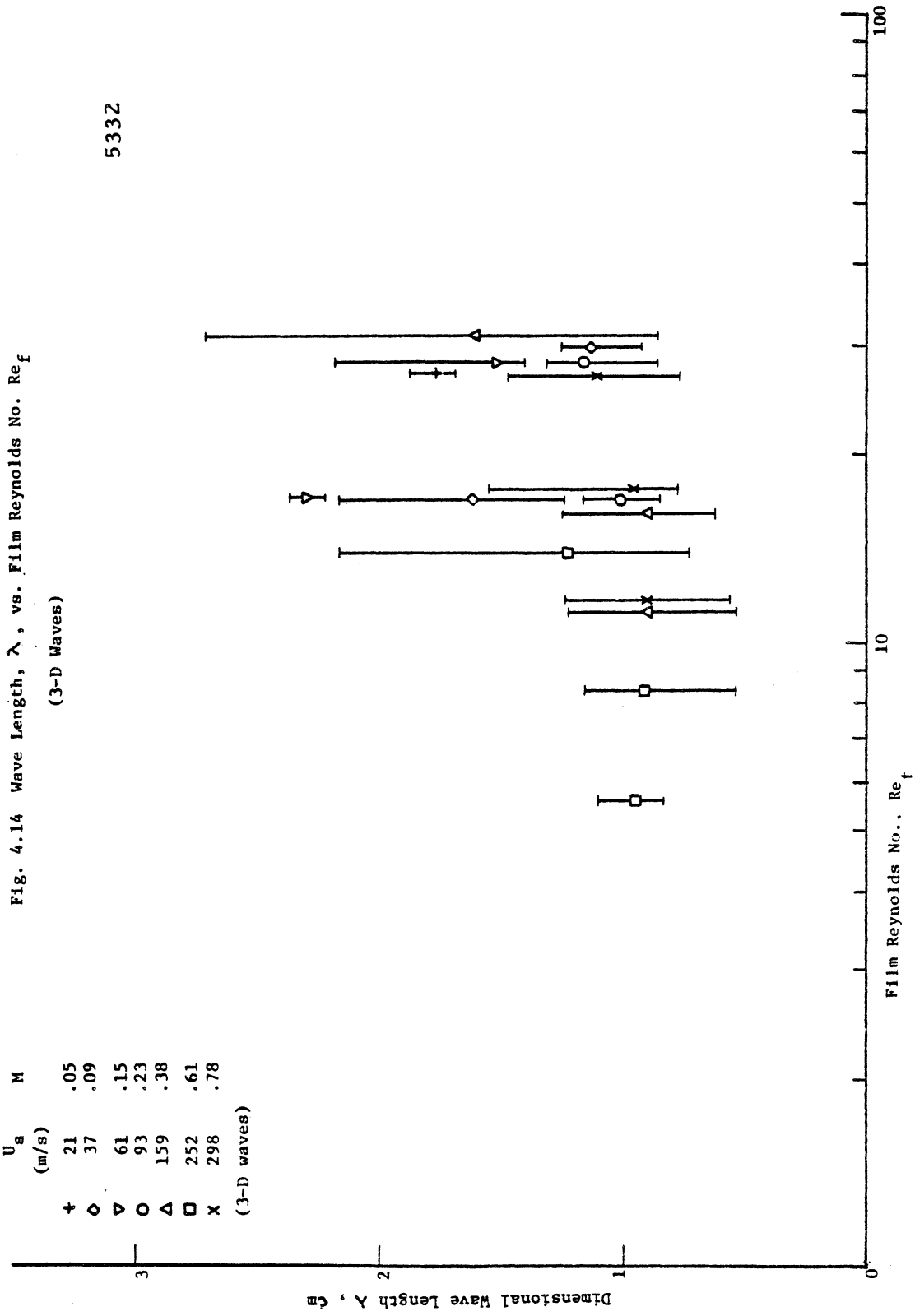
5332
Fig. 4.14 Wave Length, λ , vs. Film Reynolds No. Re_f
(3-D Waves)
U_g (m/s) M
+ 21 .05
◇ 37 .09
▽ 61 .15
○ 93 .23
△ 159 .38
□ 252 .61
x 298 .78
(3-D waves)
Dimensional Wave Length λ , cm
0
1
2
3
10
100
Film Reynolds No., Re_f

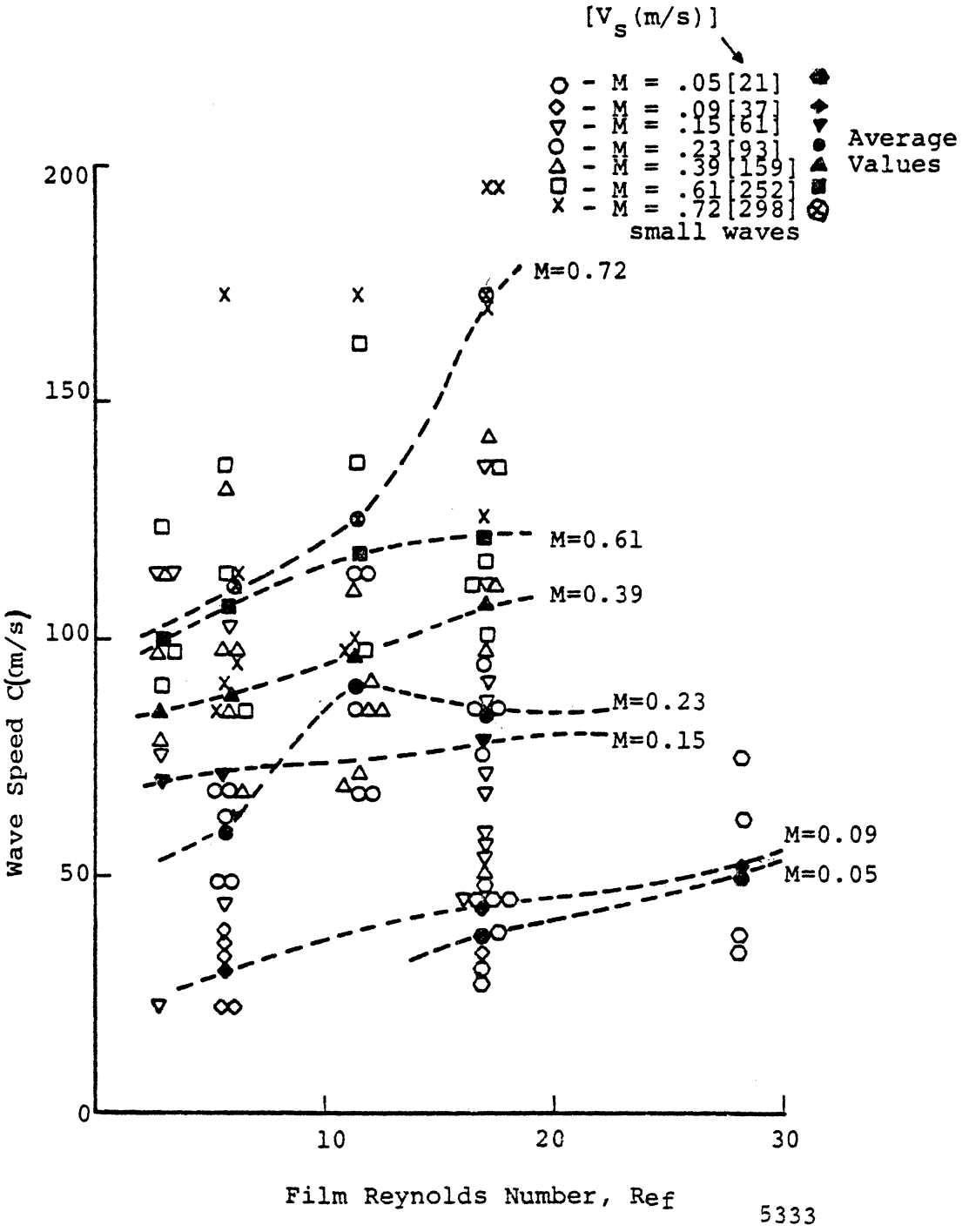

Fig. 4.15.a Wave Propagation Speed, C, vs Film Reynolds No. Re_f
(2-D waves)

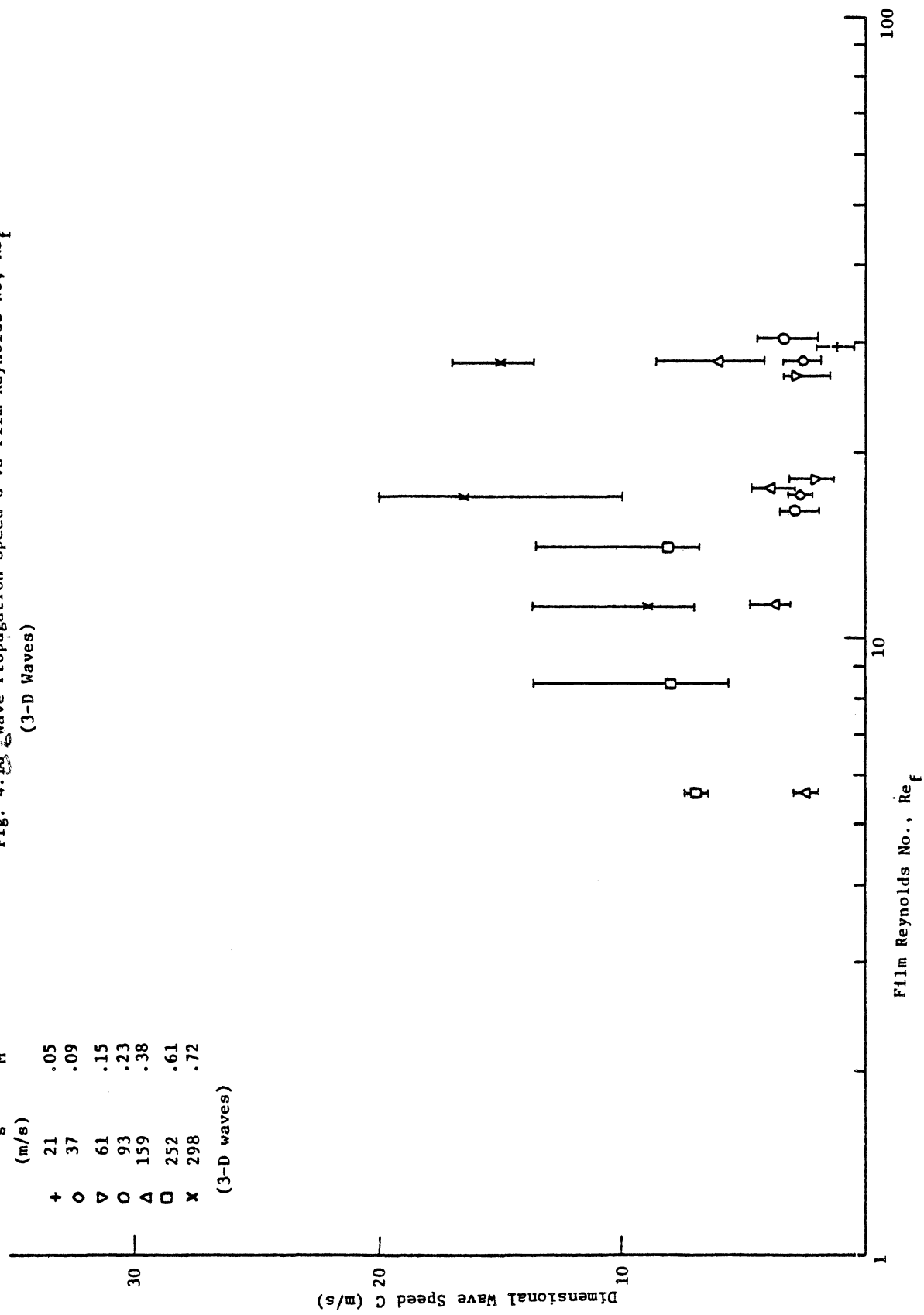

Fig. 4.16 Wave Propagation Speed C vs Film Reynolds No, Re_f
(3-D Waves)

from the high-speed motion picture frames.

The wave propagation speed, C, increases with both M and Re_f for two-dimensional waves (Fig. 4.15.a). Solid symbols represent average values, while open symbols are individual points. To help clarify the operative wave-propagation mechanisms, the celerity of capillary-gravity wave Vc has been computed (Table 4.6).

The classical solution for combined capillary and gravity waves (long waves), Vc, is expressed as[C17,L6]

$$V_c = [\frac{g}{k} + \sigma \frac{k}{\rho_f}]^{1/2} \qquad (4.25)$$

where g is gravitational acceleration and $k = 2\pi/\lambda$ is wave number.

Comparing measured wave speed, C, with capillary wave speed, V_c, it is found that the measured speed is 1.86 ± 0.36 x that calculated from the conventional capillary-gravity model for author's two-dimensional waves. Thus the celerity of the two-dimensional waves is in reasonably good agreement with the classical capillary gravity model.

Recently Wurz[W14] proposed a two-dimensional film wave propagation speed model, compared with his own experimental data. Using "universal" velocity profiles (laminar and laminar-turbulent) for the film, two limiting correlations are suggested; $C^* = 2^{3/2} Re_f^{1/2}$

and

$$C^* = 2^{9/4} 9^{-1/3} Re_f^{1/3}$$

Table 4.6 FILM WAVE CHARACTERISTICS (2-D WAVE)

V_s (m/s) Steam Velocity	q_2 (cm^2/s) Specific Liquid Flow Rate	h (mils) Film Thickness	V_f' (cm/s) Interfacial Film Velocity	λ (cm) Wave Length	C (cm/s) Wave Propagation Speed	Vc (cm/s) Capillary Wave Speed $\left(\frac{\lambda g}{2\pi}+\frac{\sigma}{\lambda\rho}\frac{2\pi}{\lambda}\right)^{\frac{1}{2}}$	W_λ Weber Number $\left(\frac{\rho_s V_s^2 \lambda}{\sigma}\right)$	W_h Weber Number $\left(\frac{\rho_s V_s^2 h}{\sigma}\right)$	τ_i $\left(\frac{dyne}{cm^2}\right)$ Interfacial Shear Stress	Re_f Film Reynolds Number $\left(\frac{V_f h}{\nu_f}\right)$	k (cm^{-1}) Wave Number	$\propto$ Non-Dimensional Wave Number (kh)	C/V_f Non-Dimensional Wave Speed	W_f Weber Number $\left(\frac{\rho_s V_f^2 h}{\sigma}\right)$ x10^{+4}	G Inverse Froude Number $\left(\frac{gh}{V_f^2}\right)$ x10^{+3}	$\propto_c$ Cut-Off Wave Number	C/V_c Non-dimensional Wave speed	$C^* = C/\sqrt{\tau_i/\rho}$ Non-dimensional Wave speed (W14) (Wurz)
	.005	3.5	1.17					.061	2.0	1.4				1.68	639	0.037		
	.010	3.5	2.34					.061	2.0	2.8				6.71	160	0.070		
	.021	4.7	3.49					.082	2.1	5.6				20.0	96.5	0.092		
				.923	49.0	22.3	6.34	.113	2.4	16.9	6.81	.112	6.47	130.4	28.4	0.156	2.2	31.0
21.4 (M=0.05)				1.23	38.0	19.3	8.45	"	"	"	5.11	.084	5.02	"	"	"	2.0	24.5
	.063	6.5	7.57	1.46	45.6	17.7	10.0	"	"	"	4.30	.071	6.02	"	"	"	2.6	29.4
				.769	31.1	24.4	5.28	"	"	"	8.17	.135	4.11	"	"	"	1.3	20.1
				2.15	27.4	14.6	14.8	"	"	"	2.92	.048	3.62	"	"	"	1.9	17.7
				.615	62.0	27.3	4.23	.156	2.8	28.2	10.2	.231	6.73	264	26.2	0.174	2.3	37.1
				.577	34.2	28.2	3.96	"	"	"	10.9	.246	3.71	"	"	"	1.2	20.4
				.185	76.0	49.8	1.27	"	"	"	34.0	.769	8.25	"	"	"	1.5	45.4
	.104	8.9	9.21		38.0			"	"	"			4.13	"	"	"		22.7

Table 4.6 FILM WAVE CHARACTERISTICS (2 - D WAVE)

V_s (m/s) Steam Velocity	q_2 (cm^2/s) Specific Liquid Flow Rate	h (mils) Film Thickness	V_f (cm/s) Interfacial Film Velocity	λ (cm) Wave Length	C (cm/s) Wave Propagation Speed	Vc (cm/s) Capillary Wave Speed $\left(\frac{\lambda g}{2\pi}+\frac{\sigma 2\pi}{\lambda \rho}\right)^{\frac{1}{2}}$	W_λ Weber Number $\left(\frac{\rho_s V_s^2 \lambda}{\sigma}\right)$	W_h Weber Number $\left(\frac{\rho_s V_s^2 h}{\sigma}\right)$	τ_i $\left(\frac{dyne}{cm^2}\right)$ Interfacial Shear Stress	Re_f Film Reynolds Number $\left(\frac{V_f h}{\nu_f}\right)$	k (cm^{-1}) Wave Number	α Non-Dimensional Wave Number (kh)	C/V_f Non-Dimensional Wave Speed	W_f Weber Number $\left(\frac{\rho_s V_f^2 h}{\sigma}\right)$ x10^{+4}	G Inverse Froude Number $\left(\frac{gh}{V_f^2}\right)$ x10^{+3}	α_c Cut-Off Wave Number	C/V_c Non-dimensional Wave speed	$C^* = C/\sqrt{\tau_i/\rho}$ Non-dimensional Wave speed (W14) (Wurz)
	.010	2.4	3.42					.123	4.9	2.8				9.8	51.3	.10		
	.021	3.7	4.43	.385	34.2	34.5	7.74	.189	5.6	5.6	16.3	.153	7.72	25.4	47.1	.115	1.0	14.5
				.231	36.0	44.5	4.64	"	"	"	27.2	.256	8.13	"	"	"	0.8	15.2
				.385	38.0	34.5	7.74	"	"	"	16.3	.153	8.58	"	"	"	1.1	16.1
				.231	22.6	44.5	4.64	"	"	"	27.2	.256	5.10	"	"	"	0.5	9.6
				.308	22.8	38.6	6.19	"	"	"	20.4	.192	5.15	"	"	"	0.6	9.6
36.6 (M= 0.089	0.063	6.4	7.69	.462	46.3	31.5	9.28	.327	7.0	16.9	13.6	.221	6.02	132.5	27.1	0.176	1.5	17.6
				.385	52.5	34.5	7.74	"	"	"	16.3	.265	6.83	"	"	"	1.5	19.8
				.385	45.6	34.5	7.74	"	"	"	16.3	.265	5.93	"	"	"	1.3	17.2
				.462	36.0	31.5	9.28	"	"	"	13.6	.221	4.68	"	"	"	1.1	15.6
	.104	8.5	9.65	.385	52.5	34.5	7.74	.434	4.4	28.2	16.3	.352	5.44	277	"	0.182	1.5	
	.005		2.56					.227	19	1.4				3.7	61.0	0.088		
61.0 (M= 0.15)	.010	1.6	5.13		21.4			"	12	2.8			4.17	14.7	15.2	0.097		6.2

Table 4.6 FILM WAVE CHARACTERISTICS (2 - D WAVE)

V_s (m/s) Steam Velocity	q_2 (cm^2/s) Specific Liquid Flow Rate	h (mils) Film Thickness	V_f (cm/s) Interfacial Film Velocity	λ (cm) Wave Length	C (cm/s) Wave Propagation Speed	V_c (cm/s) Capillary Wave Speed $\left(\frac{\lambda g}{2\pi}+\frac{2\pi\sigma}{\lambda\rho}\right)^{\frac{1}{2}}$	W_λ Weber Number $\left(\frac{\rho_s V_s^2 \lambda}{\sigma}\right)$	W_h Weber Number $\left(\frac{\rho_s V_s^2 h}{\sigma}\right)$	τ_i $\left(\frac{dyne}{cm^2}\right)$ Interfacial Shear Stress	Re_f Film Reynolds Number $\left(\frac{V_f h}{\nu_f}\right)$	k (cm^{-1}) Wave Number	$\propto$ Non-Dimensional Wave Number (kh)	C/V_f Non-Dimensional Wave Speed	W_f Weber Number $\left(\frac{\rho_s V_f^2 h}{\sigma}\right)$ $\times 10^{+4}$	G Inverse Froude Number $\left(\frac{gh}{V_f^2}\right)$ $\times 10^{+3}$	$\propto_c$ Cut-Off Wave Number	C/V_c Non-dimensional Wave speed	$C^* = C/\sqrt{\tau_i/\rho}$ Non-dimensional Wave speed (W14) (Wurz)
61.0 (M=0.15)	.010	1.6	5.13		114			.227	12	2.8			22.2	14.7	15.2	0.097		32.9
				.539	76.0	29.2	30.1	"	"	"	11.7						2.6	21.9
	.021	2.4	6.83	.923	44.2	22.3	51.5	.340	15	5.6	6.81	.042	6.47	38.8	12.9	.198	2.0	11.4
				.385	37.0	34.5	21.5	"	"	"	16.3	.099	5.42	"	"	"	1.1	9.6
				.385	34.2	34.5	21.5	"	"	"	16.3	.099	5.01	"	"	"	1.0	8.8
	.063	4.0	12.3	.539	91.3	29.2	30.1	.567	20	16.9	11.7	.119	7.42	212	6.61	.312	3.1	13.7
				.385	87.7	34.5	21.5	"	"	"	16.3	.166	7.13	"	"	"	2.5	19.6
				.539	57.0	29.2	30.1	"	"	"	11.7	.119	4.63	"	"	"	2.0	12.8
				.308	72.0	39.6	17.2	"	"	"	20.4	.207	5.85	"	"	"	1.8	16.1
				.577	46.6	28.2	32.2	"	"	"	10.9	.111	3.79	"	"	"	1.7	10.4
				.539	59.5	29.2	30.1	"	"	"	11.7	.119	4.83	"	"	"	2.0	13.3
				.539	53.3	29.2	30.1	"	"	"	11.7	.119	4.35	"	"	"	1.8	11.9
	.104	5.5	14.9	.385	137	39.5	21.5	.780	22	"	16.3	.228	9.2	427	6.19	.561	3.5	29.2
				.462	114	31.5	25.8	"	"	"	13.6	.190	7.65	"	"	"	3.6	24.3
				.385	68.4	39.5	21.5	"	"	"	16.3	.228	4.59	"	"	"	1.7	14.6

Table 4.6 FILM WAVE CHARACTERISTICS (2 - D WAVE)

V_s (m/s) Steam Velocity	q_2 (cm^2/s) Specific Liquid Flow Rate	h (mils) Film Thickness	V_f (cm/s) Interfacial Film Velocity	λ (cm) Wave Length	C (cm/s) Wave Propagation Speed	Vc (cm/s) Capillary Wave Speed $\left(\frac{\lambda g}{2\pi}+\frac{2\pi\sigma}{\lambda\rho}\right)^{\frac{1}{2}}$	W_λ Weber Number $\left(\frac{\rho_s V_s^2 \lambda}{\sigma}\right)$	W_h Weber Number $\left(\frac{\rho_s V_s^2 h}{\sigma}\right)$	τ_i $\left(\frac{dyne}{cm^2}\right)$ Interfacial Shear Stress	Re_f Film Reynolds Number $\left(\frac{V_f h}{\nu_f}\right)$	k (cm^{-1}) Wave Number	α Non-Dimensional Wave Number (kh)	C/V_f Non-Dimensional Wave Speed	W_f Weber Number $\left(\frac{\rho_s V_f^2 h}{\sigma}\right)$ x10^{+4}	G Inverse Froude Number $\left(\frac{gh}{V_f^2}\right)$ x10^{+3}	α_c Cut-Off Wave Number	C/V_c Non-dimensional Wave speed	$C^*=C/\sqrt{\tau_i/\rho}$ Non-dimensional Wave speed (W14) (Wurz)
93.3 (M=0.23)	.021	1.5	10.9	.269	68.4	41.2	35.1	.497	29	5.6	23.4	.089	6.28	62.4	3.17	.372	1.7	12.7
				.231	68.4	44.5	30.1	"	"	"	27.2	.104	6.28	"	"	"	1.5	12.7
				.269	62.2	41.2	35.1	"	"	"	23.4	.089	5.71	"	"	"	1.5	11.6
				.308	48.9	38.6	40.2	"	"	"	20.4	.078	4.50	"	"	"	1.3	9.1
				.269	48.9	41.2	35.1	"	"	"	23.4	.089	4.50	"	"	"	1.2	9.1
	.042	2.1	15.7	.192	85.6	48.8	25.1	.697	31	11.3	32.7	.174	5.45	181	2.13	.534	1.8	15.4
				.308	114	38.6	40.2	"	"	"	20.4	.109	7.26	"	"	"	3.0	20.5
				.231	68.4	44.5	30.1	"	"	"	27.2	.145	4.36	"	"	"	1.5	12.3
				.308	114	44.5	40.2	"	"	"	20.4	.109	7.26	"	"	"	2.6	20.4
				.192	68.4	48.8	25.1	"	"	"	32.7	.174	4.36	"	"	"	1.4	12.4
	.063	2.6	18.9	.323	85.6	37.6	42.2	.863	32.7	16.9	19.5	.129	5.45	32.5	1.82	.55	2.3	14.9
				.308	85.6	38.6	40.2	"	"	"	20.4	.135	5.45	"	"	"	2.2	14.9
				.269	76.0	41.2	35.1	"	"	"	23.4	.155	4.02	"	"	"	1.8	13.3
				.308	95.1	38.6	40.2	"	"	"	20.4	.135	5.03	"	"	"	2.5	16.6
	.104	3.4	24.1					1.13	35.3	28.2				691	1.46	.70		

Table 4.6 FILM WAVE CHARACTERISTICS (2 - D WAVE)

V_s (m/s) Steam Velocity	q_2 (cm^2/s) Specific Liquid Flow Rate	h (mils) Film Thickness	V_f (cm/s) Interfacial Film Velocity	λ (cm) Wave Length	C (cm/s) Wave Propagation Speed	Vc (cm/s) Capillary Wave Speed $\left(\frac{\lambda g}{2\pi}+\frac{\sigma 2\pi}{\lambda \rho}\right)^{\frac{1}{2}}$	W_λ Weber Number $\left(\frac{\rho_s V_s^2 \lambda}{\sigma}\right)$	W_h Weber Number $\left(\frac{\rho_s V_s^2 h}{\sigma}\right)$	τ_i $\left(\frac{dyne}{cm^2}\right)$ Interfacial Shear Stress	Re_f Film Reynolds Number $\left(\frac{V_f h}{\nu_f}\right)$	k (cm^{-1}) Wave Number	α Non-Dimensional Wave Number (kh)	C/V_f Non-Dimensional Wave Speed	W_f Weber Number $\left(\frac{\rho_s V_f^2 h}{\sigma}\right)$ x10^{+4}	G Inverse Froude Number $\left(\frac{gh}{V_f^2}\right)$ x10^{+3}	α_c Cut-Off Wave Number	C/V_c Non-dimensional Wave speed	$C^* = C/\sqrt{\tau_i/\rho}$ Non-dimensional Wave speed (W14) (Wurz)
159 (M=0.39)	.010	.7	11.7	1.77	114		671	.674	76.3	2.8	3.55	.006	9.74	33.5	1.28	.478	5.0	13.1
				.385	114		146	"	"	"	16.3	.029	9.74	"	"	"	3.4	13.1
				.385	97.8		146	"	"	"	16.3	.029	8.36	"	"	"	2.9	11.2
				.385	114		146	"	"	"	16.3	.029	9.74	"	"	"	3.4	13.1
	.021	1.0	16.4	.269	132	41.2	102	.963	79.5	5.6	23.4	.059	8.05	94.1	.930	.560	3.2	14.8
				.192	85.6	48.8	72.8	"	"	"	32.7	.083	5.22	"	"	"	1.8	9.6
				.192	97.8	48.8	72.8	"	"	"	32.7	.083	5.96	"	"	"	2.0	10.9
				.177	68.4	50.8	67.1	"	"	"	32.7	.083	4.17	"	"	"	1.4	7.7
				.169	97.8	52.0	64.1	"	"	"	32.7	.083	5.96	"	"	"	1.9	11.0
	.042	1.4	23.4	.154	97.8	54.5	58.4	1.35	83.2	11.26	40.8	.145	4.18	268	.639	.794	1.8	10.7
				.154	85.6	54.5	58.4	"	"	"	40.8	.145	3.66	"	"	"	1.6	9.4
				.185	72.0	49.8	70.1	"	"	"	34.0	.121	3.08	"	"	"	1.5	7.9
				.185	85.6	49.8	70.1	"	"	"	34.0	.121	3.66	"	"	"	1.7	9.4
				.139	91.3	57.5	52.7	"	"	"	45.2	.161	3.90	"	"	"	1.6	10.0
				.139	68.8	57.5	52.7	"	"	"	45.2	.161	2.94	"	"	"	1.2	7.5

Table 4.6 FILM WAVE CHARACTERISTICS (2 - D WAVE)

V_s (m/s) Steam Velocity	q_2 (cm^2/s) Specific Liquid Flow Rate	h (mils) Film Thickness	V_f (cm/s) Interfacial Film Velocity	λ (cm) Wave Length	C (cm/s) Wave Propagation Speed	V_c (cm/s) Capillary Wave Speed $\left(\frac{\lambda g}{2\pi}+\frac{2\pi\sigma}{\lambda\rho}\right)^{\frac{1}{2}}$	W_λ Weber Number $\left(\frac{\rho_s V_s^2 \lambda}{\sigma}\right)$	W_h Weber Number $\left(\frac{\rho_s V_s^2 h}{\sigma}\right)$	τ_i $\left(\frac{dyne}{cm^2}\right)$ Interfacial Shear Stress	Re_f Film Reynolds Number $\left(\frac{V_f h}{\nu_f}\right)$	k (cm^{-1}) Wave Number	$\propto$ Non-Dimensional Wave Number (kh)	C/V_f Non-Dimensional Wave Speed	W_f Weber Number $\left(\frac{\rho_s V_f^2 h}{\sigma}\right)$ x10^{+4}	G Inverse Froude Number $\left(\frac{gh}{V_f^2}\right)$ x10^{+3}	$\propto_c$ Cut-Off Wave Number	C/V_c Non-dimensional Wave speed	$C^* = C/\sqrt{\tau_i/\rho}$ Non-dimensional Wave speed (W14) (Wurz)
	.063	1.7	28.9	.115	143	63.0	43.6	1.64	86.1	16.9	54.6	.236	4.95	268	.639	.794	2.3	15.4
				.123	114	61.0	46.6	"	"	"	51.1	.221	3.95	"	"	"	1.9	12.3
				.192	97.8	48.8	72.8	"	"	"	32.7	.141	3.38	"	"	"	2.0	10.5
				.215	79.6	46.1	81.5	"	"	"	29.2	.126	2.75	"	"	"	1.7	8.6
	.104	2.2	37.3	.				2.12	90.9	28.2				1070	1.58	1.084		
	.010	0.3	13.7	.092	124	70.4	87.6	.726	182.0	2.8	68.3	.052	9.05	19.7	.400	.282	1.8	9.2
				.077	97.8	77.1	73.3	.726	"	"	81.6	.062	7.14	"	"	"	1.3	7.3
				.108	91.3	65.2	103	"	"	"	58.2	.044	6.66	"	"	"	1.4	6.8
252 (M=0.61)	.021	0.4	20.5	.092	137	70.4	87.6	.967	184.4	5.6	68.3	.069	6.68	58.8	2.38	.420	2.0	10.1
				.077	85.6	77.1	73.3	"	"	"	81.6	.083	4.18	"	"	"	1.1	6.3
				.069	114	81.3	65.7	"	"	"	91.1	.093	5.56	"	"	"	1.4	8.4
	.042	0.65	25.2	.069	163	81.3	65.7	1.57	190.5	11.26	91.1	.150	6.47	145	.256	.516	2.0	11.8
				.077	132	77.1	73.3	"	"	"	81.6	.135	5.24	"	"	"	1.7	9.6
				.100	97.8	67.6.	95.3	"	"	"	62.8	.104	3.88	"	"	"	1.5	7.1
				.092	118	70.4	87.6	"	"	"	68.3	.113	4.68	"	"	"	1.7	8.6

Table 4.6 FILM WAVE CHARACTERISTICS (2 - D WAVE)

V_s (m/s) Steam Velocity	q_2 (cm^2/s) Specific Liquid Flow Rate	h (mils) Film Thickness	V_f (cm/s) Interfacial Film Velocity	λ (cm) Wave Length	C (cm/s) Wave Propagation Speed	Vc (cm/s) Capillary Wave Speed $\left(\frac{\lambda g}{2\pi} + \frac{2\pi\sigma}{\lambda\rho}\right)^{\frac{1}{2}}$	W_λ Weber Number $\left(\frac{\rho_s V_s^2 \lambda}{\sigma}\right)$	W_h Weber Number $\left(\frac{\rho_s V_s^2 h}{\sigma}\right)$	τ_i $\left(\frac{dyne}{cm^2}\right)$ Interfacial Shear Stress	Re_f Film Reynolds Number $\left(\frac{V_f h}{\nu_f}\right)$	k (cm^{-1}) Wave Number	α Non-Dimensional Wave Number (kh)	C/V_f Non-Dimensional Wave Speed	W_f Weber Number $\left(\frac{\rho_s V_f^2 h}{\sigma}\right)$ x10^{+4}	G Inverse Froude Number $\left(\frac{gh}{V_f^2}\right)$ x10^{+3}	α_c Cut-Off Wave Number	C/V_c Non-dimensional Wave speed	$C^* = C/\sqrt{\tau_i/\rho}$ Non-dimensional Wave speed (W14) (Wurz)
	.063	0.75	32.8	.100	101	67.6	95.3	1.82	193.0	16.9	62.8	.120	3.08	282	.174	.556	1.5	7.3
				.092	114	70.4	87.6	"	"	"	68.3	.130	3.48	"	"	"	1.6	8.2
				.092	137	70.4	87.6	"	"	"	68.3	.130	4.18	"	"	"	2.0	9.9
	.104	1.0	41.0					2.43	200.0	28.2				588	.149	.696		
	.021	0.6	27.3	.064	85.6	84.5	82.3	1.96	310	5.6	98.2	.150	3.14	157	.201	1.122	1.0	4.9
				.067	171	82.4	89.3	"	"	"	93.8	.143	6.26	"	"	"	2.1	9.7
				.103	91.3	89.0	137	"	"	"	61.0	.093	3.34	"	"	"	1.0	5.2
				.116	114	62.9	155	"	"	"	54.2	.083	4.18	"	"	"	1.8	6.5
				.064	95.1	84.5	82.3	"	"	"	98.2	.150	3.48	"	"	"	1.1	5.4
298 (M=0.72)	.042	0.8	41.0	.077	172	77.0	103	2.72	340	11.26	81.6	.166	4.20	471	.119	1.674	2.2	9.3
					97.8			"	"	"			2.39	"	"	"		5.3
				.092	105	70.4	123	"	"	"	68.3	.139	2.56	"	"	"	1.5	5.7
	.063	1.0	49.2	.051	196	94.4	67.9	3.38	380	16.9	123	.312	3.98	847	.103	1.670	2.1	10.1
				.062	171	86.2	82.6	"	"	"	101	.257	3.48	"	"	"	2.0	8.8
				.077	127	77.1	103	"	"	"	81.6	.207	2.58	"	"	"	1.7	6.5

Table 4.6 FILM WAVE CHARACTERISTICS (2 - D WAVE)

V_s (m/s) Steam Velocity	q_2 (cm^2/s) Specific Liquid Flow Rate	h (mils) Film Thickness	V_f (cm/s) Interfacial Film Velocity	λ (cm) Wave Length	C (cm/s) Wave Propagation Speed	Vc (cm/s) Capillary Wave Speed $\left(\frac{\lambda g}{2\pi} + \frac{2\pi\sigma}{\lambda\rho}\right)^{\frac{1}{2}}$	W_λ Weber Number $\left(\frac{\rho_s V_s^2 \lambda}{\sigma}\right)$	W_h Weber Number $\left(\frac{\rho_s V_s^2 h}{\sigma}\right)$	τ_i $\left(\frac{dyne}{cm^2}\right)$ Interfacial Shear Stress	Re_f Film Reynolds Number $\left(\frac{V_f h}{\nu_f}\right)$	k (cm^{-1}) Wave Number	α Non-Dimensional Wave Number (kh)	C/V_f Non-Dimensional Wave Speed	W_f Weber Number $\left(\frac{\rho_s V_f^2 h}{\sigma}\right)$ x10^{+4}	G Inverse Froude Number $\left(\frac{gh}{V_f^2}\right)$ x10^{+3}	α_c Cut-Off Wave Number	C/V_c Non-dimensional Wave speed	$C^* = C/\sqrt{\tau_i/\rho}$ Non-dimensional Wave speed (W14) (Wurz)
	.063	1.0	49.2	.092	196	70.4	123	3.38	380	16.9	68.3	.173	3.98	847	.103	1.670	2.8	10.1
	.104	1.2	68.3					4.06	430	28.2				1960	.064	2.316		

where

$$C^* = C/U_\tau = C/\sqrt{\tau_i/\rho_f}$$

Most of author's high subsonic data (M = 0.61) falls into his limiting "envelope" (Fig. 4.15.b). However Wurz's model does not adequately explain the lower subsonic portion of author's data. For this range of data, a more accurate estimate or measurement of the interfacial shear stress appears necessary. Alternatively a more sophisticated model may be required.

However, the propagation speed of three-dimensional waves (Fig. 4.16 and Table 4.7) is much greater (C/Vc = 32.2 ± 20.7) and the data more scattered, especially for high Mach numbers. Their speed is the order of ~10 m/s, while that of two dimensional waves is ~ 1 m/s.

The basic wave initiation and growth mechanisms are yet in question. No adequate calculating model for the three dimensional wave celerity is yet available. As shown in Fig. 4.17 and 4.18, dimensionless wave speeds $C'=C/V_f \geq 1$, i.e., the wave velocity is always greater than the liquid surface velocity, so that as expected, the waves are always progressing downstream.

Since wave propagation speed is always much smaller than the average steam velocity, a resonance mechanism of the type suggested by Phillips[P5] is not applicable to the present case. Turbulent steam pressure fluctuations with wave lengths comparable to those here observed would have velocities much larger than the wave velocities observed.

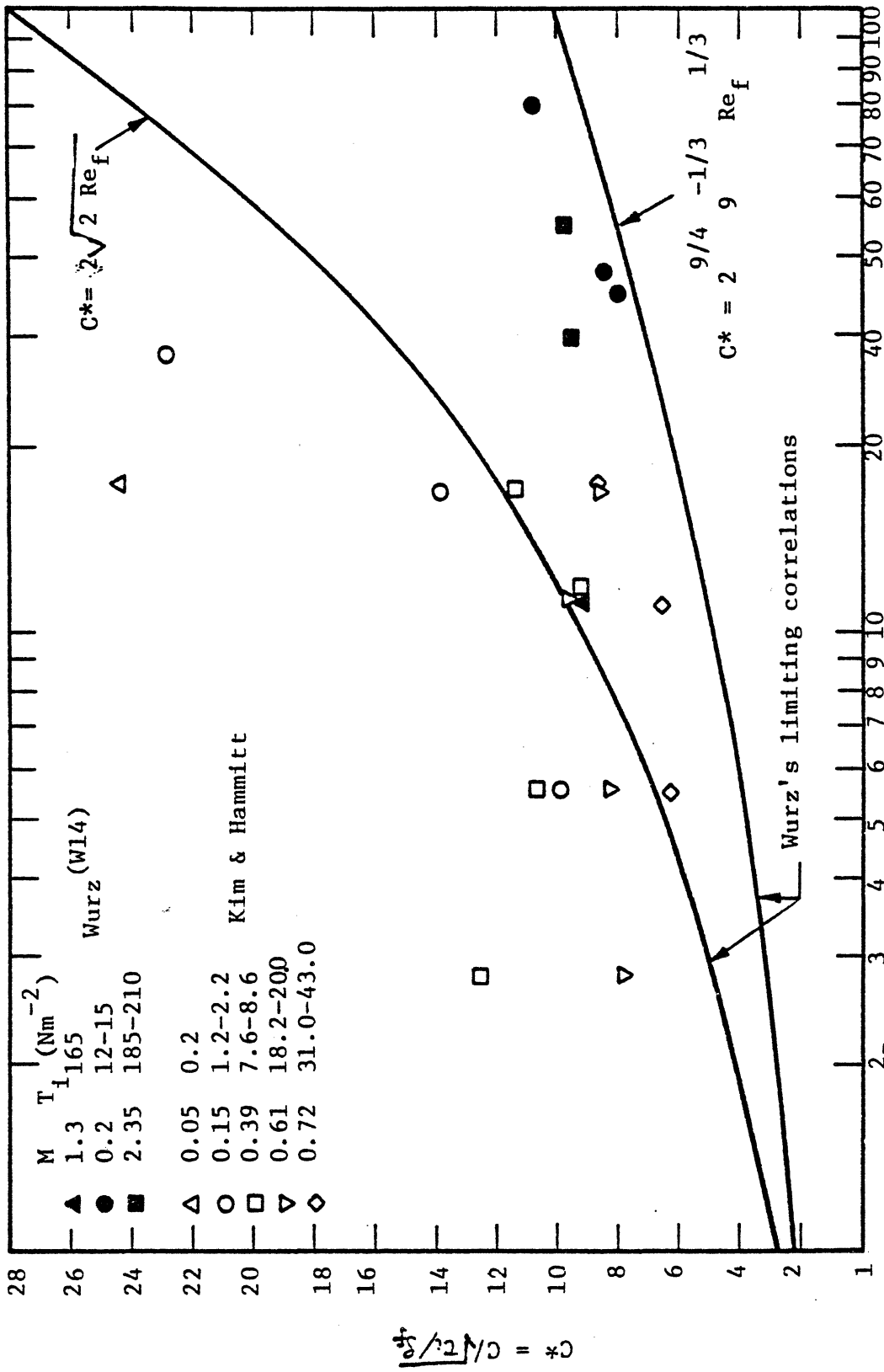

Fig. 4.15.b Non-Dimensional Wave Propogation Velocity, C*, vs. Film Reynolds Number, Re_f.

Table 4.7 FILM WAVE CHARACTERISTICS (3 - D WAVE)

V_s (m/s) Steam Velocity	q_2 (cm²/s) Specific Liquid Flow Rate	h (mils) Film Thickness	V_f (cm/s) Interfacial Film Velocity	λ (cm) Wave Length	C (cm/s) Wave Propagation Speed	V_c (cm/s) Capillary Wave Speed $\left(\frac{\lambda}{2\pi}\sqrt{\frac{\sigma 2\pi}{\lambda \rho}}\right)^{\frac{1}{2}}$	W_λ Weber Number $\left(\frac{\rho_s V_s^2 \lambda}{\sigma}\right)$	W_h Weber Number $\left(\frac{\rho_s V_s^2 h}{\sigma}\right)$	τ_i $\left(\frac{\text{dyne}}{\text{cm}^2}\right)$ Interfacial Shear Stress	Re_f Film Reynolds Number $\left(\frac{V_f h}{\nu_f}\right)$	k (cm^{-1}) Wave Number	α Non-Dimensional Wave Number (kh)	C/V_f Non-Dimensional Wave Speed	W_f Weber Number $\left(\frac{\rho_s V_f^2 h}{\sigma}\right)$ $\times 10^{+4}$	G Inverse Froude Number $\left(\frac{gh}{V_f^2}\right)$ $\times 10^{+3}$	α_c Cut-Off Wave Number	C/V_c Non-dimensional Wave speed	$C^* = C/\sqrt{\tau_i/\rho}$ Non-dimensional Wave speed (W14) (Wurz)
36.6 (M= .089)	.104	8.5	9.65	1.23	342	19.3	24.7	.434	4.4	23.2	5.11	1.43	35.4	277	27.1	.192	17.7	163.0
				1.16	254	19.9	23.3	"	"	"	5.42	1.52	26.3	"	"	"	12.8	121.0
				1.08	244	20.6	21.7	"	"	"	5.82	1.63	25.3	"	"	"	11.8	116.3
				1.16	171	19.9	23.3	"	"	"	5.42	1.52	17.7	"	"	"	8.6	81.5
				.923	228	22.3	18.6	"	"	"	6.81	1.91	23.6	"	"	"	10.2	108.7
				1.16	274	19.9	23.3	"	"	"	5.42	1.52	28.4	"	"	"	13.8	130.6
61.0 (M=.15)	.005	1.6	2.56					.227	10	1.41				3.7	61.0	.088		
	.010	1.6	5.13					.227	12	1.41				14.7	15.2	.097		
	.021	2.4	6.83					.340	15	5.63				38.8	12.9	.198		
	.063	4.0	12.3	2.31	298	14.1	129	.567	20	16.9	2.72	.358	24.2	212	6.61	.312	21.1	66.6
					152			"	"	"				"	"	"		34.0
	.104	5.5	14.9	1.54	342	17.2	86.0	.780	22	28.1	4.08	.739	23.0	427	6.19	.561	20.0	72.9
				1.08	342	20.6	60.3	"	"	"	5.82	1.05	23.0	"	"	"	16.6	72.9
				2.16	274	14.6	121	"	"	"	2.91	.527	18.4	"	"	"	18.8	58.5
				1.39	228	18.2	77.6	"	"	"	4.52	.819	15.3	"	"	"	12.5	48.6

Table 4.7 FILM WAVE CHARACTERISTICS (3 - D WAVE)

V_s (m/s) Steam Velocity	q_2 (cm^2/s) Specific Liquid Flow Rate	h (mils) Film Thickness	V_f (cm/s) Interfacial Film Velocity	λ (cm) Wave Length	C (cm/s) Wave Propagation Speed	V_c (cm/s) Capillary Wave Speed $\left(\frac{\lambda g}{2\pi} + \frac{2\pi\sigma}{\lambda\rho}\right)^{\frac{1}{2}}$	W_λ Weber Number $\left(\frac{\rho_s V_s^2 \lambda}{\sigma}\right)$	W_h Weber Number $\left(\frac{\rho_s V_s^2 h}{\sigma}\right)$	τ_i $\left(\frac{dyne}{cm^2}\right)$ Interfacial Shear Stress	Re_f Film Reynolds Number $\left(\frac{V_f h}{\nu_f}\right)$	k (cm^{-1}) Wave Number	α Non-Dimensional Wave Number (kh)	C/V_f Non-Dimensional Wave Speed	W_f Weber Number $\left(\frac{\rho_s V_f^2 h}{\sigma}\right)$ x10^{+4}	G Inverse Froude Number $\left(\frac{gh}{V_f^2}\right)$ x10^{+3}	α_c Cut-Off Wave Number	C/V_c Non-dimensional Wave speed	$C^* = C/\sqrt{\tau_i/\rho}$ Non-dimensional Wave speed (W14) (Wurz)
	.104	5.5	14.9	3.85	228	10.9	215	.780	22	28.1	1.63	.296	15.3	427	6.19	.561	2.3	48.6
	.010	1.0	8.2					.333		2.82								
	.021	1.5	10.9					.500	29	5.6				62.4	3.17	.372		
	.042	2.1	15.7					.700	31	11.3				181	2.13	.534		
				.923	274	24.4	121	.866	32.7	16.9	6.81	.583	14.5	32.5	1.82	.550	11.2	47.9
				.846	214	30.0	111	"	"	"	7.43	.636	11.3	"	"	"	7.1	37.4
	.063	2.6	18.9	1.15	342	23.2	151	"	"	"	5.46	.468	18.1	"	"	"	14.7	59.8
				.923	342	24.4	121	"	"	"	6.81	.583	18.1	"	"	"	14.6	59.8
93.3				1.08	342	23.5	141	"	"	"	5.82	.498	18.1	"	"	"	14.6	59.8
(M=.23)				1.00	171	23.9	131	1.13	35.3	28.1	6.28	.704	7.10	691	1.46	.700	7.2	28.8
				.846	228	25.0	111	"	"	"	7.43	.832	9.46	"	"	"	9.1	38.4
				.923	456	24.4	121	"	"	"	6.81	.763	18.9	"	"	"	18.7	76.8
				1.15	342	23.2	151	"	"	"	5.46	.612	14.2	"	"	"	14.7	57.6
	.104	3.4	24.1	2.08	342	22.9	272	"	"	"	3.02	.338	14.2	"	"	"	14.9	57.6
					228			"	"	"			9.46	"	"	"		38.4

Table 4.7 FILM WAVE CHARACTERISTICS (3 - D WAVE)

V_s (m/s) Steam Velocity	q_2 (cm^2/s) Specific Liquid Flow Rate	h (mils) Film Thickness	V_f (cm/s) Interfacial Film Velocity	λ (cm) Wave Length	C (cm/s) Wave Propagation Speed	Vc (cm/s) Capillary Wave Speed $\left(\frac{\lambda g}{2\pi}+\frac{\sigma 2\pi}{\lambda \rho}\right)^{\frac{1}{2}}$	W_λ Weber Number $\left(\frac{\rho_s V_s^2 \lambda}{\sigma}\right)$	W_h Weber Number $\left(\frac{\rho_s V_s^2 h}{\sigma}\right)$	τ_i $\left(\frac{dyne}{cm^2}\right)$ Interfacial Shear Stress	Re_f Film Reynolds Number $\left(\frac{V_f h}{\nu_f}\right)$	k (cm^{-1}) Wave Number	α Non-Dimensional Wave Number (kh)	C/V_f Non-Dimensional Wave Speed	W_f Weber Number $\left(\frac{\rho_s V_f^2 h}{\sigma}\right)$ x10^{+4}	G Inverse Froude Number $\left(\frac{gh}{V_f^2}\right)$ x10^{+3}	α_c Cut-Off Wave Number	C/V_c Non-dimensional Wave speed	$C^* = C/\sqrt{\tau_i/\rho}$ Non-dimensional Wave speed (W14) (Wurz)
	.104	3.4	24.1	.923	274	24.4	121	1.13	35.3	28.1	6.81	.763	11.4	691	1.46	.700	11.2	46.2
				1.29	228	22.9	168	"	"	"	4.87	.546	9.46	"	"	"	10.0	38.4
	.010	0.7	11.7					.675	76.3	2.81				33.5	1.28	.478		
	.021	1.0	16.4		274			.964	79.5	5.63			16.7	94.1	.930	.560		30.7
	.042	1.4	23.4	.539	342	29.4	204	1.35	83.2	11.3	11.7	.538	14.6	268	.639	.794	11.6	37.5
				1.23	342	23.0	466	"	"	"	5.11	.236	14.6	"	"	"	14.9	37.5
159 (M=.39)				1.23	456	23.0	466	"	"	"	5.11	.236	19.5	"	"	"	19.8	50.0
				.616	342	27.7	234	"	"	"	10.2	.471	14.6	"	"	"	12.4	37.5
	.063	1.7	28.9	1.23	456	23.0	466	1.64	86.1	16.9	5.11	.286	15.8	268	.639	.794	19.8	49.1
				.769	428	25.7	292	"	"	"	8.17	.458	14.8	"	"	"	16.7	46.7
				.923	342	24.4	351	"	"	"	6.81	.381	11.8	"	"	"	14.0	36.9
				.615	326	27.7	233	"	"	"	10.2	.572	11.3	"	"	"	11.8	35.1
	.104	2.2	37.3	1.85	684	22.6	702	2.12	90.9	28.2	3.40	.246	18.3	1070	1.58	1.084	30.3	71.7
				1.54	428	22.6	584	"	"	"	4.08	.296	11.5	"	"	"	18.9	44.9
				2.69	684	23.9	1020	"	"	"	2.34	.169	18.3	"	"	"	28.6	71.7

Table 4.7 FILM WAVE CHARACTERISTICS (3 - D WAVE)

V_s (m/s) Steam Velocity	q_2 (cm²/s) Specific Liquid Flow Rate	h (mils) Film Thickness	V_f (cm/s) Interfacial Film Velocity	λ (cm) Wave Length	C (cm/s) Wave Propagation Speed	V_c (cm/s) Capillary Wave Speed $\left(\frac{\lambda g}{2\pi} + \frac{2\pi\sigma}{\lambda\rho}\right)^{\frac{1}{2}}$	W_λ Weber Number $\left(\frac{\rho_s V_s^2 \lambda}{\sigma}\right)$	W_h Weber Number $\left(\frac{\rho_s V_s^2 h}{\sigma}\right)$	τ_i $\left(\frac{\text{dyne}}{\text{cm}^2}\right)$ Interfacial Shear Stress	Re_f Film Reynolds Number $\left(\frac{V_f h}{\nu_f}\right)$	k (cm^{-1}) Wave Number	$\propto$ Non-Dimensional Wave Number (kh)	C/V_f Non-Dimensional Wave Speed	W_f Weber Number $\left(\frac{\rho_s V_f^2 h}{\sigma}\right)$ x10^{+4}	G Inverse Froude Number $\left(\frac{gh}{V_f^2}\right)$ x10^{+3}	$\propto_c$ Cut-Off Wave Number	C/V_c Non-dimensional Wave speed	$C^* = C/\sqrt{\tau_i/\rho}$ Non-dimensional Wave speed (W14) (Wurz)
				1.92	684	22.7	728	2.12	90.9	28.2	3.27	.237	18.3	1070	1.58	1.084	30.1	71.7
				1.39	684	22.7	527	"	"	"	4.52	.328	18.3	"	"	"	30.1	71.7
				1.23	856	23.0	466	"	"	"	5.11	.370	23.0	"	"	"	37.2	89.8
				1.69	684	22.6	641	"	"	"	3.72	.270	18.3	"	"	"	30.1	71.7
	.104	2.2	37.3	2.15	684	23.0	815	"	"	"	2.92	.212	18.3	"	"	"	29.7	71.7
				.846	570	25.0	321	"	"	"	7.43	.538	15.3	"	"	"	22.8	59.8
				.923	684	24.4	351	"	"	"	6.81	.493	18.3	"	"	"	28.0	71.7
				1.15	570	23.2	436	"	"	"	5.46	.396	15.3	"	"	"	24.2	59.8
				1.62		22.6	614	"	"	"	3.88	.281		"	"	"		
	.010	0.3	13.7					.725	182.0	1.41				19.7	.400	.282		
	.021	0.4	20.5					.966	184.4	2.79				58.8	2.38	.420		
				1.00	684	23.9	953	1.57	190.5	5.62	6.28	.135	27.1	145	.256	.516	28.6	49.6
252	.042	0.65	25.2	1.08	684	23.5	1030	"	"	"	5.82	.125	27.1	"	"	"	29.1	49.6
(M=.61)				.846	684	25.0	806	"	"	"	7.43	.159	27.1	"	"	"	27.4	49.6

Table 4.7 FILM WAVE CHARACTERISTICS (3 - D WAVE)

V_s (m/s) Steam Velocity	q_2 (cm²/s) Specific Liquid Flow Rate	h (mils) Film Thickness	V_f (cm/s) Interfacial Film Velocity	λ (cm) Wave Length	C (cm/s) Wave Propagation Speed	V_c (cm/s) Capillary Wave Speed $\left(\frac{\lambda g}{2\pi} + \frac{2\pi\sigma}{\lambda\rho}\right)^{\frac{1}{2}}$	W Weber Number $\left(\frac{\rho_s V_s^2 \lambda}{\sigma}\right)$	W_h Weber Number $\left(\frac{\rho_s V_s^2 h}{\sigma}\right)$	τ_i $\left(\frac{\text{dyne}}{\text{cm}^2}\right)$ Interfacial Shear Stress	Re_f Film Reynolds Number $\left(\frac{V_f h}{\nu_f}\right)$	k (cm^{-1}) Wave Number	α Non-Dimensional Wave Number (kh)	C/V_f Non-Dimensional Wave Speed	W_f Weber Number $\left(\frac{\rho_s V_f^2 h}{\sigma}\right)$ x10 +4	G Inverse Froude Number $\left(\frac{gh}{V_f^2}\right)$ x10 +3	α_c Cut-Off Wave Number	C/V_c Non-dimensional Wave speed	$C^* = C/\sqrt{\tau_i/\rho}$ Non-dimensional Wave speed (W14) (Wurz)
252 (M=.61)	.063	0.75	32.8	1.00	1370	23.9	953	1.81	193.0	8.44	6.28	.155	41.8	282	.174	.556	57.3	98.6
				1.15	1370	23.2	1100	"	"	"	5.46	.135	41.8	"	"	"	59.1	98.6
				.769	684	25.7	733	"	"	"	8.17	.202	20.9	"	"	"	26.6	49.2
				.769	684	25.7	733	"	"	"	8.17	.202	20.9	"	"	"	26.6	49.2
				1.15	684	23.2	1100	"	"	"	5.46	.135	20.9	"	"	"	29.5	49.2
				.539	570	29.4	513	"	"	"	11.7	.288	17.4	"	"	"	19.4	41.0
				1.08	570	20.6	1030	"	"	"	5.82	.144	17.4	"	"	"	27.7	41.0
				.923	684	22.3	879	"	"	"	6.81	.168	20.9	"	"	"	30.7	49.2
	.104	1.0	41.0	.769	1360	25.7	733	2.42	200.0	14.1	8.17	.269	33.2	588	.149	.696	52.9	96.2
				1.15	856	23.2	1100	2.42	"	"	5.46	.180	20.9	"	"	"	36.9	60.5
				.846	1140	25.0	806	"	"	"	7.43	.245	27.8	"	"	"	45.6	80.6
				2.15	684	23.0	2050	"	"	"	2.92	.096	16.7	"	"	"	29.7	48.4
				.769	684	25.7	733	"	"	"	8.17	.269	16.7	"	"	"	26.6	48.4
				.923	684	22.2	879	"	"	"	6.81	.224	16.7	"	"	"	30.7	48.4
				.731	684	26.1	696	"	"	"	8.60	.283	16.7	"	"	"	26.2	48.4

Table 4.7 FILM WAVE CHARACTERISTICS (3 - D WAVE)

V_s (m/s) Steam Velocity	q_2 (cm^2/s) Specific Liquid Flow Rate	h (mils) Film Thickness	V_f (cm/s) Interfacial Film Velocity	λ (cm) Wave Length	C (cm/s) Wave Propagation Speed	Vc (cm/s) Capillary Wave Speed $\left(\frac{\lambda g}{2\pi} + \frac{2\pi\sigma}{\lambda\rho}\right)^{\frac{1}{2}}$	W_λ Weber Number $\left(\frac{\rho_s V_s^2 \lambda}{\sigma}\right)$	W_h Weber Number $\left(\frac{\rho_s V_s^2 h}{\sigma}\right)$	τ_i $\left(\frac{dyne}{cm^2}\right)$ Interfacial Shear Stress	Re_f Film Reynolds Number $\left(\frac{V_f h}{\nu_f}\right)$	k (cm^{-1}) Wave Number	$\propto$ Non-Dimensional Wave Number (kh)	C/V_f Non-Dimensional Wave Speed	W_f Weber Number $\left(\frac{\rho_s V_f^2 h}{\sigma}\right)$ x10^{+4}	G Inverse Froude Number $\left(\frac{gh}{V_f^2}\right)$ x10^{+3}	$\propto_c$ Cut-Off Wave Number	C/V_c Non-dimensional Wave speed	$C^* = C/\sqrt{\tau_i/\rho}$ Non-dimensional Wave speed (W14) (Wurz)
				2.08	684	22.9	1980	2.42	200.0	14.1	3.02	.100	16.7	588	.149	.696	29.9	48.4
	.104	1.0	41.0	1.31	684	22.8	1250	"	"	"	4.80	.158	16.7	"	"	"	30.0	48.4
				1.31	769	22.8	1250	"	"	"	4.80	.158	18.5	"	"	"	55.3	53.0
				1.39	684	18.2	1320	"	"	"	4.52	.149	16.7	"	"	"	37.6	48.8
	.021	0.6	27.3					2.03	310	5.62				157	.201	1.122		
				.615	684	27.7	819	2.71	340	11.3	10.2	.269	16.7	471	.119	1.674	24.7	37.1
				.577	1370	28.5	770	"	"	"	10.9	.287	33.4	"	"	"	48.1	74.3
				.846	684	30.0	1130	"	"	"	7.43	.196	16.7	"	"	"	22.8	37.1
	.042	0.8	41.0	.846	684	30.0	1130	"	"	"	7.43	.196	16.7	"	"	"	22.8	37.1
298				.846	684	30.0	1130	"	"	"	7.43	.196	16.7	"	"	"	22.8	37.1
(M=.72)				1.23	1370	19.3	1640	"	"	"	5.11	.135	33.4	"	"	"	71.0	74.3
				.615	684	27.2	819	"	"	"	10.2	.269	16.7	"	"	"	25.2	37.1
				.769	1370	25.7	1020	3.37	380	16.9	8.17	.269	22.7	847	.103	1.670	53.3	70.3
	.063	1.0	49.2	.923	1010	24.4	1230	"	"	"	6.81	.224	20.5	"	"	"	41.4	51.8
				1.54	2280	22.6	2050	"	"	"	4.08	.134	40.6	"	"	"	100.9	117.0

Table 4.7 FILM WAVE CHARACTERISTICS (3 - D **WAVE**)

V_s (m/s) Steam Velocity	q_2 (cm^2/s) Specific Liquid Flow Rate	h (mils) Film Thickness	V_f (cm/s) Interfacial Film Velocity	λ (cm) Wave Length	C (cm/s) Wave Propagation Speed	Vc (cm/s) Capillary Wave Speed $\left(\frac{\lambda g}{2\pi} + \frac{2\pi\sigma}{\lambda\rho}\right)^{\frac{1}{2}}$	W_λ Weber Number $\left(\frac{\rho_s V_s^2 \lambda}{\sigma}\right)$	W_h Weber Number $\left(\frac{\rho_s V_s^2 h}{\sigma}\right)$	τ_i $\left(\frac{dyne}{cm^2}\right)$ Interfacial Shear Stress	Re_f Film Reynolds Number $\left(\frac{V_f h}{\nu_f}\right)$	k (cm^{-1}) Wave Number	$\propto$ Non-Dimensional Wave Number (kh)	C/V_f Non-Dimensional Wave Speed	W_f Weber Number $\left(\frac{\rho_s V_f^2 h}{\sigma}\right)$ x10 +4	G Inverse Froude Number $\left(\frac{gh}{V_f^2}\right)$ x10 +3	$\propto_c$ Cut-Off Wave Number	C/V_c Non-dimensional Wave speed	$C^* = C/\sqrt{\tau_i/\rho}$ Non-dimensional Wave speed (W14) (Wurz)
298 (M=.72)	.063	1.0	49.2	.846	3420	25.0	1130	3.37	380	16.9	7.43	.245	69.5	847	.103	1.670	136.8	175.4
				.846	3420	25.0	1130	"	"	"	7.43	.245	69.5	"	"	"	136.8	175.4
				1.00	1140	23.9	1330	"	"	"	6.28	.207	23.2	"	"	"	47.7	58.8
				.923	3420	24.4	1230	"	"	"	6.81	.224	69.5	"	"	"	140.2	175.4
				.769	1370	25.7	1020	"	"	"	8.17	.269	27.9	"	"	"	53.3	70.3
	.104	1.2	68.3	1.46	1710	22.6	1950	4.07	430	28.1	4.30	.170	25.0	1960	.046	2.316	75.7	82.5
				1.15	1370	23.2	1530	"	"	"	5.46	.216	20.1	"	"	"	59.1	66.1
				1.15	1370	23.2	1530	"	"	"	5.46	.216	20.1	"	"	"	59.1	66.1
				1.31	1710	22.8	1750	"	"	"	4.80	.190	25.0	"	"	"	75.0	82.5
				1.15	1710	23.2	1530	"	"	"	5.46	.216	20.1	"	"	"	73.7	82.5
				1.08	1370	23.5	1440	"	"	"	5.82	.230	20.1	"	"	"	58.3	66.1
				.769	1370	25.7	1020	"	"	"	8.17	.323	20.1	"	"	"	53.3	66.1
				.846	1370	25.0	1130	"	"	"	7.43	.294	20.1	"	"	"	54.8	66.1
				.846	1370	25.0	1130	"	"	"	7.43	.294	20.1	"	"	"	54.8	66.1
				1.15	1710	23.2	1530	"	"	"	5.46	.216	25.0	"	"	"	73.7	82.5

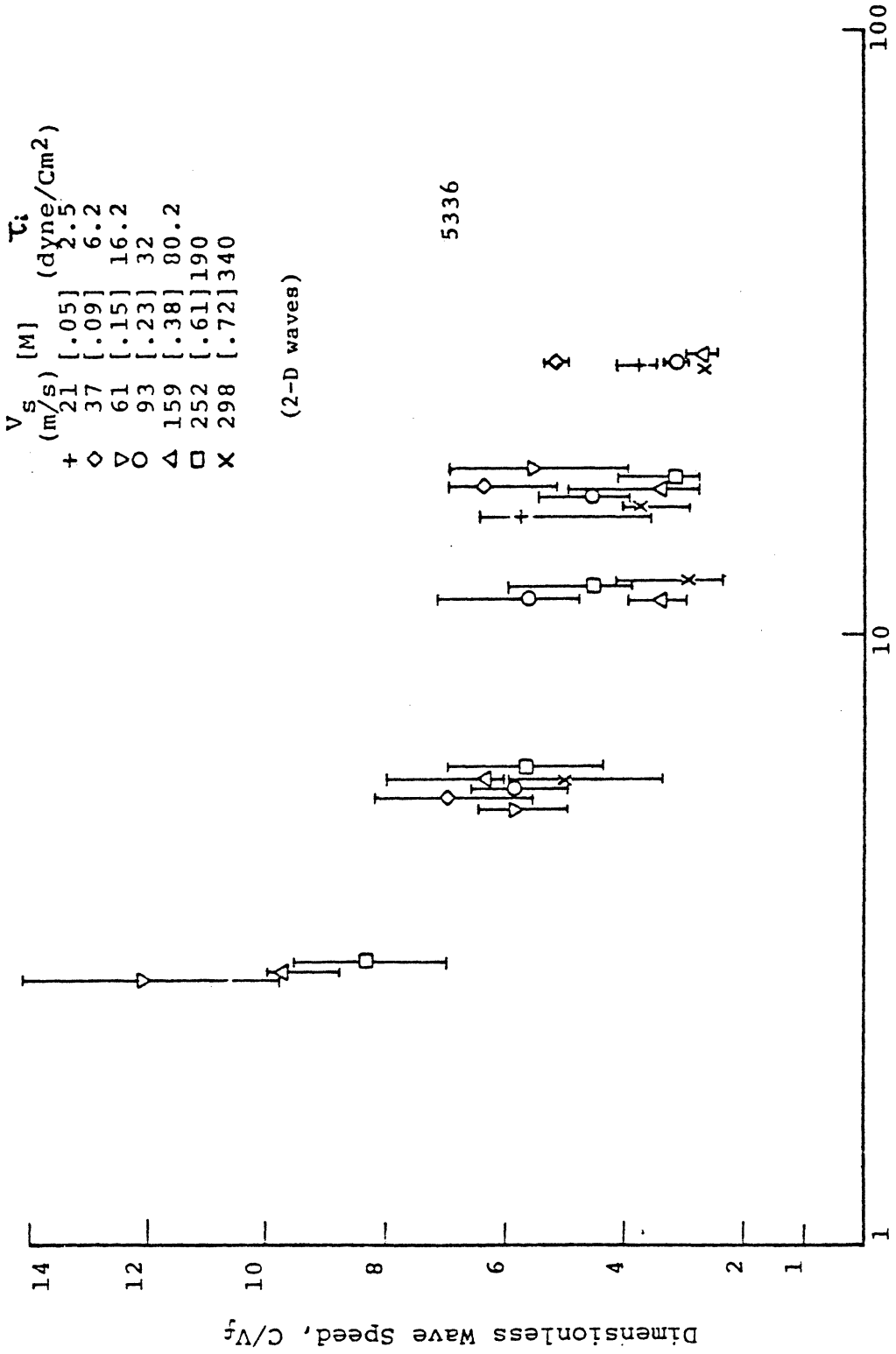

Fig. 4.17 Dimensionless Wave Speed vs Film Reynolds No. (2_{-D} waves)

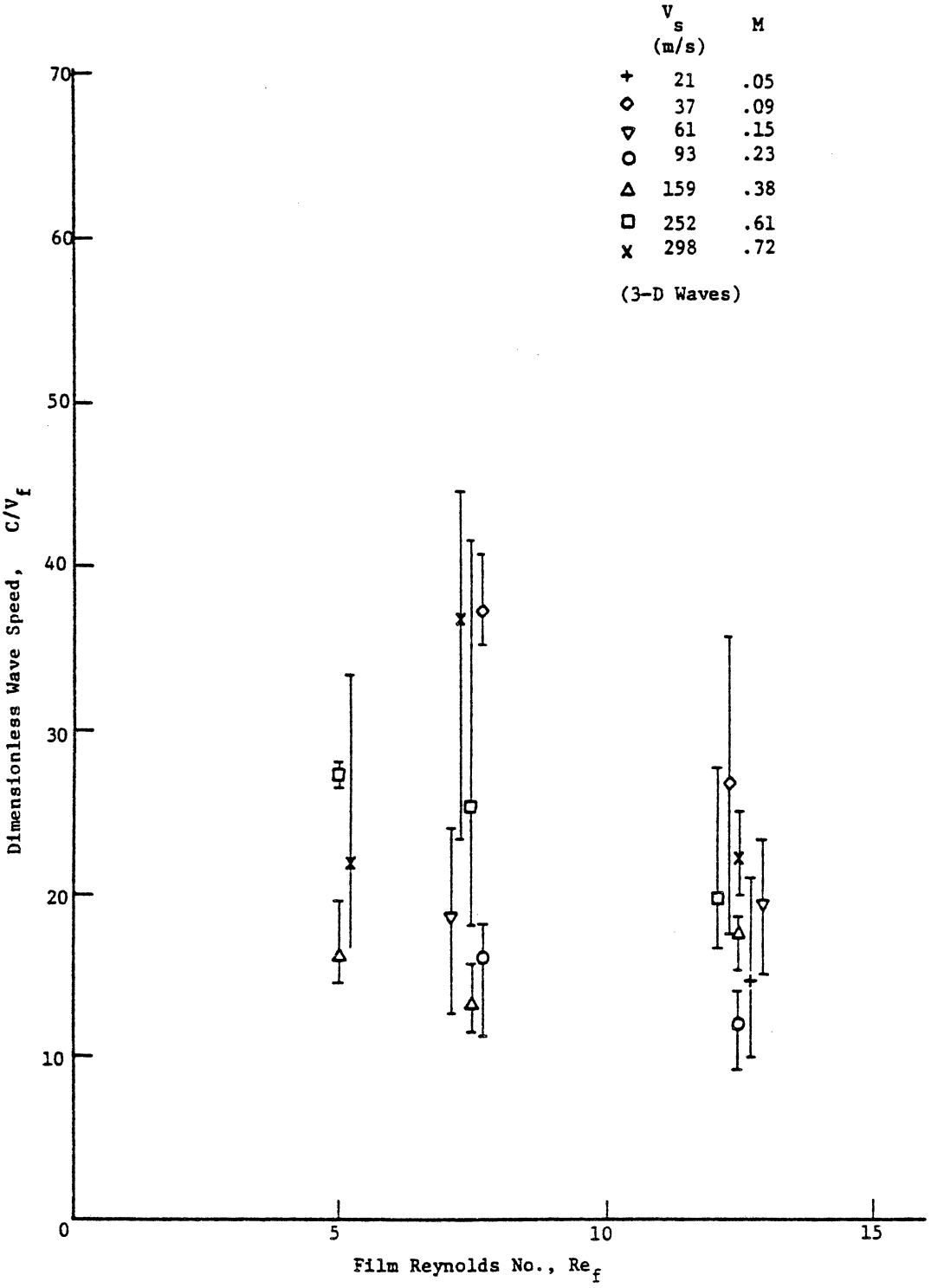

Fig. 4.18 Dimensionless Wave Speed vs Film Reynolds No. (3-D waves)

Thus only a very weak coupling to this type is possible.

The mechanism responsible for wave generation in thick film liquid flows (author's case is thin film) is understood as follows. Disturbance in the steam velocity field caused by the waves creates pressure and shear variations over the wavy surface. These transfer energy from the steam to the liquid film. If the rate at which energy is transmitted to the waves by these mechanisms is not larger than the rate of viscous dissipation in the liquid, the waves will decay.

In thick film cases, shear perturbations are very small compared to pressure perturbations.[C7,C10] Therefore, the contribution of the shear perturbation as an instability factor can be neglected. Based upon the pressure perturbation mechanism alone, Cohen-Hanratty,[C7] Nachtsheim,[N6] and Nayfeh-Saric[N3] formulated stability analyses for thick liquid films below a horizontal cocurrent gas flow.

To evaluate the pressure perturbation magnitudes, Cohen-Hanratty used the Jeffreys[J2] and Miles[M6] models. One of the important findings of the Cohen-Hanratty analysis is that viscous dissipation at the interface is predominant for short wavelengths (compared to their height), while viscous dissipation at the solid wall is important for long waves.

Because of their interest in a transpiration cooling system for missile nose-cones, the Nachtsheim and Nayfeh-Saric analyses were focused on highly supersonic gas flows over relatively thick liquid films. Their linear analyses neglected shear perturbations, and derived the rate of wave

growth and wave propagation velocity in terms of body force, surface tension and pressure perturbations. As normally expected they conclude that while surface tension is stabilizing, pressure perturbations are destabilizing, and body force can be either, depending on its direction (downward is stabilizing). They also found that films adjacent to supersonic streams are more unstable than those adjacent to subsonic streams.

In later non-linear analyses, Nayfeh-Saric[N4,N5] and Saric-Nayfeh-LeKoudis[S3] modified these conclusions. According to their non-linear theory,[N4,N5] linear unstable disturbancies do not grow indefinitely, but achieve steady-state amplitudes in the supersonic case, provided disturbance layer is larger than the subsonic layer.

For very thin films, a quite different stability mechanism was suggested by Craik[C10]. According to his analysis, small wave-like disturbances become unstable when the normal stress component in phase with the wave slope is sufficient to overcome the resistance to motion of the liquid surface due to gravity and surface tension. He also held that the destabilizing role of the tangential stress component became important for very thin films, and that instability may occur whatever the velocity of the gas stream is, provided the film is sufficiently thin. It is appropriate to examine the wave behavior in author's experiment using the Craik model.[C10] He assumed a two dimensional wave of the sinusoidal form, where $\alpha = k\,h =$

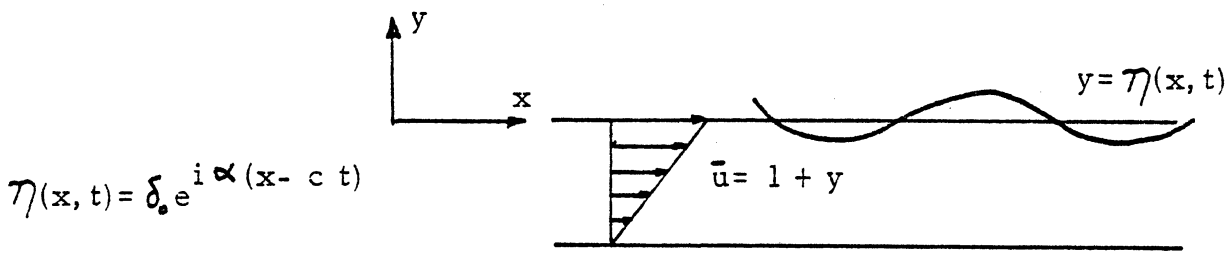

$\frac{2\pi}{\lambda}$ h is the (real) non-dimensional wave number and C is the non-dimensional wave velocity, which may be complex. The non dimensional wave amplitude δ_o was assumed to be sufficiently small for the problem to be linearized.

Using a perturbation stream function with the linearized Navier-Stokes equations, the Orr-Sommerfeld equation is obtained. This is a fourth-order differential equation for the perturbation stream function. To solve it Craik assumed a perturbation solution in powers of dimensionless wave number α. To specify the required 4 boundary conditions he used the Benjamin[B4] expressions for shear and pressure perturbation stresses at the wavy interface, together with no-slip, no-penetration conditions at the solid wall. In Benjamin's derivation for perturbation stresses over a wavy wall, it was assumed that the disturbances introduced into the gas flow by the waves do not interact with the turbulence in the gas.

Substituting a power solution for the perturbation stream function into the four boundary conditions, he obtained four homogeneous equations, whose determinant should vanish in order for the equations to be consistent.

Neglecting the higher order terms, he obtained,

$$T\alpha^2 + G - \Pi + \frac{3i\Sigma}{2\alpha} = (1-c)\left(\frac{3}{i\alpha Re_f} + \frac{6}{5}(1-c) - \frac{7}{8} + \frac{27}{5}\frac{2}{i Re_f} \right) \tag{4.26}$$

where

$T = \frac{\sigma}{\rho_f V_f^2 h}$ reciprocal Weber number

$G = \frac{g h}{V_f^2}$ reciprocal Froude number

$\alpha = k h = \frac{2\pi}{\lambda} h$ dimensionless wave number

$\Pi = \Pi_r + i\Pi_i$ pressure perturbation (Benjamin, 1959 (B4))

$\Sigma = \Sigma_r + i\Sigma_i$ shear perturbation (Benjamin, 1959 (B4))

$C = C_r + iC_i$ dimensionless wave speed normalized by film velocity, V

$Re_f = \frac{V_f h}{\nu_f}$ film Reynolds number

On separating the real and imaginary parts,

$$\frac{6}{5}(C_r-1)^2 + \frac{7}{8}(C_r-1) - (Ci/\alpha Re_f)(3+\frac{27}{5}\alpha^2+\frac{6}{5}\alpha Re_f C_i) = T\alpha^2 + G - \Pi_r - (3\Sigma_i/2\alpha) \quad (4.27)$$

$$C_i\left[\frac{12}{5}(C_r-1)+\frac{7}{8}\right] + \left[(C_r-1)/\alpha Re_f\right](3+\frac{27}{5}\alpha^2) = -\Pi_i(3\Sigma_r/2\alpha) \quad (4.28)$$

From Eqs. (4.27) and (4.28), the rate of wave amplification $\alpha C_i Re_f$ and wave velocity, C_r, can be found.

$$\alpha C_i Re_f = \frac{(\alpha Re_f)^2}{3}(\Pi_r + \frac{3}{2}\frac{\Sigma_i}{\alpha} - T\alpha^2 - G) \quad (4.29)$$

$$C_r - 1 = \frac{-\frac{7}{8}(\alpha C_i Re_f) - \alpha Re_f \Pi_i + \frac{3}{2} Re_f \Sigma_r}{3 + \frac{27}{5}\alpha^2 + \frac{12}{5}\alpha C_i Re_f} \quad (4.30)$$

It is seen from Eq. (4.29) that instability occurs when

$$\Pi_r + \frac{3}{2}\frac{\Sigma_i}{\alpha} > T\alpha^2 + G$$

i.e. when the effect of the surface stresses is sufficient to overcome the restoring forces of surface tension and

gravity. Although the pressure perturbation component Π_r is generally much greater than the shear perturbation component Σ_i, the effect of the variable shear stress cannot be neglected when α is small. The term in Σ_i becomes dominant for sufficiently thin films. Because of this, instability is more likely to occur for sufficiently thin films. The present author defines this as the "shear perturbation mechanism". These results are in good qualitative agreement with the author's experimental observations reported in section 4 of Chapter IV, that waves always exist over the entire range of the experiment including even the rivulet film flow regime.

One can explain this wave formation mechanism in the following way:

The component of normal stress, Π_r, is in phase with the wave displacement, and it attempts to deform the liquid surface by exerting an upward force upon the crests and a downward force upon the troughs of small periodic disturbances. Also, the tangential stress component, Σ_i, is in phase with the wave slope, and it has the effect of accelerating the liquid on the windward slopes while retarding that on the leeward slopes. This mechanism tends to displace liquid toward the crests and away from the troughs of existing wavelets, thereby increasing their amplitude. The thinner the mean film compared to the wave amplitudes, the more effective is this mechanism . Thus it should be highly effective in author's case.

Compared with the pressure perturbation instability mechanism for thicker films, the shear perturbation mechanism is a entirely different one from the pressure perturbation mechanism.

In the pressure perturbation mechanism instability is caused by an irreversible energy transfer from the vapor flow to the disturbance through the stress components represented by Π_i and Σ_r. The flow becomes unstable when film viscous dissipation is less than energy input. This energy transfer takes place through non-conservative forces, provided by the normal stress component in phase with the wave slope, and the tangential stress component in phase with the wave displacement (articles 348-350 in Lamb's "Hydrodynamics" [L6]). However, the stress components causing the instability in the shear perturbation mechanism are Π_r and Σ_i (Appendix B) both of which act conservatively on the wave.

The disturbance growth rate $\propto C_i R$, calculated from Eq. (4.29), is shown in Fig. 4.19 . It is essentially a frequency-response curve for infinitesimal initial conditions. Very large wave number disturbances (greater than the critical wave number, α_c) remain stable because of the dominant effect of surface tension. The smaller wave number disturbances are unstable because of the controlling effect of the tangential and normal perturbation stresses.

A precise estimate of perturbation stresses is essential. Author's calculations of the normal (Π), and tangential (Σ)

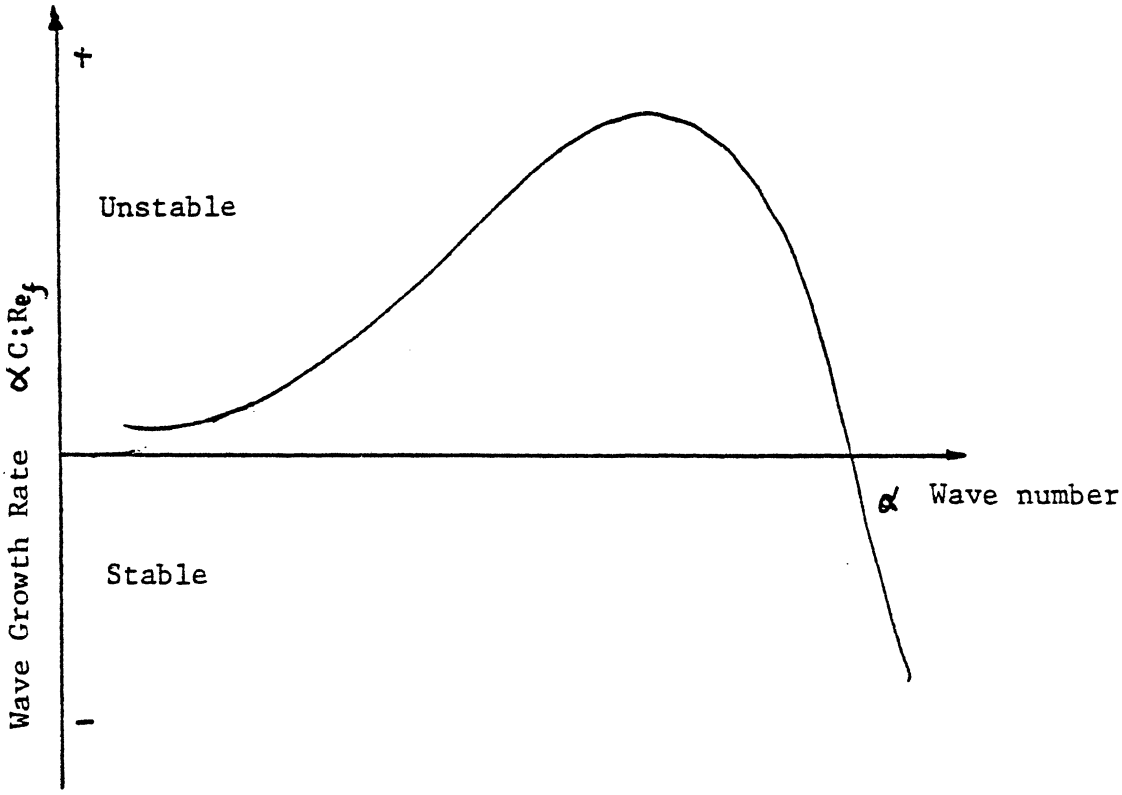

Fig. 4.19 Disturbance Wave Growth Rate as a Function of Wave Number

perturbation stresses based on Benjamin's [B4] analysis, with listing of related computer programs, are given in Appendix B.

Figure 4.20 compares author's observed wave numbers with the critical wave numbers calcualted from Eq . (4.29). Since the analysis is based on a linear small perturbation theory, it is applicable only to the small two-dimensional wave regime.

Most of the observed wave numbers for high steam velocity are smaller than the calculated critical wave numbers, and hence are in the unstable region, (Fig. 4.20).

However, the observed wave numbers for low steam velocities (21 and 37 m/s) are either larger than, or in the range of, the calculated critical values. These are in the relatively stable region indicated in Fig. 4.19. Comparing with the flow regimes in author's "map" (Fig. 4.2), most of the measured wave numbers are in the unstable region. Obviously there are inherent uncertainties in calculating the critical wave numbers. First the analysis is based on a small perturbation linear analysis and a "universal" turbulent steam velocity profile. Second the estimate of interfacial shear (see Section B, Chapter IV)may involve errors. Nevertheless, the results of Fig. 4.20 seem reasonably acceptable for such a highly complex problem.

E. FILM ENTRAINMENT

For very large waves, as already mentioned, entrainment from the wave crests occurs. Good understanding of all

Fig. 4.20 Comparison of Measured Wave Number, α with Analytic Critical Wave Number (C10), α_c (2-D wave)

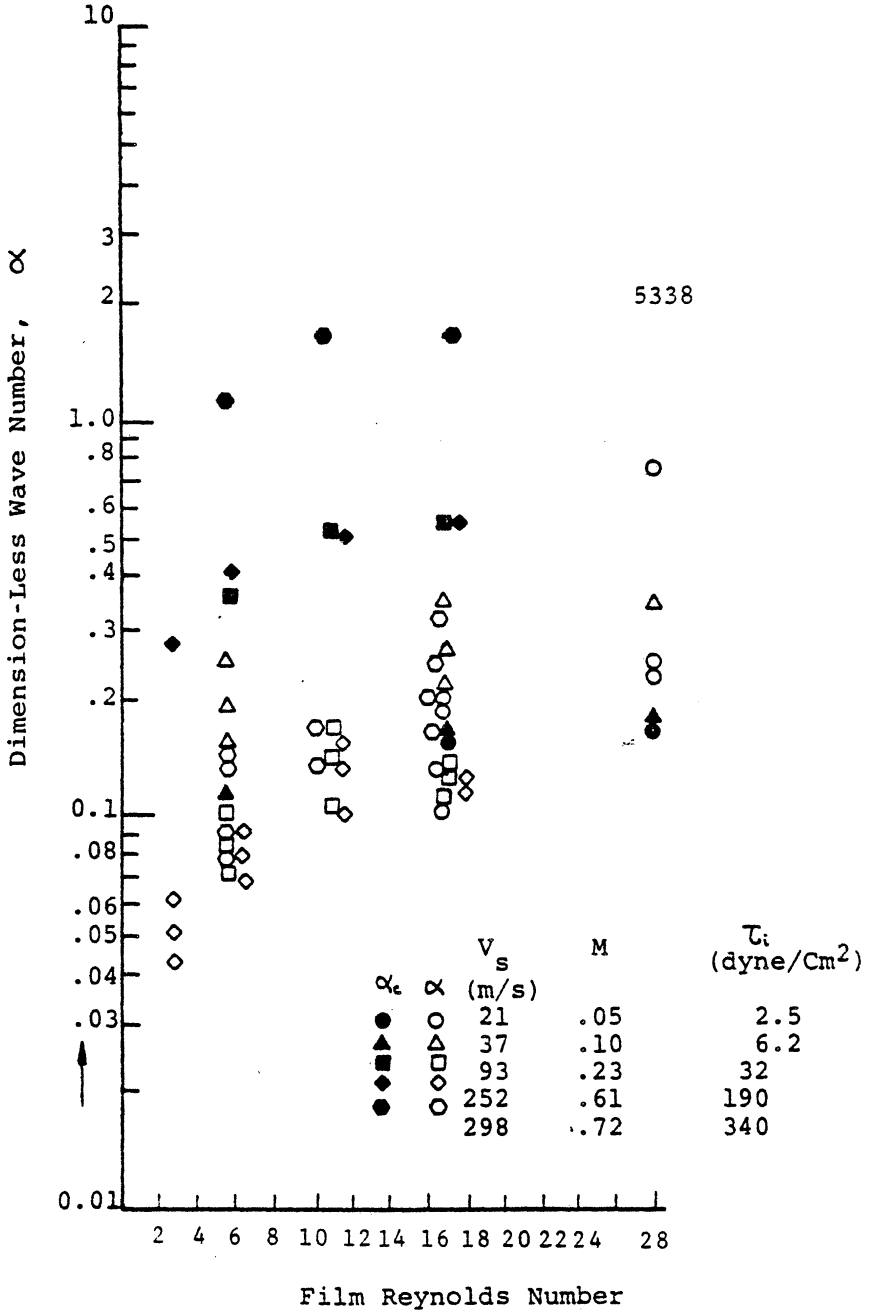

pertinent liquid entrainment mechanisms is important for both steam turbine blade erosion and moisture performance effects, as well as numerous other applications. These include annular duct flows important in many chemical process applications. Thus the critical condition for the onset of such entrainment has been studied by many researchers in both vertical[S4,G7,G8] and horizontal ducts.[V2,W1]

VISUAL OBSERVATION

Plates #5.4 to 5.7 and 6.4 to 6.7 of Fig. 4.1 reveal such liquid film entrainment. The interfacial structure is characterized by a series of liquid flow surges, i.e. large waves. The surface becomes then highly agitated, with sudden increases in liquid film thickness. Imposed on this main wave structure are complex smaller wavelets resulting from a chaotic tumbling at the wave front, like an ocean breaker. The entrained liquid droplets usually appear frothy (i.e., not well-defined). Sometimes several clear large droplets are seen together.

Author's high speed motion pictures show some features of the surface entrainment mechanisms. They include "splashing" of the liquid interface, after the impingement of a large liquid droplet. Most of the surface droplet entrainment, however, was observed to occur following rapid acceleration, lifting, and then shattering of small complex ripples present at the top of large waves. The bursting of air bubbles trapped in the liquid, as suggested by other researchers,[B7,N7,W14] was not observed here.

In author's "map" (Fig. 4.2), the transition between wavy-film and entrainment regimes is shown. As liquid flow rate decreases, the steam velocity for surface entrainment increases. For high steam velocities, or for thin films, a limiting behavior was observed for which the critical conditions are insensitive to changes in steam velocity, i.e., there is a limiting liquid flow rate below which no surface entrainment occurs ($\sim$0.07 cm^3/sec cm).

Similarly, a minimum steam velocity for entrainment even for large liquid flow rates is expected. However, it was not possible to test this possibility due to facility limitations on minimum steam velocity.

COMPARISON WITH OTHER RESULTS

Author's critical steam velocity criterion for surface entrainment is compared to other results in Fig. 4.21. There are numerous studies concerning such entrainment inception for two-phase annular flow in vertical pipes (Z2,S4,C18,U1). Much less experimental data is available for horizontal channels. It is of course necessary that experiments be reasonably similar for meaningful comparison. The channel heights of Van Rossum (V2) and Woodmansee-Hanratty (W2) were 10 cm and 2.5 cm respectively, while author's is 4 cm. Thus they are of the same general magnitude. The ratio of liquid film thickness to channel height has an important effect on critical gas phase velocity for entrainment. However, for relatively very thin films, as in author's case, precise value of this ratio becomes less important. The

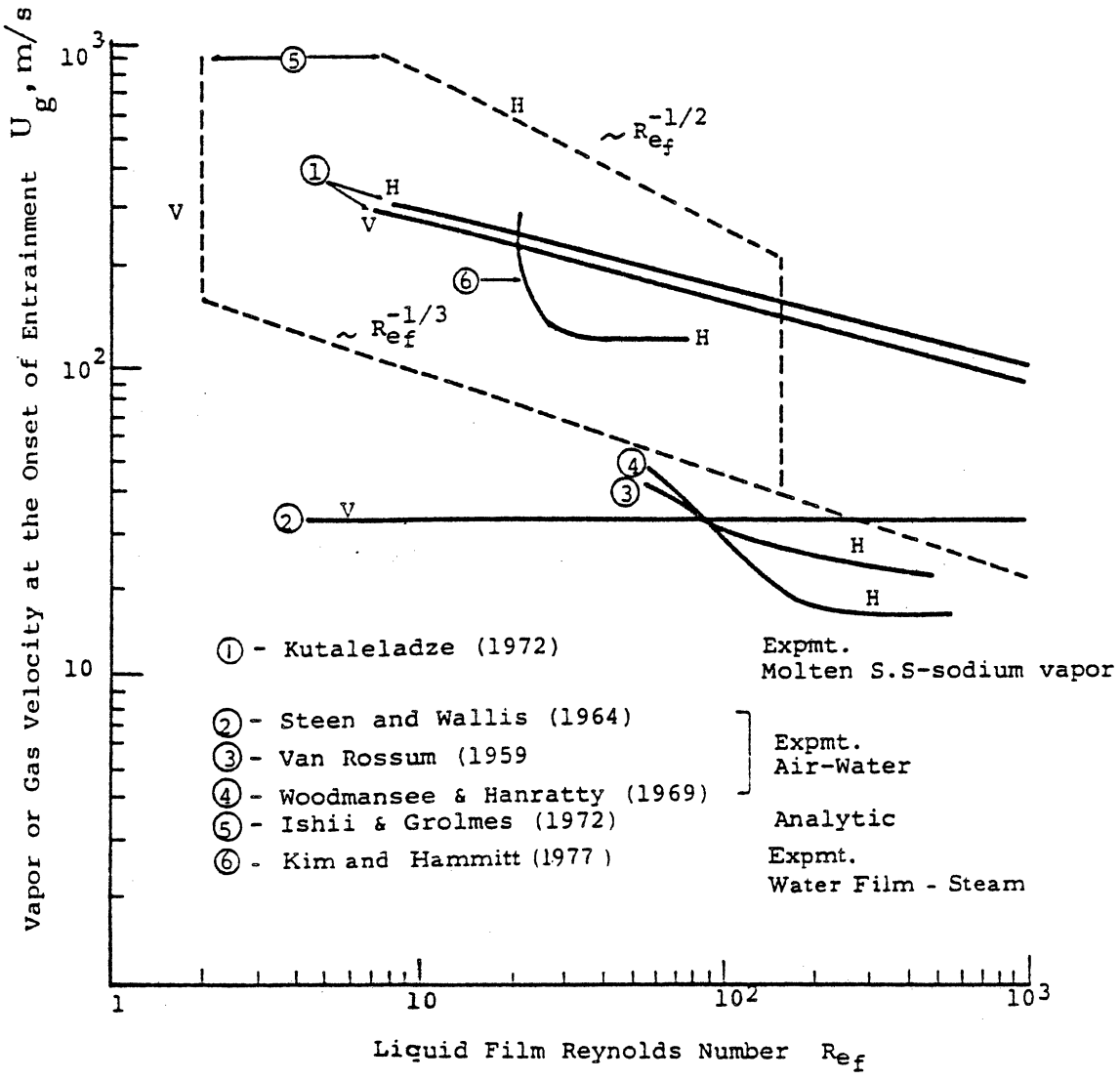

Fig. 4.21 Comparison of Various Entrainment Inception Criteria

U_g vs Re_f

experimental data ③ (V2) and ④ (W2) in Fig. 4.21 can thus be properly compared with author's results 6 for which the critical steam velocity is much higher.

Except for Zhivaikin (Z2) ①, (using sodium vapor and molten stainless-steel) and the author ⑥, fluids were air and water. The analytical correlation ⑤ (I2) is discussed in the next section. The air-water experiments ② (S4) for annular upward pipe flow indicate that the entrainment air velocity is constant with liquid flow rate. The cause for this discrepancy with horizontal geometry results is unknown.

ENTRAINMENT MECHANISMS

Wicks and Duckler (W5) proposed an empirical entrainment correlation for upward vertical annular flow as observed by Collier and Hewitt. (C15) Hughmark (H6) proposed a completely empirical correlation based on the experiments of various other researchers. (C15,A3,C18)

More recently, a theoretical correlation was proposed by Ishii and Grolmes. (I2) Based on Zuber's analysis, (Z3) they analyzed a smooth roll-wave geometry with an internal flow in the roll-wave crest. They then assumed that interfacial shear stresses at the wave crests induce a velocity within the wave of the same general magnitude as the film velocity, with a linear velocity profile within the wave-crest. To express the roll wave amplitude, they used a modified Hughmark (H6) correlation for the friction coefficient, and concluded that the critical non-dimensional gas velocity for entrainment was proportional to $Re_f^{-1/3}$ for a relatively

thick film ($Re_f > 160$).

For low film Reynolds number, based on assumed similarity between droplet disintegration (critical droplet Weber number[H15] concept) and liquid film entrainment, they derived an expression showing that critical non-dimensional gas velocity is proportional to $Re_f^{-1/2}$.

As discussed in Section IV-D, the shear perturbation instability predominates for very thin films. However, the analysis applies for wave generation inception rather than film entrainment. Author observed entrainment to occur from the wave crests, i.e., from the thickest part of the liquid film. Therefore, the pressure-perturbation mechanism, important for thick films, is here the most probable entrainment mechanism.

From author's photographic studies, the crests of the large waves, when entrainment is observed, are usually not smooth, but composed of many small wavelets. Thus Ishii and Grolmes'[I2] assumption of smooth wave crests and linear velocity profiles within the waves is questionable.

In any studies of critical conditions, it can be concluded that film entrainment will occur whenever the destabilizing components of hydrodynamic forces applied to the surface (pressure and shear) are not balanced by the stabilizing components, such as primarily surface tension and gravity. A completely comprehensive analysis is unfortunately not yet available, and probably impossible in the present state of the art.

Figure 4.22 is a schematic of wave profiles before entrainment commences. For large wave amplitudes, the steam streamline network around the waves is contracted, so that a pressure reduction at the wave crests will occur. This negative pressure differential, P_k, at the crest is proportional to $\rho_s(U_s-C)^2$. P_k should also increase, in general, with increasing wave amplitude, A, (due to increased streamline curvature), and decrease with increasing wave length, λ. Then for correlation purposes, it might be assumed that A and λ effects are linear. Then:

$$P_k \propto \rho_s (U_s-C)^2 \left(\frac{A}{\lambda}\right) \tag{4.31}$$

where U_s is the average vapor velocity, C wave propagation velocity, A amplitude and λ wave-length. The surface tension stress, P_s can be expressed as

$$P_s \propto \frac{\sigma}{\lambda} \left(\frac{A}{\lambda}\right) \tag{4.32}$$

where σ is surface tension. In cases with high velocities and thin films (such as authors), the gravity term is negligible compared to P_s, if λ is small.

Following these arguments, entrainment should occur whenever,

$$P_k \gtrsim P_s$$

or

$$\frac{\rho_s (U_s - c)^2}{\sigma} \gtrsim \text{const} \tag{4.33}$$

According to this model the critical condition is affected by steam or liquid viscosity only, as they affect wavelength, λ. Author's observations and others[Z4,M11]

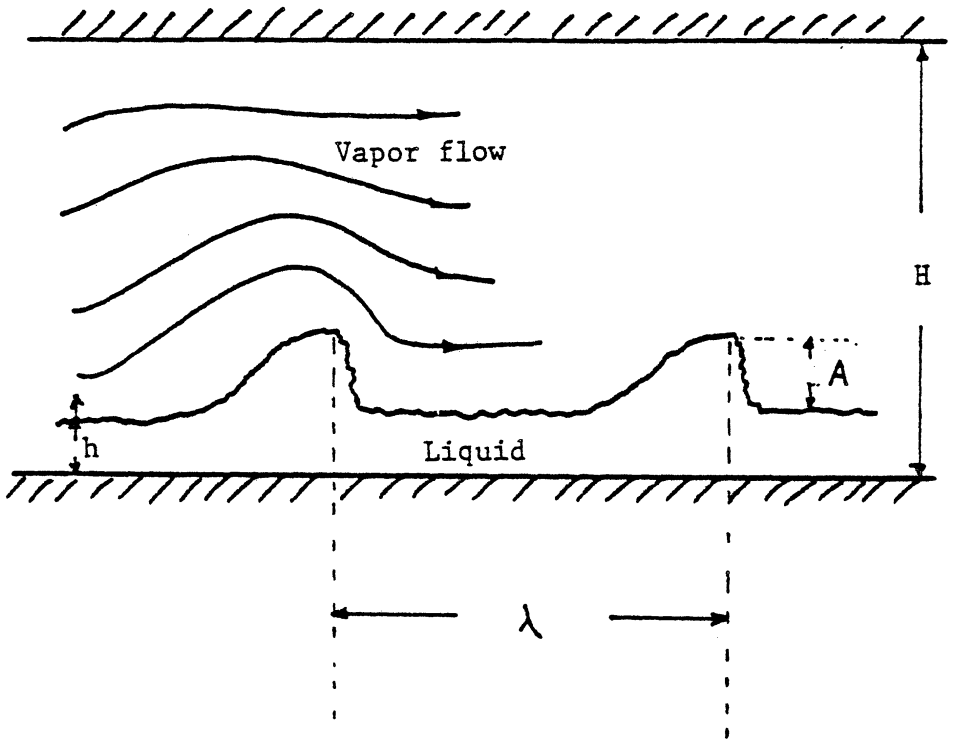

h : mean film thickness

λ : wave length

a : wave amplitude

H : channel height

Fig. 4.22 Schematic of 3-D Wave Formation in Entrainment Regime

show that λ is a strong function of film thickness, h. Due to viscous damping at the solid plate, the wavelength λ, cannot be sustained, if it is too long compared to the film thickness, h. Assuming that approximately, $\lambda \propto h$, Eq. (4.33) becomes

$$\frac{\rho_s (U_s-C)^2 h}{\sigma} \gtrsim K \qquad (4.34)$$

Combining Eq. (4.17) for h with Eq. (4.34), a critical non-dimensional relationship is obtained:

$$(U_s-C) \frac{\mu_f}{\sigma} \sqrt{\frac{\rho_s}{\rho_f}} \gtrsim \frac{K}{0.6} \sqrt{\frac{f_i}{2}} \, Re_f^{-1/2} \qquad (4.35)$$

where f_i is friction factor.

The constant in Eq. (4.34) is similar to a critical Weber number for film entrainment.[V2,W2] Two different critical Weber numbers were defined, i.e., We_h based on average film thickness h, and We_p based on the maximum wave height h_p. Data from Van Rossum[V2] and Woodmansee-Hanratty[W2] together with author's results are listed in Table 4.8. Their critical Weber number, We_h, are of the same order as author's. The critical air velocities found by Van Rossum and Woodmansee-Hanratty , however, are much less than the critical steam velocities of present author, while their Re_f values are much higher. From Van Rossum,[V2] the maximum limiting critical Weber number was found to be 17. This is not comparable, for causes unknown, to either W-H[W2] data or author's.

The critical Weber numbers, We_h, for entrainment agree

reasonably well in all cases, in spite of the use of different gases and geometries.

Using an average K = 2.5 (Table 4.8) friction coefficient f_i = 0.005 (Table 4.2 and Ref. W8), the critical condition of Eq. (4.35) becomes

$$(U_s - C)\frac{\mu_f}{\sigma}\sqrt{\frac{\rho_s}{\rho_f}} \gtrsim 0.21\ Re_f^{-1/2} \qquad (4.36)$$

Although the wave propagation velocity C is relatively variable, it is always much smaller than steam velocity, U_s (Table 4.7). Therefore, the steam velocity U_s itself is used rather than the relative steam velocity, U_s-C, in calculating the critical non-dimensional gas phase velocities. Eq. (4.36) then becomes

$$U_s \frac{\mu_f}{\sigma}\sqrt{\frac{\rho_s}{\rho_f}} \gtrsim 0.21\ Re_f^{-1/2} \qquad (4.37)$$

This relation is plotted in Fig. 4.23 . For given Re_f, author's critical non-dimensional steam velocity is much smaller than that predicted from Ishii-Grolmes[I2] shown as ⑤ in Fig. 4.23 . Their results are primarily for data from vertical pipe flows, with little data for horizontal flows. They based their analysis on the similarity between droplet disintegration (i.e., critical Weber number We_h = 22 from Hinze's[H15]) and film entrainment in this Re_f range.

Therefore, the critical gas velocity for entrainment in Eq. 4.37) is appropriate for the horizontal duct data (curve ③, ④, ⑥ in Fig. 4.23). However, a comparison of the measured critical data and predictions based on the proposed

U (m/s)	Re_f	We_h	We_p	
45	68	3.7	-	
38	69	2.9	-	
30	83	2.1	-	Woodmansee
27	89	1.9	-	& Hanratty
24	99	1.7	5.5	(1969)
21	117	1.5	5.3	
12	305	1.1	5.5	
8	2065	1.8	4.6	
2	82	6	-	
2.5	78	3.8	-	Van Rossum
3.0	60	3.0	-	(1959)
above 25	below 20	17.0	-	
66	52	-	-	
93.3	34	-	-	W. Kim
159	28	2.12	-	& F.G. Hammitt
252	22	1.52	8.2	(1977)
298	17	3.38	15.2	

$$W_h = \frac{\rho_s (U_s - c)^2 h}{\sigma}$$

$$W_p = \frac{\rho_s (U_s - c)^2 h_p}{\sigma}$$

$$Re_f = \frac{2q}{\nu_f}$$

Table 4.8 COMPARISON OF CRITICAL WEBER NUMBER FOR ENTRAINMENT OR ROLLWAVE FORMATION

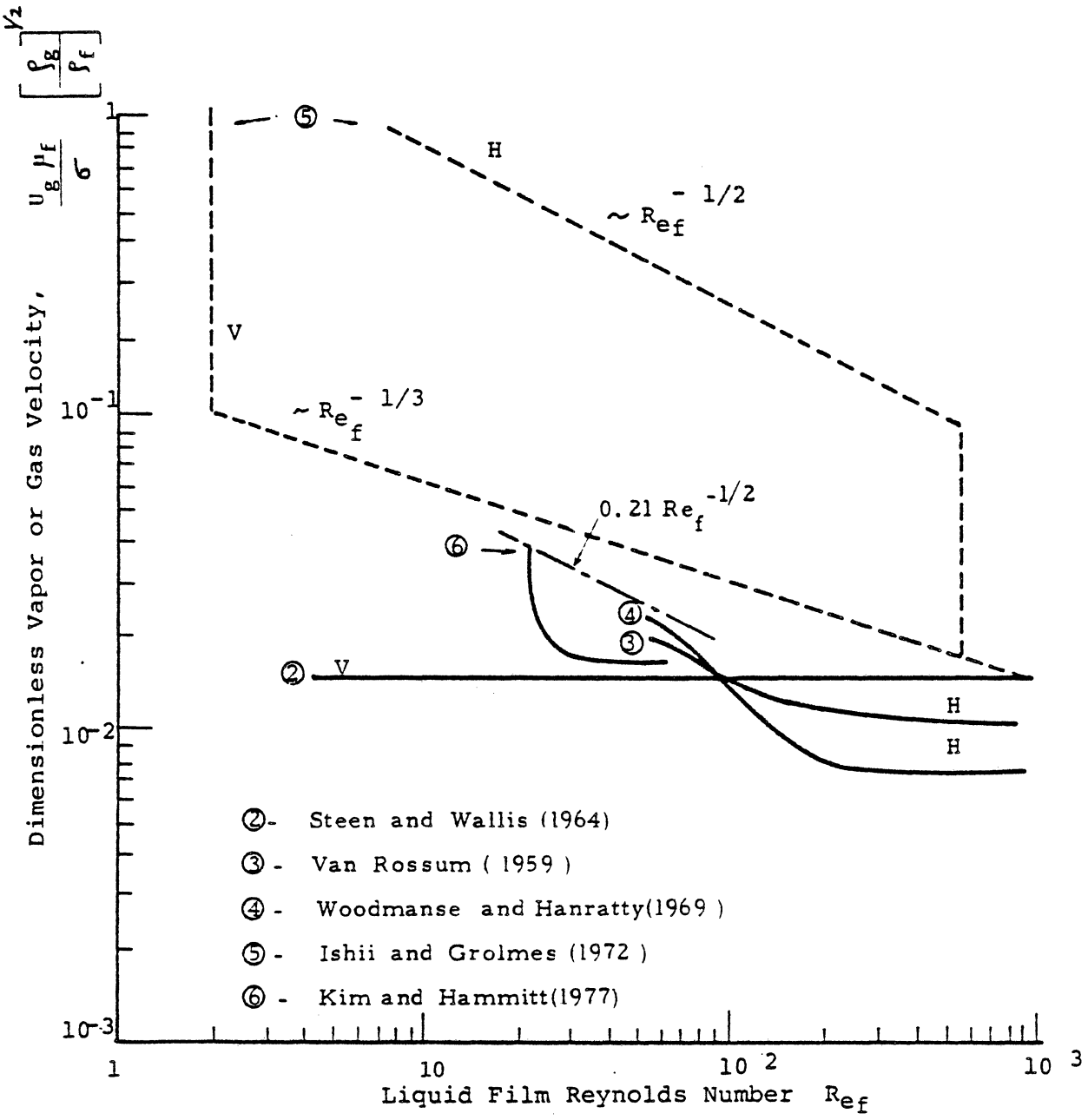

Fig. 4.23 Comparison of Various Entrainment Inception Criteria $\frac{U_g \mu_f}{\sigma}\left[\frac{\rho_g}{\rho_f}\right]^{1/2}$ vs Re_f

mechanism is limited not only by the lack of detailed information on the large wave shape, but also by an inability to adequately calculate the pressure variations over waves of arbitrary shape and size.

CHAPTER V

FORMATION OF LIQUID FINGERS AND SECONDARY DROPLETS

The characteristics of the liquid phase motion in the wake behind the trailing edge are very important from the erosion viewpoint, since the upper size limits and velocities of droplets reaching downstream rotor blades are directly influenced. Such information is crucial for the prediction of droplet impact blading erosion rates.

Liquid shed from the stator blades enters a highly complex flow region. Author's high-speed motion pictures of the blade wake region show a region of liquid "fingers." These grow relatively slowly, but extend deep into the wake before disintegrating into droplets, which then are rapidly accelerated by the high-velocity steam. Larger droplets then rapidly become unstable, disintegrating into a spray of much finer droplets. These processes are obviously closely involved with the blade erosion problem.

A. CHARACTERISTICS OF FINGER FORMATION

1. Visual Observations

Still photographs (Fig. 5.1) show typical finger shapes, as well as droplet distributions down stream of the finger region. Stream conditions and liquid flow rates, as well as location of each photograph, are listed in Table 5.1. The two concentric circles in some of the photos indicate a pressure tap in the far wall of the test section. The diameter of the inner circle(0.95 cm) provides a useful scale, since the lens focal length is long compared to the test section

Table 5.1: FLOW CONDITIONS AND LOCATION OF LEFT END OF EACH PHOTOGRAPHS FOR FIGURE 5.1

Plate No	Steam Velocity U_s, m/s	Mach No	Liquid Flow Rate q $cm^3/s.cm$	Location of Left End of each Photo X, cm	Features
P1.1	144	0.35	0.043	0	Bubbly Fingers
P1.2	144	0.35	0.043	0	Wide Base Fingers
P1.3	144	0.35	0.043	5	Disc Shape Droplet
P1.4	144	0.35	0.043	10	Large Droplet
P2.1	227	0.55	0.043	0	Finger and Droplet Shed
P2.2	227	0.55	0.043	0	Finger and Droplet Shed
P2.3	227	0.55	0.043	5	Disc Shape Droplet
P2.4	227	0.55	0.043	10	Small Droplet
P3.1	309	0.75	0.043	0	Liquid Sheet And Fingers
P3.2	309	0.75	0.043	0	Finger
P3.3	309	0.75	0.043	5	Cluster of Droplet
P3.4	309	0.75	0.043	10	Droplet
P4.1	144	0.35	0.083	0	Complicated Fingers
P4.2	144	0.35	0.083	0	Fingers
P4.3	144	0.35	0.083	5	Clear Droplet
P4.4	144	0.35	0.083	10	Droplet
P5.1	227	0.55	0.083	0	Fingers
P5.2	227	0.55	0.083	0	Finger and Sheet
P5.3	227	0.55	0.083	5	Droplet
P5.4	227	0.55	0.083	10	Droplet
P6.1	309	0.75	0.083	0	Liquid Sheet with Holes
P6.2	309	0.75	0.083	0	Finger and Sheet
P6.3	309	0.75	0.083	5	Droplet
P6.4	309	0.75	0.083	10	Droplet
P7.1	144	0.35	0.167	0	Fingers
P7.2	144	0.35	0.167	0	Fingers
P7.3	144	0.35	0.167	5	Large Droplet
P7.4	144	0.35	0.167	10	Droplet
P8.1	227	0.55	0.167	0	Finger and Sheet

Table 5.1: cont'd

Plate No	Steam Velocity U_s, m/s	Mach No	Liquid Flow Rate q $cm^3/s.cm$	Location of Left End of each Photo X, cm	Features
P8.2	227	0.55	0.167	0	Finger and Sheet
P8.3	227	0.55	0.167	5	Droplet
P8.4	227	0.55	0.167	10	Droplet
P9.1	309	0.75	0.167	0	Sheet and Fingers Disc Droplet
P9.2	309	0.75	0.167	0	S heet and Fingers
P9.3	309	0.75	0.167	5	Cluster of Droplets
P9.4	309	0.75	0.167	10	Droplets

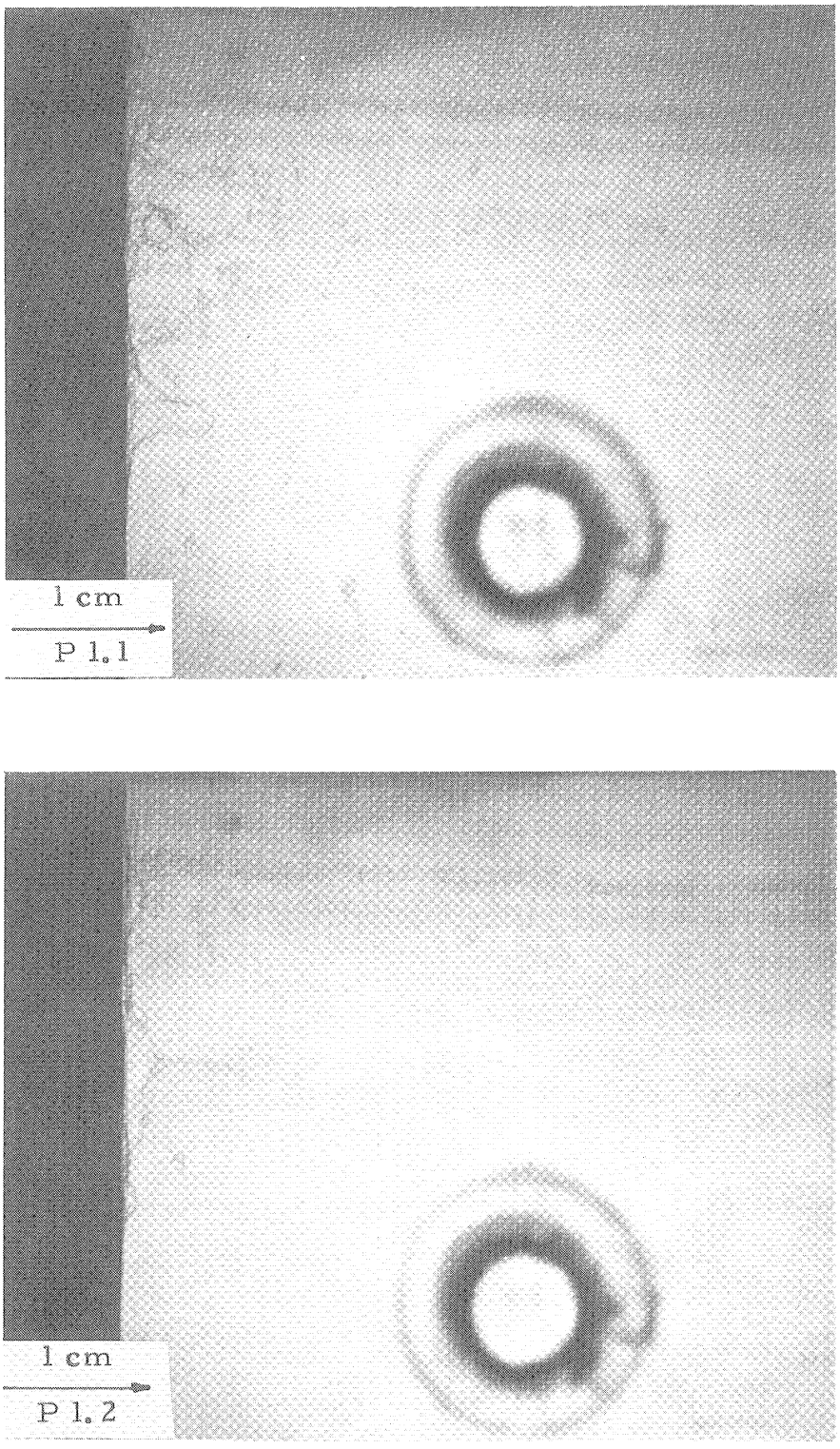

Fig. 5.1 Phtographs of Finger Formation and Secondary Droplet Formation

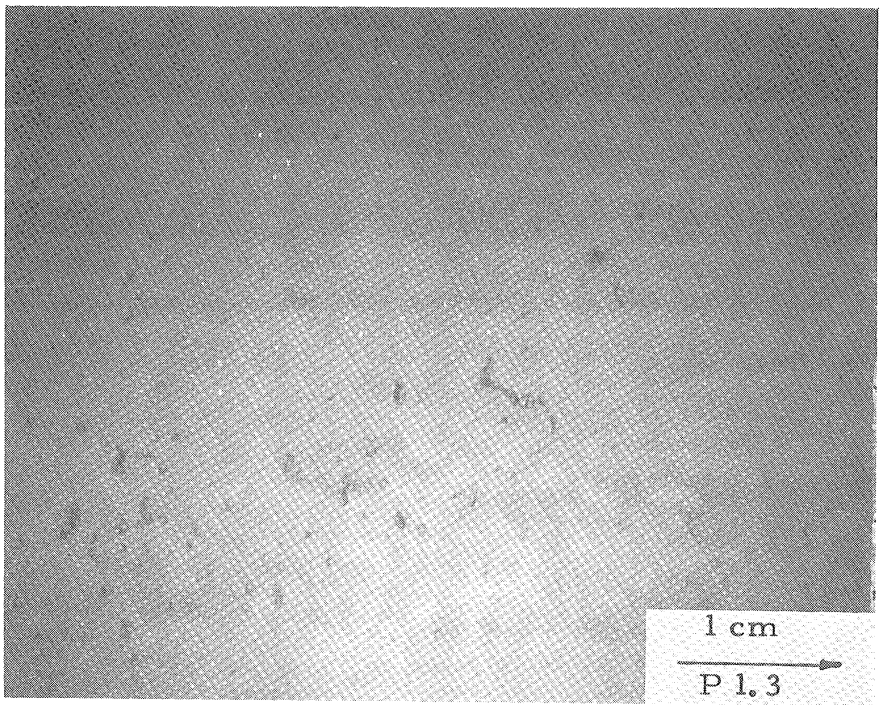

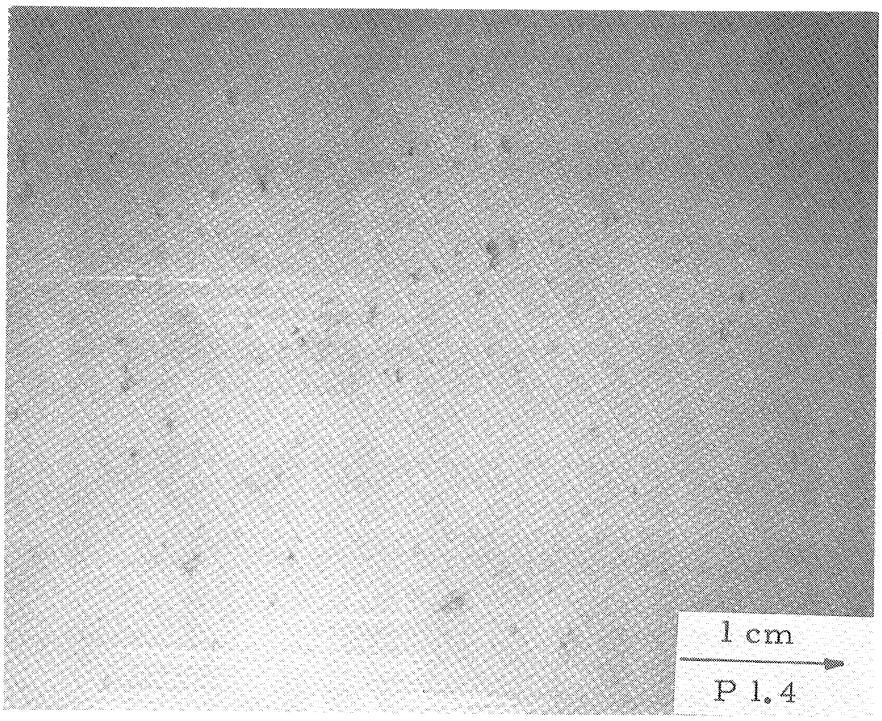

Fig. 5.1 Continued 5400

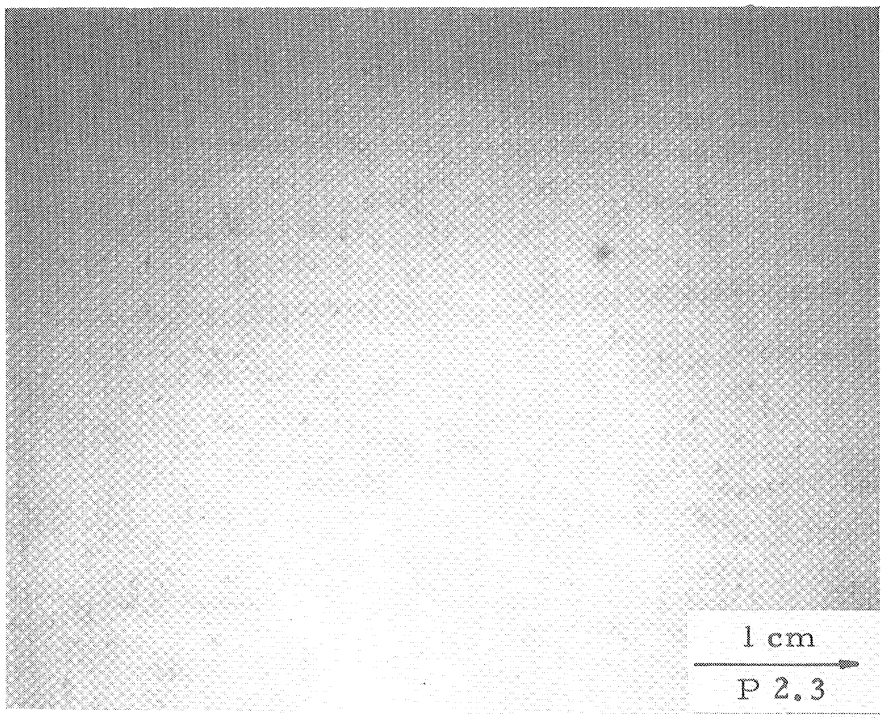

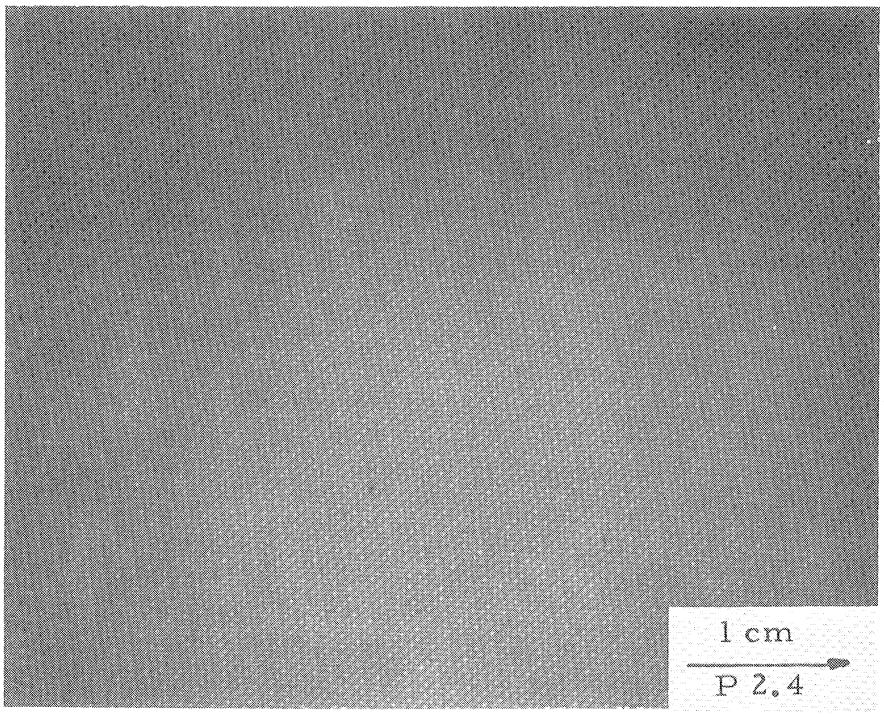

Fig. 5.1 Continued 5401

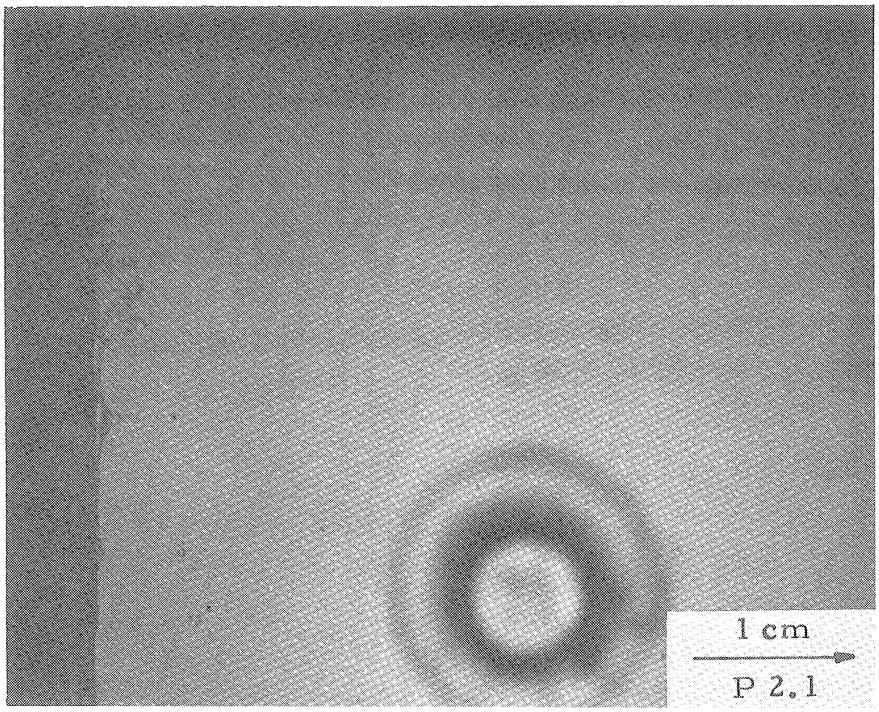

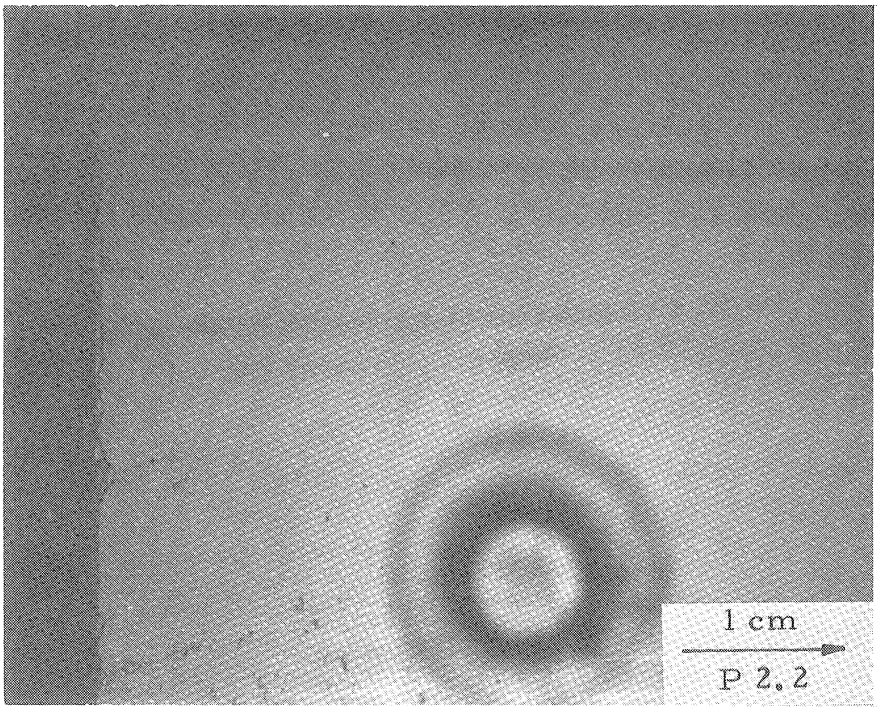

Fig. 5.1 Continued

5402

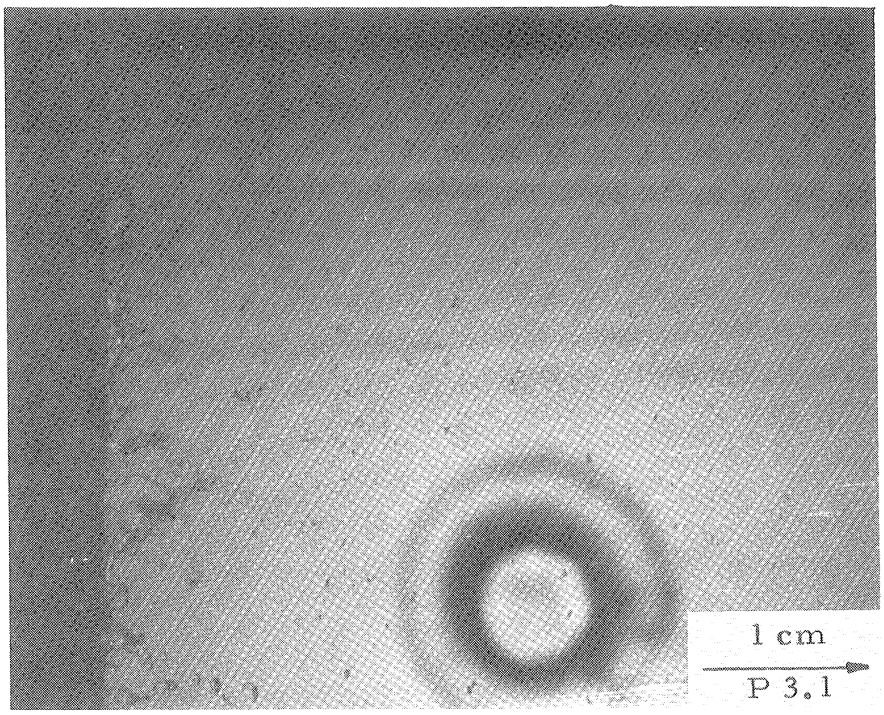

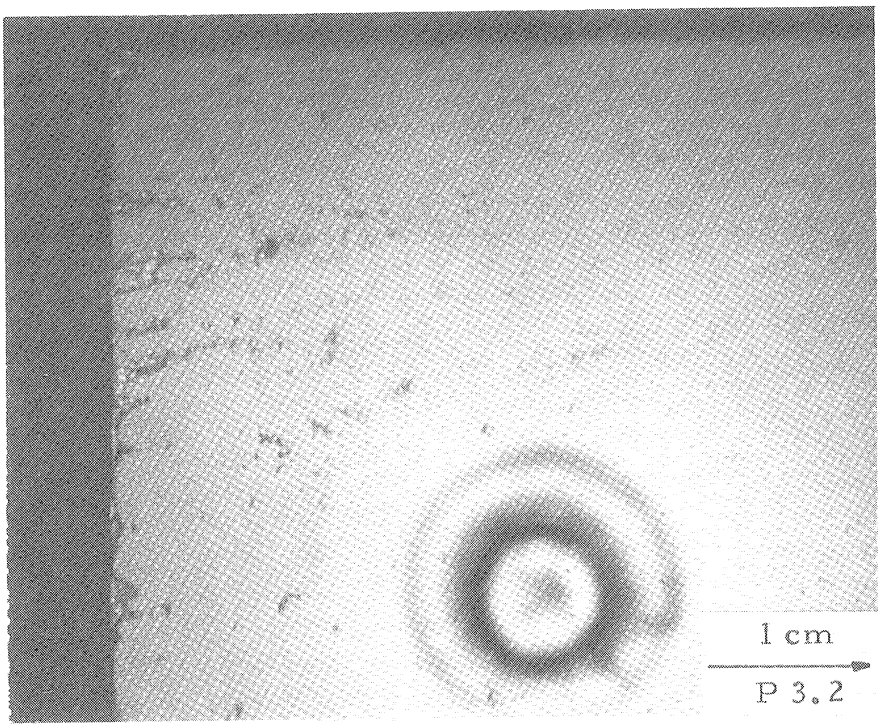

Fig. 5.1 Continued

5403

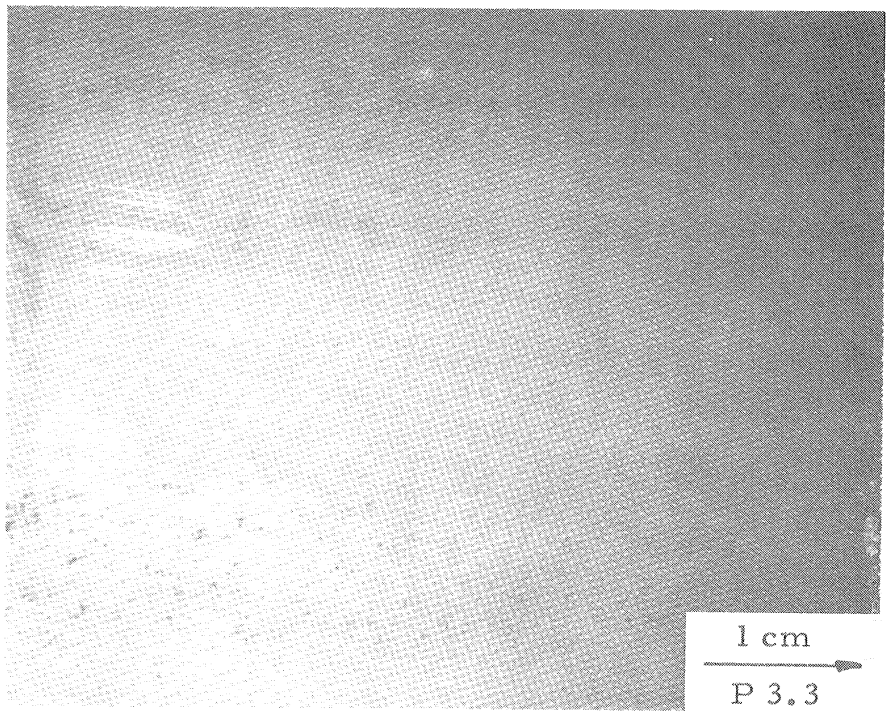

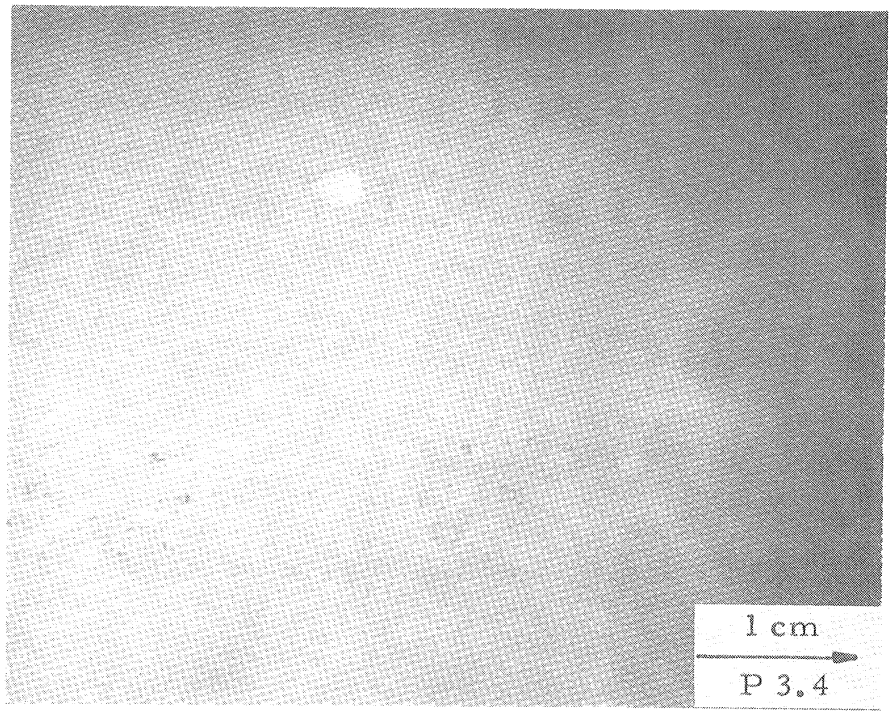

Fig. 5.1 Continued

5404

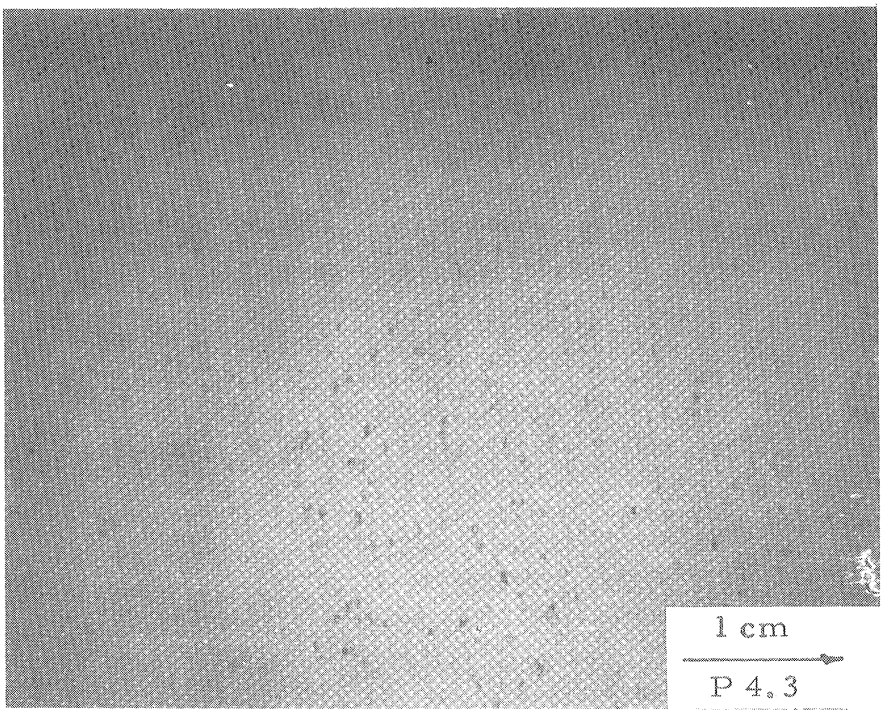

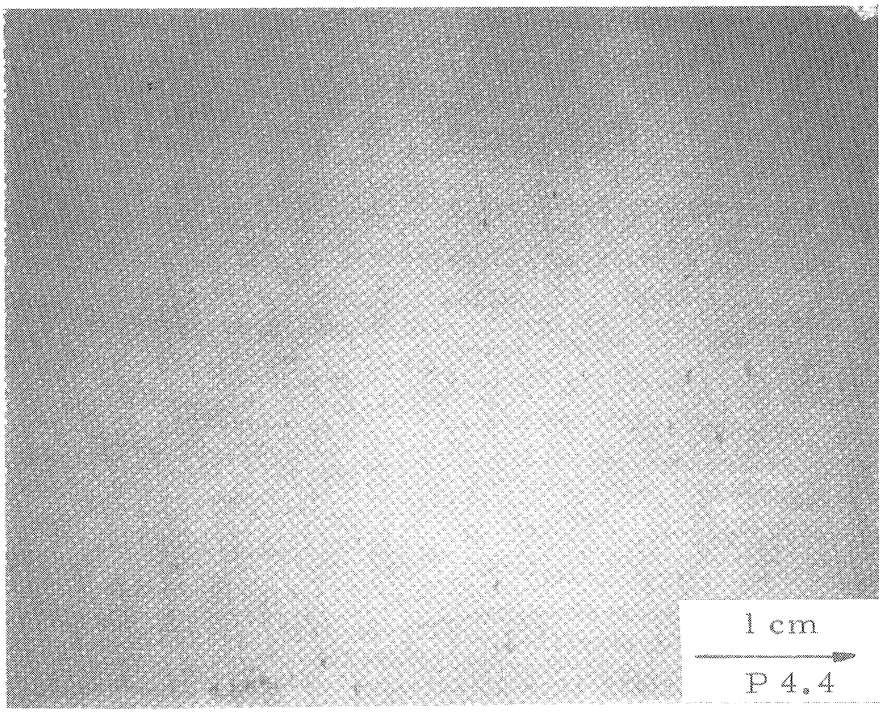

Fig. 5.1 Continued

5405

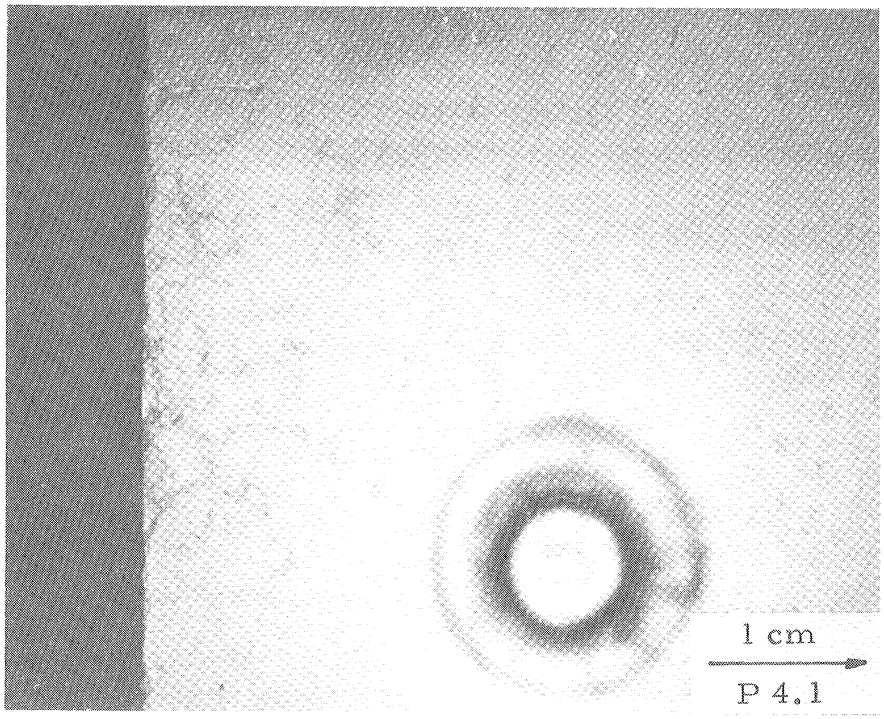

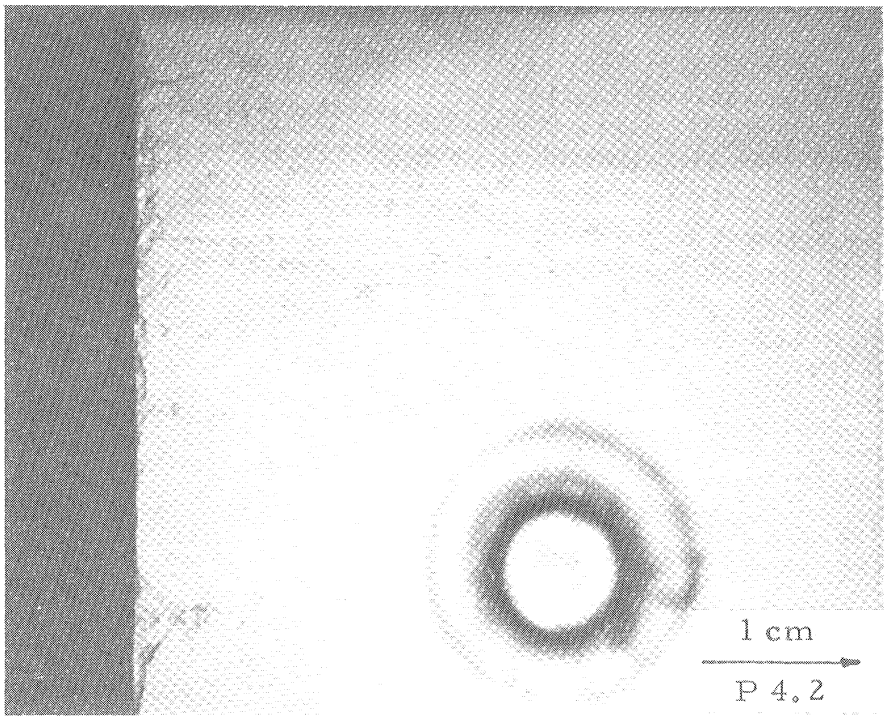

Fig. 5.1 Continued 5406

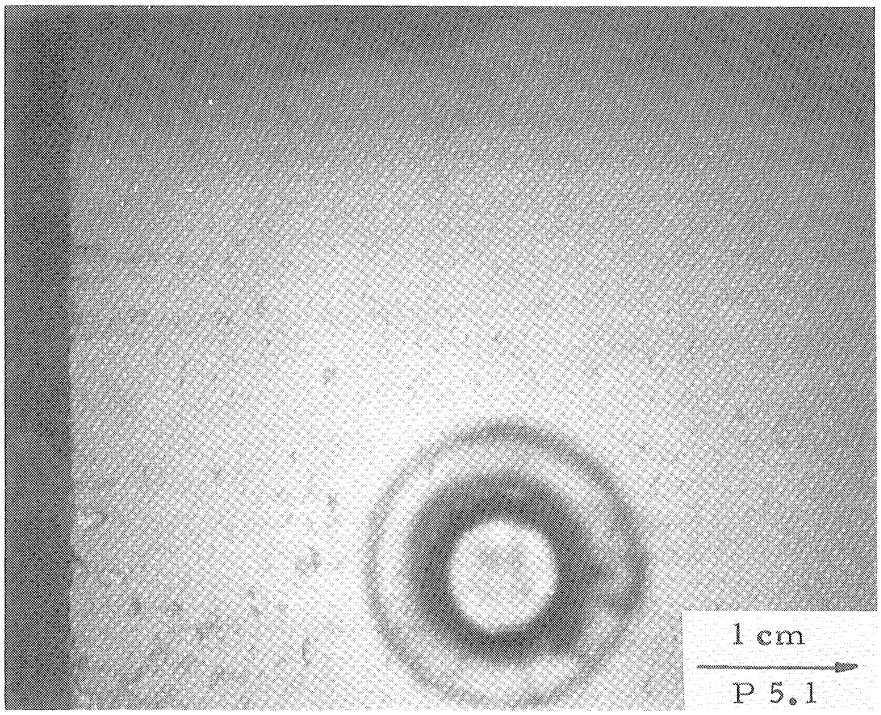

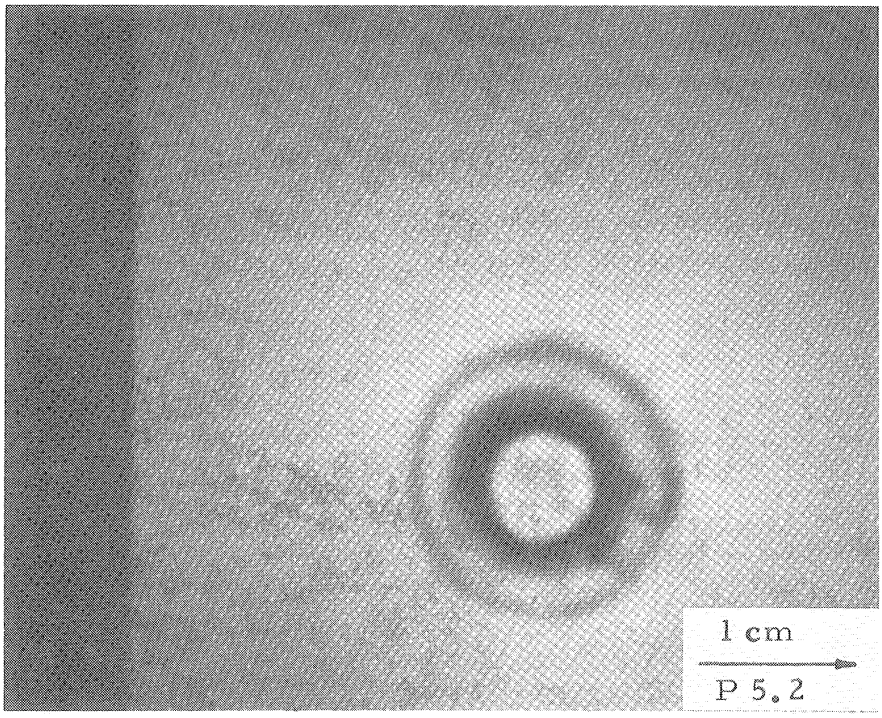

Fig. 5.1 Continued 5407

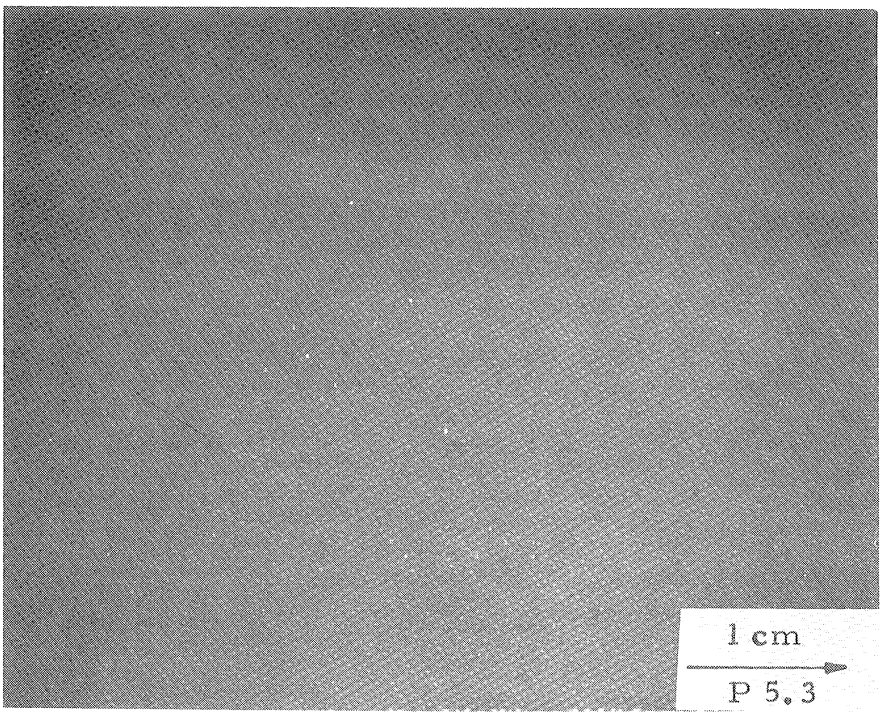

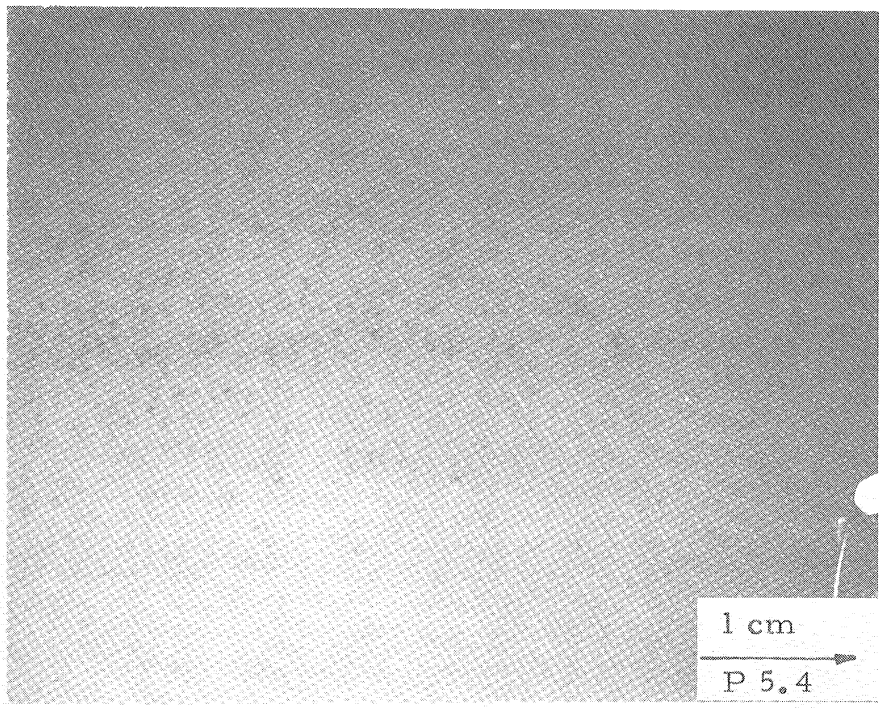

Fig. 5.1 Continued 5408

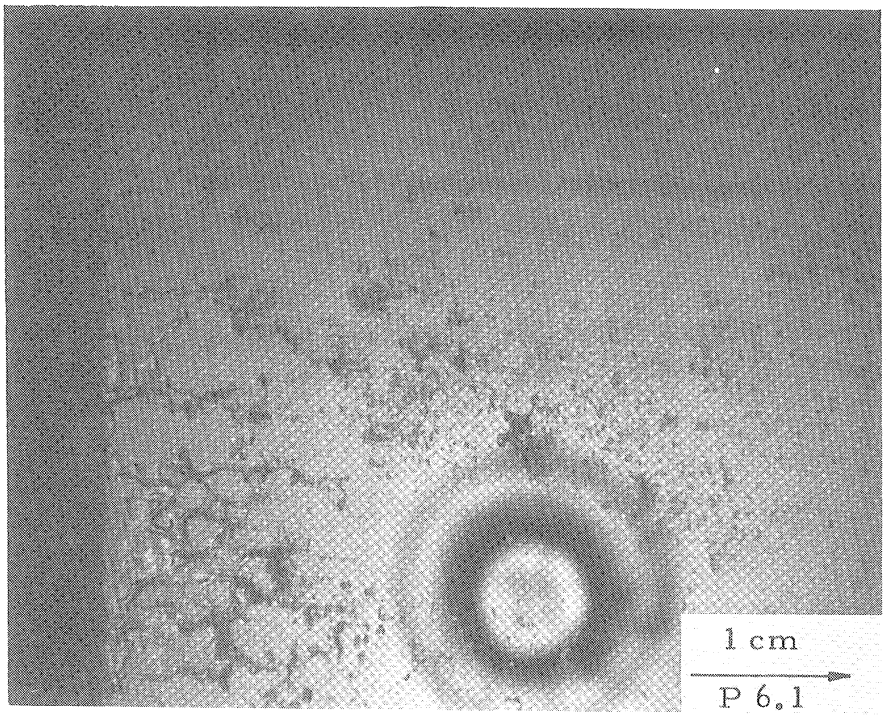

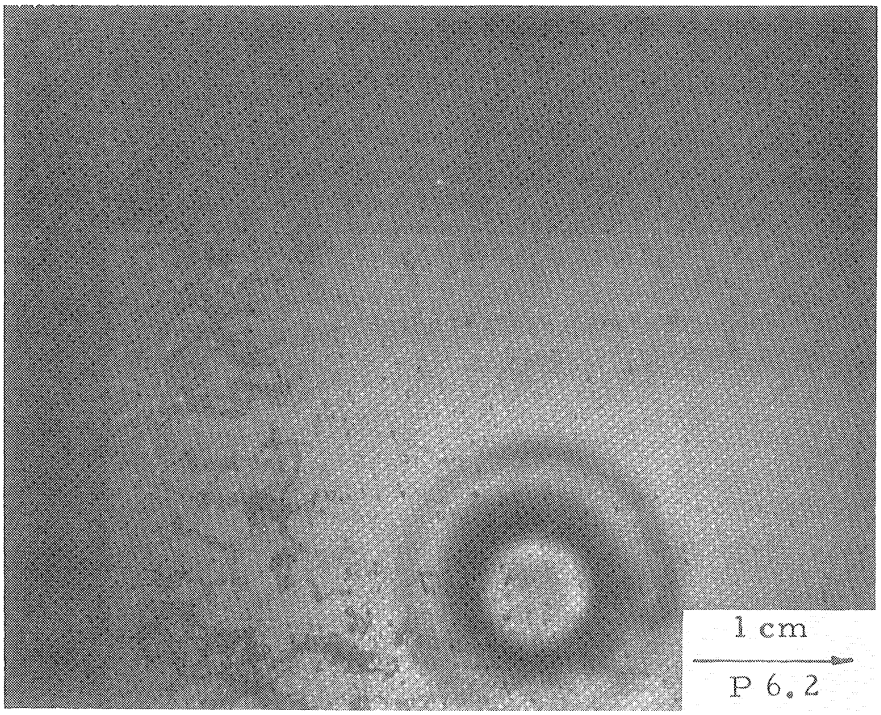

Fig. 5.1 Continued 5409

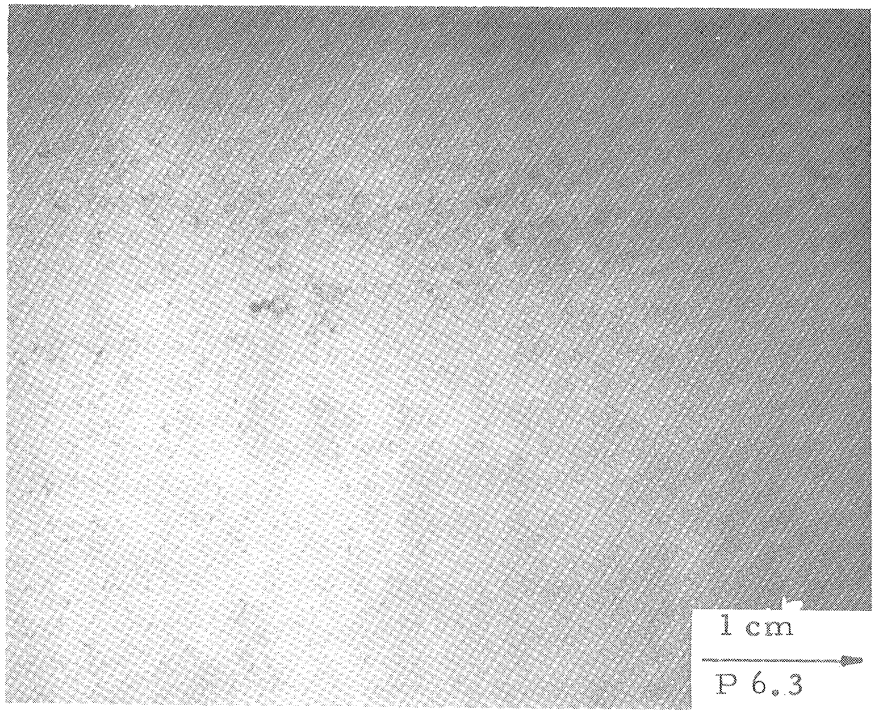

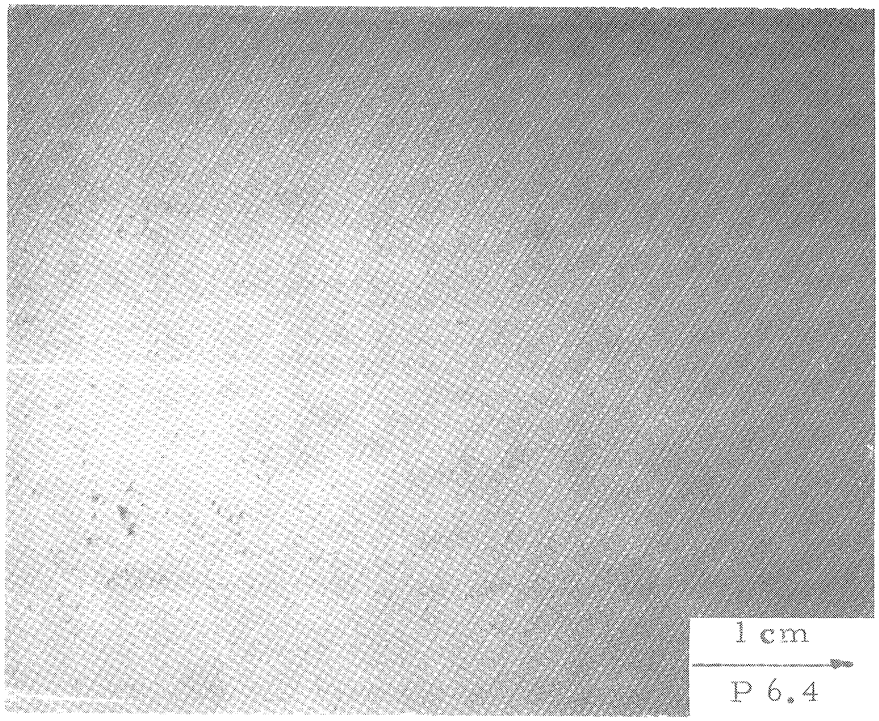

Fig. 5.1 Continued 5410

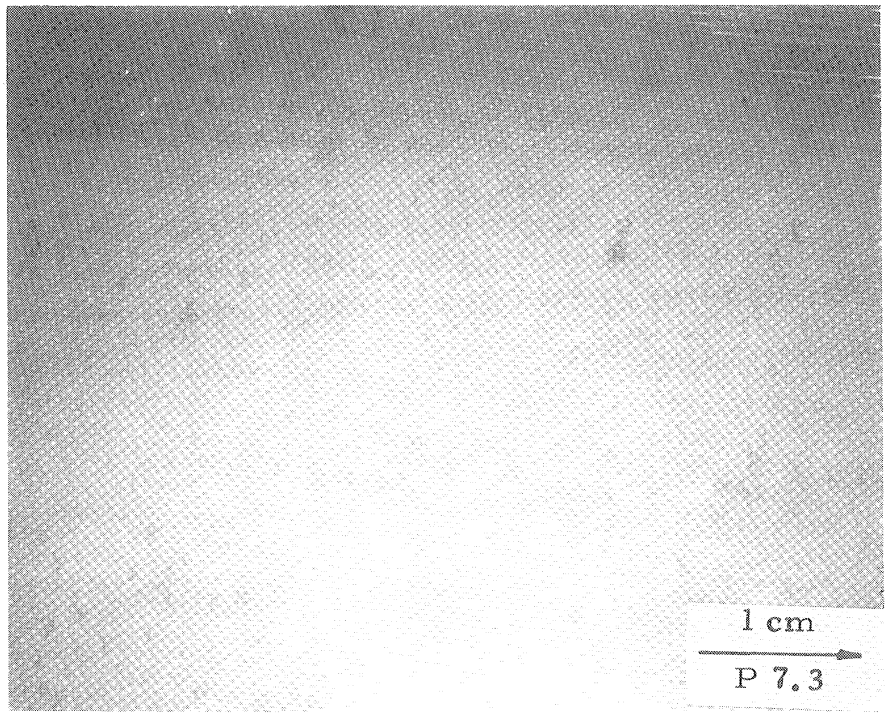

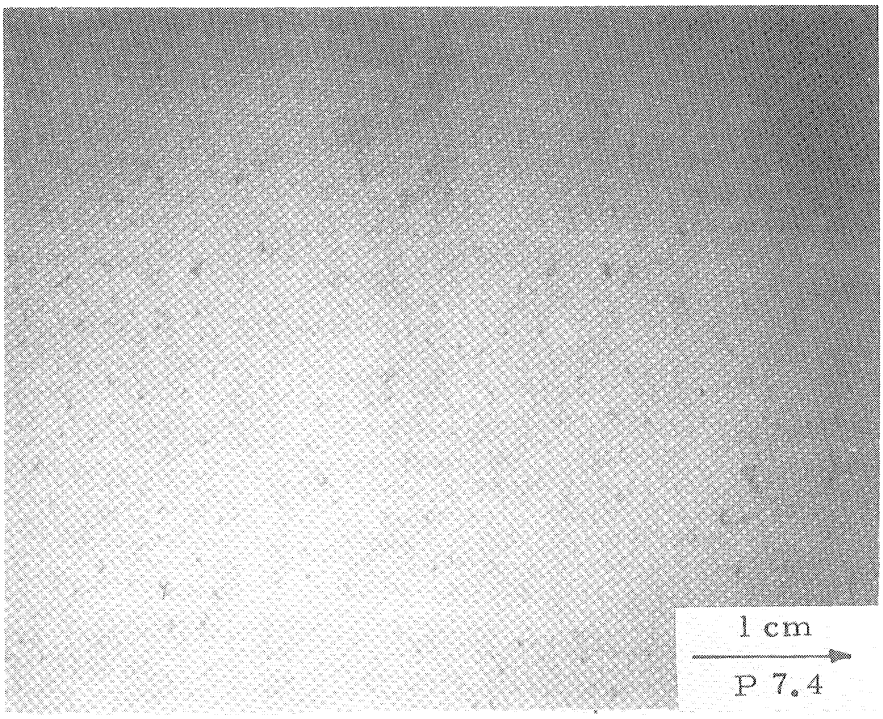

Fig. 5.1 Continued 5411

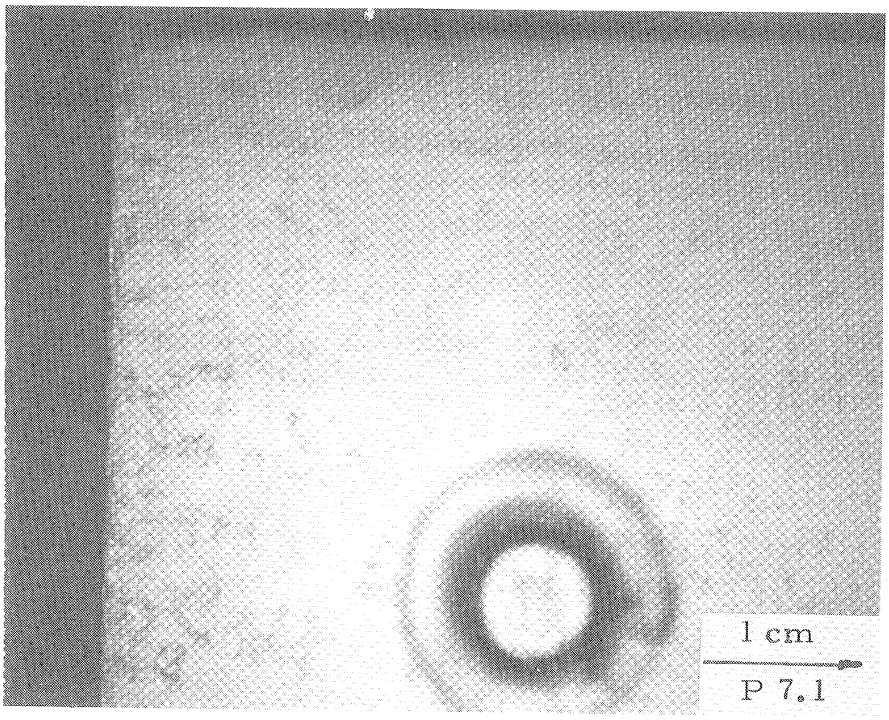

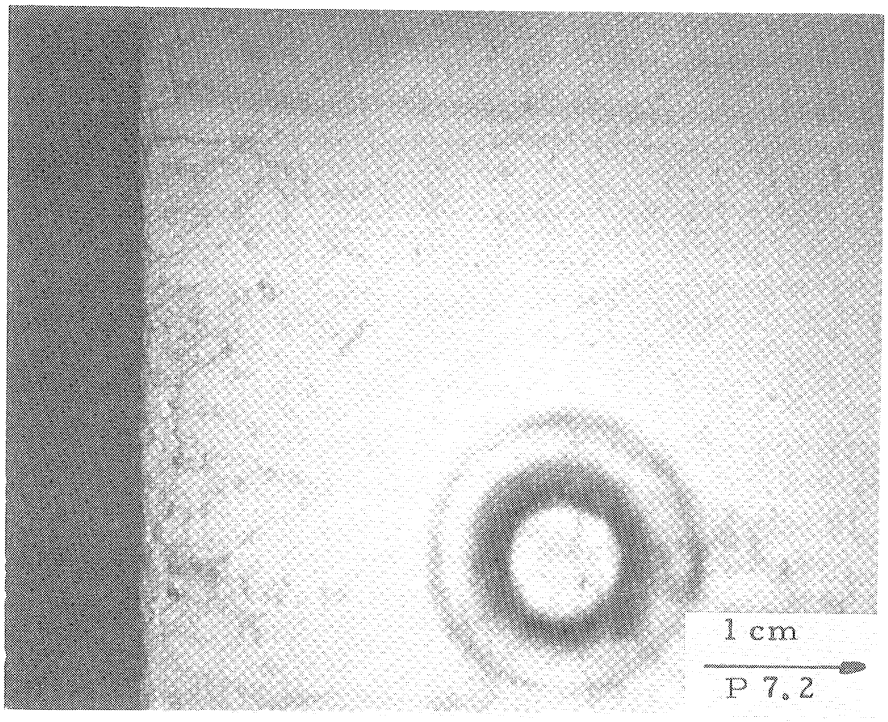

Fig. 5.1 Continued 5412

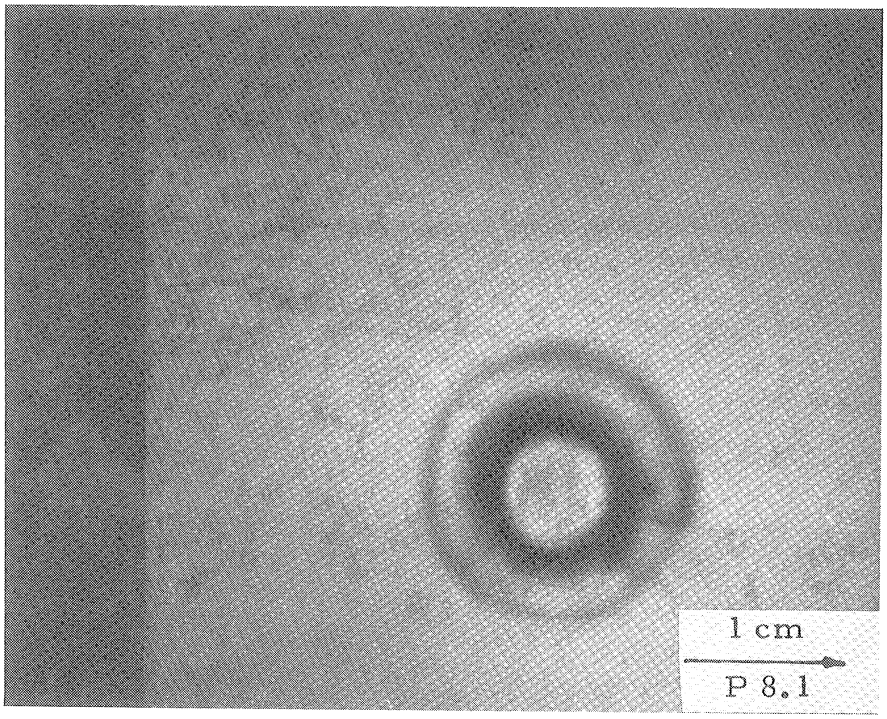

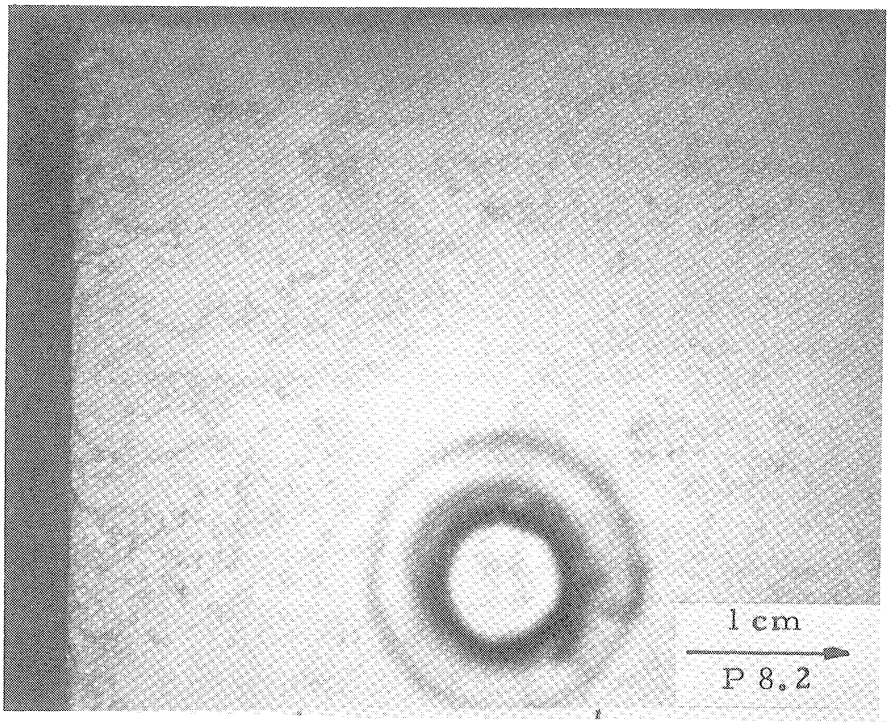

Fig. 5.1 Continued 5413

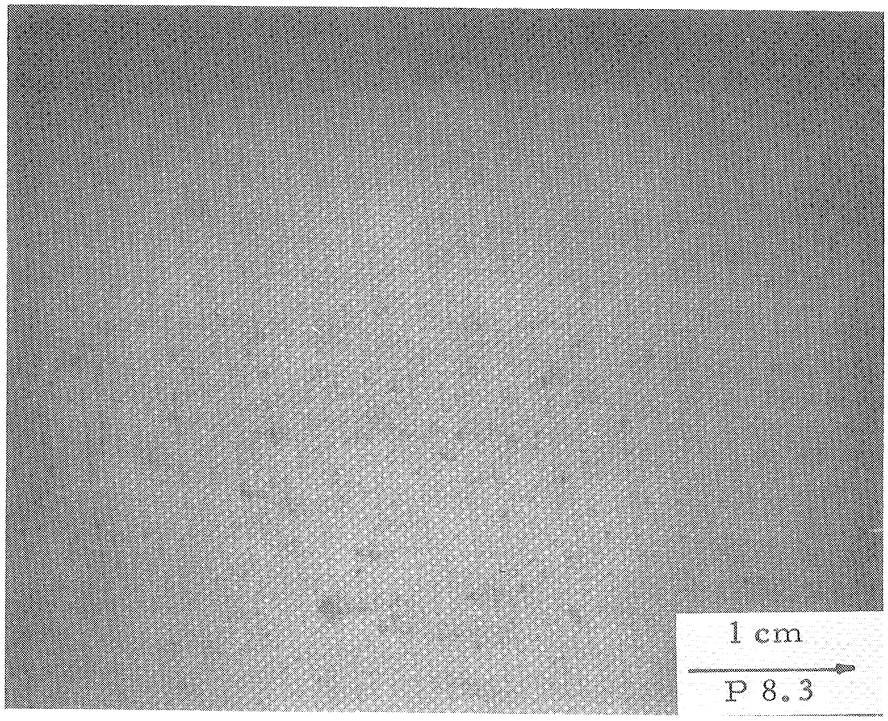

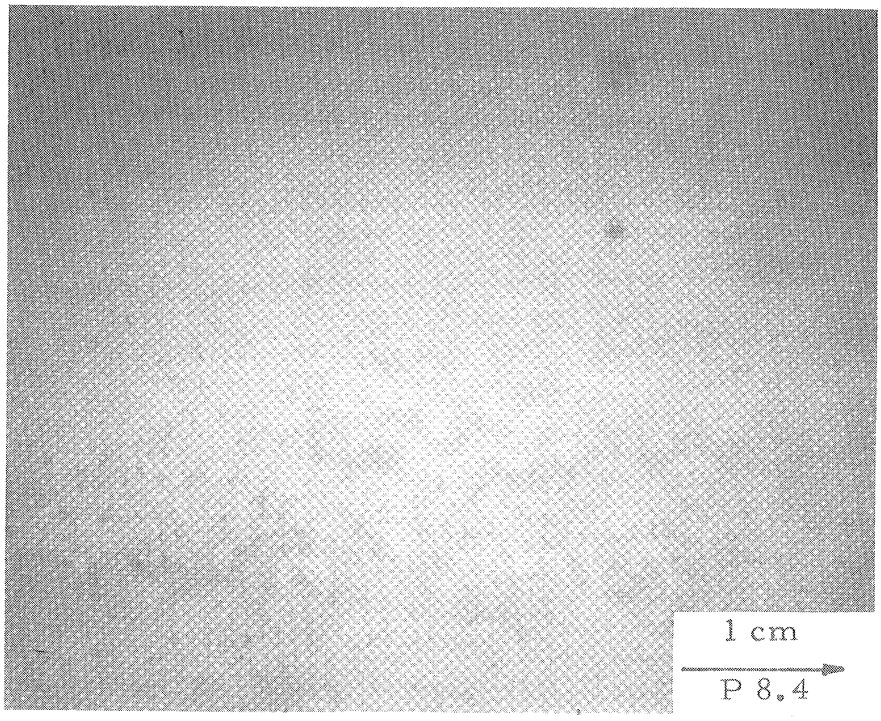

Fig. 5.1 Continued

5414

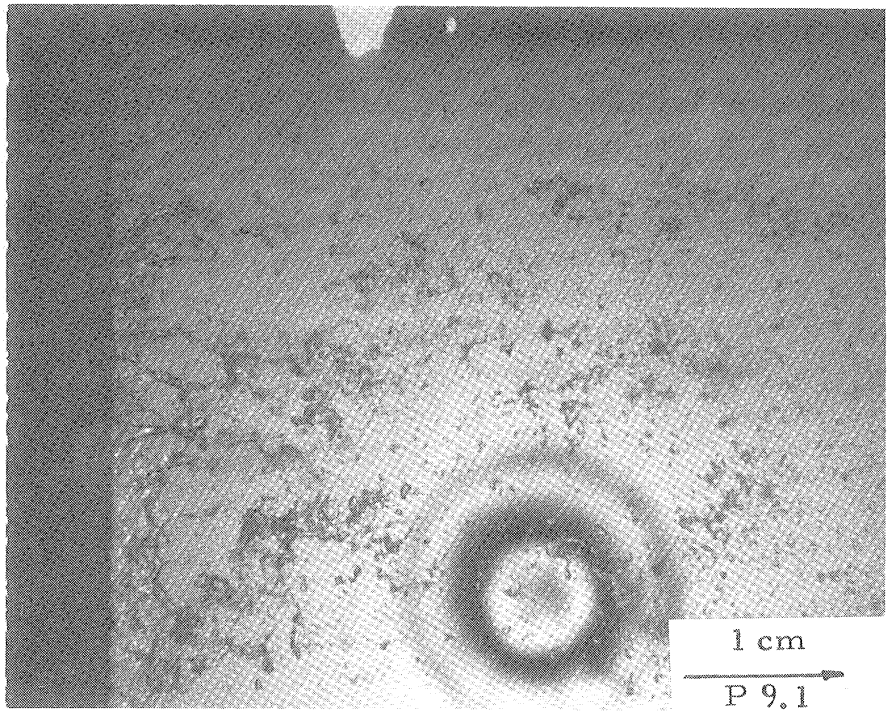

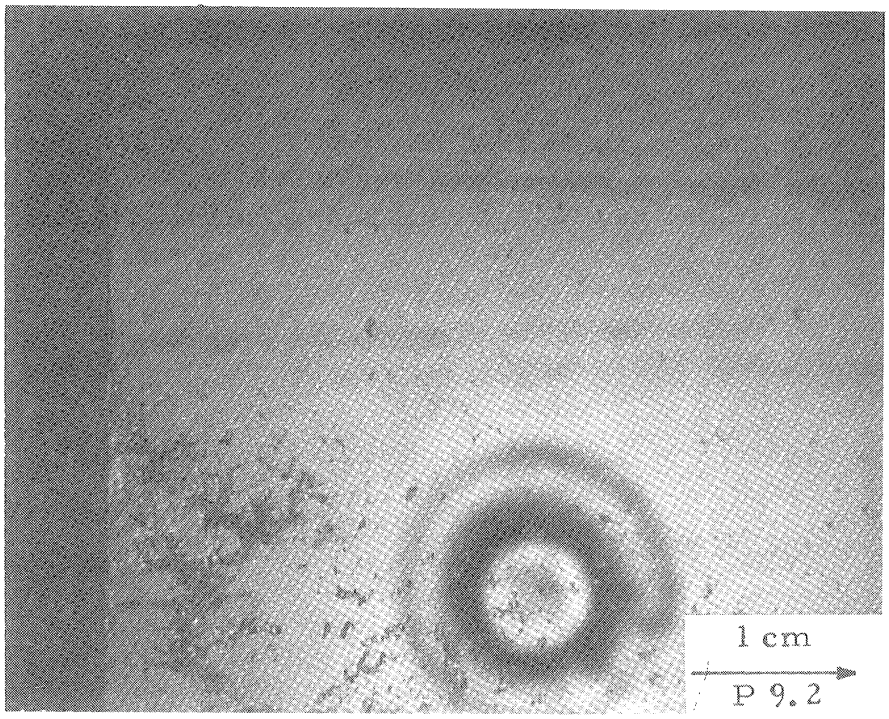

Fig. 5.1 Continued

5415

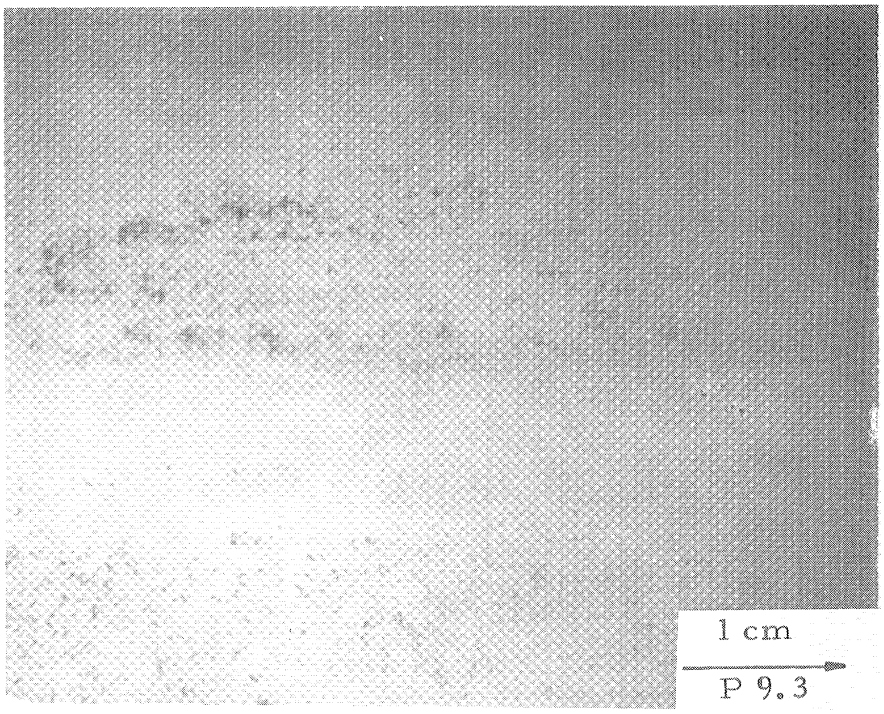

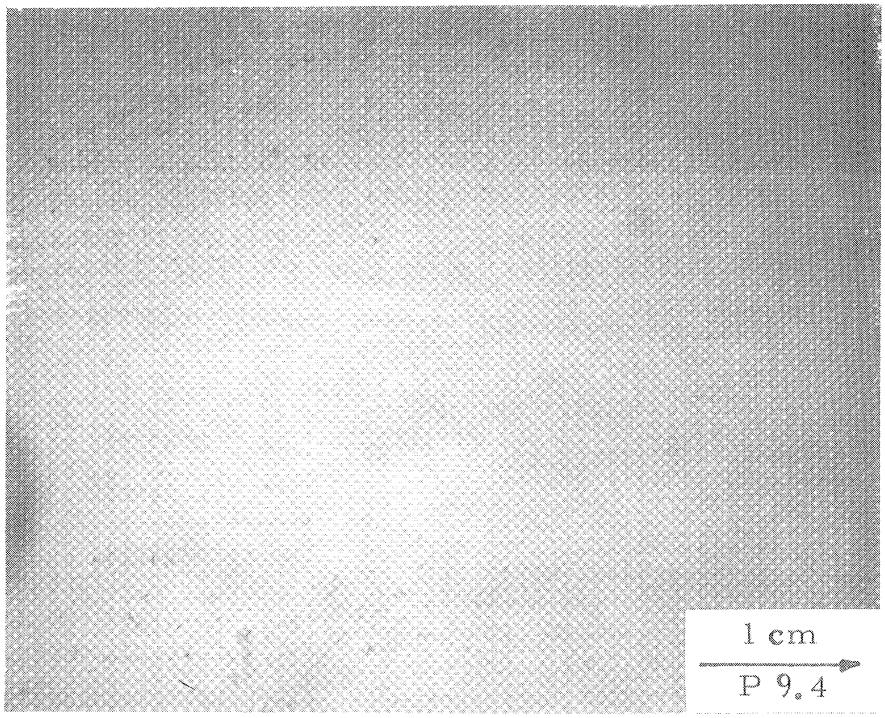

Fig. 5.1 Continued 5416

width, so that little optical distortion is involved. Flow is from left to right.

Finger shape varies with steam velocities at fixed liquid flow rate. One finger in plate #1.1 of Fig. 5.1 appears, e.g., as an approximate conical tube, with wide base commencing at the trailing edge. Other fingers appear more as cylindrical spikes of smaller diameters aligned with the flow axis. Plate #1.2 (Fig. 5.1), with the same flow conditions as Plate #1.1, shows one long spike-like finger and others of irregular shape (upper part of photo). The liquid sheet from which the fingers are formed, is wavy in the transverse direction, no doubt affecting the location, formation frequency, and size of these fingers. As steam velocity is increased, more and smaller fingers are observed. (Plates #2.1, 2.2, 3.1, and 3.2 of Fig. 5.1).

Detailed study of the fingers is necessary to understand resultant droplet formation. Finger lengths, L, and the distances between them, λ_f, vary with steam velocity and film flow rate. (Plates #2.2 and 3.2 of Fig. 5.1).

As shown by the photos, fingers of differing lengths exist at any given time. The maximum observed finger length, L, is here called the "characteristic" finger length.

One finds that maximum finger length, L, and finger wave length, λ_f, (average distance between fingers) decreases as steam velocity increases (see plates #1.2, 2.2, and 3.2) at fixed liquid flow rate.

With higher liquid flow rates, more complex finger

patterns appear along with more complicated liquid film patterns (i.e. waves, etc). As steam velocity is increased at fixed liquid flow rate, more fingers appear. Larger fingers are very unstable, and do not extend so far axially as do the smaller fingers, appearing at lower liquid flow rates. Sometimes several holes appear in such fingers. At inception, they may be of triangular shape with thick cylindrical boundaries (plate #6.1). These grow to more nearly circular shapes probably because of surface tension, before the finger disintegrates. Plates #5.2 and 6.1 show this intermediate process and the final shattering.

Author defines maximum finger length, L, as axial distance from blade trailing edge to downstream end of the finger. For the highest liquid flow rate (plates #7, 8 and 9), the blade trailing-edge flow appears in total chaos, and of extreme complexity, so that L and λ_f cannot be measured. However, they are still well discernable for lower steam velocities, even at higher steam velocities, except for the exact instant of finger disruption.

2. Reduction of Experimental Photographic Results

Finger formation at the blade trailing edge has been recorded (as already discussed) using both a still polaroid camera, and Fastax high-speed movie camera. The better optics of the still camera enables better observation of the forms occurring at the trailing edge, but cannot provide any information on the flow kinetics. However, the time-dependent processes at the trailing edge were measured

by the high-speed motion picture camera at 5000 Hz.

In most cases, every 80th frame (every 16 ms of real time) was examined with a calibrated viewer-screen. Observer error was estimated to be $\pm$ 15%, for the same film comparing 5 different observers.

Finger formation dependent parameters are maximum finger length, L(t), and finger wave length, $\lambda_f(t)$. The number of fingers, N, was counted for a given transversal length, X. Then $\lambda_f = X/N$.

Typical measurements of maximum finger length, L(t), as a function of time, are shown in Figs. 5.2 to 5.4. For all liquid flow rates, upper limit of maximum finger length, L_u, decreases as U_s is increased. For all U_s average of L increases as liquid flow rate is increased. Also there exist somes "dead" periods before a new finger is formed after one is shed.

The number distribution of maximum finger length, L, was investigated for all flow conditions. Finger length was measured in 2100 frames (70 frames on each of 30 rolls of 100 ft. length). Thus samples used are statistically meaningful and reproducible. The number of maximum fingers in each length increment was normalized by the total number of observations for a given flow condition. Typical maximum finger size distributions are shown in Figs. 5.5 to 5.9.

The largest number of finger lengths (number peak) occurs between 2.5 and 4 mm for all steam velocities for

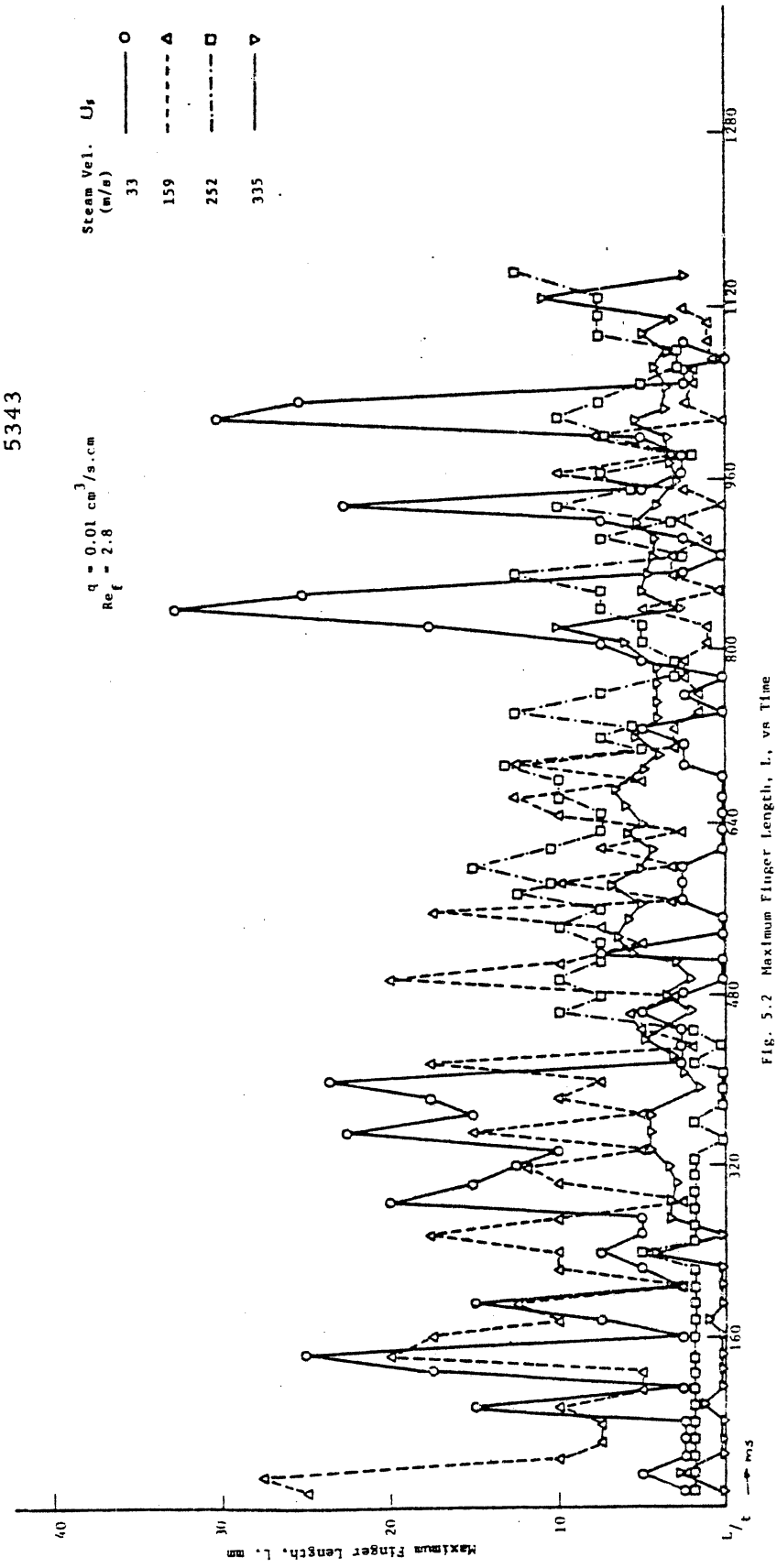

Fig. 5.2 Maximum Finger Length, L_f vs Time

5344

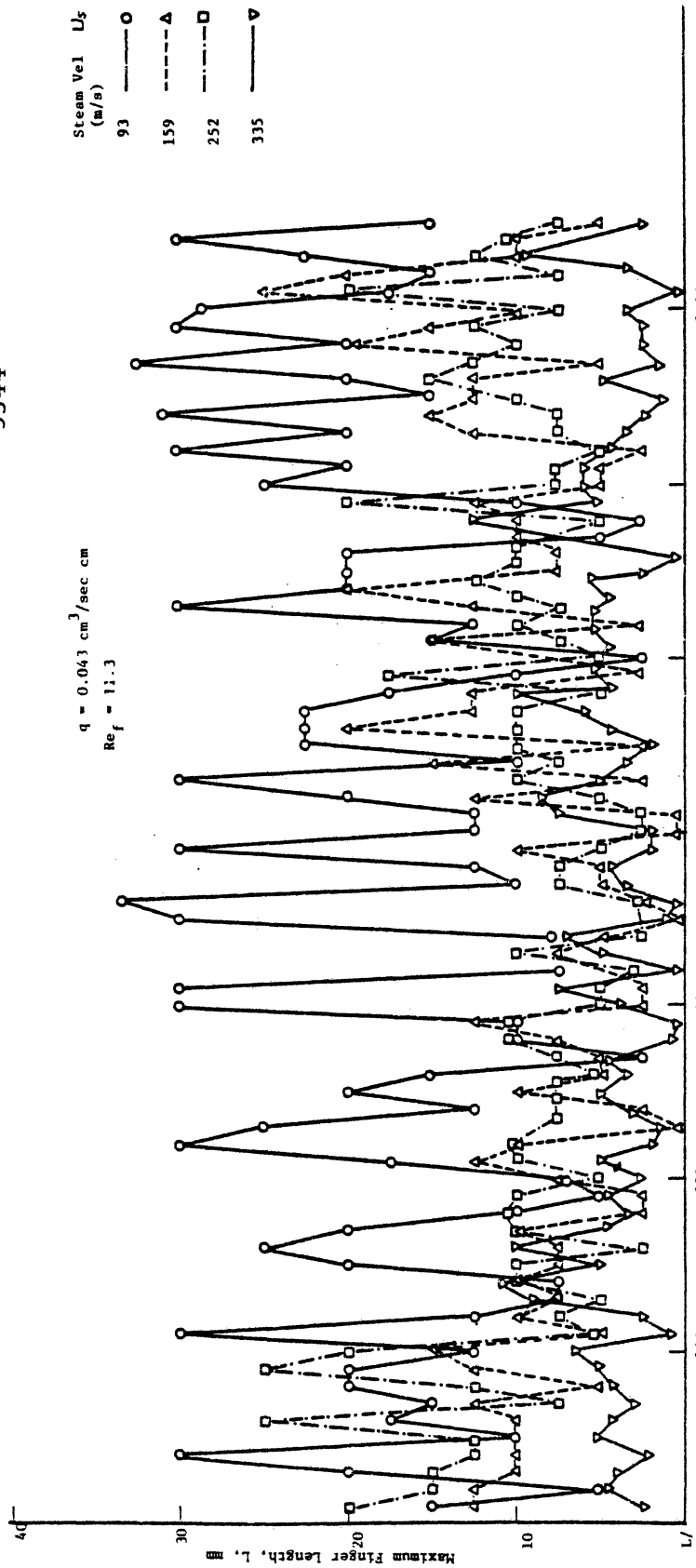

Fig. 5.3 Maximum Finger Length, l. vs Time

5345

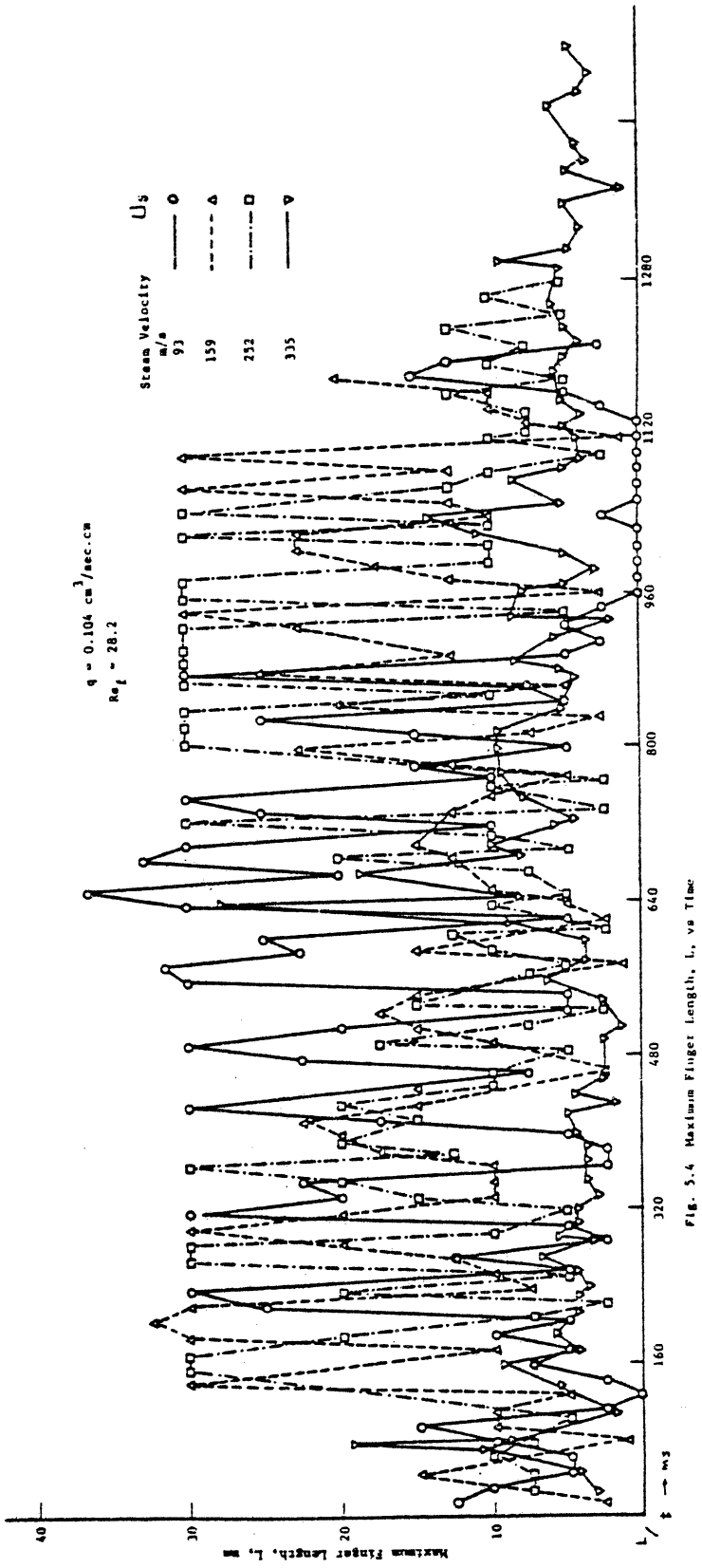

Fig. 5.4 Maximum Finger Length, L_f, vs Time

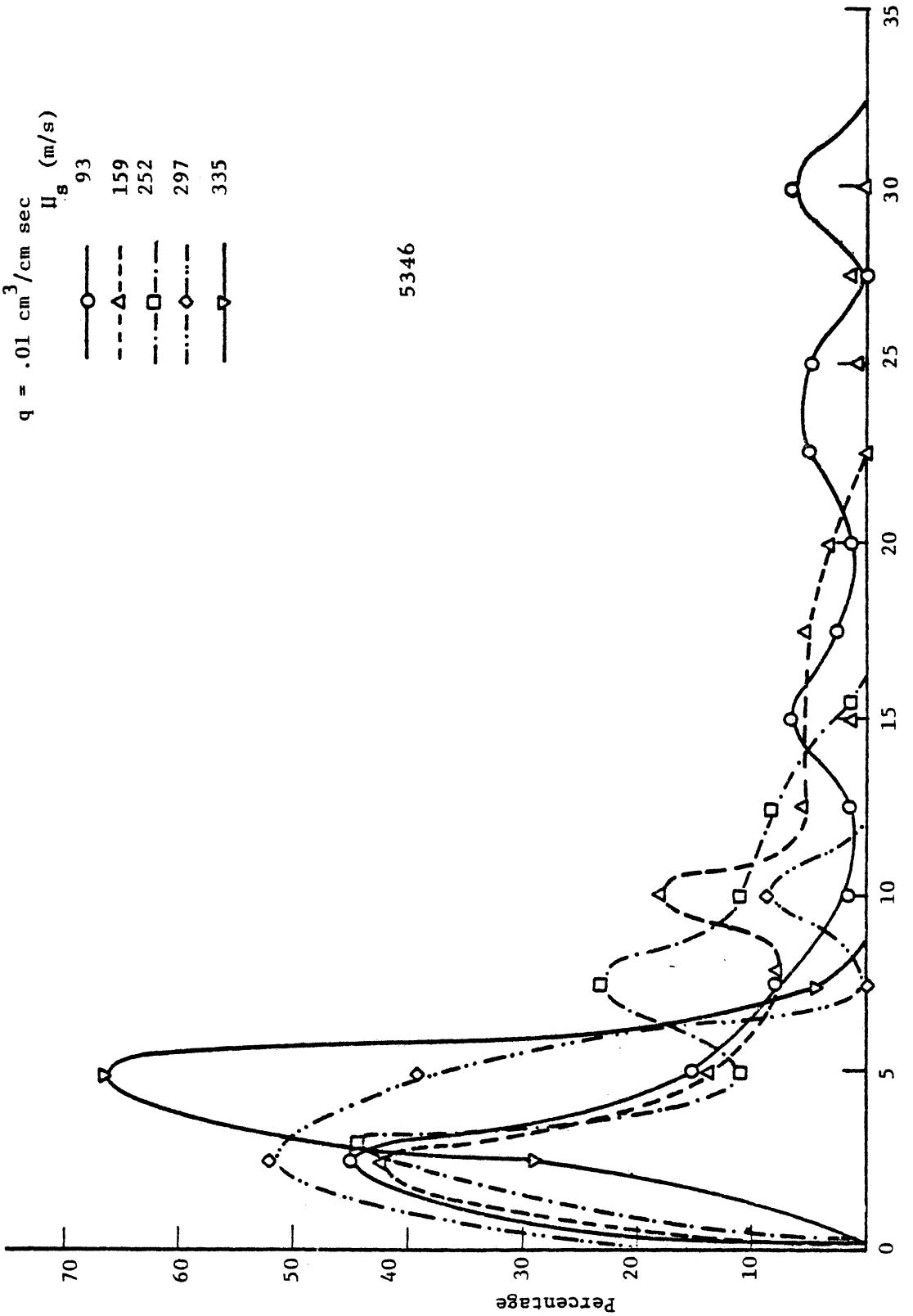

Fig. 5.5 Finger Length Distribution

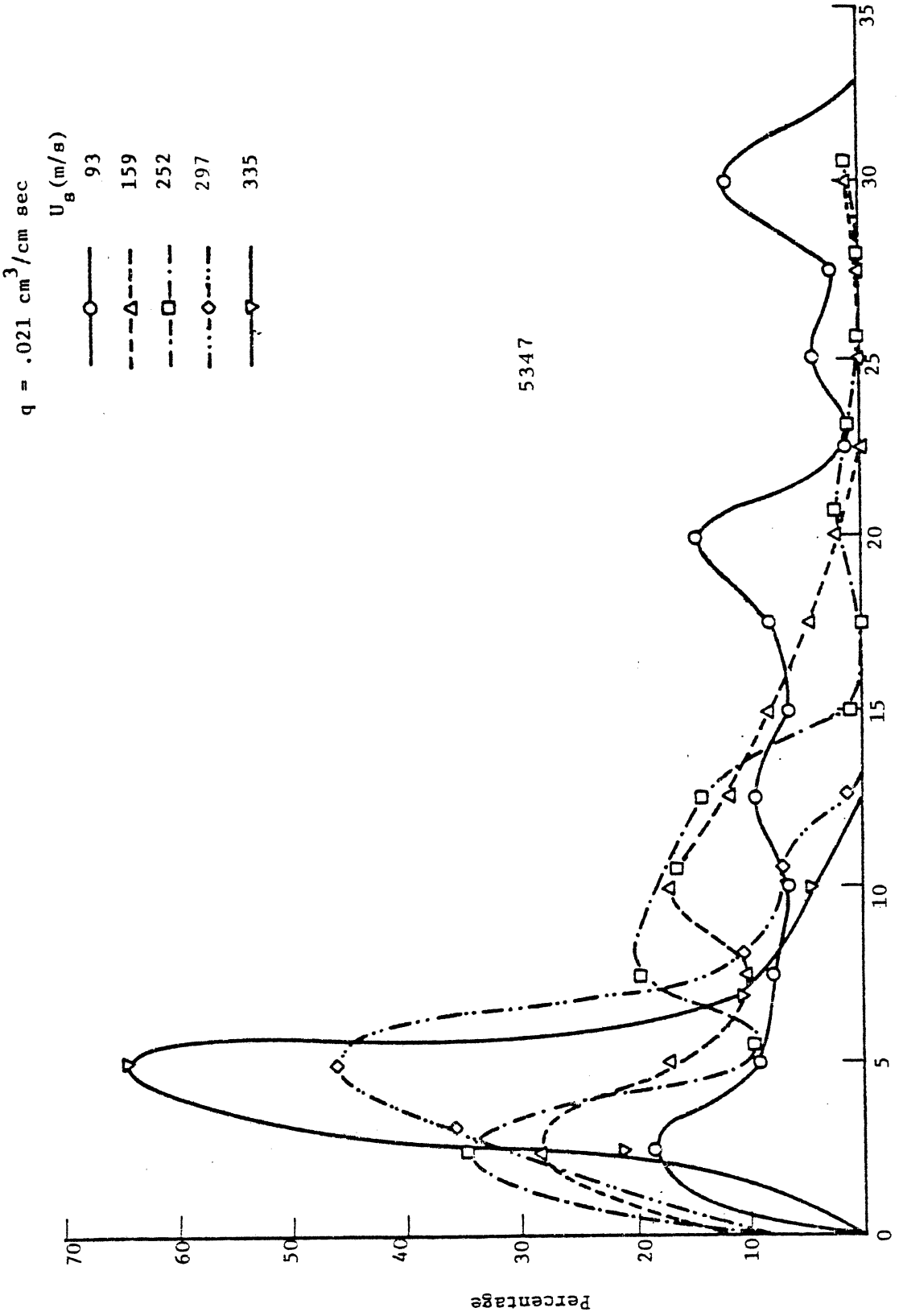

Fig. 5.6 Finger Length Distribution

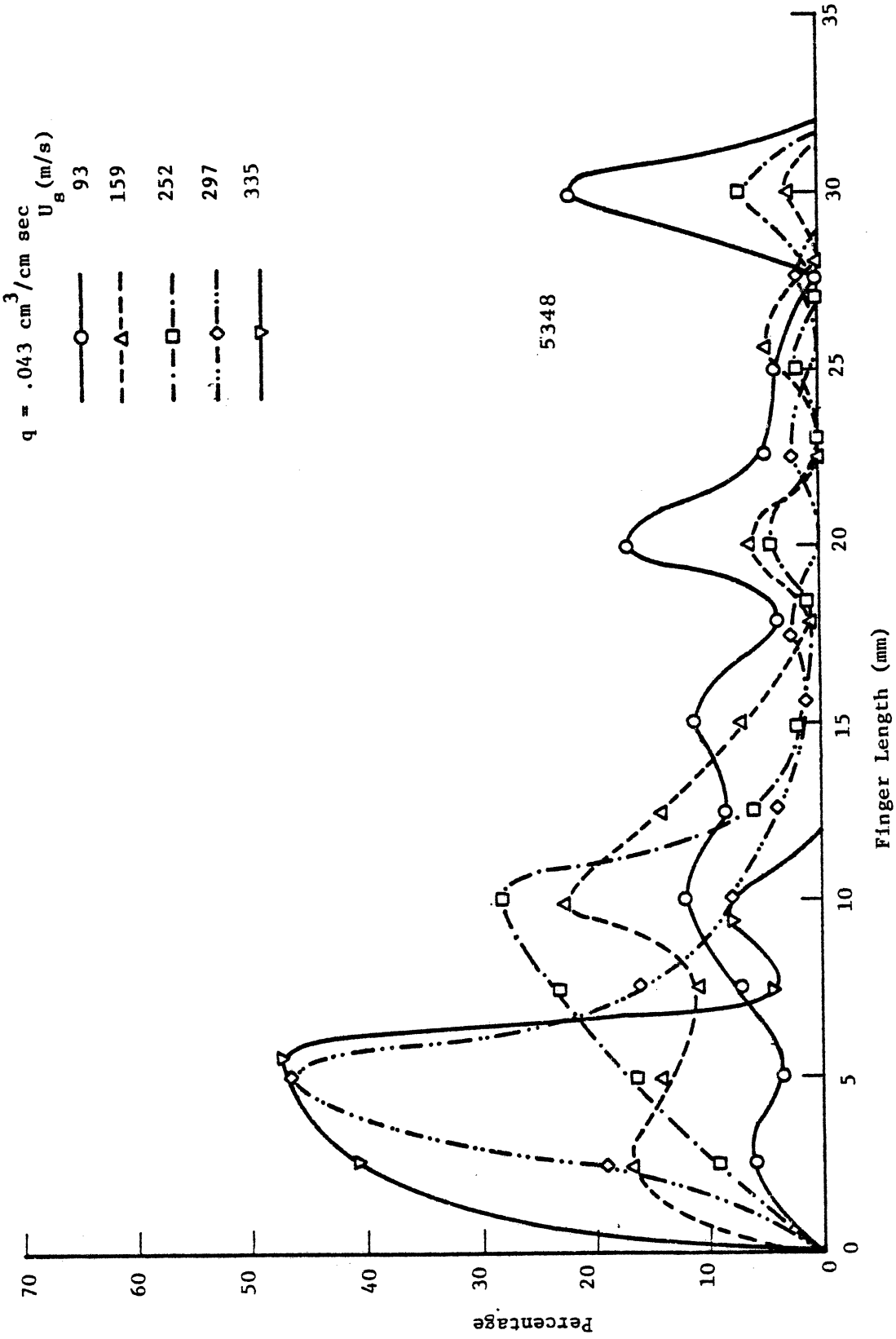

Fig. 5.7 Finger Length Distribution

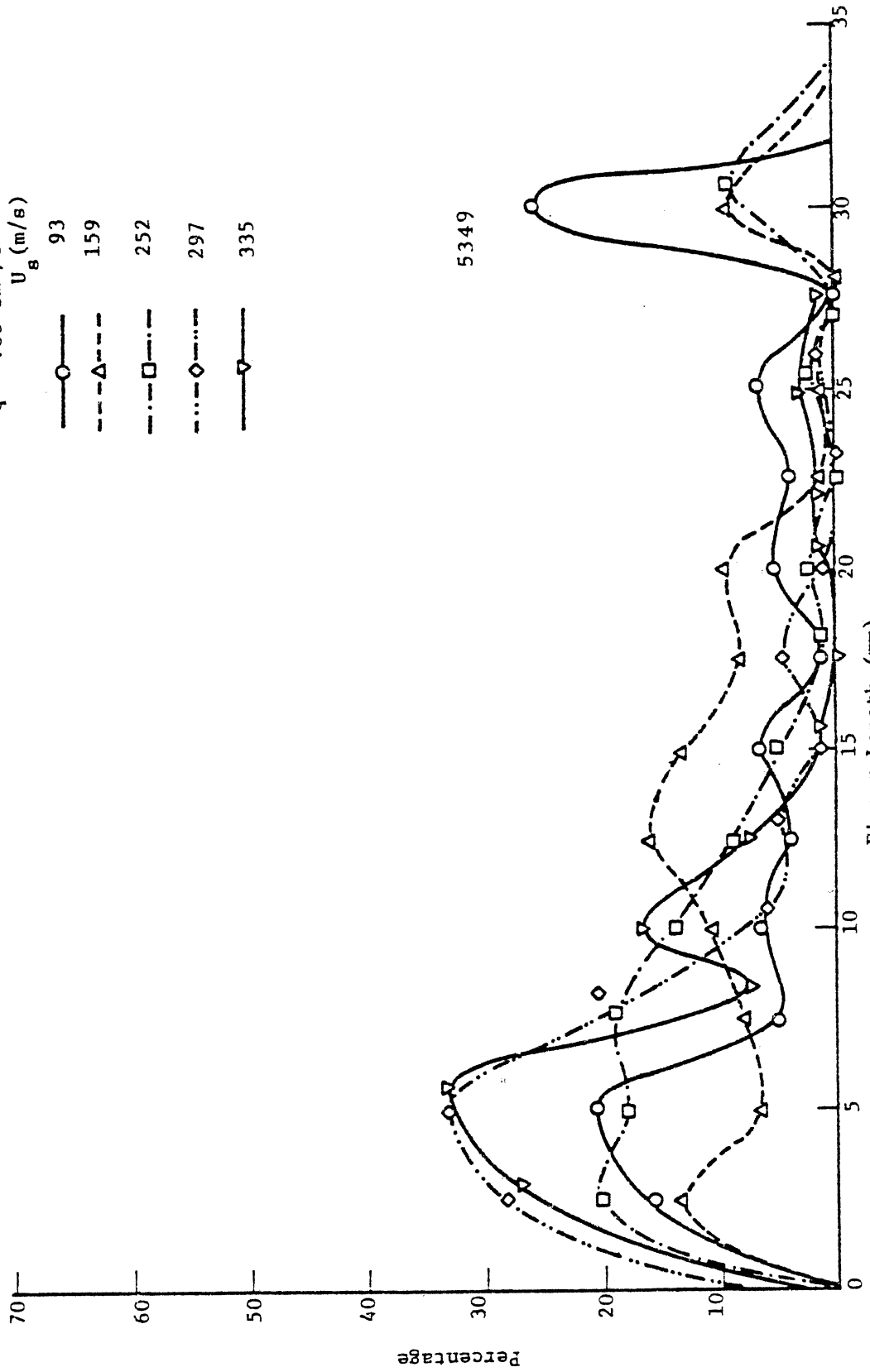

Fig. 5.8 Finger Length Distribution

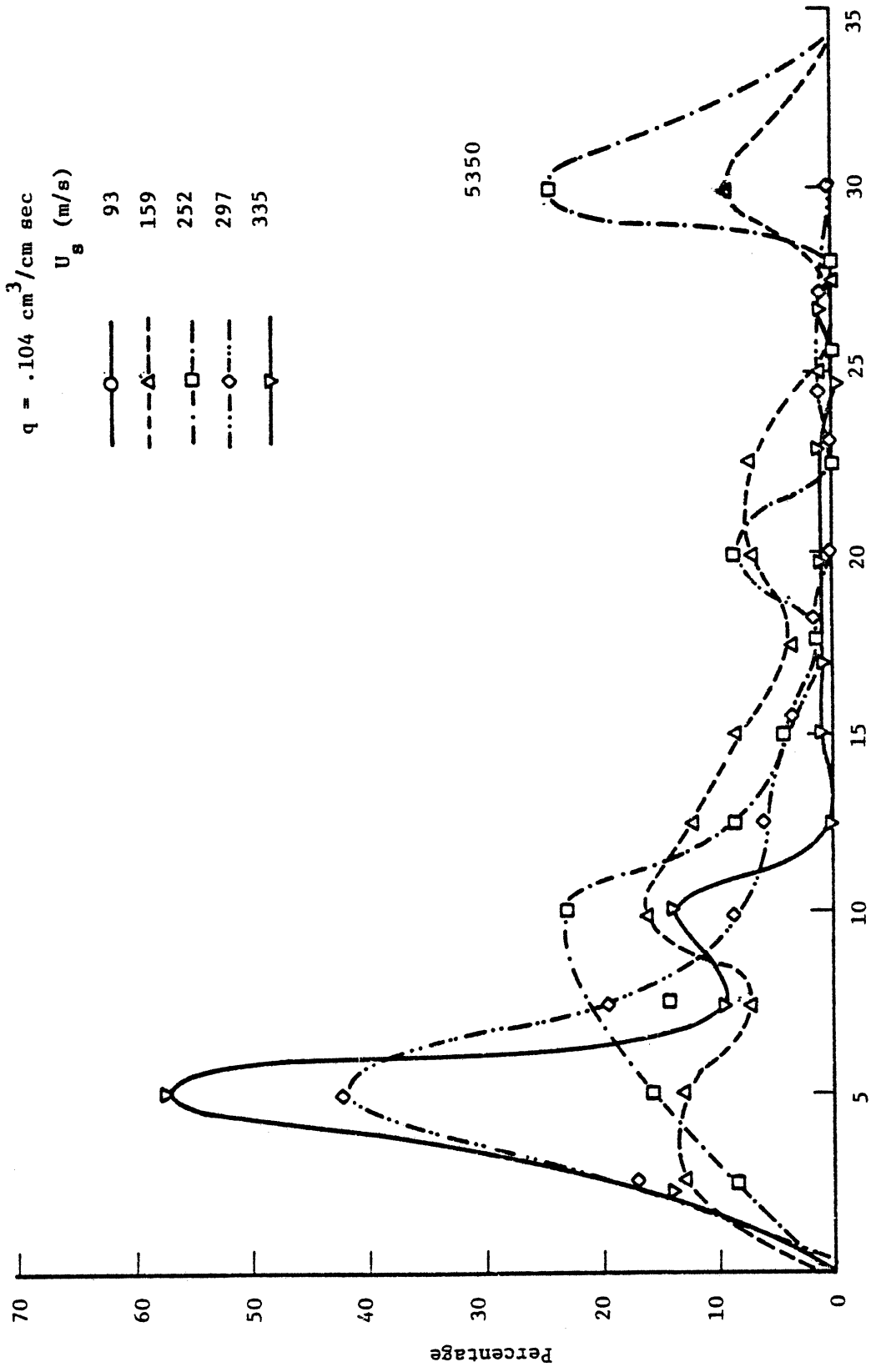

Fig. 5.9 Finger Length Distribution

liquid flow rate, q = 0.010 $cm^3/cm.sec$ (Fig. 5.5). The number peak density increases with increase of steam velocity. This is presumably due to increased finger instability as steam velocity is increased.

An increase in number peak length was also observed at higher liquid flow rate and lower steam velocity (Fig. 5.7 for q = 0.043 $cm^3/cm.sec$). For higher liquid flow rate (Fig. 5.9, q = 0.104 $cm^3/cm.sec$), an increase of number peak L at higher steam velocity was found. For two higher steam velocities (297 and 335 m/s), no peak shift was noted. Time-average maximum finger length, $\bar{L}$ was calculated from the distribution curves in Figs. 5.5-5.9.

Figure 5.10 shows the dependence of $\bar{L}$ on the various flow parameters. At a given steam velocity, $\bar{L}$ always increases with increase of liquid flow rate, q. An increase of U_s at fixed q gives a decrease in $\bar{L}$ in the low U_s region. However, all L's are strongly increased by increasing steam velocity from 297 to 335 m/s. Minima of $\bar{L}$ for all liquid flow rates are observed (Fig. 5.10) at U_s = 297 m/s. The reason for the occurence of these minima is unknown at this time. It cannot involve shock-wave phenomena since the steam velocity is well subsonic (M = 0.72). The data scatter (Fig. 5.10) is reduced for increasing U_s and decreasing q. The bar indicates the full observed range of data.

The frequency of appearance of fingers longer than $\bar{L}$ has been computed from the L vs. t curves (Figs. 5.2-5.4), dividing the time increment for a particular data

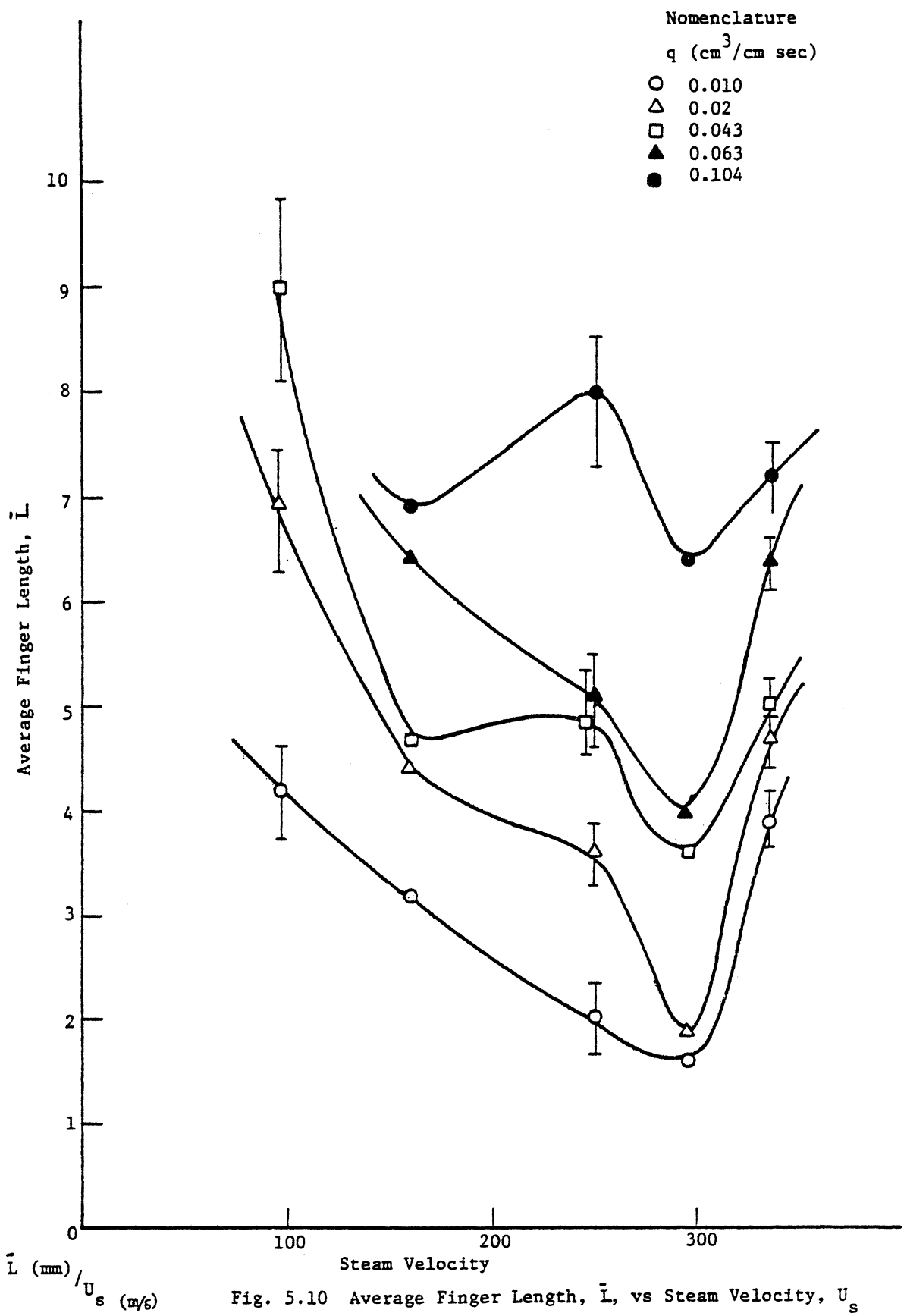

Fig. 5.10 Average Finger Length, $\bar{L}$, vs Steam Velocity, U_s

set by the total number of peaks found therein. This gives the average interval, ΔT, between the appearance of fingers larger than the time averaged finger length, $\bar{L}$.

Figure 5.11 shows ΔT vs. U_s. In general, ΔT increases with increasing U_s, and decreases with an increase of q. The general dependency of ΔT on U_s for fixed q can be explained as follows. An increase of U_s causes a thinning of the vapor boundary layer along the blade, and at the trailing edge. It also leads to an increase of interfacial shear (Table 4.2). Both vapor boundary layer thinning and increased shear stress enhances liquid removal at the trailing edge, due to increased entrainment, because of the closer approach of high velocity steam with consequent greater shear stress. It thus requires a longer time for sufficient liquid to be accumulated for the next such removal. For given U_s, a given quantity of liquid of course accumulates more quickly for increased q, as shown by data (Fig. 5.11). An unexplained deviation from the general trends occurs for q = 0.021 $cm^3/cm \cdot sec$ (Fig. 5.11). ΔT increases with increasing U_s up to U_s = 250 m/s and decreases thereafter, while for all other q, ΔT always increases with increasing U_s.

Two finger Strouhal numbers have been here defined, based on film and steam velocities respectively,

$$S_{f_1} = \frac{\bar{L}}{\Delta T \, V_f} \qquad (5.1)$$

and

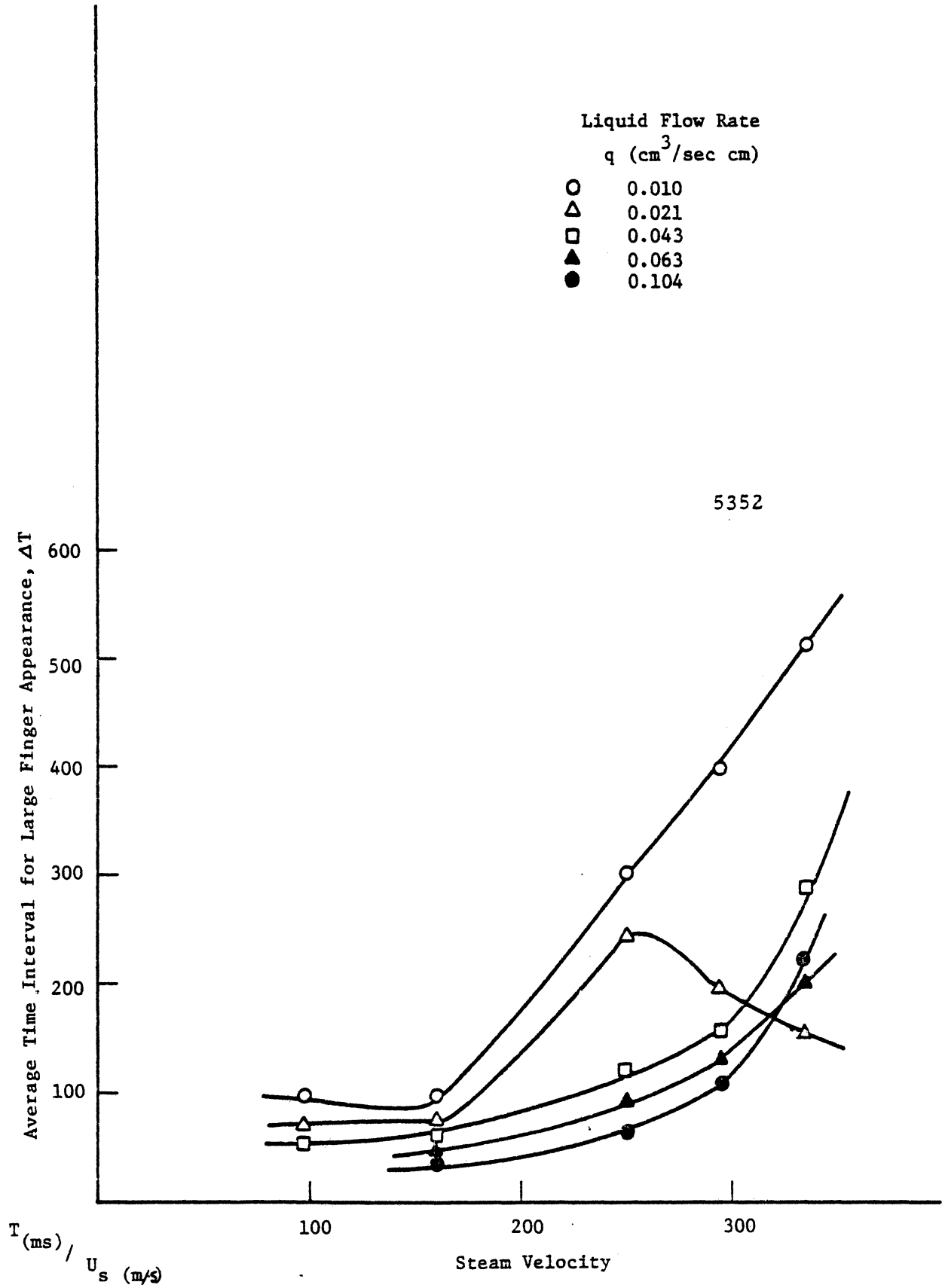

Fig. 5.11 Average Time Interval for Large Finger Appearance, ΔT, vs Steam Velocity, U_s

$$S_{f_2} = \frac{\bar{L}}{\Delta T\, U_s} \qquad (5.2)$$

to correlate finger formation frequencies. Figures 5.12 and 5.13 show the relation between S_{f_1}, S_{f_2} and steam Reynolds Number, Re_s. In general, S_{f_1} and S_{f_2} decrease as Re_s increases. Also for fixed Re_s, both S_{f_1} and S_{f_2} increase with film Reynolds number, Re_f. S_{f_1} and S_{f_2} differ by the ratio of film to steam velocity. S_{f_1}, then, varies from 0.04 to 0.93, thus being in the same range as Strouhal numbers measured in other experiments. On the other hand, S_{f_2} is $\sim 10^{-4}$, and thus not consistent with usual S data.

The finger shedding phenomenon seems obviously closely related to vortex-shedding from a circular cylinder. Such results by Roshko[(R3)] show a Strouhal number increase with Re up to S = 0.21 at Re = 10^3. No futher increase of S occurs for a further Re increase. Here,

$$S = \frac{nD}{V} \quad \text{and} \quad Re = \frac{VD}{\nu}$$

where n = vortex shedding frequency

D = cylinder diameter.

Author's Strouhal number trends with Re_s (Figs. 5.12 and 5.13) differ considerably from those for cylinders. Both S_{f_1} and S_{f_2} decrease with increasing Re_s. Thus the similarity between these processes is limited.

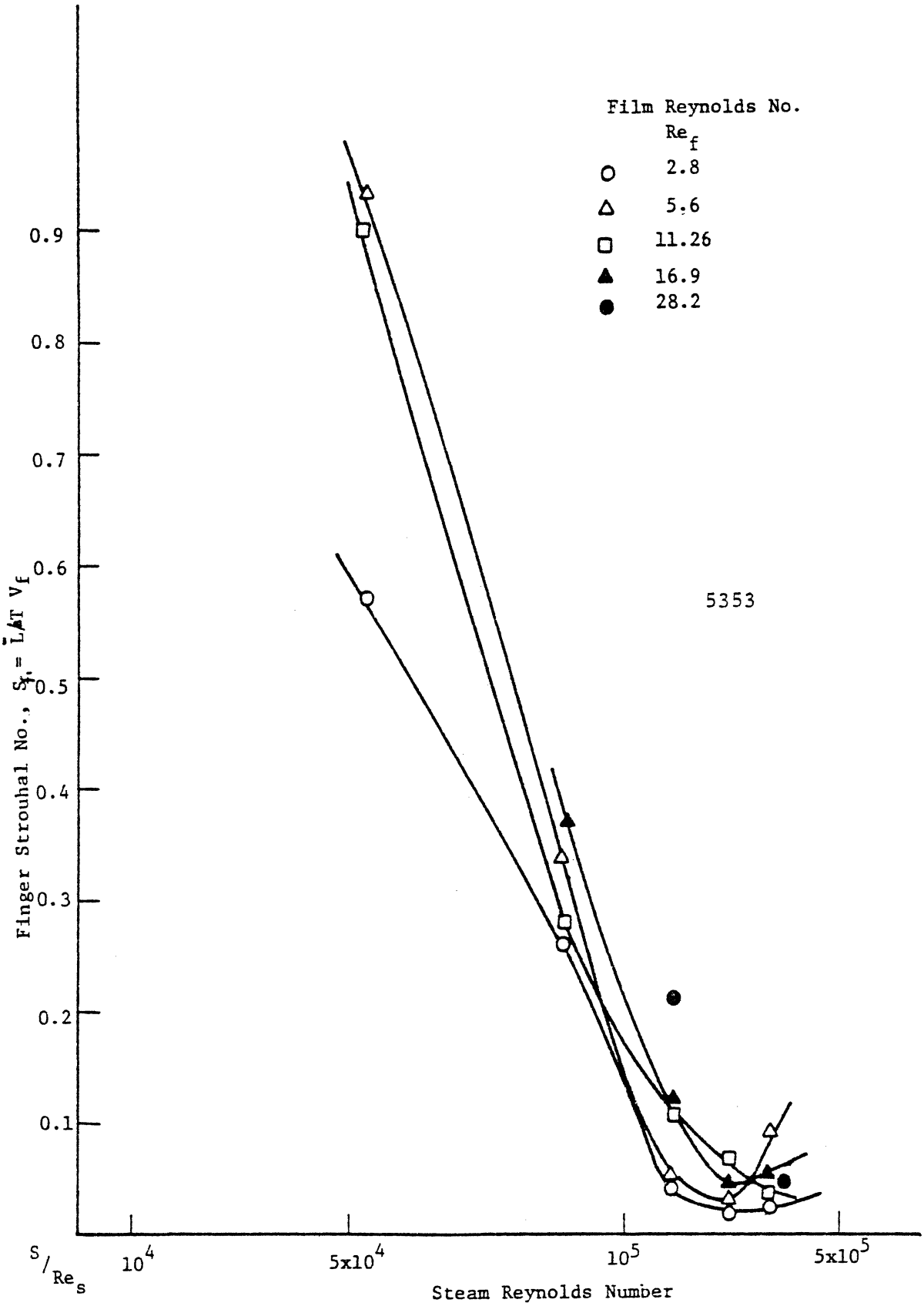

Fig. 5.12 Finger Strouhal No. $S_{f'}$ vs Steam Reynolds No. Re_s

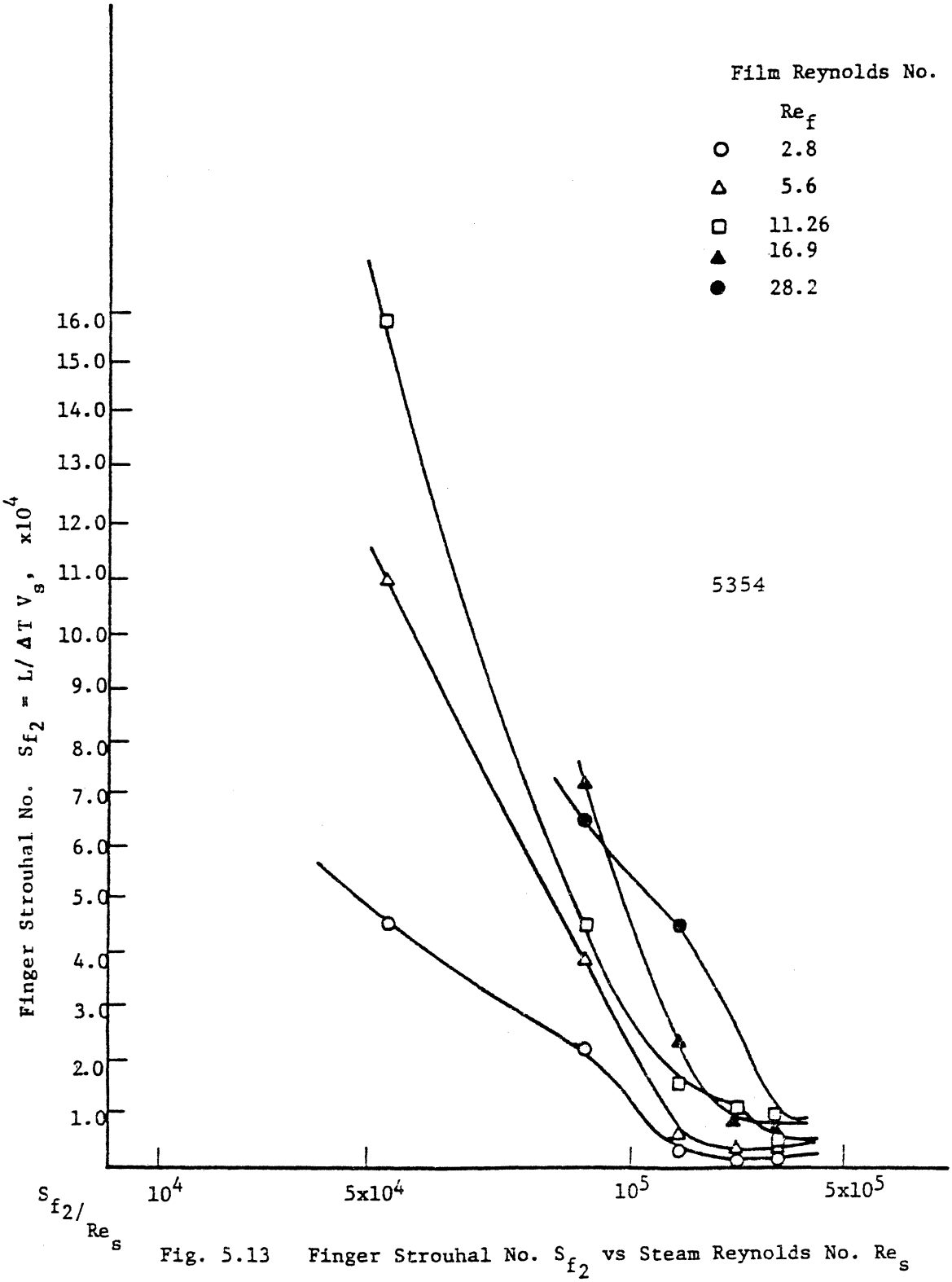

Fig. 5.13 Finger Strouhal No. S_{f_2} vs Steam Reynolds No. Re_s

Reference (B.9) provides a good summary of Strouhal number and Reynolds number correlations for various geometries. There, Strouhal number for flow past a thin flat plate (as author's case) is given as 0.156, which falls within author's range for S_{f_1} (Fig. 5.12). Since S_{f_1} is based on liquid rather than steam velocity, it appears that the vortex shedding in the steam in not a major factor for finger formation frequency.

Presumably liquid finger shedding is related to a balance between the driving forces and the stabilizing effect of surface tension. To study these effects, two new dimensionless parameters have been selected, the first being a non-dimensional time, τ:

$$\tau = \frac{U_s \Delta T}{\bar{L}} \left(\frac{\rho_s}{\rho_f}\right)^{1/2}$$

Physically, τ is the finger formation "period", normalized by a parameter having units of time formed from maximum finger length and densities of vapor and liquid. A rearrangement as below shows the physics more clearly

$$\tau = \left(\frac{U_s^2 \rho_s}{(\bar{L}/\Delta T)^2 \rho_f}\right)^{1/2}$$

$\bar{L}/\Delta T$ can be interpreted as a "deformation velocity" for the fingers. The numerator is the square root of dynamic pressure of the vapor flow acting on the finger, and the denominator is a measure of the deformation stress upon the

liquid finger.

The other nondimensional parameter here used is Weber number where

$$We_s = \frac{\rho_s U_s^2 \bar{L}}{\sigma} \tag{5.5}$$

In this case We_s is the ratio of the driving vapor dynamic pressure to the stabilizing surface tension stress for the finger. Plots of τ vs. We_s for various film Reynolds numbers, are shown in Fig. 5.14. The peak in τ is reduced, and the corresponding value of We_s also increases, as Re_f is increased to $Re_f \cong 8.4$. For higher Re_f, no peak in τ occurred. Rather it increased smoothly with increasing Re_f. Thus, surface tension appears more important for low than high Re_f, as would be expected.

Another important length parameter, mentioned earlier, is the finger wave-length, λ_f, i.e., the average distance between fingers. It was measured by counting the number of fingers, N observed in individual Fastax frames, and dividing the transversal distance along the trailing edge by N. Plots of N vs. time are shown in Figs. 5.15-5.17. In general, the number of fingers was found to increase with steam velocity.

Corresponding finger wave lengths, λ_f, are plotted in Fig. 5.18 as a function of steam velocity. λ_f ranges between 3 and 13 mm for the whole experimental range. Finger wave-lengths decreases for increasing steam velocity, except for highest steam velocity, indicating a minimum

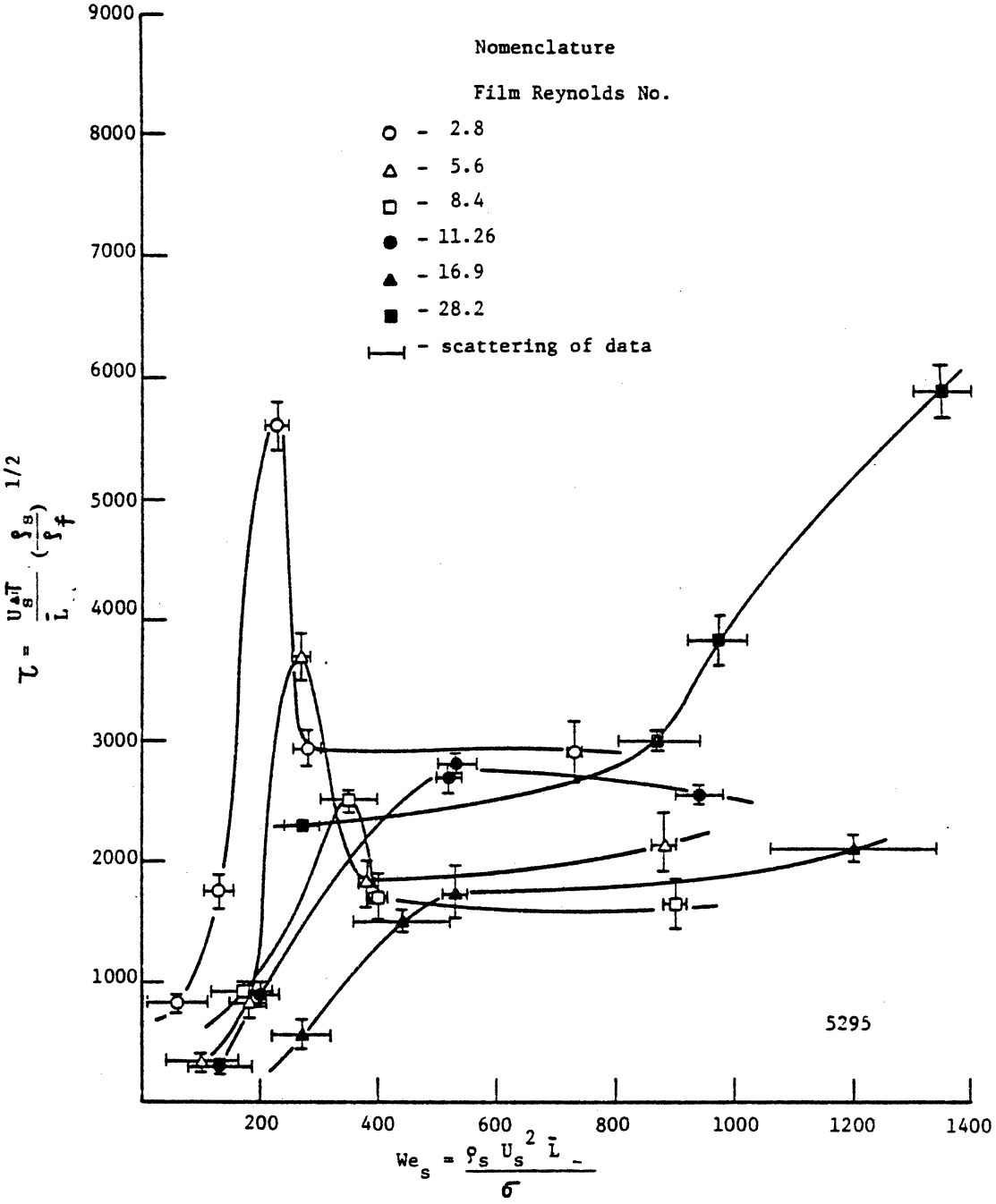

Fig. 5.14 Non-Dimensional Time and Weber Number for Finger

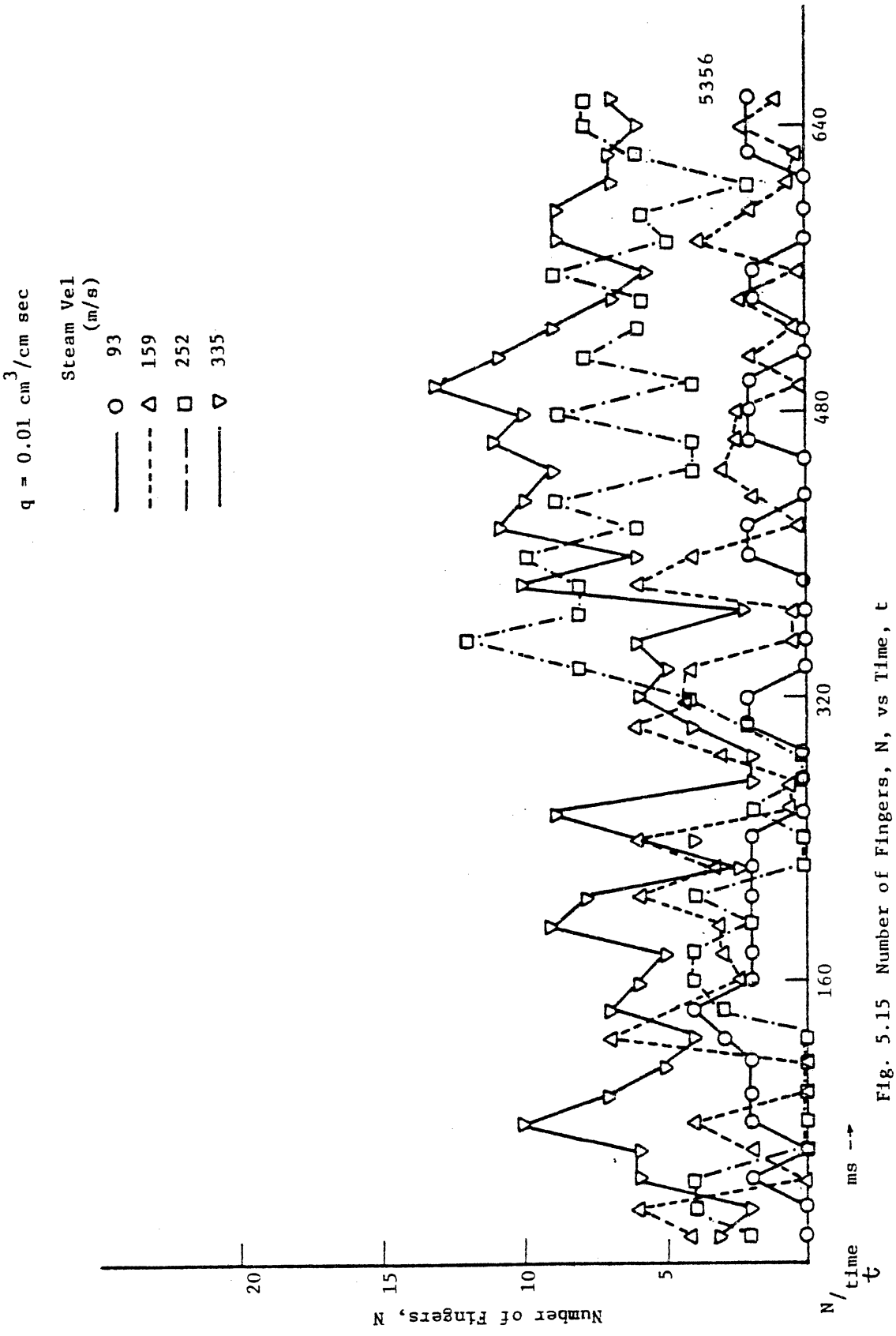

Fig. 5.15 Number of Fingers, N, vs Time, t

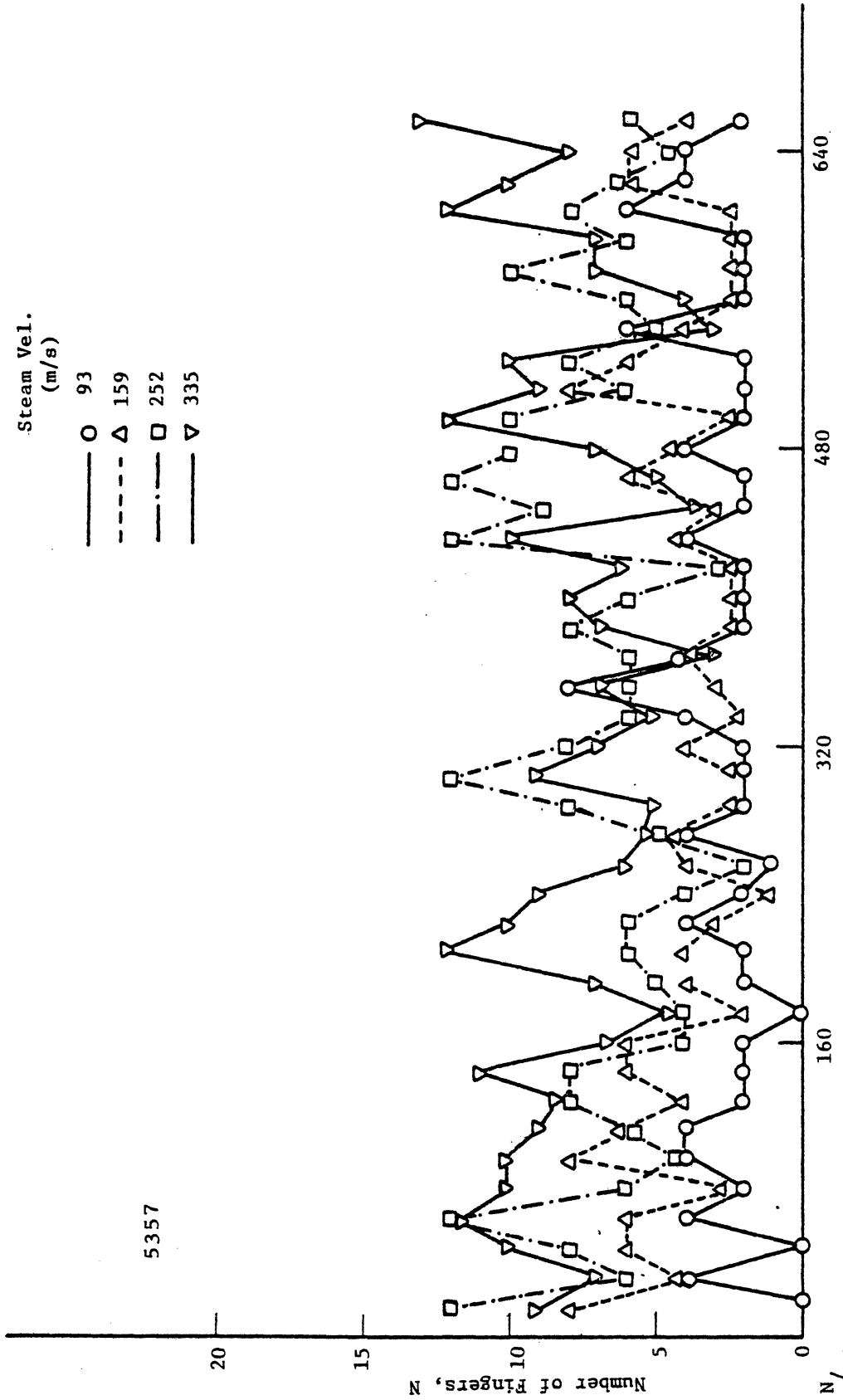

Fig. 5.16 Number of Fingers, N, vs Time, t

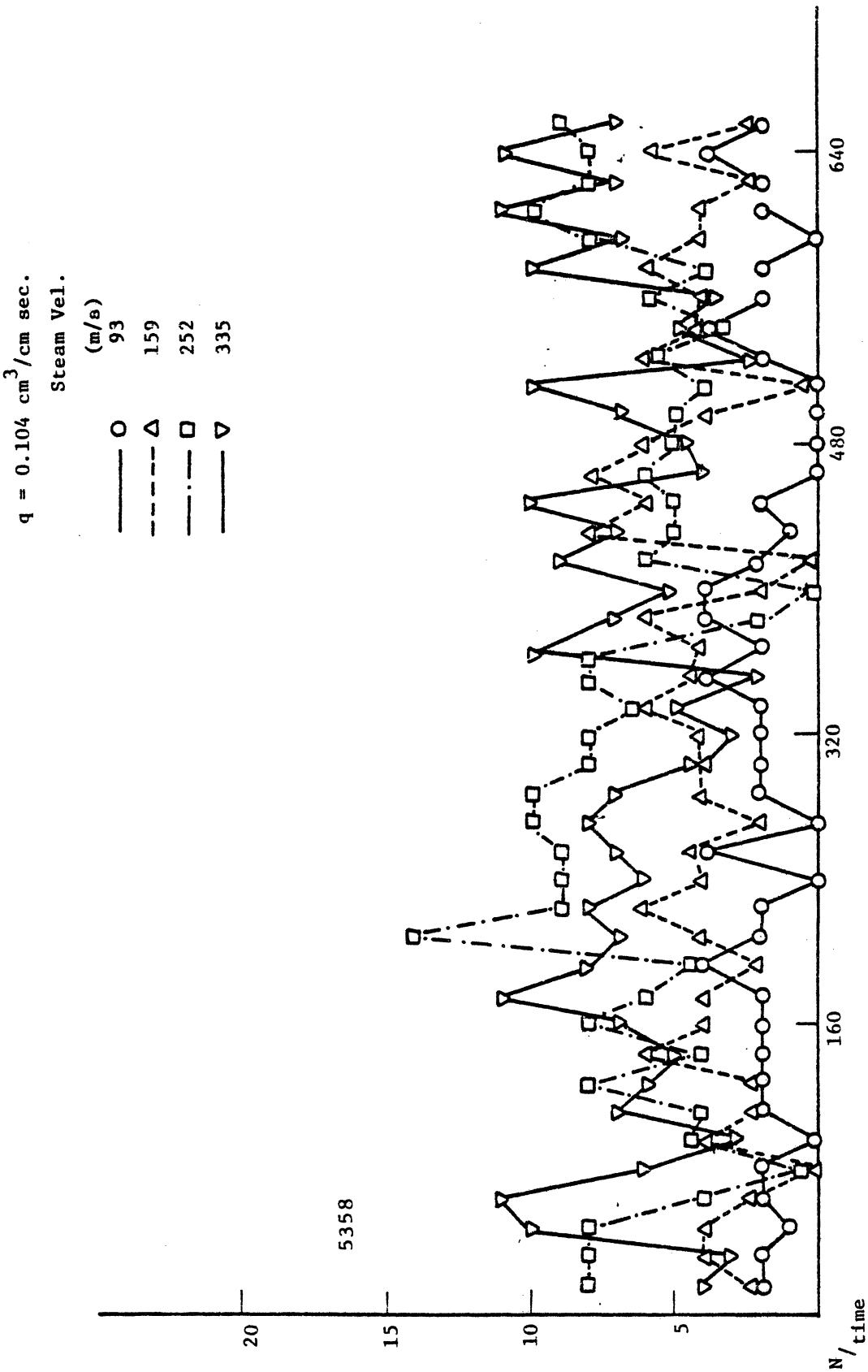

Fig. 5.17 Number of Fingers, N, vs Time, t

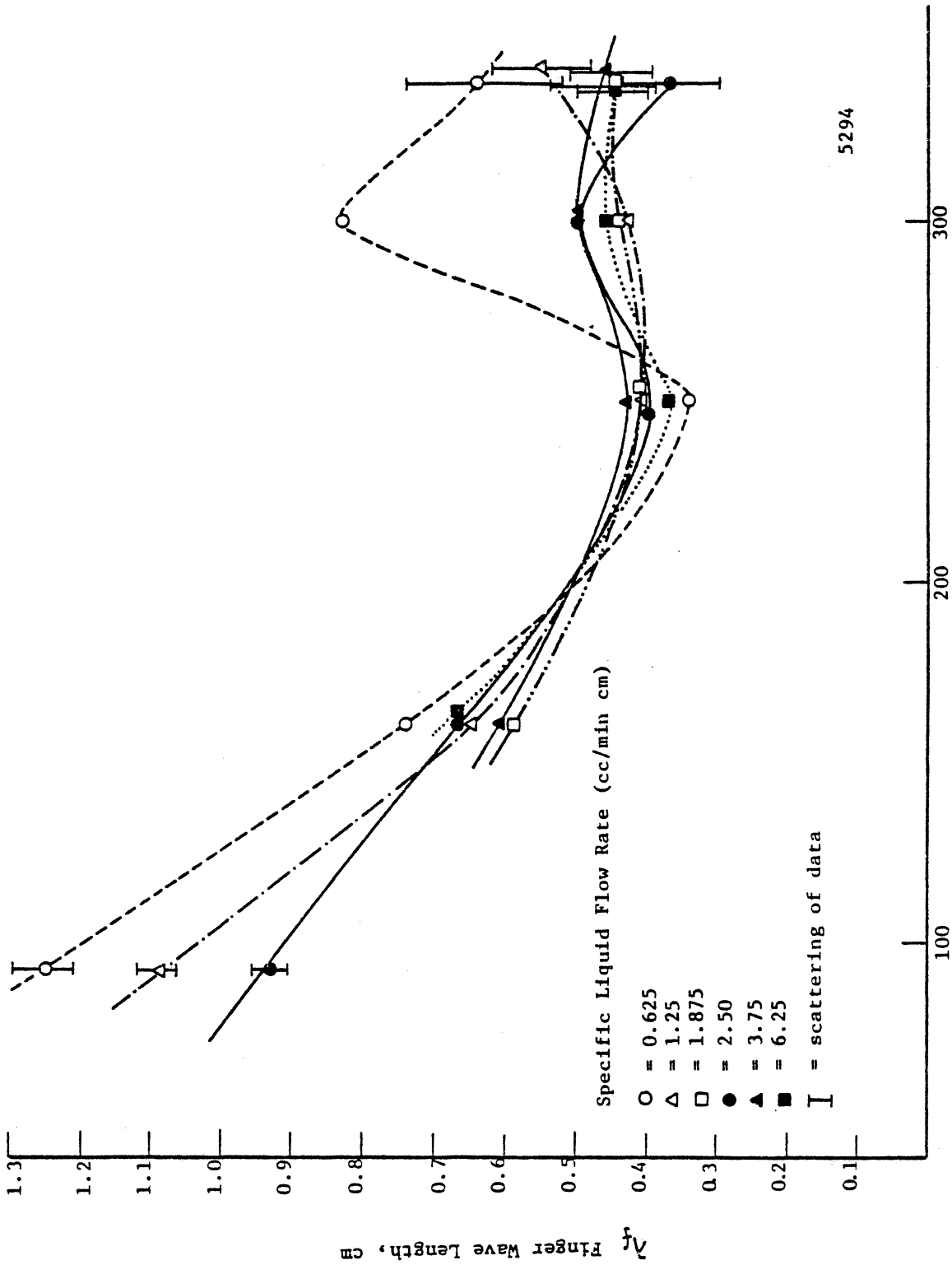

Fig. 5.18 Finger Wavelength vs Steam Velocity

with steam velocity. It is likely that the fingers become increasingly unstable, attaining smaller widths, as steam velocity is increased. This may result primarily from steam turbulence.

A non-dimensional finger length, L* is here defined as:

$$L^* = \frac{\bar{L}}{\lambda_f} \tag{5.6}$$

i.e., a ratio between average finger length and transversal distance between fingers. In general L* increases with Re_f at fixed Re_s (Fig. 5.19). Fluctuations with increasing Re_s are similar at each Re_f. These may be due to overall facility resonances depending upon steam velocity.

All finger formation parameters are listed in Table 5.2. Complete raw data and parameters are also available in our previous reports,[N9,T6,B10,B11] all done under author's supervision.

No results similar to author's current observations appear to exist in the literature, so that no comparisons with other data are possible. Thus author has made a "first attempt" which has obtained comprehensive experimental data. Later investigators will hopefully provide more complete theoretical understanding than obtained here, using this data as a basis.

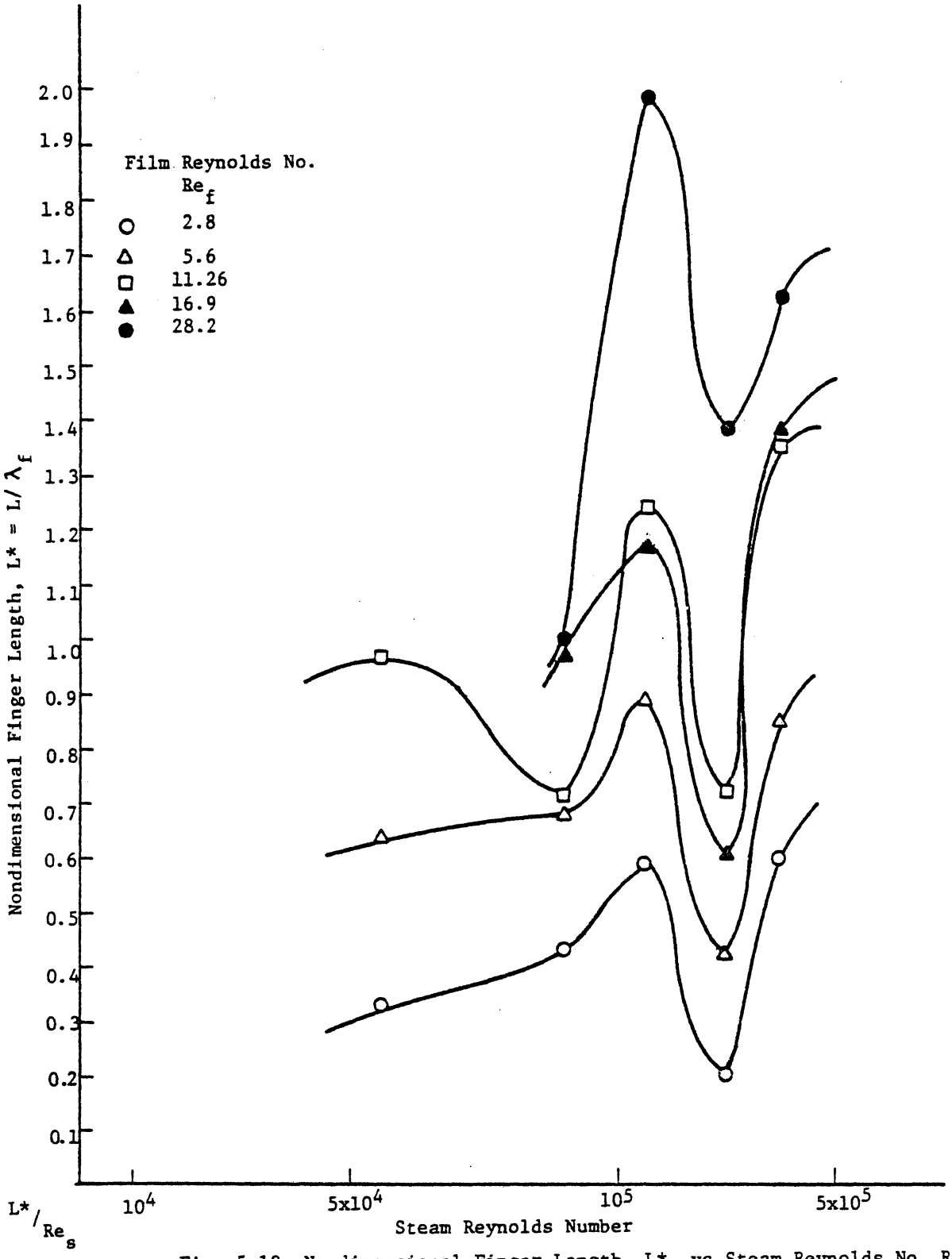

Fig. 5.19 Nondimensional Finger Length, L*, vs Steam Reynolds No. Re_s

Table 5.2: TRAILING EDGE PARAMETERS

V_s m/s	q cm^2/s	V_f cm/s	h mils	λ_f cm	$\bar{L}$ cm	Re_f	Re_s x10^{-3}	t s	We_s	We_f	S_1	S_2 x10^4	$\bar{L}^*$
93	.010	7.45	1.1	1.25	.418	2.8	53.3	.098	60.3	.33	.572	4.58	.33
"	.021	10.93	1.5	1.09	.697	5.6	"	.068	101	1.19	.936	11.00	.64
"	.043	16.40	2.0	.93	.900	11.26	"	.061	129.8	3.46	.900	15.87	.97
158.5	.010	13.67	.6	.74	.320	2.8	90.9	.089	134.3	.85	.26	2.24	.43
"	.021	18.22	.9	.65	.440	5.6	"	.072	184.5	2.09	.34	3.91	.68
"	.031	22.36	1.1	.59	.427	8.4	"	.056	180.4	3.05	.34	4.80	.72
"	.043	25.23	1.3	.66	.468	11.26	"	.067	197.18	4.26	.28	4.46	.71
"	.063	30.75	1.6	.66	.643	16.9	"	.057	268.5	8.69	.37	7.18	.97
"	.104	39.10	2.1	.66	.643	28.2	"	.073	268.5	14.04	.23	5.67	.97
252	.010	16.40	.5	.34	.202	2.8	144	.300	211.1	.78	.04	0.26	.59
"	.021	27.33	.6	.41	.364	5.6	"	.245	380.2	3.88	.05	0.54	.89
"	.031	35.14	.7	.41	.382	8.4	"	.103	401.3	6.74	.11	1.53	.93
"	.043	36.40	.9	.40	.495	11.26	"	.118	517.3	9.37	.11	1.59	1.24
"	.063	49.20	1.0	.43	.508	16.9	"	.087	528.0	17.57	.12	2.34	1.18
"	.104	58.60	1.4	.37	.823	28.2	"	.067	866.0	40.37	.21	4.88	2.22
297	.010	20.5	.4	.83	.162	2.8	170	.393	238.9	.97	.02	0.14	.20
"	.021	32.8	.5	.425	.180	5.6	"	.188	265.4	2.77	.03	0.33	.42
"	.031	41.0	.6	.44	.243	8.4	"	.159	353.9	5.84	.04	0.55	.55
"	.043	46.9	.7	.50	.360	11.26	"	.104	531.0	11.31	.07	1.11	.72
"	.063	61.5	.8	.50	.300	16.9	"	.131	442.5	16.21	.04	0.83	.60
"	.104			.46	.64	28.2	"		943.9				1.58

Table 5.2: TRAILING EDGE PARAMETERS

V_s m/s	q cm^2/s	V_f cm/s	h mils	λ_f cm	$\bar{L}$ cm	Re_f	Re_s $x10^{-3}$	t s	We_s	We_f	S_1	S_2	$\bar{L}^*$
335	.010	27.3	.3	.64	.387	2.8	192	.506	732.0	4.14	.03	0.24	.60
"	.021	32.8	.5	.55	.468	5.6	"	.152	882.4	7.19	.09	0.88	.85
"	.031	41.0	.6	.46	.481	8.4	"	.152	901.1	11.55	.08	0.98	1.05
"	.041	46.9	.7	.37	.504	11.26	"	.282	938.8	15.84	.04	0.56	1.36
"	.063	61.5	.8	.46	.639	16.9	"	.200	1201.4	20.08	.05	0.92	1.39
"	.104	82.0	1.0	.45	.724	28.2	"	.220	1351.7	69.55	.04	0.78	1.61

B. SECONDARY DROPLET MOTION

Due to drag forces from the vapor flow in the trailing edge wake, the "secondary" droplets detached from the fingers are rapidly accelerated. From the viewpoint of turbine blade erosion, direct measurement of droplet acceleration in the wake region is most important. As the droplets approach steam velocity, their normal impact velocity, important for erosion, upon the next rotating blade row will be reduced. (See Fig. 1.6).

For higher steam velocities, many of the larger drops were observed shattered into much smaller droplets, within a distance of 4 cm downstream from the trailing edge. Droplet size distribution data as a function of position is also very important for erosion, defining the probable upper limit of droplet size reaching the next rotating row.

Droplet break-up time, t_b, is here defined as the time-span between droplet formation from the liquid fingers and their disintegration.

1. DROPLET ACCELERATION

Using frame by frame studies of the Fastax pictures (as for the finger formation data) the trajectories of large liquid droplets were recorded under various steam and liquid flow conditions. Droplet size and position from the trailing edge were recorded every 5 frames (every 1 ms). Values of the second time derivative of position were determined using the following equation,

$$\left(\frac{\Delta^2 x}{\Delta t^2}\right)_i = \frac{x_{i+1} + 2x_i - x_{i-1}}{(\Delta t)^2} \qquad (5.7)$$

The "second divided difference" (here used) is the best approximation for the second derivative, if differences of higher order are not known.(D6,W13) This procedure allows identification of those position values containing significant errors. The second divided difference can then be recalculated neglecting the questionable data points. When position values are thus neglected, the time intervals are not equal. The second divided difference can then be written:

$$\left(\frac{\Delta^2 x}{\Delta t^2}\right)_i = \frac{\dfrac{x_{i+1} - x_i}{t_{i+1} - t_i} - \dfrac{x_i - x_{i-1}}{t_i - t_{i-1}}}{\dfrac{t_{i+1} + t_{i-1}}{2}} \qquad (5.8)$$

The steam and liquid flow conditions for which data on accelerations and break-up time were obtained are listed in Table 5.3. All data on droplet size and position were stored on the computer tape. Details of computer programs used and output obtained are found in Appendix C.

The time-averaged accelerations of droplets under various steam and liquid flow conditions are listed in Table 5.3. and plotted in Fig. 5.20 . Observed droplet accelerations range from $\sim 3 \times 10^4$ to $\sim 3.5 \times 10^5$ cm/sec^2 ($\sim$30 to 350 "g"), and increase with steam velocity, as would be expected.

Considering the nature of the phenomena observed, a sta-

U_s cm/s / q $\frac{cm^3}{cm\ s}$	9300			15850			25150			29720			33530		
	Am. cm/s^2	As. cm/s^2	$\bar{R}$	Am cm/s^2	As cm/s^2	$\bar{R}$	Am cm/s^2	As. cm/s^2	$\bar{R}$	Am cm/s^2	As cm/s^2	$\bar{R}$	Am cm/s^2	As cm/s^2	$\bar{R}$
.010	25550	37855	.782	75144	109893	.699	287500	244372	1.418	-	-	-	290390	363203	.910
.021	28780	30893	1.010	104906	117845	.983	294750	159862	2.059	312187	310066	1.152	303406	465454	.700
.032	-	-	-	82940	88814	.966	246000	215681	1.262	333750	311230	1.270	345000	528665	.690
.043	23454	42556	.775	69542	87936	.791	270000	161763	1.820	209117	312999	.770	356625	512930	.699
.063	-	-	-	80275	102841	.828	193593	198627	.953	189140	332318	.625	255374	509915	.606
.083	22117	30593	.727	-	-	-	-	-	-	-	-	-	-	-	-
.104	-	-	-	65203	90400	.746	147187	185582	.964	-	-	-	295833	478515	.680

TABLE 5.3; COMPARISON OF EXPERIMENTAL, Am, AND SERAFINI (S6), As, DROPLET ACCELERATIONS. $\bar{R} = (Am/As)$ ALL VALUES ARE AVERAGE VALUES FOR THE CONDITIONS SHOWN.

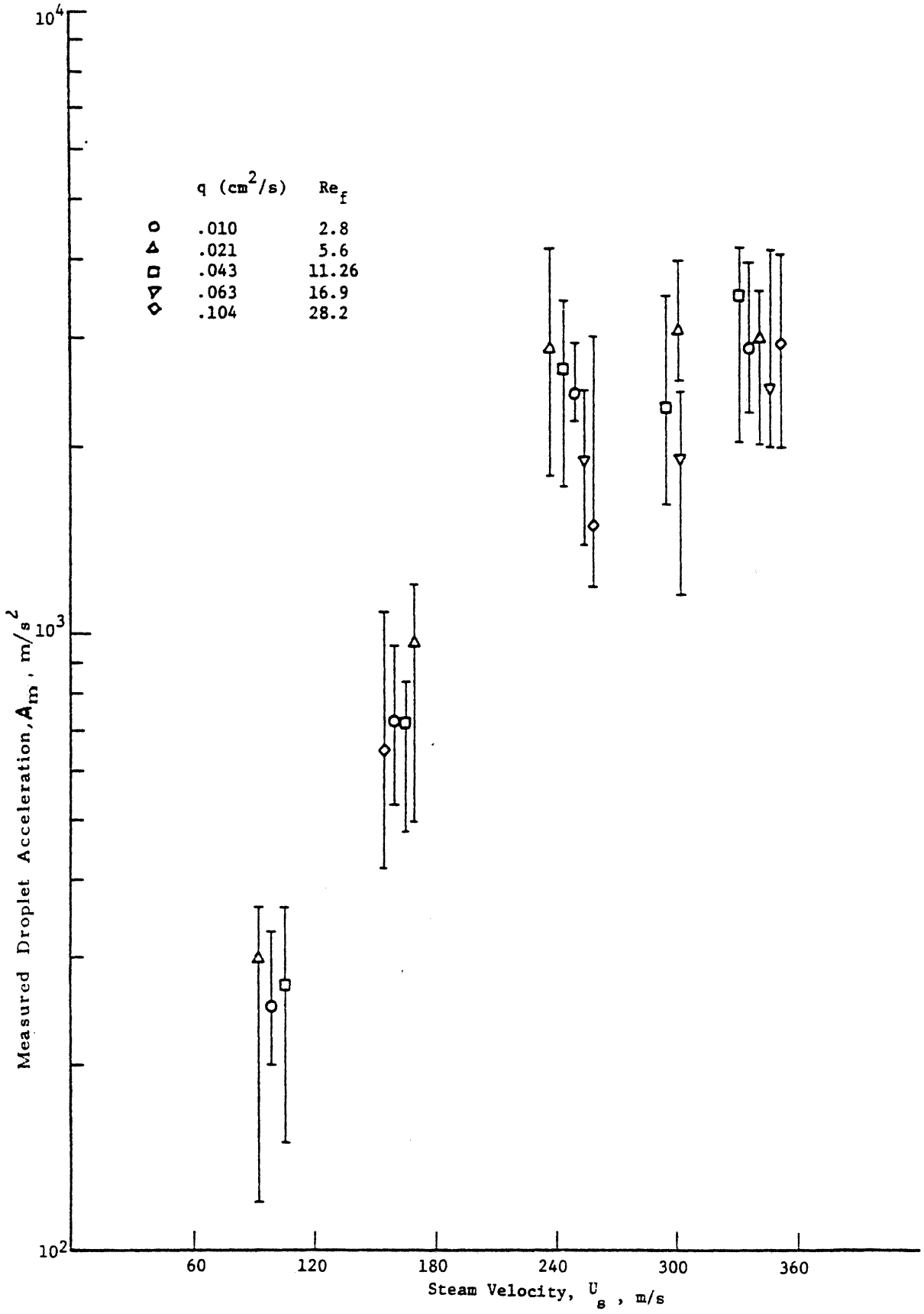

Fig. 5.20 Measured Droplet Acceleration as a Function of Steam Velocity

tistical method of data reduction was necessary and desirable. Thus a linear regression analysis was conducted. Full details of the analysis are given elsewhere (M14). The full output of the statistical analysis is given in Appendix D. An important result of this analysis is that droplet accelerations are largely unaffected by changes of liquid flow rate for all steam velocities. This is particularly true for low velocities. (Fig. 5.21)

THEORETICAL CONSIDERATIONS

Three important assumptions were needed to obtain an analytical expression for droplet acceleration. First, spherical drops were necessarily assumed, though many are severely distorted. An equivalent droplet diameter was defined as that of a disc of the same area perpendicular to the flow direction.

Next, the local vapor velocity was assumed to be the mean steam velocity at the blade exit plane.

Finally, the only force upon the droplets was assumed to be steam drag. One then obtains the following equation,

$$\rho_f \mathcal{V}_c \frac{dU}{dt} = C_D A_D \frac{\rho_s U_r^2}{2} \qquad (5.9)$$

where,

ρ_f = density of liquid droplet

ρ_s = density of vapor

$\mathcal{V}_c$ = volume of droplet $(= \frac{\pi D^3}{6})$

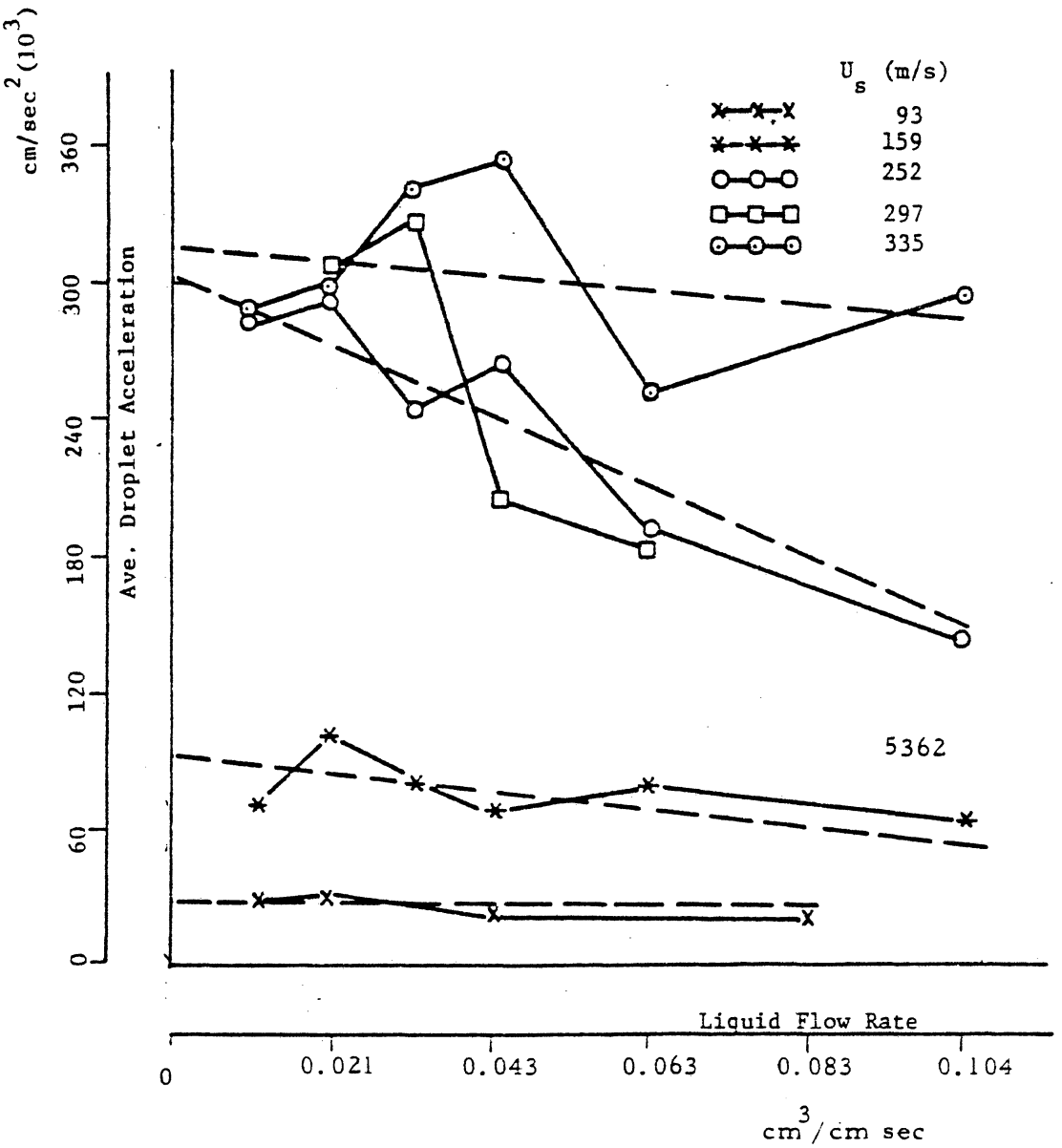

Fig. 5.21 Average Observed Droplet Acceleration versus Liquid Flow Rate at Various Steam Velocities. Dotted lines show regression analysis results. Note: Slopes of regression lines were not found to be significantly different than zero. See Statistical Analysis.

$\frac{dU}{dt}$ = droplet acceleration

C_D = Drag Coefficient

A_D = Projected area of droplet in the axial direction ($= \frac{\pi}{4} D^2$)

U_r = Relative velocity of droplet ($= U_s - U$)

Rearranging Eq. (5.9), droplet acceleration for drops of equivalent diameter, D, is $\frac{dU}{dt} = \frac{3}{4} \frac{\rho_s}{\rho_f} \frac{C_D}{D} U_r^2$ (5.10)

Many empirical results are available for C_D. As stated in Chapter II, all calculations of C_D were based on droplet acceleration due to uniform flow around a single droplet. No direct measurements of droplet acceleration in the wake region (as in the author's case) were found in the literature.

Author's wake-droplet regime is complicated by the presence of many droplets together. Because of spontaneous condensation in the "Wilson zone" combined with secondary droplets formation, a droplet size distribution exists in the wake. The drag for a given droplet will be influenced by other droplets. Such droplet "shielding" should thus be considered for a more precise analysis.

The drag coefficient shield effect was apparently first considered by Tam[T2]. He derived a statistical formula for the drag exerted on a cloud of spherical particles of given

size distribution. He concluded that the individual particle drag depends significantly only on the first three moments of the distribution function. However, no experimental verification yet exists. Tam's solution is not used by present author, because it is applicable only to very low Reynolds numbers.

Instead three different already published [C14,A1,S6] empirical correlations were compared with author's data. These are:

$$1) \quad C_D = \frac{24}{Re_D}\left(1 + \left(\frac{Re_D}{60}\right)^{5/9}\right)^{9/5} \tag{5.11}$$

$0 < Re_D < 3000$ (Churchill & Usagi [C14])

$$2) \quad C_D = 0.292\,(1 + 9.06/\sqrt{Re_D})^2 \tag{5.12}$$

$0 < Re_D < 5000$ (Abraham [A1]),

and

$$3) \quad C_D = \frac{24}{Re_D}\,(1 + 0.17\,Re_D^{2/3}) \tag{5.13}$$

$0 < Re_D < 6000$ (Serafini [S6]),

where droplet Reynolds number, Re_D, is defined as

$$Re_D = \frac{U_r\,D}{\nu_s} \tag{5.14}$$

These three empirical correlations were substituted into Eq. (5.9), and comparisons with author's data made.

(Appendix E). Calculated accelerations, using Eqs. (5.11 - 5.13) were compared with those measured (Fig. 5.22). For low acceleration, i.e., low steam velocity, the differences between measured and calcualted accelerations, using any of the C_D correlations are small. However, for higher steam velocities, the calculated accelerations using any of the C_D correlations are larger than those measured. The Serafini correlation fits best the present data. Therefore it alone has been used in the following.

2. Observed Droplet Decelerations

Author defines an acceleration ratio, R,

$$R = \frac{A_m}{A_s} \tag{5.15}$$

where A_m is measured acceleration and A_s that calculated from Serafini's C_D correlation (Eqn. 5.13). Time averaged results ($\bar{R}$) are listed in Table 5.3. One finds $\bar{R} < 1$ for high liquid flow rates ($q \geq 0.043$) and for the highest steam velocity (U_s = 335 m/s) for any value of q. For fixed flow conditions, abrupt oscillations in R with respect to time are found (Appendix C and Figs. 5.23 and 5.24). The wake droplets are not continuously accelerated, but actually decelerate at times and exhibit "back-flow" moving against the mean vapor flow. Several of our high-speed movies show this intermittent droplet directional change. To be more explicit, droplets detaching from a liquid finger move a short distance ($\sim$ 2 cm) down stream, then reverse

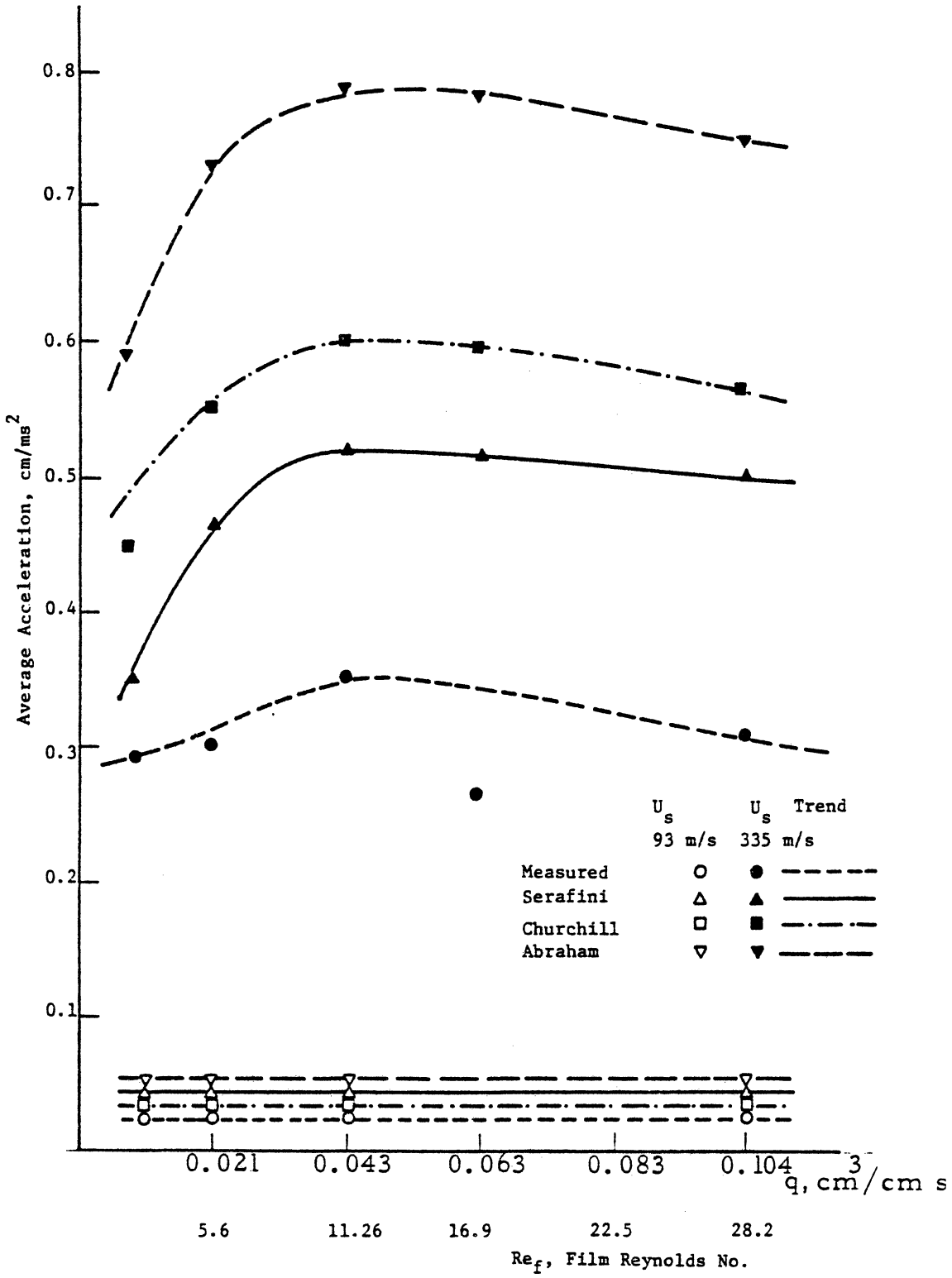

Fig. 5.22 Comparison of Average Measured Acceleration and those using other Correlations of C_D

direction, moving a short distance (~2 cm) upstream. These negative accelerations are shown in Figs. 5.23 and 5.24 .

The only plausible mechanism for this droplet deceleration and motion reversal appears to be periodic vortex shedding from the relatively blunt blade trailing edge. Figure 5.25 is a schematic of the hypothesized flow pattern. If an individual vortex is not aligned precisely with a droplet center (see lower portion of Fig. 5.25), then such a droplet will experience an additional (upstream or downstream) relative velocity and drag due to the velocity field of that particular vortex. For such upstream relative velocity, it would be momentarily decelerated. Even though this hypothesized mechanism is consistent with author's data, vortex measurements have not been possible. Nevertheless it does appear the only plausible explanation for the observations.

Some related parameters can be deduced. Average time interval Δt between decelerations, calculated from the R vs. t curves (Figs. 5.23 and 5.24), is a measure of the vortex shedding frequency. A calculation of Δt was possible only for low steam velocities (U_s = 93 and 159 m/s). For higher steam velocity, the droplets disintegrated too rapidly for accurate measurements of this type. Values of Δt and related parameters are listed in Table 5.4. Two non-dimensional parameters(S_B and Re_D) were selected to correlate the droplet deceleration frequency. These numbers are defined below.

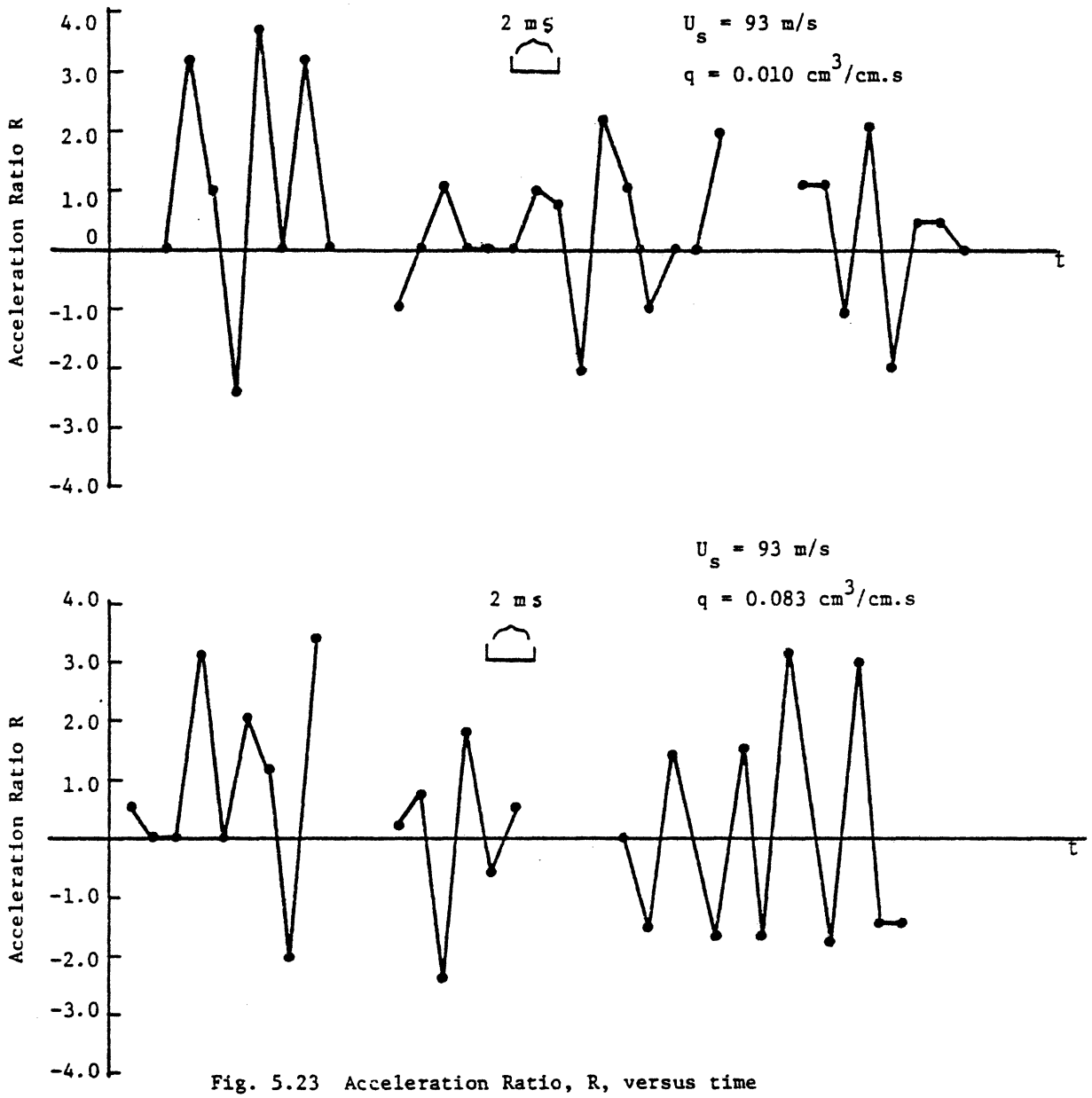

Fig. 5.23 Acceleration Ratio, R, versus time

$$R = A_m / A_s$$

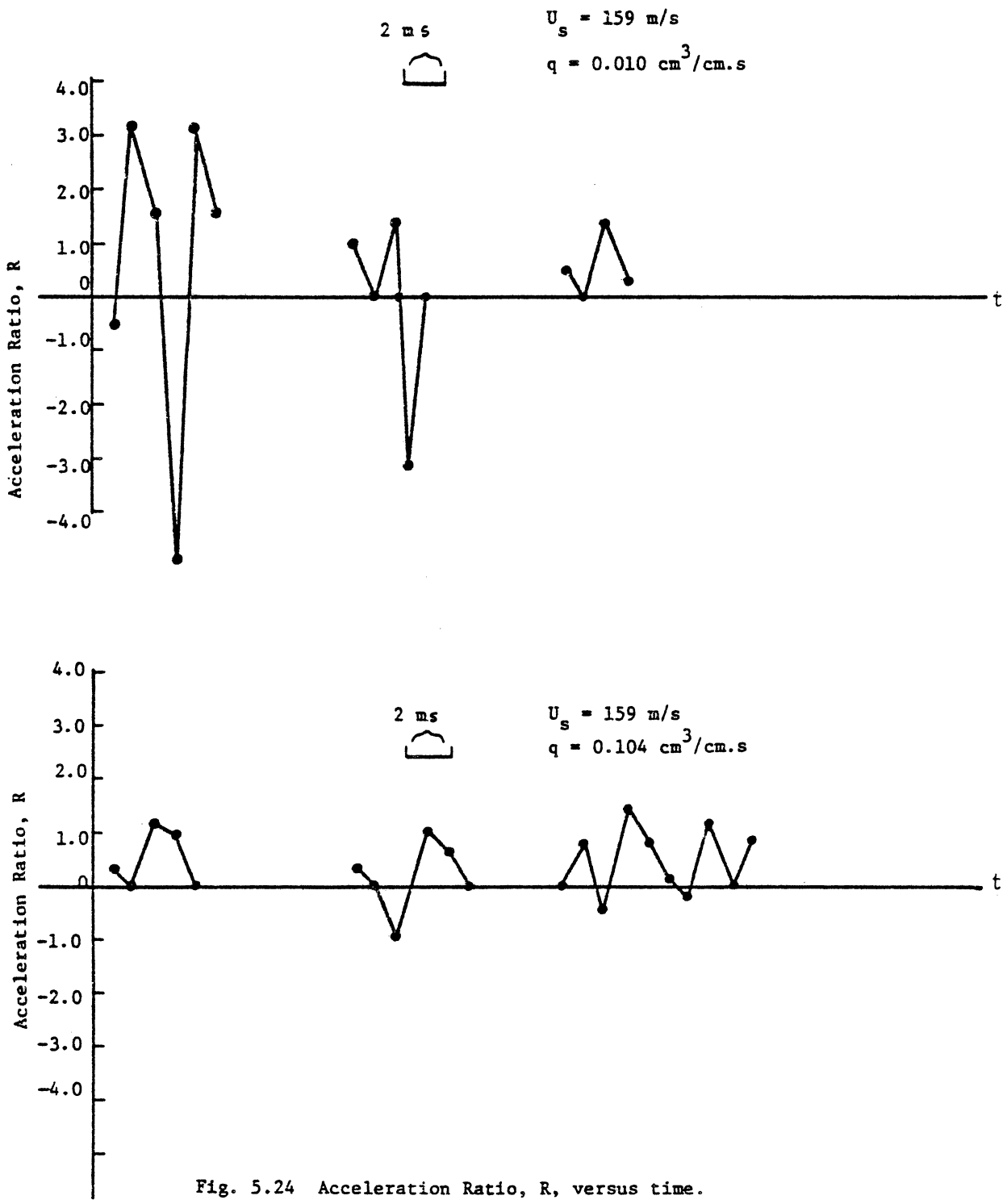

Fig. 5.24 Acceleration Ratio, R, versus time.

$$R = A_m / A_s$$

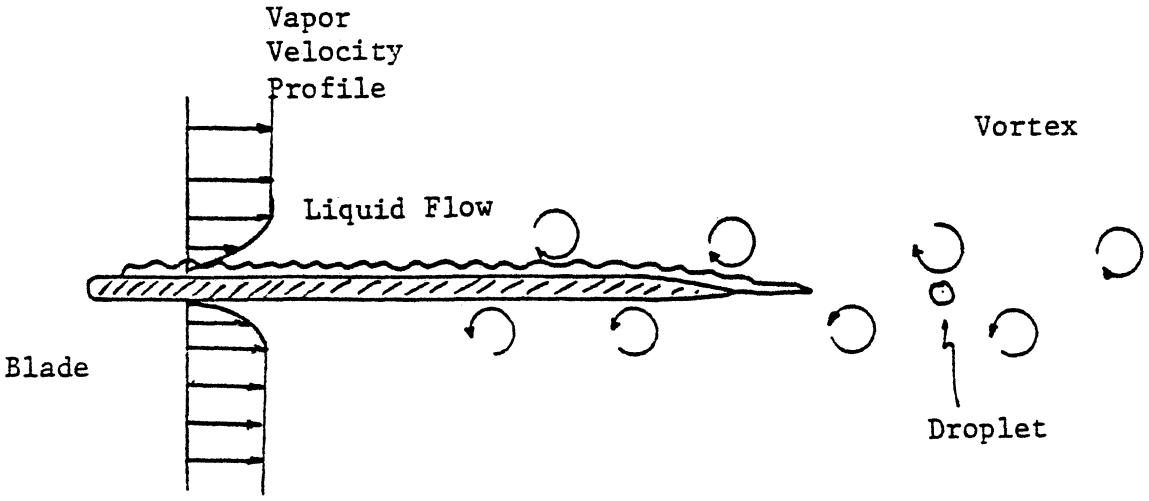

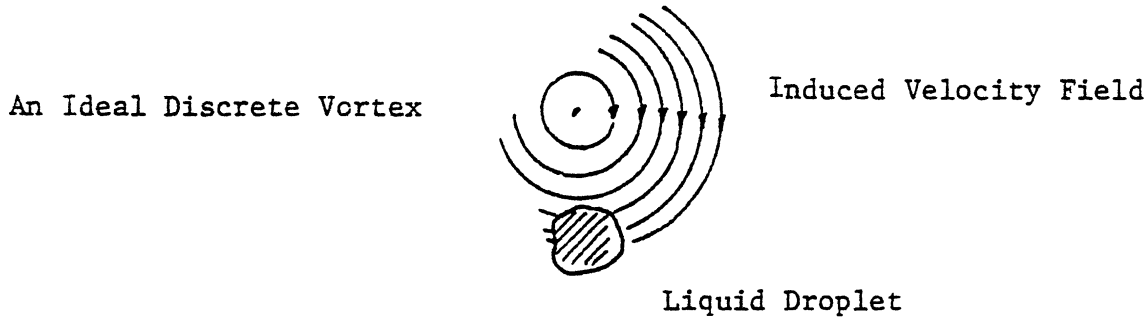

Fig. 5.25 Schematic of Vortex Generation from the Trailing Edge of the Blade

U_s m/s	q $\frac{cm^3}{cm\ sec}$	D cm	A_m cm/s^2	R $\frac{A_m}{A_s}$	V_i m/s	Γ m^2/s	Δt $10^{-3}s$	V_f cm/s	S_{v_s}	S_{v_f}	Re_D	S_B	$S_{B_{v_f}}$
93	.010	.11	27550	.78	4487	7.573	2.669	7.45	.00403	6.03	958.2	.01611	20.110
93	.021	.12	28780	1.01	55.20	9.293	3.248	10.93	.00331	2.82	1036.5	.01324	11.266
93	.043	.09	23454	.78	51.16	8.594	4.556	16.4	.00236	2.54	970.4	.00944	5.353
93	.083	.12	22116	.73	43.23	7.262	2.397	25.75	.00538	1.94	1156.0	.01794	6.479
159	.010	.08	75144	.70	74.34	12.489	2.333	13.67	.00216	2.51	1364.7	.0108	12.522
159	.021	.08	104906	.98	63.11	10.602	3.500	18.22	.00144	1.25	1316.3	.00719	6.255
159	.031	.09	82940	.97	70.76	11.887	3.942	22.36	.00144	1.02	1541.6	.00638	4.522
159	.043	.07	69542	.79	44.24	7.432	4.083	25.23	.00140	.874	1526.1	.00616	3.870
159	.063	.09	79275	.83	63.30	10.634	4.200	30.75	.00135	.697	1443.3	.00599	5.088
159	.104	.09	65203	.75	58.68	9.859	4.306	39.05	.00131	.535	1506.3	.00584	2.370

U_s: steam velocity

q : specific liquid flow rate

D : average drop diameter

a_m: measured acceleration

$\frac{a_s}{a_m}$: acceleration ratio

V_i : induced velocity

Γ : vortex strength ; $\oint \bar{u} \cdot d\bar{s}$

B : blade thickness = .4cm

ΔT : periodicity of deceleration

V_f : velocity of film

S_{v_s} : Strouhal number ($\frac{D}{U_s \Delta t}$).

S_{v_f} : Strouhal number ($\frac{D}{V_f \Delta t}$)

Re_D : ($\frac{U_s D}{\nu_s}$)

S_B : ($\frac{B}{\Delta t\ U_s}$)

$S_{B_{v_f}}$: ($\frac{B}{\Delta T V_f}$)

Table 5.4: Parameters Concerning the Periodic Deceleration of Droplet in the Wake Region.

$$S_B = \frac{B}{U_s \Delta t} \qquad \text{Strouhal number} \qquad (5.16)$$

$$Re_D = \frac{D\, U_s}{\nu_s} \qquad \text{Droplet Reynolds Number} \qquad (5.17)$$

where B is blade thickness, Δt periodicity of deceleration, and D effective droplet diameter.

S_B is plotted against Re_D in Fig. 5.26. Although data scatter is large, the solid lines show the general trends. S_B decreases as U_s increases from 93 to 159 m/s. This is due to the increase in both U_s and Δt. (Average Δt = 3.1 ms for U_s = 9.3 m/s and 3.8 ms for U_s = 159 m/s).

For a given steam velocity, S_B increases with increasing Re_D, remaining roughly constant at a higher Re_D. The present observation of droplet wake deceleration is apparently the first such reported. Thus no comparison with other experimental or theoretical results is possible.

3. Disintegration Time for Droplets

For high steam velocities, many of the large droplets were observed to undergo initial acceleration and then disintegrate into a mist of much finer particles. Break-up time, t_b, is here defined as the time between droplet formation (from the liquid fingers) and droplet disintegration into either an amorphous mass or numerous smaller droplets.

One of these disintegration processes is "disc" disintegration. Analogous behavior has been observed in shock tubes.(L8, H8, H15, J1, N8, W8) An intially almost

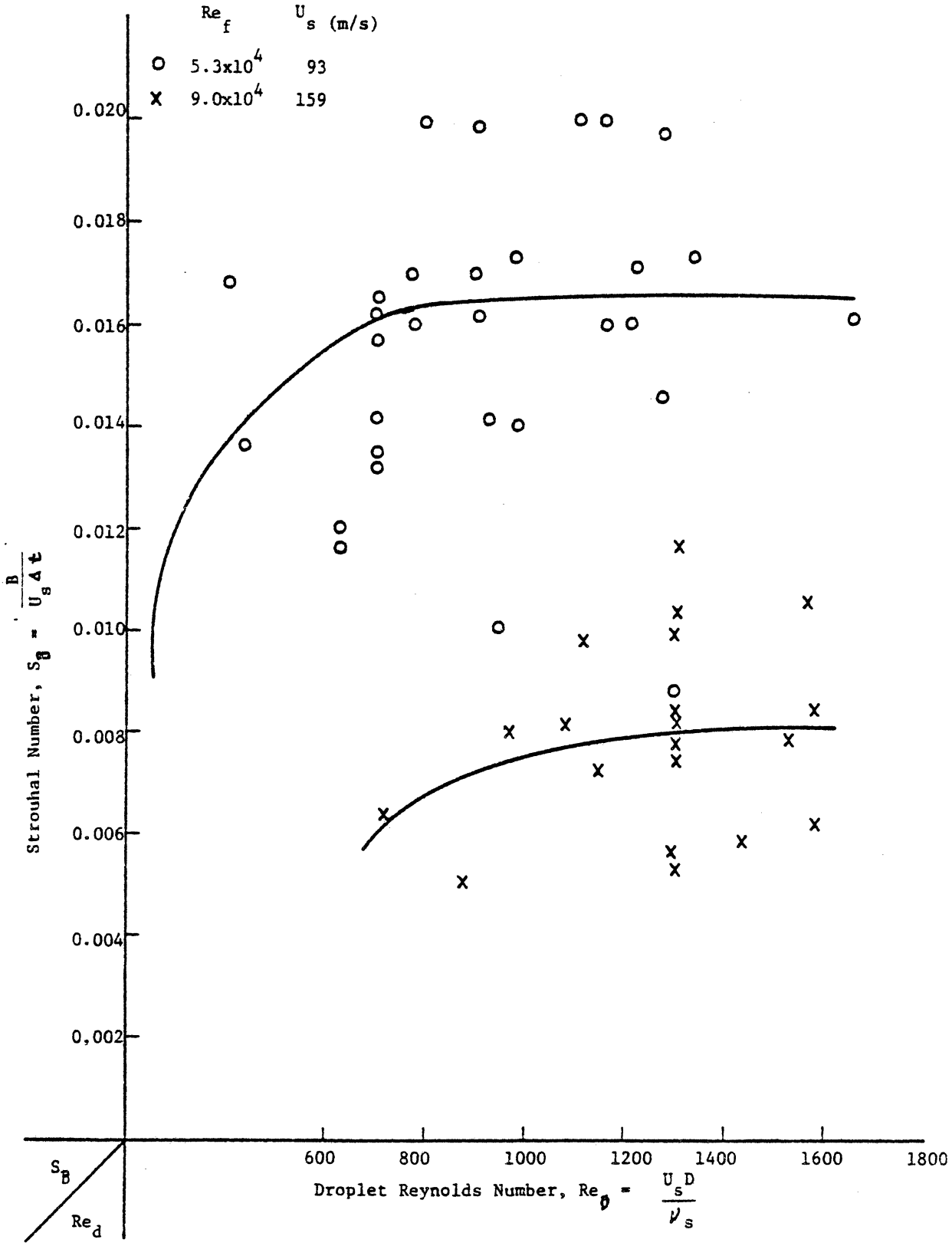

Fig. 5.26 Strouhal Number, S_B, versus Droplet Reynolds Number, Re_B

spherical droplet assumes a disc shape with axis parallel to flow direction. Upon further acceleration, it breaks into several smaller droplets.

Another disintegration mode here observed is the "club" or "claviform" process[H16, K11]. A droplet is formed around and behind a long liquid jet ("club" or "claviforn"). Break-up of the "club" then occurs with the residual droplets also quickly disintegrating. Further details are provided elsewhere[H16, K11].

In the case of supersonic aircraft rain-erosion, two additional modes of droplet break-up have been suggested[A4, R4, E1, K12, W9, W10, R5, B8] involving shock effects. Passing through a shock wave, droplets are either flattened (normal to the axis), with smaller droplets stripped from the circumference, or almost instantly torn apart.

Generally these other investigators use geometries different from author's. Liquid droplets of known size are often injected perpendicular to the flow. Shock waves may or may not occur. Author's droplets are formed from the liquid fingers previously discussed and shock waves are not involved (M<1).

Author's droplet disintegration data have been described using the following non-dimensional variables;

(1) Weber number, We_b, i.e. the ratio between steam dynamic liquid surface tension effects, here defined as,

$$We_b = \frac{\rho_s \, Ur^2 \, D_o}{\sigma}$$

Steam density, ρ_s, and velocity, U_r, relative to the droplet, are used. D_o is the original droplet diameter and σ the liquid surface tension.

(2) A non-dimensional break-up time, T_b, i.e., droplet lifetime before break-up, normalized to consider droplet size and both droplet and steam densities. T_b, used previously (A4, W9,W10,R5,B8), is defined:

$$T_b = \frac{U_r\, t_b}{D_o} \left(\frac{\rho_s}{\rho_f}\right)^{1/2} \tag{5.19}$$

where t_b is the pre-disintegration droplet lifetime. ρ_f and ρ_s are liquid and steam densities. The square of T_b is the ratio of dynamic steam pressure to a deformation droplet stress. This concept was discussed for finger formation.

(3) Q is non-dimensional flow around a droplet, already defined elsewhere (A4,B8,R5,W9,W10). It is the ratio of dynamic steam pressure on the droplet surface to upstream dynamic steam pressure, and is defined:

$$Q = \frac{\rho_g\, U_g^2}{\rho_s\, U_s^2} \tag{5.20}$$

Here ρ_g and U_g are local steam density and velocity and ρ_s and U_s the corresponding upstream values. Here $\rho_g \simeq \rho_s$. Then Q becomes:

$$Q = \left(\frac{U_g}{U_s}\right)^2 \tag{5.21}$$

Since Q is a locally varying quantity, a characteristic Q_m is its maximum. For low to moderate subsonic flows over a sphere, potential flow gives for a maximum, $Q_m = 9/4$ (see Arts. 92-96 in Ref. L6 and Section 15.30-15.53 in Ref. M13).

However, for high subsonic velocities as in some of author's cases, empirical results are required. A simple empirical expression for Q_m [R5], is

$$Q_m = 0.78 + \frac{1.47}{1 + 2.1\ M^{3.4}} \quad ; \quad 0 \lesssim M \lesssim 3.5 \qquad (5.22)$$

where M is steam Mach number.

Combining Eqs. 5.19 and 5.21, non-dimensional time, T_b, can be modified [W10, R5, B8] as in the following:

$$T_b\ Q_m^{1/2} = \frac{U_r\ t_b}{D_o} \left(\frac{\rho_s}{\rho_f}\right)^{1/2} \frac{U_g}{U_s} \qquad (5.23)$$

Then with the assumption that $U_r \tilde{=} U_s$, valid for the present tests, Eq. (5.23) becomes:

$$T_b\ Q_m^{1/2} = \frac{U_g t_b}{D_o} \left(\frac{\rho_s}{\rho_f}\right)^{1/2} \qquad (5.24)$$

The modified non-dimensional break-up time, (Eq. 5.2) can be physically interpreted as the square root of the ratio of maximum local dynamic pressure on the droplet surface to the accompanying droplet deformation stress.

$T_b Q_m^{1/2}$ is plotted against We_b in Figs. 5.27 - 5.30, and is found to be roughly inversely proportional to We_b. The proportionality constants increase with increasing steam velocity.

Experimental data obtained elsewhere in shock tubes [N8, H16, H17, A4, R5, B8] shows the non-dimensional break-up time, Eq. (5.19) or (5.24), to be approximately proportional to $We_b^{-1/4}$.

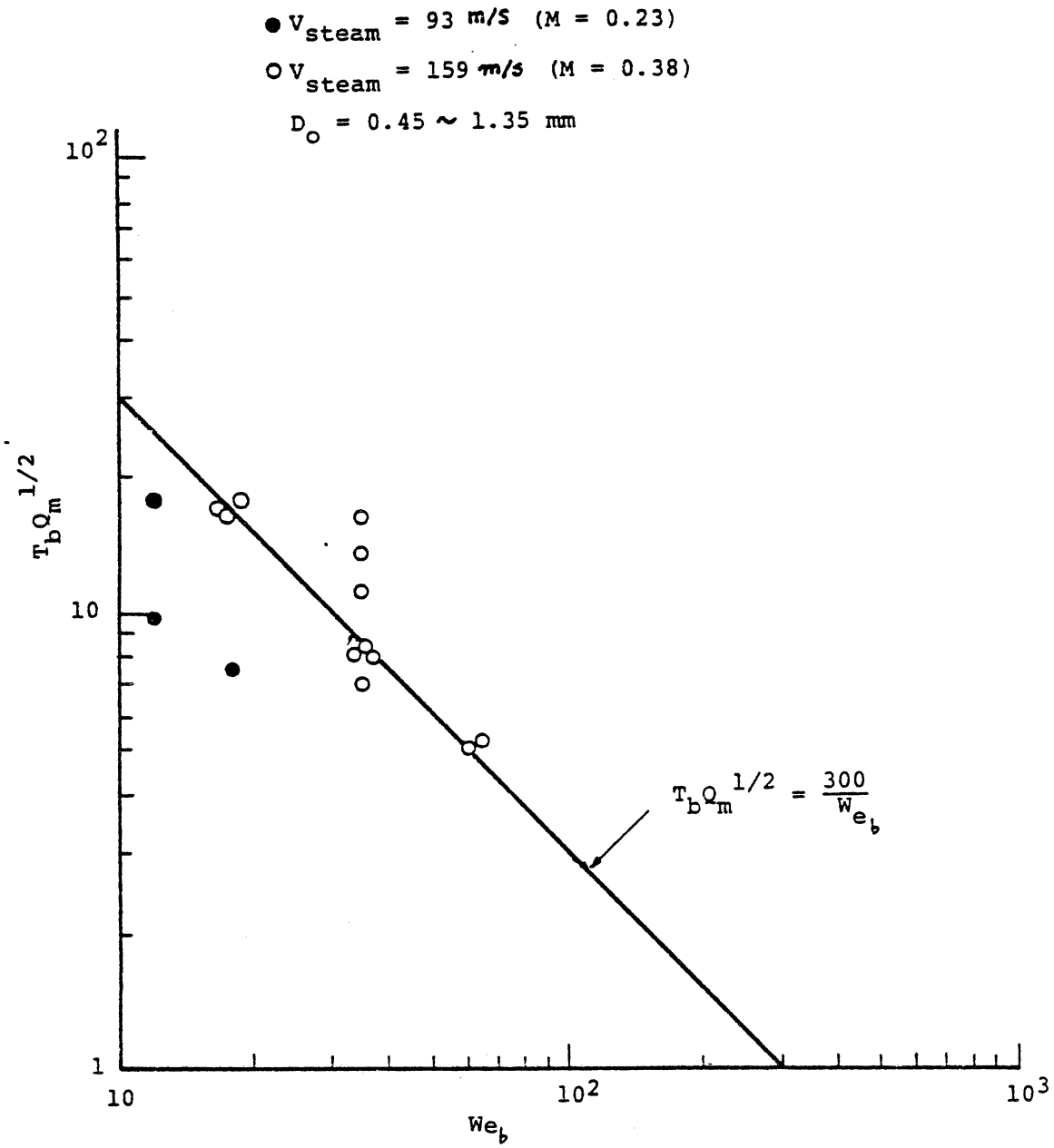

Fig. 5.27 Nondimensional Drop Breakup Time vs Droplet Weber No.

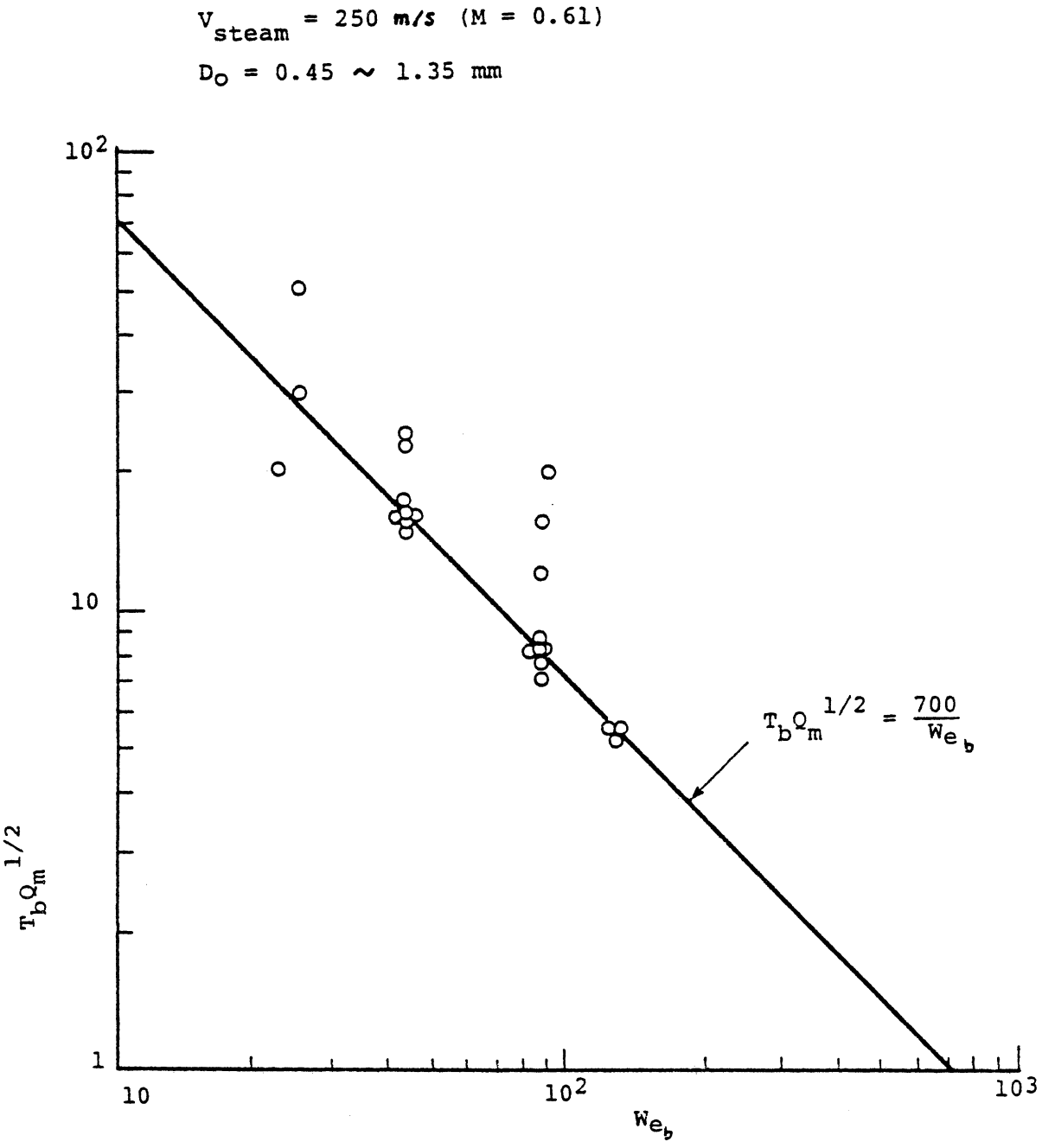

Fig. 5.28 Nondimensional Drop Breakup Time vs Droplet Weber No.

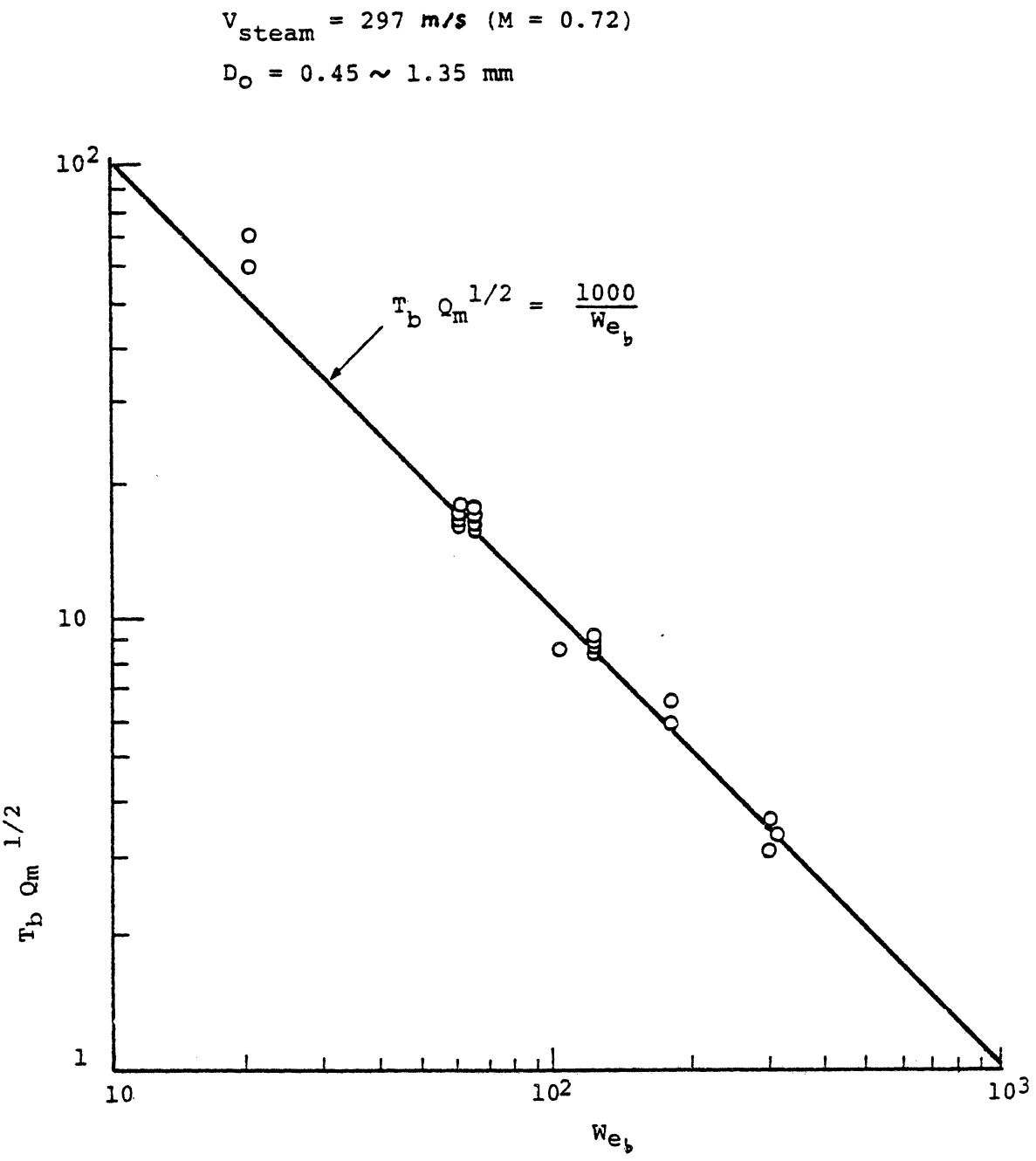

Fig. 5.29 Nondimensional Drop Breakup Time vs Droplet Weber No.

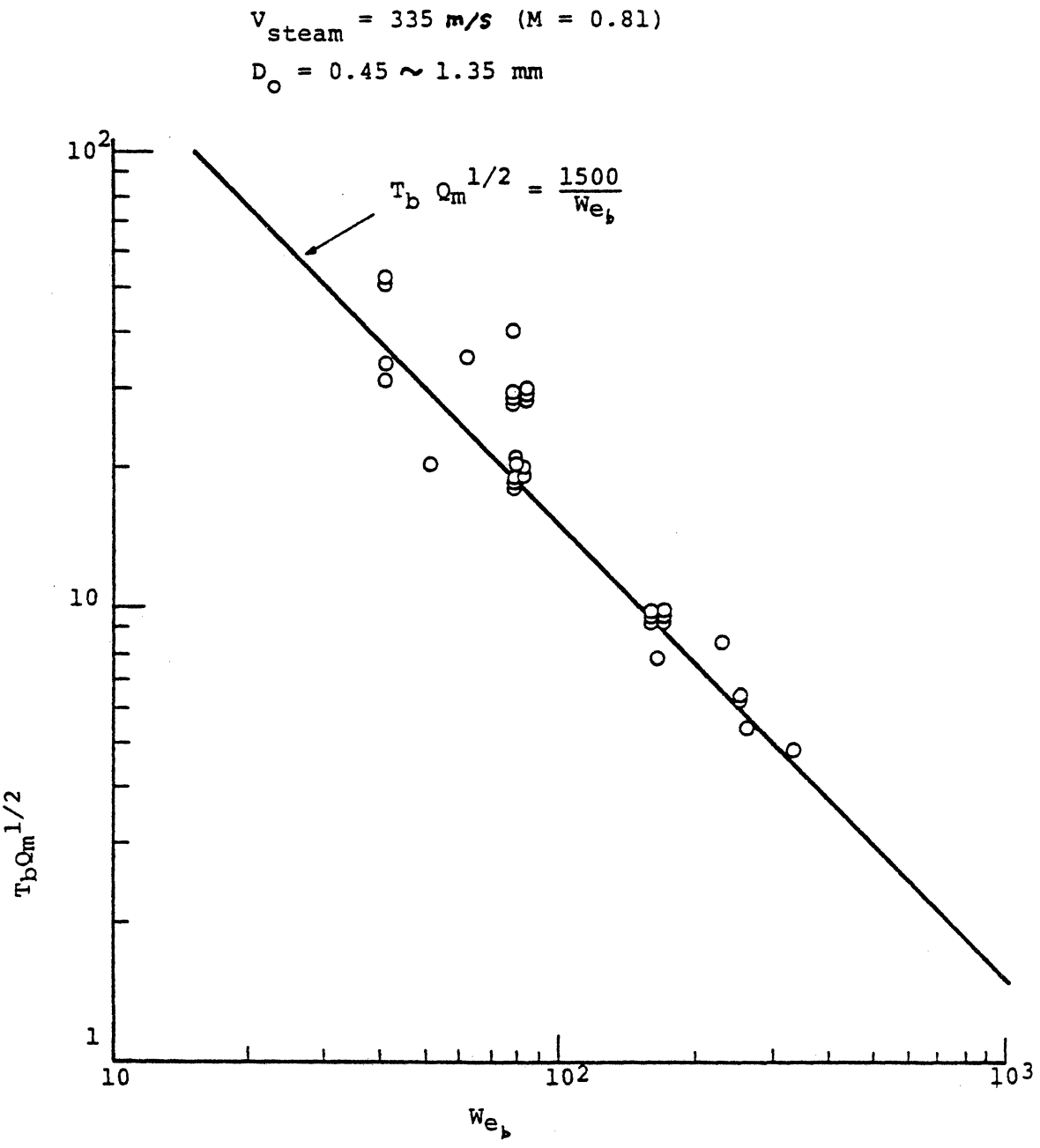

Fig. 5.30 Nondimensional Drop Breakup Time vs Droplet Weber No.

Figure 5.31 compares the shock tube data with that of present tests. The solid line is a previously proposed[R5] empirical correlation of the shock tube data. Author's data are shown as circles.

The exponent difference in droplet Weber number dependence can be explained by considering the wave growth model on the droplet surface proposed by previous investigators.[B8,R5] It is therefore concluded that an inverse We_b dependence (as found by author) is primarily due to a Kelvin-Helmholtz instability [C17,L6] near the equator of the droplet. A $We_b^{-1/4}$ dependency (from shock tube data) is due to the prevailing Rayleigh-Taylor instability [C17,L6] near the pole of the droplet.

Details of the wave growth analyses originally suggested by previous researchers [617,L6,R5,B8] are given in Appendix G.

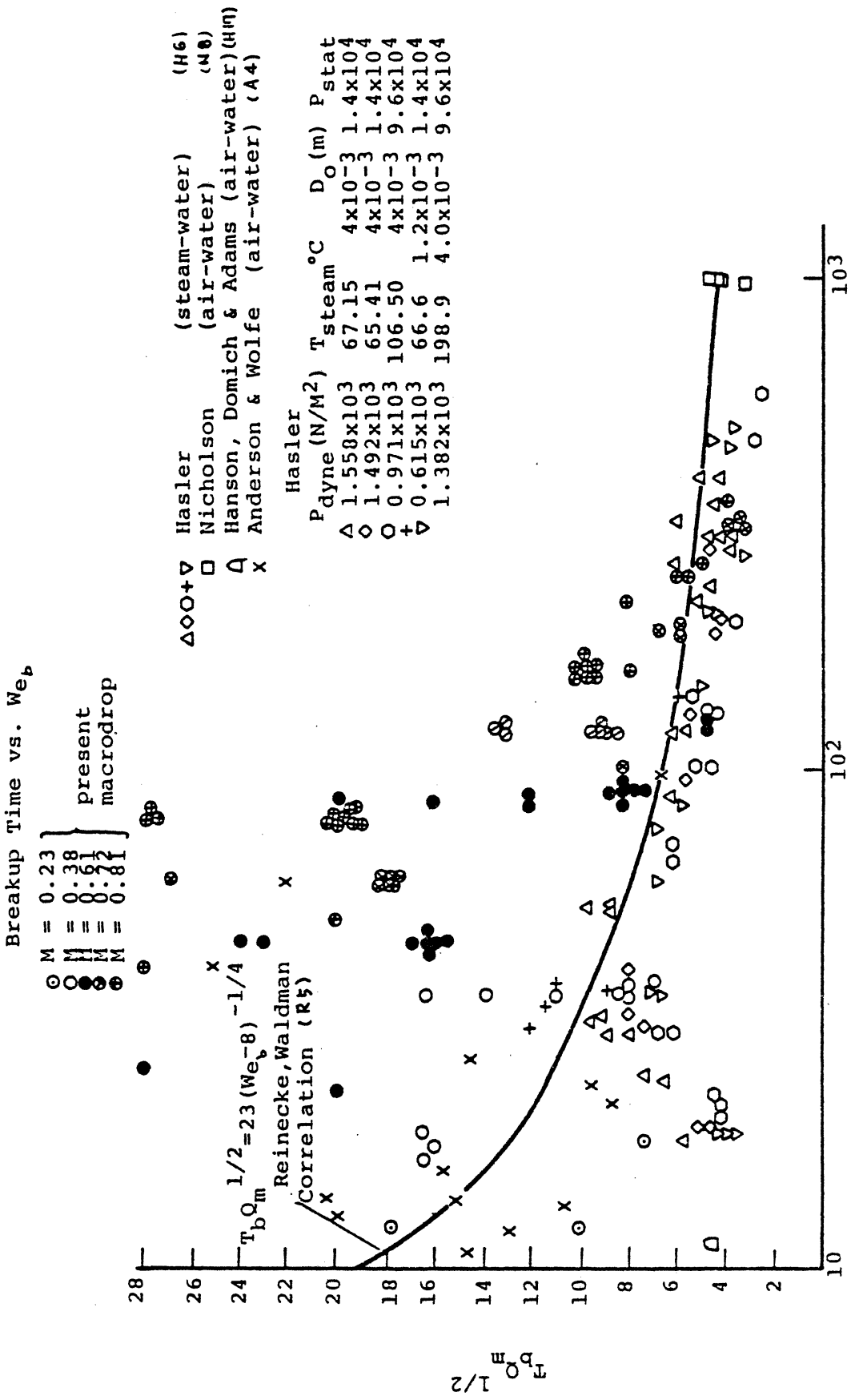

Fig. 5.31 Nondimensional Breakup Time vs Droplet Weber No.
(Comparison between shock tube experimental data and author's data)

CHAPTER VI

CONCLUSIONS

Phenomena leading to large steam turbine blading erosion have been investigated experimentally. These include the behavior of thin liquid films, and their subsequent break-up into droplets and fingers at the trailing edge of a stationary blade, here modelled by a thin flat plate.

Based primarily on photographic results, a film "Transition Map" for various flow regimes has been made. Three different film flow regimes were observed: rivulet, wavy films, and an entrainment regime corresponding to more vigorous wave action.

Liquid film thicknesses were measured as a function of time and position using electrical conductivity microgages. A best empirical correlation for author's film thickness data is: $h^+ = 0.6\ Re_f^{1/2}$, where h^+ is a non-dimensional film thickness and Re_f film Reynolds number. Few previous correlations for this very thin film range exist. However, an extrapolation of Hughmark's thick-film correlation[H6] along with some data from Collier-Hewitt[C13] give a prediction higher than author's correlation for given Re_f. Film entrainment at author's high steam velocities may be partially responsible for this discrepancy.

The author obtained the critical conditions for rivulet flow experimentally. Comparison with existing theoretical analyses shows that the wetting contact angles required in the analyses are much smaller than measured for static

or one curvature condition. Modifications of these analyses are suggested based on author's observations. First, the flow geometry around the filament or dry spot stagnation points should be considered in more detail. Author's photographs show that there is an abrupt bulge in the film near the stagnation point, instead of a smooth decrease in film thickness from upstream as had been previously assumed.

Also, film wave characteristics should be more carefully considered. Photographs from the present study show that some waviness always exists in the rivulet flow regime. These wavelets will certainly affect the dynamic forces causing film separation.

For the usual thick film analysis, the contribution of pressure perturbations to film instability with respect to wave generation is usually dominant, and that of shear perturbations negligible. For thin films (author's case) shear perturbations[C10] become relatively more important as film thickness decreases. Since author's photos always show some waviness even in the rivulet flow regime (which corresponds to the thinnest films), it is believed that the thin film shear perturbation mechanism is most important for author's case.

Measured two-dimensional wave propagation speed has been compared with Wurz's[W14] model, which well correlates author's high subsonic data. However this is not true for low subsonic data. All the two-dimensional wave celerity data is better explained by the classicial capillary-gravity

wave model.

For the film entrainment regime, both experimental and theoretical criteria are found. Liquid film entrainment was photographically observed to involve a rapid acceleration, lifting, and then shattering of small complex "wavelets" at the crests of larger waves. There is a limiting liquid flow rate below which no surface entrainment occurs ($\lesssim 0.07$ $cm^3/sec.cm$).

Based on author's thickness measurements, a correlation for critical entrainment conditions is found. This correlates the horizontal duct data better, including author's, than previous correlations.[I2] However, confidence in author's correlation is limited by the present lack of detailed information on actual shapes of larger waves, and the present inability to accurately calculate pressure variations over waves of arbitrary shape and size.

At the trailing edge, liquid finger length, L, and finger wavelength, λ_f, have been measured photographically. The upper limit of L for all time-spans decreases as steam velocity is increased. Also "dead" periods, while no finger is forming, are observed. Finger shedding frequency decreases with increasing steam velocity, U_s, and increases with an increase of liquid flow rate. The dependence of shedding frequency on U_s is explained by boundary layer thinning with increasing shear stress. It has been found that Karman vortex-shedding in the steam is not a controlling factor in finger formation.

A peak in nondimensional finger shedding period, τ, was found for lower film Reynolds number ranges. The peak value of τ is reduced, and the corresponding values of We_s is increased as Re_f is increased up to an intermediate value, $Re_f = 8.4$. For higher Re_f, no such peaks were observed. Rather τ then increases smoothly with increasing We_s.

Non-dimensional finger length, L*, normalized by transverse finger wavelength, λ_f, was found to increase with Re_f at fixed Re_f. These fluctuations could be due to various overall system resonances, which may themselves depend upon steam velocity. Since author's finger formation observations are apparently the first reported, no comparison with other related studies is possible.

Measured droplet accelerations were compared with those calculated using Serafini's empirical drag coefficient. However, author's wake-droplet behavior is complicated by the presence of many droplets together, i.e., significant "shielding" may exist.

Deceleration of droplets which sometimes reverse direction completely and move against the main stream, was observed. This phenomenon can be explained by the reverse velocity field induced by vortex shedding in the steam. A Strouhal number, S_B, considering the periodicity of deceleration, increases with increasing drop Reynolds number, Re_d, remaining roughly constant at higher Re_d. This general behavior is consistent with most vortex-shedding observations.

Disintegration time for the larger range of drops observed was measured along with characteristic droplet disintegration shapes (disc and "club" forms). Non-dimensional break-up time, T_b, is found to be proportional to We_b^{-1}. However, shock-tube data shows $T_b \propto We_b^{-1/4}$. These dependencies are explained using surface wave growth theory.

REFERENCES

A

A1. Abraham, F. F., "Functional Dependence of Drag Coefficient of a Sphere on Reynolds Number," Physics of Fluids, Vol. 13, pp. 2194-2195, 1970.

A2. Allen, J. M., "Evaluation of Compressible-Flow Preston Tube Calibrations," NASA TN D-7190, 1973.

A3. Alia, P., Cravanolo, L., Hassid, A. and Petrocchi, E., "Liquid Volume Fraction in Adiabatic Two-Phase Vertical Upflow - Round Conduit," CISE Rept. R-105, 1965.

A4. Anderson, W. and Wolfe, H., "Aerodynamic Breakup of Liquid Drops," Proceedings of 5th International Shock Tube Symposium, sponsored by the Div. of Fluid Dynamics of the Amer. Phy. Soc., April 1965.

A5. Austrow, J., "Trailing Edge Observations of the Steam Tunnel Experiments," DRDA Rept. No. UMICH 014571-19-I, April, 1978.

B

B1. Baumann, K., "Some Recent Developments in Large Steam Turbine Practice," Eng., vol. III, p. 435, 1921.

B2. Bankoff, G. S., "Minimum Thickness of a Draining Liquid Film," Int. J. Heat Mass Transfer, 14, 2143, 1971.

B3. Brown, C. and Matin, S. A., "The Effect of Finite Metal Conductivity on the Condensation Heat Transfer to Falling Water Rivulets on Vertical Heat-Transfer, Trans. ASME, J. of Heat Transfer, pp. 69-76, 1971.

B4. Benjamin, T. B., "Wave Formation in Laminar Flow Down an Inclined Plane," J. of Fluid Mech., 2, p. 554-575, 1957.

B5. Brumfield, L. K. and Theofanous, T. G., "On the Prediction of Heat Transfer Across Turbulent Liquid Films," J. of Heat Trans., Trans. ASME, pp. 496-502, 1976.

B6. Benjamin, T. B., "Shearing Flow Over a Wavy Boundary," J. Fluid Mech., vol. 6, pp. 161-205, 1959.

B7. Blanchard, D. C. and Woodcock, A. H., Tellus, vol. 9, pp. 2, 1957.

B8. Barber, J. P., "Water Drop Break Up/Impact Damage Thresholds," AFML-TR-76-126.

B9. Blevins, R. D., "Flow Induced Vibration," Van Nostrand Reinhold Co., 1977.

B10. Blome, S., "Wet Steam Tunnel Observations of Fingers at Trailing Edge," DRDA Rept. No. UMICH 014571-8-I, April 1977.

C

C1. Cohen, L. S. Hanratty, T. J., "Effects of Waves at a Gas-Liquid Interface on a Turbulent Air Flow," J. Fluid Mech., vol. 31, p. 467-479, 1968.

C2. Crane, R. I., "Deposition of Fog Drops on Low Pressure Steam Turbine Blades," Inst. J. Mech. Sci., vol. 15, pp. 613-631, 1973.

C3. Cole, J. E., and Dobbins, R. A., "Propagation of Sound Through Atmospheric Fog," J. Atmos. Sci., vol. 27, May 1970.

C4. Chu, K. J., Dukler, A. E., "Statistical Characteristics of Thin Wavy Films," A.I.Ch.E. J., vol. 20, no. 4, pp. 695-1706, July 1974, and vol. 21, no. 3, pp. 583-593, May 1975.

C5. Chun, K. R. and Seban, R. A., "Performance Prediction of Falling Film Evaporators," J. Heat Trans., Trans. ASME, pp. 391-396, 1971.

C6. Chun, K. R. and Seban, R. A., "Heat Transfer to Evaporating Liquid Films," J. Heat Trans., Trans. ASME, pp. 391-396, 1971.

C7. Cohen, L. S. and Hanratty, T. J., "Generation of Waves in the Concurrent Flow of Air and a Liquid," A.I.Ch.E. J., pp. 138-144, 1965.

C8. Cohen, L. S. and Hanratty, T., "Height of a Liquid Film in a Horizontal Concurrent Gas-Liquid Flow," A.I.Ch.E. J., pp. 290-291, 1966.

C9. Cohen, L. S. and Hanratty, T., "Effect of Waves at a Gas Liquid Interface on a Turbulent Air Flow," J. Fluid Mech., vol. 31, pp. 467-479, 1968.

C10. Craik, A.D.D., "Wind-Generated Waves in Thin Liquid Films," J. Fluid Mech., vol. 26, pp. 369-392, 1966.

C11. Chang, I. D. and Russell, P. E., "Stability of a Liquid Layer Adjacent of a High-Speed Gas Stream," The Physics of Fluids, vol. 8, no. 6, pp. 1018-1026, 1965.

C12. Charvonia, D. A., "A Study of the Mean Thickness of the Liquid Film and the Characteristics of the Interfacial Surface in Annular Two-Phase Flow in a Vertical Pipe," Purdue Rept. I-59-1, 1959.

C13. Collier, J. G. and Hewitt, G. F., "Data on the Vertical Flow of Air-Water Mixtures in the Annular and Dispersed Flow Regions-Part B: Film Thickness and Entrainment Data and Analysis of Pressure Drop Measurements," UKAEA, AERE, 3455, 1960.

C14. Churchill, S. W. and Usagai, R., "A General Expression for the Correlation of Rates of Transfer and Other Phenomena," A.I.Ch.E. J., vol. 18, no. 6, pp. 1121-1128, 1972.

C15. Collier, J. G. and Hewitt, G. F., "Film Thickness Measurements," ASME paper no. 64-WA-HT-41.

C16. Chien, S. F. and Ibele, W., "Pressure Drop and Liquid Film Thickness of Two-Phase Annular and Annular-Mist Flows," ASME paper no. 62-WA-170, 1960.

C17. Chandrasekhar, S., "Hydrodynamic and Hydromagnetic Stability," Oxford Univ. Press, 1961.

C18. Cousins, L. B., Denton, W. H., and Hewitt, G. F., "Liquid Mass Transfer in Annular Two-Phase Flow," Symp. on Two-Phase Flow," Exter, England, 1965.

C19. Christie, D. G., Hayward, G. W., Lowe, H. J., MacDonald, A. N. and Sculpher, P., "The Formation of Water Drops Which Cause Turbine Blade Erosion," Inst. of Mech. Engr, Thermodynamics and Fluids Mechanics Convention, Liverpool, England, April, 1966.

D

D1. Deich, M. E., "Investigation of the Velocity of Sound and Decrement of Attenuation of Sound-Waves in Two-Phase Media," Proc. Inst. Fluid Flow Mach., nos. 29-31, pp. 141-159, 1966.

D2. Denny, V. E., Mills, A. F. and Jusionis, V. J., "Laminar Film Condensation from a Steam-Air Mixture Undergoing Forced Flow Down a Vertical Surface," J. Heat Trans., Trans. ASME, pp. 297-304, 1971.

D3. Duckler, A. E., "Fluid Mechanics and Heat Transfer in Vertical Falling Film Systems," Chem. Engr. Prog. Symp., ser. 65, 1-10, 1960.

D4. Depooter, K., Brundrett, E. and Strong, A. B., "The Calibration of Preston Tubes in Transpired Turbulent

Boundary Layers," J. Fluid Engr., Trans. ASME, vol. 100, pp. 10-16, 1978.

D5. Dodd, K. N., "On the Disintegration of Water Drops in an Air Stream," J. Fluid Mech., vol. 9, pp. 175, 1960.

D6. deNevers, N., "Rate Data and Derivatives," A.I.Ch.E.J., vol. 12, no. 6, pp. 1110-1115, Nov. 1966.

E

E1. Engel, O. G., "Fragmentation of Waterdrops in the Zone Behind an Air Shock," J. Res. NBS, vol. 60, no. 3, Mar. 1958.

F

F1. Fenyes, Peter, "Liquid Film Thickness Measurement, Design and Use of a Conductance Probe," DRDA Rept. No. UMICH 12449-6-I, Dec. 1974.

F2. Fillipov, G. A., Povarov, O. A. and Pryakhin, V. V., "Investigation and Calculation of Wet Steam Turbines," (Russian), Moscow, 1973.

G

G1. Gyarmathy, G. and Meyer, H., "Spontane Kondensation," Forsch V.D.I., no. 508, 1965.

G2. Gyarmathy, G., Burkhard, H-P, Lesch, F. and Siegenthaler, A., "Spontaneous Condensation of Steam at High Pressures: First Experimental Results," Instn. Mech. Engrs., London, Conf. on Heat and Fluid Flow in Steam and Gas Turbine Plant, Univ. Warwick, April 3-5, 1973, paper C 66/73, pp. 182-186.

G3. Gyarmathy, G., "Zur Wachstumsgeschwindigkeit kleiner Flussigkeit in einer ubersattigten Atmosphare," Zeitschrift Fur Angewandt Mathematik und Physik (ZAMP), vol. 14, no. 3, 1963, pp. 280-293.

G4. Gardner, G. C., "Events Leading to Turbine Blade Erosion," Proc. Inst. Mech. Eng., vol. 178, pt. 1, no. 23, pp. 593-624, 1964.

G5. Ganic, E. N. and Rohsenow, W. M., "On the Mechanism of Liquid Drop Deposition in Two-Phase Flow," ASME paper no. 76-WA/HT-18, 1976.

G6. Gregor, W. and Rumpf, H., "Velocity of Sound in Two-Phase Media," Int. J. Multiphase Flow, vol. 1, pp. 753-769, 1975.

G7. Gater, R. A. and L'Ecuyer, M. R., "A Fundamental

Investigation of the Phenomena that Characterize Liquid-Film Cooling," Inst. J. Heat Mass Trans., vol. 13, pp. 1925-1939, 1970.

G8. Gill, L. E. and Hewitt, G. F., "Sampling Probe Studies of Gas Core in Annular Two-Phase Flow III," UKAEA Rept. AERE-M 1202, 1966.

H

H1. Hill, P. G., "Condensation of Water Vapor During Supersonic Expansion in Nozzle," J. Fluid Mech., vol. 25, 1966, pp. 593-620.

H2. Hartley, D. E. and Murgatroyd, W., "Criteria for the Break-up of Thin Liquids Layers Flowing Isothermally over a Solid Surface," Int. J. Heat Mass Transfer 7, 1003, 1964.

H3. Hobler, T., "Minimal Surface Wetting in a Centrifugal Force Field," Chemia Stosow 2B, 265, 1968.

H4. Hewitt, G. F. and Lacey, P. M.C., "The Breakdown of the Liquid Film in Annular Two-Phase Flow," Int. J. Heat Mass Transfer, vol. 8, pp. 781-791, 1965.

H5. Hewitt, G. F., Kearsey, H. A., Lacey, P.M.C. and Pulling, D. J., "Burn Out and Nucleation in Climbing Film Flow," Int. J. Heat Mass Transfer, vol. 8, pp. 793-814, 1965.

H6. Hughmark, G. A., "Film Thickness, Entrainment and Pressure Drop in Upward Annular and Dispersed Flow," A.I. Ch.E. J., vol. 19, no. 5, pp. 1062-1065, 1973.

H7. Henstock, W. H. and Hanratty, T. J., "The Interfacial Drag and the Height of the Wall Layer in Annular Flows," A.I.Ch.E. J., vol. 22, no. 6, pp. 990-1000, 1976.

H8. Hinze, J. O., "Fundamentals of the Hydrodynamic Mechanism of Splitting in Dispersion Process," A.I.Ch.E. J., 1, 289, 1955.

H9. Hammitt, F. G., Keller, A., Ernst, G., "Steam Tunnel Initial Operation and Results," DRDA Report no. UMICH 012449-1-T, Jan. 1974.

H10. Hammitt, F. G., Hwang, J. B., Mancuso, A., Krause, D., and Blome, S., "Liquid Film Thickness Tests - Wet Steam Tunnel," DRDA Report no. UMICH 012449-9-T, June 1975.

H11. Hammitt, F. G., Hwang, J-B and Kim, W., "Liquid Film Thickness Measurements in University of Michigan Wet Steam Tunnel," 1976 ASME Cavitation and Multiphase Flow

Forum, May 1976.

H12. Head, M. R. and Rechenberg, I., "The Preston Tube as a Means of Measuring Skin Friction," J. Fluid Mech., vol. 14, pp. 1-17, 1962.

H13. Hewitt, G. F. and Hall-Taylor, N. S., "Annular Two-Phase Flow," pp. 136-148, Pergamon Press, N.Y., 1970.

H14. Hartley, D. E. and Roberts, D. C., "A Correlation of Pressure Drop Data Two-Phase Annular Flow in Vertical Channels," Nuclear Res. Memo Q6, Queen Mary College, Univ. of London, 1961.

H15. Hinze, J. O., "Critical Speeds and Sizes of Liquid Globules," Appl. Sci. Res., vol. A1, pp. 273, 1949.

H16. Hassler, G., "Breakup of Large Water Drops Under the Influence of Aerodynamic Forces in a Steady Stream of Steam at Subsonic Velocities," Proc. of 3rd Intl' Conf. on Rain Erosion and Related Phenomena, Hartley Whitney, Hampshire,England, Aug. 1970.

H17. Hanson, A., Domich, E., and Adams, H., "Shock Tube Investigation of the Break up of Drops by Air Blasts," The Physics of Fluid, vol. 6, no. 8, pp. 1070-1080, Aug. 1963.

H18. Hammitt, F. G., Lihn, D. N., Tully, J. E., Ernst, G. C., Hwang, J-B, Krause, D. A. and Bhatt, N. R., "Film Thickness Electrical Conductivity Gages - Detailed Utilization Procedure for U-M Wet Steam Tunnel," DRDA Report no. UMICH 012449-16-I, April 1975.

H19. Hewitt, G. F., King, R. D. and Lovegrove, P. C., "Techniques for Liquid Film and Pressure Drop Studies in Annular Two-Phase Flow," Atomic Energy Res. Est., R3931, 1962.

H20. Hammitt, F. G., Kim, W. and Bou-Maroun, A., "Thin Shear Driven Water Film Disintegration and Wavelet Celerity," DRDA Report no. UMICH 014571-13-I, Jan. 1978.

I

I1. Ihnatowicz, E., Gunkowski, S. and Mikielewica, J., "Experimental Study of Evaporation and Breakdown of Thin Liquid Films Driven by Shear Stress," ASME Winter Annual Meeting, Atlanta, Ga., Nov. 27-Dec. 2, 1977.

I2. Ishii and Grolmes, "Inception Criteria for Droplet Entrainment in Two-Phase Concurrent Film Flow," A.I.Ch.E. J, vol. 21, no. 2, pp. 308-318, 1975.

J

J1. Jenkins, D. C., and Booker, J. D., "Time Required for High-Speed Air Streams to Disintegrate Water Drops," Aero. Res. Council Current Papers, C.P. No. 827.

J2. Jeffreys, H., "Resonant Phenomena in Gravity Waves," Proc. Royal Soc., A107, 189, 1925.

K

K1. Khoshaim, B. H. and Ryley, D. J., "Rivulet Flow Over Steam Turbine Blade," CERI meeting, Ft. Lauderdale, Fla., Oct. 18-20, 1976.

K2. Krantz, W. B., and Zollars, R., "The Linear Hydrodynamic Stability of Film Flow Down a Vertical Cylinder," A.I.Ch.E. J, vol. 22, no. 5, pp. 930-934, 1976.

K3. Kutateladze, S.S., "Elements of the Hydrodynamics of Gas Liquid System," Fluid Mech. - Soviet Res. 1 (4), 29, 1972.

K4. Kim, W. and Hammitt, F. G., "Observation of Liquid Fingers and Drop Formation from Trailing Edge of Simulated Turbine Blade in Wet Steam," DRDA Report no. UMICH 014571-14-I, April 1978.

K5. Krzyzanowski, J., "Wet-Steam Tunnel Facility-Design and Program of Investigations," DRDR Report no. UMICH 03371-18-T, June 1972.

K6. Kim, W., Hammitt, F. G. and Krzecskowski, S., "Investigation of the Behavior of Thin Liquid Film with Co-Current Steam Flow," Two-Phase Transport and Reactor Safety, Proc. Two-Phase Flow and Heat Transfer Sym. Workshop, Oct. 18-20, 1976, Ft. Lauderdale, Fla, vol. IV, pp. 1213-1230, Hemisphere Publ. Co., 1978.

K7. Kim, W., Hammitt, F. G., Blome, S., and Hamed, H., "Thin Shear Driven Water Film Wavelet Characteristics," 1977 ASME Cavitation and Multiphase Flow Forum, June 1977.

K8. Krzeczkowski, S., Kim, W. and Hammitt, F. G.,"Investigation of Secondary Liquid Phase Structure in Steam Wake," submitted to ASME, J. Fluid Mech.

K9. Kordyban, E., "Interfacial Shear in Two-Phase Wavy Flow in Closed Horizontal Channels," J. Fluid Engr., Trans. ASME, pp. 97-102, June, 1974.

K10. Kosky, P. G., "Thin Liquid Films Under Simultaneous Shear and Gravity Forces," Inst. J. Heat Mass Transf.,

vol. 14, pp. 1220-1224, 1971.

K11. Krzeczkowski, S. and Hammitt, F. G., "Experimental Investigation of Liquid Droplet Break-Up Duration," Cavitation and Multiphase Flow Forum, 1977.

K12. Krause, W. E., "Water Drop Deformation and Fragmentation Due to Shock Wave Impact," Ph.D. thesis, Univ. of Florida, 1970.

K13. Kim, W. and Hammitt, F. G., "Observations of Liquid Finger and Drop Formation from the Trailing Edge of Simulated Turbine Blade in Wet Steam," DRDA Report no. UMICH 014571-14-I, April 1978.

L

L1. Lin, S. P., "Instability of a Liquid Film Flowing Down an Inclined Plane," The Physics of Fluids, vol. 10, no. 2, pp. 308-313, 1967.

L2. Lin, S. P., "Finite Amplitude Stability of a Parallel Flow with a Free Surface," J. Fluid Mech., vol. 36, pp. 113-126, 1969.

L3. Lin, S. P., "Profile and Speed of Finite Amplitude Waves in a Falling Liquid Layer," The Physics of Fluids, vol. 14, no. 2, 1971.

L4. Levich, V. G., "Physiochemical Hydrodynamics," Prentice-Hall, Englewood Cliffs, N.J., 1962.

L5. Levy, S., "Prediction of Two-Phase Angular Flow With Liquid Entrainment," Int. J. Heat Mass Trans., vol. 9, pp. 101-188, 1966.

L6. Lamb, H., "Hydrodynamics," Dover Publications, 1932.

L7. Langmuin, I. and Blodgett, K. B., "Mathematical Investigation of Water Droplet Trajectories," Tech. Rept. No. 5418, Air Materials Command, AAF, Feb. 1946.

L8. Lane, W. R., "Shatter of Drops in Streams of Air," Ind. and Engr. Chem., vol. 43, pp. 1312, 1951.

M

M1. Miller, E. H., Schofield, P., "The Performance of Large Steam Turbine Generators with Water Reactors," ASME Winter Annual Meeting, N.Y., Nov. 26-30, 1972.

M2. Moses, C. A. and Stein, G. D., "On the Growth of Steam Droplets Formed in a Laval Nozzle Using Both Static Pressure and Light Scattering Measurements," Condensation in High-Speed Flows, ASME Jt. Appl. Mech. Fluid

Fluid Eng. and Bioeng. Conf., Yale Univ., New Haven, Conn., June 15-17, 1977.

M3. Mikielewicz, J. and Moszynski, J. R., "Minimum Thickness of a Liquid Film Flowing Vertically Down a Solid Surface," Inst. J. Heat and Mass Transfer, vol. 19, no. 7, pp. 771-776, 1976.

M4. Miles, J. W., "The Hydrodynamic Stability of a Thin Film of Liquid in Uniform Shearing Motion," J. Fluid Mech., 13, p. 433-448, 1962.

M5. Miles, J. W., "On the Generation of Surface Waves by Shear Flows," J. Fluid Mech., 13, p. 433-448, 1962.

M6. Miles, J. W., "On the Generation of Surface Waves by Shear Flows, Part I, II and III," J. Fluid Mech., vol. 3, pp. 185-204, 1957, vol. 6, pp. 568-582, 1959, vol. 6, pp. 583-598, 1959.

M7. Mills, A. F. and Chung, D. K., "Heat Transfer Across Turbulent Falling Films," Int. J. Heat Mass Transfer, vol. 16, pp. 694-696, 1973.

M8. Mikielewicz, J. and Moszynski, J. R., "Breakdown of a Shear Driven Liquid Film," Trans. Inst. Fluid Flow Machinery, Polish Acad. of Sci., vol. 66, pp. 3-10, 1975.

M9. Mancuso, A., Hammitt, F. G., Blome, S. and Hwang, J-B, "Data Reduction Procedures - Steam Tunnel Film Thickness Tests," DRDA Report no. UMICH 012449-20-Ia.

M10. Mikielewicz, J. and Hammitt, F. G., "Generalized Characteristics of Electrical Conductance Film Thickness Gages, " Prace IMP, pp. 87-95, 1977.

M11. Miya, M., Woodmansee, D. E. and Hanratty, T. J., "A Model for Roll Waves in Gas-Liquid Flow," Chem. Eng. Sci., vol. 26, pp. 1915-1931, 1971.

M12. Murgatroyd, W., "The Role of Shear and Form Forces in the Stability of a Dry Patch in Two-Phase Film Flow," Int. J. Heat Mass Transfer, v. 8, pp. 297-301, 1965.

M13. Milne-Thomson, L. M., "Theoretical Hydrodynamics," The MacMillan Co., 1960.

M14. Margle, J. T., "Investigation of Secondary Liquid Phase Droplet Accelerations," DRDA Report no. UMICH 014571-17-I, April, 1978.

M15. Moszynski, J. R., Personal Communication, 1978.

N

N1. Norman, W. S. and McIntyre, V., "Heat Transfer to a Liquid Film on a Vertical Surface," Trans. Inst. Chem. and Chem. Engrs., v. 38, 301, 1960.

N2. Nusselt, W., ZVD 1, 60, 541 and 569, 1916.

N3. Nayfeh, A. H. and Saric, W. C., "Stability of a Liquid Film," AIAA J., vol. 9, no. 4, pp. 750-752, 1971.

N4. Nayfeh, A. H. and Saric, W. C., "Non-Linear Kelvin-Helmholtz Instability," J. Fluid Mech., vol. 46, pp. 209-232, 1971.

N5. Nayfeh, A. H. and Saric, W. C., "Nonlinear Stability of a Liquid Film Adjacent to a Supersonic Stream," J. Fluid Mech., vol. 58, pp. 39-51, 1973.

N6. Nachtsheim, P. R., "Stability of Crosshatched Wave Patterns in Thin Liquid Films Adjacent to Supersonic Streams," The Physics of Fluids, vol. 13, pp. 2432-2447, 1970.

N7. Newitt, D. M., Dombrowski, N. and Knelman, F. H., "Liquid Entrainment: I, The Mechanism of Drop Formation from Gas or Vapor Bubbles," Trans. Inst. Chem. Eng., vol. 32, p. 244, 1954.

N8. Nicholson, J. E., "Drop Breakup by Airstream Impact," published in Rain Erosion and Associated Phenomena," RAE Report N68-19401-427, Farnborough, England, 1967.

N9. Niedzielski, R. J., "Computer Analysis Programs, Computer Graphic," DRDA Report no. UMICH 014571-15-I, Ap. 1978.

O

O1. Orell, A. and Bankoff, S. G., "Formation of A Dry Spot in a Horizontal Liquid Film Heated from Below," Int. J. Heat Mass Transfer 14, 1834, 1971.

P

P1. Petr, V., "Measurement of an Average Size and Number of Droplets during Spontaneous Condensation of Supersaturated Steam," Instn. Mech. Engr., London, Thermodynamics and Fluid Mechanics Group Convention, Univ. Glasgow, Mar. 23-25, 1970, paper 10, pp. 73-79.

P2. Petr, V., "The Propagation of Small Disturbances in Wet-Steam," Fifth Nat. Conf. Czech. Sii-Eng. Soc., Mech. Eng. Grp., Pilsen, Oct. 1972.

P3. Preston, J. H., "The Determination of Turbulent Skin Friction by Means of Pitot Tubes," J. Royal Aero Soc., vol. 58, pp. 109-121, 1954.

P4. Patel, V. C., "Calibration of the Preston Tube and Limitations on its Use in Pressure Gradients," J. Fluid Mech., vol. 23, pp. 185-208, 1956.

P5. Phillips, O. M., "Resonant Phenomena in Gravity Waves," J. Fluid Mech., 2, p. 417, 1957.

P6. Pouchot, W. D., Kothman, R. E., 2nd ed., "Basic Investigation of Turbine Erosion Phenomena," NASA CR-1830, Nov. 1971.

R

R1. Ryley, D. J. and Tubman, K. A., "Spontaneous Condensation in High-Pressure Expanding Steam," Proc. Inst. for Turbomachinery Res., Gdansk, Polish Aca. Sci., vol. 70-72, 1976, pp. 273-284.

R2. Reynolds, W. C. and Potter, M. C., "J. Fluid Mech., 27, 465, 1967.

R3. Roshko, A., "On the Development of Turbulent Wakes from Vortex Streets," NASA Rept. 1191, 1954

R4. Ranger, A. and Nicholls, J., "Aerodynamic Shattering of Liquid Drops," AIAA J., vol. 7, no. 2, Feb. 1969.

R5. Reinecke, W. G., Waldman, G. D., McKay, W. L. and Ziering, M. B., "Shock Layer Shattering of Water Drops and Ice Crystals in Reentry Flight," AFNL-TR-75-71.

S

S1. Smith, T. N. and Tait, R. W. F., "Interfacial Shear Stress and Momentum Transfer in Horizontal Gas-Liquid Flow," Chem. Eng. Sci, vol. 21, pp. 63-75, 1966.

S2. Saric, W. S. and Marshall, B. W., "An Experimental Investigation of the Stability of a Thin Liquid Layer Adjacent to a Supersonic Stream," AIAA J, vol. 9, no. 8, pp. 1546-19553, 1971.

S3. Saric, W. S. and Nayfeh, A. H. and Lekoudis, S. G., "Experiments on the Stability of Liquid Films Adjacent to Supersonic Boundary Layers," J. Fluid Mech., vol. 77, pp. 63-80, 1976.

S4. Steen, D. A. and Wallis, G. B., "The Transition From Annular to Annular-Mist Cocurrent Two-Phase Down Flow," AEC Rept. NYO-3114-2, 1964.

S5. Sherman, P., Klein, J. S., and Tribus, M., "Determination of Drop Trajectories by Means of an Extension of Stokes' Law," Eng. Res. Inst., Air Res. and Dev. Command, USAF, Univ. Mich., Apr. 1952, Contract No. AF 18(600)-51.

S6. Serafini, J. S., "Impingement of Water Droplets on Wedges and Doublewedge Airfoil at Supersonic Speeds," NACA Report no. 1159, 1954.

S7. Simpson, R. L. and Whitten, D. G., "Preston Tubes in the Transpired Turbulent Boundary Layer," AIAA J, vol. 6, pp. 1776-1777, 1968.

S8. Schlichting, H., "Boundary Layer Theory," N.Y., McGraw-Hill, 1960.

S9. Smith, A., Kent, R. P. and Armstrong, R. L., "Erosion of Steam Turbine Blade Shield Materials," ASTM Special Tech. Publ. no. 408, Mar. 1967.

S10. Spink, L. K., "Principles of Flow Meter Engineering," Foxborough Co., Foxborough, Mass., 1958.

T

T1. Traupel, W., "Zur Theorie der Nassdamfturbine," Schweiz. Bauzg, vol. 77, pp. 324, 1959.

T2. Tam, C. K. W., "The Drag on a Cloud of Spherical Particles in Low Reynolds Number Flow," J. Fluid Mech., vol. 38, part 3, pp. 537-546, 1969.

T3. Tailby, S. R. and Portalski, S., "The Hydrodynamics of Liquid Films Flowing on a Vertical Surface," Trans. Inst. Chem. Engr. (London), 38, pp. 324-330, 1960.

T4. Tyler, A. L. and Salt, D. L., "Periodic Discontinuities in the Acceleration of Spheres in Free Flight," ASME paper no. 77-WA/FE-3.

T5. Tseng, R., "Investigation of the Acceleration of Droplets in a Steam Wake Behind a Stationary Turbine Blade," DRDA Rept. no. UMICH 014571-19-I, Apr. 1978.

T6. Trier, E. and Blome, S., "Wet Steam Tunnel Trailing Edge Observations," DRDA Rept. no. UMICH 014571-7-I, June 1977.

Y

Y1. Yellot, J. I., "Supersaturated Steam," Trans. ASME, vol. 56, 1934, pp. 411-430.

Y2. Yellot, J. I. and Holland, C. K., "The Condensation of Flowing Steam," Trans. ASME, vol. 59, 1937, pp. 171-183.

Y3. Yih, C. S., Proc. 2nd U.S. Congress, Appl. Mech., ASME, p. 623, 1954.

Y4. Yih, C. S., "Stability of Liquid Flow Down an Inclined Plane," Physics of Fluids, vol. 6, no. 3, pp. 321-334, 1963.

Y5. Yablonik, R. and Khaimov, V. A., "Determination of the Velocity of Inception of Droplet Entrainment in Two-Phase Flow," Fluid Mech. Soc. Res. 1 (1), p. 130, 1972.

U

U1. Ueda, T. and Tanaka, T., "Studies of Liquid Film Flow in Two-Phase Annular and Annular-Mist Flow Regions; Pt 1 and 2", Trans. JSME, vol. 39, no. 325, p. 2842, 1973.

V

V1. Valha, J. and Ryley, D. J., "Optical Studies of Nucleation in High-Pressure Expanding Steam," Condensation in High-Speed Flows, ASME Jt. App. Mech. Fluids Eng. and Bioeng. Conf., Yale Univ., June 15-17, 1977, pp. 27-42.

V2. Van Rossum, J. J., "Experimental Investigation of Horizontal Liquid Films," Chem. Eng. Sci, vol. 11, pp. 35-52, 1959.

W

W1. Woodmansee, D. E. and Hanratty, T. J., "Base Film Over Which Roll Waves Propagate," A.I.Ch.E J, pp. 712-716, 1969.

W2. Woodmansee, D. E. and Hanratty, T. J., "Mechanisms for the Removal of Droplets from a Liquid Surface by a Parallel Air Flow," Chem. Eng. Sci, vol 24, pp. 299-307, 1969.

W3. Woodmansee, D. E. and Hanratty, T. J., "A Model for Roll Waves in Gas-Liquid Flow," Chem. Eng. Sci, vol. 26, pp. 1915-1931, 1971.

W4. Wurz, D., "Flow Behavior of Thin Water Films Under the Effect of a Cocurrent Air Flow of Moderate to High Subsonic Velocities," Proc. of 3rd Int'l Conf. on Rain Erosion and Associated Phenomena, pp. 727-745, England, 1970

W5. Wicks, M. and Dukler, A. E., "Entrainment and Pressure Drop in Concurrent Gas-Liquid Flow: 1. Air-Water in Horizontal Flow," A.I.Ch.E J. 6, 463, 1960.

W6. Wilson, C. T. R., "Condensation of Water Vapor in the Presence of Dust-Free Air and Other Gases," Phil. Trans. Roy. Soc., London, A189, 1897, pp. 265-307.

W7. Wallis, G. B., "The Onset of Droplet Entrainment in Annular Gas-Liquid Flow," G.E. Rept. 62 GL 127, 1962.

W8. Wallis, G. B., "One-Dimensional Two-Phase Flow," pp. 320, 345-351, 376-391, McGraw-Hill, N.Y., 1969.

W9. Wolfe, H. E., "Photographic Study of the Break-up of Liquid Drops," J. SMPTE, vol. 75, pp. 738, 1966.

W10. Waldman, G. and Reinecke, W., "Particle Trajectories, Heating and Breakup in Hypersonic Shock Layers," AIAA J, vol. 9, no. 6, pp. 1040-1048, June, 1971.

W11. Waldman, G., Reinecke, W. and Glenn, D., "Raindrop Breakup in the Schock Layer of a High-Speed Vehicle," AIAA J, vol. 10, no. 9, pp. 1200-1204, Sept. 1972.

W12. Wegenka, M., "Multiphase Flow and Cavitation Computer Analysis Program," DRDA Rept. no. UMICH 014571-11-I, Dec. 1977.

W13. Whitaker, Sir Edmund and Robinson, G., "Interpolation with Unequal Intervals of the Argument," The Calculus of Observations, 4th ed., Blackie & Sons, Ltd., London, 1944, pp. 20-34.

W14. Wurz, D. E., "Subsonic and Supersonic Gas-Liquid Film Flow," Proc. AIAA Annual Meeting, Seattle, Wash., July 1978.

Z

Z1. Zuber, N. and Staub, F. W., "Stability of Dry Patches Forming in Liquid Film Flowing Over Heated Surfaces," Int. J. Heat Mass Transfer, 9, 897, 1966.

Z2. Zhivaikan, L. Y., "Liquid Film Thickness in Film-Type Units," Intern. Chem. Eng. 2 (3), 337, 1962.

Z3. Zuber, N., "On the Atomization and Entrainment of Liquid Films in Shear Flow," G.E. Rept. 62 CL 153, 1962.

Z4. Zanelli, S. and Hanratty, T. J., "Relationship of Entrainment to Wave Structure on a Liquid Film," Inter. Symp. Two-Phase Flow, paper 2-1, Haifa, Israel, Aug. 1971.

APPENDIX A

DESIGN, CALIBRATION AND GENERALIZED CHARACTERISTICS OF 'ELECTRICAL CONDUCTANCE FILM THICKNESS GAGES

The behavior of thin film is of considerable interest because the gas-liquid interface is often the controlling feature for heat-mass transfer. The most important parameter for the investigation in this line of interest is the thickness of film and variation of its values with respect to time.

Various techniques to measure film thickness have been developed before i.e., hold-up measurement,[T3] radioactive absorption and emission, conductance probe, needle contact method. Light absorption and Fluorescence-Spectrometer method and so on. An extensive review on film thickness measurement technique was provided by Collier and Hewitt.[C13]

Among many possible techniques, an electrical conductance gage was employed at the University of Michigan Steam Tunnel facility. The unique feature of the gage is that no part of it protrudes into either the liquid or the gas. The gage has been successfully utilized to study the interface wave characteristics and the thickness of a liquid film flowing over a horizontal plate with a high-speed vapor flow over the liquid face.

The gage consists of 3 concentric parts; i.e., a center conducting electrode of radius r_1, an insulating ring of outside radius r_2, and finally a conducting infinite plate. (Figs. A1 and A2). Electrical connections are made to the center electrode and the plate.

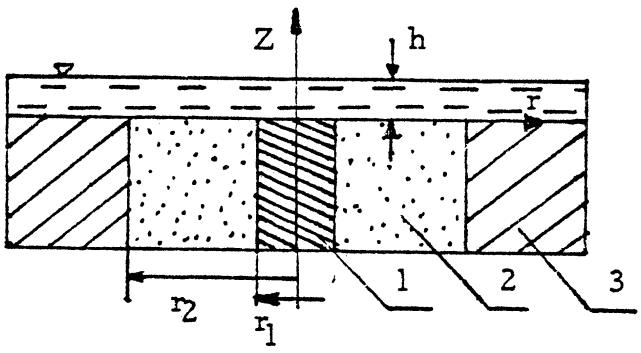

Fig. A1 : Schematic Representation of Conductance Probe

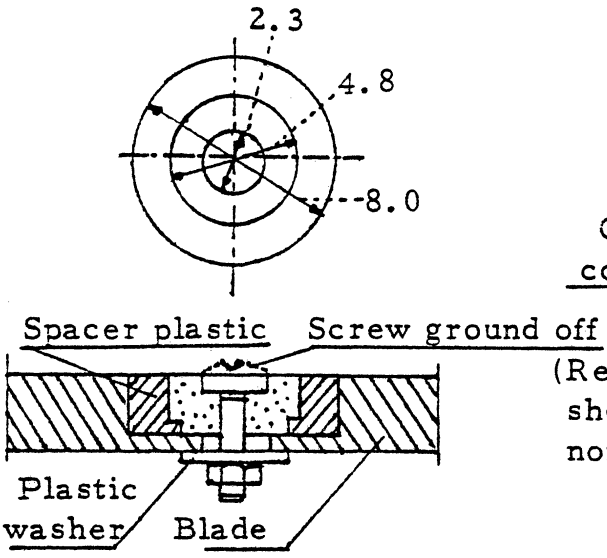

Fig. A2: Design Drawing of Gauge

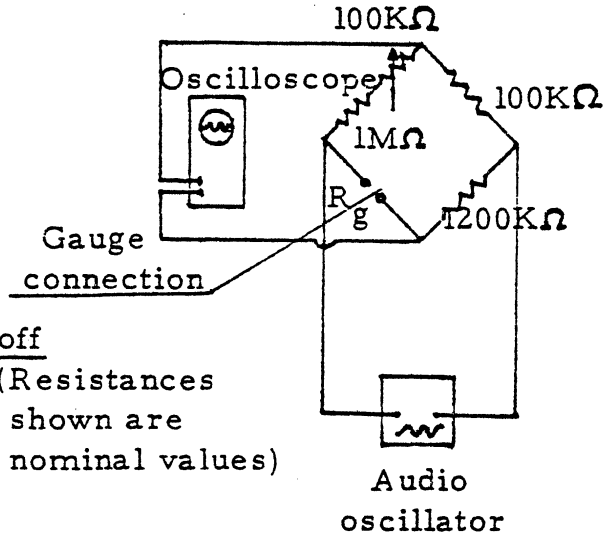

Fig. A3: Wheatstone Bridge and Related Equipment

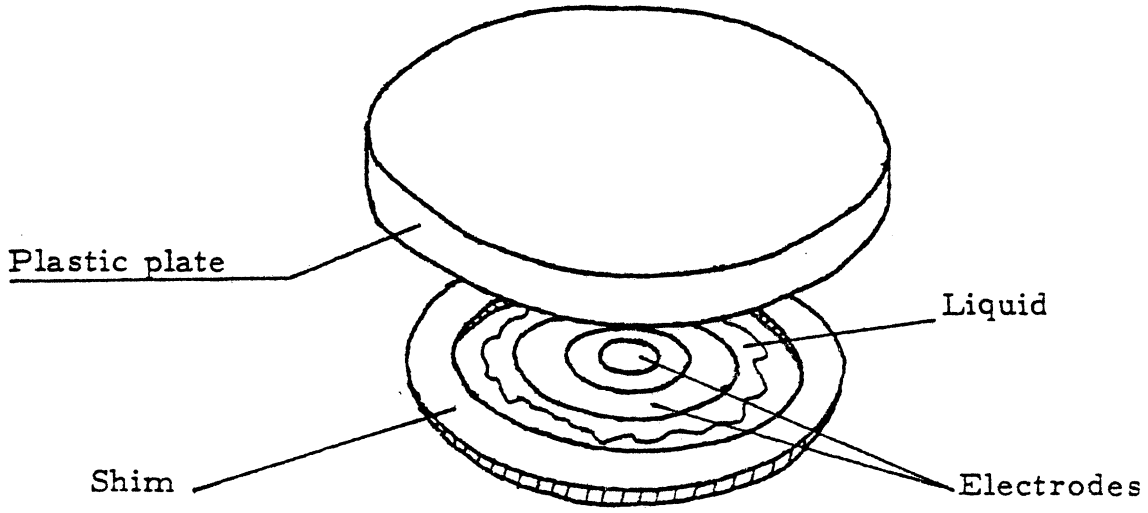

Fig. A4: Schematic of Calibration Method

Mikielewicz and Hammitt,[10] sovling Laplace equation for electrical potential distribution in the film, concluded that,

$$i = C_g\, h\, \sigma\, \Delta u \qquad (A.1)$$

where,

$i = \pi\, \sigma r_1^2 j$ - electric current

σ - specific conductivity of liquid

j - density of electrical current flow

C_g - geometric constant of the gage

h - film thickness

Δu - electrical potential difference between r_1 and r_2

Based on the experimental results of Collier and Hewitt,[C13]

$$C = 2.918\, \sigma\, h \qquad (A.2)$$

where C is the film conductivity between the probe electrodes, they assumed the following relation for this range of thickness.

$$C = C_g\, \sigma\, f(h) \qquad (A.3)$$

where f(h) is unknown function of film thickness, which can be easily established experimentally by calibrating the gages.

The design of our gage is shown in Fig. A2 . Collier and Hewitt (1964) pointed out the importance of gage size. As the gage is reduced in size, the local sensitivity is increased while the maximum measureable thickness is decreased. They suggested that electrode spacing should be about 10 times the maximum expected film thickness. Thus the diameter of the center electrode was chosen to be 2.3 mm, and the outside diameter of insulating ring 4.8 mm.

Measurements were conducted using an out-of-balance Wheatstone bridge (Fig. A3), excited by an A-C audio oscillator. Frequency of 1 KHz was used, producing a sinusoidal wave amplitude of 10 volts. The bridge output voltage was fed to an oscilloscope. The output voltage was a function of the film resistance. Known film thicknesses were obtained by placing a pre-measured circular shim around the gage (Fig. A.4), putting a few drops of water on the gage, and finally setting a circular non-conducting plate over fixed shims, trapping the water over the gage, and squeezing to the desired shim thickness. Measurements were made with distilled water and 0.05% salt (by mass) addition. This solution strength was necessary to avoid variations in water conductivity, at the different temperatures required, ranging from 70° to 150°F. (~ 21 to 66°C).

Typical calibration curves are shown in Fig. A.5 . The function, f(h), depending only on film thickness for a given gage, was found using values from calibration curves. The resulting function f(h), along with the dependence upon the factor C_g versus temperature, are presented in Figs. A.6 and A.7 . The small scatter of data points shown on Figs. A.6 and A.7 indicates the general precision level of calibration, and the realism of the calculating procedure used. Function f(h) is general for all gages, but the factor C_g is different for various gages.

One can obtain the thickness of liquid film, using the generalized characteristic curves of Fig. A.6 and A.7 .

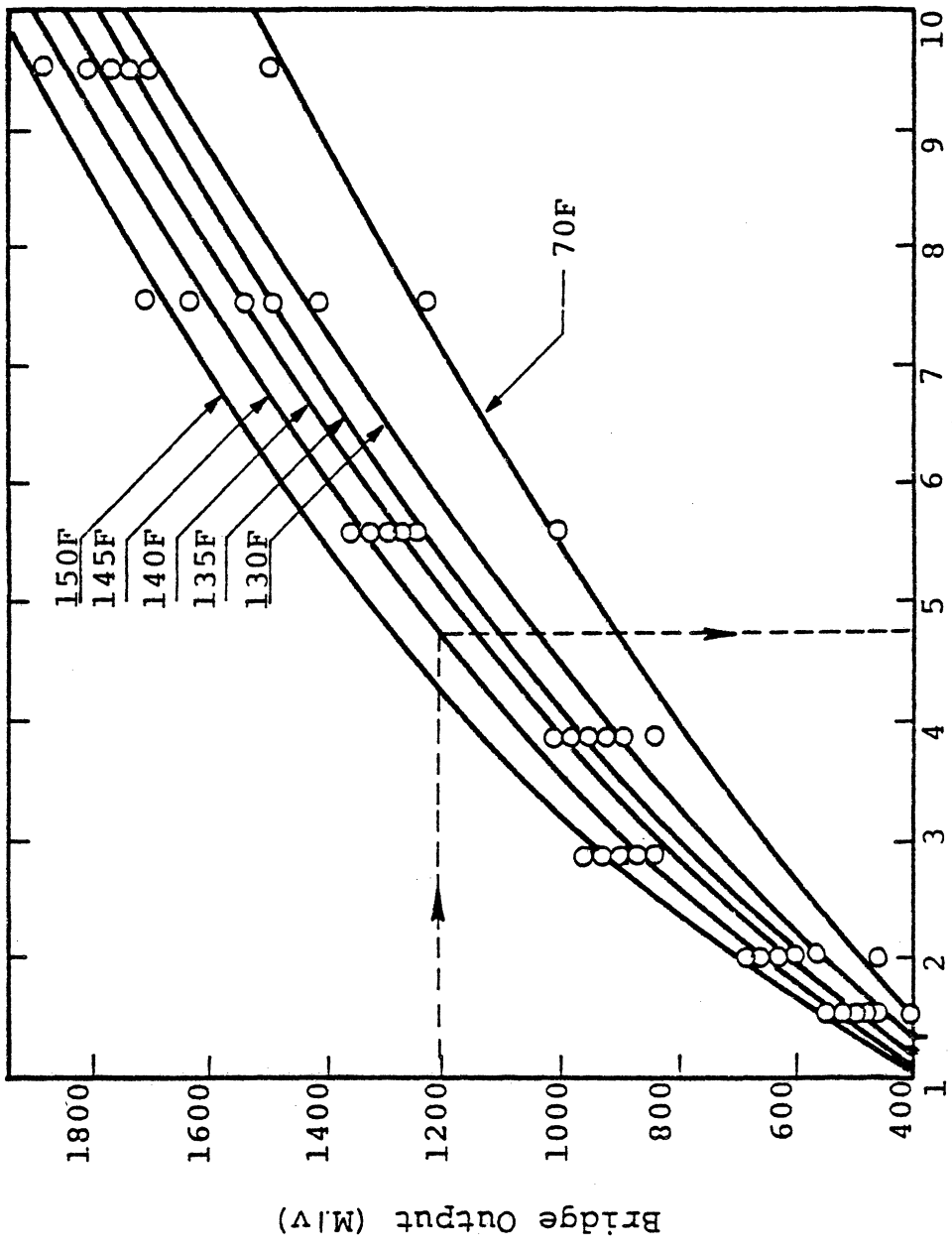

Fig. A5 Typical Calibration Curves (Gauge No. 1)

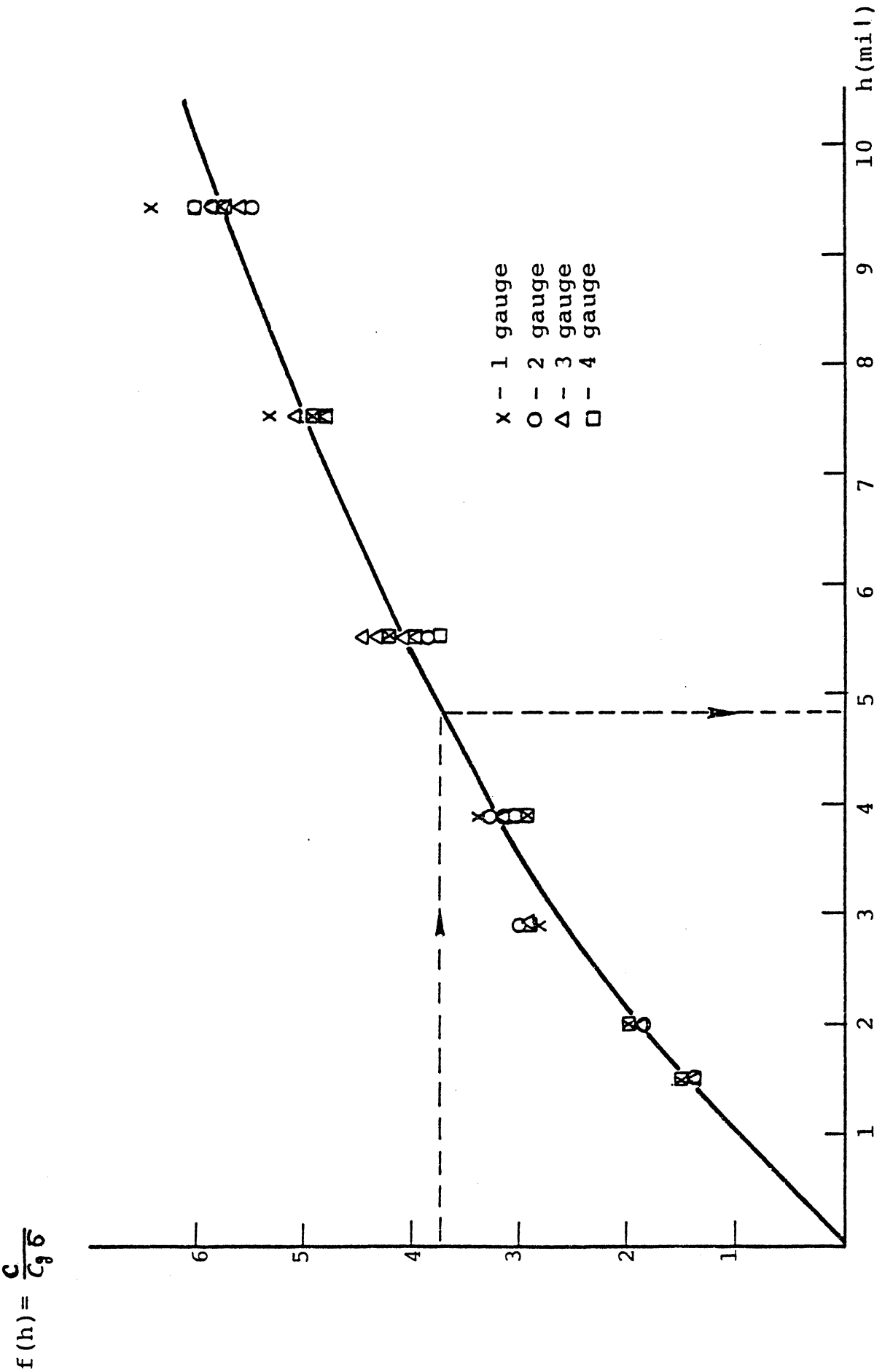

Fig. A6 Dependence of f(h) on Film Thickness, h for Gauges No. 1,2,3,4

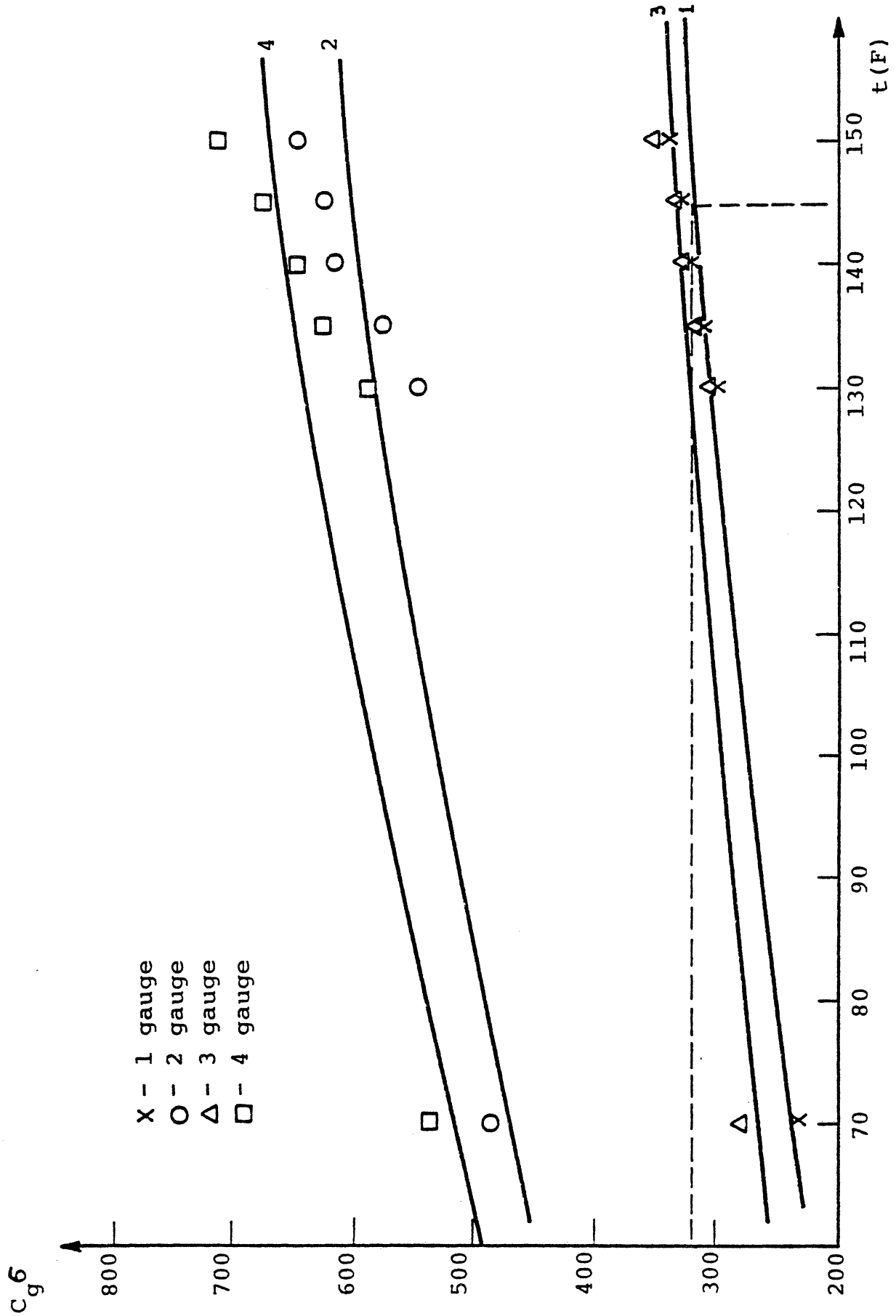

Fig. A7 Dependence of Product of Geometric Factor and Water Conductance on Temperature for Gauges No. 1,2,3, and 4.

For example, if the output of the Wheatstone bridge is 1200 mV and the temperature of the film is 145°F (63°C), one can find directly from the calibration curve (Fig. A.5) the thickness of the film, 4.75 mils (≈ 121 μm).

The same result can be obtained using the generalized characteristic. For film temperature of 145°F, the corresponding factor C_g (Fig. A.7) is 320. Dividing output of bridge (1200 mV) by value of factor C_g (320), one can find the value of the function f(h), and the measured thickness of the film equals about 4.75 mils (Fig. A.6). The procedure is shown by the dotted lines on Figs. A.6 and A.7 . Using this generalized characteristic, one can easily see the influence of temperature on the thickness measurement.

Error of correlating experimental data of film thickness is given in Table A.1 .

Thickness μm	Predicted measured value of $f_t(h)$	Minimum measured value of $f_m(h)$	Maximum measured value of $f_m(h)$	Range of error $\frac{f_t - f_m}{f_t}$ %
39.37	39.37	38.1	40.64	+ 3.1
50.80	50.80	48.26	53.34	∓ 5.0
73.66	69.85	69.85	78.74	0, ∓ 12.6
99.06	86.36	76.20	88.90	-11.8, +14.6
140.97	107.95	96.52	116.84	-10.6, +8.3
191.77	132.08	121.92	137.16	-7.7, +3.8
240.03	147.32	142.24	154.94	-3.4, +5.2

Table A1. Error of Thickness Gage Calibration

APPENDIX B

CALCULATION OF NORMAL AND TANGENTIAL PERTURBATION STRESSES UPON WAVY FILM

Estimates of normal and tangential perturbation stresses upon the wavy films from the parallel gas phase flow is extremely important for author's present data on wavy film characteristics.

Based on the Benjamin's analysis[B4], Craik[C10] simplified the expression for perturbation stresses. Author's wavy film data has been compared with Craik's[C10] theoretical analysis.

Introducing normal II, and tangential Σ, perturbation stress parameters, he solved the "Orr-Sommerfeld" equation for perturbation velocity stream function.

$$II = \frac{2\alpha}{Re_f f_i} [I - \sqrt{3}S + i(f_i - s)] \tag{B.1}$$

$$\Sigma = \frac{(4\beta . I)}{\sqrt{3} f_i} e^{i\pi/3} \alpha^3 (\alpha Re_f)^{-4/3} \tag{B.2}$$

where,

$$I = \int_o \left(\frac{U}{U_o}\right)^2 e^{-\alpha Y} d(\alpha y) = 2\int_o^{H/2h} \left(\frac{2yh}{H}\right)^{2/\eta} e^{-\alpha y} d(\alpha y) \tag{B.3}$$

$$s = 0.644\ I \tag{B.4}$$

$$\Delta = \frac{21}{f_i} \left(\frac{\mu_s}{\mu_f}\right)^{2/3} (\alpha Re_f)^{-2/3} \alpha^2 \tag{B.5}$$

$$\frac{4\beta}{\sqrt{3}} = 2.744 \left(\frac{\nu_s}{\nu_f}\right)^{2/3} \left(\frac{\rho_s}{\rho_f}\right)^{1/3} \tag{B.6}$$

$\alpha = kh = \frac{2\pi h}{\lambda}$ Nondimensional wave number

$Re_f = \frac{V_f h}{\nu_f} = \frac{2q}{\nu_f}$ Film Reynolds number

f_i	Friction coefficient estimated in Section B of Chapter IV
I	Integral representing the effect of turbulence gas velocity profile using $1/\eta$ rule
h	film thickness
H	Height of the channel ($\cong$ 4 cm)

Subscript s and f represent steam and liquid properties used. Finally he obtained wave growth rate and wave propagation velocity as follows:

$$\alpha C_i Re_f = \frac{(\alpha Re_f)^2}{3}[II_r + \frac{3\Sigma_i}{\alpha} - T\alpha^2 - G] \tag{B.7}$$

$$C_r - 1 = -\frac{\frac{7}{8}(\alpha C_i Re_f) - \alpha Re_f II_i + \frac{3}{2}(Re_f \Sigma_r)}{3 + \frac{27}{5}\alpha^2 + \frac{12}{5}(\alpha C_i Re_f)} \tag{B.8}$$

where,

$$T = \frac{\sigma}{\rho_f V_f^2 h}$$

$$G = \frac{gh}{V_f^2}$$

and subscript r and i indicate real and imaginary part respectively. Critical (or cut-off) wave number can be obtained by setting $\alpha C_i Re_f = 0$. List of computer program and output are as follows,

```
MICHIGAN TERMINAL SYSTEM FORTRAN G(21.8)          MAIN          06-22-78        15:51

              C     *****  PRESSURE-SHEAR PERTUABATION PROGRAM  *****
              C     THIS PROGRAM SOLVES AN INTEGRAL TO DETERMINE WAVE STABILITY.
              C     TWO DIFFERENT FUNCTIONS ARE INTEGRATED BY THE SUBROUTINE DCAL
              C     ..................................................................
 0001               REAL X(180),Y(180),Z(180),INPS,ITPS,H,Q,INTENS
 0002               REAL*8 RP(4)
 0003               COMPLEX*16 IP(4)
 0004               INTEGER NPS/120/
 0005               COMMON ALPHA,R,INTENS,SH,T,G
              C      ****  PRINT INITIAL HEADING  ****
 0006               F(A)=(A/C)**(2./7.)*EXP(-A)
 0007               WRITE(6,1000)
 0008            1000 FORMAT('1',T15,'SOLUTION TO PRESSURE-SHEAR PERTUABATION AT A LIQUI
                     1D -GAS INTERFACE',///)
 0009               WRITE(6,2000)
 0010            2000 FORMAT('ALPHA',6X,'R',9X,'INTENS',7X,'RNPS',7X,'INPS',7X,'RTPS',7X
                     *,'ITPS',7X,'GROWRATE',6X,'CR-1',2X,'3*ITPS/ALPHA',2X,'WB',4X,'REAL
                     * SOLN',//)
 0011               WRITE(6,201)
 0012            201  FORMAT('V=21.4',4X,'Q=0.063')
              C      ***  READ COMMON PARAMETERS  ***
 0013               M=1
 0014            1    READ(5,2004) SH,V,R,ALPHA,WB,G,H
 0015            2004 FORMAT(6F10.5,2F10.8,F10.5)
 0016               SH=0.00254*SH
 0017               T=1./WB
 0018               C=(ALPHA*H)/(2.*SH)
 0019               IF ( C .GE. 180.) C=180.
              C      ***  SOLVE EQUATION ONE BY INTEGRATION  ***
 0020               DO 10 I=1,NPS
 0021               X(I)=(C/NPS)*(I-1)
 0022            10   Y(I)=F(X(I))
 0023               CALL QTFG(X,Y,Z,NPS)
 0024               INTENS=2*Z(120)
 0025               CALL STRESS(RNPS,INPS,RTPS,ITPS,DD,ALPAR,CRMNS1,TT)
 0026               M=M+1
 0027               IF(M .EQ. 6) WRITE(6,202)
 0028            202  FORMAT(//'V=21.4',4X,'Q=0.104')
 0029               IF (M .EQ. 9) WRITE(6,203)
 0030            203  FORMAT(//,'V=36.6',4X,'Q=0.021')
 0031               IF ( M .EQ. 14) WRITE(6,204)
 0032            204  FORMAT(//,'V=36.6',4X,'Q=0.063')
 0033               IF (M .EQ. 18) WRITE(6,205)
 0034            205  FORMAT(//,'V=36.6',4X,'Q=0.104')
 0035               IF( M .EQ. 19) WRITE(6,206)
 0036            206  FORMAT(//,'V=61.0',4X,'Q=2.4')
 0037               IF(M .EQ. 22) WRITE(6,207)
 0038            207  FORMAT(//,'V=61.0',4X,'Q=0.063')
 0039               IF (M .EQ. 29) WRITE(6,208)
 0040            208  FORMAT(//,'V=61.0',4X,'Q=0.104')
 0041               IF(M .EQ. 32) WRITE(6,209)
 0042            209  FORMAT(//,'V=93.3',4X,'Q=0.021')
 0043               IF (M .EQ. 37) WRITE(6,210)
 0044            210  FORMAT(//,'V=93.3',4X,'Q=0.042')
 0045               IF (M .EQ. 42) WRITE(6,211)
```

```
MICHIGAN TERMINAL SYSTEM FORTRAN G(21.8)          MAIN          06-22-78        15:51

0046          211  FORMAT(//,'V=93.3',4X,'Q=0.063')
0047               IF (M .EQ. 46) WRITE(6,212)
0048          212  FORMAT(//,'V=159',4X,'Q=0.010')
0049               IF (M .EQ. 50) WRITE(6,213)
0050          213  FORMAT(//,'V=159',4X,'Q=0.021')
0051               IF (M .EQ. 55) WRITE(6,214)
0052          214  FORMAT(//,'V=159',4X,'Q=0.042')
0053               IF(M .EQ. 65) WRITE(6,215)
0054          215  FORMAT(//,'V=252',4X,'Q=0.010')
0055               IF(M .EQ. 68) WRITE(6,216)
0056          216  FORMAT(//,'V=252',4X,'Q=0.021')
0057               IF (M .EQ. 71) WRITE(6,217)
0058          217  FORMAT(//,'V=252',4X,'Q=0.042')
0059               IF(M .EQ. 75) WRITE(6,218)
0060          218  FORMAT(//,'V=252',4X,'Q=0.063')
0061               IF(M .EQ. 78) WRITE(6,219)
0062          219  FORMAT(//,'V=298',4X,'Q=0.021')
0063               IF(M .EQ. 83) WRITE(6,220)
0064          220  FORMAT(//,'V=298',4X,'Q=0.042')
0065               IF(M .EQ. 85) WRITE(6,221)
0066          221  FORMAT(//,'V=298',4X,'Q=0.063')
0067               IF ( M .GE. 89) GO TO 300
0068               RP(1)=3.*ITPS
0069               RP(2)=RNPS-G
0070               RP(3)=0.0
0071               RP(4)=-T
0072               CALL ZPOLY(3,RP,IP,IR)
0073               RR=DREAL(IP(1))
0074               WRITE(6,2001) ALPHA,R,INTENS,RNPS,INPS,RTPS,ITPS,ALPAR,CRANS1,TT,W
                  *B,RR
0075          2001 FORMAT(12(E10.3,1X))
0076               GO TO 1
0077           300 STOP
0078               END
 *OPTIONS IN EFFECT*   ID,EBCDIC,SOURCE,NOLIST,NODECK,LOAD,NOMAP
 *OPTIONS IN EFFECT*   NAME = MAIN     , LINECNT =       57
 *STATISTICS*     SOURCE STATEMENTS =       78,PROGRAM SIZE =     5160
 *STATISTICS*   NO DIAGNOSTICS GENERATED
NO ERRORS IN MAIN
```

```
MICHIGAN TERMINAL SYSTEM FORTRAN G(21.8)              STRESS          06-22-78        15:52

   0001               SUBROUTINE STRESS(RNPS,INPS,RTPS,ITPS,DD,ALPAR,CRMNS1,TT)
   0002               REAL INPS,ITPS,INTENS,FRC
   0003               COMMON W,R,INTENS,SH,T,G
              C**THIS SUBROUTINE CALCULATES THE NORMAL AND SHEAR STRESS
   0004               FD=1.0
   0005               SV=0.93
   0006               FV=0.0074
   0007               SD=0.00011
   0008               FRC=0.005*(1+SH/5.33)
   0009               DA=(2*INTENS)/FRC
   0010               DB=(SV/FV)**(2./3.)                                          1
   0011               DC=((W*R)**(-2./3.))*(W**2)                                  1
   0012               DD=DA*DB*DC                                                  1
   0013               S=0.644*DD*INTENS                                            1
   0014               RNPSA=(2.*W)/(R*FRC)                                         1
   0015               RNPSB=INTENS-S*SQRT(3.)                                      1
   0016               RNPS=RNPSA*RNPSB                                             1
   0017               INPS=((2.*W)/(R*FRC))*(FRC-S)                                1
   0018               BA=(SV/FV)**(2./3.)                                          1
   0019               BB=(SD/FD)**(1./3.)                                          1
   0020               U=2.744*BA*BB                                                1
   0021               RTPS=(U*0.5/FRC)*(W**3.)*((W*R)**(-4./3.))                   1
   0022               ITPS=RTPS*SQRT(3.)                                           1
   0023               TT=3.*ITPS/W                                                 1
   0024               ALPAR=(W*R)**2.*(RNPS+3.*ITPS/W-T*W**2.-G)/3.                1
   0025               CAA=(-7./8.)*ALPAR-W*R*INPS+(3./2.)*R*RNPS                   1
   0026               CAB=3.+(27./5.)*W**2.+(12./5.)*ALPAR                         1
   0027               CRMNS1=CAA/CAB                                               1
   0028          201  FORMAT(E12.5)                                                1
   0029               RETURN                                                       1
   0030               END                                                          1
    *OPTIONS IN EFFECT*   ID,EBCDIC,SOURCE,NOLIST,NODECK,LOAD,NOMAP
    *OPTIONS IN EFFECT*   NAME = STRESS   , LINECNT =       57
    *STATISTICS*     SOURCE STATEMENTS =       30,PROGRAM SIZE =     1408
    *STATISTICS*  NO DIAGNOSTICS GENERATED
NO ERRORS IN STRESS


$RUN -LOAD+NAAS:SSP+NAAS:OLDLIB
EXECUTION BEGINS   15:52:11
```

SOLUTION TO PRESSURE-SHEAR PERTURBATION AT A LIQUID -GAS INTERFACE

ALPHA	B	INTENS	RNPS	INPS	RTPS	ITPS	GROWRATE	CR-1	3*ITPS/ALPHA	WD	REAL SOLN
V=21.4	Q=0.063										
0.112E+00	0.169E+02	0.837E+00	-0.167E+03	-0.978E+02	0.197E+00	0.342E+00	-0.190E+03	0.859E+01	0.915E+01	0.133E-01	0.153E+00
0.840E-01	0.169E+02	0.914E+00	-0.102E+03	-0.596E+02	0.122E+00	0.212E+00	-0.635E+02	0.163E+02	0.756E+01	0.130E-01	0.156E+00
0.710E-01	0.169E+02	0.962E+00	-0.756E+02	-0.446E+02	0.923E-01	0.160E+00	-0.332E+02	0.239E+02	0.676E+01	0.130E-01	0.159E+00
0.135E+00	0.169E+02	0.789E+00	-0.230E+03	-0.134E+03	0.269E+00	0.467E+00	-0.384E+03	0.566E+01	0.104E+02	0.130E-01	0.152E+00
V=21.4	Q=0.104										
0.483E-01	0.169E+02	0.107E+01	-0.374E+02	-0.223E+02	0.481E-01	0.833E-01	-0.711E+01	0.658E+02	0.520E+01	0.130E-01	0.167E+00
0.231E+00	0.282E+02	0.734E+00	-0.298E+03	-0.173E+03	0.333E+00	0.576E+00	-0.413E+04	0.791E+00	0.749E+01	0.264E-01	0.145E+00
0.246E+00	0.282E+02	0.719E+00	-0.331E+03	-0.192E+03	0.370E+00	0.640E+00	-0.522E+04	0.646E+00	0.781E+01	0.264E-01	0.145E+00
V=36.6	Q=0.021										
0.769E+00	0.282E+02	0.460E+00	-0.194E+04	-0.112E+04	0.247E+01	0.428E+01	-0.305E+06	-0.286E+00	0.167E+02	0.264E-01	0.165E+00
0.153E+00	0.560E+01	0.625E+00	-0.123E+04	-0.714E+03	0.145E+01	0.251E+01	-0.291E+03	0.136E+02	0.492E+02	0.254E-02	0.153E+00
0.256E+00	0.560E+01	0.509E+00	-0.272E+04	-0.158E+04	0.342E+01	0.592E+01	-0.183E+04	0.432E+01	0.694E+02	0.254E-02	0.163E+00
0.153E+00	0.560E+01	0.625E+00	-0.123E+04	-0.714E+03	0.145E+01	0.251E+01	-0.291E+03	0.136E+02	0.492E+02	0.254E-02	0.153E+00
0.256E+00	0.560E+01	0.509E+00	-0.272E+04	-0.158E+04	0.342E+01	0.592E+01	-0.183E+04	0.432E+01	0.694E+02	0.254E-02	0.163E+00
V=36.6	Q=0.063										
0.192E+00	0.560E+01	0.574E+00	-0.176E+04	-0.102E+04	0.212E+01	0.366E+01	-0.663E+03	0.827E+01	0.573E+02	0.254E-02	0.156E+00
0.221E+00	0.169E+02	0.667E+00	-0.522E+03	-0.303E+03	0.613E+00	0.106E+01	-0.238E+04	0.176E+01	0.144E+02	0.133E-01	0.153E+00
0.265E+00	0.169E+02	0.625E+00	-0.701E+03	-0.407E+03	0.829E+00	0.144E+01	-0.461E+04	0.108E+01	0.163E+02	0.133E-01	0.154E+00
0.265E+00	0.169E+02	0.625E+00	-0.701E+03	-0.407E+03	0.829E+00	0.144E+01	-0.461E+04	0.108E+01	0.163E+02	0.133E-01	0.154E+00
V=36.6	Q=0.104										
0.221E+00	0.169E+02	0.667E+00	-0.522E+03	-0.303E+03	0.613E+00	0.106E+01	-0.238E+04	0.176E+01	0.144E+02	0.133E-01	0.153E+00
V=61.0	Q=2.4										
0.352E+00	0.282E+02	0.625E+00	-0.578E+03	-0.335E+03	0.672E+00	0.116E+01	-0.188E+05	0.103E+00	0.992E+01	0.277E-01	0.151E+00
0.420E-01	0.560E+01	0.833E+00	-0.105E+03	-0.622E+02	0.168E+00	0.291E+00	-0.156E+01	0.116E+04	0.208E+02	0.388E-02	0.208E+00
0.990E-01	0.560E+01	0.626E+00	-0.445E+03	-0.259E+03	0.702E+00	0.122E+01	-0.421E+02	0.363E+02	0.368E+02	0.388E-02	0.205E+00
V=61.0	Q=0.063										
0.990E-01	0.560E+01	0.626E+00	-0.445E+03	-0.259E+03	0.702E+00	0.122E+01	-0.421E+02	0.363E+02	0.368E+02	0.388E-02	0.205E+00
0.119E+00	0.169E+02	0.702E+00	-0.136E+03	-0.794E+02	0.219E+00	0.379E+00	-0.171E+03	0.769E+01	0.954E+01	0.212E-01	0.210E+00
0.166E+00	0.169E+02	0.624E+00	-0.234E+03	-0.137E+03	0.381E+00	0.659E+00	-0.587E+03	0.359E+01	0.119E+02	0.212E-01	0.211E+00
0.119E+00	0.169E+02	0.702E+00	-0.136E+03	-0.794E+02	0.219E+00	0.379E+00	-0.171E+03	0.769E+01	0.954E+01	0.212E-01	0.210E+00
0.207E+00	0.169E+02	0.575E+00	-0.333E+03	-0.194E+03	0.550E+00	0.952E+00	-0.131E+04	0.211E+01	0.138E+02	0.212E-01	0.215E+00
0.111E+00	0.169E+02	0.718E+00	-0.121E+03	-0.707E+02	0.195E+00	0.337E+00	-0.131E+03	0.899E+01	0.911E+01	0.212E-01	0.210E+00
0.119E+00	0.169E+02	0.702E+00	-0.136E+03	-0.794E+02	0.219E+00	0.379E+00	-0.171E+03	0.769E+01	0.954E+01	0.212E-01	0.210E+00
V=61.0	Q=0.104										
0.119E+00	0.169E+02	0.702E+00	-0.136E+03	-0.794E+02	0.219E+00	0.379E+00	-0.171E+03	0.769E+01	0.954E+01	0.212E-01	0.210E+00
0.228E+00	0.169E+02	0.625E+00	-0.493E+03	-0.286E+03	0.646E+00	0.112E+01	-0.237E+04	0.164E+01	0.147E+02	0.427E-01	0.170E+00
0.190E+00	0.169E+02	0.667E+00	-0.366E+03	-0.213E+03	0.476E+00	0.825E+00	-0.122E+04	0.258E+01	0.130E+02	0.427E-01	0.169E+00

```
V=93.3     Q=0.021
0.228E+00  0.169E+02  0.625E+00 -0.493E+03 -0.286E+03  0.646E+00  0.112E+01 -0.237E+04  0.164E+01  0.147E+02  0.427E-01  0.170E+00
0.890E-01  0.560E+01  0.544E+00 -0.261E+03 -0.153E+03  0.588E+00  0.102E+01 -0.189E+02  0.497E+02  0.343E+02  0.624E-02  0.292E+00
0.104E+00  0.560E+01  0.509E+00 -0.330E+03 -0.193E+03  0.762E+00  0.132E+01 -0.332E+02  0.343E+02  0.381E+02  0.624E-02  0.300E+00
0.890E-01  0.560E+01  0.544E+00 -0.261E+03 -0.153E+03  0.588E+00  0.102E+01 -0.189E+02  0.497E+02  0.343E+02  0.624E-02  0.292E+00
0.780E-01  0.560E+01  0.573E+00 -0.213E+03 -0.125E+03  0.472E+00  0.818E+00 -0.116E+02  0.694E+02  0.314E+02  0.624E-02  0.288E+00

V=93.3     Q=0.042
0.890E-01  0.560E+01  0.544E+00 -0.261E+03 -0.153E+03  0.588E+00  0.102E+01 -0.189E+02  0.497E+02  0.343E+02  0.624E-02  0.292E+00
0.174E+00  0.130E+01  0.469E+00 -0.107E+05 -0.619E+04  0.126E+02  0.218E+02 -0.176E+03  0.460E+02  0.376E+03  0.181E-01  0.153E+00
0.109E+00  0.130E+01  0.574E+00 -0.537E+04 -0.311E+04  0.578E+01  0.100E+02 -0.341E+02  0.127E+03  0.275E+03  0.181E-01  0.140E+00
0.145E+00  0.130E+01  0.510E+00 -0.827E+04 -0.478E+04  0.930E+01  0.161E+02 -0.940E+02  0.680E+02  0.333E+03  0.181E-01  0.146E+00
0.109E+00  0.130E+01  0.574E+00 -0.537E+04 -0.311E+04  0.578E+01  0.100E+02 -0.341E+02  0.127E+03  0.275E+03  0.181E-01  0.140E+00

V=93.3     Q=0.063
0.174E+00  0.130E+01  0.469E+00 -0.107E+05 -0.619E+04  0.126E+02  0.218E+02 -0.176E+03  0.460E+02  0.376E+03  0.181E-01  0.153E+00
0.129E+00  0.169E+02  0.584E+00 -0.113E+03 -0.664E+02  0.250E+00  0.433E+00 -0.172E+03  0.630E+01  0.101E+02  0.325E-02  0.287E+00
0.135E+00  0.169E+02  0.574E+00 -0.122E+03 -0.713E+02  0.270E+00  0.467E+00 -0.203E+03  0.567E+01  0.104E+02  0.325E-02  0.288E+00
0.155E+00  0.169E+02  0.543E+00 -0.151E+03 -0.881E+02  0.340E+00  0.588E+00 -0.335E+03  0.411E+01  0.114E+02  0.325E-02  0.293E+00

V=159    Q=0.010
0.135E+00  0.169E+02  0.574E+00 -0.122E+03 -0.713E+02  0.270E+00  0.467E+00 -0.203E+03  0.567E+01  0.104E+02  0.325E-02  0.288E+00
0.600E-02  0.280E+01  0.103E+01 -0.472E+01 -0.323E+01  0.166E-01  0.287E-01  0.904E-03 -0.658E+01  0.143E+02  0.335E-02  0.447E+00
0.290E-01  0.280E+01  0.625E+00 -0.786E+02 -0.468E+02  0.229E+00  0.396E+00 -0.832E-01 -0.116E+03  0.410E+02  0.335E-02  0.378E+00
0.290E-01  0.280E+01  0.625E+00 -0.786E+02 -0.468E+02  0.229E+00  0.396E+00 -0.832E-01 -0.116E+03  0.410E+02  0.335E-02  0.378E+00

V=159    Q=0.021
0.290E-01  0.280E+01  0.625E+00 -0.786E+02 -0.468E+02  0.229E+00  0.396E+00 -0.832E-01 -0.116E+03  0.410E+02  0.335E-02  0.378E+00
0.590E-01  0.560E+01  0.545E+00 -0.997E+02 -0.589E+02  0.296E+00  0.513E+00 -0.269E+01  0.237E+03  0.261E+02  0.941E-02  0.386E+00
0.830E-01  0.560E+01  0.469E+00 -0.164E+03 -0.965E+02  0.524E+00  0.907E+00 -0.953E+01  0.669E+02  0.328E+02  0.941E-02  0.414E+00
0.830E-01  0.560E+01  0.469E+00 -0.164E+03 -0.965E+02  0.524E+00  0.907E+00 -0.953E+01  0.669E+02  0.328E+02  0.941E-02  0.414E+00
0.830E-01  0.560E+01  0.469E+00 -0.164E+03 -0.965E+02  0.524E+00  0.907E+00 -0.953E+01  0.669E+02  0.328E+02  0.941E-02  0.414E+00

V=159    Q=0.042
0.830E-01  0.560E+01  0.469E+00 -0.164E+03 -0.965E+02  0.524E+00  0.907E+00 -0.953E+01  0.669E+02  0.328E+02  0.941E-02  0.414E+00
0.145E+00  0.113E+02  0.418E+00 -0.151E+03 -0.882E+02  0.523E+00  0.905E+00 -0.118E+03  0.821E+01  0.187E+02  0.268E-01  0.450E+00
0.145E+00  0.113E+02  0.418E+00 -0.151E+03 -0.882E+02  0.523E+00  0.905E+00 -0.118E+03  0.821E+01  0.187E+02  0.268E-01  0.450E+00
0.121E+00  0.113E+02  0.459E+00 -0.119E+03 -0.698E+02  0.387E+00  0.670E+00 -0.636E+02  0.124E+02  0.166E+02  0.268E-01  0.422E+00
0.121E+00  0.113E+02  0.459E+00 -0.119E+03 -0.698E+02  0.387E+00  0.670E+00 -0.636E+02  0.124E+02  0.166E+02  0.268E-01  0.422E+00
0.161E+00  0.113E+02  0.394E+00 -0.171E+03 -0.100E+03  0.622E+00  0.108E+01 -0.167E+03  0.646E+01  0.201E+02  0.268E-01  0.472E+00
0.161E+00  0.113E+02  0.394E+00 -0.171E+03 -0.100E+03  0.622E+00  0.108E+01 -0.167E+03  0.646E+01  0.201E+02  0.268E-01  0.472E+00
0.236E+00  0.169E+02  0.351E+00 -0.168E+03 -0.982E+02  0.685E+00  0.119E+01 -0.822E+03  0.160E+01  0.151E+02  0.268E-01  0.529E+00
0.221E+00  0.169E+02  0.366E+00 -0.157E+03 -0.917E+02  0.614E+00  0.106E+01 -0.672E+03  0.190E+01  0.144E+02  0.268E-01  0.508E+00
0.141E+00  0.169E+02  0.469E+00 -0.898E+02 -0.527E+02  0.290E+00  0.503E+00 -0.151E+03  0.561E+01  0.107E+02  0.268E-01  0.420E+00

V=252    Q=0.010
0.126E+00  0.169E+02  0.494E+00 -0.766E+02 -0.450E+02  0.241E+00  0.417E+00 -0.102E+03  0.729E+01  0.993E+01  0.268E-01  0.408E+00
0.520E-01  0.280E+01  0.298E+00 -0.701E+02 -0.417E+02  0.605E+00  0.105E+01 -0.772E-01 -0.102E+03  0.605E+02  0.197E-02  0.111E+01
0.620E-01  0.280E+01  0.256E+00 -0.781E+02 -0.464E+02  0.812E+00  0.141E+01 -0.121E+00 -0.117E+03  0.680E+02  0.197E-02  0.133E+01

V=252    Q=0.021
0.440E-01  0.280E+01  0.338E+00 -0.607E+02 -0.362E+02  0.458E+00  0.794E+00 -0.380E-01 -0.857E+02  0.541E+02  0.197E-02  0.969E+00
```

```
0.690E-01  0.560E+01  0.299E+00 -0.429E+02 -0.256E+02  0.385E+00  0.667E+00 -0.733E+00 -0.276E+03  0.290E+02  0.588E-02  0.116E+01
0.830E-01  0.560E+01  0.255E+00 -0.481E+02 -0.286E+02  0.524E+00  0.907E+00 -0.119E+01 -0.213E+04  0.328E+02  0.588E-02  0.140E+01


V=252     Q=0.042
0.930E-01  0.560E+01  0.232E+00 -0.520E+02 -0.309E+02  0.633E+00  0.110E+01 -0.163E+01  0.479E+03  0.354E+02  0.588E-02  0.156E+01
0.150E+00  0.113E+02  0.232E+00 -0.497E+02 -0.294E+02  0.553E+00  0.958E+00 -0.305E+02  0.109E+02  0.192E+02  0.145E-01  0.144E+01
0.135E+00  0.113E+02  0.255E+00 -0.469E+02 -0.278E+02  0.464E+00  0.804E+00 -0.233E+02  0.138E+02  0.179E+02  0.145E-01  0.128E+01
0.104E+00  0.113E+02  0.317E+00 -0.393E+02 -0.234E+02  0.301E+00  0.521E+00 -0.115E+02  0.257E+02  0.150E+02  0.145E-01  0.990E+00


V=252     Q=0.063
0.113E+00  0.113E+02  0.298E+00 -0.421E+02 -0.249E+02  0.345E+00  0.598E+00 -0.146E+02  0.208E+02  0.159E+02  0.145E-01  0.106E+01
0.120E+00  0.169E+02  0.317E+00 -0.278E+02 -0.166E+02  0.222E+00  0.384E+00 -0.257E+02  0.111E+02  0.961E+01  0.282E-01  0.103E+01
0.130E+00  0.169E+02  0.298E+00 -0.297E+02 -0.177E+02  0.254E+00  0.439E+00 -0.325E+02  0.917E+01  0.101E+02  0.282E-01  0.111E+01


V=298     Q=0.021
0.130E+00  0.169E+02  0.298E+00 -0.297E+02 -0.177E+02  0.254E+00  0.439E+00 -0.325E+02  0.917E+01  0.101E+02  0.282E-01  0.111E+01
0.150E+00  0.560E+01  0.232E+00 -0.161E+03 -0.942E+02  0.140E+01  0.243E+01 -0.267E+02  0.205E+02  0.486E+02  0.157E-01  0.113E+01
0.143E+00  0.560E+01  0.232E+00 -0.144E+03 -0.843E+02  0.130E+01  0.225E+01 -0.209E+02  0.238E+02  0.471E+02  0.157E-01  0.117E+01
0.930E-01  0.560E+01  0.325E+00 -0.103E+03 -0.605E+02  0.633E+00  0.110E+01 -0.613E+01  0.707E+02  0.354E+02  0.157E-01  0.801E+00
0.830E-01  0.560E+01  0.352E+00 -0.920E+02 -0.543E+02  0.524E+00  0.907E+00 -0.430E+01  0.102E+03  0.328E+02  0.157E-01  0.739E+00


V=298     Q=0.042
0.150E+00  0.560E+01  0.232E+00 -0.161E+03 -0.942E+02  0.140E+01  0.243E+01 -0.267E+02  0.205E+02  0.486E+02  0.157E-01  0.113E+01
0.166E+00  0.113E+02  0.255E+00 -0.766E+02 -0.450E+02  0.655E+00  0.113E+01 -0.660E+02  0.742E+01  0.205E+02  0.471E-01  0.111E+01


V=298     Q=0.063
0.139E+00  0.113E+02  0.298E+00 -0.687E+02 -0.405E+02  0.487E+00  0.844E+00 -0.416E+02  0.110E+02  0.182E+02  0.471E-01  0.921E+00
0.312E+00  0.169E+02  0.232E+00 -0.141E+03 -0.825E+02  0.109E+01  0.189E+01 -0.115E+04  0.775E+00  0.182E+02  0.847E-01  0.100E+01
0.257E+00  0.169E+02  0.232E+00 -0.895E+02 -0.525E+02  0.790E+00  0.137E+01 -0.468E+03  0.146E+01  0.160E+02  0.847E-01  0.115E+01
0.207E+00  0.169E+02  0.256E+00 -0.655E+02 -0.385E+02  0.551E+00  0.954E+00 -0.213E+03  0.264E+01  0.138E+02  0.847E-01  0.109E+01
EXECUTION TERMINATED    15:52:29  T=.91  RC=0       $.29


$SIGNOFF
```

APPENDIX C

COMPUTER PROGRAM FOR DATA REDUCTION ON ACCELERATION AND BREAK-UP TIME OF DROPLETS

WATERDROP is a computer program developed to analyze liquid droplet behavior as observed in steam tunnel. The size, orientation and kinematics of a droplet are determined by analyzing four basic parameters in a film frame of movie film. The equations used in the program are developed and presented in section B.1, Chapter V. The experimental results physically define the particle in each observation frame. The experimental and analytical accelerations calculated are compared in the program to determine if the theoretical relations can be used to predict the actual acceleration for a specific particle size and steam velocity.

A basic understanding of the program requires a knowledge of how it categorizes experimental data. Each data point belongs to three interrelated groups or sets as shown in Fig. C1 . In general, each point is classified to be in a set. A set includes all of the data taken at a specific liquid flow rate and steam velocity. The next major

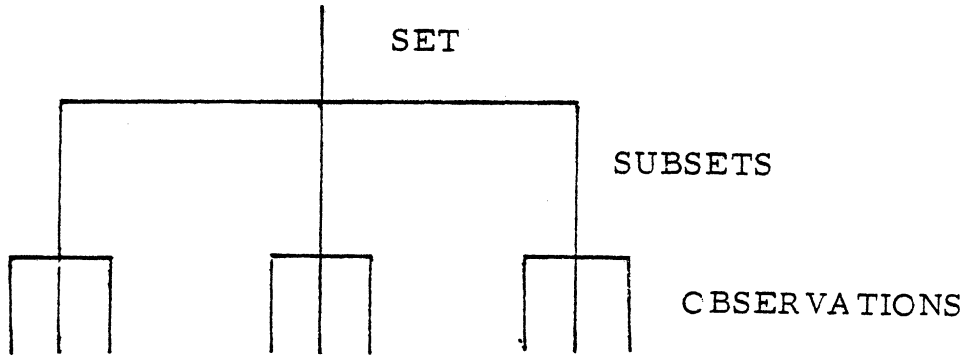

Fig. C1 WATERDROP Data point categories

classification is a subset. A subset includes all of the data points describing a specific particle motion from the time it was first observed until it either disintegrates or vanishes from view. The last group is the observation. The instantaneous size and position of a particle in a reference frame is recorded.

SUBSET RESULTS

A sample listing of these results are given. Each subset has experimental results printed under the twelve headings at the top of the computer printout. The metric CGS units used in the program are listed below each heading. The first six columns define the particle postion and size, while the last six columns define its motion.

The second set of headings lists the calculation results and the comparison between experimental and analytical accelerations according to Serafini correlations[S6]. The last four columns allow a direct comparison of the experimental and analytical accelerations in three ways. First, the experimental acceleration is reprinted directly after the theoretical to allow a comparison at each observation. Second, the difference between these accelerations is printed. Third, a ratio between them is printed to allow an order of magnitude comparison.

Statistics of the subset experimental accelerations are printed next. The arithmetic mean, the mean deviation, and the standard deviation of all accelerations in a subset show an average value and how it varies. The arithmetic mean of

the acceration ratio is also printed to show the average value for the subset.

Information in the last four lines of the subset results define the operating conditions for the subset. Steam flow rate and velocity are given in both metric and English units for clarity. Particle density, steam density, and the kinematic viscosity of the steam are printed to further define the flow conditions. Movie film framing rate and a data conversion factor are given to show the equivalence factors necessary to convert the raw laboratory data into usable results. The last line describes the particle stability, and the elapsed time and position of the observation.

SET RESULTS

The program determines an average value for experimental acceleration and acceleration ratio for each flow and velocity condition. A sample listing from these printouts are also listed. The arithmetic mean, mean deviation,* and standard deviation are calculated for the average experimental accelerations of each subset. In addition, the arithmetic mean of all average acceleration ratios from each subset is printed. The average experimental accelerations from all subsets are printed to keep all the average values on a single page.

---

*Mean deviation = $\dfrac{|X_1-\bar{X}| + |X_2-\bar{X}| + \ldots + |X_n-\bar{X}|}{n}$

WATERDROP VARIABLE AND SUBSCRIPTS LIST

Variable Name	Description of Variable
ABAR(II)	Average acceleration for each subset
ACCEL(J)	EXperimental accelerations from three successive film observations
ARATIO(J)	Ratio of experimental to analytic acceleration for each observation
AREA(J)	Water particle area at each observation
ARR(II)	Average ratio of experimental acceleration ratios of a subset
ARSUM	Sum of all experimental acceleration ratios of a subset
ASUM	Sum of all experimental accelerations in a subset
ATOT	Total sum of experimental acceleration for a subset
ATOTB	Average experimental acceleration of a set
CD(J)	Analytic drag coefficient at each observation
CON	Equivalence factor for converting feet to centimeters
CONFAC	Equivalence factor for converting film measured quantities to centimeters
DELA(J)	Change in acceleration in four consecutive observations
DELV(J)	Change in velocity in three consecutive observations
DELX(J)	Change in displacement between two consecutive observations
DIA(I)	Diameter of the particle at each observation
DTAVG	Average change in time in experimental acceleration calculation

Variable Name	Description of Variable
DVM	Mean deviation of experimental acceleration calculation
FILMV	Velocity of the film
FN(I)	Number of film frames between observations
K1	A test point to determine whether a particle was observed to split
MASS(J)	Mass of the particle at each observation
MEANDV	Mean deviation of experimental acceleration for each subset
N	Total number of data points in a subset
NPL	One less than the total number of data points
NP2	Two less than the total number of data points
P14	One-fourth of the constant
Q	Steam flow rate
QCHECK	Test point to determine the equality of two flow rates
RBAR	Average acceleration ratio for a set
RE(J)	Reynolds number for each observation
RHOS	Steam density
RHOW	Water density
RSUM	Sum of acceleration ratios for a set
SD	Absolute value of the difference between average experimental accelerations of a set and of a subset
SFLOW	Steam flow rate
SIGMA	Standard deviation of experimental acceleration for each subset
SMD	Sum of the differences between experimental and average acceleration for each set

Variable Name	Description of Variable
SMD2	Square of the sums of the experimental and average acceleration difference for each subset
STDV	Standard deviation of the experimental acceleration for each set
SUMDIF	Absolute value of the difference between the average and experimental acceleration in each subset
SUMD2	Square of the sum of the experimental and average acceleration difference for each subset
SUMMD	Sum of the experimental and average acceleration difference for each subset
SVEL	Steam velocity
T(I)	Water particle thickness
TD(J)	Elapsed time between observations
TOTHRD	A constant, 0.6666...
TTOL	Total particle observation time
UDOTW(J)	Analytic Acceleration
V	Steam velocity
VCHECK	A test point to determine the equality of two steam velocities
VEL(J)	Velocity between two consecutive observations
VISNU	Kinematic viscosity of the steam
VOL(J)	Volume of an observed particle

Subscript Character	Description of Subscript
I	Input reading iteration
II	Set calculation iteration
J	Subset calculation iteration
JJ	Average set calculation iteration
K	Output printing iteration

WATERDROP FLOW CHART

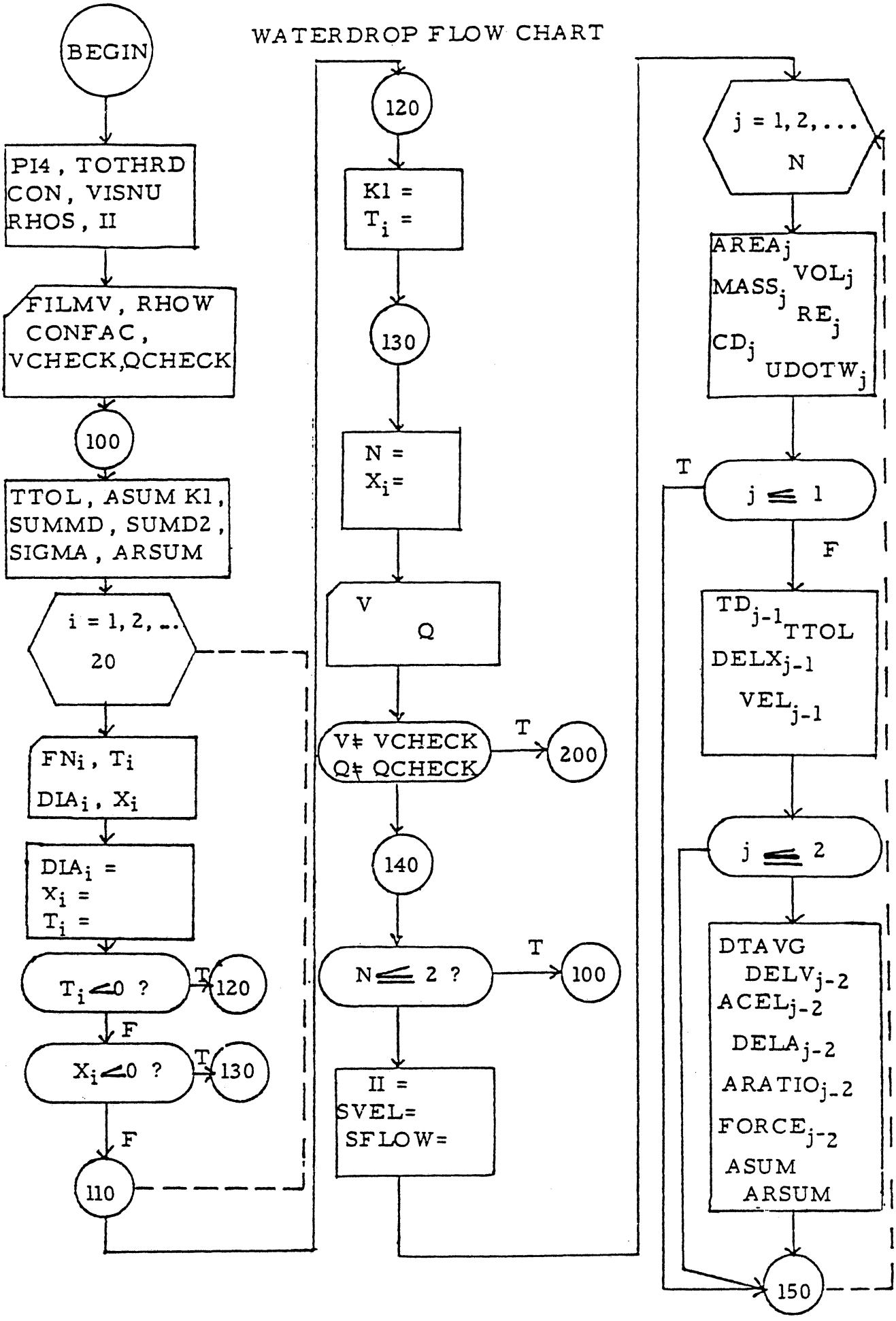

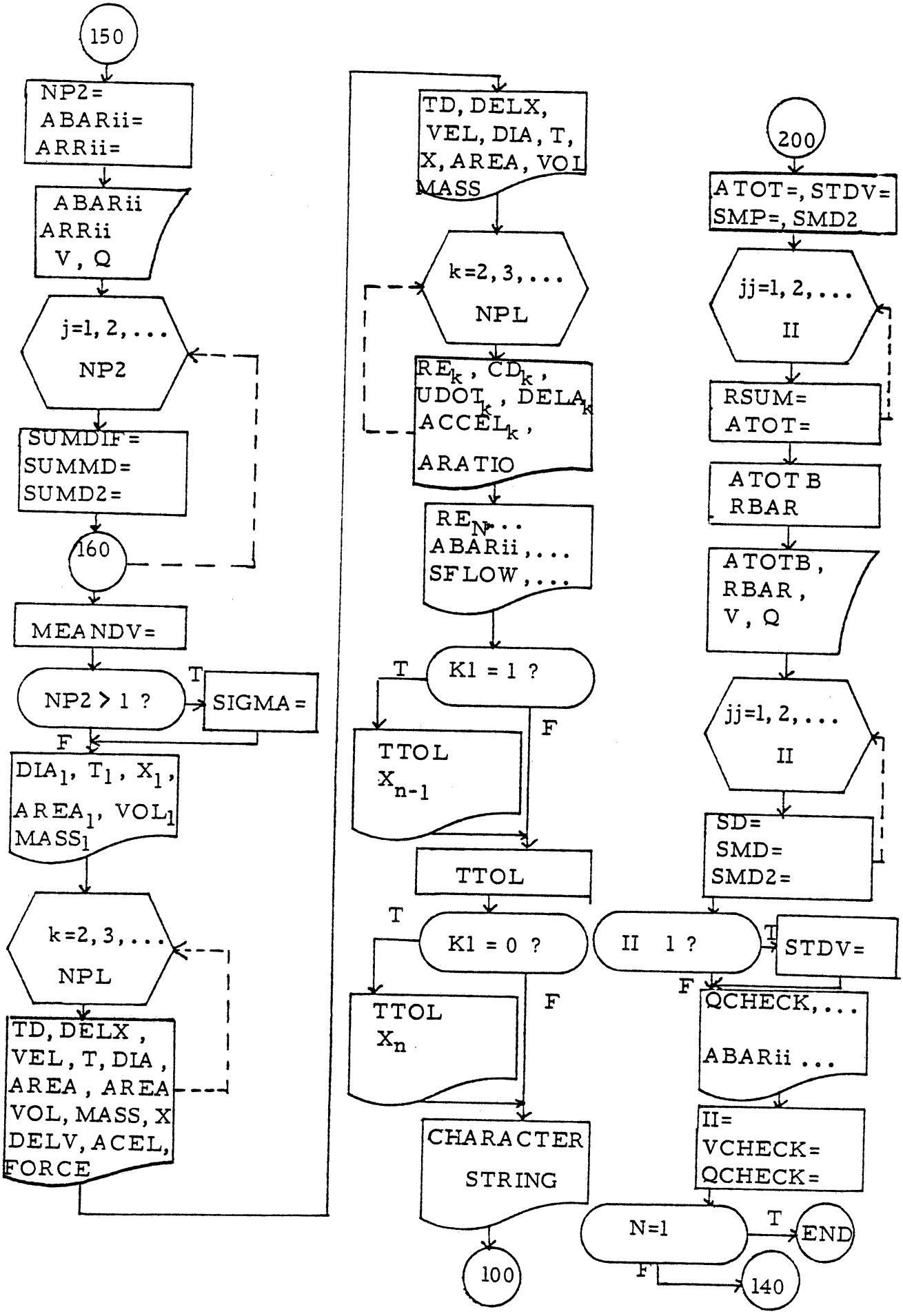
150
NP2=
ABARii=
ARRii=
ABARii
ARRii
V, Q
j=1, 2, ...
NP2
SUMDIF=
SUMMD=
SUMD2=
160
MEANDV=
NP2 > 1 ?
T
SIGMA=
F
DIA1, T1, X1,
AREA1, VOL1
MASS1
k=2, 3, ...
NPL
TD, DELX,
VEL, T, DIA,
AREA, AREA
VOL, MASS, X
DELV, ACEL,
FORCE
TD, DELX,
VEL, DIA, T,
X, AREA, VOL
MASS
k=2, 3, ...
NPL
REk, CDk,
UDOTk, DELAk
ACCELk,
ARATIO
REN...
ABARii, ...
SFLOW, ...
T
K1 = 1 ?
F
TTOL
Xn-1
TTOL
T
K1 = 0 ?
F
TTOL
Xn
CHARACTER
STRING
100
200
ATOT=, STDV=
SMP=, SMD2
jj=1, 2, ...
II
RSUM=
ATOT=
ATOTB
RBAR
ATOTB,
RBAR,
V, Q
jj=1, 2, ...
II
SD=
SMD=
SMD2=
II 1 ?
T
STDV=
F
QCHECK, ...
ABARii ...
II=
VCHECK=
QCHECK=
N=1
T
END
F
140

WATERDROP PROGRAM LISTING

```
C                    WATERDROP
C    ****      A WATER-PARTICLE DATA REDUCTION PROGRAM  ****
C    ****    THIS PROGRAM IS TO DETERMINE THE VELOCITY,ACCELERATION,
C    ****    AND FORCE ON A WATER PARTICLE AS IT TRAVELS THRU A
C    ****    STEAM TUNNEL. IT ALSO CALCULATES AN ANALYTIC
C    ****    ACCELERATION BY THE FOLLOWING RELATION:
C
C                                                              2
C           DU    2A                  2/3    3  DENSITY   VELOCITY
C           -- = -- ( 1.0 + 0.17*RE     ) -  -------  --------
C           DT    RE                       4   RATIO   DIAMETER
C
C.....................................................................
      IMPLICIT REAL*8 (A-H,M,O-Z)
      DIMENSION ACEL(18),AREA(20),DELV(18),DELX(20), DIA(20),MASS(20),
     1  T(20),TD(20),VEL(20), VOL(20),X(20), FORCE(18),ABAR(100),
     2 FN(20), RE(20), CD(20), UDOTW(20), DELA(18), ABATIO(18),ARE(99)
      PI4  = DARSIN(1.0D0)/2.
      CON     =  30.48
      TOTHRD  =  2. / 3.
      VISNU   =  .93469634
      RHOS    =  .00011135215
      READ(5,540) FILMV, RHOW, CONFAC, VCHECK, QCHECK
      II      =  0.0
  100 TTOL=0.
      K1=0.
      ASUM  =  0.0
      SUMD    =  0.0
      SUMD2   =  0.0
      SIGMA   =  0.0
      ARSUM   =  0.0
C    ****  READ ONE SUBSET OF DATA  ****
      DO 110 I=1,20
      READ(5,540)  FN(I), DIA(I), T(I), X(I)
C    **** CONVERT THE DATA TO METRIC DIMENSIONS  ****
      DIA(I)  = CONFAC*DIA(I)
      T(I)    = CONFAC*T(I)
      X(I)    = CONFAC*X(I)
C    **** TEST TO SEE IF THE PARTICLE SPLIT  ****
      IF( T(I) .LT. 0.0 ) GO TO 120
C    ****  TEST TO SEE IF THIS IS THE LAST DATA POINT OF THE SET  ****
      IF( X(I) .LT. 0.0 ) GO TO 130
  110 CONTINUE
  120 K1=1
      T(I) =DABS(T(I))
  130 N = I
      X(N) =DABS(X(N))
      READ(5,540) V, Q
      IF( V .NE. VCHECK .OR. Q .NE. QCHECK ) GO TO 200
  140 IF( N .LE. 2 ) GO TO 100
      II    =   II + 1
C    **** CALCULATING OPERATIONS ****
      SVEL    =  V*CON
      SFLOW   =  Q*60. / CON**3
C    ****  ITERATIVE SUBSET CALCULATIONS  ****
```

```
      DO 150 J=1,N
      AREA(J)    = PI4*DIA(J)**2
      VOL(J)     = AREA(J)*T(J)*16. / 3.
      MASS(J)    = VOL(J)*RHOW
      RE(J)      =  DIA(J) * SVEL / VISNU
      CD(J)    =  24. / RE(J) *( 1. + 0.17*RE(J)**TOTHRD)
      UDOTW(J)=  CD(J) * RHOS/RHOW *3./4. /DIA(J) *SVEL**2
      IF( J .LE. 1 ) GO TO 150
      TD(J-1) =PW(J) / FILMV
      TTOL    = TTOL + TD(J-1)
      DELX(J-1)= X(J) - X(J-1)
      VEL(J-1)   = DELX(J-1)/TD(J-1)
      IF( J .LE. 2 ) GO TO 150
      DTAVG   =  (TD(J-1) + TD(J-2)) / 2.
       DELV(J-2)= VEL(J-1) - VEL(J-2)
       ACEL(J-2)= DELV(J-2)/2./DTAVG
       DELA(J-2)   =UDOTW(J-1) -ACEL(J-2)
       ARATIO(J-2)= ACEL(J-2) / UDOTW(J-1)
       FORCE(J-2)= ACEL(J-2)*MASS(J-1)
      ASUM    =  ACEL(J-2) + ASUM
      ARSUM    =  ARATIO(J-2) + ARSUM
  150 CONTINUE
C     **** SUBSET STATISTICS CALCULATIONS ****
      NP2 =   N - 2
      ABAR(II)  =  ASUM / NP2
      ARR(II) =  ARSUM / NP2
C     **** STORE SUBSET RESULTS FOR PLOTTING ****
      WRITE(1,660) ABAR(II),ARR(II), VCHECK, QCHECK
      DO 160 J=1,NP2
      SUMDIF  =  DABS( ACEL(J) - ABAR(II) )
      SUMMD   =  SUMDIF + SUMMD
  160 SUMD2   =  SUMDIF**2 + SUMD2
      MEANDV  =  SUMMD / NP2
      IF( NP2 .GT. 1 ) SIGMA  =DSQRT( SUMD2 / (NP2 - 1. ))
C    **** PRINT OUT RESULTS OF THE SET ****
      WRITE(6,550)  DIA(1), T(1),AREA(1), VOL(1), MASS(1), X(1)
      NPL=  N- 1
      DO 180 K=2,NPL
  180 WRITE(6,560) TD(K-1),DELX(K-1),VEL(K-1), DIA(K), T(K), AREA(K),
     1 VOL(K),MASS(K), X(K), DELV(K-1), ACEL(K-1),FORCE(K-1)
      WRITE(6,560) TD(NPL),DELX(NPL), VEL(NPL), DIA(N), T(N), AREA(N),
     1 VOL(N), MASS(N), X(N)
C     **** PRINT ANALYTIC RESULTS AND COMPARISONS ****
      WRITE(6,610) RE(1), CD(1), UDOTW(1)
      DO 190 K=2,NPL
  190 WRITE(6,570) RE(K), CD(K), UDOTW(K), ACEL(K-1),DELA(K-1), ARATIO(K-1)
      WRITE(6,570) RE(N), CD(N), UDOTW(N)
      WRITE(6,650) ABAR(II), MEANDV, SIGMA, ARR(II)
      WRITE(6,620) SFLOW,Q,V,SVEL,RHOW,RHOS,VISNU,FILMV,CONFAC
      IF( K1 .EQ. 1 ) WRITE(6,580) TTOL,X(N-1)
      TTOL  = TTOL  + TD(J)
      IF( K1 .EQ. 0 ) WRITE(6,590) TTOL, X(N)
      WRITE(6,600)
C    **** GO READ ANOTHER DATA SET ****
      GO TO 100
C     **** PERFORM SET STATISTICS CALCULATIONS ****
  200 ATOT    =  0.0
      SMD     =  0.0
      SMD2    =  0.0
      STDV =0.0
```

```
      RSUM    =  0.0
      DO 220 JJ=1,II
      RSUM    =  ARR(JJ)  + RSUM
  220 ATOT    =  ABAR(JJ) + ATOT
      ATOTB   =  ATOT / II
      RBAR    =  RSUM / II
      WRITE(2,660) ATOTB, RBAR, VCHECK, QCHECK
      DO 240 JJ=1,II
      SD      =  DABS( ABAR(JJ) - ATOTB )
      SMD     =  SD + SMD
  240 SMD2    =  SD**2 + SMD2
      IF( II .GT. 1 ) STDV=DSQRT( SMD2/ (II-1))
      DVR     =  SMD / II
      WRITE(6,630) QCHECK,VCHECK,ATOTB,RBAR,DVR,STDV,II
C     ****  PRINT SET STATISTICS  ****
      WRITE(6,640) (ABAR(I),I=1,II)
C     ****  STORE SET RESULTS FOR PLOTTING  ****
      WRITE(6,600)
      II  =  0.0
      VCHECK =  V
      QCHECK =  Q
C     ****  CHECK FOR AN END OF THE DATA SETS  ****
      IF( N .EQ. 1 )  CALL EXIT
      GO TO 140
C    ****  INPUT AND OUTPUT FORMATS  ****
  540 FORMAT(6(F10.5))
  550 FORMAT('1',1X,'DIAMETER',T13,'THICKNESS', T27,'AREA', T36,'VOLUME'
     1,T48,'MASS', T57,'POSITION', T68,'DELTA TIME', T80,'DELTA X', T91,
     2'VELOCITY', T102,'DEL VEL', T111,'ACCELERATION', T125,'FORCE'/
     3T3,'( CM )', T14,'( CM )',T26,'(CM**2)', T36,'(CM**3)', T46,
     4'(GRAMS)', T55,'(CM FROM FIN)', T69,'(SECONDS)' ,T80,'( CM )',T91,
     5'(CM/SEC)', T102,'(CM/SEC)', T111,'(CM/SEC**2)', T124,'(DYNES)'///
     6 2F11.5,F11.7,2F11.8,F11.5)
  560 FORMAT(T56,F11.4 ,F11.6,F11.3/ 2F11.5,F11.7,2F11.8,F11.5,F11.7,
     1 T99,F11.4,F11.1)
  570 FORMAT(F13.5,T17,F10.8,F12.1,F13.2,F15.3,T70,F10.4/)
  580 FORMAT('  THE PARTICAL WAS OBSERVED TO BREAK UP AT ',F10.5,' SECON
     1DS AND ',F10.5,' CM. FROM THE END OF FIN.')
  590 FORMAT(' THE PARTICAL WAS NOT OBSERVED TO BREAK UP IN ',F10.5,
     1' SECONDS OR ',F10.5,' CM. FROM THE END OF THE FIN.')
  600 FORMAT(66('* '))
  610 FORMAT('-',T5,'REYNOLDS',T20,'DRAG',T31,'ANALYTIC',T42,
     1 'EXPERIMENTAL',T56,'ACCELERATION',T70,'ACCELERATION'/
     2 T6,'NUMBER',T17,'COEFFICIENT',T29,'ACCELERATION',T42,
     3 'ACCELERATION',T57,'DIFFERENCE',T73,'RATIO'/T30,'(CM/SEC**2)',
     4 T42,'(CM/SEC**2)',T56,'(CM/SEC**2)'//F13.5,T17,F10.8,F12.1/)
  620 FORMAT(/' FLOW RATE =  ',F10.5,' CFM OR ',F10.5,' CM**3/SEC ',
     1 T55,'STEAM VELOCITY = ', F10.5,' FT/SEC OR ',F10.1,' CM/SEC ',
     2 /'PARTICLE DENSITY = ',F10.5,T38,'STEAM DENSITY = ',F11.10,
     3  ' GM/CM**3',T80,'KINEMATIC VISCOSITY = ',F10.8,' CM**2/SEC'/
     4 'FILM VELOCITY =',F6.0,' FRAMES/SEC              DATA CONVERSION',
     5 ' FACTOR = ',F6.3)
  630 FORMAT('1',66('* '),///T10,'AVERAGE EXPERIMENTAL ACCELERATION ',
     1 'STATISTICS FOR A FLOW RATE OF ',F3.0,' CM**3/MIN AND STEAM ',
     2 'VELOCITY ',F4.0,' FT/SEC',///T40,'STATISTICS OF EXPERIMENTAL',
     3' ACCELERATION'///,T30,'ARITHMATIC MEAN  = ',T60,F20.8//
     9T30,'ACCELERATION RATIO  = ',T65,F15.11//
     4T30,'MEAN DEVIATION  = ',T60,F20.8//
     5T30,'STANDARD DEVIATION  = ',T60,F20.8///T40,'AVERAGE ',
     6 'ACCELERATION OF ',I3,' DATA SETS'///)
```

```
640 FORMAT(6F20.8//)
650 FORMAT(//T40,'STATISTICS OF EXPERIMENTAL ACCELERATION'//
   1T10,'ARITHMATIC MEAN  = ',F12.3,T45,'MEAN DEVIATION  = ',F12.3,
   2T80,'STANDARD DEVIATION  = ',F12.3/T35,'AVERAGE ACCELERATION ',
   3 'RATIO  = ',F20.13)
660 FORMAT(4(F15.5,','))
    END
```

DIAMETER (CM)	THICKNESS (CM)	AREA (CM**2)	VOLUME (CM**3)	MASS (GRAMS)	POSITION (CM FROM FIN)	DELTA TIME (SECONDS)	DELTA X (CM)	VELOCITY (CM/SEC)	DEL VEL (CM/SEC)	ACCELERATION (CM/SEC**2)	FORCE (DYNES)
0.13500	0.09000	0.0143139	0.00687066	0.00687066	0.45000						
						0.0010	0.045000	45.000			
0.13500	0.09000	0.0143139	0.00687066	0.00687066	0.49500				45.0000	22500.0	154.590
						0.0010	0.090000	90.000			
0.13500	0.13500	0.0143139	0.01030599	0.01030599	0.58500				0.0	0.0	0.0
						0.0010	0.090000	90.000			
0.18000	0.09000	0.0254469	0.01221451	0.01221451	0.67500				-45.0000	22500.0	274.827
						0.0010	0.135000	135.000			
0.13500	0.09000	0.0143139	0.00687066	0.00687066	0.81000				-0.0000	-0.0	-0.000
						0.0010	0.135000	135.000			
0.13500	0.04500	0.0143139	0.00343533	0.00343533	0.94500				90.0000	45000.0	154.590
						0.0010	0.225000	225.000			
0.13500	0.09000	0.0143139	0.00687066	0.00687066	1.17000				0.0000	0.0	0.000
						0.0010	0.225000	225.000			
0.13500	0.09000	0.0143139	0.00687066	0.00687066	1.39500				90.0000	45000.0	309.180
						0.0010	0.315000	315.000			
0.09000	0.09000	0.0063617	0.00305363	0.00305363	1.71000				45.0000	22500.0	68.707
						0.0010	0.360000	360.000			
0.13510	0.04500	0.0143139	0.00343533	0.00343533	2.07000				-45.0000	-22500.0	-77.295
						0.0010	0.315000	315.000			
0.13500	0.04500	0.0143139	0.00343533	0.00343533	2.38500						

REYNOLDS NUMBER	DRAG COEFFICIENT	ANALYTIC ACCELERATION (CM/SEC**2)	EXPERIMENTAL ACCELERATION (CM/SEC**2)	ACCELERATION DIFFERENCE (CM/SEC**2)	ACCELERATION RATIO
1342.69688	0.38770317	21131.7			
1342.69688	0.38770317	21131.7	22500.00	-1368.300	1.0648
1342.69688	0.38770317	21131.7	0.0	21131.700	0.0
1790.25250	0.34961752	14283.7	22500.00	-9216.290	1.5752
1342.69688	0.38770317	21131.7	-0.00	21131.700	-0.0000
1342.69688	0.38770317	21131.7	45000.00	-23868.300	2.1295
1342.69688	0.38770317	21131.7	0.00	21131.700	0.0000
1342.69688	0.38770317	21131.7	45000.00	-23868.300	2.1295
895.13125	0.45015930	36803.8	22500.00	14303.841	0.6113
1342.69688	0.38770317	21131.7	-22500.00	43631.700	-1.0648
1342.69688	0.38770317	21131.7			

STATISTICS OF EXPERIMENTAL ACCELERATION

ARITHMATIC MEAN = 15000.000 MEAN DEVIATION = 18333.333 STANDARD DEVIATION = 22500.000

AVERAGE ACCELERATION RATIO = 0.7151749322211

FLOW RATE = 0.01059 CFM OR 5.00000 CM**3/SEC STEAM VELOCITY = 305.00000 FT/SEC OR 9296.4 CM/SEC

DIAMETER (CM)	THICKNESS (CM)	AREA (CM**2)	VOLUME (CM**3)	MASS (GRAMS)	POSITION (CM FROM FIN)	DELTA TIME (SECONDS)	DELTA X (CM)	VELOCITY (CM/SEC)	DEL VEL (CM/SEC)	ACCELERATION (CM/SEC**2)	FORCE (DYNES)
0.09000	0.04500	0.0063617	0.00152681	0.00152691	0.49500						
						0.0010	0.180000	180.000			
0.04500	0.04500	0.0015904	0.00038170	0.00038170	0.67500				45.0000	22500.0	8.588
						0.0010	0.225000	225.000			
0.04500	0.04500	0.0015904	0.00038170	0.00038170	0.90000				135.0000	67500.0	25.765
						0.0010	0.360000	360.000			
0.09000	0.09000	0.0063617	0.00305363	0.00305363	1.26000				-0.0000	-0.0	-0.000
						0.0010	0.360000	360.000			
0.04500	0.04500	0.0015904	0.00038170	0.00038170	1.62000				45.0000	22500.0	8.588
						0.0010	0.405000	405.000			
0.04500	0.04500	0.0015904	0.00038170	0.00038170	2.02500				180.0000	90000.0	34.353
						0.0010	0.585000	585.000			
0.09000	0.09000	0.0063617	0.00305363	0.00305363	2.61000						

REYNOLDS NUMBER	DRAG COEFFICIENT	ANALYTIC ACCELERATION (CM/SEC**2)	EXPERIMENTAL ACCELERATION (CM/SEC**2)	ACCELERATION DIFFERENCE (CM/SEC**2)	ACCELERATION RATIO
895.13125	0.45015999	36803.8			
447.56563	0.58700872	95984.5	22500.00	73484.454	0.2344
447.56563	0.58700872	95984.5	67500.00	28484.454	0.7032
895.13125	0.45015999	36803.8	-0.00	36803.841	-0.0000
447.56563	0.58700872	95984.5	22500.00	73484.454	0.2344
447.56563	0.58700872	95984.5	90000.00	5984.454	0.9377
895.13125	0.45015999	36803.8			

STATISTICS OF EXPERIMENTAL ACCELERATION

ARITHMATIC MEAN = 40500.000 MEAN DEVIATION = 30600.000 STANDARD DEVIATION = 36971.273
AVERAGE ACCELERATION RATIO = 0.4219433271900

FLOW RATE = 0.01059 CFM OR 5.00000 CM**3/SEC STEAM VELOCITY = 305.00000 FT/SEC OR 9296.4 CM/SEC
PARTICLE DENSITY = 1.00000 STEAM DENSITY = .0001135215 GM/CM**3 KINEMATIC VISCOSITY = 0.93469632 CM**2/SEC
FILM VELOCITY = 5000. FRAMES/SEC DATA CONVERSION FACTOR = 0.450
THE PARTICAL WAS NOT OBSERVED TO BREAK UP IN 0.00700 SECONDS OR 2.61000 CM. FROM THE END OF THE FIN.
* *

```
PARTICLE DENSITY =    1.00000        STEAM DENSITY = .0001135215 GM/CM**3        KINEMATIC VISCOSITY = 0.93469632 CM**2/SEC
FILM VELOCITY = 5000. FRAMES/SEC             DATA CONVERSION FACTOR =  0.450
THE PARTICAL WAS NOT OBSERVED TO BREAK UP IN    0.01100 SECONDS OR    2.38500 CM. FROM THE END OF THE FIN.
* * * * * * * * * * * * * * * * * * * * * * * * * * * * * * * * * * * * * * * * * * * * * * * * * * * * * * * * * * * * * * * * *
```

AVERAGE EXPERIMENTAL ACCELERATION STATISTICS FOR A FLOW RATE OF 5. CM**3/MIN AND STEAM VELOCITY 305. FT/SEC

STATISTICS OF EXPERIMENTAL ACCELERATION

ARITHMATIC MEAN =	26928.01339286
ACCELERATION RATIO =	0.78721570486
MEAN DEVIATION =	14922.36328125
STANDARD DEVIATION =	17834.16571408

AVERAGE ACCELERATION OF 16 DATA SETS

61875.00000000	40500.00000000	52500.00000000	30000.00000000	37500.00000000	22500.00000000
11250.00000000	15000.00000000	40500.00000000	22500.00000000	6000.00000000	18000.00000000
45000.00000000	0.0	8035.71428571	19687.50000000		

DIAMETER (CM)	THICKNESS (CM)	AREA (CM**2)	VOLUME (CM**3)	MASS (GRAMS)	POSITION (CM FROM FIN)	DELTA TIME (SECONDS)	DELTA X (CM)	VELOCITY (CM/SEC)	DEL VEL (CM/SEC)	ACCELERATION (CM/SEC**2)	FORCE (DYNES)
0.09000	0.09000	0.0063617	0.00305363	0.00305363	0.36000						
						0.0010	0.180000	180.000			
0.09000	0.04500	0.0063617	0.00152681	0.00152681	0.54000				45.0000	22500.0	34.353
						0.0010	0.225000	225.000			
0.09000	0.09000	0.0063617	0.00305363	0.00305363	0.76500				45.0000	22500.0	68.707
						0.0010	0.270000	270.000			
0.09000	0.09000	0.0063617	0.00305363	0.00305363	1.03500				90.0000	45000.0	137.413
						0.0010	0.360000	360.000			
0.09000	0.09000	0.0063617	0.00305363	0.00305363	1.39500				180.0000	90000.0	274.827
						0.0010	0.540000	540.000			
0.09000	0.09000	0.0063617	0.00305363	0.00305363	1.93500						

REYNOLDS NUMBER	DRAG COEFFICIENT	ANALYTIC ACCELERATION (CM/SEC**2)	EXPERIMENTAL ACCELERATION (CM/SEC**2)	ACCELERATION DIFFERENCE (CM/SEC**2)	ACCELERATION RATIO
1526.12541	0.37010119	87953.6			
1526.12541	0.37010119	87953.6	22500.00	65453.645	0.2558
1526.12541	0.37010119	87953.6	22500.00	65453.645	0.2558
1526.12541	0.37010119	87953.6	45000.00	42953.645	0.5116
1526.12541	0.37010119	87953.6	90000.00	-2046.355	1.0233
1526.12541	0.37010119	87953.6			

STATISTICS OF EXPERIMENTAL ACCELERATION

ARITHMATIC MEAN = 45000.000 MEAN DEVIATION = 22500.000 STANDARD DEVIATION = 31819.805
AVERAGE ACCELERATION RATIO = 0.5115331458401

FLOW RATE = 0.03178 CFM OR 15.00000 CM**3/SEC STEAM VELOCITY = 520.00000 FT/SEC OR 15849.6 CM/SEC
PARTICLE DENSITY = 1.00000 STEAM DENSITY = .0001135215 GM/CM**3 KINEMATIC VISCOSITY = 0.93469632 CM**2/SEC
FILM VELOCITY = 5000. FRAMES/SEC DATA CONVERSION FACTOR = 0.450
THE PARTICAL WAS OBSERVED TO BREAK UP AT 0.00500 SECONDS AND 1.93500 CM. FROM THE END OF FIN.
* *

AVERAGE EXPERIMENTAL ACCELERATION STATISTICS FOR A FLOW RATE OF 15. CM**3/MIN AND STEAM VELOCITY 520. FT/SEC

STATISTICS OF EXPERIMENTAL ACCELERATION

ARITHMATIC MEAN =	82940.21739130
ACCELERATION RATIO =	1.02963352162
MEAN DEVIATION =	49834.59357278
STANDARD DEVIATION =	71393.81289208

AVERAGE ACCELERATION OF 23 DATA SETS

67500.00000000	120000.00000000	135000.00000000	202500.00000000	54000.00000000	90000.00000000
52500.00000000	90000.00000000	101250.00000000	90000.00000000	45000.00000000	58500.00000000
-90000.00000000	157500.00000000	146250.00000000	270000.00000000	-11250.00000000	75000.00000000
49500.00000000	73125.00000000	41250.00000000	45000.00000000	45000.00000000	

DIAMETER (CM)	THICKNESS (CM)	AREA (CM**2)	VOLUME (CM**3)	MASS (GRAMS)	POSITION (CM FROM FIN)	DELTA TIME (SECONDS)	DELTA X (CM)	VELOCITY (CM/SEC)	DEL VEL (CM/SEC)	ACCELERATION (CM/SEC**2)	FORCE (DYNES)
0.09000	0.04500	0.0063617	0.00152681	0.00152681	0.18000						
0.04500	0.04500	0.0015904	0.00038170	0.00038170	0.36000	0.0010	0.180000	180.000			
0.04500	0.04500	0.0015904	0.00038170	0.00038170	0.49500	0.0010	0.135000	135.000	-45.0000	-22500.0	-8.588
0.04500	0.04500	0.0015904	0.00038170	0.00038170	0.81000	0.0010	0.315000	315.000	180.0000	90000.0	34.353
0.04500	0.04500	0.0015904	0.00038170	0.00038170	1.35000	0.0010	0.540000	540.000	225.0000	112500.0	42.942
0.04500	0.04500	0.0015904	0.00038170	0.00038170	2.25000	0.0010	0.900000	900.000	360.0000	180000.0	68.707

REYNOLDS NUMBER	DRAG COEFFICIENT	ANALYTIC ACCELERATION (CM/SEC**2)	EXPERIMENTAL ACCELERATION (CM/SEC**2)	ACCELERATION DIFFERENCE (CM/SEC**2)	ACCELERATION RATIO
2421.25666	0.31375316	187682.0			
1210.62833	0.40264004	481705.4	-22500.00	504205.413	-0.0467
1210.62833	0.40264004	481705.4	90000.00	391705.413	0.1868
1210.62833	0.40264004	481705.4	112500.00	369205.413	0.2335
1210.62833	0.40264004	481705.4	180000.00	301705.413	0.3737
1210.62833	0.40264004	481705.4			

STATISTICS OF EXPERIMENTAL ACCELERATION

ARITHMATIC MEAN = 90000.000 MEAN DEVIATION = 56250.000 STANDARD DEVIATION = 84187.291
AVERAGE ACCELERATION RATIO = 0.1868361815152

FLOW RATE = 0.10594 CFM OR 50.00000 CM**3/SEC STEAM VELOCITY = 925.00000 FT/SEC OR 25146.0 CM/SEC
PARTICLE DENSITY = 1.00000 STEAM DENSITY = .0001135215 GM/CM**3 KINEMATIC VISCOSITY = 0.93469632 CM**2/SEC
FILM VELOCITY = 5000. FRAMES/SEC DATA CONVERSION FACTOR = 0.450
THE PARTICAL WAS OBSERVED TO BREAK UP AT 0.00500 SECONDS AND 2.25000 CM. FROM THE END OF FIN.
* *

AVERAGE EXPERIMENTAL ACCELERATION STATISTICS FOR A FLOW RATE OF 50. CM**3/MIN AND STEAM VELOCITY 825. FT/SEC

STATISTICS OF EXPERIMENTAL ACCELERATION

ARITHMATIC MEAN =	147187.50000000
ACCELERATION RATIO =	1.02707793883
MEAN DEVIATION =	66796.87500000
STANDARD DEVIATION =	78985.61690948

AVERAGE ACCELERATION OF 8 DATA SETS

202500.00000000	202500.00000000	75000.00000000	90000.00000000	112500.00000000	90000.00000000
101250.00000000	213750.00000000				

APPENDIX D

STATISTICAL LINEAR REGRESSION ANALYSIS OF DROPLET ACCELERATION

Due to the nature of the physical phenomenon under consideration and the large amount of experimental data collected, certain statistical tools were used to better understand the experimental results. Reduction of the initial raw data (Appendix C) resulted in 855 droplet accelerations for the flow conditions outlined in Table 5.3 . These 855 cases were broken into 327 subsets for which average droplet accelerations were obtained.

When performing a first-order regression of E.A. (Experimental Acceleration) on Q the 327 data set was arranged into the following cases corresponding to constant steam velocity, U_s, and stored in data file "AVGACCEL";

Cases	U_s (ft/sec)
1-45	305
46-129	520
130-185	825
186-246	975
247-327	1100

In a similar manner the "327" data set was rearranged in order to perform a first-order regression of E.A. on U_s with liquid flow rate, Q, being held constant. These are stored on data file "QACCEL".

Cases	Q (cm^3/min)
1-3	0
4-58	5
59-130	10
131-198	15
199-250	20
251-294	30
295-302	40
303-327	50

MIDAS "REGRESSION" command was used to perform the regression analyses mentioned throughout the test.

From the MIDAS results, it is found that E.A. is not affected by changing Q. However, it is seen that E.A. is strong function of U_s. For example, "goodness of fit," R-SQR shows that for Q = 15, there is a variation of 76% in E.A., which can be explained by the variation in U_s. Full details of this analysis is available from on of our previous reports.(M14) Regression analysis output is followed.

REGRESSION OF E.A. ON @ at CONST. Us

VARIABLE LABELS

DATA FILE: AVGACCEL

AA- Ave. "327" DATA SET
Acceleration, Ft/Sec

R- ACCEL, RATIO (Measured/Senafini)

U- Steam Velocity, Ft/Sect

Q- Liquid Flow rate, cm^3/min

```
RES


CØMMAND
?HIST V=AA CASES=1-45 ØP=HIST%
 INTERVAL EXPRESSIØN -- #INT:(MIN,MAX)  (MIN,MAX)/WIDTH  #PER/(MIN,MAX)
=


 HISTØGRAM  CASES=CASE#:1-45

 MIDPØINT   HIST%  CØUNT FØR 1.AA  (EACH X= 1)

  0.         20.0     9 +XXXXXXXXX
  676.67     46.7    21 +XXXXXXXXXXXXXXXXXXXX
  1353.3     22.2    10 +XXXXXXXXXX
  2030.0      8.9     4 +XXXX
  2706.7      0.      0 +
  3383.4      0.      0 +
  4060.0      2.2     1 +X

  TØTAL              45  (INTERVAL WIDTH= 676.67)


 CØMMAND
?HIST V=AA CASES=1-45 ØP=HIST%
 INTERVAL EXPRESSIØN -- #INT:(MIN,MAX)  (MIN,MAX)/WIDTH  #PER/(MIN,MAX)
=*


 HISTØGRAM  CASES=CASE#:1-45

 MIDPØINT   HIST%  CØUNT FØR 1.AA  (EACH X= 1)

  0.         20.0     9 +XXXXXXXXX
  676.67     46.7    21 +XXXXXXXXXXXXXXXXXXXX
  1353.3     22.2    10 +XXXXXXXXXX
  2030.0      8.9     4 +XXXX
  2706.7      0.      0 +
  3383.4      0.      0 +
  4060.0      2.2     1 +X

  TØTAL              45  (INTERVAL WIDTH= 676.67)


 CØMMAND
?DESCRIBE V=AA CASES=1-45


 DESCRIPTIVE MEASURES  CASES=CASE#:1-45

      VARIABLE        N  MINIMUM     MAXIMUM       MEAN      STD DEV
```

```
   1.AA              45  0.          4060.0      851.28      735.72

 CØMMAND
?DIST V=AA CASES=1-45 PRØB=.5

 DISTRIBUTIØNAL ANALYSIS  CASES=CASE#:1-45

 CUMULATIVE SAMPLE DISTRIBUTIØN ØF 1.AA  N= 45 ØUT ØF 45
1.00000   +                                                    *
                                                  * *
                                               *
 .90000   +                        3  *
                                2
 .80000   +
                               3
 .70000   +                   **
                             *
                         3
 .60000   +
                       2
                       2
 .50000   +          —— *
                     2
                    *
 .40000   +          3
                    *
 .30000   +          5

 .20000   +     *
                2
                *
 .10000   +    **
               *
              **
0.          +
            +----+----+----+----+----+----+----+----+----+
           0.                  1624.0              3248.0     AA
                    812.01              2436.0               4060.0

  PRØB   QUANTILE

 .5000   632.73

 CØMMAND
?REGRESS V=AA;Q CASES=1-45
```

```
 LEAST SQUARES REGRESSIØN  CASES=CASE#:1-45

 ANALYSIS ØF VARIANCE ØF 1.AA  N= 45 ØUT ØF 45

      SØURCE              DF  SUM SQRS    MEAN SQR    F-STAT     SIGNIF

      REGRESSIØN           1  .25527 +6  .25527 +6  .46589       .4985
      ERRØR               43  .23561 +8  .54793 +6
      TØTAL               44  .23816 +8
```

MULT R= .10353 R-SQR= .01072 SE= 740.22

VARIABLE	PARTIAL	CØEFF	STD ERRØR	T-STAT	SIGNIF
CØNSTANT		944.69	175.80	5.3736	.0000
4.Q	-.10353	-5.9627	8.7357	-.68256	.4985

CØMMAND
?

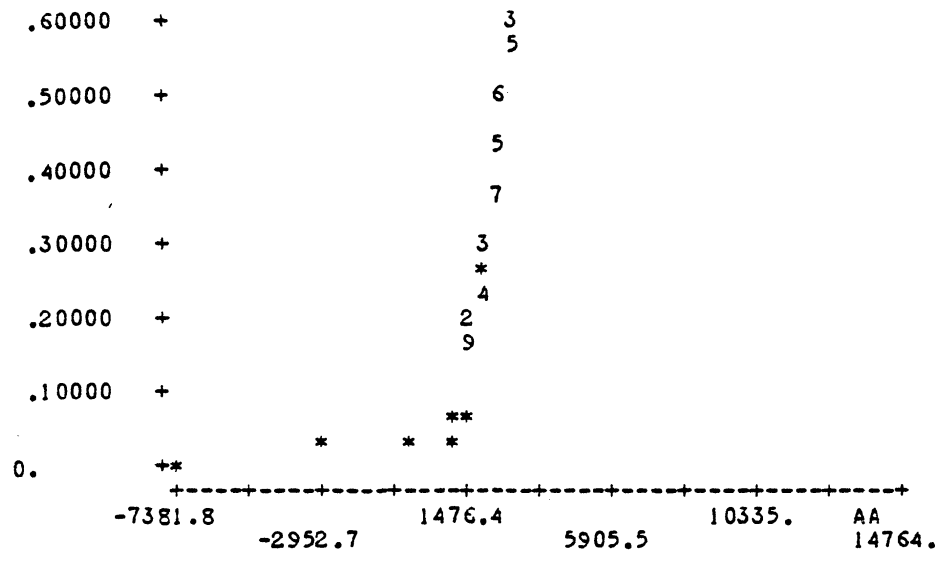

PRØB	QUANTILE
.5000	2509.8

```
 CØMMAND
?REGRESS V=AA;Q CASES46-=46-129

 LEAST SQUARES REGRESSIØN  CASES=CASE#:46-129

 ANALYSIS ØF VARIANCE ØF 1.AA  N= 84 ØUT ØF 84

      SØURCE              DF  SUM SQRS    MEAN SQR    F-STAT    SIGNIF

      REGRESSIØN           1  .11675 +8  .11675 +8  2.0719      .1538
      ERRØR               82  .46205 +9  .56347 +7
      TØTAL               83  .47372 +9

      MULT R= .15699  R-SQR= .02464 SE= 2373.8

      VARIABLE     PARTIAL    CØEFF     STD ERRØR    T-STAT    SIGNIF

      CØNSTANT                3402.7      446.23     7.6255     .0000
    4.Q            -.15699   -29.388      20.417    -1.4394     .1538

 CØMMAND
?
```

```
?HIST V=AA CASES=130-185 ØP=HIST%
 INTERVAL EXPRESSIØN -- #INT:(MIN,MAX)  (MIN,MAX)/WIDTH  #PER/(MIN,MAX)
=

 HISTØGRAM  CASES=CASE#:130-185

 MIDPØINT   HIST%  CØUNT FØR 1.AA  (EACH X= 1)

  738.19      1.8     1 +X
  2952.8      8.9     5 +XXXXX
  5167.3     19.6    11 +XXXXXXXXXX
  7381.9     28.6    16 +XXXXXXXXXXXXXXX
  9596.5     23.2    13 +XXXXXXXXXXXXX
  11811.     12.5     7 +XXXXXXX
  14026.      3.6     2 +XX
  16240.      1.8     1 +X

  TØTAL              56  (INTERVAL WIDTH= 2214.6)


 CØMMAND
?DESV-SCRIBE V=AA CASES=130-185

 ERRØR -- INVALID CØMMAND:  "DESSCRIBE"
 CØMMAND CANCELLED


 CØMMAND
?DESCRIBE V=AA CASES=130-185


 DESCRIPTIVE MEASURES  CASES=CASE#:130-185

      VARIABLE        N  MINIMUM    MAXIMUM      MEAN     STD DEV

    1.AA              56  738.19     16240.     7871.8     3195.2


 CØMMAND
?DIST V=AA CASES=130-185 PRØB=.5


 DISTRIBUTIØNAL ANALYSIS  CASES=CASE#:130-185


 CUMULATIVE SAMPLE DISTRIBUTIØN ØF 1.AA  N= 56 ØUT ØF 56
 1.00000   +                                                    *
                                                          * *
                                                        3
  .90000   +                                          3
```

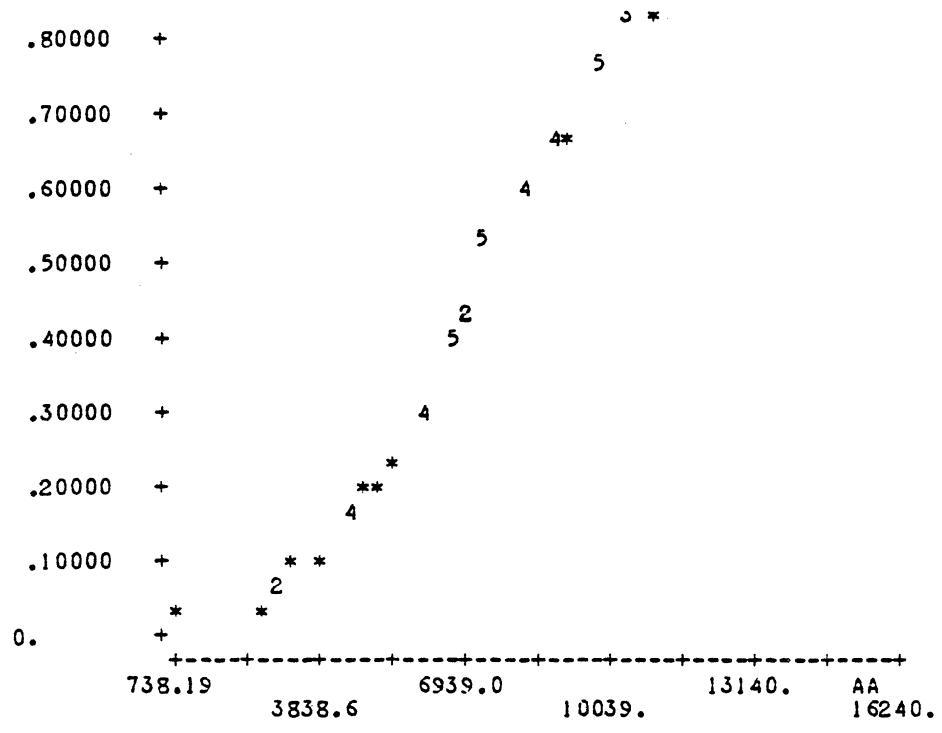

PRØB	QUANTILE
.5000	7381.9

```
 CØMMAND
?REGRESS V=AA;Q CASES=130-185

 LEAST SQUARES REGRESSIØN  CASES=CASE#:130-185

 ANALYSIS ØF VARIANCE ØF 1.AA  N= 56 ØUT ØF 56

      SØURCE              DF  SUM SQRS    MEAN SQR    F-STAT    SIGNIF

      REGRESSIØN           1  .12325 +9  .12325 +9  15.185     .0003
      ERRØR               54  .43828 +9  .81163 +7
      TØTAL               55  .56153 +9

      MULT R= .46849  R-SQR= .21949 SE= 2848.9

      VARIABLE     PARTIAL     CØEFF     STD ERRØR    T-STAT    SIGNIF

      CØNSTANT                9991.2      663.89     15.050     .0000
    4.Q            -.46849   -104.57      26.835    -3.8968     .0003

 CØMMAND
?
```

```
HIST V=AA CASES=186-246 I←ØP=HIST%
INTERV@L EXPRESSIØN -- #INT:(MIN,MAX)  (MIN,MAX)/WIDTH  #PER/(MIN,MAX)
=


HISTØGRAM  CASES=CASE#:186-246

MIDPØINT   HIST%  CØUNT FØR 1.AA  (EACH X= 1)

 2214.6      1.6     1 +X
 4640.0     26.2    16 +XXXXXXXXXXXXXXXX
 7065.5     31.1    19 +XXXXXXXXXXXXXXXXXXX
 9491.0     13.1     8 +XXXXXXXX
 11916.     14.8     9 +XXXXXXXXX
 14342.      8.2     5 +XXXXX
 16767.      3.3     2 +XX
 19193.      1.6     1 +X

 TØTAL              61  (INTERVAL WIDTH= 2425.5)


 CØMMAND
?DESCRIBE V=186-246#
?DESCRIBE V=AAB← CASES=186-246


 DESCRIPTIVE MEASURES  CASES=CASE#:186-246

     VARIABLE         N  MINIMUM     MAXIMUM       MEAN      STD DEV

   1.AA               61  2214.6      19193.      8525.5      3661.7


 CØMMAND
?DIST V=AA CASES=186-246 PRØB=.5


 DISTRIBUTIØNAL ANALYSIS  CASES=CASE#:186-246


 CUMULATIVE SAMPLE DISTRIBUTIØN ØF 1.AA  N= 61  ØUT ØF 61
1.00000   +                                                2       *
                                                        *
                                                  3 *
 .90000   +
                                              4 *
 .80000   +                             4
                                      *
 .70000   +                        2
                                5
```

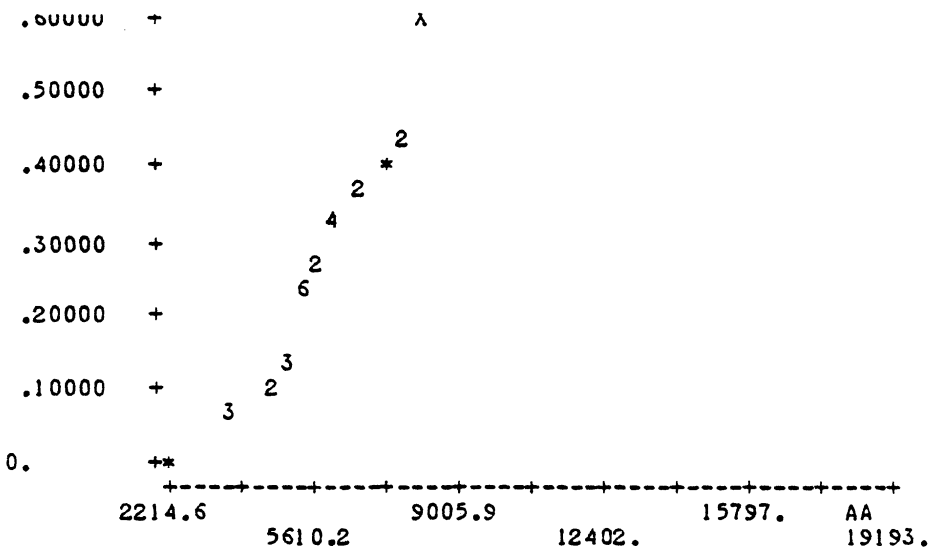

PRØB QUANTILE

.5000 8120.1

```
 CØMMAND
?REGRESS V=AA;Q CASES=186-246

 LEAST SQUARES REGRESSIØN  CASES=CASE#:186-246

 ANALYSIS ØF VARIANCE ØF 1.AA  N= 61 ØUT ØF 61

      SØURCE              DF  SUM SQRS    MEAN SQR    F-STAT    SIGNIF

      REGRESSIØN           1  .26170 +9  .26170 +9  28.446     .0000
      ERRØR               59  .54280 +9  .92000 +7
      TØTAL               60  .80450 +9

      MULT R= .57035  R-SQR= .32530 SE= 3033.1

      VARIABLE     PARTIAL    CØEFF     STD ERRØR   T-STAT    SIGNIF

      CØNSTANT                13526.     1014.8     13.328     .0000
    4.Q             -.57035  -265.25     49.733    -5.3335     .0000

 CØMMAND
?
```

```
 HIST#
?HIST V=AA CASES=247-327 ØP=HISTZ
 INTERVAL EXPRESSIØN -- #INT:(MIN,MAX)  (MIN,MAX)/WIDTH  #PER/(MIN,MAX)
=

 HISTØGRAM  CASES=CASE#:247-327

 MIDPØINT   HISTZ  CØUNT FØR 1.AA  (EACH X= 1)

  2952.8     1.2     1 +X
  5085.3    12.3    10 +XXXXXXXXXX
  7217.8    22.2    18 +XXXXXXXXXXXXXXXXXX
  9350.4    25.9    21 +XXXXXXXXXXXXXXXXXXXXX
 11483.     19.8    16 +XXXXXXXXXXXXXXXX
 13615.      2.5     2 +XX
 15748.      9.9     8 +XXXXXXXX
 17881.      3.7     3 +XXX
 20013.      1.2     1 +X
 22146.      1.2     1 +X

  TØTAL             81  (INTERVAL WIDTH= 2132.5)

 CØMMAND
?DESCRIBE V=AA CASES=247-327

 DESCRIPTIVE MEASURES  CASES=CASE#:247-327

     VARIABLE        N  MINIMUM     MAXIMUM      MEAN      STD DEV

   1.AA              81  2952.8      22146.     10201.      3819.4
```

```
 CØMMAND
?REGRESS V=AA;Q CASES=247-2-327

 LEAST SQUARES REGRESSIØN  CASES=CASE#:247-327

 ANALYSIS ØF VARIANCE ØF 1.AA  N= 81 ØUT ØF 81

     SØURCE            DF  SUM SQRS    MEAN SQR   F-STAT    SIGNIF

     REGRESSIØN         1  .45454 +7  .45454 +7  .30890     .5799
     ERRØR             79  .11625+10  .14715 +8
     TØTAL             80  .11670+10

     MULT R= .06241  R-SQR= .00389 SE= 3836.0

     VARIABLE     PARTIAL    CØEFF     STD ERRØR   T-STAT    SIGNIF

     CØNSTANT              10512.      703.91     14.934     .0000
   4.Q            -.06241  -17.273     31.079    -.55579     .5799
```

```
 CØMMAND
?DIST V=AA CASES=247-327 PØ←RØB=.5

 DISTRIBUTIØNAL ANALYSIS  CASES=CASE#:247-327

 CUMULATIVE SAMPLE DISTRIBUTIØN ØF 1.AA  N= 81 ØUT ØF 81
1.00000   +                                                *       *
                                                        3
                                                     5
 .90000   +
                                                  3
                                              * *
 .80000   +                                5
                                        4
 .70000   +                         6
                                  9*
 .60000   +
 .50000   +                    5
                            52
 .40000   +
                         7
 .30000   +
                        6
 .20000   +            3*
                    2*
 .10000   +       3*
                *
                3
0.          +*
           +----+----+----+----+----+----+----+----+----+----+
         2952.8              6791.3              10630.              14469.              18307.     AA
                                                                                                    22146.

  PRØB  QUANTILE
 .5000  9596.5

 COMMAND
?
```

```
 REGRESS V=AA;Q
 CASES TØ SELECT
=ALL

 LEAST SQUARES REGRESSIØN

 ANALYSIS ØF VARIANCE ØF 1.AA  N= 327 ØUT ØF 327

      SØURCE              DF  SUM SQRS    MEAN SQR    F-STAT    SIGNIF

      REGRESSIØN           1  .71320 +8  .71320 +8  3.3347      .0688
      ERRØR              325  .69509+10  .21387 +8
      TØTAL              326  .70222+10

      MULT R= .10078  R-SQR= .01016 SE= 4624.6

      VARIABLE     PARTIAL    CØEFF     STD ERRØR   T-STAT    SIGNIF

      CØNSTANT                6998.8     450.21     15.546     .0000
    4.Q             -.10078  -37.216     20.380    -1.8261     .0688

 CØMMAND
?TRANS
 TRANSFØRMATIØN EXPRESSIØN  (E.G., V9=V2+V5  ØR  V10=SQRT(V8)  )
=V10=LØG10(AA)  L=LA

 ERRØR -- SYNTAX:  "V10=LØG10(AA)  L=LA"
 ENTER NEW VALUE FØR TRANSFØRMATIØN EXPRESSIØN  (E.G., V9=V2+V5  ØR
 V10=SQRT(V8)  )
=

 ERRØR -- ILLEGAL VALUE

 THE EXPRESSIØN STARTS WITH "VK=", WHERE 0 < K < 10000; THE RIGHT-SIDE
MAY BE:  "A", "A ØP B", "FCN", "FCN(A)", "FCN(A,B)", WHERE A AND B ARE
 VARIABLES AND/ØR CØNSTANTS WITH DECIMAL PØINTS, FCN IS FUNCTIØN NAME.

 ENTER NEW VALUE FØR TRANSFØRMATIØN EXPRESSIØN  (E.G., V9=V2+V5  ØR
 V10=SQRT(V8)  )
=V20=LØG10(AA)
 LABEL FØR THE RESULT VARIABLE(S)
=LAA

 LØG10 TRANSFØRMATIØN

      VARIABLE  TØTAL  VALID   MISS

   20.LAA         327    323       4

 CØMMAND
?REGRESS V=LAA;Q CASESE←=ALL
```

```
LEAST SQUARES REGRESSIØN

ANALYSIS ØF VARIANCE ØF 20.LAA  N= 323 ØUT ØF 327

     SØURCE              DF  SUM SQRS    MEAN SQR    F-STAT    SIGNIF

     REGRESSIØN           1  .39460      .39460      1.9284     .1659
     ERRØR              321  65.685      .20463
     TØTAL              322  66.080

     MULT R= .07728  R-SQR= .00597 SE= .45236

     VARIABLE      PARTIAL    CØEFF     STD ERRØR    T-STAT    SIGNIF

     CØNSTANT                3.6946      .44400 -1  83.211    0.
   4.Q             -.07728  -.27783 -2  .20007 -2 -1.3887     .1659

 CØMMAND
?DIST V=LAA CASES=ALL ØP=←HIST%

 ERRØR -- INVALID KEYWØRD:  "ØP=HIST%"

 DISTRIBUTIØNAL ANALYSIS

 CUMULATIVE SAMPLE DISTRIBUTIØN ØF 20.LAA  N= 323 ØUT ØF 327
 1.00000   +                                                    52*
                                                               X
                                                             9
  .90!
 $.07 USED.  CØNTINUE(YES/NØ)%0200 DATA CHECK.
?%0200 DATA CHECK.
??#
#
RES
  "Y" ØR "N"?N

 CØMMAND
?HIST=V#
?HIST V=LAA CASES=ALL ØP=HIST%
 INTERVAL EXPRESSIØN -- #INT:(MIN,MAX)  (MIN,MAX)/WIDTH  #PER/(MIN,MAX)
=

 HISTØGRAM

 MIDPØINT   HIST%  CØUNT FØR 20.LAA  (EACH X= 2)

  1.8682      .6     2 +X
  2.0139     0.      0 +
  2.1596     0.      0 +
  2.3053      .6     2 +X
  2.4510     1.2     4 +XX
  2.5967     1.9     6 +XXX
  2.7424     3.1    10 +XXXXX
  2.8882     1.5     5 +XXX
  3.0339     2.5     8 +XXXX
  3.1796     6.8    22 +XXXXXXXXXXX
  3.3253     7.7    25 +XXXXXXXXXXXXX
  3.4710     7.7    25 +XXXXXXXXXXXXX
```

```
 3.6167      9.6     31 +XXXXXXXXXXXXXXXXX
 3.7624     13.0     42 +XXXXXXXXXXXXXXXXXXXX
 3.9081     17.6     57 +XXXXXXXXXXXXXXXXXXXXXXXXXXX
 4.0539     19.2     62 +XXXXXXXXXXXXXXXXXXXXXXXXXXXXX
 4.1996      5.9     19 +XXXXXXXXX
 4.3453       .9      3 +XX

 MISSING              4
 TØTAL              327  (INTERVAL WIDTH= .14571)


 CØMMAND
?READ

 NØTE.  THIS DATASET CURRENTLY HAS 5 VARIABLES AND 327 CASES
 FILE CØNTAINING DATA ØR  *  TØ ENTER DATA HERE
=WGABAR
 FØRMAT SPECIFICATIØN ØR  *  TØ ENTER DATA SEPARATED BY CØMMAS
=:←*
 VARIABLES TØ READ (E.G., 1-10)
=1-4
 LABELS CØRRESPØNDING TØ THESE VARIABLES ØR  *  FØR STANDARD LABELS
=AAC,RC,U,Q
 CASES TØ ASSIGN TØ THE DATA BEING READ (E.G., 1-98)
=1-327


 READ ØBSERVATIØNS 1-327
 VARIABLES BY CASE

 327 CASES READ FØR 4 VARIABLES

 CASES CHANGED FØR 4 EXISTING VARIABLES


 CØMMAND
?REGRESS V=AAC;Q CASES=ALL


 LEAST SQUARES REGRESSIØN


 ANALYSIS ØF VARIANCE ØF 1.AAC  N= 327 ØUT ØF 327

      SØURCE              DF  SUM SQRS    MEAN SQR    F-STAT     SIGNIF

      REGRESSIØN           1  .66258+11  .66258+11  3.3347       .0688
      ERRØR              325  .64576+13  .19869+11
      TØTAL              326  .65238+13

      MULT R= .10078  R-SQR= .01016 SE= .14096 +6


      VARIABLE      PARTIAL    CØEFF     STD ERRØR    T-STAT     SIGNIF

      CØNSTANT                .21332 +6  13722.      15.546       .0000
    4.Q             -.10078  -1134.4      621.19    -1.8261      .0688


 CØMMAND
?TRANS
 TRANSFØRMATIØN EXPRESSIØN  (E.G., V9=V2+V5  ØR  V10=SQRT(V8)  )
=V30=LØG10(AAC)
 LABEL FØR THE RESULT VARIABLE(S)
=LAAC
```

```
LØG10 TRANSFØRMATIØN

     VARIABLE  TØTAL  VALID   MISS

  30.LAAC        327    323      4


 CØMMAND
?REGRESS V=LAAC;Q CASES=ALL


 LEAST SQUARES REGRESSIØN


 ANALYSIS ØF VARIANCE ØF 30.LAAC  N= 323 ØUT ØF 327

      SØURCE              DF  SUM SQRS    MEAN SQR    F-STAT    SIGNIF

      REGRESSIØN           1  .39460      .39460      1.9284     .1659
      ERRØR              321  65.685      .20463
      TØTAL              322  66.080

      MULT R= .07728  R-SQR= .00597 SE= .45236


      VARIABLE     PARTIAL    CØEFF     STD ERRØR    T-STAT    SIGNIF

      CØNSTANT                5.1786     .44400 -1  116.64    0.
    4.Q            -.07728  -.27783 -2  .20007 -2 -1.3887     .1659


 CØMMAND
?SIGNØFF

 ERRØR -- INVALID CØMMAND:  "SIGNØFF"
 CØMMAND CANCELLED


 CØMMAND
?STØP
 USE $RES TØ RE-ENTER MIDAS
#SIGNØFF
#ØDLU 15:39:40-17:22:21 FRI MAR 31/78
#TERM,NØRMAL,UNIV
#ELAPSED TIME      102.685 MIN.          $2.40
#CPU TIME USED       3.021 SEC.           $.49
#CPU STØR VMI        4.116 PAGE-MIN.      $.24
#WAIT STØR VMI     141.476 PAGE-HR.
#DRUM READS        5806
#APPRØX. CØST ØF THIS RUN IS     $3.23
#DISK STØRAGE      128      PAGE-HR.       $.01
#APPRØX. REMAINING BALANCE.     $73.29
(@
```

REGRESSION OF $\sqrt{EA}$ ON Us AT CONST @

VARIABLE LABELS

DATA FILE: QACCEL

V1.AA - A AVG ACCEL. Ft/sec^2

V2.R - ACCEL RATIO

V3.U - STEAM VELOCITY, Ft/sec

V4.Q - LIQUID FLOW RATE, cm^3/min

V20.SRAA - SQUARE ROOT AVG. ACCEL, $\sqrt{Ft/sec^2}$

```
 SIGNON ODLU
#ENTER USER PASSWORD.
?STEAM
#TERM,NORMAL,UNIV
#**LAST SIGNON WAS: 00:19:25   TUE APR 04/78
# USER "ODLU" SIGNED ON AT  17:27:51 ON WED APR 05/78
#F
 AVGACCEL  CUMACCEL  LF        LINEFIT   MDPRDATA  PFILE     PLOTI
 PLOT2     QACCEL    TDATA     TEMP      WATERDROP WD        WDATA
 WDGRAF    WG        WGABAR    WGAVG
#LIST QACCEL
>     1          19192.91406          0.75839       1100.00000          0.0
>     2          15501.96875          0.61254       1100.00000          0.0
 >     3           7381.89063          0.29169        1100.00000          0.0
 >     4           2030.01978          2.24796         305.00000          5.0
 >     5           1328.74023          1.10043         305.00000          5.0
 >     6           1722.44116          1.42648         305.00000          5.0
 >    !
>ATTN!
*RUN STAT:_:MIDAS
 EXECUTION BEGINS


 M I D A S
 STATISTICAL RESEARCH LABORATORY
 UNIVERSITY OF MICHIGAN
 17:30:46
 APR  5, 1978


 COMMAND
?READ
 FILE CONTAINING DATA OR  *  TO ENTER DATA HERE
=*_QACCEL
 FORMAT SPECIFICATION OR  *  TO ENTER DATA SEPARATED BY COMMAS
=4(F15.5,1X)
 VARIABLES TO READ (E.G., 1-10)
=1-4
 LABELS CORRESPONDING TO THESE VARIABLES OR  *  FOR STANDARD LABELS
=AA,R,U,Q
 CASES TO ASSIGN TO THE DATA BEING READ (E.G., 1-98)
=1-327


 READ OBSERVATIONS 1-327
 VARIABLES BY CASE

 327 CASES READ FOR 4 VARIABLES


 COMMAND
?WRITE V=ALL CASES=1-6
```

```
 FILE TO RECEIVE DATA OR  *  TO WRITE DATA HERE
=*
 FORMAT SPECIFICATION OR  *  TO LIST DATA WITH HEADINGS
=*

 WRITE OBSERVATIONS  CASES=CASE#:1-6
 VARIABLES BY CASE

 1.          2.          3.          4.
 AA          R           U           Q

  19193.      .75839      1100.0      0.

  15502.      .61254      1100.0      0.

  7381.9      .29169      1100.0      0.

  2030.0      2.2480      305.00      5.0000

  1328.7      1.1004      305.00      5.0000

  1722.4      1.4265      305.00      5.0000

 6 CASES WRITTEN FOR 4 VARIABLES

 COMMAND
?DESCRIBE V=AA CASES=ALL

 DESCRIPTIVE MEASURES

      VARIABLE          N  MINIMUM     MAXIMUM       MEAN      STD DEV

    1.AA              327 -7381.8      22146.      6322.2      4641.2

 COMMAND
?DIST V=AA CASES=ALL PROB=NOGRAPH:.25,.5,.75

 DISTRIBUTIONAL ANALYSIS

 CUMULATIVE DISTRIBUTION OF 1.AA  N= 327 OUT OF 327

   PROB   QUANTILE

  .2500   2399.1

  .5000   5659.4

  .7500   9596.5

 COMMAND
```

```
HIST V=AA CASES=ALL OP=HISTZ
INTERVAL EXPRESSION -- #INT:(MIN,MAX)  (MIN,MAX)/WIDTH  #PER/(MIN,MAX)
=


HISTOGRAM

MIDPOINT   HISTZ  COUNT FOR 1.AA  (EACH X= 2)

-7381.8       .3      1 +X
-5741.4       0.      0 +
-4101.0       0.      0 +
-2460.6       .3      1 +X
-820.14       .6      2 +X
 820.28     15.9     52 +XXXXXXXXXXXXXXXXXXXXXXXXX
 2460.7     16.2     53 +XXXXXXXXXXXXXXXXXXXXXXXXXX
 4101.1     10.7     35 +XXXXXXXXXXXXXXXXX
 5741.5      9.5     31 +XXXXXXXXXXXXXXXX
 7381.9     15.0     49 +XXXXXXXXXXXXXXXXXXXXXXXX
 9022.4      9.5     31 +XXXXXXXXXXXXXXXX
 10663.      7.6     25 +XXXXXXXXXXXXX
 12303.      6.1     20 +XXXXXXXXXX
 13944.      2.8      9 +XXXXX
 15584.      3.1     10 +XXXXX
 17224.      1.5      5 +XXX
 18865.       .6      2 +X
 20505.      0.       0 +
 22146.       .3      1 +X

 TOTAL              327  (INTERVAL WIDTH= 1640.4)


 COMMAND
?REGRESS V=AA;U CASES=ALL OPTION=MEANZERO


 LEAST SQUARES REGRESSION


 ANALYSIS OF VARIANCE OF 1.AA  N= 327 OUT OF 327

      SOURCE              DF  SUM SQRS    MEAN SQR    F-STAT     SIGNIF

      REGRESSION           1  .16705+11  .16705+11   1607.8     0.
      ERROR              326  .33871+10  .10390 +8
      TOTAL              327  .20092+11

      OPT:  MEANZERO  R-SQR= .57491 SE= 3223.4

      VARIABLE      PARTIAL     COEFF     STD ERROR   T-STAT     SIGNIF

    3.U              .91182    8.6755      .21636     40.098     0.

 COMMAND
```

```
REGRESS V=AA;U CASES=ALL

LEAST SQUARES REGRESSION

ANALYSIS OF VARIANCE OF 1.AA  N= 327 OUT OF 327

     SOURCE              DF  SUM SQRS    MEAN SQR    F-STAT     SIGNIF

     REGRESSION           1  .40371+10  .40371+10   439.55      .0000
     ERROR              325  .29851+10  .91848 +7
     TOTAL              326  .70222+10

     MULT R= .75823  R-SQR= .57491 SE= 3030.6

     VARIABLE      PARTIAL     COEFF     STD ERROR   T-STAT     SIGNIF

     CONSTANT                -3204.5     484.32    -6.6164      .0000
   3.U              .75823    12.325      .58787     20.965      .0000

 COMMAND
?
```

```
?SCATTER V=AA;U CASES=ALL

 SCATTER PLOT
           N= 327 OUT OF 327  1.AA VS. 3.U
AA
 22146.    +                                                       *

           +                                                       2

                                                         2         3
 16240.    +                                           *           5
                                                       *           3
                                                     2 *           *
           +                                         * 3           *
                                                     3 *           5
                                                     4 *           X
 10335.    +                                         2 2           X
                                                     6 2           7
                                 2                   * X           X
           +                                         7 3           7
                                 *                   5 2           4
                                 6                   6 X           6
 4429.2    +*                    5                   5 5           4
                                 X                   2 3
            2                    X                   3 *           *
           +X                    X
            X                    *                   *
            *                    *
-1476.3    +
                                  .
                                  *
           +

-7381.8    +                     *
           +----+----+----+----+----+----+----+----+----+----+
         305.00                623.00               941.00     U
                  464.00                782.00               1100.0

 COMMAND
?
```

```
 TRANS
 TRANSFORMATION EXPRESSION  (E.G., V9=V2+V5  OR  V10=SQRT(V8)  )
=V20=SQRT(AA) LABELS=SRAA

 ERROR -- SYNTAX:  "V20=SQRT(AA) LABELS=SRAA"
 ENTER NEW VALUE FOR TRANSFORMATION EXPRESSION  (E.G., V9=V2+V5  OR
 V10=SQRT(V8)  )
=V20=SQRT(AA)
 LABEL FOR THE RESULT VARIABLE(S)
=SRAA


 SQRT TRANSFORMATION

      VARIABLE  TOTAL  VALID   MISS

   20.SRAA        327    324      3


 COMMAND
?WRITE V=S_ALL CASES=1-6
 FILE TO RECEIVE DATA OR  *  TO WRITE DATA HERE
=*
 FORMAT SPECIFICATION OR  *  TO LIST DATA WITH HEADINGS
=*


 WRITE OBSERVATIONS  CASES=CASE#:1-6
 VARIABLES BY CASE

 1.          2.          3.          4.          20.
 AA          R           U           Q           SRAA

  19193.      .75839      1100.0      0.          138.54

  15502.      .61254      1100.0      0.          124.51

  7381.9      .29169      1100.0      0.          85.919

  2030.0      2.2480      305.00      5.0000      45.056

  1328.7      1.1004      305.00      5.0000      36.452

  1722.4      1.4265      305.00      5.0000      41.502

 6 CASES WRITTEN FOR 5 VARIABLES


 COMMAND
?DESCRIBE V=SRAA CASES=ALL


 DESCRIPTIVE MEASURES

      VARIABLE         N  MINIMUM     MAXIMUM       MEAN      STD DEV

   20.SRAA           324  0.          148.81       73.991      30.692


 COMMAND
?
```

```
HIST V=SRAA CASES=ALL OP=HIST%
INTERVAL EXPRESSION -- #INT:(MIN,MAX)  (MIN,MAX)/WIDTH  #PER/(MIN,MAX)
=


HISTOGRAM

MIDPOINT   HIST%  COUNT FOR 20.SRAA  (EACH X= 1)

 0.          .3     1 +X
 8.2675      .6     2 +XX
 16.535     3.4    11 +XXXXXXXXXXX
 24.802     4.9    16 +XXXXXXXXXXXXXXXX
 33.070     3.4    11 +XXXXXXXXXXX
 41.337     7.7    25 +XXXXXXXXXXXXXXXXXXXXXXXX
 49.605     9.0    29 +XXXXXXXXXXXXXXXXXXXXXXXXXXXX
 57.872     7.7    25 +XXXXXXXXXXXXXXXXXXXXXXXX
 66.140     6.5    21 +XXXXXXXXXXXXXXXXXXX
 74.407     9.3    30 +XXXXXXXXXXXXXXXXXXXXXXXXXXXX
 82.675     8.3    27 +XXXXXXXXXXXXXXXXXXXXXXXXX
 90.942    12.0    39 +XXXXXXXXXXXXXXXXXXXXXXXXXXXXXXXXXXXX
 99.209     8.6    28 +XXXXXXXXXXXXXXXXXXXXXXXXXX
 107.48     7.1    23 +XXXXXXXXXXXXXXXXXXXXX
 115.74     5.2    17 +XXXXXXXXXXXXXXXXX
 124.01     3.4    11 +XXXXXXXXXXX
 132.28     1.5     5 +XXXXX
 140.55      .6     2 +XX
 148.81      .3     1 +X

 MISSING             3
 TOTAL             327  (INTERVAL WIDTH= 8.2675)


 COMMAND
?DIST V=R_SRAA CASES=ALL PROB=NOGRAPH:.25,.5,.75


 DISTRIBUTIONAL ANALYSIS


 CUMULATIVE DISTRIBUTION OF 20.SRAA  N= 324 OUT OF 327

   PROB  QUANTILE

  .2500  49.605

  .5000  76.847

  .7500  97.962


 COMMAND
?
```

```
?REGRESS V=SRAA;U CASES=ALL OP=MEANZERO

 LEAST SQUARES REGRESSION

 ANALYSIS OF VARIANCE OF 20.SRAA  N= 324 OUT OF 327

      SOURCE              DF  SUM SQRS    MEAN SQR    F-STAT    SIGNIF

      REGRESSION           1  .19801 +7  .19801 +7  6527.6     0.
      ERROR              323  97979.      303.34
      TOTAL              324  .20781 +7

      OPT:  MEANZERO  R-SQR= .68150 SE= 17.417

      VARIABLE     PARTIAL     COEFF     STD ERROR   T-STAT    SIGNIF

    3.U             .97614   .94625 -1  .11712 -2  80.794     0.

 COMMAND
?
```

```
?SCATTER V=SRAA;U

 SCATTER PLOT
            N= 324 OUT OF 327  20.SRAA VS. 3.U
?RAA
 148.81   +                                                          *
                                                                     ?
          +
                                                  *          2       R
                                                             *       3
 119.05   +                                       2          *       *
                                                  4          4       6
                                                  3          4       4
          +                                       *          4       7
                                                  7          4       X
                          2                       5          5       7
 89.289   +                                       4          X       7
                                                  7          *       7
                          *                       5          2       4
          +               2                       5          6       3
                          5                       2          9       4
           *              5                       4          2       3
 59.526   +              9                       2          3
                         X                       2                  *
                         X                       *
          +3             X                                  *
           4             X
           7             2
 29.763   +*             *
           X                                      *
           9
          +6
           2

 0.       +*
          +----+----+----+----+----+----+----+----+----+----+
         305.00          464.00          623.00          782.00          941.00          U
                                                                                        1100.0

 COMMAND
?
```

```
HIST V=R_SRAA CASES=1-3 I=*

HISTOGRAM  CASES=CASE#:1-3

MIDPOINT    COUNT FOR 20.SRAA  (EACH X= 1)

 85.918         1 +X
 138.54         2 +XX

 TOTAL          3  (INTERVAL WIDTH= 52.621)

 COMMAND
?DIST V=SRAA CASES=1-3 PROB=NOGRAPH;.25,.5,.75

 DISTRIBUTIONAL ANALYSIS  CASES=CASE#:1-3

 CUMULATIVE DISTRIBUTION OF 20.SRAA  N= 3 OUT OF 3

   PROB  QUANTILE

  .2500  85.918

  .5000  124.51

  .7500  138.54

 COMMAND
?DESCRIBE V=SRAA CASES=1-3

 DESCRIPTIVE MEASURES  CASES=CASE#:1-3

      VARIABLE         N  MINIMUM     MAXIMUM       MEAN      STD DEV

   20.SRAA             3  85.918      138.54       116.33      27.249

 COMMAND
?
```

```
REGRESS V=SRAA;U CASES=1-3 OP=MEANZERO

LEAST SQUARES REGRESSION  CASES=CASE#:1-3

ANALYSIS OF VARIANCE OF 20.SRAA  N= 3 OUT OF 3

     SOURCE              DF  SUM SQRS    MEAN SQR    F-STAT     SIGNIF

     REGRESSION           1  40592.      40592.      54.670      .0178
     ERROR                2  1485.0      742.49
     TOTAL                3  42077.

     OPT:  MEANZERO  R-SQR= .00000 SE= 27.249

     VARIABLE      PARTIAL     COEFF     STD ERROR   T-STAT     SIGNIF

   3.U              .98220    .10575      .14302 -1  7.3939      .0178
```

```
 COMMAND
?SCATTER V=SRAA;U CASES=1-3

 SCATTER PLOT  CASES=CASE#:1-3

 INVALID INTERVAL FOR 3.U:  1100.0, 1100.0

 N= 0 OUT OF 3  20.SRAA VS. 3.U

 COMMAND
?
```

```
SCATTER V=SRAA;U CASES=4-58

SCATTER PLOT  CASES=CASE#:4-58
          N= 54 OUT OF 55  20.SRAA VS. 3.U
SRAA
 130.30   +                                                        *
                                                                   *
                                                  *
          +                                                        *
                                                                   *

 104.24   +                                       *               *
                                                  *               2
                                                  2               2
          +                                       3               *
                                                  *               2
                                                                  *
 78.181   +
                          *                                       2

          +               2                                       *
                          3
                          *
 52.120   +               2
                          *
           2              *
          +*              *
           4
           *
 26.060   +4
           *
           2
          +*

 0.       +*
          +----+----+----+----+----+----+----+----+----+----+----+
         305.00          464.00          623.00          782.00          941.00          U
                                                                                        1100.0

 COMMAND
?
```

```
HIST V=SRAA CASES=4-58 OP=HISTZ I=*

HISTOGRAM  CASES=CASE#:4-58

MIDPOINT   HISTZ  COUNT FOR 20.SRAA  (EACH X= 1)

 0.          1.9      1 +X
 18.614     14.8      8 +XXXXXXXX
 37.229     18.5     10 +XXXXXXXXXX
 55.843     14.8      8 +XXXXXXXX
 74.458     11.1      6 +XXXXXX
 93.072     25.9     14 +XXXXXXXXXXXXXX
 111.69      7.4      4 +XXXX
 130.30      5.6      3 +XXX

 MISSING               1
 TOTAL                55  (INTERVAL WIDTH= 18.614)

 COMMAND
?DIST V=SRAA CASES=4-58 PROB=NOGRAPH;.25,.5,.75

 DISTRIBUTIONAL ANALYSIS  CASES=CASE#:4-58

 CUMULATIVE DISTRIBUTION OF 20.SRAA  N= 54 OUT OF 55

   PROB  QUANTILE

  .2500  36.452

  .5000  64.677

  .7500  94.118

 COMMAND
?
```

```
DESCRIBE V-SRAA_____=SRAAA_ CASES=4-58

DESCRIPTIVE MEASURES  CASES=CASE#:4-58

     VARIABLE          N  MINIMUM     MAXIMUM       MEAN      STD DEV

  20.SRAA              54  0.          130.30       65.850      33.073
```

```
 COMMAND
?REGRESS V=SRAA;U CASES=AL__4-58 OP=MEANZERO

LEAST SQUARES REGRESSION  CASES=CASE#:4-58

ANALYSIS OF VARIANCE OF 20.SRAA  N= 54 OUT OF 55

     SOURCE              DF  SUM SQRS    MEAN SQR    F-STAT     SIGNIF

     REGRESSION           1  .27783 +6  .27783 +6  1029.8       .0000
     ERROR               53  14299.     269.79
     TOTAL               54  .29213 +6

     OPT:  MEANZERO  R-SQR= .76080 SE= 16.425

     VARIABLE      PARTIAL    COEFF      STD ERROR    T-STAT    SIGNIF

   3.U              .97522   .95737 -1  .29834 -2   32.090      .0000
```

```
 COMMAND
?
```

```
SCATTER V=SRAA;U CASES=59-130

SCATTER PLOT  CASES=CASE#:59-130
          N= 72 OUT OF 72  20.SRAA VS. 3.U
SRAA
 124.51   +                                                  *
                                    *          3
          +                         2
                                    *          2          2
                                               2          4
 101.32   +                         *          2          3
                                    *          *
          +              *                     2
                                               3          3
                                    *                     2
                                    *
 78.141   +                         2          *          *
                   *
                   2
          +        *
            *
                   2
 54.958   +        3
                   5
            *      3
          +
                   2
            *
 31.775   +

          +3
            3
 8.5918   +*
          +----+----+----+----+----+----+----+----+----+----+
         305.00          623.00          941.00          U
                  464.00          782.00          1100.0

 COMMAND
?DESCRIBE V=SRAA CASES=59-130

 DESCRIPTIVE MEASURES  CASES=CASE#:59-130

      VARIABLE          N  MINIMUM     MAXIMUM       MEAN      STD DEV

   20.SRAA              72  8.5918      124.51       77.396      30.637

 COMMAND
?
```

```
HIST V=SRAA CASES=59-130 OP=HISTZ I=*

HISTOGRAM  CASES=CASE#:59-130

MIDPOINT   HISTZ  COUNT FOR 20.SRAA  (EACH X= 1)

 8.5918     2.8     2 +XX
 23.081     6.9     5 +XXXXX
 37.571     4.2     3 +XXX
 52.060    18.1    13 +XXXXXXXXXXXXX
 66.549     6.9     5 +XXXXX
 81.039    12.5     9 +XXXXXXXXX
 95.528    23.6    17 +XXXXXXXXXXXXXXXXX
 110.02    22.2    16 +XXXXXXXXXXXXXXXX
 124.51     2.8     2 +XX

 TOTAL             72  (INTERVAL WIDTH= 14.489)

 COMMAND
?DIST V=SRAA CASES=59-130 PROB=NOGRAPH;.25,.5,.75

 DISTRIBUTIONAL ANALYSIS  CASES=CASE#:59-130

 CUMULATIVE DISTRIBUTION OF 20.SRAA  N= 72 OUT OF 72

   PROB  QUANTILE

  .2500  52.026

  .5000  85.918

  .7500  101.66

 COMMAND
?
```

```
REGRESS V=SRAA;U CASES=59-130 OP=MEANZERO

LEAST SQUARES REGRESSION  CASES=CASE#:59-130

\NALYSIS OF VARIANCE OF 20.SRAA  N= 72 OUT OF 72

     SOURCE              DF  SUM SQRS    MEAN SQR    F-STAT     SIGNIF

     REGRESSION           1  .48093 +6  .48093 +6  2007.4      .0000
     ERROR               71  17010.     239.58
     TOTAL               72  .49794 +6

     OPT:  MEANZERO  R-SQR= .75104 SE= 15.478

     VARIABLE      PARTIAL    COEFF     STD ERROR   T-STAT     SIGNIF

   3.U              .98277   .10040     .2240R -2  44.804      .0000
```

```
 COMMAND
?
```

```
SCATTER V=SSR__S_RAA;U CASES=131-198

SCATTER PLOT  CASES=CASE#:131-198
          N= 66 OUT OF 68  20.SRAA VS. 3.U
SRAA
 138.54   +                                                        *
                                                      2
          +                           *                           *
                                                                  *

 118.19   +                                          *           *
                                      *
                                                     *           3
          +                           *              *           *
                                                     2           *
                                                                 2
 97.838   +                           *              *           3
           *                          2              *           *
                                                     *           *
          +
                                      3                          *
           *                          *
 77.488   +                                          *
                                      *
           2
          +*                          4              *           *
           *

 57.138   +*
           3
           2
          +*
           2
           2
 36.788   +4
          +----+----+----+----+----+----+----+----+----+----+
        520.00              752.00              984.00     U
                  636.00              868.00               1100.0

 COMMAND
?
?
?DESCRIBE V=SRAA CASES=131-198

 DESCRIPTIVE MEASURES  CASES=CASE#:131-198

      VARIABLE          N  MINIMUM     MAXIMUM       MEAN      STD DEV

   20.SRAA             66  36.788       138.54      84.547      27.825

 COMMAND
```

```
 RE#
?HIST V=SRAA CASES=131-198 OP=HIST% I=*

 HISTOGRAM  CASES=CASE#:131-198

 MIDPOINT   HIST%  COUNT FOR 20.SRAA  (EACH X= 1)

  36.788    10.6     7 +XXXXXXX
  49.507    10.6     7 +XXXXXXX
  62.226    13.6     9 +XXXXXXXXX
  74.944     6.1     4 +XXXX
  87.663    12.1     8 +XXXXXXXX
  100.38    22.7    15 +XXXXXXXXXXXXXXX
  113.10    15.2    10 +XXXXXXXXXX
  125.82     7.6     5 +XXXXX
  138.54     1.5     1 +X

  MISSING             2
  TOTAL              68  (INTERVAL WIDTH= 12.719)

 COMMAND
?DIST V=SRAA CASES=131-198 PROB=NOGRAPH;.25,.5,.75

 DISTRIBUTIONAL ANALYSIS  CASES=CASE#:131-198

 CUMULATIVE DISTRIBUTION OF 20.SRAA  N= 66 OUT OF 68

   PROB  QUANTILE

  .2500  66.552

  .5000  85.918

  .7500  105.23

 COMMAND
?REGRESS V=SRAA;U CASES=131-198 OP=MEANZERO
```

```
 LEAST SQUARES REGRESSION  CASES=CASE#:131-198

 ANALYSIS OF VARIANCE OF 20.SRAA  N= 66 OUT OF 68

      SOURCE              DF  SUM SQRS    MEAN SQR   F-STAT    SIGNIF

      REGRESSION           1  .50215 +6  .50215 +6  1635.1     .0000
      ERROR               65  19962.     307.10
      TOTAL               66  .52211 +6

      OPT:  MEANZERO  R-SQR= .60911 SE= 17.524

      VARIABLE      PARTIAL    COEFF     STD ERROR   T-STAT    SIGNIF

    3.U              .98070   .10115     .25016 -2  40.437     .0000
```

```
 COMMAND
```

```
?
?
?SCATTER V=SRAA CASES=199-250

 ERROR -- WRONG # OF VARS:  "SRAA"
 ENTER NEW VALUE FOR VARIABLES -- VERTICAL; HORIZONTAL
 SRAA;U


 SCATTER PLOT  CASES=CASE#:199-250
           N= 52 OUT OF 52  20.SRAA VS. 3.U
 SRAA
  130.30   +                                                    *
                                                               2
                                                    *
           +
                                                               *
  108.45   +                                  *        *
                                                               *
                                              *                *
           +                                  *                2
                                              *        2
                                                       3       *
  86.599   +
                                              *        *       *

           +                                  *        2
                                                       2
                                                       *
  64.748   +                                           *
                                                       2

           +              2
                          2
                          3                            *
  42.897   +              *
            *             *

           +2
            *
            4
  21.046   +2
           +----+----+----+----+----+----+----+----+----+----+
          305.00          623.00          941.00     U
                   464.00          782.00          1100.0


 COMMAND
?#
?#
?DESCRIBE V=SRAA CASES=199-250


 DESCRIPTIVE MEASURES  CASES=CASE#:199-250

      VARIABLE          N  MINIMUM     MAXIMUM       MEAN      STD DEV

   20.SRAA              52  21.046      130.30      71.219      31.705


 COMMAND
?
```

```
?#
?HIST V=SRAA CASES=199-250 OP=HIST% I=*

 HISTOGRAM  CASES=CASE#:199-250

 MIDPOINT   HIST%  COUNT FOR 20.SRAA  (EACH X= 1)

  21.046     13.5     7 +XXXXXXX
  36.653      9.6     5 +XXXXX
  52.261     15.4     8 +XXXXXXXX
  67.869     13.5     7 +XXXXXXX
  83.477     17.3     9 +XXXXXXXXX
  99.085     17.3     9 +XXXXXXXXX
  114.69      5.8     3 +XXX
  130.30      7.7     4 +XXXX

  TOTAL              52  (INTERVAL WIDTH= 15.608)

 COMMAND
?DIST V=SRAA CASES=199-250 PROB=NOGRAPH;.25,.5,.75

 DISTRIBUTIONAL ANALYSIS  CASES=CASE#:199-250

 CUMULATIVE DISTRIBUTION OF 20.SRAA  N= 52 OUT OF 52

   PROB  QUANTILE

  .2500  47.059

  .5000  71.884

  .7500  94.118

 COMMAND
?
```

```
?#
?#
?REGRESS V=SRAA;U CASES=199-250 OP=MEANZERO

 LEAST SQUARES REGRESSION  CASES=CASE#:199-250

 ANALYSIS OF VARIANCE OF 20.SRAA  N= 52 OUT OF 52

      SOURCE              DF  SUM SQRS    MEAN SQR    F-STAT     SIGNIF

      REGRESSION           1  .30189 +6  .30189 +6   1173.1      .0000
      ERROR               51  13124.     257.34
      TOTAL               52  .31502 +6

      OPT:  MEANZERO  R-SQR= .74400 SE= 16.042

      VARIABLE      PARTIAL    COEFF     STD ERROR   T-STAT     SIGNIF

    3.U              .97895   .91948 -1  .26845 -2  34.251      .0000

 COMMAND
?
```

```
#
?#
?SCATTER V=SRAA CAS____;U CASES=251-294

 SCATTER PLOT  CASES=CASE#:251-294
           N= 44 OUT OF 44  20.SRAA VS. 3.U
 SRAA
 127.44   +                                                  *
          +
          +                                    *
 107.38   +                                                  *
          +                                                  *
          +                                                  2
          +                                    *        3    *
 87.330   +                                                  3
          +                                    *
          +                                    *        *    *
          +                                    *        *
           *                                   *        6    2
 67.277   +                                    *
           *                                                *
          +*
           *                                                *
           2
 47.223   +
           *
          +2
           *
 27.170   +                                    *
          +----+----+----+----+----+----+----+----+----+----+
         520.00              752.00              984.00     U
                   636.00              868.00              1100.0

 COMMAND
?DESCRIBE V=SRAA CASES=251-294

 DESCRIPTIVE MEASURES  CASES=CASE#:251-294

      VARIABLE          N  MINIMUM     MAXIMUM       MEAN      STD DEV

   20.SRAA              44  27.170      127.44      73.952      21.166

 COMMAND
?
```

```
?
?
?HIST V=SRAA CASES=251-294 OP=HISTZ I=*

 HISTOGRAM  CASES=CASE#:251-294

 MIDPOINT   HISTZ  COUNT FOR 20.SRAA  (EACH X= 1)

  27.170      4.5     2 +XX
  43.881     11.4     5 +XXXXX
  60.592     13.6     6 +XXXXXX
  77.303     38.6    17 +XXXXXXXXXXXXXXXXX
  94.014     25.0    11 +XXXXXXXXXXX
  110.73      4.5     2 +XX
  127.44      2.3     1 +X

  TOTAL              44  (INTERVAL WIDTH= 16.711)

 COMMAND
?DIST V=SRAA CASES=* PROB=NOGRAPH;:_*

 ERROR -- INVALID CONSTANT:  "NOGRAPH;*"
 ENTER NEW VALUE FOR PROBABILITY POINTS
=NOGRAPH;.5,.25,.75

 DISTRIBUTIONAL ANALYSIS  CASES=CASE#:251-294

 CUMULATIVE DISTRIBUTION OF 20.SRAA  N= 44 OUT OF 44

    PROB  QUANTILE

   .5000  71.884

   .2500  60.753

   .7500  88.040

 COMMAND
?
```

```
?REGRESS V=SRAA;U CASES=251-294 OP=MEANZERO

LEAST SQUARES REGRESSION  CASES=CASE#:251-294

ANALYSIS OF VARIANCE OF 20.SRAA  N= 44 OUT OF 44

     SOURCE              DF  SUM SQRS    MEAN SQR    F-STAT     SIGNIF

     REGRESSION           1  .24816 +6  .24816 +6  909.49      .0000
     ERROR               43  11733.     272.86
     TOTAL               44  .25989 +6

     OPT:  MEANZERO  R-SQR= .42784 SE= 16.518

     VARIABLE      PARTIAL    COEFF     STD ERROR   T-STAT    SIGNIF

   3.U              .97717   .83657 -1  .27740 -2  30.158     .0000
```

```
 COMMAND
?
```

```
?#
?#
?SCATTER V=SRAA CASES=295-302

 ERROR -- WRONG # OF VARS:  "SRAA"
 ENTER NEW VALUE FOR VARIABLES -- VERTICAL; HORIZONTAL
 SRAA,_;U

 SCATTER PLOT  CASES=CASE#:295-302

 INVALID INTERVAL FOR 3.U:  305.00, 305.00

 N= 0 OUT OF 8  20.SRAA VS. 3.U

 COMMAND
?DESCRIBE V=SRAA CASES=*

 DESCRIPTIVE MEASURES  CASES=CASE#:295-302

      VARIABLE          N  MINIMUM     MAXIMUM       MEAN      STD DEV

   20.SRAA              8  9.0565      42.959      24.830      11.166

 COMMAND
?DIST V=SRAA CASES=* PROB=NOGRAPH;.25,.5,.75

 DISTRIBUTIONAL ANALYSIS  CASES=CASE#:295-302

 CUMULATIVE DISTRIBUTION OF 20.SRAA  N= 8 OUT OF 8

    PROB   QUANTILE

  .2500   16.384

  .5000   22.184

  .7500   25.616

 COMMAND
?
```

```
#
?#
?HIST V=SRAA CASES=* OP=* I=*

 HISTOGRAM  CASES=CASE#:295-302

 MIDPOINT    COUNT FOR 20.SRAA  (EACH X= 1)

  9.0565        2 +XX
 26.008         4 +XXXX
 42.959         2 +XX

  TOTAL         8  (INTERVAL WIDTH= 16.951)
```

```
 COMMAND
?REGRESS V=SRAA;U CASES=* OP=MEANZERO

 LEAST SQUARES REGRESSION  CASES=CASE#:295-302

 ANALYSIS OF VARIANCE OF 20.SRAA  N= 8 OUT OF 8

      SOURCE              DF  SUM SQRS    MEAN SQR    F-STAT     SIGNIF

      REGRESSION           1  4932.1      4932.1      39.557      .0004
      ERROR                7  872.77      124.68
      TOTAL                8  5804.8

      OPT:  MEANZERO  R-SQR= .00000 SE= 11.166

      VARIABLE     PARTIAL    COEFF     STD ERROR   T-STAT     SIGNIF

    3.U             .92176   .81409 -1  .12944 -1  6.2895      .0004
```

```
 COMMAND
?
```

```
SCATTER V=SRAA CASES=303-327

ERROR -- WRONG # OF VARS:  "SRAA"
ENTER NEW VALUE FOR VARIABLES -- VERTICAL; HORIZONTAL
SRAA;U


SCATTER PLOT  CASES=CASE#:303-327
          N= 25 OUT OF 25  20.SRAA VS. 3.U
SRAA
 148.81   +                                                    *
          +
          +                                                   *
 126.07   +
          +
 103.32   +                                                   *
                                    *
          +                                                  *
          +
                                    *                        *
 80.571   +                         *                        *
                                                             *
          +                                                  *
                                                             *
                                    *
 57.824   +*                        *
           2                        *
          +*
           2
           *
 35.076   +*
          +----+----+----+----+----+----+----+----+----+----+
        520.00              752.00              984.00     U
                636.00              868.00               1100.0


 COMMAND
?DESCRIBE V=SRAA CASES=*


 DESCRIPTIVE MEASURES  CASES=CASE#:303-327

      VARIABLE          N  MINIMUM     MAXIMUM       MEAN      STD DEV

   20.SRAA              25  35.076      148.81       70.386      28.315


 COMMAND
?
```

```
 DI__HIST V=SRAA CASES=* OP=HISTZ I=*___ I=*

 HISTOGRAM  CASES=CASE#:303-327

 MIDPOINT   HISTZ  COUNT FOR 20.SRAA  (EACH X= 1)

  35.076     16.0     4 +XXXX
  57.824     44.0    11 +XXXXXXXXXXX
  80.571     20.0     5 +XXXXX
  103.32     12.0     3 +XXX
  126.07      4.0     1 +X
  148.81      4.0     1 +X

  TOTAL              25  (INTERVAL WIDTH= 22.748)

 COMMAND
?DIST V=SRAA CASES=* PROB=NOGRAPH;.25,.5,.75

 DISTRIBUTIONAL ANALYSIS  CASES=CASE#:303-327

 CUMULATIVE DISTRIBUTION OF 20.SRAA  N= 25 OUT OF 25

   PROB  QUANTILE

  .2500  48.981

  .5000  60.753

  .7500  83.742

 COMMAND
?

#
```

```
?#
?#
?REGRESS V=SRAA;U CASES=* OP=MEANZERO

 LEAST SQUARES REGRESSION  CASES=CASE#:303-327

 ANALYSIS OF VARIANCE OF 20.SRAA  N= 25 OUT OF 25

      SOURCE              DF  SUM SQRS    MEAN SQR    F-STAT    SIGNIF

      REGRESSION           1  .13409 +6  .13409 +6   357.18     .0000
      ERROR               24  9009.8     375.41
      TOTAL               25  .14310 +6

      OPT:  MEANZERO  R-SQR= .53178 SE= 19.375

      VARIABLE     PARTIAL    COEFF     STD ERROR   T-STAT    SIGNIF

    3.U             .96801   .85139 -1  .45049 -2  18.899     .0000

 COMMAND
?
```

APPENDIX E

COMPARISON OF EXPERIMENTAL DROPLET ACCELERATIONS WITH THOSE USING SERAFINI, ABRAHAM AND CHURCHILL'S EMPIRICAL CORRELATIONS FOR THE DRAG COEFFICIENT, C_D

VARIABLE NAME	DESCRIPTION OF VARIABLE
AA(M)	Analytical acceleration as calculated by Abraham
AABAR	Average of all Abraham accelerations for a particular steam velocity and flow rate
AASM	Sum of all Abraham accelerations for a particular steam velocity and flow rate
ABAR(M)	Average of the measured accelerations for one droplet
AC(M)	Analytical acceleration as calculated by Churchill
ACBAR	Average of all Churchill accelerations for a particular steam velocity and flow rate
ACCSM	Sum of all the measured accelerations for a particular steam velocity and flow rate
ACEL(J)	Measured acceleration of one droplet for three successive film readings
ACSM	Sum of all the Churchill accelerations for a particular steam velocity and flow rate
AS(M)	Analytical acceleration as calculated by Serafini
ASBAR	Average of all measured accelerations for a particular steam velocity and flow rate
ASUM	Sum of all the measured accelerations for one droplet
CDA(M)	Abraham's expression for the drag coefficient
CDC(M)	Churchill's expression for the drag coefficient
CDS(M)	Serafini's expression for the drag coefficient
CON	Constant conversion factor, 30.48, the number of cm/sec in one ft/sec.

VARIABLE NAME	DESCRIPTION OF VARIABLE
CONFAC	Constant conversion factor, .45, the number of centimeters in one measured screen unit
DELV(J)	The difference between two consecutively measured velocities
DELX(J)	The difference between two consecutively measured distances
DIA(J)	The diameter of the water droplet for a particular observation
DPBAR	The average of all the diameters for a particular steam velocity and flow rate
DPSM	The sum of all the diameters for a particular steam velocity and flow rate
DPSUM	The sum of all the diameters observed for a particular droplet
DRPU(M)	The average of all diameters observed for a particular droplet
DTAVG	The average time between each successive observation
FILMV	The film speed at which the pictures were taken
FIVNIN	Constant, which equals 5/9.
FN(I)	Number of frames between each successive observation
IM2	The number of observations in a set minus two
M	A counter which checks how many different cases were observed for each steam velocity and flow rate
Q	Flow rate of water entering the test section
QCHECK	A control that is used to see if the flow rate has changed
RA(M)	The ratio of measured acceleration to Abraham acceleration, for a particular water droplet
RABAR	The average of all measured/Abraham acceleration ratios for a particular steam velocity and flow

VARIABLE NAME	DESCRIPTION OF VARIABLE
	rate
RASM	The sum of all measured/Abraham acceleration ratios for a particular steam velocity and flow rate
RBAR	The average of all measured/Serafini acceleration ratios for a particular water droplet
RC(M)	The ratio of measured acceleration to Churchill acceleration for a particular water droplet
RCBAR	The average of all measured/Churchill acceleration ratios for a particular steam velocity and flow rate
RCSM	The sum of all measured/Churchill acceleration ratios for a particular steam velocity and flow rate
RE(M)	Reynolds number for a particular water droplet
REBAR	The average of all Reynolds numbers for a particular steam velocity and flow rate
RESUM	The sum of all Reynolds numbers for a particular steam velocity and flow rate
RHOW	Density of water
RS(M)	The ratio of measured acceleration to Serafini acceleration for a particular water droplet
RSUM	The sum of all measured/Serafini acceleration ratios for a particular steam velocity and flow rate
SEBAR	Average of all Serafini accelerations for a particular steam velocity and flow rate
SVEL	Steam velocity in cm/sec.
T(I)	Thickness of the water droplet for a particular observation
TD(J)	Elapsed time between observations
TOTHRD	Constant, which equals 2/3
TTOL	Total time that observations on a particular

VARIABLE NAME	DESCRIPTION OF VARIABLE
	drop were made
V	Steam Velocity
VEECK	A control which checks if the steam velocity has changed
VEL(J)	Measured velocity of one droplet for two successive film readings
X(I)	Distance an individual particle was away from the edge of the blade

```
$SIG ODLU T=3 P=20
$R *FTN 5=WDATA
C     ******************** ACCELERATION RATIC PROGRAM ******************
C     THIS PROGRAM CALCULATES THE MEASURED ACCELERATION AND THREE
C     ANALYTIC ACCELERATIONS:SERAFINI, CHURCHILL, AND ABRAHAM.
C     IT ALSO FINDS THE ACCELERATION RATICS AND DETERMINES AVERAGE
C     VALUES FOR EACH STEAM VELOCITY AND FLOW RATE.
C     ***********************************************************************
      DIMENSION ACEL(20),FN(20),DIA(20),T(20),X(20),TD(20),DELX(20),
     1 VEL(20),DELV(20),ABAR(25),DRPU(25),RE(25),CDS(25),AS(25),RS(25),
     2 CDA(25),AA(25),RA(25),CDC(25),AC(25),RC(25)
      WRITE(6,199)
      TOTHRD=2./3.
      ANIN=9./5.
      FIVNIN=5./9.
      CON=30.48
      READ(5,101) FILMV,RHOW,CONPAC,VCHECK,QCHECK
      M=0.0
    1 ASUM=0.0
      TTOL=0.0
      DPSUM=0.0
C     ***** READ THE DATA FOR EACH OBSERVATION *****
      DO 110 I=1,20
      READ(5,101) FN(I),DIA(I),T(I),X(I)
      DPSUM=DPSUM+DIA(I)
      IF(T(I) .LT. 0.0) GO TO 120
      IF(X(I) .LT. 0.0) GO TO 130
  110 CONTINUE
  120 T(I)=ABS(T(I))
  130 X(I)=ABS(X(I))
      READ(5,101) V,Q
      IF(I .EQ. 2) GO TO 1
C     ***** CHECK TO SEE IF THERE ARE NEW CONDITIONS *****
      IF(V.NE.VCHECK .OR.Q.NE.QCHECK) GO TO 160
  100 M=M+1
      DRPU(M)=DPSUM/I*.45
C     ***** CALCULATE THE MEASURED ACCELERATION *****
      DO 150 J=2,I
      TD(J-1)=0.001
      TTOL=TTOL+TD(J-1)
      DELX(J-1)=(X(J)-X(J-1))*0.45
      VEL(J-1)=DELX(J-1)/TD(J-1)
      IF(J .EQ.2) GO TO 150
      DTAVG=(TD(J-1)+TD(J-2))/2.0
      DELV(J-2)=VEL(J-1)-VEL(J-2)
      ACEL(J-2)=DELV(J-2)/2./DTAVG
      ASUM=ACEL(J-2)+ASUM
  150 CONTINUE
      IM2=I-2
      ABAR(M)=ASUM/IM2
      SVEL=V*CON
C     ***** CALCULATE THE ANALYTIC ACCELERATIONS *****
      RE(M)=V*DRPU(M)*32.61
      CDS(M)=24./RE(M)*(1.+0.17*RE(M)**TOTHRD)
      AS(M)=(CDS(M)*0.75)*.0001135/DRPU(M)*SVEL**2
      RS(M)=ABAR(M)/AS(M)
      CDA(M)=.292*((1.+(9.06/(2*RE(M))**.5))**2)
      AA(M)=(CDA(M)*0.75)*.0001135/DRPU(M)*SVEL**2
      RA(M)=ABAR(M)/AA(M)
      CDC(M)=24./RE(M)*((1.+(RE(M)/60)**FIVNIN)**ANIN)
```

```
      AC(M)=(CDC(M)*.75)*.C001135/DBPU(M)*SVEL**2
      RC(M)=ABAR(M)/AC(M)
      WRITE(6,200) V,Q,DBPU(M),RE(M),ABAR(M),AS(M),BS(M),AA(M),BA(M),
     1 AC(M),RC(M)
      GO TO 1
C     ***** DETERMINE AVERAGES *****
  160 DPSM=0.0
      RESUM=0.0
      ACCSM=0.0
      SESUM=0.0
      RSUM=0.0
      AASM=0.0
      RASM=0.0
      ACSM=0.0
      RCSM=0.0
      DO 170 N=1,M
      DPSM=DPSM+DBPU(N)
      RESUM=RESUM+RE(N)
      ACCSM=ACCSM+ABAR(N)
      SESUM=SESUM+AS(N)
      RSUM=RSUM+BS(N)
      AASM=AASM+AA(N)
      RASM=RASM+BA(N)
      ACSM=ACSM+AC(N)
      RCSM=RCSM+RC(N)
  170 CONTINUE
      DPBAR=DPSM/M
      REBAR=RESUM/M
      ASBAR=ACCSM/M
      SEBAR=SESUM/M
      RBAR=RSUM/M
      AABAR=AASM/M
      RABAR=RASM/M
      ACBAR=ACSM/M
      RCBAR=RCSM/M
      WRITE (6,201) QCHECK,DPBAR,REBAR,ASBAR,SEBAR,RBAR,AABAR,
     1 RABAR,ACBAR,RCBAR
      M=0.0
      VCHECK=V
      QCHECK=Q
      IF(I.EQ.1) CALL EXIT
      GO TO 100
  101 FORMAT(6(F10.5))
  199 FORMAT ('1','STEAM',4X,'FLOW',3X,'DROP',4X,'REYNOLDS',3X,
     1 'MEASURED',5X,'SERAFINI   SERAFINI    ABRAHAM   ABRAHAM',3X,
     2 'CHURCHILL',2X,'CHURCHILL'/'VELOCITY',2X,'RATE DIAMETER',
     3 3X,'NUMBER',2X,'ACCELERATION ACCELERATICN',2X,'RATIO',3X,
     4 'ACCELERATION  RATIO  ACCELERATICN',3X,'RATIO'/'(FEET/S)',
     5 1X,'(CC/M)  (CM)',13X,'(CM/SEC**2)  (CM/SEC**2)',
     6 11X,'(CM/SEC**2)',11X,'(CM/SEC**2)')
  200 FORMAT ('0',1X,F6.1,3X,F4.1,2X,F6.4,3X,F8.3,1X,F11.3,3X,
     1 F10.3,3X,F6.3,3X,F10.3,3X,F6.3,2X,F10.2,4X,F6.3)
  201 FORMAT ('0','**AVG FOR Q=',F3.0,1X,F6.4,3X,F8.3,1X,F11.3,3X,
     1 F10.3,3X,F6.3,3X,F10.3,3X,F6.3,2X,F10.2,4X,F6.3)
      END
$ENDFILE
$R -LOAD 5=WDATA
$ENDFILE
$SIG
```

STEAM VELOCITY (FEET/S)	FLOW RATE (CC/M)	DROP DIAMETER (CM)	REYNOLDS NUMBER	MEASURED ACCELERATION (CM/SEC**2)	SERAFINI ACCELERATION (CM/SEC**2)	RATIO	ABRAHAM ACCELERATION (CM/SEC**2)	RATIO	CHURCHILL ACCELERATION (CM/SEC**2)	RATIO
305.0	5.0	0.0975	969.738	61874.953	32969.531	1.877	32030.258	1.932	42732.91	1.448
305.0	5.0	0.0900	895.143	40499.949	36796.660	1.101	35184.652	1.151	46961.88	0.862
305.0	5.0	0.0900	895.143	52499.957	36796.621	1.427	35184.633	1.492	46961.81	1.118
305.0	5.0	0.0900	895.143	30000.008	36796.660	0.815	35184.652	0.853	46961.88	0.639
305.0	5.0	0.0956	951.089	37499.977	33859.242	1.108	32767.145	1.144	43720.39	0.858
305.0	5.0	0.0956	951.089	37499.977	33859.242	1.108	32767.145	1.144	43720.39	0.858
305.0	5.0	0.1260	1253.199	22499.969	23213.598	0.969	23777.996	0.946	31691.73	0.710
305.0	5.0	0.1350	1342.713	11249.969	21127.598	0.532	21962.758	0.512	29267.38	0.384
305.0	5.0	0.1350	1342.713	14999.965	21127.598	0.710	21962.758	0.683	29267.38	0.513
305.0	5.0	0.0643	639.388	40500.012	58492.781	0.692	52493.148	0.772	70244.75	0.577
305.0	5.0	0.0450	447.572	22499.984	95965.688	0.234	81025.875	0.278	108885.81	0.207
305.0	5.0	0.1350	1342.713	6000.000	21127.617	0.284	21962.758	0.273	29267.40	0.205
305.0	5.0	0.0900	895.143	17999.973	36796.660	0.489	35184.652	0.512	46961.88	0.383
305.0	5.0	0.0900	895.143	44999.969	36796.660	1.223	35184.652	1.279	46961.88	0.958
305.0	5.0	0.0900	895.143	0.001	36796.660	0.000	35184.652	0.000	46961.88	0.000
305.0	5.0	0.0787	783.250	8035.691	44211.266	0.182	41196.277	0.195	55033.64	0.146
305.0	5.0	0.0900	895.143	19687.492	36796.660	0.535	35184.652	0.560	46961.88	0.419
**AVG FOR Q= 5.		0.0963	958.202	27549.848	37854.715	0.782	35778.723	0.807	47797.92	0.605
305.0	10.0	0.1237	1230.822	123750.063	23791.879	5.201	24277.504	5.097	32359.11	3.824
305.0	10.0	0.0900	895.143	67499.938	36796.621	1.834	35184.633	1.918	46961.81	1.437
305.0	10.0	0.0990	984.657	37500.082	32286.652	1.161	31463.141	1.192	41973.14	0.893
305.0	10.0	0.0900	895.143	11249.973	36796.660	0.306	35184.652	0.320	46961.88	0.240
305.0	10.0	0.0990	984.657	11249.977	32286.652	0.348	31463.164	0.358	41973.11	0.268
305.0	10.0	0.1087	1081.630	2249.981	28388.996	0.079	28198.461	0.080	37602.10	0.060
305.0	10.0	0.1215	1208.443	8437.492	24395.758	0.346	24797.535	0.340	33054.10	0.255
305.0	10.0	0.1150	1143.793	6428.551	26299.715	0.244	26426.887	0.243	35232.34	0.182
305.0	10.0	0.0844	839.197	11249.977	40208.293	0.280	37965.684	0.296	50693.89	0.222
305.0	10.0	0.1109	1101.713	8181.813	27683.238	0.296	27601.867	0.296	36803.90	0.222

**AVG FOR Q=10.		0.1042	1036.519	28779.754	30893.418	1.010	30256.324	1.014	40361.51	0.760
305.0	20.0	0.0900	895.143	17999.973	36796.660	0.489	35184.652	0.512	46961.88	0.383
305.0	20.0	0.1600	1591.365	19285.703	16761.746	1.151	18084.617	1.066	24093.04	0.800
305.0	20.0	0.1000	994.603	32142.848	31844.957	1.009	31095.617	1.034	41480.80	0.775
305.0	20.0	0.1125	1118.928	44999.969	27102.238	1.660	27109.320	1.660	36145.03	1.245
305.0	20.0	0.1200	1193.523	33750.000	24813.371	1.360	25156.207	1.342	33533.53	1.006
305.0	20.0	0.0450	447.572	19285.676	95965.563	0.201	81025.813	0.238	108885.88	0.177
305.0	20.0	0.1181	1174.876	22499.969	25353.141	0.887	25618.730	0.878	34151.73	0.659
305.0	20.0	0.0900	895.143	13499.973	36796.660	0.367	35184.652	0.384	46961.88	0.287
305.0	20.0	0.0950	944.873	16071.383	34165.176	0.470	33019.957	0.487	44059.30	0.365
305.0	20.0	0.0450	447.572	14999.965	95965.563	0.156	81025.813	0.185	108885.88	0.138
**AVG FOR Q=20.		0.0976	970.358	23453.523	42556.480	0.775	39250.523	0.779	52515.87	0.584
305.0	40.0	0.0900	895.143	56249.984	36796.660	1.529	35184.652	1.599	46961.88	1.198
305.0	40.0	0.0675	671.357	15000.008	54679.961	0.274	49507.641	0.303	66219.50	0.227
305.0	40.0	0.1309	1302.024	19999.969	22033.504	0.908	22753.770	0.879	30323.62	0.660
305.0	40.0	0.0975	969.738	45000.016	32969.531	1.365	32030.258	1.405	42732.91	1.053
305.0	40.0	0.1294	1286.767	18749.988	22390.852	0.837	23064.613	0.813	30738.83	0.610
305.0	40.0	0.0787	783.250	11250.000	44211.227	0.254	41196.258	0.273	55033.70	0.204
305.0	40.0	0.1800	1790.285	2500.012	14280.930	0.175	15821.797	0.158	21077.14	0.119
305.0	40.0	0.1558	1549.285	8181.813	17384.426	0.471	18645.242	0.439	24840.59	0.329
**AVG FOR Q=40.		0.1162	1155.981	22116.453	30593.352	0.727	29775.500	0.734	39741.00	0.550
520.0	5.0	0.0787	1335.378	135000.063	105488.875	1.280	109529.500	1.233	145959.94	0.925
520.0	5.0	0.0630	1068.302	52499.977	143097.000	0.367	141775.375	0.370	189064.31	0.278
520.0	5.0	0.0900	1526.145	-224997.000	87936.500	-2.559	94000.813	-2.394	125237.25	-1.797
520.0	5.0	0.0900	1526.146	67499.938	87936.438	0.768	94000.750	0.718	125237.06	0.539
520.0	5.0	0.0900	1526.146	168749.875	87936.438	1.919	94000.750	1.795	125237.06	1.347
520.0	5.0	0.0900	1526.146	112500.000	87936.438	1.279	94000.750	1.197	125237.06	0.898
520.0	5.0	0.0450	763.073	127500.000	227116.563	0.561	210583.938	0.605	281370.75	0.453
520.0	5.0	0.0900	1526.146	112499.938	87936.438	1.279	94000.750	1.197	125237.06	0.898
520.0	5.0	0.0720	1220.917	112500.000	119215.313	0.944	121441.250	0.926	161871.19	0.695

520.0	5.0	0.0900	1526.146	82499.875	87936.438	0.938	94000.750	0.878	125237.06	0.659
520.0	5.0	0.0900	1526.145	45000.000	87936.500	0.512	94000.813	0.479	125237.25	0.359
520.0	5.0	0.0900	1526.146	101249.938	87936.438	1.151	94000.750	1.077	125237.06	0.808
520.0	5.0	0.0675	1144.609	84374.938	130208.188	0.648	130857.250	0.645	174458.31	0.484
**AVG FOR Q= 5.		0.0805	1364.725	75144.375	109893.500	0.699	112783.813	0.671	150355.38	0.504
520.0	10.0	0.0900	1526.146	97499.938	87936.438	1.109	94000.750	1.037	125237.06	0.779
520.0	10.0	0.0675	1144.609	157500.125	130208.188	1.210	130857.250	1.204	174458.31	0.903
520.0	10.0	0.0525	890.252	84374.938	183732.438	0.459	175494.438	0.481	234244.19	0.360
520.0	10.0	0.0900	1526.146	172499.875	87936.438	1.962	94000.750	1.835	125237.06	1.377
520.0	10.0	0.0900	1526.146	82500.000	87936.438	0.938	94000.750	0.878	125237.06	0.659
520.0	10.0	0.0900	1526.146	157499.813	87936.438	1.791	94000.750	1.676	125237.06	1.258
520.0	10.0	0.0900	1526.146	101249.938	87936.438	1.151	94000.750	1.077	125237.06	0.808
520.0	10.0	0.0900	1526.146	90000.000	87936.438	1.023	94000.750	0.957	125237.06	0.719
520.0	10.0	0.0900	1526.145	73124.938	87936.500	0.832	94000.813	0.778	125237.25	0.584
520.0	10.0	0.0450	763.073	82499.938	227116.563	0.363	210583.938	0.392	281370.75	0.293
520.0	10.0	0.0675	1144.609	135000.000	130208.188	1.037	130857.250	1.032	174458.31	0.774
520.0	10.0	0.0750	1271.788	270000.000	112751.688	2.395	115855.000	2.330	154407.63	1.749
520.0	10.0	0.0900	1526.146	67500.188	87936.438	0.768	94000.750	0.718	125237.06	0.539
520.0	10.0	0.0450	763.073	74999.938	227116.563	0.330	210583.938	0.356	281370.75	0.267
520.0	10.0	0.0900	1526.145	90000.000	87936.500	1.023	94000.813	0.957	125237.25	0.719
520.0	10.0	0.0900	1526.146	74999.938	87936.438	0.853	94000.750	0.798	125237.06	0.599
520.0	10.0	0.0750	1271.788	50625.000	112751.688	0.449	115855.000	0.437	154407.63	0.328
520.0	10.0	0.0750	1271.788	73124.938	112751.688	0.649	115855.000	0.631	154407.63	0.474
520.0	10.0	0.0900	1526.145	50625.016	87936.500	0.576	94000.813	0.539	125237.25	0.404
520.0	10.0	0.0600	1017.431	112499.938	152984.563	0.735	150071.625	0.750	200170.06	0.562
**AVG FOR Q=10.		0.0776	1316.299	104906.000	117845.813	0.983	119500.750	0.943	159344.88	0.708
520.0	15.0	0.0975	1653.324	67500.000	78860.563	0.856	85813.375	0.787	114320.63	0.590
520.0	15.0	0.0810	1373.532	119999.875	101512.500	1.182	106043.188	1.132	141305.63	0.849
520.0	15.0	0.0900	1526.146	135000.000	87936.438	1.535	94000.750	1.436	125237.06	1.078
520.0	15.0	0.0750	1271.788	202500.125	112751.688	1.796	115855.000	1.748	154407.63	1.311

520.0	15.0	0.0900	1526.145	54000.012	87936.500	0.614	94000.813	0.574	125237.25	0.431
520.0	15.0	0.0900	1526.145	90000.000	87936.500	1.023	94000.813	0.957	125237.25	0.719
520.0	15.0	0.1012	1716.913	52499.977	74915.188	0.701	82215.125	0.639	109524.88	0.479
520.0	15.0	0.0900	1526.146	89999.938	87936.438	1.023	94000.750	0.957	125237.06	0.719
520.0	15.0	0.0900	1526.146	101250.063	87936.438	1.151	94000.750	1.077	125237.06	0.808
520.0	15.0	0.0900	1526.146	90000.000	87936.438	1.023	94000.750	0.957	125237.06	0.719
520.0	15.0	0.0900	1526.145	44999.938	87936.500	0.512	94000.813	0.479	125237.25	0.359
520.0	15.0	0.0900	1526.145	58499.961	87936.500	0.665	94000.813	0.622	125237.25	0.467
520.0	15.0	0.0750	1271.788	-90000.125	112751.688	-0.798	115855.000	-0.777	154407.63	-0.583
520.0	15.0	0.0787	1335.378	157499.938	105488.875	1.493	109529.500	1.438	145959.94	1.079
520.0	15.0	0.1350	2289.219	146249.938	50697.652	2.885	59468.723	2.459	79233.44	1.846
520.0	15.0	0.0900	1526.146	270000.000	87936.438	3.070	94000.750	2.872	125237.06	2.156
520.0	15.0	0.1012	1716.914	-11250.000	74915.125	-0.150	82215.063	-0.137	109524.69	-0.103
520.0	15.0	0.0900	1526.146	74999.938	87936.438	0.853	94000.750	0.798	125237.06	0.599
520.0	15.0	0.0900	1526.145	49500.000	87936.500	0.563	94000.813	0.527	125237.25	0.395
520.0	15.0	0.0750	1271.788	73124.938	112751.688	0.649	115855.000	0.631	154407.63	0.474
520.0	15.0	0.1012	1716.913	41249.969	74915.188	0.551	82215.125	0.502	109524.88	0.377
520.0	15.0	0.0900	1526.145	44999.957	87936.500	0.512	94000.813	0.479	125237.25	0.359
520.0	15.0	0.0900	1526.145	44999.969	87936.500	0.512	94000.813	0.479	125237.25	0.359
**AVG FOR	Q=15.	0.0909	1541.627	82939.813	88814.250	0.966	94655.125	0.897	126117.13	0.673
520.0	20.0	0.0900	1526.146	82499.938	87936.438	0.938	94000.750	0.878	125237.06	0.659
520.0	20.0	0.0900	1526.145	71249.938	87936.500	0.810	94000.813	0.758	125237.25	0.569
520.0	20.0	0.0900	1526.145	84374.938	87936.500	0.959	94000.813	0.898	125237.25	0.674
520.0	20.0	0.0900	1526.145	78749.938	87936.500	0.896	94000.813	0.838	125237.25	0.629
520.0	20.0	0.0900	1526.145	44999.973	87936.500	0.512	94000.813	0.479	125237.25	0.359
520.0	20.0	0.0900	1526.145	53999.973	87936.500	0.614	94000.813	0.574	125237.25	0.431
520.0	20.0	0.0900	1526.145	67499.938	87936.500	0.768	94000.813	0.718	125237.25	0.539
520.0	20.0	0.0900	1526.146	67500.000	87936.438	0.768	94000.750	0.718	125237.06	0.539
520.0	20.0	0.0900	1526.146	74999.938	87936.438	0.853	94000.750	0.798	125237.06	0.599
**AVG FOR	Q=20.	0.0900	1526.145	69541.563	87936.438	0.791	94000.750	0.740	125237.06	0.555

520.0	30.0	0.0900	1526.145	76499.938	87936.500	0.870	94000.813	0.814	125237.25	0.611
520.0	30.0	0.0450	763.073	112499.875	227116.563	0.495	210583.938	0.534	281370.75	0.400
520.0	30.0	0.0990	1678.760	90000.000	77239.813	1.165	84338.313	1.067	112354.56	0.801
520.0	30.0	0.0900	1526.146	97500.000	87936.438	1.109	94000.750	1.037	125237.06	0.779
520.0	30.0	0.0900	1526.146	82500.000	87936.438	0.938	94000.750	0.878	125237.06	0.659
520.0	30.0	0.0900	1526.145	29999.945	87936.500	0.341	94000.813	0.319	125237.25	0.240
520.0	30.0	0.0771	1308.125	44999.973	108498.625	0.415	112157.375	0.401	149469.06	0.301
520.0	30.0	0.0900	1526.145	44999.977	87936.500	0.512	94000.813	0.479	125237.25	0.359
520.0	30.0	0.0900	1526.145	56249.969	87936.500	0.640	94000.813	0.598	125237.25	0.449
520.0	30.0	0.0900	1526.146	157500.000	87936.438	1.791	94000.750	1.676	125237.06	1.258
**AVG FOR	Q=30.	0.0851	1443.297	79274.938	102041.000	0.828	106508.500	0.780	141985.38	0.586
520.0	50.0	0.0900	1526.146	59999.977	87936.438	0.682	94000.750	0.638	125237.06	0.479
520.0	50.0	0.0900	1526.145	73124.938	87936.500	0.832	94000.813	0.778	125237.25	0.584
520.0	50.0	0.0975	1653.324	106874.938	78860.563	1.355	85813.375	1.245	114320.63	0.935
520.0	50.0	0.0900	1526.145	44999.984	87936.500	0.512	94000.813	0.479	125237.25	0.359
520.0	50.0	0.0900	1526.145	67499.875	87936.500	0.768	94000.813	0.718	125237.25	0.539
520.0	50.0	0.0900	1526.145	58499.973	87936.500	0.665	94000.813	0.622	125237.25	0.467
520.0	50.0	0.0900	1526.145	73124.938	87936.500	0.832	94000.813	0.778	125237.25	0.584
520.0	50.0	0.0731	1239.993	37499.988	116717.438	0.321	119287.125	0.314	158992.63	0.236
**AVG FOR	Q=50.	0.0888	1506.273	65203.055	90399.563	0.746	96138.125	0.697	128092.06	0.523
825.0	5.0	0.1050	2824.838	450000.000	152311.813	2.954	187948.688	2.394	250509.06	1.796
825.0	5.0	0.0900	2421.290	337499.750	187645.250	1.799	223069.188	1.513	297231.13	1.135
825.0	5.0	0.0562	1513.306	247499.813	355236.188	0.697	379027.438	0.653	504983.19	0.490
825.0	5.0	0.0450	1210.646	269999.750	481610.813	0.561	489730.063	0.551	652785.75	0.414
825.0	5.0	0.1050	2824.838	247500.250	152311.813	1.625	187948.688	1.317	250509.06	0.988
825.0	5.0	0.0600	1614.194	292500.250	325359.813	0.899	352153.813	0.831	469149.06	0.623
825.0	5.0	0.1050	2824.838	225000.000	152311.813	1.477	187948.688	1.197	250509.06	0.898
825.0	5.0	0.0750	2017.741	270000.000	240260.813	1.124	273602.000	0.987	364491.56	0.741
825.0	5.0	0.1050	2824.838	247499.625	152311.813	1.625	187948.688	1.317	250509.06	0.988
**AVG FOR	Q= 5.	0.0829	2230.723	287499.750	244372.875	1.418	274374.875	1.196	365630.50	0.897

825.0	10.0	0.1200	3228.387	224999.500	127160.250	1.769	162178.063	1.387	216234.50	1.041
825.0	10.0	0.0750	2017.741	427500.000	240260.813	1.779	273602.000	1.562	364491.56	1.173
825.0	10.0	0.1500	4035.485	314999.750	94093.750	3.348	126981.438	2.481	169428.56	1.859
825.0	10.0	0.0900	2421.290	180000.000	187645.250	0.959	223069.188	0.807	297231.13	0.606
825.0	10.0	0.1350	3631.935	292500.250	108464.500	2.697	142492.250	2.053	190055.50	1.539
825.0	10.0	0.1050	2824.838	202499.875	152311.813	1.330	187948.688	1.077	250509.06	0.808
825.0	10.0	0.1050	2824.838	382500.000	152311.813	2.511	187948.688	2.035	250509.06	1.527
825.0	10.0	0.0750	2017.741	179999.750	240260.813	0.749	273602.000	0.658	364491.56	0.494
825.0	10.0	0.0900	2421.290	360000.250	187645.250	1.919	223069.188	1.614	297231.13	1.211
825.0	10.0	0.1350	3631.935	382499.750	108464.500	3.526	142492.250	2.684	190055.50	2.013
**AVG FOR	Q=10.	0.1080	2905.546	294749.563	159861.688	2.059	194338.188	1.636	259023.56	1.227
825.0	15.0	0.0900	2421.290	224999.625	187645.250	1.199	223069.188	1.009	297231.13	0.757
825.0	15.0	0.1350	3631.935	281249.938	108464.500	2.593	142492.250	1.974	190055.50	1.480
825.0	15.0	0.0600	1614.194	494999.500	325359.813	1.521	352153.813	1.406	469149.06	1.055
825.0	15.0	0.0900	2421.290	269999.750	187645.250	1.439	223069.188	1.210	297231.13	0.908
825.0	15.0	0.0600	1614.194	404999.500	325359.813	1.245	352153.813	1.150	469149.06	0.863
825.0	15.0	0.0750	2017.742	359999.500	240260.375	1.498	273601.813	1.316	364490.81	0.988
825.0	15.0	0.0900	2421.290	202500.000	187645.250	1.079	223069.188	0.908	297231.13	0.681
825.0	15.0	0.0900	2421.290	135000.063	187645.250	0.719	223069.188	0.605	297231.13	0.454
825.0	15.0	0.1012	2723.951	168750.063	159991.500	1.055	195679.875	0.862	260792.94	0.647
825.0	15.0	0.0900	2421.290	135000.000	187645.250	0.719	223069.188	0.605	297231.13	0.454
825.0	15.0	0.1200	3228.387	225000.000	127160.250	1.769	162178.063	1.387	216234.50	1.041
825.0	15.0	0.0900	2421.290	135000.375	187645.250	0.719	223069.188	0.605	297231.13	0.454
825.0	15.0	0.0600	1614.194	225000.125	325359.813	0.692	352153.813	0.639	469149.06	0.480
825.0	15.0	0.0562	1513.306	134999.875	355236.188	0.380	379027.438	0.356	504983.19	0.267
825.0	15.0	0.1200	3228.387	292500.000	127160.250	2.300	162178.063	1.804	216234.50	1.353
**AVG FOR	Q=15.	0.0885	2380.934	245999.625	214681.313	1.262	247335.313	1.056	329574.69	0.792
825.0	20.0	0.1500	4035.485	179999.750	94093.750	1.913	126981.438	1.418	169428.56	1.062
825.0	20.0	0.1050	2824.838	202499.500	152311.813	1.330	187948.688	1.077	250509.06	0.808
825.0	20.0	0.0900	2421.290	292499.750	187645.250	1.559	223069.188	1.311	297231.13	0.984

825.0	20.0	0.1350	3631.935	360000.000	108464.500	3.319	142492.250	2.526	190055.50	1.894
825.0	20.0	0.0750	2017.741	269999.500	240260.813	1.124	273602.000	0.987	364491.56	0.741
825.0	20.0	0.0900	2421.290	315000.250	187645.250	1.679	223069.188	1.412	297231.13	1.060
**AVG FOR	Q=20.	0.1075	2892.095	269999.625	161736.875	1.820	196193.625	1.455	261491.00	1.092
825.0	30.0	0.0750	2017.741	382499.500	240260.813	1.592	273602.000	1.398	364491.56	1.049
825.0	30.0	0.1125	3026.613	179999.938	138747.063	1.297	174141.313	1.034	232145.44	0.775
825.0	30.0	0.0675	1815.967	213749.938	277213.250	0.771	308121.500	0.694	410466.00	0.521
825.0	30.0	0.1050	2824.838	22500.121	152311.813	0.148	187948.688	0.120	250509.06	0.090
825.0	30.0	0.0990	2663.418	142499.938	164930.875	0.864	200621.875	0.710	267367.06	0.533
825.0	30.0	0.0750	2017.741	247500.000	240260.813	1.030	273602.000	0.905	364491.56	0.679
825.0	30.0	0.0900	2421.290	202499.875	187645.250	1.079	223069.188	0.908	297231.13	0.681
825.0	30.0	0.0900	2421.290	157499.875	187645.250	0.839	223069.188	0.706	297231.13	0.530
**AVG FOR	Q=30.	0.0892	2401.111	193593.375	198626.750	0.953	233021.875	0.809	310491.50	0.607
825.0	50.0	0.1200	3228.387	202499.875	127160.250	1.592	162178.063	1.249	216234.50	0.936
825.0	50.0	0.1200	3228.387	292499.750	127160.250	2.300	162178.063	1.804	216234.50	1.353
825.0	50.0	0.0900	2421.290	75000.000	187645.250	0.400	223069.188	0.336	297231.13	0.252
825.0	50.0	0.0525	1412.420	89999.938	390248.063	0.231	410140.625	0.219	546495.25	0.165
825.0	50.0	0.1012	2723.951	112500.000	159991.500	0.703	195679.875	0.575	260792.94	0.431
825.0	50.0	0.0900	2421.290	90000.000	187645.250	0.480	223069.188	0.403	297231.13	0.303
825.0	50.0	0.1275	3430.159	101250.000	117164.250	0.864	151716.063	0.667	202321.44	0.500
825.0	50.0	0.0900	2421.290	213749.813	187645.250	1.139	223069.188	0.958	297231.13	0.719
**AVG FOR	Q=50.	0.0989	2660.896	147187.375	185582.375	0.964	218887.375	0.776	291721.25	0.582
975.0	10.0	0.0600	1907.684	315000.000	427957.438	0.736	481070.313	0.655	640864.75	0.492
975.0	10.0	0.0900	2861.525	405000.000	247062.688	1.639	305834.438	1.324	407645.88	0.994
975.0	10.0	0.0900	2861.525	359999.750	247062.688	1.457	305834.438	1.177	407645.88	0.883
975.0	10.0	0.1050	3338.446	247499.750	200604.375	1.234	258000.375	0.959	344029.75	0.719
975.0	10.0	0.0450	1430.763	179999.750	632929.000	0.284	667063.813	0.270	888813.69	0.203
975.0	10.0	0.1350	4292.285	337499.750	142919.500	2.361	195965.063	1.722	261531.38	1.290
975.0	10.0	0.0900	2861.525	269999.750	247062.688	1.093	305834.438	0.883	407645.88	0.662
975.0	10.0	0.0600	1907.684	270000.250	427957.438	0.631	481070.313	0.561	640864.75	0.421

975.0	10.0	0.0750	2384.603	314999.500	316206.813	0.996	374532.813	0.841	499038.56	0.631
975.0	10.0	0.0750	2384.604	404999.750	316206.438	1.281	374532.375	1.081	499037.75	0.812
975.0	10.0	0.1050	3338.446	247500.125	200604.375	1.234	258000.375	0.959	344029.75	0.719
975.0	10.0	0.0900	2861.525	247500.125	247062.688	1.002	305834.438	0.809	407645.88	0.607
975.0	10.0	0.0750	2384.603	404999.500	316206.813	1.281	374532.813	1.081	499038.56	0.812
975.0	10.0	0.0900	2861.525	359999.750	247062.688	1.457	305834.438	1.177	407645.88	0.883
975.0	10.0	0.0750	2384.603	337499.750	316206.813	1.067	374532.813	0.901	499038.56	0.676
975.0	10.0	0.0600	1907.684	292499.500	427957.438	0.683	481070.313	0.608	640864.75	0.456
**AVG FOR Q=10.		0.0825	2623.063	312186.813	310066.438	1.152	365596.063	0.938	487210.75	0.704
975.0	15.0	0.0750	2384.603	337499.500	316206.813	1.067	374532.813	0.901	499038.56	0.676
975.0	15.0	0.0600	1907.684	179999.750	427957.438	0.421	481070.313	0.374	640864.75	0.281
975.0	15.0	0.1050	3338.446	517500.000	200604.375	2.580	258000.375	2.006	344029.75	1.504
975.0	15.0	0.0600	1907.684	427499.750	427957.438	0.999	481070.313	0.889	640864.75	0.667
975.0	15.0	0.0600	1907.684	292500.000	427957.438	0.683	481070.313	0.608	640864.75	0.456
975.0	15.0	0.1200	3815.366	359999.500	167520.188	2.149	222849.125	1.615	297284.69	1.211
975.0	15.0	0.0750	2384.603	247500.000	316206.813	0.783	374532.813	0.661	499038.56	0.496
975.0	15.0	0.0750	2384.603	337499.750	316206.813	1.067	374532.813	0.901	499038.56	0.676
975.0	15.0	0.0600	1907.684	270000.250	427957.438	0.631	481070.313	0.561	640864.75	0.421
975.0	15.0	0.0900	2861.525	135000.000	247062.688	0.546	305834.438	0.441	407645.88	0.331
975.0	15.0	0.1350	4292.285	382499.250	142919.500	2.676	195965.063	1.952	261531.38	1.463
975.0	15.0	0.0750	2384.603	517500.000	316206.813	1.637	374532.813	1.382	499038.56	1.037
**AVG FOR Q=15.		0.0825	2623.063	333749.625	311229.875	1.270	367088.063	1.024	489174.81	0.768
975.0	20.0	0.1050	3338.446	472500.250	200604.375	2.355	258000.375	1.831	344029.75	1.373
975.0	20.0	0.0600	1907.684	247499.750	427957.438	0.578	481070.313	0.514	640864.75	0.386
975.0	20.0	0.0600	1907.684	247500.000	427957.438	0.578	481070.313	0.514	640864.75	0.386
975.0	20.0	0.0750	2384.603	269999.750	316206.813	0.854	374532.813	0.721	499038.56	0.541
975.0	20.0	0.0600	1907.684	112499.750	427957.438	0.263	481070.313	0.234	640864.75	0.176
975.0	20.0	0.0900	2861.525	157500.063	247062.688	0.637	305834.438	0.515	407645.88	0.386
975.0	20.0	0.1012	3219.214	157500.063	210703.938	0.747	268537.250	0.587	358042.75	0.440
975.0	20.0	0.0750	2384.603	269999.750	316206.813	0.854	374532.813	0.721	499038.56	0.541

975.0	20.0	0.1050	3338.446	359999.500	200604.375	1.795	258000.375	1.395	344029.75	1.046
975.0	20.0	0.1050	3338.446	247499.875	200604.375	1.234	258000.375	0.959	344029.75	0.719
975.0	20.0	0.0600	1907.684	202499.875	427957.438	0.473	481070.313	0.421	640864.75	0.316
975.0	20.0	0.0900	2861.525	146250.000	247062.688	0.592	305834.438	0.478	407645.88	0.359
975.0	20.0	0.0900	2861.525	112499.875	247062.688	0.455	305834.438	0.368	407645.88	0.276
975.0	20.0	0.0787	2503.834	168750.000	295988.375	0.570	354705.875	0.476	472658.13	0.357
975.0	20.0	0.0900	2861.525	67500.000	247062.688	0.273	305834.438	0.221	407645.88	0.166
975.0	20.0	0.0900	2861.525	134999.938	247062.688	0.546	305834.438	0.441	407645.88	0.331
975.0	20.0	0.0450	1430.763	179999.875	632929.000	0.284	667063.813	0.270	888813.69	0.203
**AVG FOR Q=20.		0.0812	2580.982	209117.063	312999.000	0.770	368636.438	0.627	491256.38	0.471
975.0	30.0	0.0750	2384.603	247500.000	316206.813	0.783	374532.813	0.661	499038.56	0.496
975.0	30.0	0.0900	2861.525	180000.000	247062.688	0.729	305834.438	0.589	407645.88	0.442
975.0	30.0	0.0562	1788.453	146250.000	467170.375	0.313	517455.938	0.283	689334.19	0.212
975.0	30.0	0.0750	2384.604	247499.875	316206.438	0.783	374532.375	0.661	499037.75	0.496
975.0	30.0	0.0600	1907.684	225000.000	427957.438	0.526	481070.313	0.468	640864.75	0.351
975.0	30.0	0.0675	2146.142	236249.688	364744.375	0.648	421385.000	0.561	561393.81	0.421
975.0	30.0	0.1050	3338.446	157499.875	200604.375	0.785	258000.375	0.610	344029.75	0.458
975.0	30.0	0.0675	2146.142	168749.875	364744.375	0.463	421385.000	0.400	561393.81	0.301
975.0	30.0	0.0600	1907.684	157500.438	427957.438	0.368	481070.313	0.327	640864.75	0.246
975.0	30.0	0.0900	2861.525	202499.813	247062.688	0.820	305834.438	0.662	407645.88	0.497
975.0	30.0	0.0900	2861.525	146250.000	247062.688	0.592	305834.438	0.478	407645.88	0.359
975.0	30.0	0.0900	2861.525	157499.875	247062.688	0.637	305834.438	0.515	407645.88	0.386
975.0	30.0	0.0750	2384.603	247500.125	316206.813	0.783	374532.813	0.661	499038.56	0.496
975.0	30.0	0.0900	2861.525	157499.750	247062.688	0.637	305834.438	0.515	407645.88	0.386
975.0	30.0	0.0900	2861.525	236249.813	247062.688	0.956	305834.438	0.772	407645.88	0.580
975.0	30.0	0.0450	1430.763	112499.875	632929.000	0.178	667063.813	0.169	888813.69	0.127
**AVG FOR Q=30.		0.0766	2436.766	189140.125	332318.563	0.625	387876.875	0.521	516854.63	0.391
1100.0	0.0	0.0600	2152.258	584999.750	521766.813	1.121	603194.438	0.970	803612.63	0.728
1100.0	0.0	0.0600	2152.258	472499.750	521766.813	0.906	603194.438	0.783	803612.63	0.588
1100.0	0.0	0.0562	2017.742	225000.063	569506.000	0.395	648537.500	0.347	863978.31	0.260

**AVG FOR Q= 0.		0.0587	2107.419	427499.625	537679.625	0.807	618308.313	0.700	823734.31	0.525
1100.0	5.0	0.0450	1614.194	157500.000	771222.625	0.204	834734.813	0.189	1112056.00	0.142
1100.0	5.0	0.0600	2152.258	382499.500	521766.813	0.733	603194.438	0.634	803612.63	0.476
1100.0	5.0	0.0600	2152.258	404999.500	521766.813	0.776	603194.438	0.671	803612.63	0.504
1100.0	5.0	0.0900	3228.387	202500.000	301417.000	0.672	384421.875	0.527	512555.94	0.395
1100.0	5.0	0.1050	3766.452	494999.250	244788.813	2.022	324569.188	1.525	432961.69	1.143
1100.0	5.0	0.1050	3766.452	247500.000	244788.813	1.011	324569.188	0.763	432961.69	0.572
1100.0	5.0	0.1050	3766.452	224999.875	244788.813	0.919	324569.188	0.693	432961.69	0.520
1100.0	5.0	0.0900	3228.387	224999.875	301417.000	0.746	384421.875	0.585	512555.94	0.439
1100.0	5.0	0.0900	3228.387	292500.000	301417.000	0.970	384421.875	0.761	512555.94	0.571
1100.0	5.0	0.0900	3228.387	517499.500	301417.000	1.717	384421.875	1.346	512555.94	1.010
1100.0	5.0	0.0900	3228.387	337499.500	301417.000	1.120	384421.875	0.878	512555.94	0.658
1100.0	5.0	0.0900	3228.387	315000.000	301417.000	1.045	384421.875	0.819	512555.94	0.615
1100.0	5.0	0.1050	3766.452	270000.000	244788.813	1.103	324569.188	0.832	432961.69	0.624
1100.0	5.0	0.0600	2152.258	134999.875	521766.813	0.259	603194.438	0.224	803612.63	0.168
1100.0	5.0	0.0750	2690.321	270000.000	385666.938	0.700	470272.250	0.574	626740.31	0.431
1100.0	5.0	0.0900	3228.387	168750.000	301417.000	0.560	384421.875	0.439	512555.94	0.329
**AVG FOR Q= 5.		0.0844	3026.612	290390.188	363203.625	0.910	443988.250	0.716	591835.06	0.537
1100.0	10.0	0.0750	2690.321	247499.750	385666.938	0.642	470272.250	0.526	626740.31	0.395
1100.0	10.0	0.0750	2690.321	337499.750	385666.938	0.875	470272.250	0.718	626740.31	0.539
1100.0	10.0	0.0562	2017.742	326250.000	569506.000	0.573	648537.500	0.503	863978.31	0.378
1100.0	10.0	0.0600	2152.258	179999.875	521766.813	0.345	603194.438	0.298	803612.63	0.224
1100.0	10.0	0.0450	1614.194	247500.125	771222.625	0.321	834734.813	0.297	1112056.00	0.223
1100.0	10.0	0.0600	2152.258	315000.000	521766.813	0.604	603194.438	0.522	803612.63	0.392
1100.0	10.0	0.0675	2421.289	314999.875	444789.313	0.708	528757.875	0.596	704548.75	0.447
1100.0	10.0	0.0600	2152.258	359999.750	521766.813	0.690	603194.438	0.597	803612.63	0.448
1100.0	10.0	0.0900	3228.387	247499.750	301417.000	0.821	384421.875	0.644	512555.94	0.483
1100.0	10.0	0.0600	2152.258	225000.125	521766.813	0.431	603194.438	0.373	803612.63	0.280
1100.0	10.0	0.0750	2690.321	337499.750	385666.938	0.875	470272.250	0.718	626740.31	0.539
1100.0	10.0	0.0600	2152.258	314999.750	521766.813	0.604	603194.438	0.522	803612.63	0.392

1100.0	10.0	0.0600	2152.258	225000.000	521766.813	0.431	603194.438	0.373	803612.63	0.280
1100.0	10.0	0.0750	2690.321	360000.000	385666.938	0.933	470272.250	0.766	626740.31	0.574
1100.0	10.0	0.0750	2690.321	472499.750	385666.938	1.225	470272.250	1.005	626740.31	0.754
1100.0	10.0	0.0900	3228.387	337499.500	301417.000	1.120	384421.875	0.878	512555.94	0.658
**AVG FOR	Q=10.	0.0677	2429.696	303046.375	465454.875	0.700	546962.188	0.583	728816.50	0.438
1100.0	15.0	0.0600	2152.258	494999.250	521766.813	0.949	603194.438	0.821	803612.63	0.616
1100.0	15.0	0.0600	2152.258	584999.750	521766.813	1.121	603194.438	0.970	803612.63	0.728
1100.0	15.0	0.0600	2152.258	337499.750	521766.813	0.647	603194.438	0.560	803612.63	0.420
1100.0	15.0	0.0600	2152.258	315000.000	521766.813	0.604	603194.438	0.522	803612.63	0.392
1100.0	15.0	0.0787	2824.838	292499.750	361035.125	0.810	445508.063	0.657	593799.38	0.493
1100.0	15.0	0.0600	2152.258	270000.000	521766.813	0.517	603194.438	0.448	803612.63	0.336
1100.0	15.0	0.0900	3228.387	314999.750	301417.000	1.045	384421.875	0.819	512555.94	0.615
1100.0	15.0	0.0600	2152.258	292500.000	521766.813	0.561	603194.438	0.485	803612.63	0.364
1100.0	15.0	0.0750	2690.321	472499.750	385666.938	1.225	470272.250	1.005	626740.31	0.754
1100.0	15.0	0.0750	2690.321	247500.125	385666.938	0.642	470272.250	0.526	626740.31	0.395
1100.0	15.0	0.0600	2152.258	359999.750	521766.813	0.690	603194.438	0.597	803612.63	0.448
1100.0	15.0	0.0600	2152.258	134999.875	521766.813	0.259	603194.438	0.224	803612.63	0.168
1100.0	15.0	0.0900	3228.387	224999.938	301417.000	0.746	384421.875	0.585	512555.94	0.439
1100.0	15.0	0.0600	2152.258	292500.000	521766.813	0.561	603194.438	0.485	803612.63	0.364
1100.0	15.0	0.0450	1614.194	382499.500	771222.625	0.496	834734.813	0.458	1112056.00	0.344
1100.0	15.0	0.0450	1614.194	427499.500	771222.625	0.554	834734.813	0.512	1112056.00	0.384
1100.0	15.0	0.0450	1614.194	382499.500	771222.625	0.496	834734.813	0.458	1112056.00	0.344
1100.0	15.0	0.0450	1614.194	382499.500	771222.625	0.496	834734.813	0.458	1112056.00	0.344
**AVG FOR	Q=15.	0.0627	2249.407	344999.313	528665.813	0.690	606809.750	0.588	808506.75	0.442
1100.0	20.0	0.0600	2152.258	517499.500	521766.813	0.992	603194.438	0.858	803612.63	0.644
1100.0	20.0	0.0600	2152.258	202500.250	521766.813	0.388	603194.438	0.336	803612.63	0.252
1100.0	20.0	0.0750	2690.321	292499.500	385666.938	0.758	470272.250	0.622	626740.31	0.467
1100.0	20.0	0.0600	2152.258	382499.750	521766.813	0.733	603194.438	0.634	803612.63	0.476
1100.0	20.0	0.0562	2017.742	281249.750	569506.000	0.494	648537.500	0.434	863978.31	0.326
1100.0	20.0	0.0600	2152.258	337500.000	521766.813	0.647	603194.438	0.560	803612.63	0.420

1100.0	20.0	0.0600	2152.258	494999.750	521766.813	0.949	603194.438	0.821	803612.63	0.616
1100.0	20.0	0.0600	2152.258	315000.000	521766.813	0.604	603194.438	0.522	803612.63	0.392
1100.0	20.0	0.0600	2152.258	247500.125	521766.813	0.474	603194.438	0.410	803612.63	0.308
1100.0	20.0	0.0600	2152.258	495000.000	521766.813	0.949	603194.438	0.821	803612.63	0.616
**AVG FOR Q=20.		0.0611	2192.612	356624.688	512930.188	0.699	594436.063	0.602	791961.50	0.452
1100.0	30.0	0.0900	3228.387	495000.000	301417.000	1.642	384421.875	1.288	512555.94	0.966
1100.0	30.0	0.0750	2690.321	359999.750	385666.938	0.933	470272.250	0.766	626740.31	0.574
1100.0	30.0	0.0750	2690.321	247499.625	385666.938	0.642	470272.250	0.526	626740.31	0.395
1100.0	30.0	0.0600	2152.258	315000.000	521766.813	0.604	603194.438	0.522	803612.63	0.392
1100.0	30.0	0.0450	1614.194	270000.000	771222.625	0.350	834734.813	0.323	1112056.00	0.243
1100.0	30.0	0.0562	2017.742	157500.000	569506.000	0.277	648537.500	0.243	863978.31	0.182
1100.0	30.0	0.0562	2017.742	191249.938	569506.000	0.336	648537.500	0.295	863978.31	0.221
1100.0	30.0	0.0900	3228.387	269999.750	301417.000	0.896	384421.875	0.702	512555.94	0.527
1100.0	30.0	0.0450	1614.194	157500.000	771222.625	0.204	834734.813	0.189	1112056.00	0.142
1100.0	30.0	0.0600	2152.258	90000.000	521766.813	0.172	603194.438	0.149	803612.63	0.112
**AVG FOR Q=30.		0.0652	2340.580	255374.688	509915.500	0.606	588231.688	0.500	783788.25	0.375
1100.0	50.0	0.0900	3228.387	517500.000	301417.000	1.717	384421.875	1.346	512555.94	1.010
1100.0	50.0	0.0600	2152.258	202500.125	521766.813	0.388	603194.438	0.336	803612.63	0.252
1100.0	50.0	0.0600	2152.258	674999.750	521766.813	1.294	603194.438	1.119	803612.63	0.840
1100.0	50.0	0.0562	2017.742	213750.000	569506.000	0.375	648537.500	0.330	863978.31	0.247
1100.0	50.0	0.0600	2152.258	134999.750	521766.813	0.259	603194.438	0.224	803612.63	0.168
1100.0	50.0	0.0600	2152.258	314999.750	521766.813	0.604	603194.438	0.522	803612.63	0.392
1100.0	50.0	0.0787	2824.838	281249.813	361035.125	0.779	445508.063	0.631	593799.38	0.474
1100.0	50.0	0.0540	1937.033	142499.875	601952.563	0.237	679042.563	0.210	904600.50	0.158
1100.0	50.0	0.0750	2690.321	180000.000	385666.938	0.467	470272.250	0.383	626740.31	0.287
**AVG FOR Q=50.		0.0660	2367.483	295832.750	478515.625	0.680	560061.875	0.567	746235.63	0.425

EXECUTION TERMINATED 15:16:01 T=1.893 RC=0 $.59

$SIG

APPENDIX F

COMPUTER PROGRAM AND OUTPUT OF DROPLET BREAK-UP TIME DATA REDUCTION LIST OF VARIABLES

VARIABLES NAME	DESCRIPTION OF VARIABLE
DIA(I)	Diameter of an individual droplet at a particular observation
DIST	The distance that the particle travelled since the last observation
DRPF	Final observed diameter of a particular droplet
DRPI	Initial observed diameter of a particular droplet
FN(I)	Number of frames between each successive observation
Q	Flow rate of water in the test section
QM	Ratio of dynamic pressure
QMTB	Square root of the dynamic pressure ratio times dimensionless break-up time
RE	Reynolds number for a particular particle
SMACH	Mach number of the steam through the test section
T(I)	Thickness of an individual droplet at a particular observation
TB	Dimensionless break-up time
THKF	Final observed thickness of a particular droplet
THKI	Initial observed thickness of a particular droplet
TIME	Real time measured between observations
V	Steam velocity in the system
VEL	Droplet velocity across the test section
WE	Weber number for a particular particle
X(I)	Distance of an individual droplet from the edge of the blade at a particular observation.

BREAK-UP TIME ANALYSIS PROGRAM

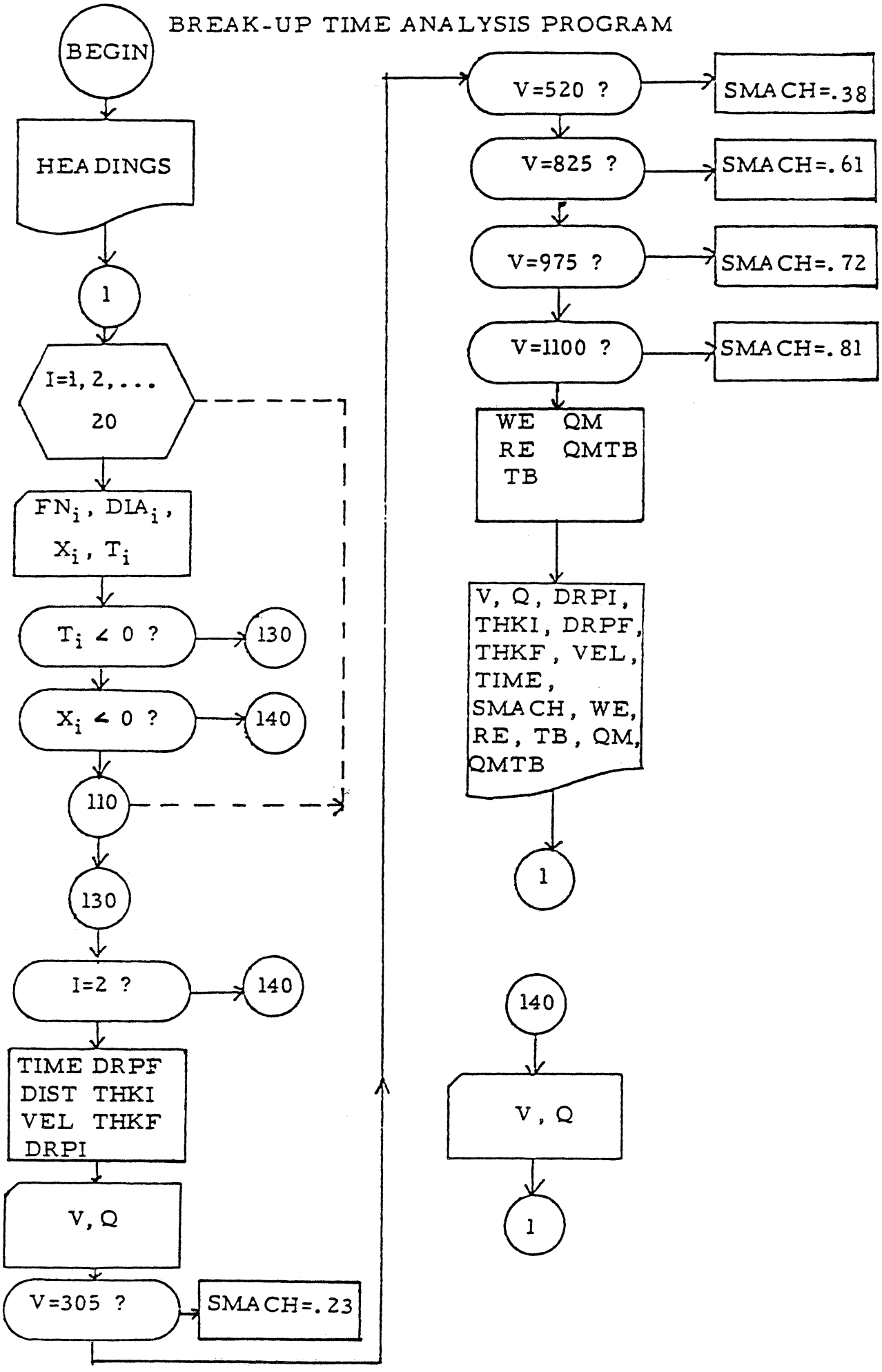

```
$SIG ODLU T=3 P=20
$R *FTN S=WDATA(2,1873)
C     ***************** BREAK-UP TIME ANALYSIS PROGRAM *****************
C     THIS PROGRAM CALCULATES THE INITIAL AND FINAL
C     DIMENSIONS OF A DROP AND ITS VELOCITY FOR SPLIT CASES ONLY.
C     IT ALSO FINDS WEBBER NUMBER, REYNOLDS NUMBER, DIMENSIONLESS
C     BREAK-UP TIME, AND THE DYNAMIC PRESSURE RATIO.
C     ***********************************************************************
      DIMENSION FN(20), DIA(20), T(20), X(20)
      WRITE(6,199)
C     ***** READ THE DATA FOR EACH OBSERVATION *****
    1 DO 110 I=1,20
      READ (5,101) FN(I), DIA(I), T(I), X(I)
      IF (T(I) .LT.0.0) GO TO 130
      IF (X(I) .LT.0.0) GO TO 140
  110 CONTINUE
  130 IF (I .EQ. 2) GO TO 140
      TIME=(I-1.0)*0.001
      DIST=(X(I)-X(1))*0.45
      VEL=DIST/TIME
C     ***** FIND THE INITIAL AND FINAL DROP DIMENSIONS *****
      DRPI=DIA(1)*0.45
      DRPF=DIA(I)*0.45
      THKI=T(1)*0.45
      THKF=ABS(T(I))*0.45
      READ(5,101) V,Q
C     ***** DETERMINE THE STEAM MACH NUMBER *****
      IF (V.EQ.305.0) SMACH=0.23
      IF(V.EQ.520.0) SMACH=0.38
      IF (V.EQ.825.0) SMACH=0.61
      IF (V.EQ.975.0) SMACH=0.72
      IF(V.EQ.1100.0) SMACH=0.81
      WE=(V**2)*DRPI*1.435E-3
      RE=V*DRPI*32.61
      TB=(TIME*V)/DRPI*0.323
      QM=0.78+1.47/(1.+2.1*SMACH**3.4)
      QMTB=SQRT(QM)*TB
      WRITE(6,200) V,Q,DRPI,THKI,DRPF,THKF,VEL,TIME,SMACH,WE,RE,TB,
     1 QM,QMTB
      GO TO 1
  140 READ(5,101) V,Q
      GO TO 1
  101 FORMAT (6(F10.5))
  199 FORMAT ('1',2X,'STEAM',4X,'FLOW',2X,'INITIAL',3X,
     1 'INITIAL',4X,'FINAL',6X,'FINAL',6X,'DROP',5X,
     2 'TOTAL MACH',5X,'WE',6X,'RE',6X,'TB',5X,'QM',4X,'QM.5TB'/
     3 2X,'VELOCITY  RATE  DIAMETER THICKNESS  DIAMETER  THICKNESS',
     4 2X,'VELOCITY   TIME NUMBER (RS*V**2 (V*DO/',
     5 1X,'(T*V/DO  PRESS'/2X,'(FEET/S) (CC/M)    (CM)',6X,
     6 '(CM)',6X,'(CM)',6X,'(CM)',5X,'(CM/S)',4X,'(SEC)',8X,
     7 '*DO/SIG)  KVIS) *RS**.5)  RATIO')
  200 FORMAT ('0',F8.3,2X,F4.1,2X,F8.5,1X,F9.5,2X,
     1 F8.5,2X,F9.5,2X,F8.3,3X,F4.3,2X,F4.2,3X,F6.2,2X,F6.1,
     2 2X,F6.3,2X,F5.3,2X,F5.2)
      END
$ENDFILE
$R -LOAD S=WDATA(2,1873)
$ENDFILE
$SIG
```

□

STEAM VELOCITY (FEET/S)	FLOW RATE (CC/M)	INITIAL DIAMETER (CM)	INITIAL THICKNESS (CM)	FINAL DIAMETER (CM)	FINAL THICKNESS (CM)	DROP VELOCITY (CM/S)	TOTAL TIME (SEC)	MACH NUMBER	WE (RS*V**2 *DO/SIG)	RE (V*DO/ KVIS)	TB (T*V/DO *RS**.5)	QM PRESS RATIO	QM**.5 TB
305.000	5.0	0.09000	0.09000	0.09000	0.09000	210.000	.006	0.21	12.01	895.1	6.568	2.229	9.81
305.000	10.0	0.09000	0.09000	0.13500	0.09000	163.636	.011	0.21	12.01	895.1	12.041	2.229	17.98
305.000	20.0	0.13500	0.04500	0.22500	0.09000	321.428	.007	0.21	18.02	1142.7	5.108	2.229	7.61
520.000	5.0	0.09000	0.09000	0.09000	0.09000	525.000	.003	0.38	34.92	1526.1	5.599	2.143	8.20
520.000	5.0	0.09000	0.09000	0.09000	0.09000	405.000	.004	0.38	34.92	1526.1	7.465	2.143	10.93
520.000	10.0	0.04500	0.04500	0.09000	0.04500	645.000	.003	0.38	17.46	763.1	11.197	2.143	16.39
520.000	10.0	0.09000	0.09000	0.09000	0.09000	306.000	.005	0.38	34.92	1526.1	9.331	2.143	13.66
520.000	15.0	0.09000	0.09000	0.09000	0.09000	495.000	.003	0.38	34.92	1526.1	5.599	2.143	8.20
520.000	15.0	0.09000	0.09000	0.09000	0.09000	277.500	.006	0.38	34.92	1526.1	11.197	2.143	16.39
520.000	15.0	0.09000	0.09000	0.13500	0.04500	295.714	.007	0.38	34.92	1526.1	13.064	2.143	19.13
520.000	15.0	0.09000	0.09000	0.09000	0.09000	315.000	.005	0.38	34.92	1526.1	9.331	2.143	13.66
520.000	20.0	0.09000	0.09000	0.09000	0.09000	414.000	.005	0.38	34.92	1526.1	9.331	2.143	13.66
520.000	20.0	0.09000	0.09000	0.09000	0.09000	262.500	.006	0.38	34.92	1526.1	11.197	2.143	16.39
825.000	5.0	0.09000	0.09000	0.11500	0.09000	945.000	.002	0.61	87.90	2421.3	5.922	1.837	8.03
825.000	5.0	0.09000	0.09000	0.09000	0.04500	877.500	.002	0.61	87.90	2421.3	5.922	1.837	8.03
825.000	5.0	0.04500	0.04500	0.09000	0.04500	660.000	.003	0.61	43.95	1210.6	17.765	1.837	24.08
825.000	5.0	0.04500	0.04500	0.04500	0.04500	585.000	.002	0.61	43.95	1210.6	11.843	1.837	16.05
825.000	5.0	0.09000	0.09000	0.11500	0.04500	607.500	.002	0.61	87.90	2421.3	5.922	1.837	8.03
825.000	5.0	0.04500	0.04500	0.09000	0.09000	697.500	.002	0.61	43.95	1210.6	11.843	1.837	16.05
825.000	5.0	0.09000	0.09000	0.11500	0.09000	675.000	.002	0.61	87.90	2421.3	5.922	1.837	8.03
825.000	5.0	0.04500	0.04500	0.09000	0.09000	765.000	.002	0.61	43.95	1210.6	11.843	1.837	16.05
825.000	5.0	0.09000	0.09000	0.11500	0.11500	877.500	.002	0.61	87.90	2421.3	5.922	1.837	8.03
825.000	10.0	0.11500	0.09000	0.11500	0.09000	1080.000	.002	0.61	131.85	3631.9	3.948	1.837	5.35
825.000	10.0	0.04500	0.04500	0.09000	0.09000	922.500	.002	0.61	43.95	1210.6	11.843	1.837	16.05
825.000	10.0	0.11500	0.11500	0.11500	0.11500	1035.000	.002	0.61	131.85	3631.9	3.948	1.837	5.35
825.000	10.0	0.09000	0.04500	0.09000	0.09000	450.000	.002	0.61	87.90	2421.3	5.922	1.837	8.03
825.000	10.0	0.09000	0.09000	0.11500	0.09000	697.500	.002	0.61	87.90	2421.3	5.922	1.837	8.03
825.000	10.0	0.09000	0.09000	0.11500	0.04500	967.500	.002	0.61	87.90	2421.3	5.922	1.837	8.03

825.000	10.0	0.09000	0.09000	0.09000	0.09000	540.000	.002	0.61	87.90	2421.3	5.922	1.837	8.01
825.000	10.0	0.13500	0.09000	0.18000	0.04500	1057.500	.002	0.61	131.85	3631.9	3.948	1.837	5.35
825.000	15.0	0.09000	0.09000	0.18000	0.09000	825.000	.003	0.61	87.90	2421.3	8.882	1.837	12.04
825.000	15.0	0.04500	0.04500	0.09000	0.09000	1170.000	.002	0.61	43.95	1210.6	11.843	1.837	16.05
825.000	15.0	0.04500	0.04500	0.09000	0.09000	810.000	.002	0.61	43.95	1210.6	11.843	1.837	16.05
825.000	15.0	0.04500	0.04500	0.13500	0.09000	765.000	.002	0.61	43.95	1210.6	11.843	1.837	16.05
825.000	15.0	0.09000	0.04500	0.09000	0.09000	450.000	.002	0.61	87.90	2421.3	5.922	1.837	8.01
825.000	15.0	0.09000	0.04500	0.13500	0.04500	765.000	.002	0.61	87.90	2421.3	5.922	1.837	8.01
825.000	15.0	0.09000	0.09000	0.09000	0.09000	630.000	.002	0.61	87.90	2421.3	5.922	1.837	8.01
825.000	15.0	0.04500	0.04500	0.04500	0.04500	585.000	.002	0.61	43.95	1210.6	11.843	1.837	16.05
825.000	15.0	0.04500	0.04500	0.09000	0.04500	300.000	.003	0.61	43.95	1210.6	17.765	1.837	24.08
825.000	15.0	0.09000	0.09000	0.18000	0.13500	607.500	.002	0.61	87.90	2421.3	5.922	1.837	8.01
825.000	20.0	0.09000	0.04500	0.09000	0.09000	697.500	.002	0.61	87.90	2421.3	5.922	1.837	8.01
825.000	20.0	0.09000	0.04500	0.09000	0.09000	855.000	.002	0.61	87.90	2421.3	5.922	1.837	8.01
825.000	20.0	0.09000	0.09000	0.09000	0.09000	855.000	.002	0.61	87.90	2421.3	5.922	1.837	8.01
825.000	30.0	0.09000	0.09000	0.18000	0.13500	600.000	.003	0.61	87.90	2421.3	8.882	1.837	12.04
825.000	30.0	0.04500	0.04500	0.09000	0.04500	570.000	.003	0.61	43.95	1210.6	17.765	1.837	24.08
825.000	30.0	0.09000	0.09000	0.13500	0.09000	506.250	.004	0.61	87.90	2421.3	11.843	1.837	16.05
825.000	30.0	0.04500	0.04500	0.09000	0.09000	472.500	.002	0.61	43.95	1210.6	11.843	1.837	16.05
825.000	30.0	0.09000	0.04500	0.09000	0.09000	562.500	.002	0.61	87.90	2421.3	5.922	1.837	8.01
825.000	50.0	0.13500	0.04500	0.09000	0.09000	652.500	.002	0.61	131.85	3631.9	3.948	1.837	5.35
825.000	50.0	0.09000	0.09000	0.09000	0.09000	416.250	.004	0.61	87.90	2421.3	11.843	1.837	16.05
825.000	50.0	0.09000	0.04500	0.04500	0.04500	414.000	.005	0.61	87.90	2421.3	14.804	1.837	20.06
825.000	50.0	0.09000	0.09000	0.18000	0.09000	615.000	.003	0.61	87.90	2421.3	8.882	1.837	12.04
825.000	50.0	0.09000	0.09000	0.09000	0.09000	472.500	.004	0.61	87.90	2421.3	11.843	1.837	16.05
825.000	50.0	0.09000	0.09000	0.18000	0.18000	405.000	.005	0.61	87.90	2421.3	14.804	1.837	20.06
975.000	10.0	0.04500	0.04500	0.09000	0.09000	1034.999	.002	0.72	61.39	1430.8	13.997	1.651	17.99
975.000	10.0	0.09000	0.04500	0.09000	0.09000	765.000	.002	0.72	122.77	2861.5	6.998	1.651	8.99
975.000	10.0	0.09000	0.09000	0.09000	0.09000	855.000	.002	0.72	122.77	2861.5	6.998	1.651	8.99
975.000	10.0	0.13500	0.04500	0.09000	0.09000	427.500	.002	0.72	184.16	4292.3	4.666	1.651	6.00

975.000	10.0	0.04500	0.04500	0.04500	0.04500	405.000	.002	0.72	61.39	1430.8	13.997	1.651	17.99
975.000	10.0	0.13500	0.09000	0.13500	0.09000	922.500	.002	0.72	184.16	4292.3	4.666	1.651	6.00
975.000	10.0	0.09000	0.09000	0.09000	0.09000	720.000	.002	0.72	122.77	2861.5	6.998	1.651	8.99
975.000	10.0	0.04500	0.04500	0.09000	0.04500	720.000	.002	0.72	61.39	1430.8	13.997	1.651	17.99
975.000	10.0	0.09000	0.04500	0.09000	0.09000	765.000	.002	0.72	122.77	2861.5	6.998	1.651	8.99
975.000	10.0	0.04500	0.04500	0.11500	0.04500	1034.999	.002	0.72	61.39	1430.8	13.997	1.651	17.99
975.000	10.0	0.09000	0.09000	0.13500	0.09000	652.500	.002	0.72	122.77	2861.5	6.998	1.651	8.99
975.000	10.0	0.04500	0.04500	0.13500	0.09000	652.500	.002	0.72	61.39	1430.8	13.997	1.651	17.99
975.000	10.0	0.04500	0.04500	0.09000	0.04500	900.000	.002	0.72	61.39	1430.8	13.997	1.651	17.99
975.000	10.0	0.04500	0.04500	0.13500	0.13500	900.000	.002	0.72	61.39	1430.8	13.997	1.651	17.99
975.000	10.0	0.04500	0.04500	0.09000	0.09000	652.500	.002	0.72	61.39	1430.8	13.997	1.651	17.99
975.000	10.0	0.04500	0.04500	0.09000	0.04500	832.500	.002	0.72	61.39	1430.8	13.997	1.651	17.99
975.000	15.0	0.04500	0.04500	0.09000	0.09000	787.500	.002	0.72	61.39	1430.8	13.997	1.651	17.99
975.000	15.0	0.04500	0.04500	0.09000	0.09000	360.000	.002	0.72	61.39	1430.8	13.997	1.651	17.99
975.000	15.0	0.09000	0.04500	0.13500	0.09000	1057.500	.002	0.72	122.77	2861.5	6.998	1.651	8.99
975.000	15.0	0.04500	0.04500	0.09000	0.09000	787.499	.002	0.72	61.39	1430.8	13.997	1.651	17.99
975.000	15.0	0.04500	0.04500	0.09000	0.09000	562.500	.002	0.72	61.39	1430.8	13.997	1.651	17.99
975.000	15.0	0.09000	0.04500	0.13500	0.09000	765.000	.002	0.72	122.77	2861.5	6.998	1.651	8.99
975.000	15.0	0.09000	0.04500	0.09000	0.09000	517.500	.002	0.72	122.77	2861.5	6.998	1.651	8.99
975.000	15.0	0.09000	0.04500	0.09000	0.09000	967.500	.002	0.72	122.77	2861.5	6.998	1.651	8.99
975.000	15.0	0.04500	0.04500	0.09000	0.04500	585.000	.002	0.72	61.39	1430.8	13.997	1.651	17.99
975.000	15.0	0.09000	0.09000	0.09000	0.09000	450.000	.002	0.72	122.77	2861.5	6.998	1.651	8.99
975.000	15.0	0.04500	0.04500	0.09000	0.04500	1057.500	.002	0.72	61.39	1430.8	13.997	1.651	17.99
975.000	20.0	0.09000	0.04500	0.13500	0.09000	1012.499	.002	0.72	122.77	2861.5	6.998	1.651	8.99
975.000	20.0	0.04500	0.04500	0.09000	0.09000	472.500	.002	0.72	61.39	1430.8	13.997	1.651	17.99
975.000	20.0	0.04500	0.04500	0.09000	0.04500	697.500	.002	0.72	61.39	1430.8	13.997	1.651	17.99
975.000	20.0	0.09000	0.09000	0.09000	0.09000	540.000	.002	0.72	122.77	2861.5	6.998	1.651	8.99
975.000	20.0	0.09000	0.09000	0.04500	0.04501	382.500	.002	0.72	122.77	2861.5	6.998	1.651	8.99
975.000	20.0	0.09000	0.09000	0.09000	0.09000	510.000	.003	0.72	122.77	2861.5	10.497	1.651	13.49
975.000	20.0	0.09000	0.09000	0.13500	0.11500	680.000	.003	0.72	122.77	2861.5	10.497	1.651	13.49

975.000	20.0	0.09000	0.04500	0.09000	0.09000	675.000	.002	0.72	122.77	2861.5	6.998	1.651	8.99
975.000	20.0	0.09000	0.09000	0.13500	0.09000	765.000	.002	0.72	122.77	2861.5	6.998	1.651	8.99
975.000	20.0	0.09000	0.09000	0.13500	0.13500	607.500	.002	0.72	122.77	2861.5	6.998	1.651	8.99
975.000	20.0	0.04500	0.04500	0.09000	0.04500	652.500	.002	0.72	61.39	1430.8	13.997	1.651	17.99
975.000	20.0	0.09000	0.09000	0.09000	0.09000	585.000	.003	0.72	122.77	2861.5	10.497	1.651	13.49
975.000	20.0	0.09000	0.09000	0.09000	0.09000	405.000	.003	0.72	122.77	2861.5	10.497	1.651	13.49
975.000	20.0	0.09000	0.04500	0.09000	0.04500	630.000	.003	0.72	122.77	2861.5	10.497	1.651	13.49
975.000	20.0	0.09000	0.09000	0.09000	0.09000	240.000	.003	0.72	122.77	2861.5	10.497	1.651	13.49
975.000	20.0	0.09000	0.09000	0.09000	0.09000	585.000	.003	0.72	122.77	2861.5	10.497	1.651	13.49
975.000	20.0	0.04500	0.04500	0.04500	0.04500	525.000	.003	0.72	61.39	1430.8	20.995	1.651	26.98
975.000	10.0	0.04500	0.04500	0.09000	0.09000	517.499	.002	0.72	61.39	1430.8	13.997	1.651	17.99
975.000	10.0	0.09000	0.09000	0.13500	0.04500	600.000	.003	0.72	122.77	2861.5	10.497	1.651	13.49
975.000	30.0	0.04500	0.04500	0.09000	0.04500	480.000	.003	0.72	61.39	1430.8	20.995	1.651	26.98
975.000	30.0	0.04500	0.04500	0.13500	0.13500	697.500	.002	0.72	61.39	1430.8	13.997	1.651	17.99
975.000	30.0	0.04500	0.04500	0.04500	0.04500	585.000	.002	0.72	61.39	1430.8	13.997	1.651	17.99
975.000	30.0	0.04500	0.04500	0.09000	0.09000	555.000	.003	0.72	61.39	1430.8	20.995	1.651	26.98
975.000	30.0	0.09000	0.09000	0.13500	0.13500	382.500	.002	0.72	122.77	2861.5	6.998	1.651	8.99
975.000	30.0	0.04500	0.04500	0.09000	0.04500	450.000	.003	0.72	61.39	1430.8	20.995	1.651	26.98
975.000	30.0	0.04500	0.04500	0.09000	0.09000	697.500	.002	0.72	61.39	1430.8	13.997	1.651	17.99
975.000	30.0	0.09000	0.09000	0.09000	0.04500	585.000	.003	0.72	122.77	2861.5	10.497	1.651	13.49
975.000	30.0	0.09000	0.09000	0.09000	0.09000	465.000	.003	0.72	122.77	2861.5	10.497	1.651	13.49
975.000	30.0	0.09000	0.04500	0.09000	0.04500	607.500	.002	0.72	122.77	2861.5	6.998	1.651	8.99
975.000	30.0	0.04500	0.04500	0.09000	0.04500	562.500	.002	0.72	61.39	1430.8	13.997	1.651	17.99
975.000	30.0	0.09000	0.09000	0.09000	0.09000	427.500	.002	0.72	122.77	2861.5	6.998	1.651	8.99
975.000	30.0	0.09000	0.04500	0.09000	0.09000	705.000	.003	0.72	122.77	2861.5	10.497	1.651	13.49
975.000	30.0	0.04500	0.04500	0.04500	0.04500	420.000	.003	0.72	61.39	1430.8	20.995	1.651	26.98
1100.000	0.0	0.04500	0.04500	0.09000	0.04500	855.000	.002	0.81	78.14	1614.2	15.791	1.506	19.38
1100.000	0.0	0.04500	0.04500	0.09000	0.09000	922.500	.002	0.81	78.14	1614.2	15.791	1.506	19.38
1100.000	0.0	0.04500	0.04500	0.09000	0.09000	510.000	.003	0.81	78.14	1614.2	23.687	1.506	29.06
1100.000	5.0	0.04500	0.04500	0.04500	0.04500	247.500	.002	0.81	78.14	1614.2	15.791	1.506	19.38

1100.000	5.0	0.04500	0.04500	0.09000	0.09000	652.500	.002	0.81	78.14	1614.2	15.791	1.506	19.38
1100.000	5.0	0.04500	0.04500	0.09000	0.09000	675.000	.002	0.81	78.14	1614.2	15.791	1.506	19.38
1100.000	5.0	0.09000	0.09000	0.09000	0.04500	382.500	.002	0.81	156.27	3228.4	7.896	1.506	9.69
1100.000	5.0	0.09000	0.04500	0.13500	0.13500	675.000	.002	0.81	156.27	3228.4	7.896	1.506	9.69
1100.000	5.0	0.09000	0.09000	0.13500	0.04500	517.500	.002	0.81	156.27	3228.4	7.896	1.506	9.69
1100.000	5.0	0.09000	0.04500	0.13500	0.04500	450.000	.002	0.81	156.27	3228.4	7.896	1.506	9.69
1100.000	5.0	0.09000	0.04500	0.09000	0.09000	540.000	.002	0.81	156.27	3228.4	7.896	1.506	9.69
1100.000	5.0	0.09000	0.04500	0.09000	0.09000	607.500	.002	0.81	156.27	3228.4	7.896	1.506	9.69
1100.000	5.0	0.09000	0.09000	0.13500	0.04500	742.499	.002	0.81	156.27	3228.4	7.896	1.506	9.69
1100.000	5.0	0.09000	0.04500	0.09000	0.09000	787.499	.002	0.81	156.27	3228.4	7.896	1.506	9.69
1100.000	5.0	0.09000	0.04500	0.09000	0.09000	720.000	.002	0.81	156.27	3228.4	7.896	1.506	9.69
1100.000	5.0	0.09000	0.09000	0.13500	0.13500	675.000	.002	0.81	156.27	3228.4	7.896	1.506	9.69
1100.000	5.0	0.04500	0.04500	0.09000	0.09000	315.000	.002	0.81	78.14	1614.2	15.791	1.506	19.38
1100.000	5.0	0.04500	0.04500	0.09000	0.09000	540.000	.002	0.81	78.14	1614.2	15.791	1.506	19.38
1100.000	5.0	0.09000	0.04500	0.13500	0.09000	495.000	.003	0.81	156.27	3228.4	11.843	1.506	14.53
1100.000	10.0	0.04500	0.04500	0.09000	0.09000	472.500	.002	0.81	78.14	1614.2	15.791	1.506	19.38
1100.000	10.0	0.09000	0.04500	0.09000	0.04500	832.500	.002	0.81	156.27	3228.4	7.896	1.506	9.69
1100.000	10.0	0.04500	0.04500	0.09000	0.09000	795.000	.003	0.81	78.14	1614.2	23.687	1.506	29.06
1100.000	10.0	0.04500	0.04500	0.09000	0.09000	495.000	.002	0.81	78.14	1614.2	15.791	1.506	19.38
1100.000	10.0	0.04500	0.04500	0.04500	0.04500	562.500	.002	0.81	78.14	1614.2	15.791	1.506	19.38
1100.000	10.0	0.04500	0.04500	0.09000	0.04500	765.000	.002	0.81	78.14	1614.2	15.791	1.506	19.38
1100.000	10.0	0.04500	0.04500	0.09000	0.09000	870.000	.003	0.81	78.14	1614.2	23.687	1.506	29.06
1100.000	10.0	0.04500	0.04500	0.09000	0.04500	900.000	.002	0.81	78.14	1614.2	15.791	1.506	19.38
1100.000	10.0	0.09000	0.04500	0.09000	0.09000	562.500	.002	0.81	156.27	3228.4	7.896	1.506	9.69
1100.000	10.0	0.09000	0.04500	0.04500	0.04500	675.000	.002	0.81	156.27	3228.4	7.896	1.506	9.69
1100.000	10.0	0.09000	0.04500	0.09000	0.04500	517.499	.002	0.81	156.27	3228.4	7.896	1.506	9.69
1100.000	10.0	0.04500	0.04500	0.09000	0.04500	450.000	.002	0.81	78.14	1614.2	15.791	1.506	19.38
1100.000	10.0	0.04500	0.04500	0.09000	0.09000	360.000	.002	0.81	78.14	1614.2	15.791	1.506	19.38
1100.000	10.0	0.04500	0.04500	0.09000	0.09000	630.000	.002	0.81	78.14	1614.2	15.791	1.506	19.38
1100.000	10.0	0.09000	0.04500	0.09000	0.04500	832.500	.002	0.81	156.27	3228.4	7.896	1.506	9.69

1100.000	10.0	0.09000	0.09000	0.09000	0.09000	787.500	.002	0.81	156.27	3228.4	7.896	1.506	9.69
1100.000	15.0	0.04500	0.04500	0.09000	0.09000	675.000	.002	0.81	78.14	1614.2	15.791	1.506	19.38
1100.000	15.0	0.04500	0.04500	0.09000	0.09000	765.000	.002	0.81	78.14	1614.2	15.791	1.506	19.38
1100.000	15.0	0.04500	0.04500	0.09000	0.04500	472.500	.002	0.81	78.14	1614.2	15.791	1.506	19.38
1100.000	15.0	0.04500	0.04500	0.09000	0.09000	495.000	.002	0.81	78.14	1614.2	15.791	1.506	19.38
1100.000	15.0	0.04500	0.04500	0.09000	0.09000	615.000	.001	0.81	78.14	1614.2	23.687	1.506	29.06
1100.000	15.0	0.04500	0.04500	0.09000	0.09000	900.000	.002	0.81	78.14	1614.2	15.791	1.506	19.38
1100.000	15.0	0.09000	0.04500	0.09000	0.09000	585.000	.002	0.81	156.27	3229.4	7.896	1.506	9.69
1100.000	15.0	0.04500	0.04500	0.09000	0.04500	652.500	.002	0.81	78.14	1614.2	15.791	1.506	19.38
1100.000	15.0	0.04500	0.04500	0.09000	0.09000	1057.500	.002	0.81	78.14	1614.2	15.791	1.506	19.38
1100.000	15.0	0.09000	0.04500	0.09000	0.09000	697.500	.002	0.81	156.27	3228.4	7.896	1.506	9.69
1100.000	15.0	0.04500	0.04500	0.09000	0.09000	585.000	.002	0.81	78.14	1614.2	15.791	1.506	19.38
1100.000	15.0	0.04500	0.04500	0.09000	0.09000	450.000	.002	0.81	78.14	1614.2	15.791	1.506	19.38
1100.000	15.0	0.09000	0.04500	0.09000	0.09000	525.000	.003	0.81	156.27	3228.4	11.843	1.506	14.53
1100.000	15.0	0.04500	0.04500	0.09000	0.04500	652.500	.002	0.81	78.14	1614.2	15.791	1.506	19.38
1100.000	15.0	0.04500	0.04500	0.04500	0.04500	742.499	.002	0.81	78.14	1614.2	15.791	1.506	19.38
1100.000	15.0	0.04500	0.04500	0.04500	0.04500	832.500	.002	0.81	78.14	1614.2	15.791	1.506	19.38
1100.000	15.0	0.04500	0.04500	0.04500	0.04500	787.499	.002	0.81	78.14	1614.2	15.791	1.506	19.38
1100.000	15.0	0.04500	0.04500	0.04500	0.04500	697.500	.002	0.81	78.14	1614.2	15.791	1.506	19.38
1100.000	20.0	0.04500	0.04500	0.09000	0.04500	742.499	.002	0.81	78.14	1614.2	15.791	1.506	19.38
1100.000	20.0	0.09000	0.04500	0.04500	0.04500	697.500	.002	0.81	156.27	3228.4	7.896	1.506	9.69
1100.000	20.0	0.04500	0.04500	0.09000	0.09000	877.500	.002	0.81	78.14	1614.2	15.791	1.506	19.38
1100.000	20.0	0.04500	0.04500	0.09000	0.04500	1012.500	.002	0.81	78.14	1614.2	15.791	1.506	19.38
1100.000	20.0	0.04500	0.04500	0.09000	0.09000	600.000	.003	0.81	78.14	1614.2	23.687	1.506	29.06
1100.000	20.0	0.04500	0.04500	0.09000	0.04500	607.500	.002	0.81	78.14	1614.2	15.791	1.506	19.38
1100.000	20.0	0.04500	0.04500	0.09000	0.09000	765.000	.002	0.81	78.14	1614.2	15.791	1.506	19.38
1100.000	20.0	0.04500	0.04500	0.09000	0.09000	585.000	.002	0.81	78.14	1614.2	15.791	1.506	19.38
1100.000	20.0	0.04500	0.04500	0.09000	0.09000	562.500	.002	0.81	78.14	1614.2	15.791	1.506	19.38
1100.000	20.0	0.04500	0.04500	0.09000	0.04500	1014.999	.002	0.81	78.14	1614.2	15.791	1.506	19.38
1100.000	10.0	0.09000	0.09000	0.09000	0.04500	1125.000	.002	0.81	156.27	3229.4	7.896	1.506	9.69

1100.000	30.0	0.09000	0.04500	0.09000	0.04500	585.000	.002	0.81	156.27	3228.4	7.896	1.506	9.69
1100.000	30.0	0.04500	0.04500	0.09000	0.04500	877.500	.002	0.81	78.14	1614.2	15.791	1.506	19.38
1100.000	30.0	0.04500	0.04500	0.09000	0.04500	855.000	.002	0.81	78.14	1614.2	15.791	1.506	19.38
1100.000	30.0	0.04500	0.04500	0.04500	0.04500	630.000	.002	0.81	78.14	1614.2	15.791	1.506	19.38
1100.000	30.0	0.04500	0.04500	0.09000	0.04500	540.000	.003	0.81	78.14	1614.2	23.687	1.506	29.06
1100.000	30.0	0.04500	0.04500	0.09000	0.04500	525.000	.003	0.81	78.14	1614.2	23.687	1.506	29.06
1100.000	30.0	0.09000	0.09000	0.09000	0.04500	855.000	.002	0.81	156.27	3228.4	7.896	1.506	9.69
1100.000	30.0	0.04500	0.04500	0.04500	0.04500	697.500	.002	0.81	78.14	1614.2	15.791	1.506	19.38
1100.000	30.0	0.04500	0.04500	0.09000	0.09000	450.000	.002	0.81	78.14	1614.2	15.791	1.506	19.38
1100.000	50.0	0.09000	0.04500	0.09000	0.04500	1012.500	.002	0.81	156.27	3228.4	7.896	1.506	9.69
1100.000	50.0	0.04500	0.04500	0.09000	0.04500	517.500	.002	0.81	78.14	1614.2	15.791	1.506	19.38
1100.000	50.0	0.04500	0.04500	0.09000	0.04500	1080.000	.002	0.81	78.14	1614.2	15.791	1.506	19.38
1100.000	50.0	0.04500	0.04500	0.09000	0.04500	705.000	.003	0.81	78.14	1614.2	23.687	1.506	29.06
1100.000	50.0	0.04500	0.04500	0.09000	0.09000	360.000	.002	0.81	78.14	1614.2	15.791	1.506	19.38
1100.000	50.0	0.04500	0.04500	0.09000	0.04500	585.000	.002	0.81	78.14	1614.2	15.791	1.506	19.38
1100.000	50.0	0.09000	0.09000	0.09000	0.04500	705.000	.003	0.81	156.27	3228.4	11.843	1.506	14.53
1100.000	50.0	0.04500	0.04500	0.09000	0.04500	596.250	.004	0.81	78.14	1614.2	31.582	1.506	38.75
1100.000	50.0	0.09000	0.04500	0.09000	0.09000	505.000	.002	0.81	156.27	3228.4	7.896	1.506	9.69

```
END OF FILE ON #DATA(2,1873) CAUSES A RETURN TO MTS.
EXECUTION TERMINATED   00:20:29  T=1.509  RC=0       $.43

$SIG
```

APPENDIX G

WAVE GROWTH THEORY ON LIQUID DROPLET SURFACE

To understand the droplet break-up mechanism, the use of unstable wave growth theory has been suggested.(B8,R5) A summary of these theories is presented here.

Considering the moving liquid droplet as the frame of reference, the following schematic describes droplet motion.

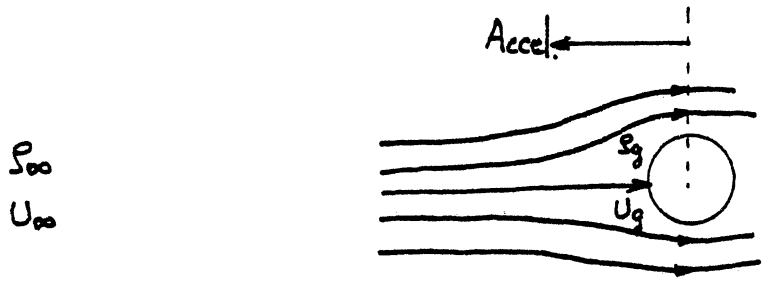

The gas-liquid interface is assumed smooth and potential flow to exist in the gas. Then wave displacement can be expressed,

$$Y = Y_o + \eta = y_o + \eta_o e^{i(kx-\sigma t)} \tag{G.1}$$

From the solution of Lamb(L6) or Chandrasekhr(C17)

$$\frac{\sigma}{k} = \frac{\rho_f U_f + \rho_g U_g}{\rho_f + \rho_g} + \left(-\frac{\rho_f \rho_g (U_g - U_f)^2}{(\rho_f + \rho_g)^2} + \frac{(\rho_f - \rho_g)\frac{g}{k} + KS}{\rho_f + \rho_g} \right)^{1/2} \tag{G.2}$$

Replacing

$$\frac{\rho_f U_f + \rho_g U_g}{\rho_f + \rho_g} = V \tag{G.3}$$

and

$$g = -A \tag{G.4}$$

where,

$$\rho_f \frac{4}{3} \pi \left(\frac{D_o}{2}\right)^3 A = C_D \left(\frac{\pi}{4} D_o^2\right) \frac{\rho_g U_\infty^2}{2}$$

$$\therefore \quad A = \frac{3}{4} C_D \left(\frac{\rho_g}{\rho_f}\right) \frac{U_\infty^2}{D_o} \tag{G.5}$$

Equation (G.2) becomes,

$$\frac{\sigma}{k} = V + \left(- \frac{\rho_f \rho_g (U_g - U_f)^2}{(\rho_f + \rho_g)^2} - \frac{(\rho_f - \rho_g) A}{(\rho_f + \rho_g) k} + \frac{kS}{\rho_f + \rho_g} \right)^{1/2} \qquad (G.6)$$

(1) (2) (3)

If the sum of terms within the square root is negative, the wave will become unstable and grow. Each term in Eq. (G.6) can be interpreted as follows:

(1) Relative velocity term between gas and liquid on the drop (Kelvin-Helmholtz term)

(2) Acceleration term due to drag (Rayleigh-Taylor term)

(3) Surface tension term

Here (1) and (2) are destabilizing factors, while (3) is stabilizing. Since $\rho_f >> \rho_g$ ($U_g >> U_f$),

$$\frac{(2)}{(1)} \cong \frac{\rho_f}{\rho_g} \frac{A}{k} \frac{1}{(U_g - U_f)^2} = \frac{\rho_f}{\rho_g} \frac{3}{4} C_D \frac{\rho_g}{\rho_f} \frac{U_\infty^2}{D_o} \frac{\lambda}{2\pi} \frac{1}{U_g^2}$$

$$\therefore \frac{(2)}{(1)} \cong \frac{3}{8} \frac{C_D}{\pi Q} \frac{\lambda}{D_o} \qquad (G.7)$$

where,

$$Q = \frac{\rho_g U_g^2}{\rho_g U_\infty^2} = \frac{\text{Dynamic pressure of gas at drop surface}}{\text{Dynamic pressure of gas ahead of drop}} \qquad (G.8)$$

$$\frac{(3)}{(1)} = \frac{2\pi}{\lambda} \frac{S}{(\rho_f + \rho_g)} \frac{(\rho_f + \rho_g)^2}{\rho_f \rho_g (U_g - U_f)^2} \cong \frac{2\pi}{\lambda} \frac{S}{\rho_g U_g^2}$$

$$\therefore \frac{(3)}{(1)} = \frac{2\pi}{\lambda} \frac{S}{\rho_g U_\infty^2 D_o} \frac{D_o}{U_g^2 / U_\infty^2} = \frac{2\pi}{\lambda} \frac{D_o}{We_b Q} \qquad (G.9)$$

where $$We_b = \frac{\rho_g U_\infty^2 D_o}{S} \qquad (G.10)$$

For unstable case, from Eq. (G.6),

$$\sigma - kV = iU_g \sqrt{\frac{\rho_g}{\rho_f}} \frac{2\pi}{\lambda} \left[1 + \frac{1}{Q}\left(\frac{3}{4}\frac{C_D}{D_o}\frac{\lambda}{2\pi} - \frac{2\pi}{\lambda}\frac{D_o}{We_b}\right)\right]^{1/2} \qquad (G.11)$$

Rearranging Eq. (G.11) the dimensionless time, T_σ is

$$T_\sigma = \frac{i2\pi}{\sigma - kV}\frac{U_\infty}{D_o}\sqrt{\frac{\rho_g}{\rho_f}} = \frac{\lambda}{D_o} Q^{-1/2}\left[1+\frac{1}{Q}\left(\frac{3}{4}\frac{C_D}{D_o}\frac{\lambda}{2\pi} - \frac{2\pi}{\lambda}\frac{D_o}{We_b}\right)\right]^{-1/2}$$

$$\cong \frac{\lambda}{D_o}\left(Q + \frac{3}{4}\frac{C_D}{2\pi}\frac{\lambda}{D_o} - \frac{2\pi}{We_b}\frac{D_o}{\lambda}\right)^{-1/2} \qquad (G.12)$$

The fastest growing wave length, λ_f, is obtained by setting,

$$\frac{\partial T_\sigma}{\partial \lambda} = 0$$

Then

$$\frac{\lambda_f}{D_o} = \frac{8\pi}{3C_D} Q \left[\left(1 + \frac{9}{4}\frac{C_D}{Q^2 We_b}\right)^{1/2} - 1\right] \qquad (G.13)$$

Also the critical (or cut-off) wavelength, λ_c is obtained by setting, $T_\sigma \longrightarrow \infty$

then

$$\frac{\lambda_c}{D_o} = \frac{4\pi Q}{3 C_D}\left[\left(1 + \frac{3 C_D}{Q^2 We_b}\right)^{1/2} - 1\right] \qquad (G.14)$$

For large vaues of We_b, two limiting cases can be obtained as,

i) $Q = 0$ (1)

$$\frac{\lambda_c}{D_o} = \frac{2\pi}{Q We_b}$$

$$\frac{\lambda_f}{D_o} = \frac{3\pi}{QWe_b}$$

$$T\sigma_f = \pi\left(\frac{3}{Q}\right)^{3/2} We_b^{-1}$$

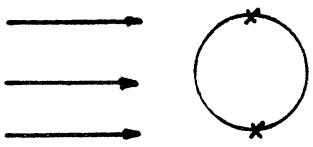

ii) $Q^2 << We_b$

$$\frac{\lambda_c}{D_o} = \frac{4\pi}{\sqrt{3C_D We_b}}$$

$$\frac{\lambda_f}{D_o} = \frac{4\pi}{\sqrt{C_D We_b}}$$

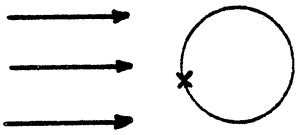

$$T\sigma_f = \frac{4\pi}{C_D^{3/4} We_b^{1/4}}$$